Burkholderia sigma factor systems with metal-responsive regulatory domains

By:

Christopher D. Banyard

A thesis submitted in partial fulfilment of the requirements for the degree of
Doctor of Philosophy

The University of Sheffield
Faculty of Medicine, Dentistry and Health, The Medical School
Department of Infection, Immunity and Cardiovascular Disease

Submission Date:
October 2019

Acknowledgments

I owe a great deal to my supervisor Dr Mark Thomas for his patience, support and guidance over the years. I would also like to thank Professor Jeff Green, for his valuable insights and encouragement. I am indebted to Dr Srdjan (Guta) Vitovski for his work and training in performing bio layer interferometry assays. I am also grateful to the BBSRC White Rose Mechanistic Biology DTP for funding this project.

There are many members of lab LU103 whom I am thankful to have worked with, and you all made the many hours spending toiling away more bearable. I am especially grateful to Dr Aaron Butt – he paved the way forward for my work and taught me everything from how to perform a β-gal assay to where the best lunch could be found (I miss our Falafel King Fridays!). I would like to thank the wider Infection, Immunity and Cardiovascular Disease department for providing all the training and resources that made this work possible.

I will be eternally grateful to all the family and friends who have supported me along the way, maybe without even realising it. I will always remember your confidence in me, when I had none. I am especially grateful to my parents, for their guidance and trust for as long as I can remember. I hope I make you proud.

Finally, I owe a special debt of gratitude to my incredible wife, Ellie. For all the times you were there, and all the times I was not, I can only apologise and thank you for your unerring faith and love.

Table of Contents

Abstract

Burkholderia pseudomallei and *Burkholderia cenocepacia* are pathogenic bacteria that are the causative agents of the deadly diseases melioidosis and 'cepacia syndrome', respectively. Both species utilise extracytoplasmic function (ECF) sigma factors, alternative subunits of bacterial RNA polymerase, to transduce extracellular signals and drive the transcription of specific genes. MbaS, from *Burkholderia pseudomallei*, and OrbS, from *Burkholderia cenocepacia,* are two iron starvation (IS) sigma factors that regulate gene clusters associated with the iron-chelating siderophores mallebaction and ornibactin, respectively.

Evidence has been presented in this study that these proteins contain on-board C-terminal regulatory extensions that transduce the presence of selected metal ions via cysteine thiol groups. Firstly, C-terminal trucnations of OrbS were assayed through colorimetric siderophore assays and promoter-reporter analyses to demonstrate that the C-terminal extension is required for sigma factor activity, and may be necessary for iron-dependent regulation. A series of gene deletions were also introduced into *B. thailandensis*, a safer surrogate species of *B. pseudomallei*, through allelic exchange to delete *mbaS* and the secondary siderophore pyochelin. Through use of these constructed mutants and promoter-reporter analyses, the target promoters of MbaS have been identified and Fur regulation of the sigma factor has been established. Using further promoter-reporter analyses and *in vitro* techniques to assay transcription activity and protein-protein interaction, it has been demonstrated that the sigma factor activity of OrbS is inhibited in the presence of Fe(II), Cu(II) and Zn(II) ions, and the sigma factor activity of MbaS is inhibited in the presence of Zn(II).

This could represent a novel regulation mechanism of a class of bacterial sigma factors.

List of tables

List of figures

Abbreviations

ABC	ATP-binding cassette
Amp	Ampicillin
APS	Ammonium persulphate
BACTH	Bacterial adenylate cyclase two-hybrid
Bcc	*Burkholderia cepacia* complex
Bce	*Burkholderia cenocepacia*
BHR	Broad host range
BLI	Bio layer interferometry
Bma	*Burkholderia mallei*
Bpc	*Burkholderia pseudomallei* complex
Bps	*Burkholderia pseudomallei*
BSA	Bovine serum albumin
BSL	Biosafety Level
Bth	*Burkholderia thailandensis*
CAA	Casamino acids
CAP	Catabolite activator protein
CAS	Chrome-azurol sulphonate
CF	Cystic fibrosis
Cm	Chloramphenicol
cPhe	DL-4-chlorophenylalanine
CRD	Cysteine-rich domain
CRE	Cysteine-rich extension
CRP	cAMP receptor protein
CTD	C-terminal domain
d.	Distilled
DMSO	Dimethylsulphoxide
DP	2,2-dipyridyl
DTPA	Diethylenetriaminepentaacetic acid (pentetic acid)
DTT	Dithiothreitol
EB	Environmental broth
ECF	Extra-cytoplasmic function
EDDHA	Ethylenediamine-N,N'-bis(2-hydroxyphenylacetic acid)
Fur$^{+/-}$	*fur* positive/negative phenotype
FURTA	Fur titration assay
Gm	Gentamicin
HDTMA	Hexadecyltrimethylammonium bromide
HEPES	4-(2-hydroxyethyl)-1-piperazineethanesulphonic acid
HGED	HEPES glycerol EDTA DTT (buffer)
IMAC	Immobilised metal ion affinity chromatography
IPTG	Isopropyl β-D-thiogalactoside
IST	Iso-sensitest
*iv*T	*in vitro* transcription
Km	Kanamycin
Lac$^{+/-}$	Lactose fermentation positive/negative phenotype
Lnx	Lennox
MALDI-TOF	Matrix-assisted laser desorption/ionisation time-of-flight
Mba$^{+/-}$	Malleobactin positive/ negative phenotype
MLST	Multi-locus sequence typing
MOPS	3-(N-morpholino)propanesulphonic acid
Mu	Miller units

NRPS	Non-ribosomal peptide synthetase
NTD	N-terminal domain
ONPG	Ortho-nitrophenyl-D-galactoside
Orb$^{+/-}$	Ornibactin positive/negative phenotype
pBBR1	pBBR1MCS
pBBR2	pBBR1MCS-2
pBBR3	pBBR1MCS-3
pBBR5	pBBR1MCS-5
PBS	Phosphate-buffered saline
PBP	Periplasmic binding protein
Pch$^{+/-}$	Pyochelin positive/negative phenotype
PKS	Polyketide synthase
RNAP	RNA polymerase
RND	Resistance-nodulation-division
Sarkosyl	N-lauroylsarcosine
SOE	Synthesis by overlap extension
T3SS	Type III secretion system
T5SS	Type V secretion system
T6SS	Type VI secretion system
T_a	Annealing temperature
T_m	Melting temperature
TAE	Tris acetate EDTA (buffer)
TBE	Tris boric acid EDTA (buffer)
TBDR	TonB-dependent receptor
TBS-T	Tris-buffered saline-tween
Tc	Tetracycline
TE	Tris EDTA (buffer)
TEMED	Tetramethylethylenediamine
Tp	Trimethoprim
TPR	Tetratrico peptide repeat
X-gal	5-bromo-4-chloro-3-indolyl-β-D-galactoside

Chapter I: Introduction

1.1 The *Burkholderia* genus

1.1.1 Characteristics of *Burkholderia*

Burkholderia is a large, diverse and complex genus comprised of over 90 species. Recently, some of these species have undergone reclassification, which is expounded upon in section 1.1.2. *Burkholderia* are Gram-negative β-proteobacteria and typically have large genomes of around 6-11 Mb with high GC content, normally organised into 2-3 chromosomes (Mannaa, Park and Seo, 2018; Depoorter *et al.*, 2016). *Burkholderia* species can be found in a variety of contexts including as pathogens, phytopathogens, symbiotic and free-living non-symbiotic strains. Identified strains are usually isolated from environmental (water, soil, fungi, plant) or clinical (animal and human) environments (Parke and Gurian-Sherman, 2001).

Species of *Burkholderia* are noted for their adaptability, accomplished through their large and gene-rich genomes containing a variety of different genes enabling survival in environments with stressful conditions (Mahenthiralingam, Urban and Goldberg, 2005; Duangurai, Indrawattana and Pumirat, 2018), resistances to many commonly used antibiotics (Rhodes and Schweizer, 2016), and genetic plasticity achieved through multiple transposable insertion sequence elements (Lessie *et al.*, 1996).

1.1.2 Taxonomy

Initially described as a *Pseudomonas* species, *Burkholderia* was identified as a distinct genus with seven species by (Yabuuchi *et al.*, 1992). The *Burkholderia* sensu lato now comprises at least 92 species and the splitting and reclassification of the genus into more closely defined groups is currently underway and may include the major genera *Burkholderia*, *Paraburkholderia*, *Caballeronia*, and the minor genera *Trinickia*, *Mycetohabitans*, and *Robbsia* (Figure 1.1).
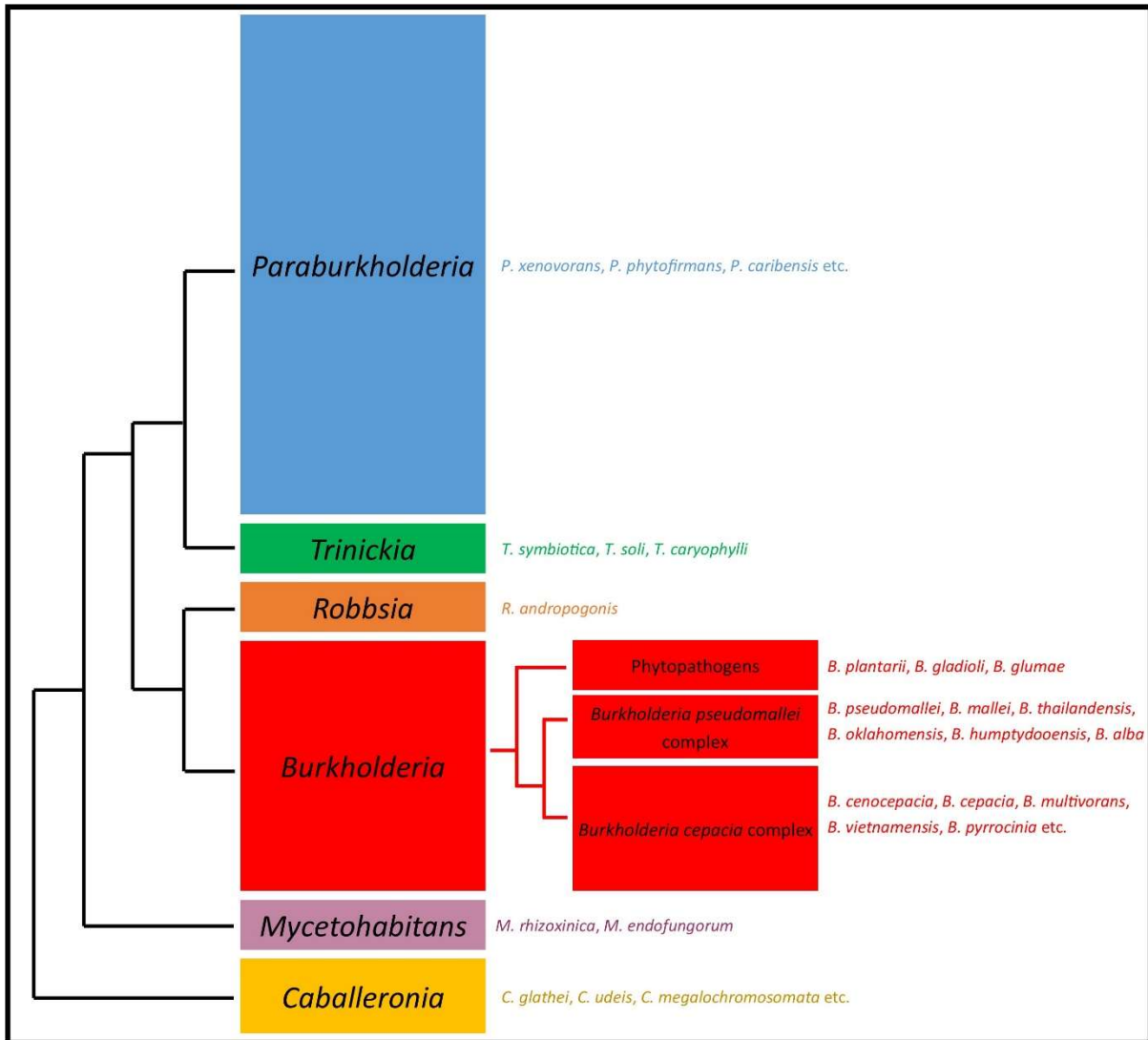
Figure 1.1. Phylogenetic tree of *Burkholderia* sensu lato

Shown genera are based upon the 16S rRNA-based phylogenetic tree constructed by (Mannaa, Park and Seo, 2018) using data from the SILVA database (https://www.arb-silva.de/). Note that alternative phylogenetic analyses (for example (Estrada-de Los Santos *et al.*, 2018)) may show different intergeneric relationships, but distinct groups remain consistent. The genus *Burkholderia* sensu stricto is expanded further to show the three intrageneric groups. Examples of representative strains are displayed next to each genus. Taxonomic positions and sizes of genus boxes are not to scale.

The species of *Burkholderia* that are capable of causing human or animal infection all fall within the genus *Burkholderia* sensu stricto; this is one of the key characteristics of the group (Estrada-de los Santos *et al.*, 2013). Compared to other *Burkholderia* sensu lato species, the *Burkholderia* sensu stricto species have genomes with higher GC content, contain genes for the virulence-associated Type III secretion system-3 (T3SS-3) and Type VI

secretion system-5 (T6SS-5) and do not have genes for Type IV secretion systems (T4SS) (Angus *et al.*, 2014). Additionally, a second flagella system used in intracellular motility is only found in *Burkholderia* sensu stricto species (French *et al.*, 2011).

Members of the newly created genus *Paraburkholderia* are often associated with plants and/or fungi, either as symbionts, phytopathogens or as free-living/endophytic species (Sawana, Adeolu and Gupta, 2014). They are closely related to the newly created *Trinickia* genus (Estrada-de Los Santos *et al.*, 2018) (can be legume nodulators or phytopathogenic) and the *Caballeronia* group (Dobritsa and Samadpour, 2016) (often free-living nitrogen-fixing endosymbionts initially described as a clade between *Burkholderia* and *Paraburkholderia*). Much is shared in common with the *Robbsia* genus which also contains a plant-pathogenic ormer *Burkholderia* species – but the type species *R. andropogonis* has a single polar sheathed flagellum and can produce rhizobitoxine (Lopes-Santos *et al.*, 2017).

Finally, the *Mycetohabitans* genus currently containing two former Burkholderia sensu stricto species, is typified by the smaller genomes (3-4 Mb) of its member species and their lifestyle as fungal endosymbionts (Estrada-de Los Santos *et al.*, 2018).

1.1.3 The *Burkholderia pseudomallei* complex

A sub-group of the *Burkholderia* genus, the *Burkholderia pseudomallei* complex (Bpc) currently contains six species. These are *B. pseudomallei* (Whitmore, 1913), *B. mallei* (Nierman *et al.*, 2004), *B. thailandensis* (Brett, DeShazer and Woods, 1998), *B. oklahomensis (Glass et al., 2006)*, *B. humptydooensis* (Tuanyok *et al.*, 2017) and *B. alba* (Lee, Kim and Park, 2018).

The complex's species are usually soil saprophytes. However, two species are also considered pathogenic. *B. pseudomallei* is the etiological agent of the human disease melioidosis (see section 1.2), and its clone *B. mallei* causes the disease glanders in equines (and in rare cases humans) (Van Zandt, Greer and Gelhaus, 2013).

The remaining four species are closely related and are considered to be non-pathogenic. However, both *B. thailandensis* and *B. oklahomensis* have been observed to cause clinical

infections in humans under extreme and rare circumstances (Glass *et al.*, 2006; Gee *et al.*, 2018).

1.1.4 *Burkholderia pseudomallei*

B. pseudomallei (*Bps*) is the causative agent of melioidosis (see section 1.2). Unlike the obligate parasite *B. mallei* (*Bma*), *Bps* is an environmental saprophyte that acts as an opportunistic pathogen of humans and other animals. It is often found in the soil in the tropics – in particular, rice paddy fields in South-East Asia. *Bps* has a large genome of 7.2 Mb, split across two chromosomes of 4 Mb and 3.2 Mb, with a high GC content of around 68% and encodes around 5,900 genes (Holden *et al.*, 2004).

Bps is considered a Category B agent for biosecurity and bioterrorism by the US Centers for Disease Control (CDC). A significant aspect of the virulence of *Bps*, and an important justification for its bioterror agent classification, is its multiple antibiotic resistances (Rhodes and Schweizer, 2016). Perhaps the most effective system of antibiotic resistance in *Bps* is through its ten multi-drug efflux pumps of the resistance-nodulation-division (RND) type, conferring resistance to six antibiotic classes (Podnecky, Rhodes and Schweizer, 2015). These are important due to their ability to export antibiotics across a combination of the cytoplasmic membrane, the periplasm and the outer membrane. Three RND family efflux pumps have been elucidated in *Bps*: AmrAB-OprA (contributing to macrolide, aminoglycoside and tetracycline resistance) (Trunck *et al.*, 2009), BpeAB-OprB (contributing to macrolide, tetracycline, chloramphenicol and fluoroquinolone resistance) (Chan *et al.*, 2004; Mima and Schweizer, 2010) and BpeEF-OprC (contributing to tetracycline, trimethoprim, chloramphenicol, fluoroquinolone and sulphamethoxozole resistance) (Kumar, Chua and Schweizer, 2006; Podnecky *et al.*, 2013). Further β-lactam resistance (more specifically carbapenems) is achieved via the type 2 metallo β-lactamase encoded from *blaNDM-1* (González *et al.*, 2016) and further trimethoprim resistance is conferred by mutations in the dihydrofolate reductase gene *folA* (Podnecky *et al.*, 2013). Additional antibiotic resistances are achieved through expressing the PenA class A β-lactamase (providing resistance to β-lactams) (Randall *et al.*, 2015), via the low permeability of the outer membrane (in particular due to the outer membrane porin Omp38 providing

resistance to polymyxin B) (Aunkham *et al.*, 2014) and by encoding a mutated form of the GyrA DNA gyrase (providing resistance to fluoroquinolones) (Rhodes and Schweizer, 2016).

Due to the hazardous nature of *Bps*, it must be handled in microbiological Containment Level 3 facilities. Therefore, it is common practice to use the closely-related but non-pathogenic surrogate species *Burkholderia thailandensis* (*Bth*), which may be handled in Containment Level 2 laboratories (see section 1.1.5).

1.1.5 *Burkholderia thailandensis*

Bth was first identified as a *Bps*-like species, isolated in the same ecological niches, which displayed a decreased relative virulence (Brett, DeShazer and Woods, 1998). The species type strain *Bth* E264 shows a high degree of genomic synteny with *Bps*, with a similar number of coding regions, distributions of protein structural families and several shared genomic islands of unusually high GC-content or bacteriophage-related genes (Yu *et al.*, 2006).

Unsurprisingly, there are several *Bps* virulence factors that are not found in the avirulent *Bth* E264. A major one of these is the bacterial cell capsule polysaccharide encoded by the *wcbA-T* genes; uncommon *Bth* strains that are able to produce a *Bps*-like capsule, such as strain E555, are also noteworthy displaying similar growth patterns to *Bps* in macrophages. However, they still cannot cause disease in murine models of disease and there are likely additional factors involved (Kovacs-Simon *et al.*, 2019).

Another important difference between *Bth* and *Bps* is the former's ability to assimilate arabinose (Smith *et al.*, 1997). The nine-gene operon conferring the ability to metabolise L-arabinose found in *Bth* is not found in *Bps*, and the reintroduction of this operon into *Bps* has been demonstrated to reduce the pathogen's virulence, most likely via the downregulation of its type III secretion system 3 (T3SS-3) (Moore *et al.*, 2004).

1.1.6 The *Burkholderia cepacia* complex

Another sub-group of the *Burkholderia* genus is the *Burkholderia cepacia* complex (Bcc). Currently, this group contains 22 reported member species based upon homology of the *B. cepacia recA* gene (Devanga, Naveen and Veeraraghavan, 2019). Member species of the Bcc, including *B. cencepacia* (*Bce*), are noted for their ability to opportunistically infect and cause disease in immunocompromised individuals. This usually manifests as a pulmonary infection, and can lead to disease known as '*Cepacia* syndrome' (more detail in section 1.3). Bcc species are also found interact non-pathogenically with plants, where their ability to perform nitrogen fixation and produce anti-fungal compounds could have useful applications in agriculture (Coenye and Vandamme, 2003).

The significant aspect of Bcc species is the multiple antimicrobial resistances that can be employed. Bcc species can display resistances to carboxypenecillins, polymyxins and 1st-generation cephalosporins (Mahenthiralingam, Urban and Goldberg, 2005). This antimicrobial resistance is brought about by a series of key factors.

Firstly, the outer membrane of Bcc species is a major factor in antibiotic resistance. A decreased permeability of this membrane relative to other bacteria can be acquired and confers an inherent resistance to many aminoglycosides and β-lactams (Moore and Hancock, 1986). Additionally, the LPS of the outer membrane can be modified by the MrgS/MrgR two-component regulatory switch imparting polymyxin resistance (Kumar *et al.*, 2016). The LPS can also lack several binding sites, providing resistance to cationic antibiotics such as aminoglycosides. In cases of prolonged infection, Bcc species have been found to lose the O-antigen component of LPS, enabling evasion from host immune recognition (Hassan, Coutinho and Sa-Correia, 2019).

As with *Bps*, many antibiotic resistances are conferred by the class A β-lactamase PenA and through multiple RND efflux pump systems (AmrAB-OprA, BpeEF-OprC and BpeAM-OprB) (Biot *et al.*, 2011). All three efflux pumps provide resistance to tetracycline, AmrAB-OprA also provides resistances to aminoglycosides and macrolides, and BpeEF-OprC provides resistances to chloramphenicol, fluoroquinones and trimethoprim-sulphamethoxazole.

1.2 Melioidosis

1.2.1 Symptoms and diagnosis

Melioidosis is a disease caused by the bacterial pathogen *Burkholderia pseudomallei* (see section 1.1.4). *Bps* is able to infect and cause melioidosis in humans and several species of animals. The environmental bacterium is found in contaminated soil and water, and infection usually occurs through skin penetration, ingestion or inhalation (Limmathurotsakul *et al.*, 2013). More details are provided in section 1.2.3.

The symptoms of severity of melioidosis can vary depending on the route of infection, the bacterial load/strain, and if the patient has any disease risk factors. The most common clinical symptom of melioidosis is bacteraemia, which occurs in 40-60% of cases. Symptoms of pneumonia are also common, and occur in around 50% of cases. In 20% of cases septic shock can befall the patient. The infection can frequently spread to other key organs, in particular the liver, kidneys, spleen and prostate (Wiersinga *et al.*, 2018).

In most cases with immunocompetent individuals, infection of *Bps* does not lead to disease, as the pathogen can be cleared by the host's humoral and cell-mediated immune response. However, infection can result in clinical symptoms of melioidosis with either acute or chronic disease (Currie, Ward and Cheng, 2010). Acute disease, which occurs in 85% of melioidosis cases, is associated with symptoms of sepsis, pneumonia and localised abscesses. On average, the incubation time of *Bps* in acute cases is nine days. The chronic disease, which occurs in 11% of cases, is a symptomatic infection that remains for more than two months. Additionally, less than 5% of cases may result in latency in which the disease is asymptomatic but not fully cleared; the symptoms of disease may occur much later than the original exposure and has been reported to be as long as 29 years (Chodimella *et al.*, 1997). To complicate diagnosis of melioidosis, many cases of the disease do not display specific symptoms. This has led to the dubbing of melioidosis as 'the great mimicker' (Yee *et al.*, 1988).

Diagnosis of melioidosis can be difficult for several reasons. These include the aforementioned occurrence of non-specific symptoms, a lack of awareness of the disease (particularly in non-endemic areas), and a lack of high-quality microbiology laboratories required for fast and specific identification of *Bps* (Wiersinga *et al.*, 2018). In endemic areas that are familiar with the disease, melioidosis can be identified based upon the common clinical symptoms and the patient's associated risk factors (Currie, 2015; Wiersinga, Currie and Peacock, 2012). In these cases, the disease can be pre-emptively treated with *Bps*-targeting antibiotics. However, in many circumstances the disease does not show specific clinical symptoms and patients do not always display known risk factors, particularly in the case of paediatric patients (Hoffmaster *et al.*, 2015).

Bacterial culture is the main method used to identify *Bps* and melioidosis. Because *Bps* is not a commensal bacterium in humans, identification of the pathogen in patients is considered a positive test for incidence of melioidosis. Blood cultures are the chief method of sample collection due to the high frequency of bacteraemia. However, these samples often need to be repeated due to low sensitivity of identification (Limmathurotsakul *et al.*, 2010a). Additionally, identification of *Bps* may be missed or mistaken by laboratory staff unfamiliar with the bacterium, or in lower-quality laboratories. Furthermore, bacterial culture techniques can take several days, which may take too long considering the potentially fast progression of melioidosis (Hoffmaster *et al.*, 2015; Wiersinga *et al.*, 2018).

There are several standard biochemical and molecule-based tests that can be used to confirm the presence of *Bps*, but these can either lack specificity or only be available in research or defence laboratories. There are several more cost-effective and specific assays for the identification of *Bps* being developed, for example the use of a protein microarray, a duplex qPCR assay and specific selective media (Dance *et al.*, 2019; Mohd Ali *et al.*, 2019; Kohler *et al.*, 2016).

1.2.2 Epidemiology

Bps and melioidosis is endemic to South-East Asia and Northern Australia. However, the disease is increasingly reported in more distant areas such as Colombia, Brazil and

equatorial Africa (Volpe-Chaves *et al.*, 2019; Birnie *et al.*, 2019; Rodriguez *et al.*, 2019). It is likely that *Bps* and melioidosis is present across most tropical regions, and the distribution of the disease is likely to increase with increased diagnosis and awareness. The pathogenic bacterium is present in contaminated soil and surface water; it is most abundant at least 10 cm below the soil surface. As a result, exposure to *Bps* can be increased during the rainy season, particularly during tropical storms, and through farming of the land, most commonly through rice farming in paddy fields (Kaestli *et al.*, 2012; Limmathurotsakul *et al.*, 2016b).

The major risk factor associated with melioidosis is diabetes mellitus, which is present in 23-60% of melioidosis cases (Currie, 2015). Diabetes has been shown to 'dampen' the host cell-mediated response through inhibiting the phagocytosis ability of macrophages, reducing the generation of CD4$^+$ regulatory T cells via lipopolysaccharide induction (resulting in loss of cytotoxic T lymphocyte protein 4) (Jenjaroen *et al.*, 2015), impairing MyD88 inflammatory signalling (specifically Toll-like receptor-mediated differentiation of myeloid cells), and dysregulation of NF-κB phosphorylation (Maniam *et al.*, 2015). Diabetes mellitus has been predicted to confer a 12-fold increased risk of melioidosis infection (Limmathurotsakul *et al.*, 2010b). Another major risk factor is exposure to contaminated soil and water, which is increased through occupation (farmers, rice paddy workers) and environmental conditions (tropical storms) (Cheng and Currie, 2005). Additional risk factors include excess alcohol consumption and the associated liver damage, chronic lung and kidney disease, thalassaemia (Fong *et al.*, 2015), prolonged steroid use and immunosuppression (Wiersinga *et al.*, 2018). In a significant proportion of cases (>80% of children and approximately 20% of adults), sufferers of melioidosis possess no known risk factors (McLeod *et al.*, 2015; Currie *et al.*, 2004).

A major modelling study from (Limmathurotsakul *et al.*, 2016b) has predicted that worldwide there are around 165,000 cases of melioidosis in humans, around 89,000 (54%) of which are fatal. This estimated mortality is similar to the more well-known disease of measles (95,600 deaths per year) and greater than those of leptospirosis (50,000 deaths per year) and dengue fever (12,500 deaths per year). Under diagnosis or mistaken diagnosis of melioidosis may be a significant problem, particularly in areas where knowledge of the pathogen and disease are not as well established. This means the reported cases of

melioidosis are much lower than those predicted (Wiersinga *et al.*, 2018; Limmathurotsakul *et al.*, 2016a).

1.2.3 Transmission and prevention

Bps is found in contaminated soil and water, and there are three main routes of infection. The infection can occur through skin penetration through cuts or wounds, through ingestion of contaminated food or water, and through inhalation of disturbed contaminated soil or water. These routes of infection are particularly pertinent for farmers or other outdoor workers in endemic areas. Melioidosis is not contagious, and transmission between humans only occurs in very rare cases (Ashdown, 1979; Wiersinga *et al.*, 2018).

Depending on how the bacteria enters the host, upon initial infection *Bps* is able to invade and replicate in epithelial cells of the mucosa or broken skin. From there, *Bps* can spread to various cell types including both phagocytic and non-phagocytic cells. Infection most commonly occurs in the respiratory system or cardiovascular system (usually bacteraemia), but infection of the gastrointestinal system, musculoskeletal system, skin and soft tissue, and elsewhere in the body is also common (Wiersinga *et al.*, 2018).

A cost-effective approach for preventing the incidence of melioidosis is the increasing of awareness of the disease. Public health advice aims to educate those at risk to avoid exposure of contaminated soil and water (Bory *et al.*, 2018; Chansrichavala *et al.*, 2015). This is especially relevant at the start of the rainy season, where tropical storms and dust clouds can be prevalent. Additionally, those who may be in contact with contaminated soil and water can be encouraged to wear protective equipment such as boots and respiratory protection. Those at risk of infection, in particular sufferers of diabetes mellitus, may also be encouraged to cease smoking to reduce potential risk (Limmathurotsakul *et al.*, 2013). Preventative measures targeting contaminated water have also been suggested. People may be urged to drink bottled water, or treat their water before consumption through boiling, chlorination or UV treatment (depending on the economic development of the area in question) (McRobb *et al.*, 2013; Howard and Inglis, 2003). However, the effectiveness of

these measures has not been determined. A lack of awareness of melioidosis and those at risk finding themselves in underdeveloped areas may limit the impact of these approaches.

Vaccination may be an effective approach for prevention of melioidosis. Currently, there are no human melioidosis vaccines available, but several are in development. Potential vaccines are either live attenuated vaccines (Titball *et al.*, 2017; Khakhum *et al.*, 2019), or subunit based vaccines (Muruato and Torres, 2016). An effective vaccine may utilise several antigens in order to combat *Bps* (Morici, Torres and Titball, 2019). Nonetheless, as a risk factor associated with melioidosis is immunosuppression, the effectiveness of a vaccine may be limited for this group.

1.2.4 Treatment

Antimicrobial therapy is the treatment used for melioidosis, and the initial diagnosis and start of antimicrobial therapy is critical. Where fast diagnosis and effective antibiotic therapy is applied, mortality rates are around 10%; where this treatment is less prompt and more limited, mortality rates increase to greater than 40% (Currie, 2015).

Bps can be eliminated by some β-lactams (meropenem, imipenem, co-amoxiclav (a combination of amoxicillin and clavulanic acid) and ceftazidime), doxycycline, chloramphenicol and trimethoprim-sulphamethoxazole. However, as *Bps* is resistant to penicillin, ampicillin, gentamicin, cephalosporins, tobramycin, streptomycin, macrolides and polymyxins, the pathogen must be correctly identified in order to apply the correct antibiotic therapy (Rhodes and Schweizer, 2016).

Initially, antibiotics are applied intravenously. Usually, meropenem or ceftazidime is used for 10-14 days, but this can be increased to around four weeks for patients with severe disease. Once symptoms have improved, the patient receives oral antibiotics (usually trimethoprim-sulphamethoxazole) for at least three months to eradicate the disease. This treatment duration can be increased for sufferers of neurological melioidosis or osteomyelitis. In cases where there are large abscesses in the liver, prostate or in muscle, or where septic arthritis or osteomyelitis has occurred, surgical drainage may be required (Wiersinga *et al.*, 2018).

1.2.5 Virulence factors

Bps possesses a large and varied array of virulence factors that enable it to infect, proliferate and avoid the immune response within a host.

Bps possesses three type III secretion systems (T3SSs), the most well-characterised of which is T3SS-3 (also known as the Bsa system) (Vander Broek and Stevens, 2017). The T3SS-3 needle tip and translocator protein components BipBCD are involved in cell invasion and intravesicular survival and escape upon contact with the host cell, the BopE effector induces actin rearrangement to assist cell invasion, and the CHBP/Cif effector inhibits cell maturation and apoptosis (Vander Broek and Stevens, 2017; Wiersinga *et al.*, 2018).

In addition to its T3SSs, *Bps* also has several type Va secretion systems (T5SSa), also known as autotransporters, that serve as virulence factors. These include BoaA and BoaB involved in cell attachment and invasion (Campos, Byrd and Cotter, 2013), BpaC required for cell adhesion (Lafontaine *et al.*, 2014) and the BimA autotransporter implicated in actin tail formation and phagosome escape (Stevens *et al.*, 2005).

Furthermore, the *Bps* genome encodes six type VI secretion systems (T6SSs), involved in a variety of virulence-associated functions. The most well-studied example is T6SS-5, which can load and inject the specialised effector VgrG5 (also known as TssI). VgrG5 has been proposed to be responsible for the fusing of adjacent macrophages, leading to multi-nucleate giant cell (MNGC) formation (Toesca, French and Miller, 2014; Shalom, Shaw and Thomas, 2007). MNGC formation is a hallmark feature of Bps infection, although its role in virulence is unclear (Burtnick *et al.*, 2011). Interestingly, this system appears to be regulated by glutathione, cysteine, pH, iron and zinc (Burtnick and Brett, 2013; Wong, Chen and Gan, 2015).

Other virulence factors used by *Bps* include, but are not limited to: the Type IV pilin subunit, PilA (Essex-Lopresti *et al.*, 2005), and the flagellin subunit FliC with functions in intracellular motility and cell adherence (DeShazer *et al.*, 1997), the oxidative stress-associated enzymes SodC, KatG, AhpC and DpsA (Loprasert *et al.*, 2004; Loprasert *et al.*, 2003b; Loprasert *et al.*, 2003a; Vanaporn *et al.*, 2011), the toxin BLF1 (Cruz-Migoni *et al.*, 2011), and several genes

associated with lipopolysaccharides that confer protection against the host immune response (Wiersinga *et al.*, 2018; Norris, Schweizer and Tuanyok, 2017).

1.3 *Cepacia* syndrome

1.3.1 Symptoms and diagnosis

'Cepacia syndrome' is a severe form of disease that can be caused by species of the Bcc (more detail in section 1.1.6). The symptoms that arise for Bcc infections can vary widely, ranging from no symptoms to severe respiratory decline, septicaemia and death (Mahenthiralingam *et al.*, 1995). Sufferers of cystic fibrosis (CF) and chronic granulomatous disease are particularly susceptible to infection by the Bcc, although infections can occur in patients without these risk factors (Hauser and Orsini, 2015).

In cases where symptoms develop to severe levels, Bcc infections may be referred to a 'Cepacia syndrome'. This disease is characterised by symptoms including rapid decline of lung and pulmonary functions, fever, septicaemia, necrotising pneumonia, leukocytosis, and increased inflammatory markers (Isles *et al.*, 1984; Sfeir, 2018). However, more uncommon symptoms have been observed including but not limited to spontaneous bacterial peritonitis (in patients with liver cirrhosis), endophthalmitis (in patients after eye trauma and / or surgery) and genito-urinary infections (Sachdeva *et al.*, 2011; Agochukwu *et al.*, 2012; Taneja *et al.*, 2017).

Bcc infections and 'Cepacia syndrome' are diagnosed based on patient symptoms and identification of the Bcc bacteria. The bacteria can be identified using specific selective agar (Henry *et al.*, 1999), *recA* specific PCR assays (Payne *et al.*, 2005), MALDI-TOF mass spectroscopy (Fehlberg *et al.*, 2013), and MLST (Spilker *et al.*, 2009). Also, antibiotic susceptibility testing is often used to identify Bcc species using ceftazidime, meropenem, trimethoprim-sulphamethoxazole or minocycline (Sfeir, 2018).

1.3.2 Epidemiology

Much like *Bps*, Bcc species are found in contaminated water, soil and moist environments. They can also be found in hospital environments, usually in the Western hemisphere, and often in the sputum of CF patients (Mahenthiralingam, Urban and Goldberg, 2005). In 2016, it was estimated that 2.7 % of CF patients have Bcc infections. However, this number is gradually decreasing year-on-year as awareness and treatment of Bcc infections increases (Salsgiver *et al.*, 2016).

Humans can be exposed to Bcc species through contaminated water. Bcc species can be found naturally in water, where they display a high survival rate. Moreover, in some countries such as China, Bcc species are utilised in agriculture, where they suppress plant pathogens, and in bioremediation, where they assist in metabolising pesticides and herbicides (Ibrahim *et al.*, 2012; McLoughlin *et al.*, 1992).

1.3.3 Transmission and prevention

All species of the Bcc are able to opportunistically infect humans, and cause symptoms that lead to 'Cepacia syndrome'. However, the most virulent of these species is *Bce*, followed by *B. multivorans* and *B dolosa*. Recently, *B. multivorans* appears to be found more commonly in infected patients than *Bce*, although with less severe symptoms (Zahariadis, Levy and Burns, 2003; Woods *et al.*, 2004; Kalish *et al.*, 2006; Miller *et al.*, 2015).

Unlike *Bps*, which does not show horizontal transmission between patients, Bcc species are able to transmit between patients via contact and / or water droplets. Patients with CF or chronic granulomatous disease are particularly vulnerable (Saiman *et al.*, 2014). Transmission can also occur via contaminated medical equipment or medications, and can lead to outbreaks of disease (Sommerstein *et al.*, 2017; Song *et al.*, 2017). Correct sterilisation and hygiene techniques within hospitals and regarding medical products can prevent outbreaks of Bcc infections.

1.3.4 Treatment

The treatment of Bcc infections suffers from a lack of published data, and usually is approached on an individual basis depending on the severity and history of infection and *in vitro* antibiotic susceptibility data (Sfeir, 2018).

Most commonly, either trimethoprim-sulphamethoxazole, ceftazidime, meropenem or doripenem is used in antibiotic therapy. The antimicrobials doxycycline and minocycline may also be used (Regan and Bhatt, 2019). However, certain antimicrobial resistance mechanisms can reduce the effectiveness of these antibiotics (more details are provided in section 1.1.6). Novel β-lactamase inhibitors can be used to overcome the effect of PenA. Avibactam (used in conjunction with ceftazidime) or vaborbactam (used in conjunction with meropenem) can support antibiotic therapy (Papp-Wallace *et al.*, 2017). However, these inhibitors do not overcome the effect of multi-drug efflux pumps. Amiloride and verapamil have been shown to increase the effectiveness of tobramycin against these efflux pumps (Cohn, Rudzienski and Putnam, 1995). A combination of antibiotics appears to be an effective antibiotic treatment strategy. The cooperation of β-lactam-ciprofloxacin-tobramycin has been demonstration to be the most consistent permutation, and shows effectiveness against the formation of biofilms, too. More recently, a novel polycationic glycopolymer has been shown to increase the effectiveness of tobramycin and meropenem against Bcc isolates (Narayanaswamy *et al.*, 2017).

1.4 Iron acquisition

1.4.1 Iron in microbiology

In almost all aerobic organisms, iron is an essential nutrient required for growth and survival. Iron is often incorporated in important proteins, including as a part of the haem cofactor, in iron-sulphur clusters, or an independent cofactor in mononuclear or dinuclear form. Its ability to transition between Fe(II), Fe(III) and Fe(IV) oxidation states make it ideal for the redox chemistry found in many metabolic processes and electron transport.

Biological iron is usually found in the oxidation states Fe(II) (ferrous) or Fe(III) (ferric) (Hider and Kong, 2010; Cassat and Skaar, 2013).

Both the mammalian host and the bacterial pathogens must engage in an iron acquisition 'arms race' in order obtain the iron each needs.

In effect, the host organism makes iron unavailable by incorporating it in various proteins. Iron is incorporated in many enzymes, and also in prosthetic groups such as haem in haemoglobin and myoglobin. Excess iron is stored in ferritin and by lactoferrin, and transported by transferrin. Additionally, Fe(III) is highly insoluble and therefore difficult to obtain. These contribute to making the internal host environment an iron-limited environment. Bacteria can utilise different mechanisms to acquire extracellular iron during infection and aid survival.

1.4.2 Siderophores

One major mechanism used by many bacterial species to acquire extracellular iron for survival is the synthesis and secretion of iron-chelating compounds called siderophores. Siderophores are low molecular weight compounds of around 0.5-1.5 kDa that bind ferric iron with high specificity and affinity. They are able to form complexes with a single ion of Fe^{3+} using bidentate ligand groups, usually via a nucleophilic oxygen as a donor atom. The most common groups found in siderophores are the bidentate catecholate, hydroxamate and hydroxycarboxylate groups, shown in Figure 1.2. The majority of ferric-siderophore complexes use three of these ligand groups to form hexadentate coordination complexes with Fe^{3+}, with an overall octahedral geometry (Hider and Kong, 2010). Usage of siderophores is an important mechanism for solubilising the normally insoluble and inaccessible ferric iron (Ratledge and Dover, 2000).
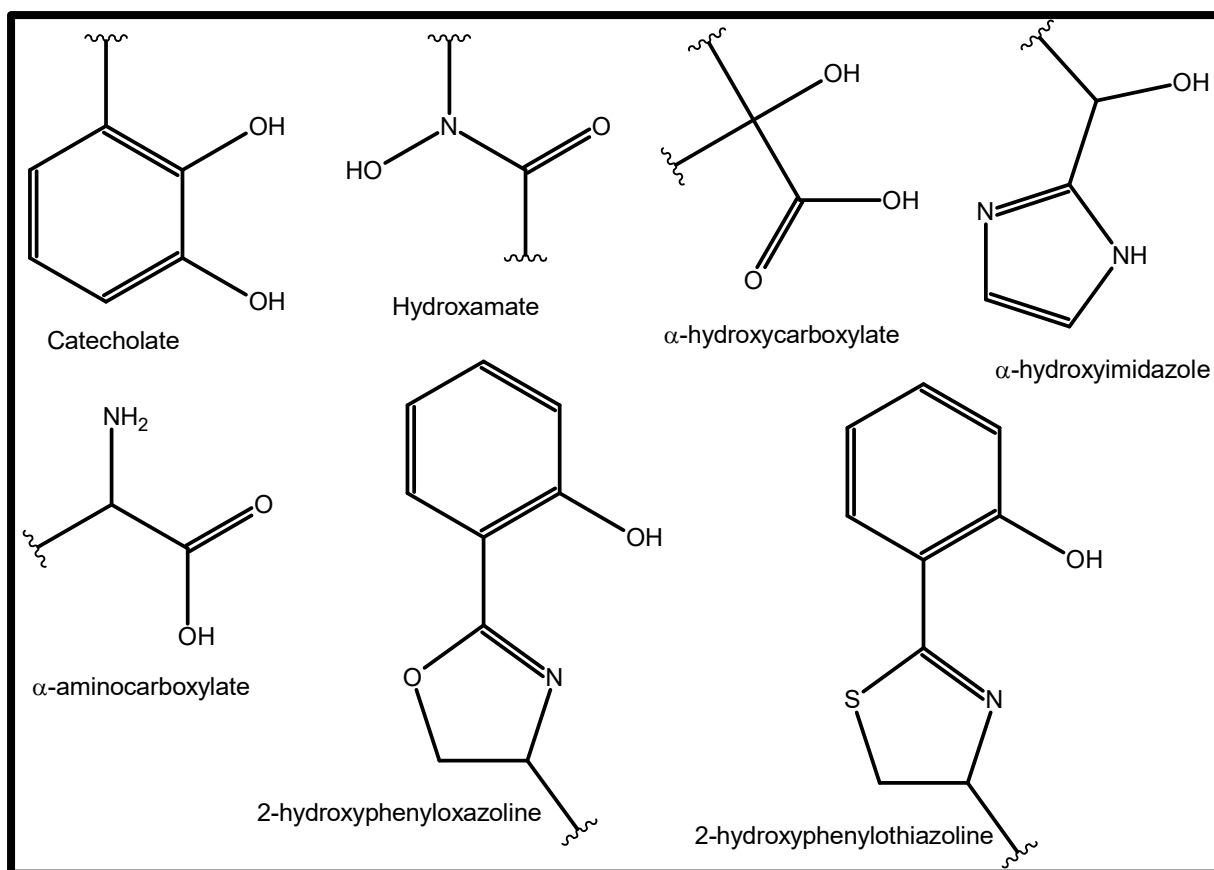
Figure 1.2. Donor ligand group of bacterial siderophores

Common bidentate ligand groups found in siderophores that are able to coordinate ferric iron. Adapted from (Hider and Kong, 2010). Note that derivatives of these functional groups may also act as metal-binding ligands in siderophores, such as with pyochelin (see section 1.4.5).

In Gram-negative bacteria, ferric-siderophore complexes are transported across the bacterial outer membrane into the periplasmic space via specific TonB-dependent receptors (TBDRs). These TBDRs are gated receptors that are energised by the proton motive force (PMF), through the action of the TonB system consisting of the three inner membrane-anchored proteins TonB, ExbB and ExbD (Bradbeer, 1993). The TBDR protein itself forms a β-barrel structure and binds a specific ferric-siderophore complex with the high affinity necessary in the iron-scarce extracellular space. The β-barrel is 'corked' by a globular 'plug' domain that is 'uncorked' upon the binding of the ferric-siderophore complex and resulting in conformational change. Once within the periplasmic space, some systems have a periplasmic binding protein (PBP) to shuttle the ferric-siderophore complex to the cytoplasmic membrane. Here, both in Gram-negative and Gram-positive bacteria, the ferric-

siderophore complex is then transported across into the bacterial cell cytoplasm by a cytoplasmic membrane transporter, usually acting in an ABC (ATP-binding cassette)-dependent mechanism. These transporters can translocate either the ferric-siderophore complex, or the free ferric ion, depending on the system. When entering the cell cytoplasm, the ferric ion is released from the complex either by reduction to Fe(II) or by hydrolysis of the siderophore (Butt and Thomas, 2017).

Most bacteria use one major siderophore to utilise extracellular iron. However, it is common to have additional secondary siderophores that may bind iron with lower affinity. These secondary siderophores may be useful under different environmental conditions, for iron storage, or for binding other metal ions (Hider and Kong, 2010).

1.4.3 Ornibactin

The major siderophore synthesised by all members of the Bcc (except for the recently identified strain *B. paludis* (Ong *et al.*, 2016)) is ornibactin. Although ornibactin is predicted to be utilised by most Bcc members (Butt and Thomas, 2017), this has only been empirically demonstrated in *B. cepacia*, *B. cenocepacia* and *B. vietnamensis* (Meyer *et al.*, 1995; Stephan *et al.*, 1993; Agnoli *et al.*, 2006; Darling *et al.*, 1998). Ornibactin synthesis and utilisation is specified by the 14-15 gene *orb* cluster that is composed of three operons (Figure 1.3 a).

Ornibactin is a tetrapeptide siderophore, formed from an L-ornithine-D-hydroxyaspartate-L-serine-L-ornithine backbone and synthesised by the NRPSs OrbI and OrbJ (Figure 1.3 b). The N-terminal ornithine is modified at the δ-amino group by hydroxylation by the oxygenase PvdA, and OrbL/OrbK-dependent acylation by a β-hydroxy acid which may have chain lengths of four, six or eight carbons leading to synthesis of ornibatin-C4, -C6 or -C8, respectively. The C-terminal ornithine is also modified by hydroxylation by PvdA and by formylation at the same δ-amino group by the transformylase PvdF. It also and undergoes amidation at the α-carboxyl group with a single molecule of putrescine. These modifications result in the assembly of a mixed type siderophore containing two hydroxamate groups and one α-hydroxycarboxylate group that chelate Fe(III) in a 1:1 stoichiometry (Figure 1.3 b).
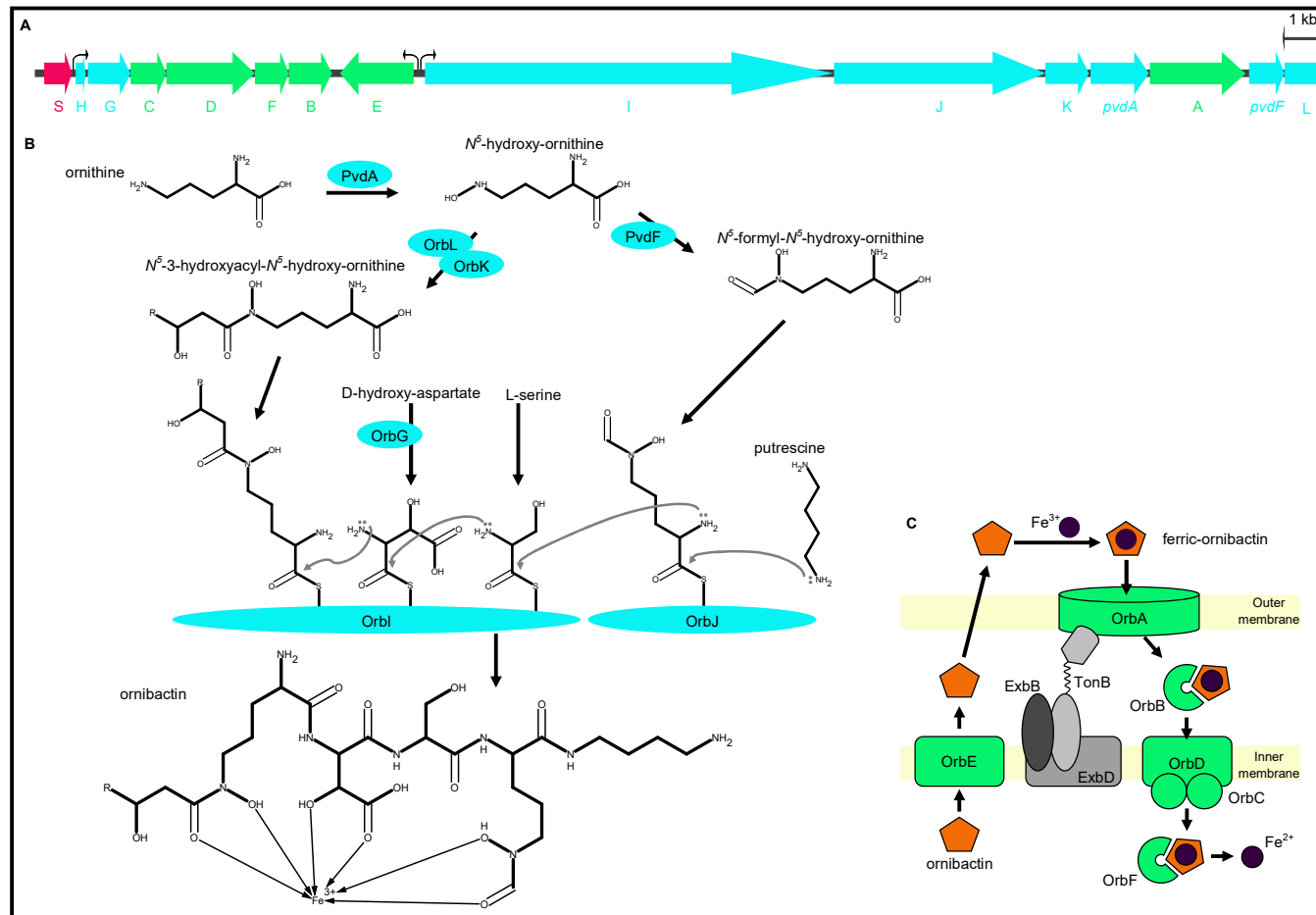
Figure 1.3. *orb* gene cluster organisation, ornibactin biosynthesis and role in iron transport

A. Organisation of *orb* genes responsible for production and utilisation of the siderophore ornibactin. Siderophore biosynthesis genes are shown in blue, siderophore transport/utilisation genes are shown in green, regulatory genes are shown in pink. The sites of the OrbS-dependent promoters are shown as curved arrows. **B.** Predicted chemical synthesis of pyochelin. Role of OrbH, an MbtH-like protein of unknown function, is not shown. **C.** Proposed ornibactin export and uptake mechanisms. Further detail provided in main body of text.

The export of ornibactin through the cytoplasmic membrane is proposed to be performed by the ABC transporter OrbE (Figure 1.3 c). The ferric-ornibactin complex is transported across the outer membrane via the TonB-dependent receptor OrbA, then across the periplasm by the PBP OrbB, and finally across the inner membrane via the ABC transporter OrbCD. Once within the cytoplasm, the iron ion is proposed to be released from ornibactin via reduction to the ferrous form by OrbF.

The *orb* gene cluster is regulated by the extracytoplasmic function (ECF) sigma factor OrbS (more detail in 1.7.2) and the global transcriptional regulator Fur (more detail in 1.5) (Agnoli *et al.*, 2006).

1.4.4 Malleobactin

Malleobactin (to be precise, malleobactin E) is the major siderophore used by all members of the Bpc. Its structure is very similar to ornibactin, differing only by the presence of an additional formyl group on the α-amino nitrogen of the N-terminal ornithine and loss of an alkyl side chain and hydroxyl group (shown in Figure 1.4).

Malleobactin is synthesised, exported and imported using genes of the *mba* gene cluster (Figure 1.4 a). The transcriptional control of these genes was demonstrated to act in the same way as the *orb* gene cluster, with the three transcriptional units regulated by a homologous ECF sigma factor, MbaS (Alice *et al.*, 2006) (more detail in 1.7.2). Synthesis of malleobactin occurs very similarly to synthesis of ornibactin, with homologous enzymes and chemical precursors (Figure 1.4 b). However, there are the following differences: the *mba* operon lacks genes homologous to *orbL/K*, so that the N-terminal molecule of ornithine is acylated by formic acid rather than with a β-hydroxycarboxylic acid; the MbaI NRPS contains a different N-terminal adenylation domain to OrbI, so that this differently modified N-terminal ornithine can be incorporated into the malleobactin structure; this peptide undergoes an additional formylation upon cyclisation by MbaI; the *mba* operon contains a hypothetical gene, *mbaM*, of unknown function (Franke, Ishida and Hertweck, 2014; Franke *et al.*, 2013).

Additionally, the malleobactin biosynthetic apparatus shows greater flexibility in comparison that of ornibactin. Eight malleobactin congeners, A-H, have been identified. Not including malleobactin C (which is readily non-enzymatically transformed from malleobactin B), the malleobactin congeners A-H were isolated in the ratio of 30:11:9:2:6:2:20 by weight (Franke, Ishida and Hertweck, 2015; Franke *et al.*, 2013). These diverse chemical structures are thought to arise due to the promiscuity of the adenylation domains of MbaI and MbaJ responsible for the incorporation diverse ornithine-derived precursors. Nonetheless, only malleobactin E contains the three bidentate ligand groups required for siderophore activity. Indeed, only this congener demonstrates siderophore activity similar to that of ornibactin by chrome azurol sulphonate (CAS) assay (Franke, Ishida and Hertweck, 2015). Another congener of malleobactin has been observed to be produced by *B. xenovorans*. In this case, the N-terminal N^5-formyl-N^5-hydroxyornithine does not undergo the additional formylation, giving rise to the malleobactin congener "malleobactin X" (Vargas-Straube *et al.*, 2016; Butt and Thomas, 2017).

The malleobactin import/export apparatus is homologous to the ornibactin apparatus, with homologous proteins corresponding to each of those encoded by the *orb* gene cluster (Figure 1.4c).

First isolated from *Bps*, malleobactin was demonstrated to bind free iron in addition to host protein-bound iron and cell-derived iron (Yang, Kooi and Sokol, 1993; Yang, Chaowagul and Sokol, 1991). Additionally, this siderophore has been demonstrated not to be essential for virulence in mouse models (Kvitko *et al.*, 2012). Interestingly, there is evidence that the malleobactin B congener may play a role in cell signalling, where it is used as a precursor in the biosynthesis of the antibiotic malleonitrone (Trottmann *et al.*, 2019a).
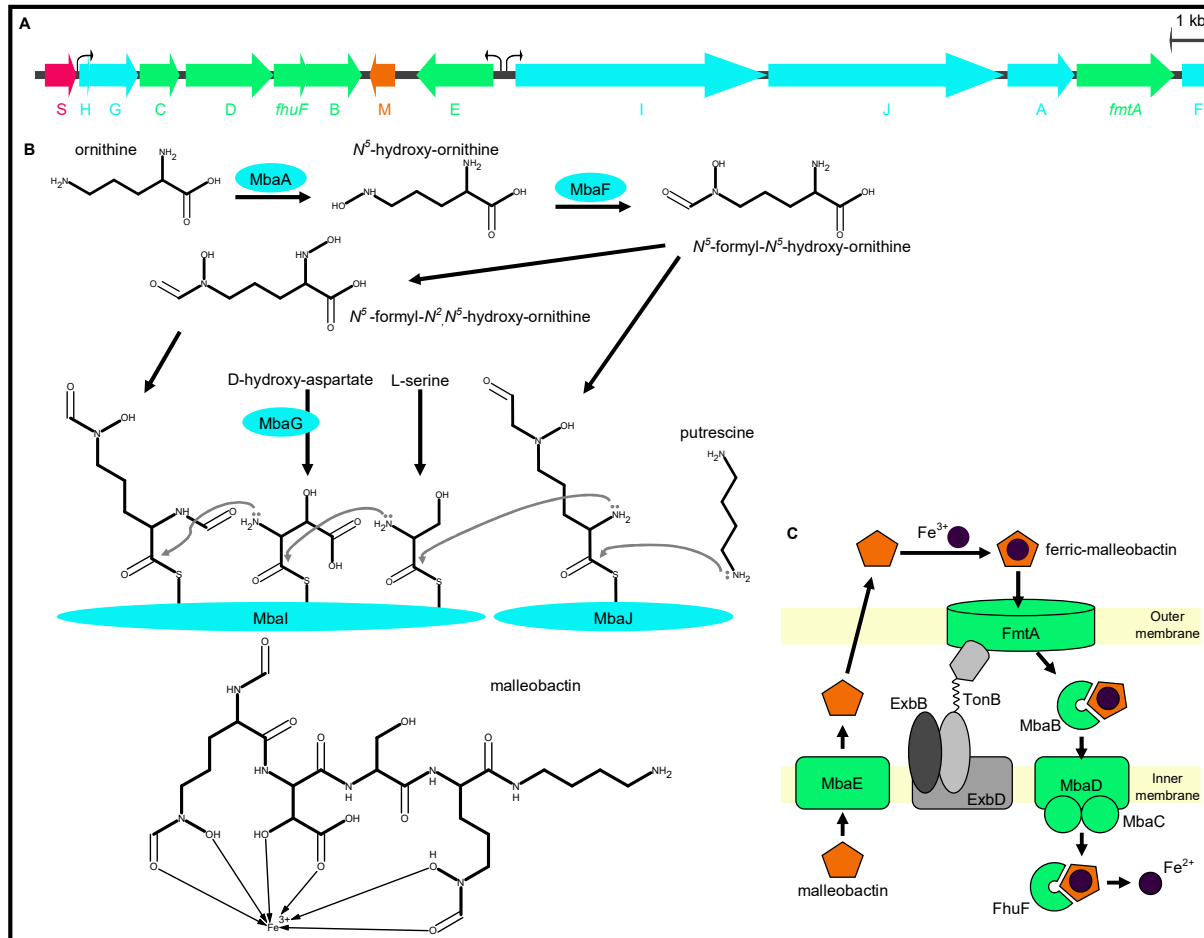
Figure 1.4. *mba* gene cluster organisation, malleobactin biosynthesis and role in iron transport

A. Organisation of *mba* genes responsible for production of the siderophore malleobactin. Siderophore biosynthesis genes are shown in blue, siderophore transport / utilisation proteins are shown in green, regulatory genes are shown in pink. The sites of the MbaS-dependent promoters are shown as curved arrows. **B.** Predicted chemical synthesis of malleobactin. Role of MbaH is not shown, and is predicted to encode an MbtH-like protein of unknown function. **C.** Proposed malleobactin export and uptake mechanisms. Further detail provided in main body of text.

1.4.5 Pyochelin

The secondary siderophore produced by most members of the Bcc, *Bps* and *Bth* (but not *Bma*) is pyochelin. It was first discovered in *Pseudomonas aeruginosa* (Liu and Shokrani, 1978). Pyochelin is a tetradentate siderophore, with one bidentate 2-hydroxyphenyl thiazoline group and one bidentate N-methylthiazolidine-4-carboxylate group. Pyochelin can bind Fe^{3+} in a 1:1 ratio using all of its ligand groups, a 2:1 ratio using two additional ligand groups from the second pyochelin molecule to form an asymmetrical octahedral complex (Tseng *et al.*, 2006), or a 1:1:1 ratio with a second siderophore, cepabactin, secreted by *B. cepacia* (Klumpp *et al.*, 2005). The association constant for ferric iron is relatively low (2.4 x 10^5 M) compared to ornibactin and malleobactin, although this value was obtained in ethanol and is likely to be higher in aqueous media (Cox and Graham, 1979).

Pyochelin is synthesised from a salicylic acid molecule and two molecules of cysteine (see Figure 1.5) (Ronnebaum and Lamb, 2018). Salicylic acid is generated from chorismic acid by the isochorismate synthase PchA and the isochorimate pyruvate lyase PchB. Salicylate is the initiating hydroxy acid, which is activated by the standalone NRPS adenylase module of PchD and loaded upon the NRPS PchE. PchE integrates a thiazoline ring, derived from one cyclised L-cysteine molecule, into the nascent compound and epimerises the conjugate before passing it on to the second NRPS PchF. PchF integrates a second thiazoline ring, derived from a second cyclised L-cysteine molecule. The standalone NRPS tailoring module of PchG reduces this second thiazoline ring to thiazolidine, before PchF uses a 'stuffed' methyltransfersase domain to methylate the ring (Ronnebaum *et al.*, 2019). Pyochelin is then released from the NRPS.

The import and export of pyochelin from the cell is less well understood than synthesis of the siderophore. PchH and PchI are predicted to be cytoplasmic ABC transporters, but have been demonstrated to be non-essential for the export of pyochelin (Reimmann *et al.*, 2001). Ferric-pyochelin is imported across the outer membrane by the TBDR FptA, and across the inner membrane by the transporter FptX. Unlike the ornibactin and malleobactin systems, the pyochelin import system appears to lack a PBP. The additional proteins FptB and FptC are also predicted to be involved in pyochelin transport, but appear to be dispensable for ferric-pyochelin uptake (Michel, Bachelard and Reimmann, 2007).
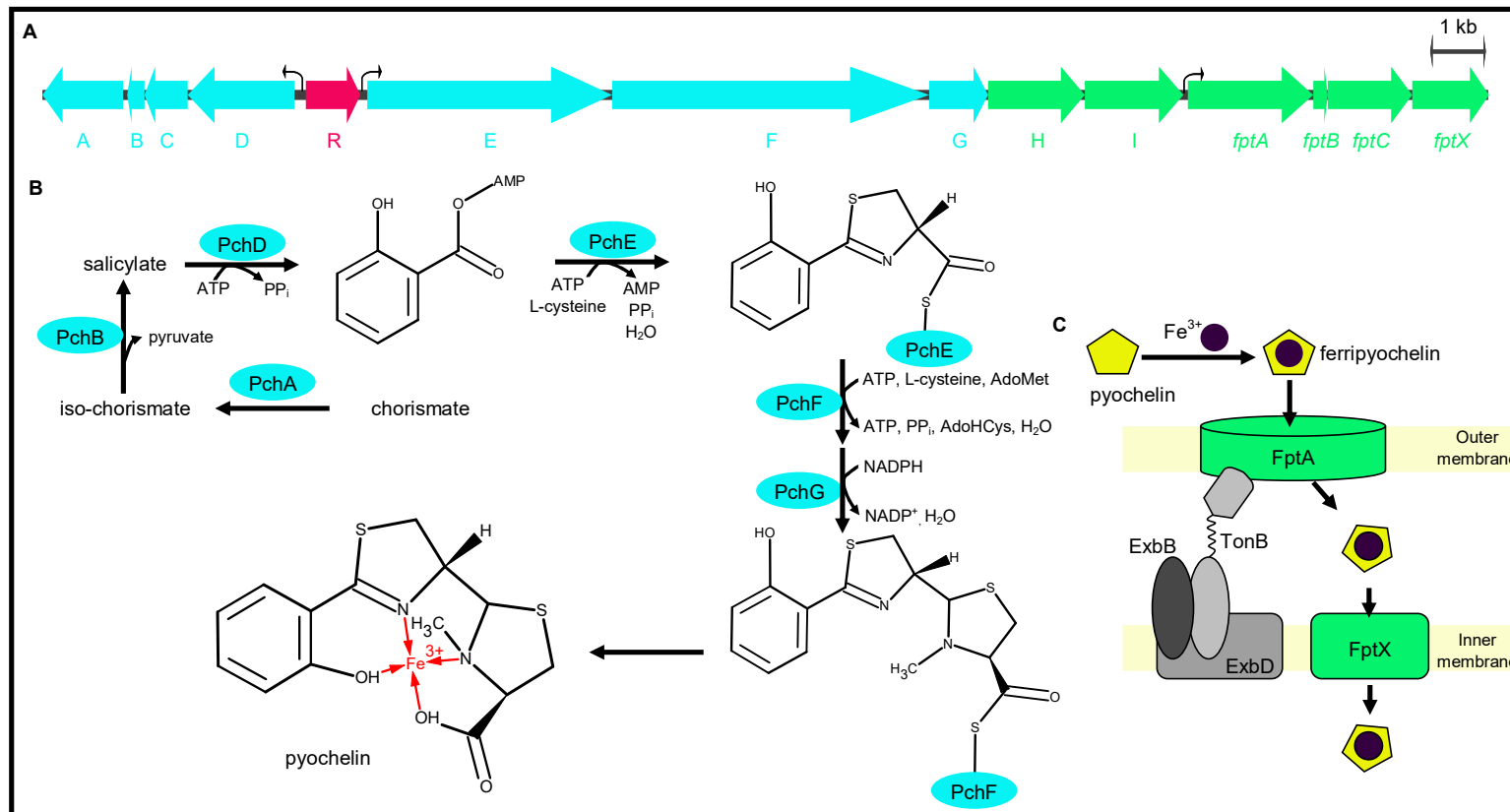
Figure 1.5. *pch* gene cluster organisation, pyochelin biosynthesis and role in iron transport

A. Organisation of *pch* genes responsible for production of the siderophore pyochelin. Siderophore biosynthesis genes are shown in blue, siderophore transport/utilisation proteins are shown in green, regulatory genes are shown in pink. The sites of the PchR-dependent promoters are shown as curved arrows. **B.** Predicted chemical synthesis of pyochelin. Role of PchC is not shown, and is predicted to encode a type II thioesterase that removes incorrectly charged substrates from the PchE-PchF NRPS complex. **C.** Proposed ferric-pyochelin uptake mechanism. Roles of the following proteins are not shown: PchH/PchI (predicted cytoplasmic membrane ABC transporters, but demonstrated not to have a role in pyochelin export (Reimmann *et al.*, 2001)), FptB and FptC (predicted to be associated with pyochelin transport, but demonstrated not be necessary for ferric-pyochelin uptake (Michel, Bachelard and Reimmann, 2007)). Further details are provided in main body of text.

Pyochelin has also been demonstrated to form complexes with other metal ions, including Cu(II), Zn(II), Ni(II), Co(II), Mo(VI), Al(III), V(IV) and V(V) (Cuppels *et al.*, 1987; Visca *et al.*, 1992; Baysse *et al.*, 2000).

The *pch* gene cluster is regulated by both the Ferric uptake regulator Fur (more detail in section 1.5), and the AraC family transcription factor, PchR. PchR is activated upon direct binding of ferric-pyochelin, and recognises the 32 bp PchR-box DNA sequence located at the promoters of the *pchDCBA*, *pchEFGHI* and *fptABCX* operons. In the absence of ferric-pyochelin, PchR is able to bind to these PchR-boxes and repress the expression of these operons. Additionally, these promoters and the *pchR* promoter are dominantly repressed by Fur (Heinrichs and Poole, 1993; Ochsner, Vasil and Vasil, 1995; Andrews, Robinson and Rodriguez-Quinones, 2003).

1.4.6 Malleilactone

A third siderophore-type compound that can be synthesised by the Bpc is the cytotoxic secondary metabolite malleilactone (also known as burkholderic acid), encoded by the polyketide synthase (PKS) *mal* gene cluster. Malleilactone has been demonstrated to be cytotoxic and antiproliferative against some human cell lines and Gram positive bacteria in cell-based assays, through an unknown mode of action (Klaus *et al.*, 2018; Trottmann *et al.*, 2019b).

Bps and *Bth* lacking the ability to produce malleilactone have been shown to be less cytotoxic to C*aenorhabditis elegans* and *Dictyostelium disoideum* compared to those producing the metabolite. Malleilactone also displays iron-chelating properties in addition to this toxicity and therefore likely functions like a siderophore, despite not having 'true' siderophore ligand groups (Biggins, Ternei and Brady, 2012).

MalR is a LuxR orphan (lacking a LuxI signal synthase partner) and is the regulatory transcription factor that controls the expression of the biosynthetic *mal* gene cluster and the production of malleilactone. Unlike most LuxR-type proteins, it does not bind acyl-homoserine lactone (AHL) and it acts upon a *lux* box-containing promoter upstream of the

mal operon (Truong *et al.*, 2015). Under regular laboratory conditions, the *mal* cluster is not expressed. But, activation of LuxR and therefore the *mal* gene cluster can be induced by sub-inhibitory levels of trimethoprim, fluoroquinolones, sulfamethoxazole, piperacillin and ceftazidime, and repressed by the AHLs N-octanoyl homoserine lactone, N-3-hydroxy-octanoyl homoserine lactone and N-3-hydroxy-decanoyl homoserine lactone via the quorum sensing regulatory protein ScmR (Truong *et al.*, 2015; Klaus *et al.*, 2018).
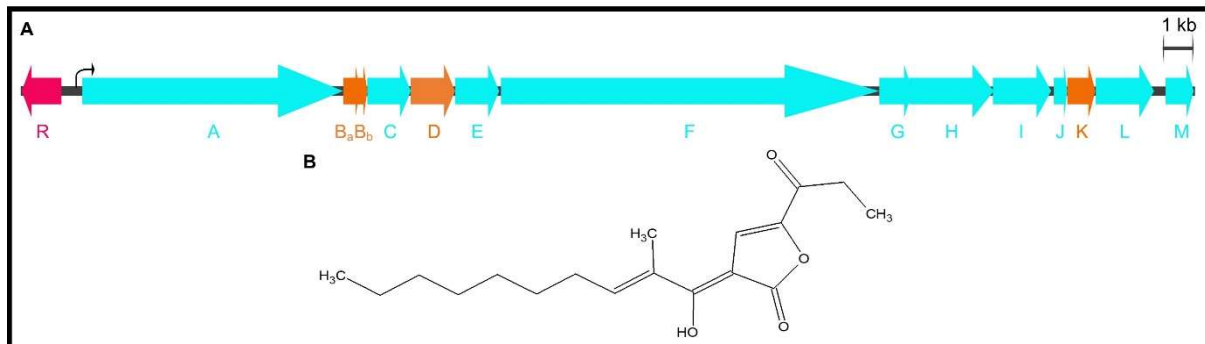
Figure 1.6. *mal* **gene cluster organisation and the structure of malleilactone**

A. Organisation of *mal* genes responsible for production of the Bpc siderophore-like compound malleilactone. Siderophore biosynthesis genes are shown in green, hypothetical proteins are shown in orange, regulatory genes are shown in pink. The site of the MalR-dependent promoter is shown as a curved arrow. **B.** Predicted chemical structure of malleilactone (Klaus *et al.*, 2018).

As production of this siderophore is not observed under standard laboratory conditions, it has not been considered in these studies with the same importance as malleobactin and pyochelin. Additionally, recent studies suggest that the reactive precursors of malleilactone are more active virulence factors and may be the primary function of this biosynthetic pathway (Trottmann *et al.*, 2019b). Additionally, it should be noted that despite being described as a siderophore-like compound, without the presence of a corresponding TBDR it does not share many of the characteristics of a siderophore.

1.4.7 Alternative *Burkholderia* iron acquisition methods

In addition to the usage of siderophores, *Burkholderia* have alternative mechanisms for acquiring iron during iron starvations conditions.

Haem is the most plentiful source of iron in the vertebrate host, making it an ideal source of iron for pathogenic bacteria. Haem can be released from haemoglobin via oxidation of the bound Fe(II) ion or proteolysis by host or pathogen proteases (Balla *et al.*, 1993; Cosgrove *et al.*, 2011). Several species of *Burkholderia*, including *Bps* and *Bce*, encode genes of the *bhu* (*Burkholderia* haem uptake) operon (Shalom, Shaw and Thomas, 2007). This five-gene operon encodes a TBDR (BhuR), a PBP (BhuT), a cytoplasmic ABC transporter formed of the membrane transporter (BhuU) and the ATPase component (BhuV), and a 'shuttle' protein (BhuS) predicted to have a role in the transport of cytoplasmic haem to haem-binding proteins and/or for degradation and release of iron (Figure 1.7). Recently, the chemo-mechanical coupling mechanism of this haem transporter has been proposed, highlighting potential conformations that may occur during internalisation of haem (Tamura *et al.*, 2019).
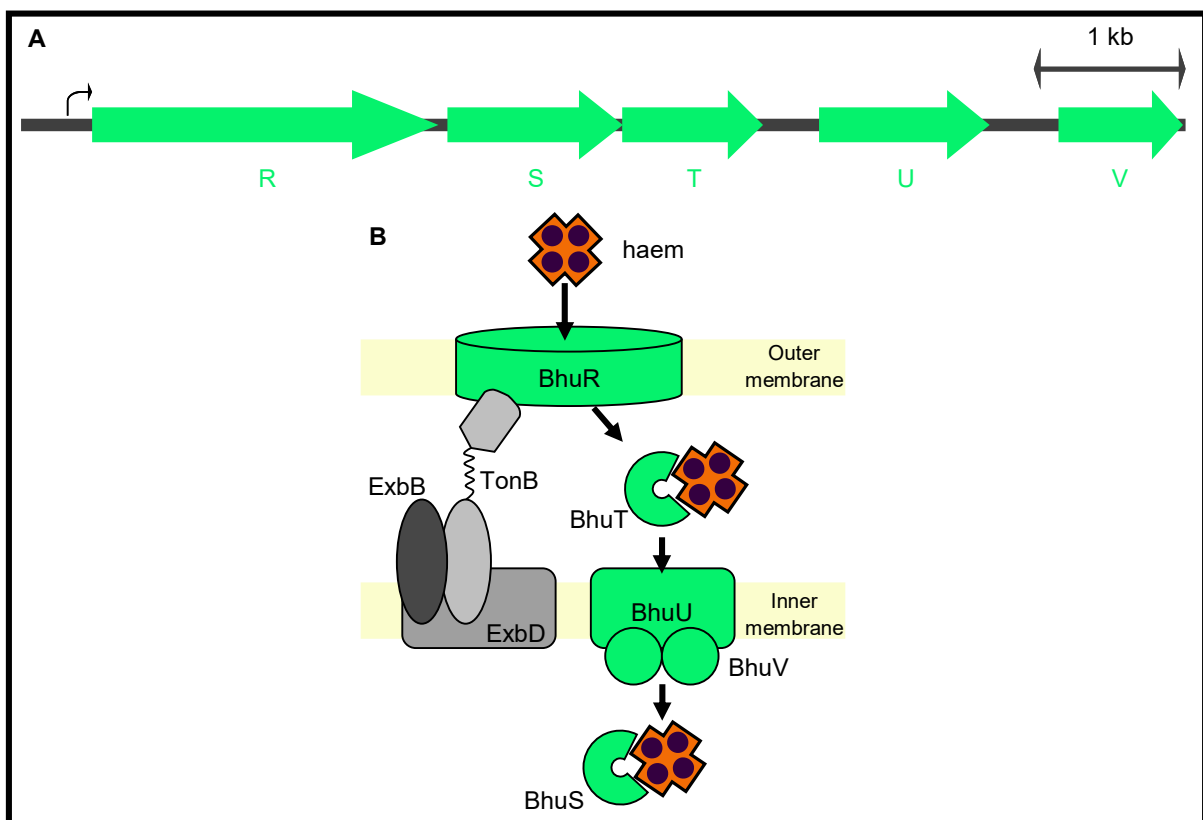
Figure 1.7. *bhu* gene operon organisation and haem uptake

A. Organisation of *bhu* genes responsible for the uptake of exogenous haem. The site of the Fur-dependent promoter is shown as a curved arrow. **B.** Proposed haem uptake mechanism. Further detail provided in main body of text.

Another abundant source of iron during infection is the iron storage protein ferritin. *Bce* has been demonstrated to be able to acquire iron from ferritin in a proteolysis-dependent process (Whitby *et al.*, 2006; Tyrrell *et al.*, 2015). Surprisingly, in *Bps*, siderophores are not required for the acquisition of ferric iron bound by ferritin suggesting the presence of another alternative ferric iron acquisition process (Kvitko *et al.*, 2012).

An alternative iron uptake mechanism present in most *Burkholderia* species and investigated in *Bce* is the FtrABCD system (Figure 1.8), that is similar to systems also observed in *Bordetella* and *Brucella* (Brickman and Armstrong, 2012; Elhassanny *et al.*, 2013) and the EfeUOB system of *E. coli* (Cao *et al.*, 2007). This system encodes a ferrous iron transporter which oxidises ferrous iron and translocates the resulting ferric iron into the cytoplasm. FtrA is a putative periplasmic protein for the transport of Fe(II). This may carry the metal ion to both the cupredoxin component FtrB and the linked ferredoxin FtrD, which facilitate the oxidation of Fe(II), and pass the resulting electron to a suitable electron acceptor and the generated ferric ion is delivered to the permease FtrC (Brickman and Armstrong, 2012; Mathew, Eberl and Carlier, 2014). The FtrABCD promoter has been shown to respond to iron, but not to low pH as is observed in *Bordetella* (Brickman and Armstrong, 2012; Mathew, Eberl and Carlier, 2014).
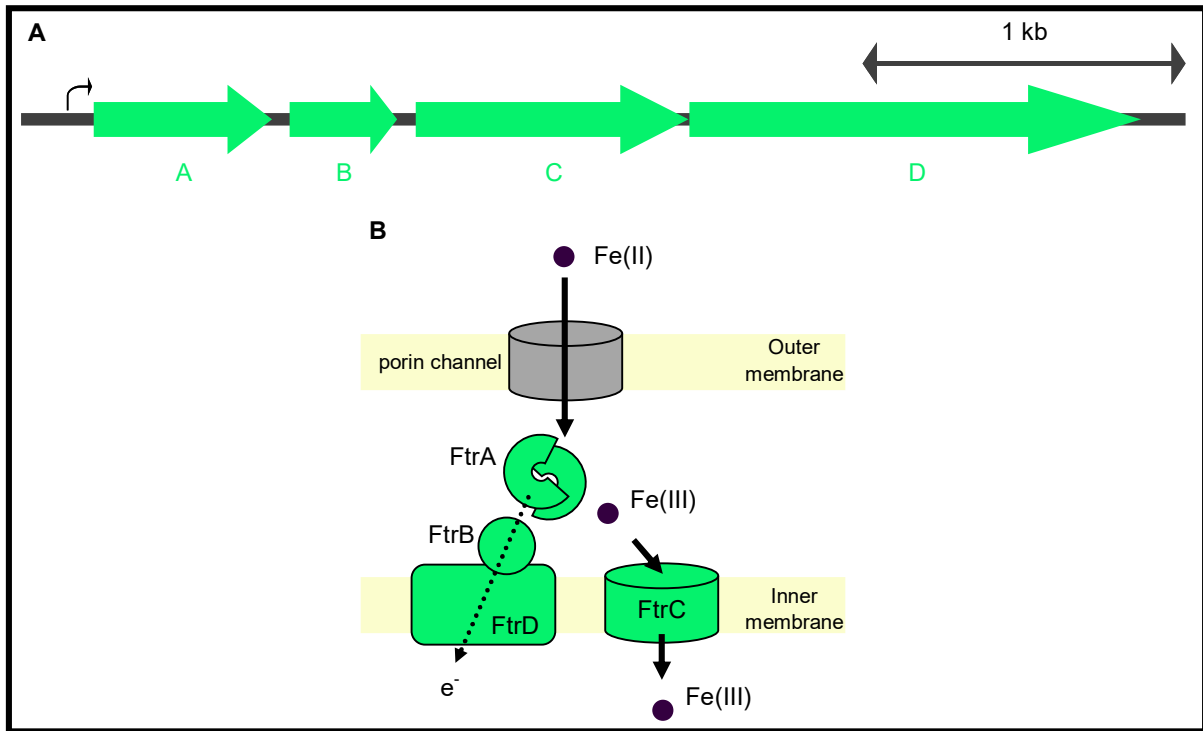
Figure 1.8. FtrABCD gene operon organisation and ferrous iron uptake

A. Organisation of FtrABCD genes responsible for the uptake of ferrous iron. The site of the putative iron-dependent promoter is shown as a curved arrow. **B.** Proposed ferrous iron uptake system. Further details are provided in main body of text.

Some species of *Burkholderia*, namely *B. multivorans*, *B. pseudomultivorans* and *B. paludis*, encode the FeoB component of the Feo ferrous iron uptake system. The Feo system is an inner membrane transport protein, used for uptake of ferrous iron into the cytoplasm. Most species of *Burkholderia*, including *Bps* and *Bce*, do not possess FeoA or FeoB (Butt and Thomas, 2017). It is not clear whether the single FeoB component present in these *Burkholderia* strains is involved in iron transport.

Finally, it has been observed that *Bps* infecting macrophages is able to downregulate the host protein iron transporter ferroportin, resulting in reduction of iron transport and a greater availability of iron within macrophages (Schmidt *et al.*, 2018). This increased iron pool may assist intracellular survival and proliferation during infection.

1.5 The Ferric Uptake Regulator (Fur)

Although iron is an essential nutrient for most microorganisms, high concentrations of Fe(II) can lead to toxicity through the formation of highly reactive and toxic superoxide radicals via Fenton reactions (Imlay, Chin and Linn, 1988). Therefore, the intracellular pool of iron must be regulated. The ferric uptake regulator (Fur) is a global transcriptional repressor protein that is found in all Gram-negative and most Gram-positive bacteria. Fur responds to high intracellular concentrations of iron to repress iron-regulated genes and maintain acceptable intracellular iron concentrations.

Initially identified in *E. coli*, Fur is a 17 kDa zinc metalloprotein (Schaffer, Hantke and Braun, 1985). Binding of transition metals, including but not limited to Fe(II), induces dimerization of Fur (Mills and Marletta, 2005; Lee and Helmann, 2007). Fur dimerization has been shown to occur via dimerization domains, and DNA interaction via a DNA binding domains (Pohl *et al.*, 2003). Additionally, Fur oligomerisation with DNA has been shown to occur, with tetramers (two Fur dimers) appearing to be particularly common (Perard *et al.*, 2016).

Fur binds DNA at specific sequences called Fur boxes, with the following consensus motif: 5'-GATAATGATAATCATTATC-3' (Baichoo and Helmann, 2002). However, Fur also displays some conformational plasticity that enable it to recognise this sequence with flexibility. These Fur boxes are located at the promoters of iron-regulated genes. Binding of the Fur dimer to this sequences occludes the promoter, preventing the association of RNAP with the DNA and repressing the transcription of the gene.

The transcription of the ECF sigma factor OrbS, which regulates the transcription of *orb* cluster genes associated with ornibactin, has been demonstrated to be regulated by Fur (Agnoli *et al.*, 2006). Additionally, the homologous sigma factor MbaS has been reported to contain a Fur box of unspecified location upstream of its gene (Alice *et al.*, 2006).

1.6 ECF sigma factors

1.6.1 Bacterial RNA polymerase

Bacterial RNAP is the enzyme complex responsible for the transcription of bacterial DNA. The catalytic core of RNAP, which is capable of transcription elongation but unable to initiate transcription, is formed of five subunits: two identical α subunits, two non-identical β subunits (β and β'), and an ω subunit (Ishihama, 1969; Gruber and Gross, 2003)(Figure 1.9). Only upon assembly with a sixth subunit, a σ factor, does core RNAP become the holoenzyme with the ability to initiate transcription.

The α subunits (35 kDa approx. each) are formed of two domains. The N-terminal domains interact to enable α dimerization, and subsequently interaction with the β and β' subunits; this is an essential step in assembly of the core enzyme. The C-terminal domains interact with DNA upstream of the gene promoter (the UP element) and can interact with a variety of transcription factors.
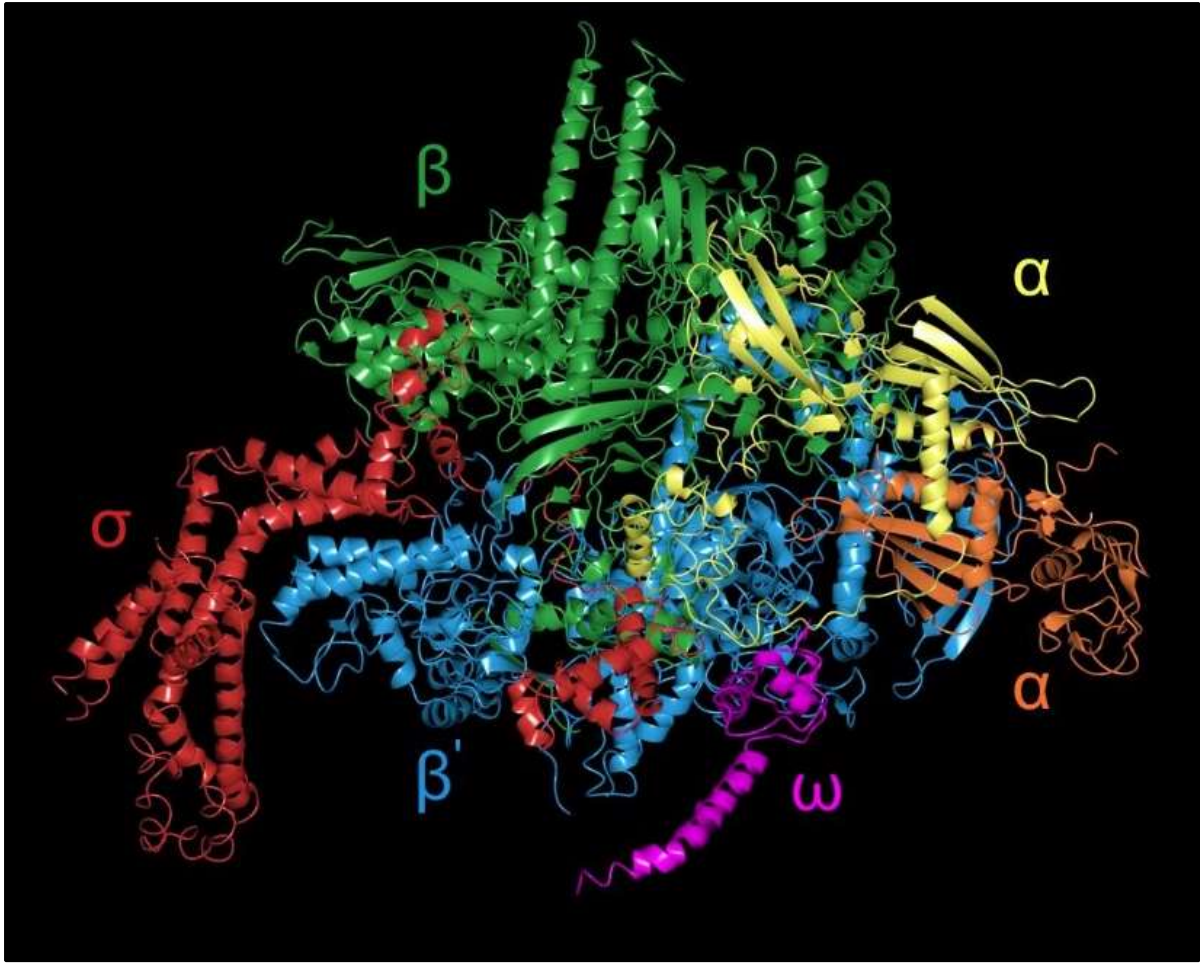
Figure 1.9. Three-dimensional Structure of *E. coli* RNA Polymerase

3D Crystal structure of *E. coli* RNAP σ^{70} holoenzyme, 3.7 Å resolution (PDB: 4YG2). Protein subunits are coloured as indicated. Image created using CCP4MG.

The large β and β' subunits (approximately 151 kDa and 155 kDa in *E. coli*, respectively) form the catalytic 'crab-claw' structure of the enzyme complex. This structure consists of a DNA-binding clamp, a channel for the DNA-RNA hybrid, and an RNA exit channel. The β' subunit contains a conserved aspartic acid catalytic triad which binds to a Mg^{2+} cofactor, and also displays structural flexibility in forming channels for the access of free NTPs into the active site (Murakami, 2013; Vassylyev *et al.*, 2002).

The ω subunit (approximately 12 kDa) is an auxiliary factor with a variety of functions. These can include stabilisation of the RNAP complex and its component subunits, and binding ppGpp as part of the stringent response.

The σ subunit is responsible for the initiation of transcription – the core enzyme cannot begin transcription of double stranded DNA without it. The sigma factor has two key roles: it recruits the RNAP holoenzyme to the target genes by interacting with specific promoters, and separates the DNA strands at the promoter (DNA melting') to generate the RNAP-promoter open complex. Additionally, sigma factors can be a target for other transcription factors, providing a further degree of modulation.

1.6.2 σ^{70} family and domain structure

Based upon protein sequence similarity, sigma factors are split into two major classes: σ^{70} and σ^{54} (or σ^{N}).

The σ^{54} factors are alternative sigma factors, and can regulate the expression of genes with functions including nitrogen metabolism, cell motility, membrane biogenesis and pathogenesis. They differ from the σ^{70} family due to their dependence on enhancer proteins and ATP hydrolysis, as well as their highly different amino acid sequence and structure. The focus hereafter will be on the σ^{70} class of sigma factors and σ^{54} factors will not be discussed in further detail.

Members of the σ^{70} sigma family are highly conserved across bacteria, and are further divided into four groups based upon their conserved domain architecture (Figure 1.10). Group 1 sigma factors are the archetypal housekeeping σ^{70}, to which the three other groups 2, 3 and 4 are related. Group 1 sigma factors are formed of four conserved helical-structured domains: $\sigma_{1.1}$, σ_2, σ_3 and σ_4. These domains are connected by flexible linkers, and are themselves comprised of regions of conserved amino acid sequence. These regions are discussed in section 1.6.3.
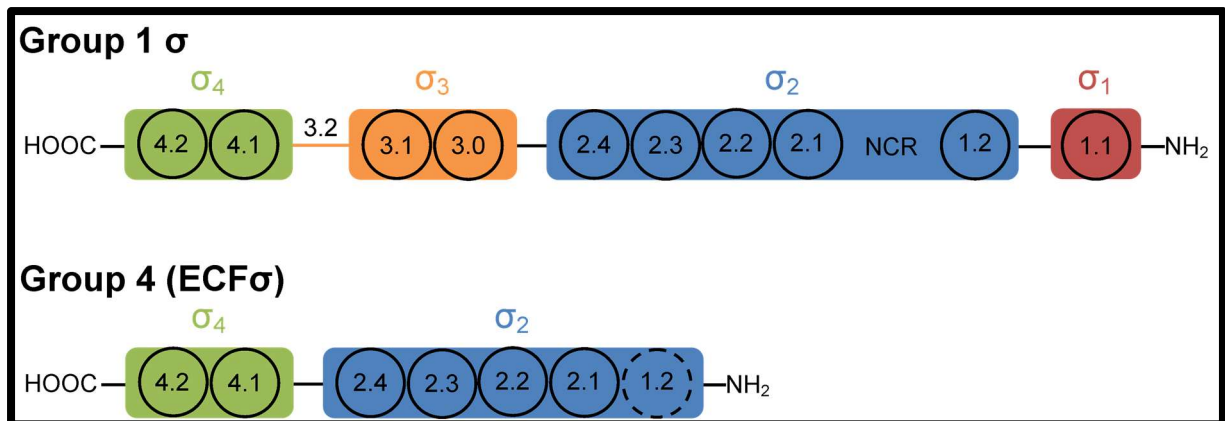
Figure 1.10. Domain structure of Group 1 and Group 4 σ70 factors.

σ70 conserved domains are shown in coloured boxes. Conserved regions are represented by circles containing their region number. Group 1 sigma factors contain all four domains. The σ_2 domain contains a non-conserved region (NCR) of variable length. A conserved 3.2 region acts as a linker between the σ_3 and σ_4 domains. Group 4 (ECF) sigma factors are smaller, containing only the σ_2 and σ_4 domains. The presence of region 1.2 in σ^{ECF} is variable, denoted by a broken circle.

Group 1 contains *E. coli* σ70 (RpoD), the primary sigma factor present in all bacteria, which is responsible for initiation of transcription at the majority of promoters in bacteria. It is largely responsible for transcription of 'house-keeping' genes. Group 1 sigma factors include all four of the σ domains. The alternative sigma factors in groups 2, 3 and 4 differ in their domain structure; they do not possess domain $\sigma_{1.1}$, have variable presence of domain σ_3 and can also differ in other aspects. Group 2 sigma factors, such as RpoS, lack the $\sigma_{1.1}$ domain, but retain the σ_3 domain, so overall show a close structural relationship to Group 1 sigma factors. Group 3 sigma factors, such as *E. coli* σ32, contain the σ_2 and σ_4 domains, and usually the σ_3 domain. Sigma factors of this group are usually associated with (a) flagellum biosynthesis, (b) the heat shock response, (c) the general stress response and (d) sporulation. Group 4 sigma factors, also referred to as the extracytoplasmic function (ECF) sigma factors, are formed of only the σ_2 and σ_4 domains. They are discussed in more detail in section 1.6.4.

1.6.3 σ⁷⁰ domain function

Domain $\sigma_{1.1}$, comprised solely of region 1.1, is an N-terminal domain of approximately 90 amino acids attached to the rest of σ^{70} via a flexible linker. $\sigma_{1.1}$ is present exclusively in group 1 sigma factors, has a high frequency of basic residues, and is formed of four α-helices. Its natively disordered state has presented difficulties in generating a crystal structure, and it has only recently been elucidated (Murakami, 2013). It was initially thought to act solely at the transcription initiation process at promoters (Vuthoori *et al.*, 2001). It is able to act as a DNA mimic and block entry into the DNA-binding channel of RNAP – its basic residues interact with the template DNA and ensure controlled entry into the complex. Further studies support that $\sigma_{1.1}$ acts as an auto-inhibitory domain that interacts with binding elements to prevent free sigma-DNA binding until holoenzyme formation (Schwartz *et al.*, 2008).

Domain σ_2, constructed of regions 1.2 to 2.4, forms an associative interface with RNAP mostly based on interactions between region 2.2 and the β' subunit (Murakami, Masuda and Darst, 2002). σ_2 also interacts with the -10 element of the promoter DNA. Regions 2.3 and 2.4 selectively bind flipped bases from single-stranded non-template DNA of the -10 promoter element using specific binding pockets, enabling stability of the opened DNA structure (Marr and Roberts, 1997). Specific interaction with the A_{-11} and T_{-7} flipped bases results from the action of conserved aromatic residues in σ^{70} (Juang and Helmann, 1994; Feklistov and Darst, 2011).

Domain σ_3 consists of regions 3.0 and 3.1, and is formed of three α helices. Region 3.0, previously known as region 2.5, is involved in the recognition and interaction with the 'extended' or upstream region of the -10 box of promoter DNA (Barne *et al.*, 1997). A conserved region, 3.2, forms a linker sequence between domains σ_3 and σ_4. Region 3.2 has been observed to fit into the RNA exit path in RNAP; part of this region (the "σ-finger") is able to interact with the DNA template strand to aid its translocation into the enzyme complex. This region is displaced when greater than four nucleotides of the *de novo* RNA strand have been synthesised, allowing RNA exit (Zhang *et al.*, 2012).

Domain σ_4, consisting of regions 4.1 and 4.2 plays at least three roles. Firstly, it forms a large interface with RNAP through interaction with the β subunit flap. Secondly, σ_4 is formed of

four α helices which fold into a helix-turn-helix motif that specifically interacts with the -35 box of the promoter DNA (Siegele *et al.*, 1989; Gardella, Moyle and Susskind, 1989; Murakami *et al.*, 2002). Thirdly, σ_4 also shows roles in interaction with transcription activator proteins that bind upstream or downstream of the -35 box (Campbell *et al.*, 2002).

1.6.4 Extracytoplasmic function (ECF) sigma factors

Group 4 sigma factors are also known as extracytoplasmic function (ECF) sigma factors. They constitute a wide and diverse family of sigma factors that frequently display a response to signals from the exterior of the cell cytoplasm (Mascher, 2013; Paget, 2015).

ECF sigma factors contain only the σ_2 and σ_4 domains, and can even lack most or all of region 1.2 and the NCR from the σ_2 domain. As a result, they are typically much smaller than group 1 sigma factors.

ECF sigma factors normally regulate their own expression. An exception is a sub-group known as the iron-starvation σ factors (see section 1.6.6). The sigma factor recognises the promoter sequence elements of its own gene, thereby giving rise to a positive feedback system. Genes encoding ECF sigma factors are often located in operons or operon-like clusters with the gene their cognate anti-sigma factor. The anti-sigma factor inhibits the ECF sigma factor in absence of the sigma factor-activating environmental stress signal (see section 1.6.5). Often, the operon includes downstream target genes when the sigma regulon is small (Matsumoto *et al.*, 2005). This ensures coordinated expression of the regulon genes.

Group 4 sigma factors recognise -35 and -10 consensus sequences promoter elements that are different to those of typical primary sigma factors (Helmann, 2002). ECF sigma factors tend to have more stringent promoter sequence requirements; unlike a σ^{70} consensus sequence, single base substitutions may not be tolerated (Staron *et al.*, 2009). The majority of ECF sigma factors also recognise promoters with an AAC motif in the -35 region, again suggesting that the diversity of gene targets results from more specific interaction elsewhere at the -10 box. At some promoters, a role for a segment of the spacer region immediately downstream of the -35 region has been implicated (Gaballa *et al.*, 2018; Agnoli

et al., 2018). Increased stringency of promoter region selection by ECF sigma factors compared to σ^{70} is also achieved by alternative DNA promoter melting during transcription initiation. In the case of *E. coli* σ^E, the opening of the DNA helix is initiated by the flipping out of a single C-10 base accommodated by the ECF sigma factor region using a dynamic loop region. This single base specificity is not observed in σ^{70}, and adds another level of stringency to promoter recognition, ensuring the redirected gene expression is restricted to the target regulons of ECF sigma factors (Campagne *et al.*, 2014).

The broad range of ECF sigma factors and their high level of diversity provide some difficulty in their categorisation. Bacterial species have on average six different ECF sigma factors, adding to the complexity. Nonetheless, ECF sigma factors were initially organised into at least 43 phylogenetically distinct major groups (Staron *et al.*, 2009). However, this classification only used predicted ECF sigmas from well-studied bacterial phyla – although 2,700 proteins were analysed, this is relatively small compared to the large range of potential ECF sigma factors. Moreover, many sigma factors were identified that could not be placed into the major groups – this issue will likely grow with the further identification of previously uncharacterised ECF sigma factor. Indeed, the number of major ECF sigma factors groups recognised has now increased to 50, yet this only encompasses roughly two thirds of all ECF sigma factor protein sequences identified (Jogler *et al.*, 2012; Mascher, 2013).

However, a small number of ECF sigma factors contain an additional domain fused to the C-terminus of σ_4. These C-terminal domains are thought to modulate the protein's activity by acting as a sensory domain, an intra- or inter-molecular auto-inhibitory domain, or a protein interaction domain (Wecke *et al.*, 2012). These C-terminal domains are not found in most ECF sigma factors.

1.6.5 Anti-sigma factors

One key characteristic of ECF sigma factors is their regulation by anti-sigma factors (Paget, 2015; Staron *et al.*, 2009). This usually occurs through inhibition of the abilty of the sigma factor to interact with core RNAP. Anti-sigma factors for ECF sigma factors are usually cytplasmic membrane-bound proteins that interact with ECF sigma factors to post-translationally regulate their activity in a variety of ways. Such anti-sigma factors contain at

least three domains: (a) a cytoplasmic sigma protein interaction module, (b) a transmembrane domain, and (c) a sensory periplasmic/extracellular module which senses the stimulus to which the sigma factor responds (Yoshimura *et al.*, 2004). Upon sensing of the specific signal (directly or indirectly via other interacting partners), the anti-sigma releases the sigma factor allowing it to associate with core RNAP. As the gene encoding the anti-sigma factor is often co-expressed with the sigma factor gene in an operon, this ensures that the sigma factor is expressed in an inactive form and with stoichiometric quantities of sigma:anti-sigma factor (Busche *et al.*, 2012). Sigma factor/anti-sigma factor systems are important as they shape the third mechanism of signal transduction in bacteria, after one- and two-component signalling systems (Staron *et al.*, 2009; Stock, Robinson and Goudreau, 2000; Ulrich, Koonin and Zhulin, 2005).

Anti-sigma factors possess a cytoplasmically-located N-terminal anti-sigma domain (ASD), forming a helical bundle which is able interact with the sigma factor to inhibit its activity. (Campbell *et al.*, 2007). In one class of sigma factor, this helical bundle is stabilised by the addition of a zinc ion – this is termed a zinc-binding anti-sigma domain (ZASD) (Campbell *et al.*, 2007). The ZASD domain contains a HX_3CX_2C motif which comprises three ligands, along with another cysteine or histidine residue elsewhere in the protein, which bind the zinc cation. Interestingly, the ZASD domain has been implicated in cytoplasmic sensing mechanisms, where it can act as a redox switch, initiating release of the sigma factor (Paget *et al.*, 2001; Bae *et al.*, 2004).

Inhibition of the sigma factor though the ASD can occur either by disruption of the interaction with DNA and/or RNAP, or by stabilising the sigma factor in an inactive conformation. Anti-sigma factors inhibit sigma factors via three interaction classes (Figure 1.11), although it is possible and probable that more as yet uncharacterised strategies exist.

Class I anti-sigma factors insert the ASD between domains σ_2 and σ_4 of the ECF sigma factor and disrupt its binding to RNAP. This mechanism of inhibition is observed in the *E. coli* σ^E/RseA sigma:anti-sigma factor pair that regulates the response to cell envelope stress (Campbell *et al.*, 2003). Another version of this mechanism using a ZASD is observed in the *Rhodobacter sphaeroides* σ^E:ChrR sigma:anti-sigma factor system that regulates the transcriptional response to reactive singlet oxygen (Campbell *et al.*, 2007).

Class II anti-sigma factors can interact around sigma factor to stabilise the compact and inactive sigma structure (Sorenson, Ray and Darst, 2004; Maillard $et\ al.$, 2014). This is the case in the σ^{CnrH}:CnrY sigma:anti-sigma factor system of $Cupriavidus\ metallidurans$ than regulates nickel and cobalt resistance. In the inhibitory complex, CnrY stabilises the σ^{CnrH} conformation that buries its DNA interaction surfaces, thereby preventing σ_2 interaction with the -10 promoter element. Furthermore, the anti-sigma factor CnrY occludes protein-protein interaction surfaces of σ^{CnrH} to inhibit RNAP holoenzyme formation (Maillard $et\ al.$, 2014).

A third way in which anti-sigma factors can act upon their ECF sigma factor partner is by the more recently discovered class III mechanism. These anti-sigma factors act simultaneously in two ways. Firstly, an ASD helix inserts between the σ_2 and σ_4 domains of the sigma factor blocking access of the DNA binding surfaces of the protein to the core promoter elements (more specifically, the σ_4 domain from the -35 promoter element). This mechanism is similar to Class I anti-sigma factors. Secondly, the rest of the ASD can bind around the sigma factor, holding it in a compact and inactive conformation that is unable to interact with DNA or associate with RNAP. This is similar to the class II system. Class III anti-sigma factors are exemplified by the σ^{BldN}:RsbN sigma:anti-sigma factor system of $Streptomyces\ venezuelae$ which regulates hyphae growth (Schumacher $et\ al.$, 2018). All of these mechanisms are used by anti-sigma factors with no strong primary sequence similarity, suggesting they have arisen through convergent evolution. There are likely to be more undiscovered methods of ECF sigma factor inactivation by anti-sigma factors.

Activation of the sigma factor via inactivation of the anti-sigma factor is also achieved in various ways. The most well studied mechanism is that of regulated proteolysis of the membrane-spanning anti-sigma factor by the process of regulated intermembrane proteolysis (RIP) (Heinrich and Wiegert, 2009). RIP consists of three proteolytic steps that result in: cleavage of the extracellular (-1) site of the anti-sigma factor, degradation of the transmembrane helix (-2) site, and further cytosolic proteolysis of the cytoplasmic domain by the ClpXP protease system to release the sigma factor. The proteases used in these steps can be fairly non-specific for the system, and several may be required at each step (Chaba $et\ al.$, 2007; Ho and Ellermeier, 2012). In this mechanism, the proteases directly or indirectly respond to activating signals. For example, in Gram-negative bacteria, DegS acts as the

initial protease involved in the degradation of the anti-sigma factor RseA. DegS acts as a periplasmic stress sensor directly responding to misfolded outer membrane protein peptides. Its activation provides the rate limiting step for the downstream release of the RseA-bound σ^E, which drives the expression of genes associated with the adjustment response to cell envelope stress (Wilken *et al.*, 2004).
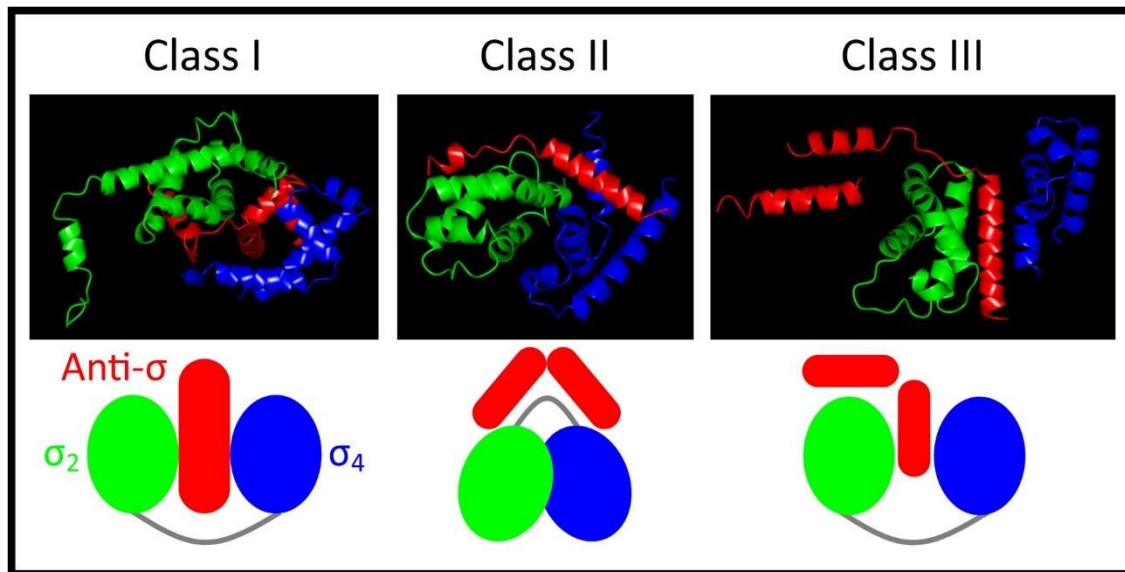
Figure 1.11. Inhibitory mechanisms of anti-sigma factors.

Mechanisms employed by anti-sigma factors for inhibiting the function of sigma factors. Class I anti-sigma factors (**left**) insert the anti-sigma domain (ASD) between the σ_2 and σ_4 domains of the sigma factor. Example shown is RseA interacting with σ^E of *E. coli* (PDB:1OR7). Class II anti-sigma factors (**centre**) bind around the σ_2 and σ_4 domains holding the sigma factor in an inactive conformation. Example shown is CnrY interacting with σ^{CnrH} of *Cupriavidus metallidurans* (PDB:4CXF). Class III anti-sigma factors (**right**) insert between the σ_2 and σ_4 domains and bind around to hold the sigma factor in an inactive conformation. Example shown is RsbN interacting with σ^{BldN} of *Streptomyces venezuelae* (PDB:6DXO).

Alternatively, anti-sigma factor inactivation can occur by allosteric means in anti-sigma factors which are not membrane bound. As discussed above, anti-sigma factors with ZASD motifs can act as direct redox sensors. In the case of the S*treptomyces coelicolor* anti-sigma factor RsrA, a ZASD-containing anti sigma factors that is not membrane bound, the ZASD motif of forms disulphide linkages between key cysteine residues when under disulphide stress. This results in the ejection the structurally significant zinc cation and stabilises the

inactive reduced form of RsrA, resulting in release of its cognate sigma factor, σ^R. σ^R then drives the expression of thioredoxin and thioredoxin reductase genes to respond to the disulphide stress (Li *et al.*, 2003). Anti-sigma factor suppression by conformational change can also occur indirectly. When the *C. metallidurans* outer membrane sensor protein CnrX detects extracellular cobalt or nickel ions, the metal binding induces allosteric changes that are transferred to the linked membrane-bound anti-sigma factor, CnrY, resulting in release of the ECF sigma factor CnrH, which then activates transcription of the appropriate metal ion resistance genes (Trepreau *et al.*, 2011).

Anti-sigma factor deactivation can also be achieved by sigma factor mimicry (Mascher, 2013). In this method, the activating signal causes the anti-sigma factor to interact with a sigma-like protein with greater affinity than the sigma factor itself, thereby releasing the sigma factor. For example, in α-proteobacteria, sigma factor EcfG (σ^{EcfG}) is bound by its anti-sigma factor, NepR, in the absence of signal (Campagne *et al.*, 2012). However, stress conditions induce the action of Pak (PhyR-activating kinase) histidine kinases, which can phosphorylate the normally inactive unphosphorylated PhyR response regulator on its C-terminal response domain. This activation induces an allosteric change in PhyR, presenting its N-terminal σ^{EcfG}-like domain, which causes NepR to undergo partner-switching to release active σ^{EcfG} (Campagne *et al.*, 2012; Francez-Charlot *et al.*, 2015).

1.6.6 Iron starvation (IS) sigma factors and cell-surface signalling (CSS)

Iron starvation (IS) sigma factors are sigma factors that belong to the groups ECF05-10, based upon the analysis of Staron et al (2009). IS sigma factors regulate the transcription of genes associated with iron acquisition. The transcription of these sigma factors are regulated by Fur (see section 1.5), and therefore the associated iron acquisition genes are only expressed under conditions of iron limitation (Baichoo and Helmann, 2002; Moraleda-Munoz *et al.*, 2019). A mechanism of sigma factor activation that is often implicated in ferric iron uptake, and regulates ECF sigma factors of the iron starvation (IS) class, is cell surface signalling (CSS)(Llamas *et al.*, 2014). This mechanism occurs in Gram-negative bacteria and involves a protein interaction cascade that links extracellular signals to the cytoplasmic

sigma factor. Three examples of IS sigma factor systems, PvdS/FpvI, FecI and FoxI, are discussed below.

The PvdS/FpvI sigma factor system of *Pseudomonas aeruginosa* is unusual in that one anti-sigma factor, FpvR, acts as an inhibitory partner for two sigma factor, PvdS and FpvI (Llamas *et al.*, 2014). *P. aeruginosa* produces a siderophore known as pyoverdine, and binding of iron-loaded pyoverdine (i.e. ferripyoverdine) to the TBDR FpvA initiates TonB-mediated active transport of the ferric-siderophore complex across the outer membrane. Binding of the ferric-siderophore complex to FpvA also stimulates the proteolytic cleavage of the linked FpvR anti-sigma factor by the RseP/MucP proteases (Visca, Imperi and Lamont, 2007), freeing the FpvI to direct further transcription of the *fpvA* gene, and PvdS to direct genes associated with pyoverdine synthesis (Edgar *et al.*, 2017).

Another IS sigma factor system is the Fec system found in many bacteria, comprising the sigma factors FecI and its anti sigma factor FecR (Braun and Mahren, 2005). In this system, the siderophore is citrate, and iron-loaded citrate is transported via the TBDR, FecA. Upon binding of extracellular ferric citrate to the FecA, an N-terminal domain of the TBDR interacts with the C-terminal domain of the linked anti-sigma factor FecR. This releases the sigma factor FecI. However, FecR appears to be essential for the activity of FecI, and thereby is more appropriately termed a sigma factor regulator (Mahren and Braun, 2003; Mettrick and Lamont, 2009). This may be due to FecR either (a) assisiting the association of FecI to core RNAP, or (b) stabilising the FecI sigma factor and/or protecting it from proteolysis (Braun, Mahren and Sauter, 2006). Thus, FecR acts as an inhibitor (anti-sigma factor) under non-inducing conditions and an activator (sigma factor) under inducing conditions. In these systems, the anti-sigma factor is referred to as a sigma factor regulatory protein.

This regulator-dependent sigma factor activation is also observed in the *P. aeruginosa* FoxI-FoxR system, and homologue of the Fec system (Bastiaansen *et al.*, 2015a). This system regulated the utilisation of ferrioxamine B. Binding the ferric-ferrioxamine to the TBDR FoxA induces the interaction of a FoxA signalling domain with a periplasmic C-terminal domain of the sigma factor regulator FoxR. Self-cleavage of FoxR, via an N-O acyl rearrangement of residues Gly191 and The192, leads to the proteolysis by the Prc/RseP proteases. After this

cleavage, a cytoplasmic domain of the sigma factor regulator, termed a pro-sigma domain, remains bound to the sigma factor to mediate its activation (Bastiaansen *et al.*, 2015b).

Other anti-sigma factor-independent mechanisms of regulation include: direct regulation by transcription factors (Hong, Paget and Buttner, 2002; Lan *et al.*, 2006), activation via phosphorylation by serine/threonine kinases (although this has not been empirically demonstrated) (Jogler *et al.*, 2012), and some mechanisms which are completely uncharacterised (Mascher, 2013).

1.7 Sigma factors with on-board regulatory domains

1.7.1 ECF sigma factors with C-terminal regulatory domains

Although the majority of ECF sigma factors are associated with an anti-sigma factor, there are several ECF groups which do not have a cognate anti-sigma factor. These sigma factors appear to be regulated in an anti-sigma factor-independent fashion (Mascher, 2013). Commonly, these ECF sigma factors have a fused regulatory C-terminal domain (CTD). Currently, there are over 15 ECF groups classified with such CTDs. However, only members of groups ECF41, ECF42, and ECF44 have been characterised.

The ECF41 group contains over 400 different sigma factors across ten bacterial phyla including Acidobacteria, Actinobacteria, Cyanobacteria, Firmicutes, and Proteobacteria (Staron *et al.*, 2009). They are hypothesised to have roles in redox homeostasis as they are often found in a genomic context with genes encoding oxioreductases, epimerases and carboxymuconolactone decarboxylases. ECF41 sigma factors have fused ~200 amino acid C-terminal extensions with a conserved SnoaL_2-like domain. This domain may have a dual role, acting as an activator and inhibitor of the ECF sigma factor. The crystal structure of σ^J from *Mycobacterium tuberculosis* suggests that the SnoaL_2 domain may act as a scaffold, holding the σ_2 and σ_4 domains in an inactive conformation under native conditions (Goutam,

Gupta and Gopal, 2017). Additionally, this regulatory CTD is also required for ECF sigma factor activity, so it also displays an activating role (Wecke *et al.*, 2012).

The ECF42 group consists of proteins that are mostly found in Actinobacteria and Proteobacteria, and are often situated near DGPF proteins (a highly-conserved but poorly-characterised protein class with an D-G-P-F motif). The very large scale of the fused CTD means that ECF42 sigma factors are larger than most other ECF sigma factors. The fused CTD contains tetratrico peptide repeats (TPRs) which are hypothesised to have a role in protein-protein interactions. Similarly to the ECF41 SnoaL_2 domain, the ECF42 TPR-containing CTD is required for the ECF sigma factor activity. However, there is less evidence demonstrating a regulatory function for the ECF42 CTD (Liu, Pinto and Mascher, 2018; Wu *et al.*, 2019).

ECF44 group sigma factors have a short cysteine-rich domain (CRD) of around 30-40 amino acids located at the C-terminus. These CRDs have been shown to act as metal-ion sensors, where the regulatory function of the CRD is activated in the presence of specific metal ions. The two characterised ECF44 sigma factors from *Myxococcus xanthus*, CorE and CorE2, have six cysteine residues within their CRDs. However, the arrangement of these cysteines is different, and this may confer different metal ion specificity. The CorE CRD has been demonstrated to interact with Cu^+ ions (which inhibit CorE) and Cu^{2+} ions (which activate CorE) (Gomez-Santos *et al.*, 2011). CorE2, with its different arrangement of cysteine residues, has been shown to be inactivated by Cd^{2+} and Zn^{2+} via its CRD (Marcos-Torres *et al.*, 2016). However, the precise step of transcription initiation that is blocked by this mechanism has not been shown i.e. it is not clear whether metal binding inhibits (a) the association of the sigma factor with core RNAP, or (b) binding of the sigma factor to DNA (in association with core RNAP).

There are examples of ECF groups that have been identified as lacking a cognate anti-sigma factor and containing a C-terminal domain that have not been characterised. In particular, the groups ECF58-62 found in Planctomycetes (formerly ECF01-Gob, ECF01-P, ECFSTK_01-04) display these characteristics and it is possible that their CTDs display a regulatory function (Jogler *et al.*, 2012; Pinto and Mascher, 2016). However, their signalling mechanisms are as yet unknown.
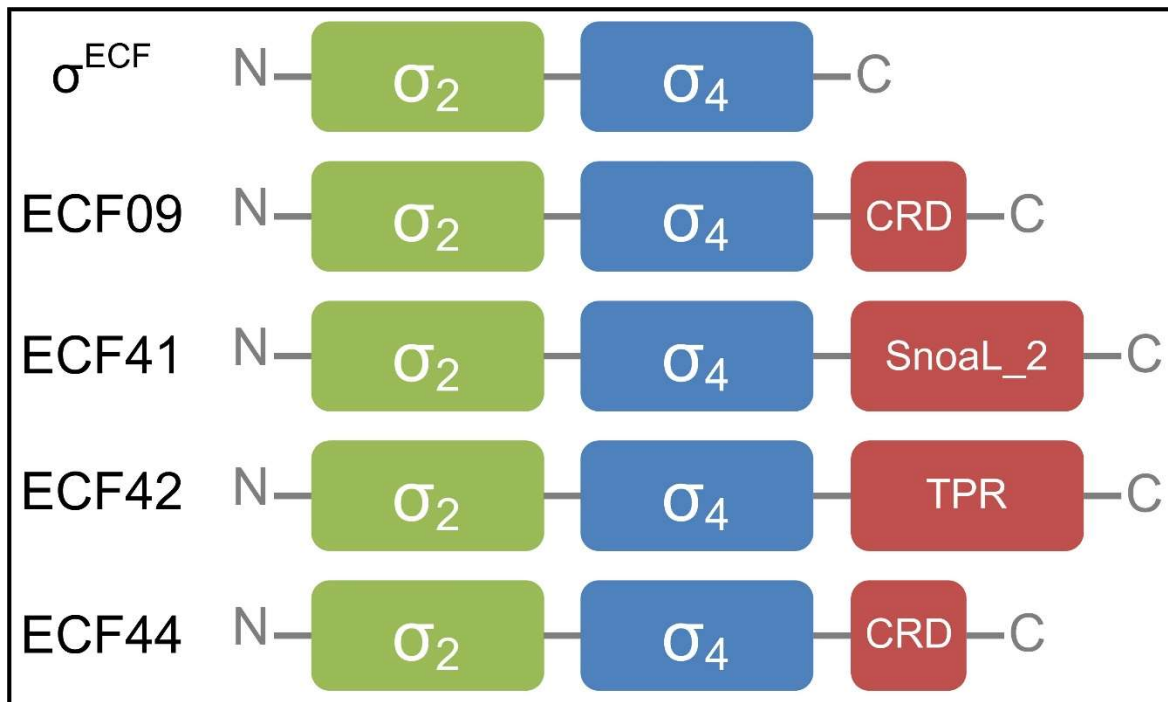
Figure 1.12. Domain architecture of characterised ECF sigma factors with putative regulatory C-terminal regions

All ECF sigma factors contain the conserved core ECF domains σ_2 and σ_4. Several classes of ECF sigma factors lack a cognate anti-sigma factor and contain a putative regulatory C-terminal region. The ECF09 sigma factors MbaS and OrbS have short C-terminal regions which constitute a C-terminal extension. ECF44 sigma factors have a short C-terminal region which constitutes a cysteine-rich domain (CRD) (Marcos-Torres *et al.*, 2016; Gomez-Santos *et al.*, 2011). ECF41 and ECF42 sigma factors have longer C-terminal regions; the ECF41 C-terminal region is a SnoaL_2-like domain, and the ECF42 C-terminal region contains tetratrico peptide repeats (TPRs) (Wu *et al.*, 2019). Domains are not shown to scale.

1.7.2 MbaS, OrbS, and the cysteine-rich extension (CRE)

MbaS and OrbS *Burkholderia* sigma factors that are members of the ECF09 group, based on sequence similarity (Staron *et al.*, 2009). Unlike other members of this group, they lack an anti-sigma factor and have a short extension at the C-terminus which may have a compensatory regulatory function. Similarly to the CRD found in ECF44 sigma factors, the C-terminal extensions of MbaS and OrbS (and the homologous *Paraburkholderia* IS sigma factor PhmE) are rich in cysteine residues (Figure 1.13). This C-terminal extension could be considered a cysteine-rich extension (CRE).

Orbs part of the *orb* gene cluster responsible for the synthesis of ornibactin in *Bce*. It was demonstrated to be a sigma factor that acted upon three OrbS-dependent promoters (P$_{orbH}$, P$_{orbE}$ and P$_{orbI}$) by RT-PCR and transcription reporter analyses. Additionally, the *orbS* promoter was shown to regulated by Fur (Agnoli *et al.*, 2006). Recently, the core elements OrbS-dependent promoters have been identified with greater precision, in addition to the transcription start site. The importance of the spacer region upon the activity of OrbS, and cross-activity between OrbS and PvdS, was also demonstrated (Agnoli *et al.*, 2018).

MbaS was originally identified as the sigma factor responsible for the transcription of the *mba* gene cluster associated with malleobactin in *Bth* (see section 1.4.4). It was demonstrated to be induced under iron-limiting conditions, likely due to regulation by Fur at an identified Fur box sequence. It was also shown to be necessary for the transcriptional activity from the *mbaI* promoter (Alice *et al.*, 2006). Several studies have been published analysing the *mba* gene cluster and malleobactin, but these have not investigated MbaS further (Franke *et al.*, 2013; Franke, Ishida and Hertweck, 2015; Trottmann *et al.*, 2019a).
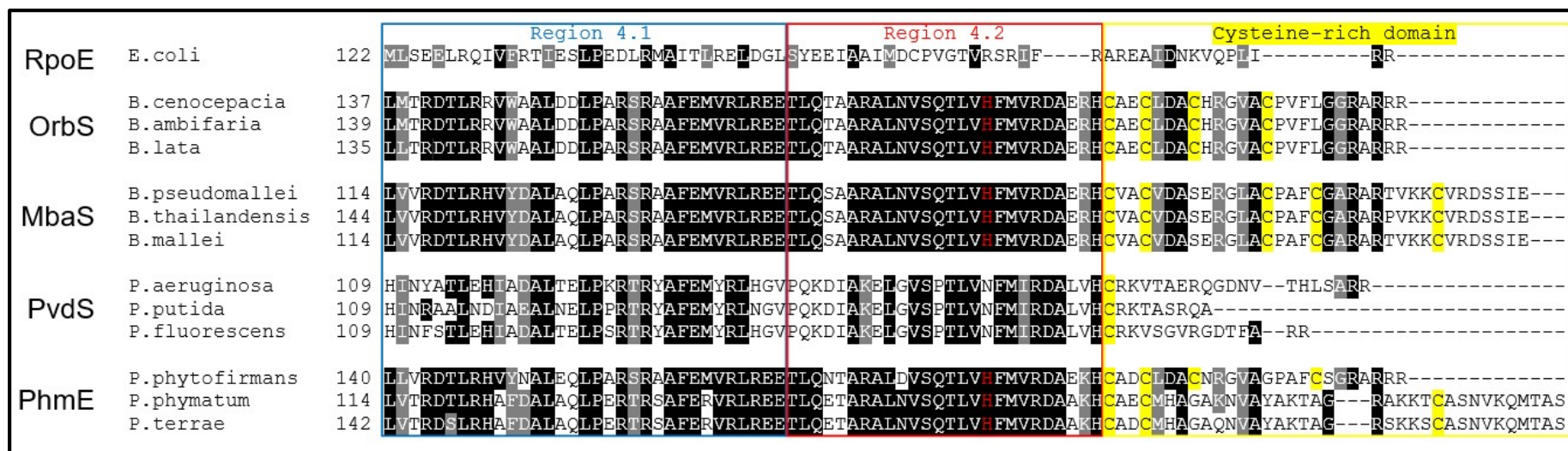
Figure 1.13. Alignment of amino acid sequences of the C-terminal extensions of ECF group sigma factors RpoE, OrbS, MbaS, PvdS and PhmE.

Sequences are aligned with Clustal-omega, amino acids that are identical in ≥70% of sequences are shown in white font highlighted in black, and amino acids that have similarity are shown in white font highlighted in grey. Conserved regions 4.1 and 4.2, based upon assignments of RpoE, are enclosed in blue and red boxes, respectively. The cysteine-rich extension (CRE) located at the C-terminus is enclosed in a yellow box, and cysteine residues in this region are highlighted in yellow. A conserved histidine residue within region 4.2 that is conserved across sigma factors containing a CRE is highlighted in red font. The iron starvation sigma factor sub-group to which sequnces belong is denoted on the left. Sequences were obtained from the following strains: *E. coli* MG1655, *B. cenocepacia* H111, *Burkholderia ambifaria* AMMD, *Burkholderia lata* 383, *B. pseudomallei* K96243, *B. thailandensis* E264, *B. mallei* ATCC23344, *P. aeruginosa* PA01, *Pseudomonas putida* KT2440, *Pseudomonas fluorescens* F113, *Paraburkholderia phytofirmans* PsJN, *Paraburkholderia phymatum* STM815, *Paraburkholderia terrae* DSM17804.

1.8 BCAM0001

Bce encodes 13 annotated ECF sigma factors across two of its three chromosomes. One of these proteins is encoded by the gene annotated as BCAM0001. It is a member of the ECF13 family, a small ECF sigma factor family found exclusively in Proteobacteria (Staron *et al.*, 2009). BCAM0001 is functionally uncharacterised.

In the BCAM0001 system, the anti-sigma factor is encoded by the originally unannotated gene BCAM0001a. The BCAM0001a gene is located downstream of the sigma factor gene, and overlaps with the BCAM0001 gene by 23 bp, suggesting that these two genes may be co-transcribed. The unusual anti-sigma factors associated with ECF13 group sigma factors are typified by their possession of ZAS domains (described in section 1.6.5). Most interesting of all, these anti-sigma factors lack the central transmembrane region and periplasmic C-terminal domains, indicating they act cytoplasmically. This group of anti-sigma factors are not well characterised. ZAS domains can act as redox sensors, with the thiol groups of conserved cysteine residues interacting with a zinc cation under favourable conditions, and forming disulphide bonds under stress conditions to eject the zinc cation and release the sigma factor. BCAM0001a also contains a ZAS domain, suggesting it could form a redox-mediated interaction with its sigma factor (Figure 1.14).

The adjacent genes to the sigma-anti-sigma factor pair, annotated as BCAM2840 and BCAM0002, are predicted to be involved in toxic metal resistance and show similarity to chromate reductases and arsenate reductases, respectively. Given that sigma factors often act on neighbouring genes, it is possible that sigma factor encoded by BCAM0001 regulates the expression of these genes, as well as its own.

```
BCAM0001a    1 -----MLPGKCTDVTRLL(13)LQVRVHLPTCSGCRAYRGQIALLRTAAKA 56
NGO1943      1 -------MKKCRDIALLL(13)ISIYMHLLFCPHCREYKRQLQTIKISLAK 54
NMB2145      1 -------MKKCRDIALLL(13)ISIYTHLLFCPYCREYKRQLQTIKRSLAK 54
RsrA         1 MSCGEPHETDCSEILDHL(13)VKFEHHFEECSPCLEKYGLEQAVKKLVKR 61
ChrR         1 -----MTIRHH-VSDALL(13)LVVATHLSLCDECRARAGALDAVGGSLME 55
ZAS motif                                   HXXXCXXC
```

Figure 1.14. Sequence alignment of selected zinc-binding anti-sigma domains (ZASDs) and BCAM0001a.

Residues with identity are shown in white font highlight in black, residues with similarity are shown in white font highlight in grey. The ZAS motif is aligned below sequences in bold font (Campbell *et al.*, 2007). Sequences were obtained from the following species: BCAM0001a, *Bce* H111; NGO1943, *Neisseria gonorrhoeae*; NMB2145, *Neisseria meningitidis*; RsrA, *Streptomyces coelicolor*; ChrR, *Rhodobacter sphaaroides*.

1.9 Hypotheses and aims

1.9.1 Hypotheses and aims of MbaS- and OrbS-related studies

Unlike the similar IS sigma factor PvdS, both MbaS and OrbS do not appear to have a cognate anti-sigma factor. Although the transcription of both *mbaS* and *orbS* has been demonstrated to be regulated by Fur, for stringent control of malleobactin/ornibactin synthesis post-translational regulation may be required.

The cysteine-rich extension (CRE) present at the C-terminal region of MbaS/OrbS may play a role in this regulation. Cysteines often play a key role in binding metal ions. In particular, by binding iron ions via thiol functional groups to form iron-sulphur clusters. Thiols also often serves as ligands for zinc. Therefore, the cysteine residues of the CRE may directly respond to metal ions, which in turn induce an inactive conformation of the sigma factor. This would allow downregulation of the siderophore-associated genes under metal-replete conditions.

This interacting metal ion is hypothesised to be Fe(II), due to the specificity of ornibactin and malleobactin for ferric iron. The bacterial cell is a reducing environment, so Fe(II) would be an appropriate signalling ion for the presence of high extracellular levels of Fe(III).

The activity of MbaS and OrbS in response to the presence of iron and other metal ions will be investigated. This will be compared to mutant forms of these proteins, with deleted or substituted residues, to examine the influence the C-terminal domain (and more specifically the cysteine residues of the CRE) has upon the regulation of the sigma factor activity.

1.9.2 Hypotheses and aims of BCAM0001-related studies

The function of the protein encoded by the gene annotated as BCAM0001 is unknown. The phenotype associated with deleting the BCAM0001 gene in *Bce* may provide some insights into the function. BCAM0001 and BCAM0001a are predicted to be a sigma-anti-sigma factor pair. This study aims to characterise this protein-protein interaction. Finally, in order to demonstrate the sigma factor activity of BCAM0001, its target promoters must be identified. More detailed hypotheses and aims are given in Chapter VI.

Chapter II: Materials and Methods

2.1 Bacteriological methods

2.1.1 Bacterial strains used in this study

The bacterial strains used in this study are shown in Table 2.1.

Table 2.1. Bacterial strains used in this study

Strain	Geneotype/Description[1]	Reference
E. coli Strains		
MC1061	hsdR araD139 Δ(ara-leu)7697 ΔlacX74 galU galK rpsL (Sm^r)	(Casadaban and Cohen, 1980)
JM83	F$^-$ ara Δ(lac-proAB) rpsL φ80dlacZΔM15 (Sm^r)	(Yanisch-Perron, Vieira and Messing, 1985)
S17-1λpir	thi proA hsdR recA RP4-2-tet::Mu-1 kan::Tn7 integrant (Tp^r Sm^r)	(Simon, Priefer and Puhler, 1983)
SM10λpir	thi thr leu tonA lacY supE recA RP4-2-tet::Mu (Tc^r Km^r)	(Simon, Priefer and Puhler, 1983)
BL21λDE3	F$^-$ ompT hsdS(r_B^- m_B^-) dcm$^+$ gal endA (λDE3) (Tc^r)	(Studier and Moffatt, 1986)
QC771	F$^-$ Δ(argF-lac)U169 rpsL (Sm^r)	(Carlioz and Touati, 1986)
QC1732	F$^-$ Δ(argF-lac)U169 rpsL Δfur::kan (Sm^r Km^r)	(Touati *et al.*, 1995)
BTH101	F$^-$ cya-99 araD139 galE15 galK16 rpsL1 hsdR2 mcrA1 mcrB1 (Sm^r)	Euromedex
CC118λpir	Δ(ara-leu) araD ΔlacX74 galE galK phoA20 thi-1 rpsE rpoB argE(Am) recA1 (λpir)	(Herrero, de Lorenzo and Timmis, 1990)
H1717	F$^-$ araD139 Δ(argF-lac)U169 rpsL150 relA1 deoC1 ptsF25 flbB5301 aroB fhuF::λplac Mu	(Hantke, 1987)
B. thailandensis Strains		
E264	Environmental isolate; prototroph	(Brett, DeShazer and Woods, 1998)
E264 Δ*mbaS*	E264 with in-frame deletion within *mbaS* (BTH_II2426)	This study
E264 Δ*pchE*	E264 with in-frame deletion within *pchE* (BTH_II1828)	This study
E264 Δ*mbaS* Δ*pchE*	E264 Δ*pchE* with in-frame deletion within *mbaS* (BTH_II2426)	This study
B. cenocepacia Strains		

OM3	KLF1-*orbI*::mini-Tn*5*Tp (*orbI*⁻ derivative of spontaneous Pch⁻ mutant of strain 715j)	(Agnoli *et al.*, 2006)
H111	CF isolate from Germany	(Gotschlich *et al.*, 2001)
H111 Δ*orbS*	H111 with in-frame deletion within *orbS* (BCAL1688)	A. T. Butt (unpublished)
H111 ΔBCAM0001a	H111 with in-frame within BCAM0001a	This study
H111 ΔBCAM0001-BCAM0001a	H111 with in-frame deletion through BCAM0001 and BCAM0001a	This study

[1] Sm^r=streptomycin resistance; Tp^r=trimethoprim resistance; Km^r=kanamycin resistance; Tc^r=tetracycline resistance.

2.1.2 Growth media

All media were made up in 300 ml glass medicine bottles. For solid media, agar powder was added to the solution at 1.5% (w/v) prior to autoclaving where required. Solutions were autoclaved for 20 minutes (except for M9 minimal media containing *p*-chlorophenylalanine, see below). Media were allowed to cool to approximately 55°C before adding media supplements and, where agar was added, before pouring 25 ml per Petri dish.

Luria-Bertani (LB) Medium

The following were dissolved in d.H$_2$O prior to autoclaving: 1.0% (w/v) tryptone, 0.5% (w/v) yeast extract, 1.0% (w/v) NaCl.

Lennox (Lnx) Medium

The following were dissolved in d.H$_2$O prior to autoclaving: 1.0% (w/v) tryptone, 0.5% (w/v) yeast extract, 0.5% (w/v) NaCl.

Environmental Broth (EB) Medium

The following were dissolved in d.H$_2$O prior to autoclaving: 0.33% (w/v) tryptone, 0.17% (w/v) yeast extract, 0.5% (w/v) NaCl.

M9 Minimal Medium

The following were added to d.H$_2$O after autoclaving: 10X M9 salts solution (see below) to a final concentration of 10% (v/v), 1 M MgSO$_4$ (filter sterilised) to a final concentration of 1 mM, 100 mM CaCl$_2$ (filter sterilised) to a final concentration of 100 μM.

10X M9 salts solution was made up by dissolving the following: 60 g anhydrous Na$_2$HPO$_4$, 30 g anhydrous KH$_2$PO$_4$, 5 g NaCl, 10 g NH$_4$Cl in water to a final volume of 1 litre.

Where each was desired, the following supplements were dissolved in d.H$_2$O prior to autoclaving: casamino acids (CAA) at a final concentration of 1% (w/v), glucose at a final concentration of 0.5% (w/v), *p*-chlorophenylalanine (cPhe) at a final concentration of 0.1% (w/v) by mixing for approximately one hour (solutions containing cPhe had a reduced autoclaving time of 15 minutes). For blue/white screeing of *E.coil* JM83 transformants containing pSNUFF3Cm derivatives, the following were added to the medium containing 0.1% (w/v) CAA after autoclaving: glycerol (final concentration of 0.5% (v/v)), thiamine (final concentration of 5 μg ml^{-1}, made up at 5 mg ml^{-1} in d.H$_2$O prior to addition), and trimethoprim (final concentration of 25 μg ml^{-1}).

CAS Medium

In order to detect and determine the presence of siderophores produced by *Bth*, media containing chrome azurol S (CAS) was used, as per the protocol of (Schywyn and Neilands, 1987). Two solutions, 'CAS mix' and Y minimal agar, were prepared and autoclaved separately.

Y minimal agar was made up by dissolving the following in 90 ml d.H$_2$O prior to autoclaving: 169 mg glutamic acid (sodium salt), 0.3 g Tris base, 100 μl MgSO$_4$·7H$_2$O (10% (w/v), 100 μl CaCl$_2$·6H$_2$O (22% w/v), 100 μl K$_2$HPO$_4$·3H$_2$O (22% w/v). The mixture was adjusted to pH 6.8, before the addition of agar powder for solid media.

CAS mix was made up in the following way: 60.5 mg of CAS powder was added to 50 ml d.H$_2$O until dissolved, followed by addition of 10 ml 1 mM FeCl$_3$·6H$_2$O (prepared by dissolution in 10 mM HCl), followed finally by addition of 40 ml

hexadecyltrimethylammonium bromide (HDTMA) solution (72.9 mg HDTMA dissolved in 40 ml d.H_2O) with stirring.

Once autoclaved and cooled to ~50 ^{o}C, 90 ml of Y minimal medium was slowly combined with 10 ml CAS mix, and mixed until homogeneous.

The resulting medium simulated iron-limiting conditions with ferric iron at a concentration of 10 µM. To prepare CAS medium with iron-replete conditions, $FeCl_3 \cdot 6H_2O$ was added immediately before pouring to give a final concentration of 60 µM.

MacConkey Medium

MacConkey agar (Difco) was dissolved into d.H_2O at a final concentration of 4% (w/v) prior to autoclaving. Selected carbohydrates were added to the medium at a final concentration of 1% (w/v) after autoclaving. For Fur titration assays (see section 2.5.2), $Fe(NH_4)_2(SO_4)_2$ was added to the medium at a final concentration of 40 µM.

2.1.3   Maintenance of bacterial cultures

Escherichia coli

E. coli cells were most commonly grown on LB-agar medium, although several other media were used where necessary for antibiotic selection or for agar plate-based assays. Agar plates harbouring *E. coli* were generally incubated overnight at 37 ^{o}C for approximately 16 hours. Overnight liquid cultures of *E. coli* were grown in LB broth, with appropriate antibiotic where required. Single colonies of *E. coli* were picked by a sterile toothpick or loop. Cultures were incubated at 37 ^{o}C (200 rpm) with aeration, for approximately 16 hours.

Burkholderia thailandensis **and** *Burkholderia cenocepacia*

Bth and *Bce* were grown on similar media to *E. coli*. Where long-term storage was required, *Bth* and *Bce* were grown on M9 minimal media with 0.5% (w/v) glucose. EB media was used for the attempted selection of *Bth fur* mutants. Agar plates harbouring *Bth* and *Bce* strains were incubated at 37 ^{o}C for approximately 24-40 hours. Overnight liquid cultures of *Bth* and

Bce were made up in LB broth, with appropriate antibiotic where required. Single colonies of *Bth* and *Bce* were picked into sterile medium by sterile toothpick or loop. Cultures were incubated at 37 °C, 200 rpm, for approximately 16 hours.

Storage of bacterial cultures

For short-term storage, bacteria were routinely stored on parafilm-sealed agar plates. Agar plates harbouring *E. coli* and *Bth* were stored at 4°C, whereas agar plates harbouring *Bce* were stored at room temperature. *Burkholderia* strains were viable for considerably longer when stored on M9 minimal medium. *E. coli* strains were viable for up to one month of storage, *Burkholderia* strains were viable up to 10 days (increased when M9 minimal medium used).

For long-term storage, bacterial suspensions were frozen in the presence of glycerol. 700 μl of overnight culture and 300 μl of 50% (v/v) glycerol were mixed in a cryovial and stored at - 80 °C. Strains were retrieved from glycerol stocks by scratching the surface of the frozen bacterial suspension with a wire loop and streaking onto a fresh agar plate to isolate single colonies.

2.1.4   Plasmid transfer into bacteria

Preparation of competent *E. coli* cells

Competent *E. coli* cells capable of uptake of plasmid DNA via transformation were prepared by the method of (Hanahan, 1983). An overnight culture of the desired *E. coli* strain was grown in LB medium. 500 μl of this was inoculated into 50 ml of LB medium and grown at 37 °C with aeration at 200 rpm until $OD_{600} \approx 0.5$, whereupon the culture was stored on ice for 15 minutes. Cells were collected by centrifugation at 3200x g for 10 minutes, and the cell pellets were resuspended in ice-chilled solution RF1 (100 mM KCl, 50 mM $MnCl_2 \cdot 4H_2O$, 30 mM potassium acetate, 10 mM $CaCl_2 \cdot 2H_2O$, 15% (v/v) glycerol, adjusted to pH 5.8 with 200 mM acetic acid) before storage on ice for 30 minutes. Cell were harvested by centrifugation

at 3200x *g* for 10 minutes, and resuspended in ice-chilled solution RF2 (200 µl MOPS [3-(N-Morpholino)propanesulfonic acid] mixed with 9.8 ml 10 mM KCl, 75 mM $CaCl_2 \cdot 2H_2O$, 15% (v/v) glycerol) followed by storage on ice for 15 minutes. 200-400 µl aliquots of these competent cells were transferred to in microcentrifuge tubes and stored immediately at -80 °C. This method was used to create stocks of the following competent *E. coli* cells: JM83, BL21λDE3, MC1061, S17-1, SM10λ*pir*, QC771, QC1732, BTH101, H1717, CC118λ*pir*.

Transformation

Transformation was the preferred means of transferring plasmid DNA into *E. coli* cells. An aliquot of competent *E. coli* cells and the stock of plasmid DNA be transferred were defrosted on ice for 20 minutes. DNA-competent cell solutions were made up in individual microcentrifuge tubes. For transformation of plasmid miniprep DNA, 1-2 µl of DNA was added to 50 µl of cells. For transformation of ligation reactions, 10-20 µl of each solution (ligation, ligation control, and vector control) was each added to 50 µl of cells. Additionally, 1-2 µl of supercoiled plasmid DNA (corresponding to the ligation reaction) was added to 50 µl of competent cells as a cell control. As a control for the antibiotic selection agar plate and/or contamination of the competent cells, 50 µl of cells with no added DNA was also included.

All DNA-competent cell suspensions were chilled on ice for 20 minutes prior to heat shock at 42 °C in a water bath for 60 seconds. Following the heat shock, suspensions were returned to ice for two minutes, whereupom 500 µl of LB broth was added to each suspension, and the suspensions were incubated at 37 °C 200 rpm for 45 minutes. 100 µl of each cell suspension were spread on agar plates with appropriate antibiotic(s) to select for the transforming plasmid, and incubated at 37 °C overnight. The remainder of the cell suspensions were stored at 4 °C overnight as a contingency measure.

Conjugation

Conjugation, using *E. coli* donor cells, was the preferred means of transferring plasmid DNA into *Burkholderia* cells. The plasmid to be transferred was initially transformed into the *E. coli* donor strain, either S17-1 or SM10λ*pir* (described in section 2.1.4: Transformation).

Overnight cultures of theplasmid-bearing *E. coli* donor strain and the recipient *Burkholderia* strain were grown in LB broth at 37 °C.

1 ml of cells were taken from the *E. coli* donor culture (henceforth known as 'donor'), and two 1 ml aliquots of the *Burkholderia* strain culture (henceforth known as 'recipient') were transferred to seperate microcentrifuge tubes. After centrifugation at 17,000x *g* for one minute, the cell pellets from the donor and recipient aliquots were resuspended in 200 µl phosphate-buffered saline (PBS). 100 µl from the donor cell suspension was taken and used to resuspend one of the recipient cell pellets. 100 µl of each of the cell suspensions was applied onto individual 0.45 µm nitrocellulose discs placed on separate agar plates (LB agar in most cases, EB agar when attempting to generate *fur* mutants) and incubated at 37 °C overnight.

The nitrocellulose discs, with a lawn of bacterial growth on them, were each transferred to 20 ml universal tubes containing 3-5 ml of PBS using sterile forceps, and the cells were resuspended by vigorous vortexing. 100-400 µl of undiluted or diluted cell suspensions were spread on selective agar plates containing appropriate antibiotics to select for the *Burkholderia* strain containing the transferred plasmid and ensuring the donor cells did not grow. Plates were incubated at 37 °C for 16-40 hours.

Provided no colonies were formed on the donor or recipient control plates, colonies on the mix plate were accepted to be *Burkholderia* bearing the conjugated plasmid.

2.1.5   Allelic exchange in *Burkholderia*

For the in-frame marker-less deletion or mutation of genes in *B. thailandensis* and *B. cenocepacia*, two gene replacement vectors were used: pEX18Tp-*pheS* (Barrett *et al.*, 2008) and pSNUFF3Cm (H. Spiewak, unpublished). These methods were particularly important when it was essential to avoid polar effects on downstream genes (such as in generating an *mbaS* mutant) and to allow multiple gene deletions to be introduced into a single strain without gaining antibiotic selectable markers and thereby restricting the ability to introduce plasmids. Additionally, for the attempted generation of marked mutants, such as the *Bth*

Δ*fur*::TpTer mutant, the pSHAFT2 gene replacement vector was used (Shastri *et al.*, 2017). This was necessary due to the strong selection for the restoration of the wild-type *fur* gene using marker-less gene deletion methods.

Generation of DNA fragments that contained in-frame deletions within the target gene was achieved using SOE-PCR (see section 2.2.6). These DNA fragments contained ≥500 bp of identical sequence with the *Burkholderia* genome on either side of the gene deletion. In the case of the Δ*fur*::TpTer allele, a TpTer cassette was also inserted within the gene deletion. The SOE-PCR generated DNA fragments were then cloned into the MCS of the desired allelic exchange vector.

The pEX18Tp-*pheS* and pSNUFF3Cm systems introduced allelic exchange using two rounds of homologous recombination. pEX18Tp-*pheS* and pSNUFF3Cm are able to introduce the mutant alleles into *Burkholderia* as the bacteria lack the ability to utilise the ColE1 origin of replication of the plasmids. Only homologous recombination between the chromosome and the plasmids, resulting in genomic integration of the plasmid, confers the specified antibiotic selection markers. The resulting co-integrant *Burkholderia* contains both the wild-type allele and the deleted/modified allele. For the second homologous recombination, a counterselection that kills co-integrant cells was implemented. Two different methods for doing this were employed, for either pEX18Tp-*pheS* system or the pSNUFF3Cm system.

For deletion of genes that were integrated into the genome using pEX18Tp-*pheS* (Figure 2.1a)), co-integrant strains were grown on M9 minimal agar containing 0.1% (w.v) DL-4-chlorophenylalanine (Sigma-Aldrich) (cPhe). Initially, the co-integrant strain was grown on M9-glucose agar containing 25 µg ml^{-1} trimethoprim. A single colony was taken, resuspended in PBS, and equal volumes of the cell solution spread on M9-glucose agar supplemented with: 25 µg ml^{-1} trimethoprim (control A); 25 µg ml^{-1} trimethoprim and 0.1% (w/v) cPhe (control B); and 0.1% (w/v) cPhe (recombination). Control A conditions should give rise to a high number of uniformly-sized colonies, control B conditions should give rise to no colonies, and the recombination conditions should give rise to a low number of variably-sized colonies. The *B. pseudomallei* mutant *pheS* gene, incorporated into the genome, is lethal when cPhe is present as it allows charging of tRNA$_{Phe}$ with cPhe. Therefore, only a second homologous recombination that results in plasmid excision enables survival.

The second crossover event resulted in either restoration of the wild-type gene, or introduction of the deleted/modified gene into the chromosome. cPhe-resistant recombinant strains were identified by parallel counter screening on agar containing chloramphenicol and trimethoprim, where sensitivity to the antibiotics indicated loss of the vector backbone.

For the deletion of genes that were integrated into the genome using pSNUFF3Cm (Figure 2.1b), the plasmid pDAI-SceI-*pheS* was introduced into the co-integrant strain by conjugation, and strains that had successfully taken up the plasmid were selected for with tetracycline resistance specified by pDAI-SceI-*pheS*. Strong expression of the I-SceI endonuclease on these plasmids introduces lethal DNA double strand breaks at the I-SceI site present on the intergrated pSNUFF3Cm plasmid, and only DNA excision via a second homologous recombination allowed survival. The second DNA crossover event resulted in either restoration of the wild-type gene, or introduction of the deleted/modified gene into the chromosome. Recombinant strains were verified by using the same means employed following application of cPhe counterselection. Mutants were then cured of the pDAI-SceI-*pheS* plasmid by two rounds of streaking on M9 minimal medium containing 0.1% (w/v) cPhe.

The pSHAFT2 system introduced allelic exchange using one round of concomitant double homologous recombination (Figure 2.1c). pSHAFT2 is able to introduce mutant alleles into *Burkholderia* as the bacteria lacks the ability to utilise the oriR6K origin of replication of the plasmid. Therefore, only homologous recombination between the chromosome and the plasmid confers the trimethoprim resistance. This recombination can occur by a single crossover event, resulting in integration of the plasmid and co-integrant formation, with both the wild-type allele and the mutant allele present. Alternatively, the recombination can occur by a double crossover event, resulting in the wild-type *fur* allele being replaced by the Δ*fur*::TpTer mutant allele. In this case, vector sequences are not permanently integrated into the genome. The desired latter case was screened for by a subsequent counter-screening for chloramphenicol sensitivity.

In all cases, PCR screening using the external primers upstream and downstream of the cloned gene fragment was used to confirm gene replacement. These PCR products also

underwent DNA sequencing and sequence analysis to verify correct gene

deletion/modification. More details can be found in sections discussing specific generation

of mutants.
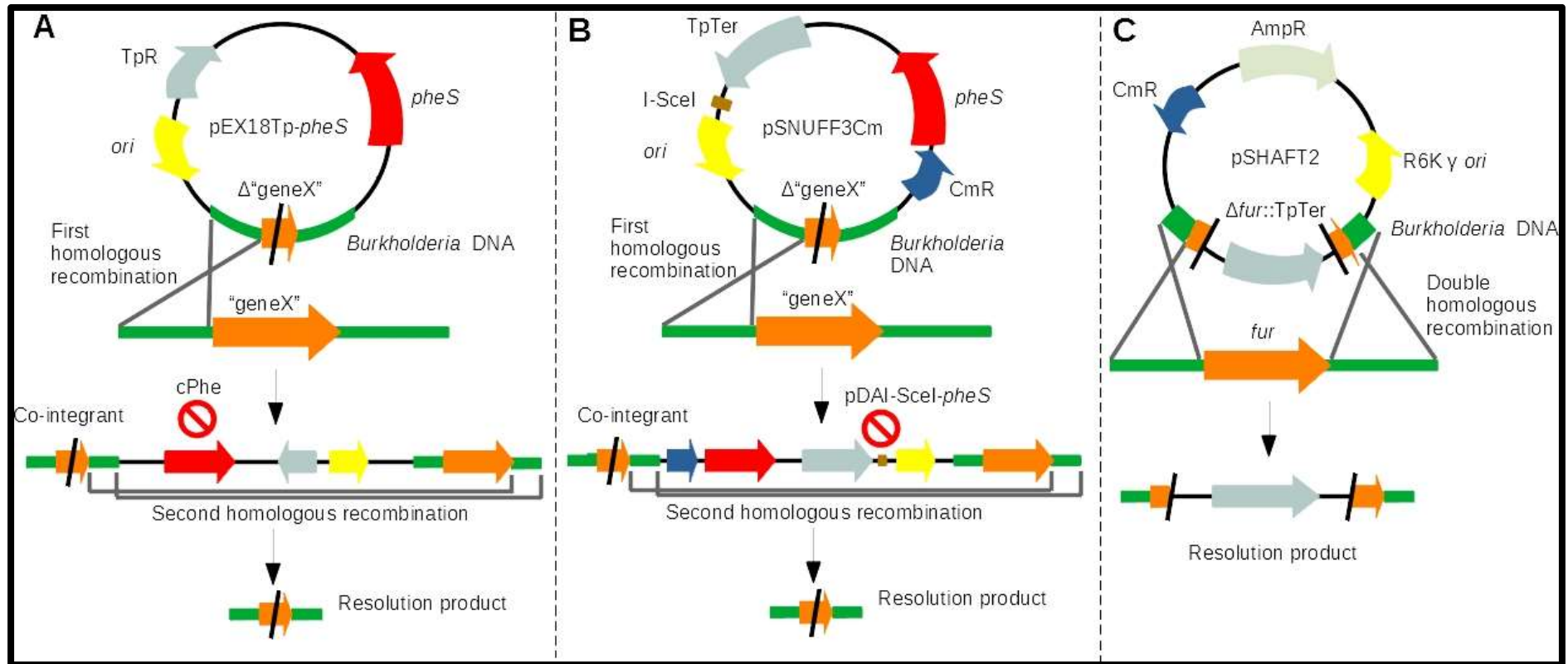
Figure 2.1. Schematic representation of *Burkholderia* allelic exchange strategies.

In all cases, allelic exchange vectors containing a mutant allele flanked by regions of *Burkholderia* DNA sequence were introduced into *Bth* or *Bce* by conjugation. Homologous recombination could occur upstream or downstream of the mutant allele. **A.** A second homologous recombination event was selected for by the presence of cPhe, which is toxic in combination with the mutant *Bps* PheS protein. **B.** A second homologous recombination event was selected for by the introduction of pDAI-SceI-*pheS*, which introduces lethal double-stranded DNA breaks. **C.** A double homologous recombination event was selected for by acquisition of trimethoprim resistance, but not ampicillin or chloramphenicol. Diagrams are not to scale. Genes are represented as annotated arrows. More detail in text.

2.1.6   Determination of bacterial growth rate

To determine the growth rate of bacterial strains in different media and under different conditions, bacterial growth curves were utilised. Firstly, overnight cultures of the assayed bacterial strain were grown at 37 °C with aeration, 200 rpm, for approximately 16 hours. 500 µl of this was inoculated into 50 ml of the desired medium. Where a single bacterial strain was assayed, these dilutions were made directly from the same overnight culture. Where different bacterial strains were assayed, the overnight cultures were first diluted with the same medium to a standard OD_{600} of 0.5 prior to inoculation. The cultures were grown at 37 °C 200 rpm. The bacterial growth rate was monitored by measuring the OD_{600} from 1 ml samples, the first taken immediately after inoculation and then every 30 minutes thereafter.

Data was plotted in GraphPad Prism to generate a growth curve, with OD_{600} values plotted on a logarithmic scale (GraphPad Prism version 7.03 for Windows, GraphPad Software, La Jolla California USA, www.graphpad.com) The growth curves were analysed by fitting to an exponential growth curve using the GraphPad Prism software (data points after the exponential growth phase were excluded), and the line of best fit was in the format:

$$y = y_0 e^{kx}$$

where $y_0 = y$ when $x = 0$

k = rate constant

The growth rate, or doubling-time, was calculated as:

$$\frac{\ln(2)}{k}$$

2.2 Polymerase Chain Reaction (PCR)

2.2.1   DNA primers

Custom DNA oligonucleotides were supplied by Eurogentec. Where possible, primers were designed to have a region of 18-20 nucleotides that was complementary to the target, a GC content of 40-60%, and a melting temperature (T_m) in the range 50-65 °C. Pairs of primers were designed to have T_ms within 5 °C of each other, and have no complementarity. Where selection of primers was limited by function, these parameters were adhered to where possible but was not always achievable. For ligation of amplicons to vectors, additional bases were added at the 5' ends of the primers that specified a restriction enzyme cleavage site and a terminal GC 'clamp'.

Primer T_m was calculated using either of the two equations:

For primers of 14-20 nucleotides in length (Wallace-Ikatura formula):

$$Tm_1(°C) = 2(A + T) + 4(G + C)$$

where A = number of adenine base pairs etc.

For primers of >20 nucleotides in length:

$$Tm_2(°C) = 81.5 + 16.6(log_{10}[0.05]) + 0.41(\%G + \%C) - (\frac{675}{n})$$

where n = total number of base pairs, %G = percentage of guanine bases in the primer etc.

The optimum annealing temperature (T_a) of primers was determined by performing multiplex PCR using a gradient of annealing temperatures, or calculated as 5 °C below the mean T_m of the primers. Template DNA used was genomic DNA from boiled cell lysates, plasmid DNA, or purified PCR product DNA. PCR products were analysed by agarose gel electrophoresis.

2.2.2   Annealing of oligonucleotides

Where only short double-stranded DNA products were required for cloning, oligonucleotides were annealed to give the desired DNA fragment the requirement for PCR. Oligonucleotides were designed to be ≤59 nucelotides in length. Annealing was performed in a microcentrifuge tube. Where two oligonucleotides were to be annealed, 45 µl of each 100 µM oligonucleotide was incubated with 10 µl of 10x annealing buffer (10 mM $MgCl_2$, 200 mM Tris pH 8.0, in d.H_2O) at 90 °C for 10 minutes, followed by room temperature for one hour. DNA products were analysed by agarose gel electrophoresis.

2.2.3   Primers used in this study

The primers used in this study are shown in Table 2.2.

Table 2.2. Primers used in this study

Primer/oligonucleotide	Sequence (5'-3')[1]
B. thailandensis E264	
ΔmbaS-A	GTATGGATCCACGATCGATTTCGGGGGCGC
ΔmbaS-B	GCATTTTTTTACCGGCCGCGCCATGGATTCTCCAGA
ΔmbaS-C	TCTGGAGAATCCATGGCGCGGCCGGTAAAAAAATGC
ΔmbaS-D	GCGCAAGCTTTCGTTCGCGATCTCGCGCAA
ΔmbaS-out-fwd	ACAGCACGGCGATCCGCT
ΔmbaS-out-rev	AGCCCGTGAAGAGCACGC
ΔpchE-A	GCATGGATCCATCGACGTGCGCATCACGTC
ΔpchE-B	CACGCCCTCCTCCATCGCGGAATCAACAGCAGACTG
ΔpchE-C	CAGTCTGCTGTTGATTCCGCGATGGAGGAGGGCGTG
ΔpchE-D	GCGCAAGCTTCATGCACCGCGTGATCGAGA
ΔpchE-out-fwd	AACTGTCTGTCGACGCAGC
ΔpchE-out-rev	ATCGACGGACAGGTGCAG
mbaS-C203+206A-B	GCGTCGACCGCCGCGACCGCGTGCCGCT
mbaS-C203+206A-C	AGCGGCACGCGGTCGCGGCGGTCGACGC
mbaS-C216+220A-B	CGCGCCCGCAAACGCCGGCGCCGCGAGC
mbaS-C216+220A-C	GCTCGCGGCGCCGGCGTTTGCGGGCGCG
mbaS-C230A-B	CGAATCGCGCACCGCTTTTTTTACCGGC
mbaS-C230A-C	GCCGGTAAAAAAAGCGGTGCGCGATTCG
mbaSmeroscreen-fwd	GGCCTTTTGCTCACATGTTC
mbaSmeroscreen-rev	GGCAAGCTCGCTGGAAAAGT
Δfur-A	TATAAAGCTTGCAGGTTGTCCGCGCCCGTC
Δfur-B	TTTGCGATAGGGGCAGTTTTTGAGATCGGTCGGATT
Δfur-C	AATCCGACCGATCTCAAAAACTGCCCCTATCGCAAA
Δfur-D	ATATGGATCCTCTTGCGTCGATCGACGTCA
Δfur-NdeI-B	TTTGCGATAGGGGCAGTTCATATGTCATTTGAGATCGGTCGGATT
Δfur-NdeI-C	AATCCGACCGATCTCAAATGACATATGAACTGCCCCTATCGCAAA

Δfur-out-fwd	CGTTCGCGTCGTTCTGATCC
Δfur-out-rev	GTTCGGCGACGTGATCGAAC
mbaS-fwd-HindIII	GCGCAAGCTTGTAACTTGCCATTGAGCAAATATC
mbaS-rev-BamHI	GCGCGGATCCCCGCGTTTACTCGATAGACG
pchE-fwd-HindIII	GCGCAAGCTTTTGAGCCCTCGAACGACCTATACA
pchE-rev-BamHI	GCATGGATCCCGAGCACGTCTTGGAAGCTC
mbaS-fwd-NdeI	GGCCCATATGATGGCGGAAGTGCTCGCTCG
pmbaS-long-fwd	GCTGAAGCTTAACGCAGGATCGTACCGC
pmbaS-long-rev	GCGCGGATCCGGATTCTCCAGATATTTGCT
pmbaS-short-fwd	AGCTTATAAATCAGATTGAGAACGATTCGCGTTTACGTTAGATTGCTTGCCATTGAGCG
pmbaS-short-rev	GATCCGCTCAATGGCAAGCAATCTAACGTAAACGCGAATCGTTCTCAATCTGATTTATA
pmbaH-long-fwd	TATAAAGCTTCGCGAGGAGACGCTGCAGAG
pmbaH-long-rev	TATAGGATCCGATCGGGAAAGCTCGCTGGA
pmbaH-short-fwd	AGCTTGCGCGGCCGGTAAAAAAATGCGTGCGCGATTCGTCTATCGAGTAAACGCG
pmbaH-short-rev	GATCCGCGTTTACTCGATAGACGAATCGCGCACGCATTTTTTTACCGGCCGCGCA
pmbaE-long-fwd	GTATAAGCTTTGCGGTCCGGCCGCACGGTT
pmbaE-long-rev	GTATGGATCCGGCGGGGCGGGAATCGTT
pmbaE-short-fwd	AGCTTCGAGCGCGGGTAAAGATTCGGCGCGCCCATTCGTCTAGCAGACTGAAGGG
pmbaE-short-rev	GATCCCCTTCAGTCTGCTAGACGAATGGGCGCGCCGAATCTTTACCCGCGCTCGA
pmbaI-long-fwd	GCACAAGCTTTTGGTCCTGCTTGGCCCGTG
pmbaI-long-rev	GCGCTCTAGAAGGGCGTGAAGTCCGTTGGA
pmbaI-short-fwd	AGCTTAACAACCCGGTAAAAAATTTCGAGCGTGATTCGTCTCACAGTTGAAGCGG
pmbaI-short-rev	GATCCCGCTTCAACTGTGAGACGAATCACGCTCGAAATTTTTTACCGGGTTGTTA
pBTHI2426-EcoRI-fwd	AATTCTATCGAGTAAACGCGGCGCGCCCGGGCGGCCGTCCTTCGAACA
pBTHI2426-HindIII-rev	AGCTTGTTCGAAGGACGGCGCGCCGGGCGCGCCGCGTTTACTCGATAG
fur-FLAG-fwd	GCGCGGATCCTTAATACTCTAGGGACGCCTAGCC
fur-FLAG-rev	GCGCAAGCTTTCATTTATCATCATCATCTTTATAATCGTGTTTGCGATAGGGGCAGT
B. cenocepacia H111	
orbSfor	GCGCAAGCTTCGGTTCGTCAGGAACATGAA
orbSrevC1	GCGCGGATCCTTACGGACAGGCGACGCCGCGAT
orbSrevC2	GCGCGGATCCTTAGGCGACGCCGCGATGGCACG
orbSrevC5	GCGCGGATCCTTAGTGGCGCTCCGCGTCGCGCA
orbSrevC6	GCGCGGATCCTTAGCGCACCATGAAATGCACGA
orbSrevC7	GCGCGGATCCTTAATGCACGAGCGTCTGCGACA
orbS-fwd-HindIII	GCGCAAGCTTGTAACTCGGAATTTGACGGAGCAG
orbS-rev-BamHI	GCGCGGATCCGTTTTTTTACCGCCGCCGCG
porbH-fwd-HindIII	AGCTTGCGGCGGCGGTAAAAAAACGCGCCGGCCAACCGTCTATCAGACAGGAGCG
porbH-fwd-HindIII	GATCCGCTCCTGTCTGATAGACGGTTGGCCGGCGCGTTTTTTTACCGCCGCCGCA
bcam1-fwd-HindIII	GCATAAGCTTATAAGCGGTCGCCTCGAGACACTG
Bcam1-rev-BamHI	TATCGGATCCGACAGCAGTCGCGTCACGTC
bcam1-fwd-FLAG	GCGCGGATCCATAAGCCTCGAGACACTGCCACCC
bcam1-rev-FLAG	GCGCAAGCTTTCATTTATCATCATCATCTTTATAATCGTACATTTCCCCGGCAGCGT
p-bcam1-fwd	GCCGAAGCTTGGCATTCTCCTTCCGGTGAG
p-bcam1-rev	TTATGGATCCGTCTGGGCGGCAGTGTCTCG
p-bcam2840-fwd	TATAAAGCTTGTCTGGGCGGCAGTGTCTCG
p-bcam2840-rev	TATAGGATCCGGCATTCTCCTTCCGGTGAG
p-bcam0002-fwd	GCATAAGCTTAGCCCTCACGAGACAGCCCT
p-bcam0002-rev	ATATGGATCCCGTTCAAGGCAGGAGGGGTG
Δbcam1-A	TTACGGATCCCCGATCTCGACGAACTCG
Δbcam1-B	CGTCAGTCCTTTTTCGCTGGGGTCGTCGTATGCGGA
Δbcam1-C	TCCGCATACGACGACCCCAGCGAAAAAGGACTGACG

Δbcam1-D	AGCCAAGCTTCGTTGAATCTGGCCCGCG
Δbcam1a-A	ATATGGATCCAAGACGCCGTGCAGGAAGCG
Δbcam1a-B	CCCACCGGACGATCCATCGTCAGTACATTTCCCCGG
Δbcam1a-C	CCGGGGAAATGTACTGACGATGGATCGTCCGGTGGG
Δbcam1a-D	GCGCAAGCTTCCTTGAACGATGATCACGAT
Δbcam1-1a-B	CCCACCGGACGATCCATCGGGGTCGTCGTATGCGGA
Δbcam1-1a-C	TCCGCATACGACGACCCCGATGGATCGTCCGGTGGG
RT-BCAL1900-fwd	CAAACACATCAGCGACGCAT
RT-BCAL1900-rev	AAGGCGGTGAGCTGCGACTT
RT-BCAL1982-fwd	GTTCACCGGCGAATACACCG
RT-BCAL1982-rev	CGGGACTCGAAGTTTAACGC
RT-BCAL2785-fwd	GCTATCGCGACATCTGCGAA
RT-BCAL2785-rev	CGGCCAGTAATTGCCGTCGA
RT-BCAL3418-fwd	CAATCCGGTCGAGCAGCTGT
RT-BCAL3418-rev	AAATTACGGGCCAGATCGGC
RT-BCAM0001-fwd	AAGACCTGGGTGTTTCGGCAT
RT-BCAM0001-rev	GAGGAATTCGCGCATCATGA
RT-BCAM0002-fwd	GATGCTCGAAATCCCGCGAG
RT-BCAM0002-rev	AACAGCGCCTTCACCGACTC
RT-BCAM0343-fwd	AATGGTGGCCGGACTATGCG
RT-BCAM0343-rev	TGTTCGAGGATCGGCATCTC
RT-BCAM2840-fwd	CCGTTGTACAGCCAGGACTA
RT-BCAM2840-rev	GAACATCTCCGGCTGACCGA
RT-BCAS0724-fwd	TTCGAGATCACGCTCAGCGA
RT-BCAS0724-rev	TCGAACACATGGCCGAGATG
RT-BCAS0725-fwd	CTCGAAACGAAGCTCGTCGA
RT-BCAS0725-rev	GAAATCGACCAGCACGACCT
RT-BCAS0726-fwd	ACCAGCGCATCGTCAATTCC
RT-BCAS0726-rev	AGAAGAACACCTGCAGCAGC
BACTH-BCAM1-fwd	GCGCTCTAGATCCGTCCGCATACGACGAC
BACTH-BCAM1-rev	GCGCGGTACCTTGTACATTTCCCCGGCAGC
BACTH-BCAM1r2-rev	GCATGGTACCTTGGTCAGGCTCACCATCCG
BACTH-BCAM1r4-fwd	GCGCTCTAGAGCAACAGCAGCAATTCTGG
BACTH-BCAM1a-fwd	GCGCTCTAGAGCTGCCGGGGAAATGTACT
BACTH-BCAM1a-rev	GCATGGTACCAAGCCCCCACCGGACGATCC
<u>Vector-specific DNA Primers</u>	
M13revBACTH	GTGTGGAATTGTGAGCGGAT
M13for2	AAGGCGATTAAGTTGGGT
T7for	ACGACTCACTATAGGGAGAC
T7rev	GCTAGTTATTGCTCAGCGGT
pEX18Tpfor2	TAGAGGATCTGCTCATGTTT
pEX18Tprev2	CGACATTACGACCTTGGAAA
catendout	GATGTGTGATAACATACTGA
pUTcatrev	AACGGTTGTGGACAACAAGC
AP10	GAACGCTCTCCTGAGTA

[1] Restriction enzyme sites underlined

2.2.4   Q$_5$ Hot Start High-Fidelity DNA Polymerase

For amplification of DNA where high-fidelity of replication was required, i.e. cloning and splicing by overlap extension (SOE) PCR (see section 2.2.6), Q$_5$ Hot Start High-Fidelity DNA Polymerase (New England Biolabs) was utilised. Reactions were made up on ice in PCR tubes with a 50 µl total volume per reaction (see Table 2.3). The DNA polymerase was the final reagent to be added shortly before PCR was initiated. PCRs were performed in either the T-100 Thermal Cycler (Bio-Rad) or the G-Storm GS1 Thermal Cycler. Reactions conditions used were based upon the manufacturer's recommended protocol (see Table 2.4).

Table 2.3. Reaction setup for one PCR reaction using Q$_5$ Hot Start High-Fidelity DNA Polymerase

Reagent	Volume per 50 µl reaction (µl)
5x Q$_5$ Reaction Buffer	10
10 mM d.NTP Mix	1
Template DNA	Variable[1]
10 µM Forward primer	2.5
10 µM Reverse primer	2.5
Q$_5$ GC Enhancer	10
Q$_5$ Polymerase (2 U/µl)	0.5
d.H$_2$O	To final volume of 50 µl
Total	**50**

[1] Approximately 1 ng-1 µg for genomic DNA, 1 pg- 1 ng for plasmid DNA

Table 2.4. Reaction steps for PCR using Q$_5$ Hot Start High-Fidelity DNA Polymerase

Step	Temperature (^{o}C)	Time (min:sec)
Initial Denaturation	98	0:30
Denaturation	98	0:10
Annealing	Variable[1]	0:30
Elongation	72	0:30 per kb
Final Elongation	72	2:00
Storage	4	-

(Denaturation, Annealing, Elongation bracketed as [2])

[1] Calculated as 5°C below the mean primer T_m, or a gradient of T_as were used
[2] Number of cycles

2.2.5   GoTaq G2 DNA Polymerase

For amplification of DNA where high-fidelity of replication was not paramount, i.e. diagnostic screening of plasmid clones or verifying allelic replacement, GoTaq G2 DNA

Polymerase (Promega) was utilised. Reactions were made up on ice in PCR tubes with a 25 μl total volume per reaction (see Table 2.5). The DNA polymerase was the final reagent to be added shortly before PCR was initiated. PCRs were performed in either the T-100 Thermal Cycler (Bio-Rad) or the G-Storm GS1 Thermal Cycler. Reactions conditions used were based upon the manufacturer's recommended protocol (see Table 2.6). In PCR screening experiments, no template DNA was added as a negative control, and 0.5 μl of appropriate plasmid or PCR product was added as template DNA as a positive control. For PCR screening of colonies, 2.5 μl of boiled lysate (as described in section2.3.3: Genomic DNA) was used as template DNA (originating from a picked single colony for *E. coli* and *Bce*, or from overnight culture for *Bth*).

Table 2.5. Reaction setup for one PCR reaction using GoTaq G2 Flexi DNA Polymerase

Reagent	Volume per 25 μl reaction (μl)
5x GoTaq Flexi Buffer	5
25 mM MgCl$_2$	1
10 mM d.NTP Mix	0.5
10 μM Forward primer	0.5
10 μM Reverse primer	0.5
DMSO	1
GoTaq G2 Flexi Polymerase (5 U/μl)	0.25
Template DNA	Variable[1]
d.H$_2$O	To final volume of 25 μl
Total	**25**

[1] Approximately <0.25 μg

Table 2.6. Reaction steps for PCR using GoTaq G2 Flexi DNA Polymerase

Step	Temperature (°C)	Time (min:sec)	
Initial Denaturation	95	2:00	
Denaturation	95	0:30	
Annealing	Variable[1]	0:30	[2]
Elongation	72	1:00 per kb	
Final Elongation	72	5:00	
Storage	4	-	

[1] Calculated as 5°C below the mean primer T_m, or a gradient of T_as were used
[2] Number of cycles

2.2.6 Splicing by Overlap Extension (SOE) PCR

SOE PCR was utilised to amplify DNA containing marker-less in-frame gene deletions or base substitutions to be cloned into the gene replacement vectors pEX18Tp-pheS, pSNUFF3Cm and pSHAFT2. A two-step process was used, and Q_5 Hot Start High Fidelity DNA Polymerase (New England Biolabs) was used for both steps. For each SOE PCR process, four primers were used as shown in Table 2.7.

Table 2.7. Primers used for general Splicing by Overlap Extension (SOE) PCR

Primer Name	Primer Description
A	Forward amplification primer. Contains a 5' *Hin*dIII site [1]
B	Reverse mutagenic primer. Complementary to primer C.
C	Forward mutagenic primer. Complementary to primer B.
D	Reverse amplification primer. Contains a 5' BamHI site. [1]

[1] When making gene deletions, primers A and D annealed ≥500 bp upstream and downstream of the gene of interest

In the first step, conventional PCR using genomic DNA as template was used. Primers A and B were used to amplify product AB, and primers C and D were used to amplify product CD. Products AB and CD were then combined in approximately equimolar amounts as template DNA (approximately 100 ng of the longest DNA product) for the second step in which amplification was carried out using primers A and D. Hybridisation at the overlapping region of single stranded DNA generated from products AB and CD and subsequent extension resulted in the generation of the full-length PCR product. Mutagenic primers were designed to produce a region of complementarity of 36 bp at the ends of PCR products AB and CD. For gene deletions, this 36 bp region contained 18 bp from the start of the gene, and 18 bp from the end of gene, to give a marker less in-frame gene deletion. For gene mutations, this 36 bp region contained the desired codon mutations at its centre.

2.2.7   Reverse transcriptase polymerase chain reaction (RT-PCR)

Reverse transcription of RNA was performed using M-MLV Reverse Transcriptase (Promega), based upon the manufacturer's recommended protocol. Approximately 2 µg of total RNA was used in each reaction. Custom primer pairs were designed to amplify a region of DNA approximately 300 bp in length. Only the reverse primer was included in the first strand cDNA synthesis step along with DMSO at a concentration of 10% (v/v) due to high GC content of *Burkholderia* DNA.

For the second strand DNA synthesis, GoTaq G2 DNA Polymerase was used. 2.5 µl of cDNA was used as template DNA per reaction. For each RT-PCR reaction, a second reaction using 0.5 µl of original RNA was used as a control of DNA contamination. T_a was selected based on the mean T_m of all primers used in the PCR. PCR products were visualised by agarose gel electrophoresis (see section 2.3.1).

2.2.8   Purification of DNA from PCR reactions

Purification of amplified DNA from PCR reactions and DNA fragments following other enzymatic reactions was achieved using the GeneJET PCR Purification Kit (Thermo-Fisher). Purification steps were followed as per the manufacturer's recommended protocol. Centrifugations were performed at 17,000x *g*.

2.3 Nucleic acids methods

2.3.1   Agarose gel electrophoresis

Agarose gel electrophoresis was used to visualise approximate molecular weight, purity, and concentration of DNA. 0.8-1.2% (w/v) agarose gels were prepared by dissolving agarose (Thermo-Fisher) in TAE buffer (0.04 M Tris, 0.1142% (w/v) acetic acid, 1 mM EDTA) and boiling using a microwave oven, then pouring the molten agarose solution into a gel cast

when cool. Conical flasks containing the gel solution were stoppered to reduce evaporation of solution. Gel volumes were 50-200 ml. Gels were allowed to set for approximately one hour prior to use.

Gels were placed in a gel tank (BioRad), the well comb removed, and submerged in TAE buffer. Typically, 5 µl of DNA samples (mixed with 1 µl of 6x loading dye (Thermo-Fisher) prior to loading) were loaded per well. PCR products generated by GoTaq G2 DNA Polymerase (Promega) already contained DNA loading dye. Larger volumes of DNA solutions were loaded where necessary i.e. for gel extraction (see section 2.3.2).

For linear DNA samples, 5 µl of GeneRuler 1 kb DNA Ladder (Thermo-Fisher) was loaded alongside samples. For supercoiled plasmid DNA, 0.5 µl of Supercoiled DNA Ladder (New England Biolabs), mixed with 4.5 µl d.H_2O and 1 µl 6x loading dye prior to loading, was loaded alongside samples.

Gel electrophoresis was performed at 80-110 V for 40-90 minutes, dependent on gel size and agarose concentration.

A DNA pre-stain, Nancy-520 (Sigma-Aldrich) or Midori Green Advanced DNA Stain (Geneflow), was added to the gel before casting at a concentration of 0.01% (v/v). Alternatively, gels were post-stained by immersion in 5 µg ml^{-1} ethidium bromide solution for approximately 30 minutes with shaking.

Gels were imaged using an EDAS 290 (Kodak) UV transilluminator.

2.3.2   DNA extraction from agarose gels

Where necessary due to the appearance of unwanted secondary PCR products or smearing following agarose gel electrophoresis, the DNA amplicon of the desired molecular weight was manually extracted from the agarose. In these situations, larger amounts of DNA were loaded, requiring larger wells to be cast in the agarose gel. Gel electrophoresis was performed as usual. Upon a UV transilluminator, the desired PCR product was manually cut from the gel with a sterile scalpel and transferred to a microcentrifuge tube. A blue light

transilluminator was used to limit UV exposure to prevent DNA damage. DNA in the excised gel slice was then extracted and purified using the QIAquick Gel Extraction Kit (QIAGEN) or the GeneJET Gel Extraction Kit (Thermo-Fisher).

2.3.3   DNA/RNA extraction

Genomic DNA

Genomic/total DNA from *E. coli* was required for PCR screening during cloning experiments, and genomic DNA from *Bth* and *Bce* was required as template DNA in PCR to generate DNA fragments for cloning and for PCR screening during allelic replacement experiments. For *E. coli* and *Bce*, a single colony was picked and resuspended in 50 µl TE buffer (10 mM Tris, 1 mM EDTA, pH 8.0). For *Bth*, a cell pellet from 1 ml of overnight culture was resuspended in 100 µl TE buffer. Cell suspensions were boiled at approximately 100 ^{o}C for 10 minutes, and centrifuged to isolate cell debris. The supernatant was used as template DNA in PCR reactions. For long-term stocks of genomic DNA, supernatant was transferred to a microcentrifuge tube, and stored at -20 ^{o}C.

Plasmid DNA

Plasmid DNA was extracted using the GeneJET Plasmid Miniprep Kit (Thermo-Fisher). Extraction and purification steps were followed as per the manufacturer's recommended protocol for centrifugation. Centrifugations were performed at 17,000x *g*. An additional wash step using 500 µl of PB buffer (QIAGEN) prior to the wash steps with the kit's 'wash buffer' was used to inactivate endonucleases in the bacterial strains bearing the plasmid. Plasmid DNA was stored at -20 ^{o}C.

For use in *in vitro* transcription assays, where high concentrations of RNase-free DNA were required, the QIAGEN Maxi Prep Kit was used according to the manufacturer's recommended protocol. A 100 ml culture was used, and QIAGEN-tip 500 were used throughout. An additional purification step was included to completely remove RNase. An equal volume of phenol-chloroform-isoamyl alcohol (25:24:1) was added to the plasmid DNA solution after the QIAGEN Maxi Prep procedure, resuspended, centrifuged and the

aqueous phase containing the plasmid DNA transferred to a clean microcentrifuge tube. 2.1x volumes of RNase-free precipitating solution (95% (v/v) ethanol, 1% (w/v) potassium acetate) was added to the DNA sample and briefly vortexed. After 10 minutes of incubation at room temperature and centrifugation for 10 minutes at 17,000x g, the DNA pellet was washed with 1 ml of RNase-free 70% (v/v) ethanol, incubated at room temperature for five minutes and centrifuged again for 10 minutes. The supernatant was removed, the pellet air-dried, and then resuspended in 0.5 ml of RNase-free TE buffer (10 mM Tris, 1 mM EDTA, pH 8.0). DNA purity and concentration was determined as described in section 2.3.5).

RNA Extraction

Extraction of RNA was performed using the NucleoSpin RNA kit (Machery-Nagel) based upon the manufacturer's recommended protocol. Bacterial cell cultures of interest were grown in LB medium at 37 °C with aeration, 200 rpm, for approximately 16 hours, before being centrifuged at 4,000x g for 10 minutes to give a cell pellet with approximately 10^9 bacterial cells. The DNase reaction mixture (prepared from the manufactuer's supplied reconstituted rDNase and Reaction Buffer for rDNase) was incubated at 37 °C for one hour, as this resulted in a superior removal of DNA contamination. Steps following the DNase reaction were performed with filter pipette tips. RNA solutions were maintained on ice trhougout the purification/extraction procedure, and stored at -20 °C for no longer than one week.

2.3.4   Plasmids used in this study

The plasmids used in this study are shown in Table 2.8. Several annotated plasmid maps of many of these plasmid constructs are shown in the Appendix.

Table 2.8. Plasmids used in this study

Plasmid	Description[1]	Reference
pBBR1MCS	Mobilisable BHR cloning vector (Cm^r)	(Kovach *et al.*, 1994)
pBBR1MCS-*orbS*	pBBR1MCS containing *orbS* gene	(Agnoli *et al.*, 2006)
pBBR1MCS-*orbS*$_{CtetraA}$	pBBR1MCS containing *orbS* gene with substitutions C196+199+203+209A	(Agnoli, 2007)
pBBR1MCS-*orbS*$_{\Delta N}$	pBBR1MCS containing *orbS* gene with residues 7-35 deleted	R. Lomax (unpublished)
pBBR1MCS-*orbS*$_{\Delta C1}$	pBBR1MCS containing *orbS* gene with residues 211-220 deleted	This study
pBBR1MCS-*orbS*$_{\Delta C2}$	pBBR1MCS containing *orbS* gene with residues 209-220 deleted	This study
pBBR1MCS-*orbS*$_{\Delta C3}$	pBBR1MCS containing *orbS* gene with residues 203-220 deleted	R. Lomax (unpublished)
pBBR1MCS-*orbS*$_{\Delta C4}$	pBBR1MCS containing *orbS* gene with residues 199-220 deleted	R. Lomax (unpublished)
pBBR1MCS-*orbS*$_{\Delta C5}$	pBBR1MCS containing *orbS* gene with residues 196-220 deleted	This study
pBBR1MCS-*orbS*$_{\Delta C6}$	pBBR1MCS containing *orbS* gene with residues 191-220 deleted	This study
pBBR1MCS-*orbS*$_{\Delta C7}$	pBBR1MCS containing *orbS* gene with residues 187-220 deleted	This study
pBBR1MCS-2	Mobilisable BHR cloning vector (Cm^r)	(Kovach *et al.*, 1995)
pBBR1MCS2-*orbS*	pBBR1MCS-2 containing *orbS* gene	(Agnoli *et al.*, 2018)
pBBR1MCS2-*orbS*$_{CtetraA}$	pBBR1MCS-2 containing *orbS* gene with substitutions C196+199+203+209A	(Agnoli, 2007)

pBBR1MCS2-$orbS_{\Delta N}$	pBBR1MCS-2 containing *orbS* gene with residues 7-35 deleted	R. Lomax (unpublished)
pBBR1MCS2-$orbS_{\Delta C1}$	pBBR1MCS-2 containing *orbS* gene with residues 211-220 deleted	This study
pBBR1MCS2-$orbS_{\Delta C2}$	pBBR1MCS-2 containing *orbS* gene with residues 209-220 deleted	This study
pBBR1MCS2-$orbS_{\Delta C3}$	pBBR1MCS-2 containing *orbS* gene with residues 203-220 deleted	This study
pBBR1MCS2-$orbS_{\Delta C4}$	pBBR1MCS-2 containing *orbS* gene with residues 199-220 deleted	This study
pBBR1MCS2-$orbS_{\Delta C5}$	pBBR1MCS-2 containing *orbS* gene with residues 196-220 deleted	This study
pBBR1MCS2-$orbS_{\Delta C6}$	pBBR1MCS-2 containing *orbS* gene with residues 191-220 deleted	This study
pBBR1MCS2-$orbS_{\Delta C7}$	pBBR1MCS-2 containing *orbS* gene with residues 187-220 deleted	This study
pBBR1MCS2-*mbaS*	pBBR1MCS-2 containing *mbaS* and 30 bp upstream DNA	This study
pBBR1MCS2-$mbaS_{CpentaA}$	pBBR1MCS-2 containing *mbaS* with substitutions C203+206+216+220+230A and 30 bp upstream DNA	This study
pBBR1MCS2-*pchE*	pBBR1MCS-2 containing *pchE* and 30 bp upstream DNA	This study
pBBR1MCS2-$orbS_{\Delta P}$	pBBR1MCS-2 containing *orbS* and 30 bp upstream DNA (no native promoter)	This study
pBBR1MCS2-$orbS_{CtetraA-\Delta P}$	pBBR1MCS-2 containing *orbS* with substitutions C196+199+203+209A and 30 bp upstream DNA (no native promoter)	This study
pBBR1MCS2-Δ*fur*::*Nde*I	pBBR1MCS-2 containing Δ*fur* with an internal *Nde*I site	This study
pBBR2MCS2-Δ*fur*::TpTer	pBBR1MCS-2 containing Δ*fur* with an inserted TpTer antibiotic resistance cassette	This study
pBBR1MCS2-BCAM0001	pBBR1MCS-2 containing the BCAM0001 gene	This study

pBBR1MCS-5	Mobilisable BHR cloning vector (Gm^r)	(Kovach *et al.*, 1995)
pBBR1MCS5-*orbS*	pBBR1MCS-5 containing *orbS* gene	This study
pBBR1MCS5-*orbS*CtetraA	pBBR1MCS-5 containing *orbS* gene with substitutions C196+199+203+209A	This study
pBBR1MCS5-*orbS*ΔC1	pBBR1MCS-5 containing *orbS* gene with residues 7-35 deleted	This study
pBBR1MCS5-*orbS*ΔC2	pBBR1MCS-5 containing *orbS* gene with residues 211-220 deleted	This study
pBBR1MCS5-*orbS*ΔC3	pBBR1MCS-5 containing *orbS* gene with residues 209-220 deleted	This study
pBBR1MCS5-*orbS*ΔC4	pBBR1MCS-5 containing *orbS* gene with residues 203-220 deleted	This study
pBBR1MCS5-*orbS*ΔC5	pBBR1MCS-5 containing *orbS* gene with residues 199-220 deleted	This study
pBBR1MCS5-*orbS*ΔC6	pBBR1MCS-5 containing *orbS* gene with residues 196-220 deleted	This study
pBBR1MCS5-*orbS*ΔC7	pBBR1MCS-5 containing *orbS* gene with residues 191-220 deleted	This study
pBBR1MCS5-*mbaS*	pBBR1MCS-5 containing the *mbaS* gene and 30 bp upstream DNA	This study
pBBR1MCS5-*mbaS*CpentaA	pBBR1MCS-5 containing the *mbaS* gene with substitutions C203+206+216+220+230A and 30 bp upstream DNA	This study
pBBR1MCS5-*orbS*ΔP	pBBR1MCS-5 containing the *orbS* gene and 30 bp upstream DNA (no native promoter)	This study
pBBR1MCS5-*orbS*CtetraA-ΔP	pBBR1MCS-5 containing the *orbS* gene with substitutions C196+199+203+209A and 30 bp upstream DNA (no native promoter)	This study
pSRK-Km	Broad host-range expression vector (Km^r)	(Khan *et al.*, 2008)

pSRK-Km-*fur*_{FLAG}	pSRK-Km containing the *Bth fur* gene modified to encode a C-terminal FLAG epitope	This study
pSRK-Km-BCAM0001_{FLAG}	pSRK-Km containing the BCAM0001 gene modified to encode a C-terminal FLAG epitope	This study
pSRK-Km-BCAM0001a_{FLAG}	pSRK-Km containing the BCAM0001a gene modified to encode a C-terminal FLAG epitope	This study
pET14b	N-terminal His-tag fusion protein vector with T7 promoter (Amp^r)	(Studier *et al.*, 1990)
pET14b-*mbaS*	pET14b containing the *mbaS* gene	This study
pET14b-*mbaS*_{CpentaA}	pET14b containing the *mbaS* gene with C203+206+216+220+230A substitutions	This study
pET14b-*orbS*	pET14b containing the *orbS* gene	A. Butt and M. Thomas (unpublished)
pET14b-*orbS*_{CtetraA}	pET14b containing the *orbS* gene with C196+199+203+209A substitutions	A. Butt and M. Thomas (unpublished)
pKAGd4	Transcriptional fusion reporter vector derived from pPR9TT (Cm^r Amp^r)	(Agnoli *et al.*, 2006)
pKAGd4-P*_{orbH}*ds6	pKAGd4 containing P$_{orbH}$ on a 42 bp DNA fragment	(Agnoli *et al.*, 2018)
pKAGd4-P*_{orbS}*	pKAGd4 containing P$_{orbS}$ on DNA fragment	(Agnoli, 2007)
pKAGd4-P*_{mbaS}*-L	pKAGd4 containing P$_{mbaS}$ on a 186 bp DNA fragment	This study
pKAGd4-P*_{mbaS}*-S	pKAGd4 containing P$_{mbaS}$ on a 53 bp DNA fragment	This study
pKAGd4-P*_{mbaH}*-L	pKAGd4 containing P$_{mbaH}$ on a 274 bp DNA fragment	This study
pKAGd4-P*_{mbaH}*-S	pKAGd4 containing P$_{mbaH}$ on a 49 bp DNA fragment	This study
pKAGd4-P*_{mbaE}*-L	pKAGd4 containing P$_{mbaE}$ on a 308 bp DNA fragment	This study
pKAGd4-P*_{mbaE}*-S	pKAGd4 containing P$_{mbaE}$ on a 49 bp DNA fragment	This study
pKAGd4-P*_{mbaI}*-L	pKAGd4 containing P$_{mbaI}$ on a 295 bp DNA fragment	This study

pKAGd4-P$_{mbaI}$-S	pKAGd4 containing P$_{mbaI}$ on a 49 bp DNA fragment	This study
pKAGd4-P$_{orbH}$-S	pKAGd4 containing P$_{orbH}$ on a 49 bp DNA fragment	This study
pKAGd4-P$_{BCAM0001}$	pKAGd4 containing P$_{BCAM0001}$ on a 369 bp DNA fragment	This study
pKAGd4-P$_{BCAM2840}$	pKAGd4 containing P$_{BCAM2840}$ on a 369 bp DNA fragment	This study
pKAGd4-P$_{BCAM0002}$	pKAGd4 containing P$_{BCAM0002}$ on a 274 bp DNA fragment	This study
pRLG770	Transcription reporter vector used in *in vitro* transcription assays (Amp^r)	(Ross *et al.*, 1990)
pRLG770-P$_{mbaH}$	pRLG770 containg the 49 bp P$_{mbaH}$ promoter	This study
pRLG770-P$_{orbH}$ds6	pRLG770 containing the P$_{orbH}$ds6 promoter (-36 to +6)	A. Butt and M. Thomas (unpublished)
pRLG770-P$_{guaB}$	pRLG770 containing the P$_{guaB}$ promoter (-133 to +36)	(Husnain and Thomas, 2008)
pEX18Tp-*pheS*	Allelic replacement vector (Tp^r)	(Barrett *et al.*, 2008)
pEX18Tp-*pheS*-Δ*mbaS*	pEX18Tp-*pheS* containing a Δ*mbaS* allele with ≥500 bp of upstream and downstream DNA sequence identical to the *Bth* genome	This study
pEX18Tp-*pheS*-*mbaS*$_{CpentaA}$	pEX18Tp-*pheS* containing a *mbaS*$_{CpentaA}$ allele with ≥500 bp of upstream and downstream DNA sequence identical to the *Bth* genome	This study
pSNUFF3Cm	Allelic replacement vector (Tp^r, Cm^r)	H. Spiewak, unpublished
pSNUFF3Cm-Δ*mbaS*	pSNUFF3Cm containing a Δ*mbaS* allele with ≥500 bp of upstream and downstream DNA sequence identical to the *Bth* genome	This study
pSNUFF3Cm-Δ*pchE*	pSNUFF3Cm containing a Δ*pchE* allele with ≥500 bp of upstream and	This study

	downstream DNA sequence identical to the *Bth* genome	
pSNUFF3Cm-*mbaS*$_{CpentaA}$	pSNUFF3Cm containing a *mbaS*$_{CpentaA}$ allele with ≥500 bp of upstream and downstream DNA sequence identical to the *Bth* genome	This study
pSNUFF3Cm-ΔBCAM0001	pSNUFF3Cm containing a ΔBCAM0001 allele with ≥500 bp of upstream and downstream DNA sequence identical to the *Bce* genome	This study
pSNUFF3Cm-ΔBCAM0001a	pSNUFF3Cm containing a ΔBCAM0001a allele with ≥500 bp of upstream and downstream DNA sequence identical to the *Bce* genome	This study
pSNUFF3Cm-ΔBCAM0001-BCAM0001a	pSNUFF3Cm containing a ΔBCAM0001-BCAM0001a allele with ≥500 bp of upstream and downstream DNA sequence identical to the *Bce* genome	This study
pDAI-SceI-*pheS*	I-SceI meganuclease expression vector (Tc^r)	(Fazli *et al.*, 2015)
pDAI-SceI-*pheS*-Km	Derivative of pDAI-SceI-*pheS* with insterted kanamycin reistance cassette (Tc^r Km^r)	S. Hussain, unpublished
p34E-TpTer	Source of TpTer cassette	(Shastri *et al.*, 2017)
pSHAFT2	Allelic replacement vector (Cm^r Amp^r)	(Shastri *et al.*, 2017)
pSHAFT2-Δ*fur*::TpTer	pSHAFT2 containing a Δ*fur*::TpTer allele with ≥500 bp of upstream and downstream DNA sequence identical to the *Bth* genome	This study
pBluescript II KS	*E. coli*-specific cloning vector (Amp^r)	(Stojiljkovic, Baumler and Hantke, 1994)
pBS-P$_{mbaS}$	pBluescript II KS containing P$_{mbaS}$ on a 186 bp DNA fragment	This study

pBS-P$_{mbaH}$	pBluescript II KS containing P$_{mbaH}$ on a 274 bp DNA fragment	This study
pBS-P$_{mbaE}$	pBluescript II KS containing P$_{mbaE}$ on a 308 bp DNA fragment	This study
pBS-P$_{mbaI}$	pBluescript II KS containing P$_{mbaI}$ on a 295 bp DNA fragment	This study
p3ZFBS	pGEM3Z containing consensus *E. coli* Fur binding site (Amp^r)	(Vanderpool and Armstrong, 2001)
pKT25	Low copy number BACTH vector, allows in-frame fusion of a gene to C-terminal coding sequence of T25 adenylate cyclase domain (Km^r)	(Karimova, Ullmann and Ladant, 2001)
pKT25-BCAM0001	pKT25 containing a protein fusion to the *Bce* BCAM0001 gene	This study
pKT25-BCAM0001-σ2	pKT25 containing a protein fusion to an N-terminal portion of the *Bce* BCAM0001 gene, including the σ2 domain	This study
pKT25-BCAM0001-σ4	pKT25 containing a protein fusion to an C-terminal portion of the *Bce* BCAM0001 gene, including the σ4 domain	This study
pKT25-BCAM0001a	pKT25 containing a protein fusion to the *Bce* BCAM0001a gene	This study
pKNT25	Low copy number BACTH vector, allows in-frame fusion of a gene to N-terminal coding sequence of T25 adenylate cyclase domain (Km^r)	(Karimova, Ullmann and Ladant, 2001)
pKNT25-BCMA0001	pKNT25 containing a protein fusion to the *Bce* BCAM0001 gene	This study
pKNT25-BCAM0001-σ2	pKNT25 containing a protein fusion to an N-terminal portion of the *Bce* BCAM0001 gene, including the σ2 domain	This study
pKNT25-BCAM0001-σ4	pKNT25 containing a protein fusion to an C-	This study

	terminal portion of the *Bce* BCAM0001 gene, including the σ4 domain	
pKNT25-BCAM0001a	pKNT25 containing a protein fusion the *Bce* BCAM0001a gene	This study
pKT25-zip	pKT25 containing a protein fusion to the leucine zipper domain of GNC4	(Karimova, Ullmann and Ladant, 2001)
pUT18	High copy number BACTH vector, allows in-frame fusion of a gene to N-terminal coding sequence of T18 adenylate cyclase domain (Amp^r)	(Karimova, Ullmann and Ladant, 2001)
pUT18-BCAM0001	pUT18 containing a protein fusion to the *Bce* BCAM0001 gene	This study
pUT18-BCAM0001-σ2	pUT18 containing a protein fusion to an N-terminal portion of the *Bce* BCAM0001 gene, including the σ2 domain	This study
pUT18-BCAM0001-σ4	pUT18 containing a protein fusion to an C-terminal portion of the *Bce* BCAM0001 gene, including the σ4 domain	This study
pUT18-BCAM0001a	pUT18 containing a protein fusion the *Bce* BCAM0001a gene	This study
pUT18C	High copy number BACTH vector, allows in-frame fusion of a gene to C-terminal coding sequence of T18 adenylate cyclase domain (Amp^r)	(Karimova, Ullmann and Ladant, 2001)
pUT18C-BCAM0001	pUT18C containing a protein fusion to the *Bce* BCAM0001 gene	This study
pUT18C-BCAM0001-σ2	pUT18C containing a protein fusion to an N-terminal portion of the *Bce* BCAM0001 gene, including the σ2 domain	This study
pUT18C-BCAM0001-σ4	pUT18C containing a protein fusion to an C-terminal portion of the *Bce* BCAM0001 gene, including the σ4 domain	This study

| pUT18C-BCAM0001a | pUT18C containing a protein fusion the *Bce* BCAM0001a gene | This study |
| pUT18C-zip | pUT18C containing a protein fusion to the leucine zipper domain of GNC4 | (Karimova, Ullmann and Ladant, 2001) |

Cm[r]=chloramphenicol resistance; Km[r]=kanamycin resistance; Gm[r]=gentamicin resistance; Amp[r]=ampicillin resistance; Tp[r]=trimethoprim resistance; Tc[r]=tetracycline resistance

2.3.5   DNA/RNA quantification

The concentration and purity of DNA/RNA was measured by a NanoDrop 2000 Spectrophotometer (Thermo Scientific). Purity of DNA and RNA was gauged by the ratio of the spectroscopic absorbance at 260/280 nm ($A\frac{260}{280}nm$). To be considered sufficiently pure, this value was approximately 1.8 for DNA and 2.0 for RNA.

2.3.6   Restriction enzyme digestion

The digestion of DNA by restriction enzymes was performed based upon the manufacturer's recommended protocol (New England Biolabs/Promega). The buffer used for the reaction was based upon the optimal activity for the selected restriction enzymes as determined by the manufacturer. Reactions were made up to 30 µl. After two hours of digestion at 37 °C, solutions underwent PCR purification (see section 0) and were visualised by agarose gel electrophoresis (see section 2.3.1) prior to further applications.

Table 2.9. Reaction components for restriction digestion of DNA

Reagent	Volume (µl)
DNA (Plasmid/PCR Product) [1]	10/20
10x Restriction Enzyme Buffer	3
Restriction Enzyme 1 (10 U/µl)	1
Restriction Enzyme 2 (10 U/µl)	1
Bovine Serum Albumin, BSA (10 mg ml^{-1})	0.5
dH$_2$O	14.5/4.5
Total	**30**

[1] Approximately 1 µg of DNA

2.3.7   DNA ligation

The ligation of digested DNA was performed using T4 DNA Ligase (Promega) based upon the manufacturer's recommended protocol. The concentration of digested DNA was measured (see section 2.3.5) and the vector DNA and DNA to be inserted into the vector was combined at a 1:3 molar ratio per reaction. Reactions were incubated at 16 °C in a heat block for approximately 16 hours.

In cloning experiments, a ligation control (containing no DNA to be inserted into the vector) and a vector control (containing no DNA to be inserted into the vector and no T4 DNA ligase) were included to account for vector self-ligation and uncut vector, respectively (see Table 2.10). Ligation reactions were used directly for transformation into competent *E. coli* cells.

Table 2.10. Reaction components for ligation of digested DNA

Reagent	Volume (µl)		
	Ligation	Ligation Control	Vector Control
Digested Vector DNA	Variable[1]	Variable[1]	Variable[1]
Digested PCR product	Variable[2]	0	0
T4 DNA ligase	1	1	0
10x DNA ligase buffer	2	2	2
d.H_2O	To final volume of 20 µl	To final volume of 20 µl	To final volume of 20 µl
Total	**20**	**20**	**20**

[1] Approximately 25 ng
[2] Approximately 75 ng

2.3.8   DNA sequencing and analysis

All newly constructed plasmids, and some PCR products, had their nucleotide sequence verified by DNA sequencing. This was performed by the University of Sheffield Medical School Core Sequencing Facility. Analysis was performed using a combination of BioEdit software (Hall, 1999) and SnapGene© software (from GSL Biotech; available at snapgene.com).

Genome sequencing was provided by MicrobesNG (http://www.microbesng.uk), which is supported by the BBSRC (grant number BB/L024209/1). Analysis was performed using Artemis software (Carver *et al.*, 2012).

2.4 Protein methods

2.4.1 Protein overexpression and extraction

The pET14b expression vector constructs were introduced into *E. coli* BL21λDE3 by transformation, and the transformed bacteria were directly inoculated into either 50 ml or 500 ml of autoinduction medium (50 mM anhydrous Na_2HPO_4, 25 mM anhydrous KH_2PO_4, 0.5% (w/v) tryptone, 0.5% (w/v) yeast extract, 0.5% (w/v) NaCl, 0.5% (v/v) glycerol, 0.05% (w/v) glucose, 0.2% (w/v) lactose, supplemented with 100 µg ml^{-1} ampicillin) (Studier, 2005). Cultures were grown with aeration at 37 °C (250 rpm) to approximately OD_{600}=1.0, then incubated at 20 °C with aeration (250 rpm) for approximately 24 hours. Cells were harvested by centrifugation at 4,000x g for 20 minutes at 4 °C. The resulting cell pellet was frozen at -20 °C.

Cell pellets were lysed in BugBuster Master Mix (Novagen) as per the manufacturer's protocol. The insoluble protein fraction possessing the ECF sigma factor was isolated by centrifugation at 16,000 xg at 4 °C for 20 mins. In order to solubilise the protein, the pellet was re-suspended in HGD buffer (Table 2.11) containing N-lauroylsarcosine (Nguyen, Jensen and Burgess, 1993) overnight at 4 °C. After centrifugation at 16,000 xg at 4 °C for 20 mins, the soluble protein fraction was removed and taken for purification by nickel-affinity chromatography.

2.4.2 Protein purification by nickel-affinity chromatography

Solubilised ECF sigma factor was purified by nickel-affinity chromatography using a 1 ml HisTrapHP column (GE Healthcare) and an ÄKTApurifer system (GE Healthcare). The solubilised protein solution was manually loaded onto the HisTrap column, washed with binding buffer (Table 2.11) prior to and after loading. The protein was then eluted by means of a gradient with elution buffer (Table 2.11). The protein typically eluted at around 60-70% of elution buffer (308-356 mM imidazole). After analysis of eluted fractions by SDS-PAGE,

fractions containing the protein were pooled and diluted two-fold in elution buffer for dialysis into storage buffer.

2.4.3   Buffer exchange of protein

For the removal of imidazole and N-lauroylsarcosine, to decrease the NaCl concentration, and to increase the glycerol concentration to facilitate the long-term storage of the ECF sigma factor protein, the purified protein samples underwent sequential dialysis into a storage buffer (Table 2.11) (Nguyen, Jensen and Burgess, 1993).

Protein samples were inserted into 8 kDa MWCO BioDesignDialysis Tubing (BioDesign Inc. of New York), and left to dialyse against 100 volumes of each buffer overnight at 4 °C with stirring. First, the protein sample was dialysed into the intermediate buffer 'dialysis 1' (Table 2.11). This buffer contained EDTA to remove any leached nickel from the IMAC column that could interfere with downstream experiments. The protein sample was the diaylsed against 'dialysis 2' buffer to remove any residual N-lauroylsarcosine, imidazole and EDTA. The protein samples were then concentrated to a total volume of 1-2 ml using the Amicon Ultra-4 10K centrifugal filter (Merck-Millipore) with 10 kDa MWCO according to the manufacturer's recommended protocol. A final dialysis against 50 volumes storage buffer was performed, and the purified protein was stored at -20 °C. These protein samples were analysed for purity and yield by SDS-PAGE (see section 2.4.4) and Bradford assay (see section 2.4.5).

Table 2.11. Protein purification buffers

| Reagents | Buffer | | | | | |
	HGD	Binding	Elution	Dialysis 1	Dialysis 2	Storage
HEPES	50 mM pH 7.4	50 mM pH 7.4	50 mM pH 7.4	50 mM pH 7.4	50 mM pH 7.4	50 mM pH 7.9
Glycerol	5% (v/v)	5% (v/v)	5% (v/v)	5% (v/v)	5% (v/v)	50% (v/v)
DTT[1]	1 mM	1 mM	1 mM	1 mM	1 mM	1 mM
NaCl	50 mM	300 mM	300 mM	50 mM	50 mM	50 mM
N-lauroylsarcosine	0.25% (w/v)	0.25% (w/v)	0.25% (w/v)	-	-	-
Imidazole	-	20 mM	500 mM	-	-	-
EDTA (pH 8.0)	-	-	-	100 µM	-	-

[1] Added fresh to buffer immediately before usage to avoid degradation

2.4.4   SDS-polyacrylamide gel electrophoresis (SDS-PAGE)

For the analysis of protein samples, sodium dodecyl sulphate polyacrylamide gel electrophoresis (SDS-PAGE) was used. 12% (w/v) SDS resolving gel was routinely used. The reagents used to make the resolving gel and stacking gel for two 8.3 cm x 7.3 cm x 0.75 mm SDS-PAGE gels are shown in Table 2.12.

Table 2.12. Reagents for casting of two 12% SDS-PAGE gels

	Volume (µl)	
Reagent	**Resolving Gel**	**Stacking Gel**
Acrylamide, 40% (Fisher Bioreagents)	3000	450
1.5 M Tris-HCl pH 8.8	2500	-
1.0 M Tris-HCl pH 6.8	-	187.5
10% (w/v) SDS	100	30
10% (w/v) APS[1]	100	30
TEMED[1]	10	3
d.H_2O	4290	2299.5
Total	**10000**	**3000**

[1] Reagents added immediately before casting

Gels were cast between two glass plates using the Mini-PROTEAN gel casting kit (BioRad). The resolving gel was cast first and levelled off with iso-butanol, allowed to polymerise for approximately 30 minutes, and the upper surface washed with d.H_2O. This was followed by casting the stacking gel and applying the comb, and was allowed to set for approximately 30 minutes. Gels were used immediately, or stored at 4 °C saturated in d.H_2O and wrapped in clingfilm for short-to-medium-term storage.

Protein samples were each prepared as a 1:1 mixture with 2x Laemmli buffer (4% (w/v) SDS, 20% (v/v) glycerol, 10% (v/v) β-mercaptoethanol, 0.004% (w/v) bromophenol blue, 125 mM Tris-HCl pH 6.8). Protein samples were denatured by incubation in a heat block at 100 °C for 10 minutes, followed by centrifugation at 17,000x *g* for 10 minutes.

Gels were immersed in running buffer, diluted from a 10x stock solution (30.3 g Tris base, 144g glycine, 10 g SDS, pH8.3 in one litre of d.H_2O). Electrophoresis was performed at 100 V for 10 minutes, or until the dye had migrated through the stacking gel, and then the voltage was increased to 150 V for approximately one hour, or until the dye had migrated through

to the bottom of the resolving gel. The gel was removed from the apparatus and stained in Coomassie blue stain solution (0.25 g Coomassie Brilliant Blue R-250, 45 ml methanol, 10 ml glacial acetic acid, 45 ml d.H$_2$O). Destaining was completed in destain solution (40 ml methanol, 10 ml glacial acetic acid, 50 ml d.H$_2$O) for 16-24 hours.

2.4.5 Measurement of protein concentration

Protein concentration was calculated using either the Bradford protein assay or estimated using a NanoDrop 1000 Spectrophotometer (Thermo Scientific).

Bradford protein assays were performed using the Bio-rad Protein Assay, using the manufactuer's instructions for the microassay procedure. A standard curve using a stock BSA solution (Promega), diluted to final concentrations of 2, 4, 6, 8 and 10 µg ml^{-1} in the same buffer as the protein sample to be assayed, was set up prior to every new protein quantification assay.

When using the Nanodrop to estimate protein concentrations, the molar extinction coefficient at 280 nm predicted using ProtParam (Gasteiger *et al.*, 2005) was input for greater accuracy.

2.4.6 Western blotting

Protein analysis by Western blotting was used to identify protein samples containing hexahistidine tags and FLAG tags. 12% SDS-PAGE was used (see section 2.4.4), but using the EZ-Run Prestained *Rec* Protein Ladder (Thermofisher) in place of the EZ-Run *Rec* Protein Ladder (Thermofisher). After electrophoresis, proteins were transferred from the SDS-PA gel onto a PVDF membrane at 25 V for 30 mins (Trans-Blot Turbo, Biorad). The membrane was washed in Tris-buffered saline-Tween, TBS-T (50 ml 10x Tris-buffered saline, 0.5 ml Tween 20, 449.5 ml d.H$_2$O) with 5% (w/v) milk powder (Fluka), and incubated at 4 °C overnight. The membrane was then washed in a series of steps at room temperature. Firstly, in TBS-T 5% milk with the primary antibody for one hour, followed by three iterative washes in TBS-T for 10 minutes each. Where required, this was followed by washing with TBS-T 5% milk with the

secondary antibody, and followed by three iterative washes in TBS-T for 10 minutes each. Chemiluminescence was initiated with EZ-ECL solutions (Biological Industries) as per the manufacturer's recommended protocol, and analysed with the ChemiDoc XRS+ Systems Imager and Image Lab software (Bio-Rad).

Table 2.13. Antibodies used for Western blot analysis

Target Protein Tag	Primary antibody	Dilution[1]	Secondary antibody	Dilution[1]
Hexahistidine	HisProbe-HRP (ThermoFisher)	1/5000	-	-
FLAG	Polyclonal rabbit anti-FLAG (Sigma)	1/5000	HRP-labelled goat anti-rabbit IgG (Vector)	1/6000

[1] Final concentration in TBS-T 5% milk

2.5 Transcription regulation methods

2.5.1   β-galactosidase assay

To examine the interaction of proteins with their putative DNA targets, β-galactosidase assays were used based upon the method of (Miller, 1972). The Z buffer used in the assay was made by dissolving 16.1 g $Na_2HPO_4 \cdot 7H_2O$, 5.5 g $NaH_2PO_4 \cdot H_2O$, 0.75 g KCl, 0.246 g $MgSO_4 \cdot 7H_2O$ in $d.H_2O$ to a final volume of 1 litre. Before use, 135 µl of β-mercaptoethanol was added per 50 ml Z buffer. This buffer was also used as the solvent to make the ONPG stock solution.

Firstly, overnight cultures of the strains to be assayed were grown in either LB or M9 medium at 37 °C for approximately 16 hours for *E. coli* or approximately 24 hours for *Burkholderia*. For each sample to be assayed, a small volume of each culture was diluted 100-fold in 3 ml of appropriate medium; for metal-limited conditions 100 µM (M9) or 175 µM (LB) 2,2-dipyridyl was added, for metal-replete conditions 50 µM of the the metal was added (more detail provided in the results sections). Three biological replicates were assayed for each strain, and for each condition. The diluted cultures were grown again at 37

ºC until OD_{600} of 0.4 for *E. coli* or 0.6 for *Burkholderia* was reached. Cultures were the then transferred to ice for 25 minutes.

For each individual cell suspension, the OD_{600} was measured using a spectrophotometer, and the volume to be used in the assay was calculated as follows:

For *E. coli*: $$Culture\ volume\ to\ be\ assayed\ (\mu l) = \frac{0.4}{OD_{600}} \times 25\ \mu l$$

For *Burkholderia*: $$Culture\ volume\ to\ be\ assayed\ (\mu l) = \frac{0.6}{OD_{600}} \times 25\ \mu l$$

Test tubes were filled with 1 ml Z buffer (minus the volume of bacterial culture to be added), 30 µl chloroform and 30 µl of 0.1% (w/v) SDS. These solutions were added gently down the side of the test tube. Subsequently, the corresponding volume of culture was added in a likewise fashion. For each culture, two technical replicates were set up, as well as two control tubes with sterile medium in place of bacterial culture. Control tubes were set up for each condition used in the assay. Once all solutions were added, each tube was vortexed for 10 seconds and incubated at 30 °C for 15 minutes in a water bath. To initiate the β-galactosidase reaction, 200 µl of 4 mg ml^{-1} ONPG (dissolved in Z buffer with β-mercaptoethanol) was added to each of the test tubes in regular recorded intervals, and the tubes immediately vortexed for one second before returning to the 30 °C water bath. When a yellow colour of sufficient intensity was judged to have developed (OD_{420} between 0.2 and 0.7) the reaction was stopped by addition of 500 µl of 1 M Na_2CO_3, immediately vortexed for one second, and the total reaction time recorded. Stopped reactions were incubated at room temperature for 10 minutes before the OD_{420} and OD_{550} were measured by spectrophotometer. The control tubes were used as blanks.

The β-galactosidase activity of each reaction was calculated, in Miller units (Mu), as:

$$Miller\ units = \frac{OD_{420} - 1.75(OD_{550})}{Time\ (min) \times Culture\ volume\ (ml) \times OD_{600}} \times 1000$$

The mean of each pair of technical replicates was taken as one biological data point. The whole experiment was usually repeated on at least one more day to provide further

experimental replicates. The mean of biological replicates across all experiments was calculated.

2.5.2   Fur titration assay (FURTA)

The Fur titration assay (FURTA) was used to analyse binding of the ferric uptake repressor protein, Fur, to gene promoters *in vivo* (Stojiljkovic, Baumler and Hantke, 1994). Promoter DNA was cloned into the high-copy number plasmid pBluescript II SK and the plasmid constructs introduced by transformation into *E. coli* H1717. *E. coli* H1717 harbours a chromosomal *fhuF-lacZ* fusion; *fhuF* contains a Fur box, and Fur binding represses the promoter, thereby decreasing *lacZ* expression, resulting in a Lac⁻ phenotype. If DNA containing another Fur-box is introduced into the bacterium on pBluescript II SK, this will titrate away Fur from the *fhuF* promoter, resulting in higher expression of the chromosomal *lacZ* gene, thereby resulting in a Lac⁺ phenotype. This was visualised *in vivo* by streaking *E. coli* H1717 on MacConkey agar supplemented with 1% (w/v) lactose, 40 µM $Fe(NH_4)_2(SO_4)_2$ and 100 µg ml⁻¹ ampicillin. Plates were incubated at 37 °C for approximately 16 hours. Introduction of a pBluescript II SK vector without a Fur box results in a Lac⁻ phenotype and white colonies. Introduction of a pBluescript II SK vector with a Fur box results in a Lac⁺ phenotype and red colonies. As a negative control, pBluescript II SK lacking any cloned promoter DNA was used; as a positive control, the plasmid p3ZFBS containing the *E. coli* consensus Fur box was used.

2.6 Protein-protein interaction methods

2.6.1   *in vitro* transcription

The *in vitro* transcription (*iv*T) assay was used to investigate the ability of ECF sigma factors to promote transcription of DNA to produce an RNA transcript using a template DNA

promoter under different conditions. It was also used to analyse the effect of metal ions upon the activity of the sigma factor.

The ECF sigma factor proteins were produced in *E. coli*, purified by IMAC and maintained in storage buffer as in the protocols outlined in sections 2.4.1 to 2.4.3. Short promoter DNA of around 50 bp in length were cloned into the plasmid pRLG770 upstream of an *rrnB* terminator region, and the plasmid construct was purified by the maxiprep procedure outlined in section 2.3.3. *E. coli* core RNA polymerase (NEB) complexed with *Burkholderia* sigma factor or holo RNA polymerase incorporating *E. coli* σ^{70} (NEB) and NTPs (Agilent) were used to perform the transcription. Radiolabelled uridine 5'-triphosphate ([α-^{32}P]UTP; 250 μCi) (PerkinElmer) was used to label the RNA transcript. Throughout all stages of the *iv*T assay filter pipette tips, UltraPure^{TM} distilled water (Invitrogen) and sterile RNase-free microcentrifuge tubes were used. Work surfaces were cleaned with RNase*Zap* (Invitrogen) prior to experimental activity.

Each reaction (25 μl) contained 5 μl 5x *E. coli* RNA Polymerase Reaction Buffer (NEB), 1 μl holo or core RNA polymerase, 0.5 μl ECF sigma factor (at a typical concentration of 40-60 μg ml^{-1} in storage buffer, see section 2.4.3), d.H$_2$O and any additional components (i.e. transition metal salts) were combined in reaction tubes and incubated at 30 $^{\circ}$C for 15 minutes to allow RNAP reconstitution. An NTP master mix was made up containing 0.5 μl each of dATP, dCTP and dGTP, 0.25 μl dUTP, and 0.25 μl [α-^{32}P]UTP (when at 100% activity, volume corrected for radioactive decay) per reaction. To initiate the transcription reaction, 1 μl of plasmid template containing the target promoter (at a typical concentration of 100-200 ng μl^{-1}) and 2 μl of NTP master mix (volume corrected for [α-^{32}P]UTP radioactive decay) were added to each reaction, and incubation continued at 30 $^{\circ}$C. The reaction was allowed to run for 5 minutes for reactions involving RNAP complexed with *E. coli* σ^{70}, and 30 minutes for reactions involving core RNAP complexed with *Burkholderia* an ECF sigma factor. The reaction was stopped by addition of 25 μl of stop buffer (95% (v/v) formamide, 4% (v/v) 0.5 M EDTA (pH 8.0), 0.01% (w/v) bromophenol blue), and 25 μl of each reaction solution was immediately loaded onto a urea polyacrylamide gel (Table 2.14).

Table 2.14. Reagents for casting of a 7 M urea 5.5% polyacrylamide gel

Reagent	Quantity
dd H_2O	3.4 ml
Acrylamide, 40% (Fisher Bioreagents)	1.372 ml
Urea	4.2 g
10X TBE buffer[1]	1 ml
10% (w/v) APS[2]	100 µl
TEMED[2]	10 µl
Final Volume	**10 ml** [3]

[1] Tris boric acid EDTA buffer (see Table 2.15)
[2] Reagents added immediately before casting
[3] Final volume is greater than the sum total volume of reagents due to solublisation of urea

The urea polyacrylamide gels were cast using 1.5 mm glass spacer plates (Biorad), and electrophoresis was performed using 0.5x TBE running buffer. After samples migrated into the gel, the wells were washed thoroughly with 0.5x TBE buffer, and the buffer in the upper chamber of the gel tank was replaced in order to remove unincorporated [α-^{32}P]UTP. Samples were electrophoresed until the bromophenol blue reached the bottom of the gel, which was cut off and discarded.

Table 2.15. Reagents for making 10x TBE Buffer

Reagent	Quantity
Tris base	54 g
Boric acid	27 g
EDTA	3.7 g
dd H_2O	500 ml

The gel was exposed to an imaging plate at 4 °C overnight, and analysed using a Fujifilm FLA3000 phosphoimager. Band intensity was calculated using the Fujifilm FLA3000 software suite as photostimulated luminescence, corrected for background luminescence.

2.6.2   Bio layer interferometry (BLI)

Bio layer interferometry (BLI) analysis was used to determine the interaction kinetics between purified ECF sigma factors and *E. coli* core RNA polymerase (NEB), and the effect of

metal ions upon this interaction. This was performed using the BLItz System using BLItz Pro 1.1 software with the 'Advanced Kinetics' mode (fortéBIO, Pall Corp., USA).

Assays were performed in RNAP buffer (40 mM Tris-HCl (pH 7.5), 150 mM KCl, 10 mM MgCl$_2$, 1 mM DTT, 0.01% (v/v) Triton X-100) made on the day of the assay. When included in the assay, metal solutions were also made on the same day as the assay. Ni-NTA Biosensors were used (fortéBIO, Pall Corp., USA), and were hydrated in RNAP buffer for a minimum of 10 minutes before use. Each assay was performed according to the steps in Table 2.16.

Table 2.16. Steps used in BLI assays

Step	Name	Time (s)	Holder type[1]	Solution
1	Initial baseline	60	Tube	RNAP buffer
2	Baseline	60	Drop	RNAP buffer
3	Loading	300	Drop	200 µg ml^{-1} His-tagged sigma factor in RNAP buffer [2]†
4	Baseline	60	Tube	RNAP buffer
5	Baseline	60	Drop	RNAP buffer (+ 25 µM M^{2+}) [3] †
6	Association	300	Drop	Core RNAP (+ 25 µM M^{2+}) [4] †
7	Dissociation	300	Tube	RNAP buffer

[1] The total volumes in each step were either 250 µl (tube) or 5 µl (drop)
[2] 1.25 µl of sigma factor, 3.75 µl of RNAP buffer
[3] 3.75 µl of RNAP buffer, 1.25 µl of either ddH$_2$O or 100 µM M^{2+} solution
[4] 3.75 µl of *E. coli* core RNAP (NEB) at varying concentrations, 1.25 µl of either ddH$_2$O or 100 µM M^{2+} solution
† Solutions were incubated at room temperature for approximately 10 minutes before assaying

For each interaction, six assays were performed with a range of concentrations of core RNAP from 62.5 nM to 2000 nM diluted in RNAP buffer.

Experimental data was analysed using the Data Analysis v9.0 software (fortéBIO, Pall Corp., USA). The dissociation rates (k_d, s^{-1}), association rates (k_a, M^{-1} s^{-1}) and the binding affinity constants (K$_D$, M) were calculated using a global analysis of the six data runs across six concentrations of core RNAP from the start of association to the end of dissociation.

2.6.3　Bacterial adenylate cyclase two-hybrid (BACTH) assay

To examine the interaction of proteins *in vivo* using a bacterial two-hybrid assay, the Bacterial Adenylate Cyclase Two-Hybrid (BACTH) System kit (Euromedex) was used. Genes or gene fragments for putative interacting proteins or domains were cloned into the provided vectors (pKT25, pKNT25, pUT18, or pUT18C) to give gene fusions to one of two subunits, T25 or T18, of the *Bordetella pertussis* adenylate cyclase (CyaA). Interaction between the two studied proteins enables close proximity between the complementary subunits T25 and T18, and the functional complementation results in CyaA activity and cyclic AMP (cAMP) synthesis. cAMP in turn binds to the *E. coli* catabolite activator protein (CAP), also known as the cAMP receptor protein (CRP). The cAMP/CAP complex activates expression of reporter genes of the *lac* and *mal* operons; this enables a phenotypic visualisation of protein-protein interaction using indicator media.

Genes or gene fragments were cloned between the *Xba*I and *Acc*65I restriction sites to give in-frame fusions to the T25 and T18 subunits. Plasmid constructs were co-transformed into the *E. coli* Δ*cya* strain BTH101, and the resulting strains were screened for their maltose phenotype on MacConkey-maltose IPTG medium following growth at 30 °C for approximately five nights.

For negative controls, each plasmid construct was concurrently assayed against the relevant empty vector, and for a positive control the control plasmids pKT25-zip and pUT18C-zip (expressing the *bona fide* interacting protein partners of the leucine zipper component of GCN4) were used. An interaction between the two test proteins gave a deep pink colour, and the absence of an interaction gave an off-white colony colour.

Chapter III: Deletion analysis of the extended N- and C-terminal domains of OrbS

3.1 Overview

As discussed in section **Error! Reference source not found.**, the iron starvation (IS) sigma factors OrbS and MbaS have unusual extended C-terminal extensions that are rich in cysteine residues. These are referred to as cysteine-rich extensions (CREs). Given the lack of a cognate anti-sigma factor, the ability of cysteine residues to coordinate metals via their thiol group (Osman and Cavet, 2010), and the observation that the cysteine-rich extended C-terminal domains of the ECF44 group sigma factors bind various metals as part of a regulatory mechanism (Gomez-Santos *et al.*, 2011; Marcos-Torres *et al.*, 2016), it was

hypothesised that the CRE found in the ECF09 sigma factors OrbS and MbaS may play a role in binding iron. This may regulate the activity of the protein.

In addition to the CRE of OrbS and MbaS, these atypical sigma factors also contain an extended N-terminal extension of 35 amino acids relative to the (IS) sigma factor homologue PvdS from *P. aeruginosa* (Figure 3.1). This, too, may play a role in the regulation of OrbS and MbaS.

Figure 3.1. Amino acid sequence alignment of OrbS and PvdS

Amino acid sequences were aligned using Clustal-Omega. Amino acids that are identical in the sequences are shown in white font highlighted in black, and amino acids that have similarity are highlighted in grey. Conserved sigma factor regions are denoted below sequences based upon previous assignments of RpoE (Gruber and Gross, 2003; Campagne *et al.*, 2014). Cysteine residues within the C-terminal region are coloured in red. Sequences were obtained from the following strains: *B. cenocepacia* H111 and *P. aeruginosa* PA01.

OrbS was the selected sigma factor used for the initial investigation into these extended N- and C-terminal extensions. Due to the high degree of homology between OrbS and MbaS, the working assumption is that most conclusions derived from OrbS should be transferrable to MbaS.

The effect of deleting these terminal extensions was investigated, with the aims of determining what length of the domains are required for the function of OrbS, and whether they play a role in the ability of OrbS to respond to iron.

Additionally, a previous preliminary analysis of OrbS-dependent promoter affinity had suggested that the substitution of all four C-terminal cysteine residues in OrbS by alanine residues may reduce the sigma factor's responsiveness to iron (Agnoli, 2007). This experiment was carried out in an *E. coli* strain harbouring an OrbS-dependent promoter-*lacZ* fusion and a plasmid expressing *orbS*. However, the function of the entire C-terminal extension upon the activity of OrbS has not been investigated. The cysteine-substituted mutant, OrbS$_{CtetraA}$, was included in this analysis to assess the importance of the four cysteine residues, both in terms of the overall function of OrbS and the sigma factor's ability to respond to iron.

Objectives:

- To construct mutant forms of OrbS containing deletions within to the extended terminal domains

- To compare the ability of these OrbS variants to initiate transcription of genes within the target regulon in *B. cenocepacia* using a phenotypic assay for siderophore production

- To compare the ability of these OrbS variants to initiate transcription of genes within the target regulon in *E. coli* using a transcription reporter assay to monitor OrbS-dependent promoter activity

- To compare the relative inhibitory effect of iron upon the OrbS variants using a transcription reporter assay to monitor OrbS-dependent activity

3.2 Construction of *orbS* variants with C-terminal truncations

The overall contribution of the C-terminal CRE upon the activity of OrbS was investigated by construction of a series of C-terminally truncated derivatives, as shown in Figure 3.2. The end-points of the truncated variants were selected to sequentially delete one, two, three

and four putative iron-binding cysteine residues (OrbS$_{\Delta C1}$-OrbS$_{\Delta C5}$). Deletions were also extended into the C-terminal helix of region 4.2 (OrbS$_{\Delta C6}$ and OrbS$_{\Delta C7}$). Furthermore, 29 residues of the extended NTD were deleted (OrbS$_{\Delta N}$), as shown in Figure 3.2. This deletion removed an internal segment of the N-terminal extension that is common to OrbS and MbaS sigma factors, but not PvdS. Finally, the effect of four cysteine-to-alanine substitutions of the four putative key cysteine residues of the CTE was investigated (OrbS$_{CtetraA}$).

OrbS	1	MAEVLDRPAAAAANPFLGSYPDLPPRAAPRARRASEPRAQ	
OrbSΔN	1	MAEVLD---------------------------EPRAQ	Δ7-35
OrbS	183	TLV FM RDAE HCAECLDACHRG ACPVFLG RARRR-	
OrbSΔC1	183	TLV FM RDAE HCAECLDACHRG ACP-----------	Δ211-220
OrbSΔC2	183	TLV FM RDAE HCAECLDACHRG A------------	Δ209-220
OrbSΔC3	183	TLV FM RDAE HCAECLDA------------------	Δ203-220
OrbSΔC4	183	TLV FM RDAE HCAE---------------------	Δ199-220
OrbSΔC5	183	TLV FM RDAE H------------------------	Δ196-220
OrbSΔC6	183	TLV FM R--------------------------	Δ191-220
OrbSΔC7	183	TLV---------------------------	Δ187-220
OrbS-CtetraA	183	TLV FM RDAE HAAEALDAAHRG AAPVFLG RARRR-	C196+199+203+209A

Figure 3.2. Sequences of OrbS deletion derivatives used for investigation of N-terminal and C-terminal extensions.

Top. The amino acid sequence of the N-terminal extension of OrbS and the truncated OrbS$_{\Delta N}$. Amino acid residues 1-40 are shown. **Bottom.** The C-terminal sequences of C-terminally truncated OrbS derivatives (cysteine residues are shown in red font). The sequence of the OrbS$_{CtetraA}$ derivative is also shown (alanine-substituted cysteines are shown in orange font). Amino acid residues 183-220 are shown.

3.2.1   Construction of pBBR1MCS-*orbS* derivatives

To investigate the effect of N- and C-terminal deletion on the activity of OrbS, the pBBR1MCS series of broad host-range expression vectors were used. These vectors have been shown to successfully express *orbS* in *E. coli* and *Bce* in previous work (Agnoli *et al.*, 2006; Agnoli *et al.*, 2018). So, pBBR1MCS was used to express the *orbS* derivative in complementation assays performed in *B. cenocepacia*.

The plasmid constructs pBBR1MCS-*orbS*, pBBR1MCS-*orbS*CtetraA, pBBR1MCS-*orbS*ΔN, pBBR1MCS-*orbS*ΔC3 and pBBR1MCS-*orbS*ΔC4 were previously constructed ((Agnoli *et al.*, 2006), (Agnoli, 2007), R. Lomax (unpublished data)). The forward primer orbSfor was used in conjunction with the following reverse primers to amplify the corresponding PCR products: orbSrevC1 (orbS$_{\Delta C1}$, 862 bp PCR product), orbSrevC2 (orbS$_{\Delta C2}$, 856 bp PCR product), orbSrevC5 (orbS$_{\Delta C5}$, 817 bp PCR product), orbSrevC6 (orbS$_{\Delta C6}$, 802 bp PCR product), and orbSrevC7 (orbS$_{\Delta C7}$, 790 bp PCR product) (Figure 3.3a). These PCR products were cloned between the *Hin*dIII and *Bam*HI sites of pBBR1MCS to give the plasmid constructs expressing *orbS* with C-terminal truncations (Figure 3.3b). These *orbS* variants contained 209 bp of upstream flanking sequence, and 97 bp of downstream flanking sequence. This included the native *orbS* promoter. The identities of these plasmid constructs was confirmed by PCR screening and DNA sequencing analysis with primers M13revBACTH and M13for2.
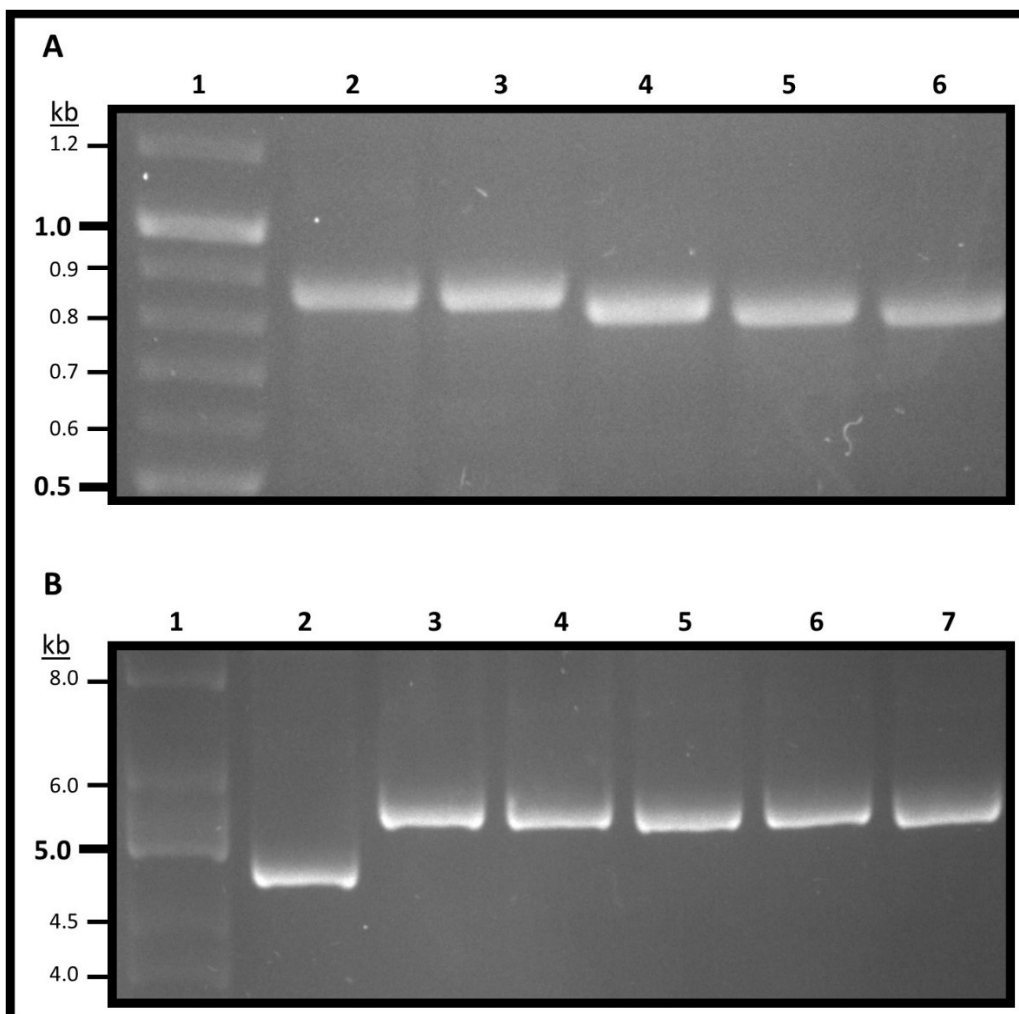
Figure 3.3. Construction of pBBR1MCS derivatives containing *orbS* with C-terminal truncations.

Agarose gel electrophoresis analysis of DNA PCR products and plasmid DNA used in construction of pBBR1MCS expressing derivatives of *orbS* with different C-terminal truncations. **A.** PCR to amplify *orbS* with C-terminal truncations. Lane 1, GeneRuler 1 kb DNA Ladder (Thermofisher); lane 2, *orbS*$_{\Delta C1}$, 862 bp PCR product; lane 3, *orbS*$_{\Delta C2}$, 856 bp PCR product; lane 4, *orbS*$_{\Delta C5}$, 817 bp PCR product; lane 5, *orbS*$_{\Delta C6}$, 802 bp PCR product; lane 6, *orbS*$_{\Delta C7}$, 790 bp PCR product. **B.** pBBR1MCS-*orbS* derivatives encoding OrbS with C-terminal truncations. Lane 1, Supercoiled ladder (NEB); lane 2, pBBR1MCS, 4.7 kb; lane 3, pBBR1MCS-*orbS*$_{\Delta C1}$, 5.5 kb; lane 4, pBBR1MCS-*orbS*$_{\Delta C2}$, 5.5 kb; lane 5, pBBR1MCS-*orbS*$_{\Delta C5}$, 5.5 kb; lane 6, pBBR1MCS-*orbS*$_{\Delta C6}$, 5.5 kb; lane 7, pBBR1MCS-*orbS*$_{\Delta C7}$, 5.5 kb.

3.2.2 Construction of pBBR1MCS2-*orbS* and pBBR1MCS5-*orbS* derivatives

The activity of the OrbS deletion derivatives in directing transcription from the OrbS-dependent promoter P$_{orbH}$ was also assayed. To achieve this, the *orbS* genes were sub-cloned into pBBR1MCS-2 and pBBR1MCS-5 so that they could be used in conjunction with the transcriptional reporter vector pKAGd4-P$_{orbH}$ds6 in β-galactosidase assays (Agnoli *et al.*, 2018). The pBBR1MCS-5 vector was used to enable assays to be performed in *E. coli* QC1732 (a kanamycin-resistant strain); the pBBR1MCS-2 vector was used as it shows greater levels of cloned gene expression compared to other vectors of the pBBR1MCS series, and therefore greater sigma factor activity in assays (however, these plasmid constructs were not used in this study). The following plasmid constructs were previously constructed: pBBR1MCS2-*orbS* (Agnoli *et al.*, 2018), pBBR1MCS5-*orbS* and pBBR1MCS2-*orbS*$_{CtetraA}$ (Agnoli 2007), pBBR1MCS2-*orbS*$_{\Delta N}$ (R. Lomax, unpublished). To construct the remaining plasmids, the pBBR1MCS plasmids underwent restriction digests with *Hind*III and *Bam*HI and the released *orbS* DNA fragments were inserted between the same sites of pBBR1MCS-2 and pBBR5MCS-5 (Figure 3.4). The identities of these plasmid constructs were confirmed by PCR screening and DNA sequencing analysis with the primers M13revBACTH and M13for2.
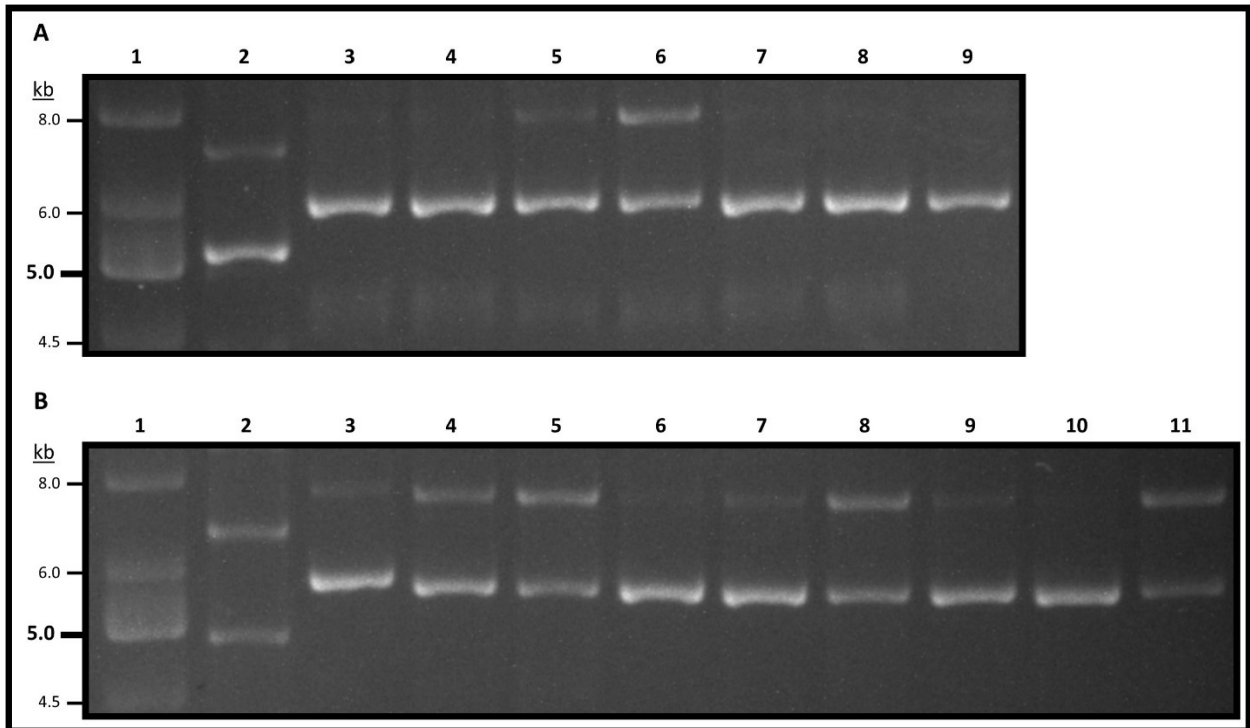
Figure 3.4. Construction of pBBR1MCS-2 and pBBR1MCS-5 derivatives containing *orbS* with terminal truncations.

Agarose gel electrophoresis analysis of constructed pBBR1MCS-2 and pBBR1MCS-5 plasmid derivatives expressing *orbS* with different C-terminal truncations. **A.** pBBR1MCS2-*orbS* derivatives with C-terminal truncations. 1: Supercoiled ladder (NEB); 2: pBBR1MCS-2, 5.1 kb; 3: pBBR1MCS2-*orbS*$_{\Delta C1}$, 6.0 kb; 4: pBBR1MCS2-*orbS*$_{\Delta C2}$, 6.0 kb; 5: pBBR1MCS2-*orbS*$_{\Delta C3}$, 5.9 kb; 6: pBBR1MCS2-*orbS*$_{\Delta C4}$, 5.9 kb; 7: pBBR1MCS2-*orbS*$_{\Delta C5}$, 5.9 kb; 8: pBBR1MCS2-*orbS*$_{\Delta C6}$, 5.9 kb; 9: pBBR1MCS2-*orbS*$_{\Delta C7}$, 5.9 kb. **B.** pBBR1MCS5-*orbS* derivatives with terminal truncations. 1: Supercoiled ladder (NEB); 2: pBBR1MCS-5, 4.7 kb; 3: pBBR1MCS5-*orbS*$_{\text{CtetraA}}$, 5.7 kb; 4: pBBR1MCS5-*orbS*$_{\Delta N}$, 5.6 kb; 5: pBBR1MCS5-*orbS*$_{\Delta C1}$, 5.6 kb; 6: pBBR1MCS5-*orbS*$_{\Delta C2}$, 5.6 kb; 7: pBBR1MCS5-*orbS*$_{\Delta C3}$, 5.6 kb; 8: pBBR1MCS5-*orbS*$_{\Delta C4}$, 5.6 kb; 9: pBBR1MCS5-*orbS*$_{\Delta C5}$, 5.5 kb; 10: pBBR1MCS5-*orbS*$_{\Delta C6}$, 5.5 kb; 11: pBBR1MCS5-*orbS*$_{\Delta C7}$, 5.5 kb.

3.3 Comparison of OrbS derivatives to complement siderophore deficient phenotype by CAS assay

Firstly, the relative activity of the truncated/substituted *orbS* derivatives was compared in a phenotypic assay. This was achieved via comparison of the ability of each *orbS* variant supplied *in trans* from pBBR1MCS to complement the KLF1 *orbS* mutant OM3, which does not produce ornibactin or pyochelin (Agnoli *et al.*, 2006). This was assessed by comparing the size of the yellow halo surrounding the bacterial growth on agar containing chrome-azurol sulphonate (CAS) (more detail in section 2.1.2).

Each of the pBBR1MCS-*orbS* derivatives, and the parental plasmid pBBR1MCS, were introduced by conjugation into OM3 using *E. coli* S17-1 donor cells. 1 µl of normalised overnight cultures grown in M9 medium supplemented with 0.5% (w/v) glucose and 50 µg ml^{-1} chloramphenicol were spotted onto CAS agar plates in triplicate, and grown at 37 $^{\circ}$C for 24 hours. Both iron-limited (10 µM $FeCl_3$) and iron-replete (60 µM $FeCl_3$) CAS agar plates were used to see if any effect of iron upon the regulation of the N- and C-terminally deleted OrbS variants could be observed.
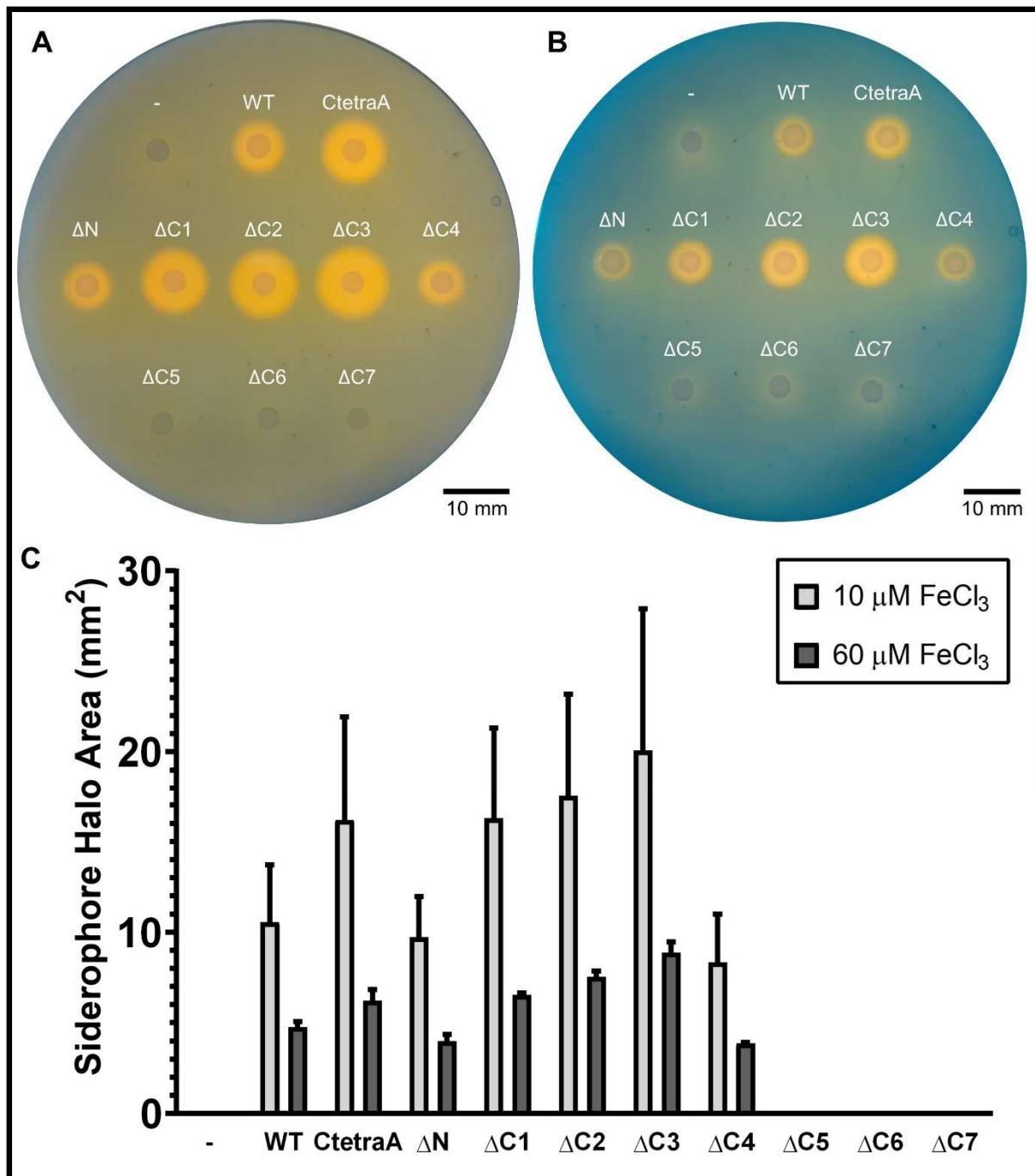
Figure 3.5. CAS assay of *B. cenocepacia* OM3 complemented with N- and C-terminally-modified OrbS derivatives.

Cultures of OM3 containing pBBR1MCS-based plasmids spotted on iron-limited and iron-replete CAS agar. Plasmids are denoted as follows: -, pBBR1MCS; WT, pBBR1MCS-orbS; CtetraA, pBBR1MCS-*orbS*$_{CtetraA}$; ΔN, pBBR1MCS-orbS$_{ΔN}$; ΔC1-7, pBBR1MCS-*orbS*$_{ΔC1}$-pBBR1MCS-*orbS*$_{ΔC7}$. **A.** CAS agar plate containing 10 μM FeCl$_3$. **B.** CAS agar plate containing 60 μM FeCl$_3$. **C.** Quantification of siderophore halo areas. The halo areas were calculated by measuring their diameters from CAS plates in triplicate. Error bars shown standard deviation (n=3).

The results presented in Figure 3.5 show that wild-type OrbS, OrbS$_{\Delta N}$, OrbS$_{CtetraA}$ and OrbS$_{\Delta C1}$-OrbS$_{\Delta C4}$ were all capable of complementing the $orbS^-$ phenotype of OM3. However, the sigma factors with more extensive deletions, i.e.OrbS$_{\Delta C5}$-OrbS$_{\Delta 7}$, appeared unable to complement the mutant.

Additionally, it was observed that OM3 containing OrbS$_{\Delta C1}$, OrbS$_{\Delta C2}$, OrbS$_{\Delta C3}$ and OrbS$_{CtetraA}$ was able to produce a larger siderophore halo than OM3 containing wild-type OrbS.

The effect of a high iron load upon the ability of these sigma factors to complement OM3 was also investigated with iron-replete agar containing 60 µM FeCl$_3$. The results show that all the complemented OM3 derivatives showed a consistent decrease in siderophore production.

3.4 Determination of the activity of N- and C-terminal deletion variants by promoter activity assays *in vivo*

Although the CAS assay provides useful qualitative detail regarding the sigma factor activity of OrbS, OrbS-dependent promoter activity measurements were used for better quantitation of this activity. Additionally, these assays could be performed in a *fur* null mutant bacterial strain to enable investigation of direct iron regulation of OrbS activity. To assay OrbS-dependent promoter activity, a transcriptional fusion of the *lacZ* reporter gene to the *orbH* promoter was used,

The pKAGd4-P$_{orbH}$ds6 promoter reporter vector (Agnoli *et al.*, 2018) and pBBR1MCS5-based vectors expressing *orbS* and *orbS* mutants encoding truncated/substituted derivatives were co-introduced into *E. coli* QC1732 (*fur*$^-$) by transformation. The assay was performed cells grown in M9 minimal salts medium supplemented with 0.5% (w/v) glucose, 0.1% (w/v) casamino acids, 50 µg ml^{-1} gentamicin, 25 µg ml^{-1} chloramphenicol and either 100 µM 2,2-

dipyridyl (iron-limited conditions) or 50 µM $FeCl_3$ (iron-replete conditions) and β-galactosidase assays were performed according to the protocol outlined in section 2.5.1. The experiment was repeated twice.
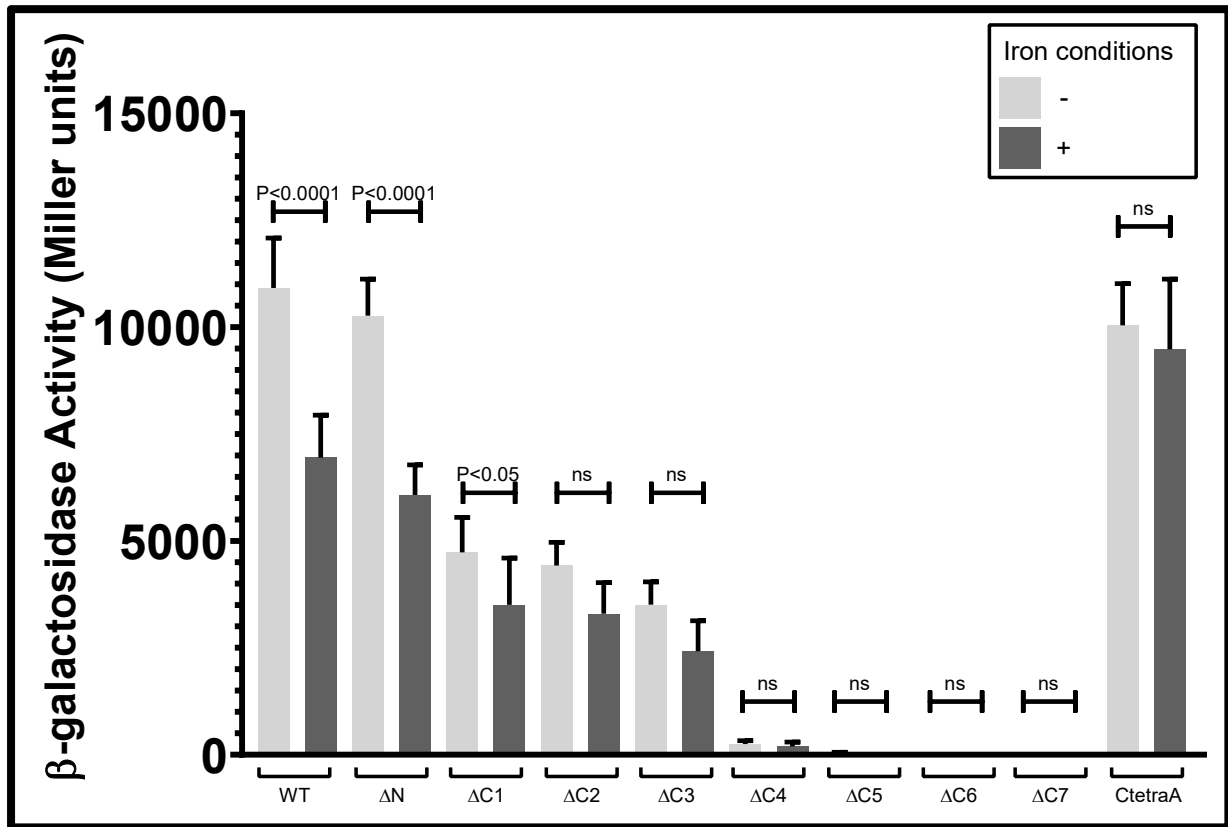
Figure 3.6. Activity of OrbS deletion derivatives at the *orbH* promoter in *E. coli* growing under iron-replete and iron-limited conditions.

β-galactosidase activity was measured in *E. coli* QC1732 harbouring pKAGd4-P*orbHds6* and pBBR5-*orbS*, pBBR5-*orbS*ΔN, pBBR5-*orbS*ΔC1-pBBR5-*orbS*ΔC7 or pBBR5-*orbS*CtetraA as denoted below data bars. All β-galactosidase activities were corrected for the background vector activity by subtraction of activity derived from *E. coli* QC1732 harbouring the plasmids pKAGd4-P*orbHds6* and pBBR1MCS-5. Growth medium was M9 minimal salts supplemented with 0.5% (w/v) glucose, 0.1% (w/v) casamino acids, 50 µg ml^{-1} gentamicin, 25 µg ml^{-1} chloramphenicol and either 100 µM 2,2-dipyridyl (light grey) or 50 µM $FeCl_3$ (dark grey). Error bars show standard deviation (n=6).

The results from the β-galactosidase assay conducted on cultures growing under iron-limiting conditions concur with those from the CAS plate assay, in that all of the OrbS truncated mutants displayed functional activity with the exception of OrbS$_{ΔC5}$, OrbS$_{ΔC6}$ and OrbS$_{ΔC7}$. OrbS$_{ΔN}$ and OrbS$_{CtetraA}$ both showed similarly high β-galactosidase activity as the wild-type, suggesting that deletion of the N-terminal extension or substitution of the four C-

terminal cysteines of the CRE has no effect on the ability of OrbS to associate with RNAP or initiate transcription of target genes. Although OrbS$_{\Delta C1}$-OrbS$_{\Delta C3}$ were able to direct transcription from P$_{orbH}$, the activity was approximately 32-43% lower than for wild-type OrbS under iron-limited conditions. OrbS$_{\Delta C4}$ was also able to direct transcription from P$_{orbH}$, but these activity was even lower – approximately 2% lower than for wild-type OrbS under iron-limited conditions.

As this assay was performed in a *fur* null mutant, the effect of direct iron-dependent regulation of OrbS activity, independently of Fur, could be investigated. There are significant differences in β-galactosidase activity under iron-limited and iron-replete conditions for OrbS ($P<0.0001$), OrbS$_{\Delta N}$ ($P<0.0001$) and OrbS$_{\Delta C1}$ ($P<0.05$), but not the others (one-way ANOVA, $F=173.8$, Sidak's multiple comparisons test).

Iron-replete conditions caused an approximately 43% decrease in the activity of wild-type OrbS. This provides initial verification that there may be a secondary mechanism for regulating OrbS in response to prevailing iron concentration, and supports previous data regarding this (Agnoli, 2007).

The P$_{orbH}$ activity in the presence of OrbS$_{\Delta N}$ was similarly decreased (by approximately 31%) during growth under iron-replete conditions, indicating that the N-terminal extension may not play a role in the putative iron-regulation mechanism. Although OrbS$_{\Delta C1}$ does also display a decrease in activity, it is a smaller decrease (approximately 35%) than that of wild-type OrbS. OrbS derivatives with more extensive C-terminal deletion show no statistically significant difference between activities in cells growing under iron-limited and iron-replete conditions.

Finally, it was observed that OrbS$_{CtetraA}$ gave rise to similarly high β-galactosidase activity in cells grown under both iron-limited and iron-replete conditions, with no statistically significant difference.

3.5 Discussion

A series of pBBR1MCS-based plasmids expressing *orbS* and derivatives of *orbS* encoding C-terminal truncations and an N-terminal deletion were constructed. All of these, with the exception of OrbS$_{\Delta C5}$, OrbS$_{\Delta C6}$, and OrbS$_{\Delta C7}$, displayed functional ability both in terms of complementation of a $\Delta orbS$ phenotype and initiation of transcription from the P$_{orbHds6}$ target promoter. Therefore, the 29 residues of the N-terminus present in OrbS are not required for OrbS-dependent transcription.

At the C-terminus, deletions extending as far as Cys199 (i.e. deletion of up to 21 amino acids from the C-terminus) also did not affect the ability of the sigma factor to initiate transcription. However, truncations extending N-terminally of Cys199 do abolish this ability, as demonstrated by the inability to complement the *orbS* mutant or initiate transcription from the *orbH* promoter. It is likely that the deleted amino acid residues in these cases provide a key role in the overall function of OrbS, particularly as they are located within the conserved region 4.2.

Also, although the OrbS$_{\Delta C4}$ mutant only has very low activity upon P$_{orbHds6}$, it is sufficient to nearly fully complement to OM3 mutant. This would suggest that though the deletion extends up to the C-terminal boundary of region 4.2, but not beyond it, there may be some destabilisation of the helix-turn-helix required for engagement with the -35 DNA element.

The residues positioned N-terminally of Cys199 are either functionally important (i.e. they are specifically required for interaction with promoter DNA and/or core RNAP) or structurally important (i.e. deletion of these residues results in an incorrectly folded sigma factor with loss-of-function). Protein structure modelling using the Phyre2 server (Kelley *et al.*, 2015) was carried out in an attempt to rationalise the effect of these N-terminal and C-terminal deletions. The overall structure of wild-type OrbS was modelled upon known structures of similar sigma factors bound by their anti-sigma factors (more specifically RpoE and NepR, among others) (Figure 3.7). Therefore, the structure shown is likely to be that of the putative inactive form, and not the structure of free OrbS or OrbS in complex with core

RNAP and/or promoter DNA. Although the core of the protein is highly conserved and modelled with relatively high reliability, the terminal extensions are not, and the reliability of these structures is low. Nonetheless, broad conclusions may be drawn about these terminal extensions.
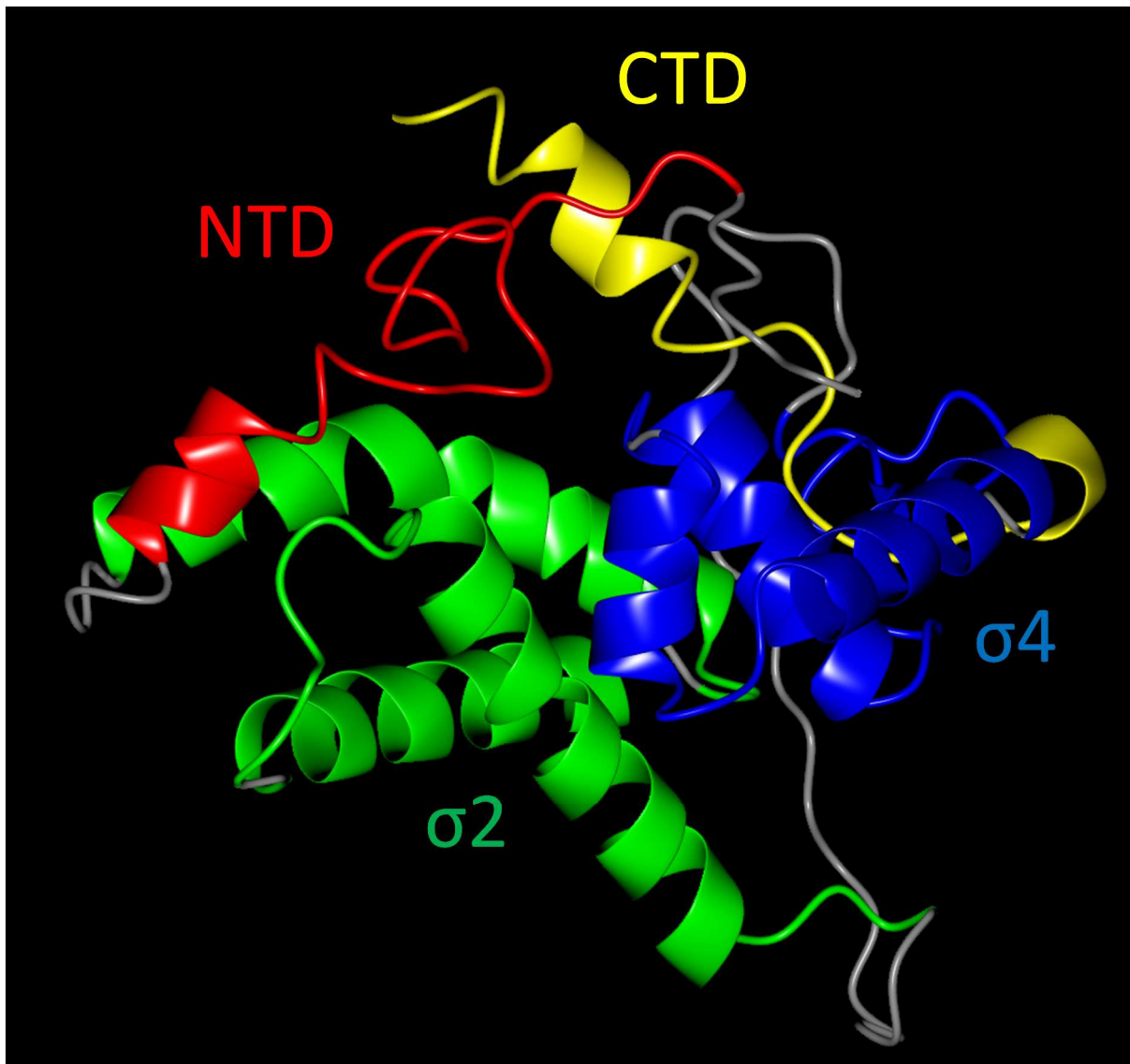
Figure 3.7. Predicted structure of OrbS.

Predicted model 3D structure of OrbS, generated using Phyre2 (Kelley *et al.*, 2015) and analysed with CCP4MG (McNicholas *et al.*, 2011). The protein structure is displayed in ribbon format. Based upon previous assignments of RpoE, domains have been coloured as follows: N-terminal extension (Arg7-Ser35), red; σ2 (Gln40-Glu114), blue; σ4 (Leu137-His195), green; C-terminal extension, yellow (Cys196-Arg220).

Firstly, in the predicted structure of OrbS, both the N-terminal extension and the C-terminal extension have been modelled to be in close proximity to each other. If OrbS, when inactivated, forms the same conformation as related sigma factors when they are inactivated by anti-sigma factors, the association between these termini may correlate to the inhibition of the sigma factor. The modelling suggests that the N- and C-terminal extensions are largely unstructured and each contain a very short α-helical region. The N-terminal extension is rich in proline residues which is consistent with its modelling as a region lacking secondary structure. The terminal extensions may adopt a different structure upon iron-binding. Nonetheless, there is a low reliability of the predicted structure of these terminal extensions. No specific conclusions can be drawn apart from the fact that the N-terminal extension is very likely to lack secondary structural elements, such as α-helices.

Next, the effect of deletion of the most of the N-terminal extension was modelled to predict what effect this may have had on the activity of OrbS (Figure 3.8).

The deletion of the N-terminal extension is predicted to have no large-scale effect on the overall fold of the protein. This affirms the data presented in Figure 3.5 and Figure 3.6, which show OrbS$_{\Delta N}$ displays very similar activity to wild-type OrbS. However, an interesting difference is predicted to occur at the C-terminus in the absence of the N-terminal extension. Without the N-terminal region, the C-terminal extension is predicted to become disordered (Figure 3.8). This is not consistent with the empirical data presented in Figure 3.6, which demonstrates that OrbS$_{\Delta N}$ retains the ability respond to iron, whereas OrbS$_{\Delta C2}$-OrbS$_{\Delta C7}$ lose this ability.
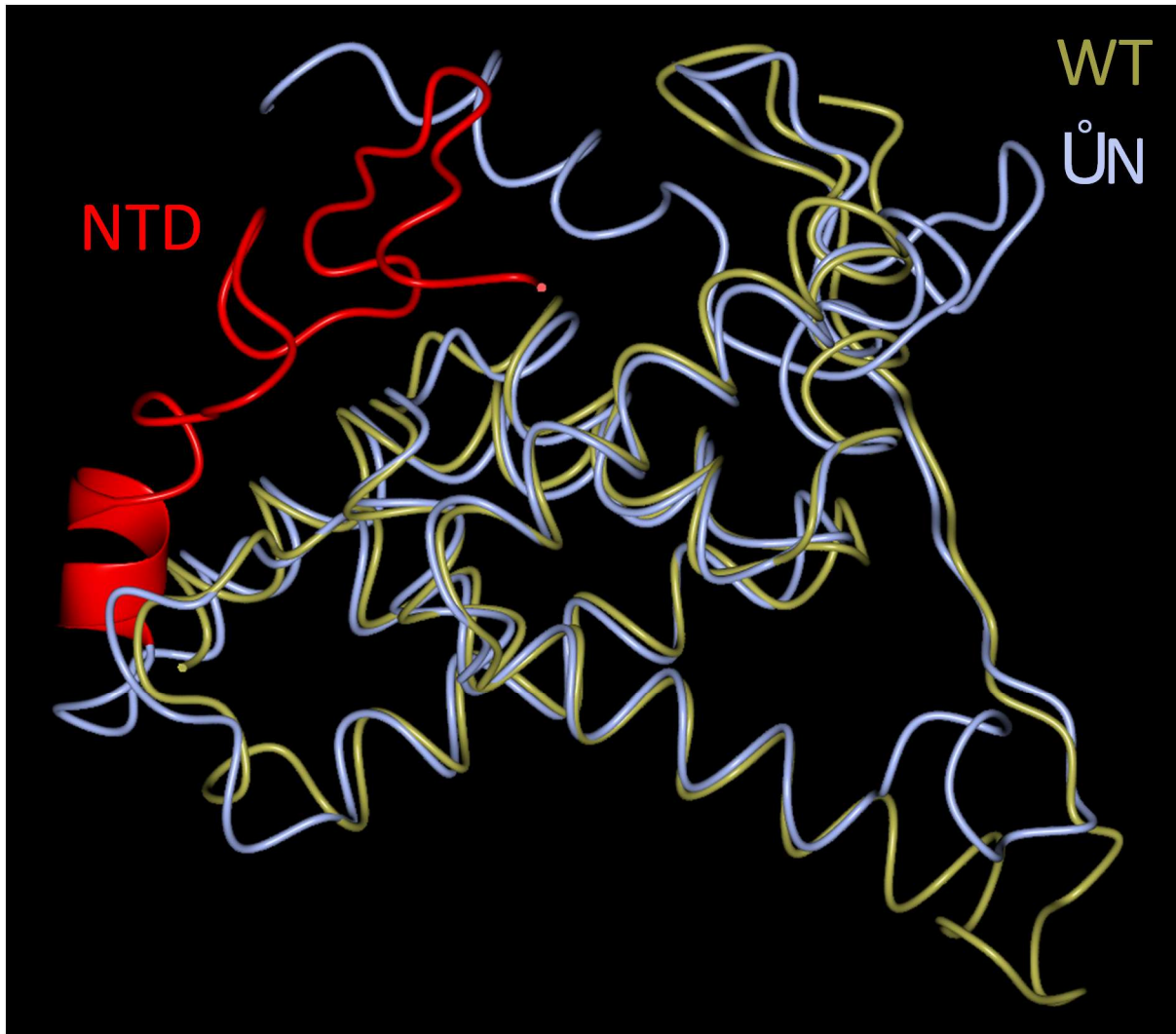
Figure 3.8. Effect of N-terminal deletion upon the predicted protein structure of OrbS.

Predicted superimposed model 3D structures of OrbS and OrbS$_{\Delta N}$, generated using Phyre2 (Kelley *et al.*, 2015) and analysed with CCP4MG (McNicholas *et al.*, 2011). The core protein structures of OrbS (gold) and OrbS$_{\Delta N}$ (ice blue) are displayed in worm format. The N-terminal extension of OrbS (Met1-Ser35) is displayed in ribbon format and coloured red.

In the presented promoter reporter analysis, there was a progressive decrease in the activity of OrbS as deletions at the C-terminus were extended (Figure 3.9). The effect of C-terminal deletion was also modelled to rationalise this data. In particular, the large 10 residue deletion of OrbS$_{\Delta C1}$ compared to OrbS has been predicted to have a significant effect upon the C-terminal extension. Not only is the predicted C-terminal α-helix lost, the peptide backbone is directed outwards at a markedly different angle. This structural disparity may account for the decrease in sigma factor activity observed in Figure 3.6.

Furthermore, successive deletion from OrbS$_{\Delta C1}$ to OrbS$_{\Delta C5}$ have the effect of shortening the C-terminal helix of region 4.2, although these deletions do not directly impinge on the helix Figure 3.1 and Figure 3.2. This may account for the decreased activity of OrbS$_{\Delta C1}$-OrbS$_{\Delta C5}$. In particular, the ΔC5 deletion that terminates immediately adjacent to the C-terminus of region 4.2 results in a much shorter α-helix and abolishes OrbS activity (Figure 3.2, Figure 3.5, Figure 3.6 and Figure 3.9). Deletion beyond ΔC5 removes key RNAP/DNA interacting residues or disrupt the structure of the helix, resulting in loss-of-function. Importantly, none of the C-terminal truncated variants are predicted to have a global effect on the overall structure of OrbS. Therefore, differences in the activity of these proteins should be specific to alterations in the structure of the C-terminal extension.

In this chapter, experiments were performed with the aim analyse the effect of iron upon the activity of OrbS and its N- and C-terminally truncated variants. This was first performed in OM3 Figure 3.5 However, this is a Fur$^+$ system. OM3 produces Fur which is able to repress the transcription of *orbS* by interacting with the Fur box sequence present in the promoter regions of the cloned *orbS* variants. Therefore, it is assumed that the action of Fur may mask any iron-dependent inhibition specific to the terminal extensions. Therefore, this decrease in siderophore production is not unexpected. This was also demonstrated with promoter reporter analysis in an *E. coli fur* null mutant Figure 3.6. In this experiment, it was observed that OrbS activity was regulated in response to prevailing iron. There was loss of this iron-dependent regulation of the activity of OrbS variants with C-terminal deletions. This could point to the CTE having a role in the iron-dependent regulation mechanism. Interestingly, the difference between OrbS$_{\Delta C1}$, which displays some iron regulation, and OrbS$_{\Delta C2}$, which does not display iron regulation, is the deletion of the Cys209 and Pro210 residues. This could imply that these residues, most likely the cysteine residue, have a role in this iron regulation.

Furthermore, this loss of iron regulation was observed upon the activity of OrbS$_{CtetraA}$. This observation strongly suggests that the four cysteine residues of the CRE play a significant role in the putative direct iron-regulation mechanism of OrbS. The predicted effect of the four cysteine-to-alanine substitutions in OrbS$_{CtetraA}$ was modelled (Figure 3.10). Overall, there is predicted to be little difference in the overall protein structure of OrbS and OrbS$_{CtetraA}$. This prediction is in accordance with the presented empirical data, in which both

OrbS and OrbS$_{CtetraA}$ display similar levels of functional activity. However, there is some structural variation in the C-terminal 15-20 residues. If this modelling is accurate, it means it is difficult to determine whether any difference between the response of OrbS and OrbS$_{CtetraA}$ to iron is specifically due to iron binding by the cysteine residues, or due to an incorrectly folded domain resulting from the substitution of the cysteines. It is also noteworthy that Cys196, Cys199 and Cys203 are predicted to be positioned in proximity to one another. The inter-atom distances are possibly viable for cooperative coordination of a metal ion such as Fe(II), although may be considered too distant. For example, in the Fur protein of *Magnetospirillum gryphiswaldense* MSR-1, bond distances between Mn(II) and coordinating amino acids are around 2.2 Å, and the distances between the amino acids are around 3-4 Å (Deng *et al.*, 2015). However, it should be noted again that (a) the modelling in this region is very unreliable, and (b) the CRE cysteines can be expected reorientate to chelate the metal ion

In conclusion, the results from these investigations into the terminal extensions have provided justification to investigate the C-terminal region of OrbS as a possible iron sensor, in particular the four conserved cysteine residues. Although the role of the N-terminal extension remains elusive, it does not appear to have a direct role in iron-dependent regulation. Therefore, the N-terminal extension will not be investigated further. Nonetheless, further examination of the role of this domain could provide interesting insights into the regulation of OrbS. Due to the high degree of similarity between OrbS and MbaS (Figure 1.13), some of the conclusions drawn here may be applicable to MbaS. More specifically, that some or all of the five cysteine residues found in the CRE of MbaS may play a role in an iron-dependent regulation mechanism. This is the focus of the investigation as described in Chapter V.
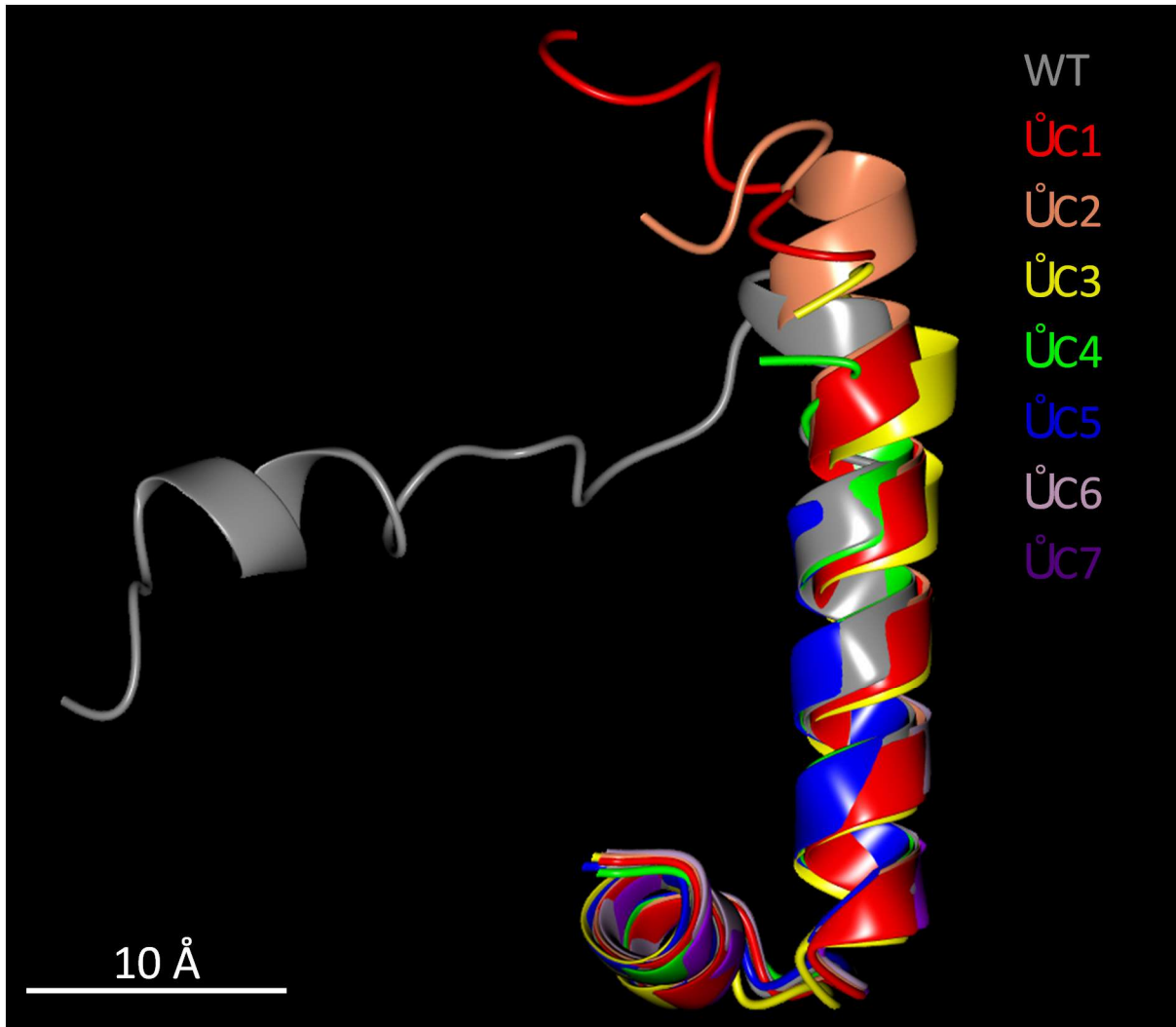
Figure 3.9. Effect of C-terminal truncation upon the predicted structure of the OrbS C-terminal extension.

Predicted superimposed 3D structural models of OrbS and OrbS$_{\Delta C1}$-OrbS$_{\Delta C7}$, generated using Phyre2 (Kelley *et al.*, 2015) and analysed using CCP4MG (McNicholas *et al.*, 2011). Amino acid residues from the region 4.2 helix-turn-helix to the C-terminus are shown (Thr170-Arg220). Structures are displayed in ribbon format, and are coloured as indicated.
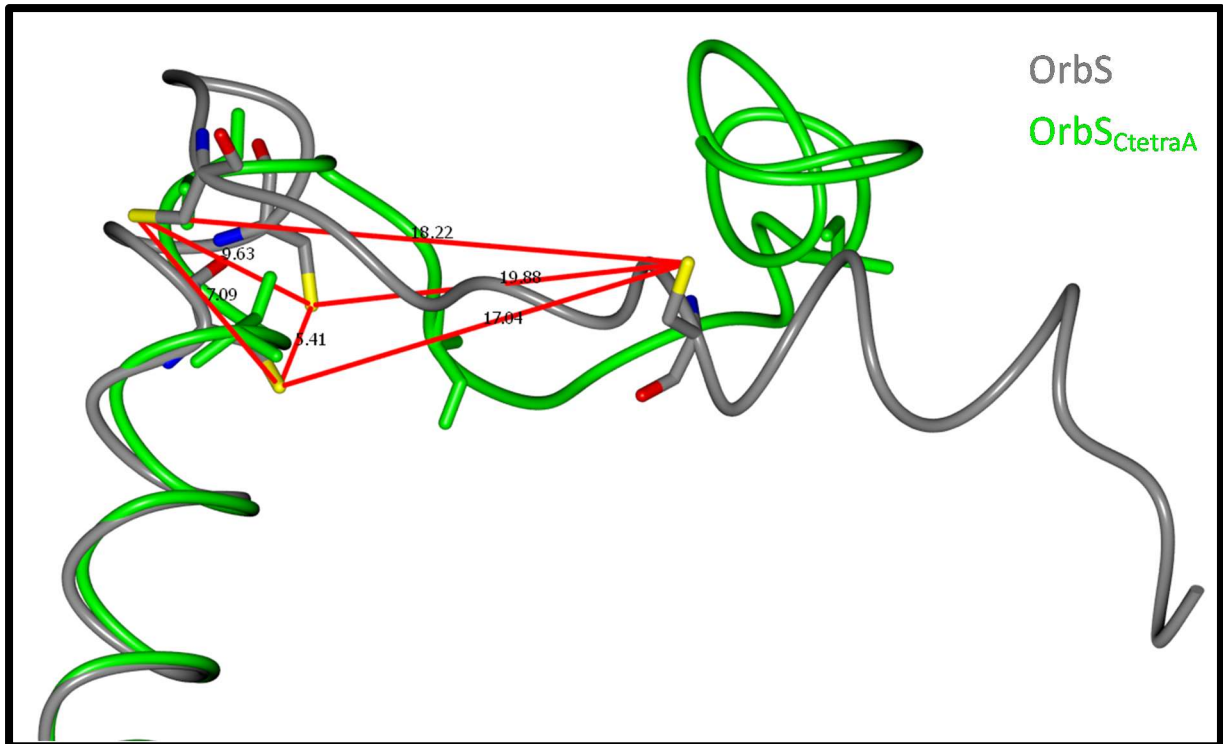
Figure 3.10. Effect of four cysteine-to-alanine substitutions upon the predicted protein structure of the OrbS C-terminal extension.

Predicted superimposed model 3D structures of OrbS and OrbS$_{CtetraA}$, generated using Phyre2 (Kelley *et al.*, 2015) and analysed using CCP4MG (McNicholas *et al.*, 2011). Amino acid residues of the CTD are shown. Peptide backbones are displayed in worm format, and are coloured as indicated. Alanine or cysteine residues at positions 196, 199, 203 and 209 are displayed in cylinder format, and atoms coloured as follows: carbon, grey (OrbS) or green (OrbS$_{CtetraA}$); oxygen, red; nitrogen, blue; sulphur, yellow. Distances between sulphur atoms of Cys196, Cys199, Cys203 and Cys209 of OrbS are shown as red lines with calculated length (Å).

Chapter IV: Generation of *Burkholderia thailandensis* E264 Mutants

4.1 Overview

For the analysis of the activity of MbaS *in vivo*, a series of gene mutations were required in the model organism *B. thailandensis* E264. Firstly, a Δ*mbaS* mutant was required to remove the genomic copy of MbaS, and allow Fur-independent MbaS (and mutant forms of MbaS) to be supplied *in trans*. Additionally, the secondary siderophore pyochelin was predicted to interfere with *in vivo* assays where the production of malleobactin was to be assayed.

Therefore, the pyochelin NRPS *pchE* gene was to be deleted. The transcription of *mbaS* is regulated by the ferric uptake regulator Fur (Alice *et al.*, 2006); therefore, the *fur* gene was also selected for deletion to remove the masking effect of Fur-dependent iron regulation. Finally, for the purpose of investigating the effect of the five conserved cysteine residues of the CRE of MbaS, mutant forms of the *mbaS* gene with selected cysteine-to-alanine substitutions were produced. These *mbaS* substitution mutants were also intended to be introduced into *Bth* E264.

Mutant alleles were amplified by SOE-PCR (described in 2.2.6) and cloned into selected allelic exchange vectors. Allelic exchange has been demonstrated to be effective at generating mutants in several species of *Burkholderia* (Barrett *et al.*, 2008; Shastri *et al.*, 2017). However, several allelic exchange vectors were employed with varying levels of success in *Bth* E264. Attempts with several different methods of allelic exchange were required to generate mutants, and these were isolated with low efficiency. For the generation of *mbaS*$_{CpentaA}$ and *fur* mutants, usage of these allelic exchange vectors was unsuccessful and it was not possible to isolate the desired mutants.

The phenotypes of isolated mutants were analysed using a variety of methods, including growth curves (see section 2.1.1), β-galactosidase assays (see section 2.5.1) and CAS assays (described in 2.1.2).

Objectives:

- To use SOE-PCR to synthesise mutant alleles of Δ*mbaS*, Δ*pchE*, Δ*fur* and *mbaS*$_{CpentaA}$

- To introduce these mutant alleles into *Bth* E264, and phenotypically characterise the isolated mutants

4.2 Construction of Δ*mbaS* gene deletion mutant

For the analysis of MbaS *in vivo* in *Bth*, an *mbaS* deletion mutant was sought after. This would enable *in trans* complementation with MbaS (and any MbaS mutants). Due to the genomic location of *mbaS* within the *mba* gene cluster, a marker-less in-frame deletion was required to avoid polar effects.

4.2.1   Construction of pEX18Tp-*pheS*-Δ*mbaS*

For the introduction of Δ*mbaS*, the pEX18Tp-*pheS* allelic exchange vector was used (Barrett *et al.*, 2008). The Δ*mbaS* mutant allele, with ≥500 bp of upstream and downstream flanking DNA, was amplified by SOE-PCR using primers ΔmbaS-A, ΔmbaS-B, ΔmbaS-C, and ΔmbaS-D to produce a 1099 bp PCR product (Figure 4.1a,b). The Δ*mbaS* allele was cloned between the *Hin*dIII and *Bam*HI sites of the MCS of pEX18Tp-*pheS* to give pEX18Tp-*pheS*-Δ*mbaS* (Figure 4.1c). The identity of the plasmid construct was confirmed by PCR screening and DNA sequencing analysis with primers M13revBACTH and M13for2.
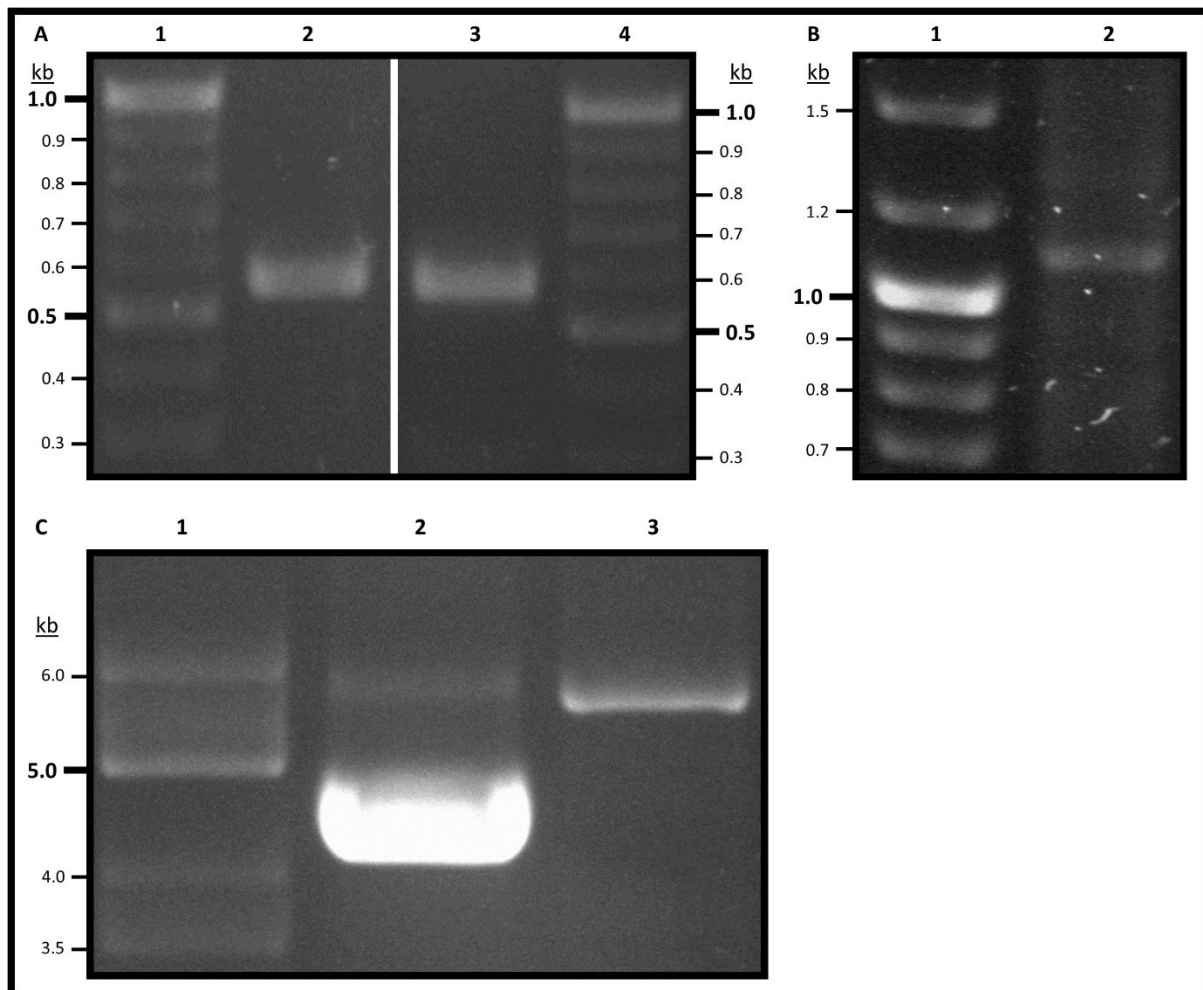
Figure 4.1. Construction of pEX18Tp-*pheS*-Δ*mbaS*

Agarose gel electrophoresis analysis of DNA PCR products and plasmid DNA used in construction of pEX18Tp-*pheS*-Δ*mbaS*. **A.** First round SOE PCR to amplify Δ*mbaS* with upstream and downstream flanking DNA. Lanes 1 and 4, GeneRuler 1 kb DNA Ladder (Thermofisher); lane 2, Δ*mbaS* 'left' flank, 554 bp PCR product; lane 3, Δ*mbaS* 'right' flank, 581 bp PCR product. **B.** Second round SOE PCR to amplify Δ*mbaS* with upstream and downstream flanking DNA. Lane 1, GeneRuler 1 kb DNA Ladder (Thermofisher); lane 2, Δ*mbaS*, 1099 bp PCR product. **C.** pEX18Tp-*pheS*-Δ*mbaS*. Lane 1, Supercoiled ladder (NEB); lane 2, pEX18Tp-*pheS*, 4.5 kb; lane 3, pEX18Tp-*pheS*-Δ*mbaS*, 5.6 kb.

4.2.2 Introduction of Δ*mbaS* into wild-type *B. thailandensis* by allelic exchange

E. coli SM10λ*pir* transformed with pEX18Tp-*pheS*-Δ*mbaS* was used as the donor strain for transfer of the mutant allele by conjugation into wild-type *Bth* E264. Resolution products were selected on M9 agar containing 25 μg ml^{-1} trimethoprim. Plasmid integration was further verified by PCR screening using the *mbaS*-specific primers ΔmbaS-A and ΔmbaS-D, and the vector specific primers pEX18Tpfor2 and pEX18Tprev2 (Figure 4.2).

The verified co-integrant strain, harbouring both *mbaS* and Δ*mbaS*, was then grown on M9-glucose agar containing 0.1% (w/v) cPhe and supplemented with 10 µM FeCl$_3$ and counter-screened on trimethoprim according to section 2.1.5 to isolate recombinant strains. Additionally, colonies were screened on CAS agar with 10 µM FeCl$_3$ to identify colonies exhibiting loss of yellow halo, indicative of loss of malleobactin production (colonies still exhibited small orange halo when grown at 30 °C, indicative of retention of pyochelin production). Positive clones underwent PCR screening with the primer pairs ΔmbaS-out-fwd/ΔmbaS-out-rev, ΔmbaS-A/ΔmbaS-D, and pEX18Tpfor2/pEX18Tprev2, to identify recombinants with the *mbaS* gene deletion and loss of the vector backbone (Figure 4.2 and Figure 4.3).
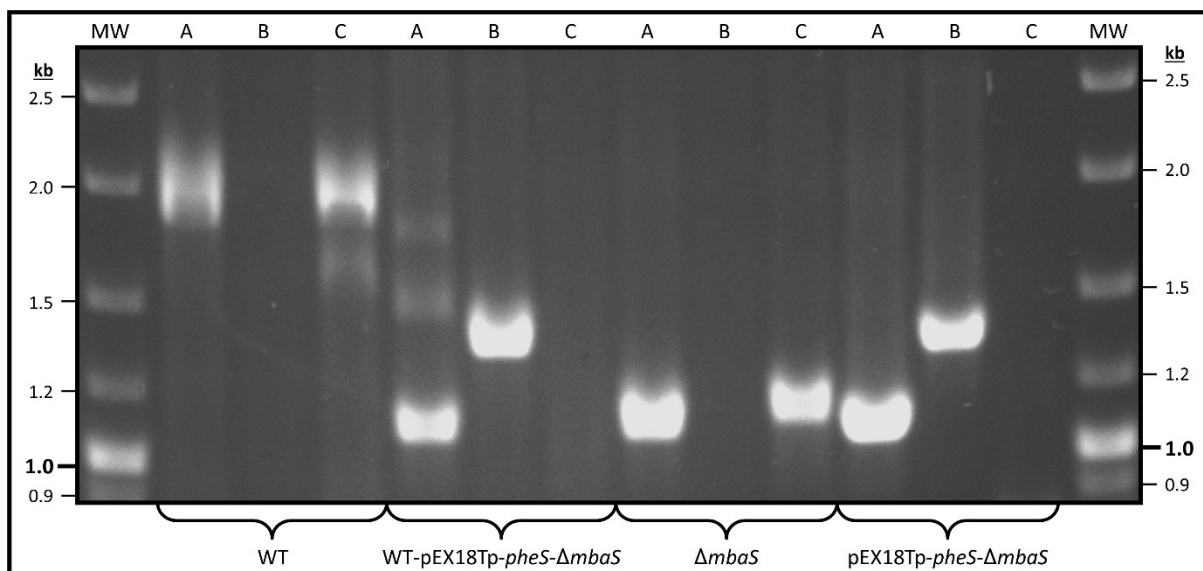
Figure 4.2. Verification of *Bth* E264 Δ*mbaS* deletion mutant by PCR screen

Agarose gel electrophoresis analysis of DNA products from PCR screening of strains during introduction of mutant Δ*mbaS* allele into *Bth* E264. The bacterial strain or plasmid from which the template DNA is extracted is denoted by brackets below. The primer pairs used in each PCR reaction are indicated by letters above lanes: A, ΔmbaS-A/ΔmbaS-D (expected molecular weights: *mbaS* = 1746 bp, Δ*mbaS* = 1092 bp); B, pEX18Tpfor2/pEX18Tprev2 (expected molecular weight 1368 bp); C, ΔmbaS-out-fwd/ΔmbaS-out-rev (expected molecular weights: *mbaS* = 1797 bp, Δ*mbaS* = 1131 bp). MW indicates GeneRuler 1 kb DNA Ladder (Thermofisher).
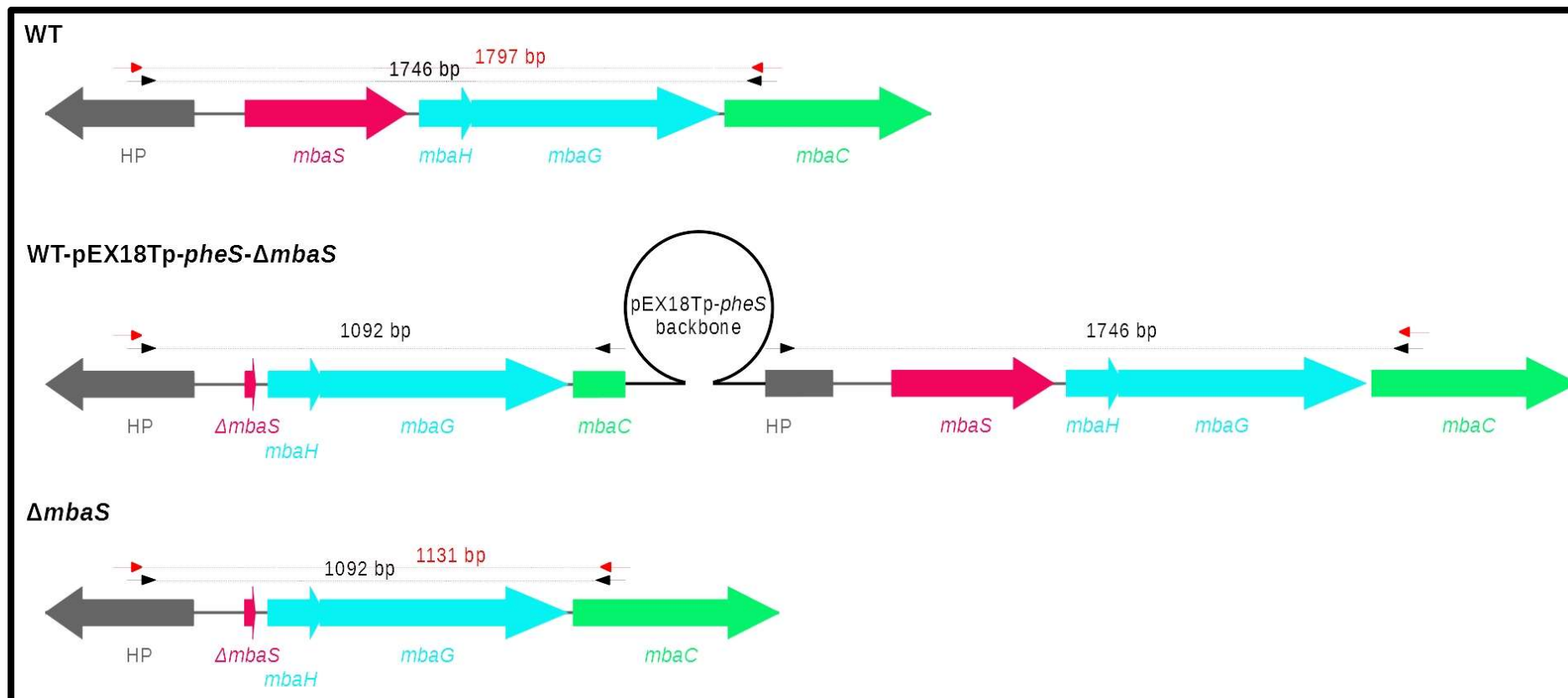
Figure 4.3. Schematic representation of *mbaS* gene deletion deletion PCR screening strategy.

Genes are shown as block arrows, and annotated with gene names below. Primer pairs, with resulting PCR product sizes, are shown above genes as arrows: black, ΔmbaS-A/ΔmbaS-D; red, ΔmbaS-out-fwd/ΔmbaS-out-rev. All genomic sizes and positions are to scale, except for the pEX18Tp-*pheS* plasmid backbone. The co-integrant strain shown results from the first homologous recombination occurring upstream of *mbaS*, but could also occur downstream and result in a different gene organisation, but the same PCR product sizes.

4.3 Construction of Δ*pchE* gene deletion mutant

Several *in vivo* experiments were planned to analyse the production of malleobactin by *Bth* as a way of evaluating the regulation of MbaS. However, *Bth* also produces a secondary siderophore, pyochelin, which was likely to interfere with the analysis of malleobactin production. Therefore, in order to remove pyochelin production, the pyochelin NRPS gene *pchE* was deleted in *Bth* by construction of a Δ*pchE* allele and allelic exchange.

4.3.1 Construction of pSNUFF3Cm-Δ*pchE*

For the introduction of Δ*pchE*, the pSNUFF3Cm allelic exchange vector was used (Spiewak, unpublished). The Δ*pchE* mutant allele, with ≥500 bp of upstream and downstream flanking DNA, was amplified by SOE-PCR using primers ΔpchE-A, ΔpchE-B, ΔpchE-C and ΔpchE-D to produce a 1088 bp PCR product (Figure 4.4a,b). The Δ*pchE* allele was cloned between the *Hin*dIII and *Bam*HI sites of the MCS of pSNUFF3Cm to give pSNUFF3-Cm-Δ*pchE* (Figure 4.4c). The identity of the plasmid construct was confirmed by PCR screening and DNA sequencing analysis with primers M13revBACTH and M13for2.
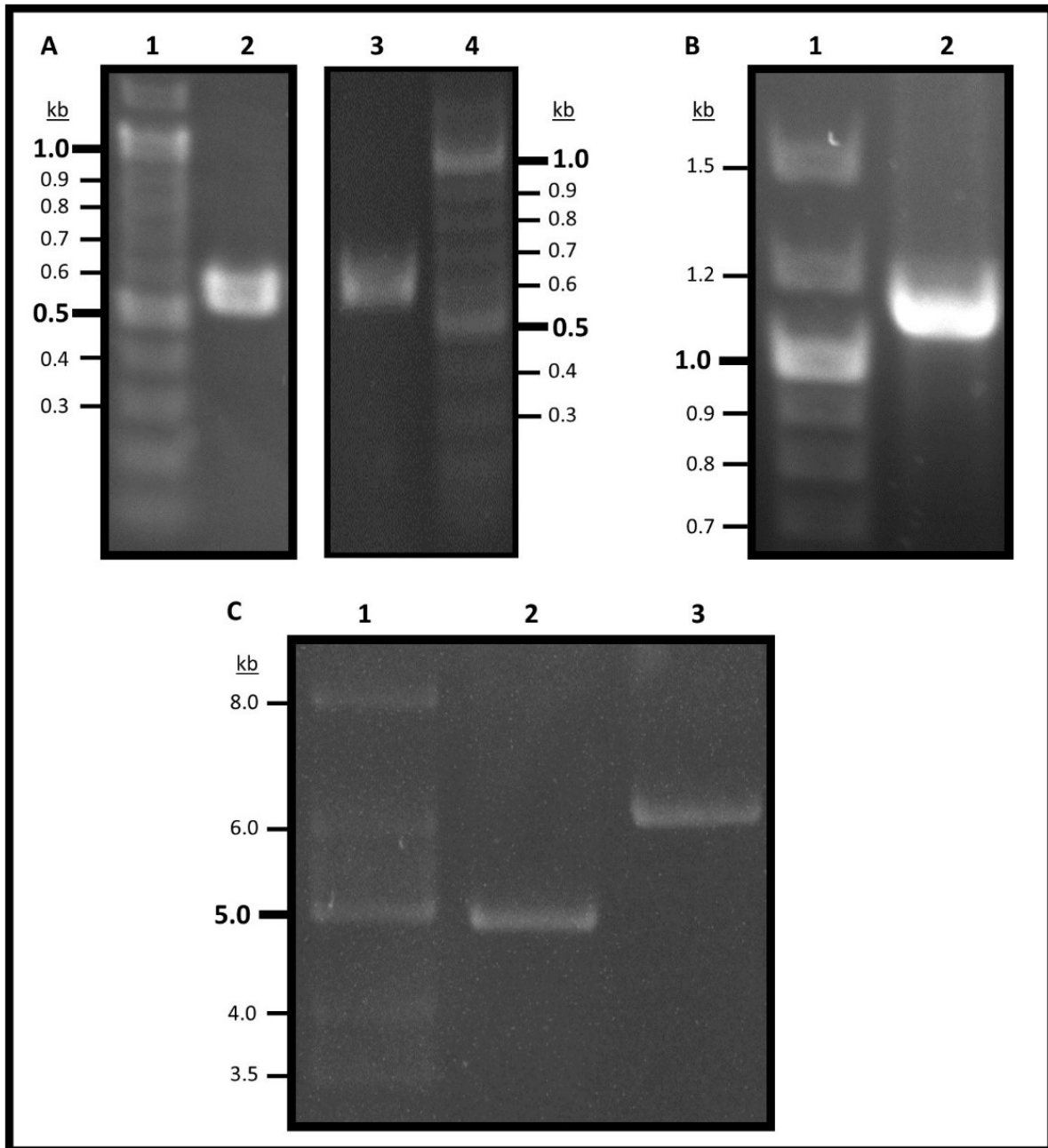
Figure 4.4. Construction of pSNUFF3Cm-Δ*pchE*

Agarose gel electrophoresis analysis of DNA PCR products and plasmid DNA used in construction of pSNUFF3Cm-Δ*pchE*. **A.** First round SOE PCR to amplify Δ*pchE* with upstream and downstream flanking DNA. Lanes 1 and 4, GeneRuler 1 kb DNA Ladder (Thermofisher); lane 2, Δ*pchE* 'left' flank, 556 bp PCR product; lane 3, Δ*pchE* 'right' flank, 568 bp PCR product. **B.** Second round SOE PCR to amplify Δ*pchE* with upstream and downstream flanking DNA. Lane 1, GeneRuler 1 kb DNA Ladder (Thermofisher); lane 2, Δ*pchE*, 1088 bp PCR product. **C.** pSNUFF3Cm-Δ*pchE*. Lane 1, Supercoiled ladder (NEB); lane 2, pSNUFF3Cm, 5.1 kb; lane 3, pSNUFF3Cm-Δ*pchE*, 6.1 kb.

4.3.2　Introduction of Δ*pchE* into wild-type *B. thailandensis* by allelic exchange

E. coli S17-1λ*pir* transformed with pSNUFF3Cm-Δ*pchE* was used as the donor strain for transfer of the mutant allele by conjugation into wild-type *Bth* E264. Resolution products were selected on Lnx agar containing 50 µg ml⁻¹ kanamycin and 50 µg ml⁻¹ chloramphenicol. Plasmid integration was further verified by PCR screening using the *pchE*-specific primers ΔpchE-A and ΔpchE-D, and the vector specific primers pEX18Tpfor2 and pEX18Tprev2.

The I-SceI endonuclease was then introduced into the verified co-integrant strain, harbouring both *pchE* and Δ*pchE*, in order to select for a second recombination event. This was achieved by introduction of pDAI-SceI-*pheS* via conjugation with *E. coli* S17-1λ*pir* donor cells. Strains that had successfully taken up pDAI-Sce-*pheS* were selected for on Lnx agar containing 50 µg ml⁻¹ gentamicin and 50 µg ml⁻¹ tetracycline. Positive clones underwent PCR screening with the primer pairs ΔpchE-out-fwd/ΔpchE-out-rev and pEX18Tpfor2/pEX18Tprev2, to identify recombinants with the *pchE* gene deletion and loss of the vector backbone (Figure 4.5).
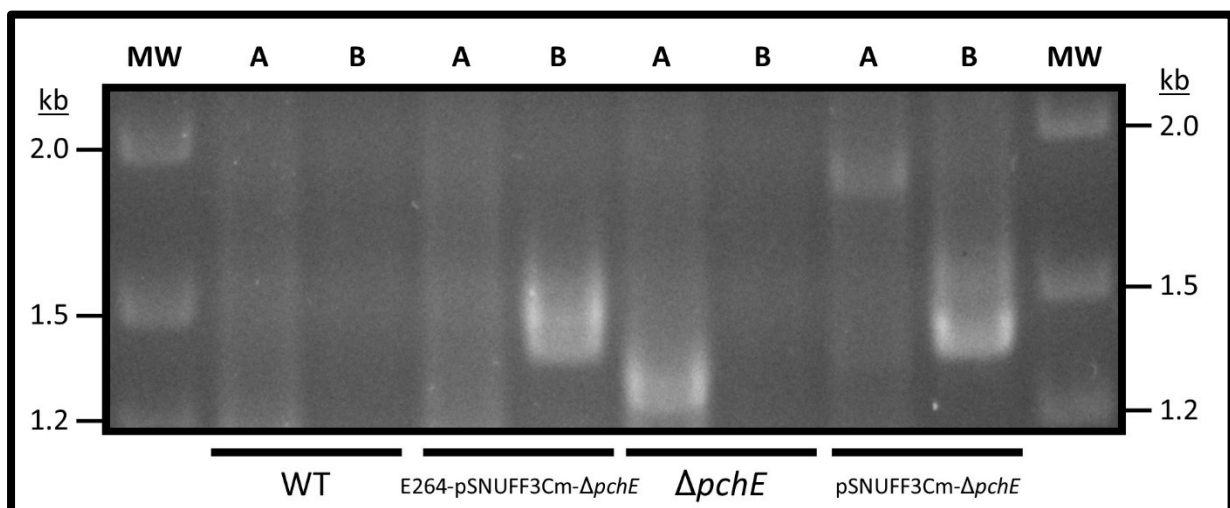
Figure 4.5. Verification of *Bth* E264 Δ*pchE* deletion mutant by PCR screen

Agarose gel electrophoresis analysis of DNA products from PCR screening of strains during introduction of mutant Δ*pchE* allele into *Bth* E264. The bacterial strain or plasmid from which the template DNA is extracted is denoted below the gel image. The primer pair used in each PCR reaction are indicated by letters above lanes: A, ΔpchE-out-fwd/ ΔpchE-out-rev (expected molecular weights: *pchE* = 5568 bp (PCR products were too large to be amplified and could not be observed), Δ*pchE* = 1224 bp). B, pEX18Tpfor2/ pEX18Tprev2 (expected molecular weight 1368 bp); MW indicates GeneRuler 1 kb DNA Ladder (Thermofisher).

4.4 Construction of Δ*mbaS* Δ*pchE* gene deletion mutant

To analyse the effect activity of MbaS supplied *in trans* in *Bth*, a mutant unable to produce pyochelin and with an *mbaS* deletion was sought after. This would enable complementation with MbaS (and any MbaS mutants), and enable the analysis of malleobactin production without the interference of pyochelin production. Again, a marker-less in-frame deletion was required to avoid polar effects. This mutant was generated by introduction of pEX18Tp-*pheS*-Δ*mbaS* (see section 4.2.1) into *Bth* E264 Δ*pchE* (see section 4.3).

4.4.1 Introduction of Δ*mbaS* into *B. thailandensis* Δ*pchE* by allelic exchange

E. coli SM10λ*pir* transformed with pEX18Tp-*pheS*-Δ*mbaS* (section 4.2.1) was used as the donor strain for transfer of the mutant allele by conjugation into *Bth* E264 Δ*pchE* (section 4.3). Resolution products were selected on M9 agar containing 25 µg ml^{-1} trimethoprim. Plasmid integration was further verified by PCR screening using the *mbaS*-specific primers ΔmbaS-A and ΔmbaS-D, and the vector specific primers pEX18Tpfor2 and pEX18Tprev2.

The verified co-integrant strain, harbouring both *mbaS* and Δ*mbaS* (and Δ*pchE*), was then grown on M9-glucose agar containing 0.1% (w/v) cPhe and supplemented with 10 µM FeCl$_3$ and counter-screened on trimethoprim according to section 2.1.5 to isolate recombinant strains. Additionally, colonies were screened on CAS agar with 10 µM FeCl$_3$ to identify colonies exhibiting loss of yellow halo, indicative of loss of malleobactin production. Positive clones underwent PCR screening with the primer pair ΔmbaS-out-fwd/ΔmbaS-out-rev to identify recombinants with the *mbaS* gene deletion, in addition to the *pchE* gene deletion (Figure 4.6).
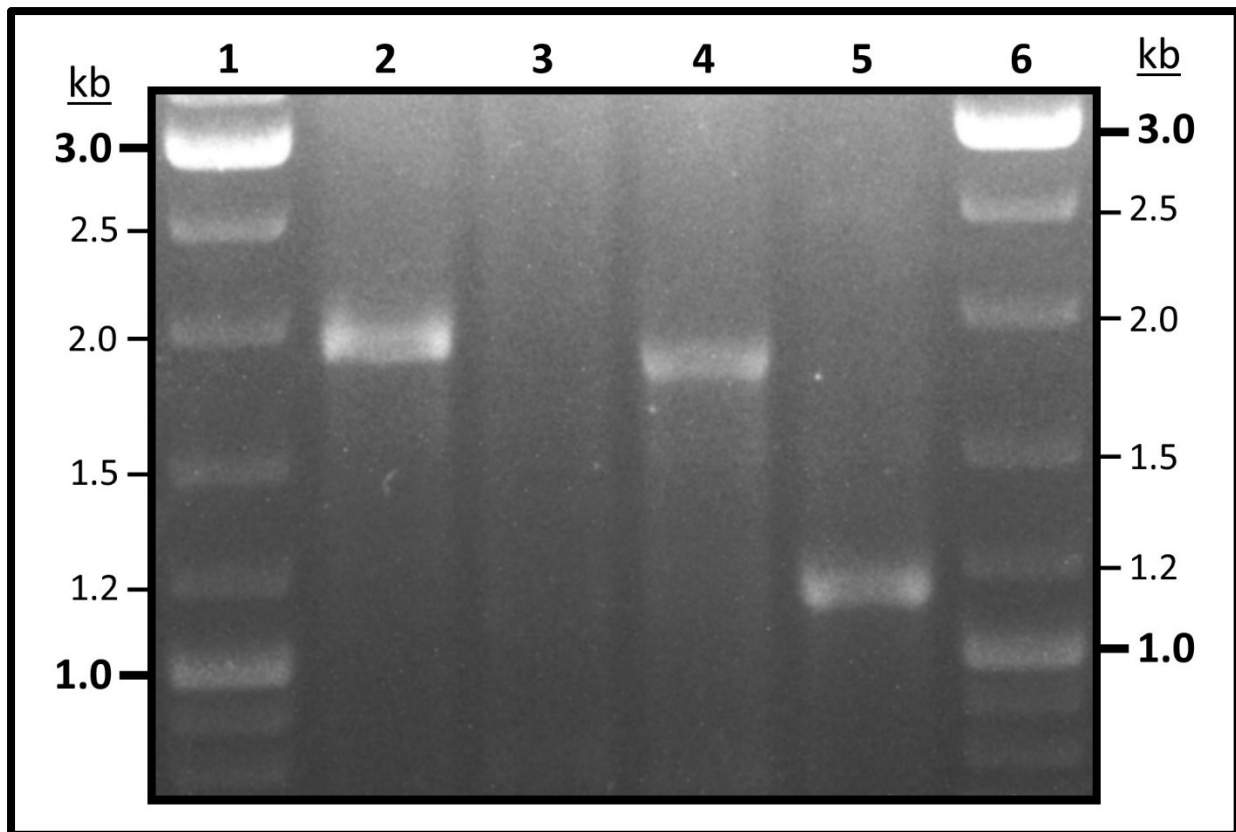
Figure 4.6. Verification of *Bth* E264 Δ*mbaS* Δ*pchE* deletion mutant by PCR screen

Agarose gel electrophoresis analysis of DNA products from PCR screening of strains during introduction of mutant Δ*mbaS* allele into *Bth* E264 Δ*pchE* using the primer pair Δmbas-out-fwd/ΔmbaS-out-rev (expected molecular weights: *mbaS* = 1797 bp, Δ*mbaS* = 1131 bp). Lanes 1 and 6, GeneRuler 1 kb DNA Ladder (Thermofisher). The bacterial strain from which the template DNA is extracted is as follows: lane 2, *Bth* E264 Δ*pchE* (original strain); lane 3, *Bth* E264 Δ*pchE*-pEX18Tp-*pheS*-Δ*mbaS* (co-integrant); lane 4, *Bth* E264 Δ*pchE* (exogonjugant restoring the wild-type *mbaS* allele); lane 5, *Bth* Δ*mbaS* Δ*pchE* (resolution product with desired gene deletion).

4.5 Attempts at construction of *mbaS*~CpentaA~ gene substitution mutants

MbaS encodes five conserved cysteine residues within its C-terminal region, which have been hypothesised to play a role in the regulation of the sigma factor via direct binding of Fe(II) (see section **Error! Reference source not found.**). To investigate the influence of these five C-terminal cysteine residues of MbaS, five cysteine-to-alanine substitutions were

introduced to construct a mutant allele, MbaS$_{CpentaA}$. This allele was attempted to be introduced into *Bth* by allelic exchange.

4.5.1   Construction of pEX18Tp-*pheS-mbaS*$_{CpentaA}$

For the introduction of Δ*mbaS*, the pEX18Tp-*pheS* allelic exchange vector was found to be successful. Therefore, this vector was initially selected for the introduction of an *mbaS* mutant allele with cysteine-to-alanine substitutions within the CRE, at positions C203, C206, C216, C220 and C230. The mutant allele was to be introduced into both *Bth* E264 Δ*mbaS* and *Bth* E264 Δ*mbaS* Δ*pchE*. This 'knock-in' mutagenesis would make the screening of potential mutants simpler, as the primers ΔmbaS-out-fwd/ΔmbaS-out-rev are expected to amplify a markedly larger PCR product from *Bth* containing the *mbaS*$_{CpentaA}$ allele compared to the Δ*mbaS* allele. Additionally, replacing MbaS with MbaS$_{CpentaA}$ is not expected to be associated with a strong phenotype change that can be screened for.

SOE-PCR was used to produce the *mbaS*$_{CpentaA}$ mutants allele. Initially, this was attempted using a single pair of long mutagenic primers, in conjugation with the primers ΔmbaS-A and ΔmbaS-D. This pair of mutagenic primers would introduce all five cysteine-to-alanine substitutions. However, attempts at producing *mbaS*$_{CpentaA}$ in the way were not successful. Therefore, it was decided to approach the five cysteine-to-alanine substitutions in three 'clusters': cluster 1 comprised the substitutions C203+206A, cluster 2 comprised the substitutions C216+220A, and cluster 3 comprised the substitution C230A.

Firstly, the *mbaS*$_{C230A}$ allele was amplified from *Bth* E264 genomic DNA by SOE-PCR using the primers ΔmbaS-A, mbaS-C230A-B, mbaS-C230A-C, and ΔmbaS-D to produce a 1765 bp PCR product (Figure 4.7a,b). This *mbaS*$_{C230A}$ allele was cloned between the *Hin*dIII and *Bam*HI sites of the MCS of pEX18Tp-*pheS* to give pEX18Tp-*pheS-mbaS*$_{C230A}$. The identity of this plasmid construct was confirmed by PCR screening and DNA sequencing analysis with primers M13revBACTH and M13for2.

Next, the *mbaS*$_{C203+206+230A}$ allele was amplified by SOE-PCR, using pEX18Tp-pheS-*mbaS*$_{C230A}$ as template DNA, with the primers ΔmbaS-A, mbaS-C203+206A-B, mbaS-C203+216A-C, and

ΔmbaS-D to produce a 1765 bp PCR product (Figure 4.7c,d). This $mbaS_{C203+206+230A}$ allele was cloned between the *Hin*dIII and *Bam*HI sites of the MCS of pEX18Tp-*pheS* to give pEX18Tp-*pheS-mbaS*$_{C203+206+230A}$. The identity of this plasmid construct was confirmed by PCR screening and DNA sequencing analysis with primers M13revBACTH and M13for2.

Finally, the $mbaS_{C203+206+216+220+230A}$ (or $mbaS_{CpentaA}$) allele was amplified by SOE-PCR, using pEX18Tp-*pheS-mbaS*$_{C203+206+230A}$ as template DNA, with the primers ΔmbaS-A, mbaS-C216+220A-B, mbaS-C216+220A-C, and ΔmbaS-D to produce a 1765 bp PCR product (Figure 4.7e,f). This $mbaS_{CpentaA}$ allele was cloned between the *Hin*dIII and *Bam*HI sites of the MCS of pEX18Tp-*pheS* to give pEX18Tp-*pheS-mbaS*$_{C230A}$ (Figure 4.7g). The identity of this plasmid construct was confirmed by PCR screening and DNA sequencing analysis with primers M13revBACTH and M13for2.

Although this was the process by which pEX18Tp-*pheS-mbaS*$_{CpentaA}$ was constructed, attempts to introduce the cysteine-to-alanine substitutions also resulted in the construction of *mbaS* mutant alleles with other arrangements of the cysteine-to-alanine substitutions. For instance, this process also yielded the alleles $mbaS_{C203+206A}$ (or $mbaS_{CdiA}$) and $mbaS_{C203+206+216+220A}$ (or $mbaS_{CtetraA}$), both of which were also inserted into pEX18Tp-*pheS*, and their cloning confirmed by PCR screening and DNA sequencing analysis with the primers M13revBACTH and M13for2.
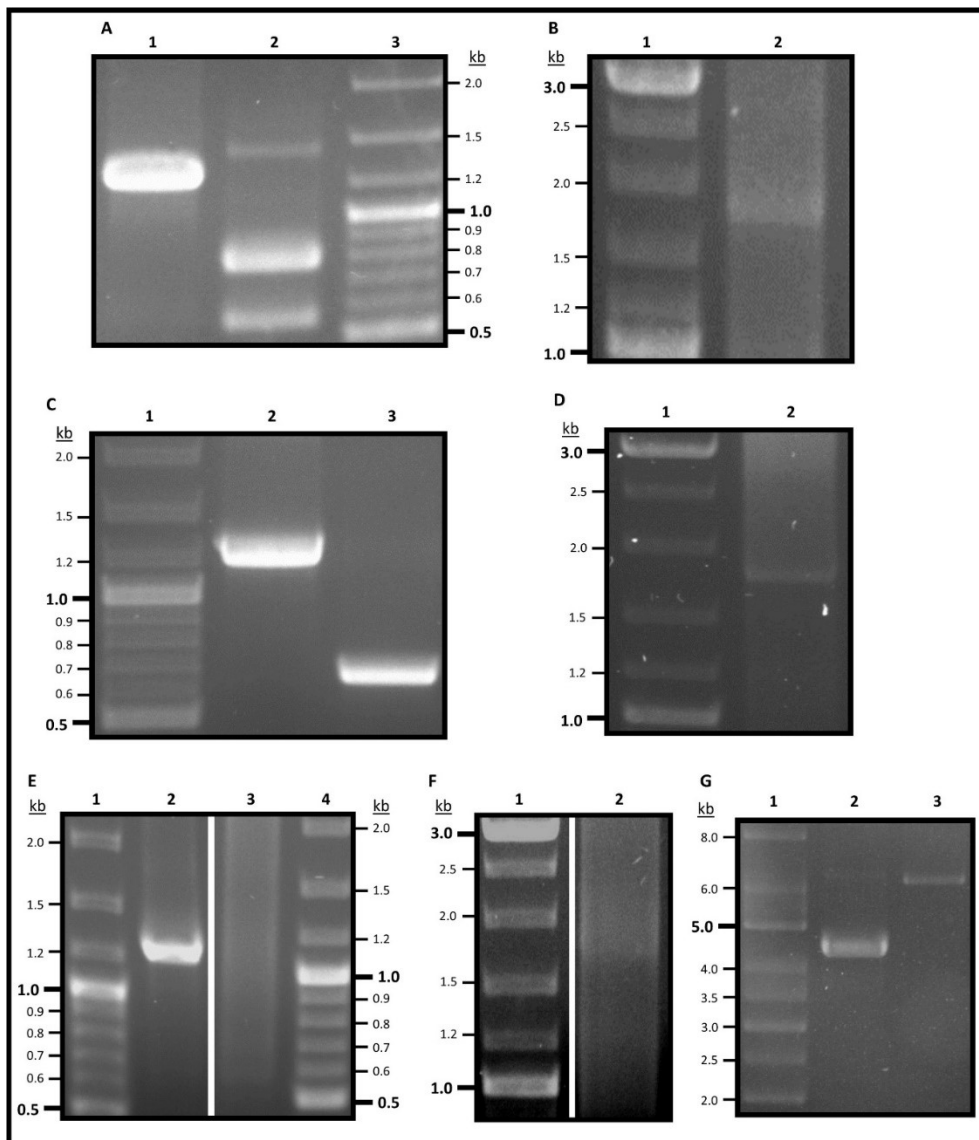
Figure 4.7. Construction of pEX18Tp-*pheS-mbaS*CpentaA

Agarose gel electrophoresis analysis of DNA PCR products and plasmid DNA used in construction of pEX18Tp-*pheS-mbaS*CpentaA. **A.** First round SOE PCR to amplify *mbaS*C230A with upstream and downstream flanking DNA. Lane 1, *mbaS*C230A 'left' flank, 1232 bp PCR product; lane 2, *mbaS*C230A 'right' flank, 561 bp PCR product; lane 3, GeneRuler 1 kb DNA Ladder (Thermofisher). **B.** Second round SOE PCR to amplify *mbaS*C230A with upstream and downstream flanking DNA. Lane 1, GeneRuler 1 kb DNA Ladder (Thermofisher); lane 2, *mbaS*C230A, 1765 bp PCR product. **C.** First round SOE PCR to amplify *mbaS*C203+206+230A with upstream and downstream flanking DNA. Lane 1, GeneRuler 1 kb DNA Ladder (Thermofisher); lane 2, *mbaS*C203+206+230A 'left' flank 1156 bp PCR product; lane 3, *mbaS*C203+206+230A 'right' flank 637 bp PCR product. **D.** Second round SOE PCR to amplify *mbaS*C203+206+230A with upstream and downstream flanking DNA. Lane 1, GeneRuler 1 kb DNA Ladder (Thermofisher); lane 2, *mbaS*C203+206+230A 1765 bp PCR product. **E.** First round SOE PCR to amplify *mbaS*CpentaA with upstream and downstream flanking DNA. Lanes 1 and 4, GeneRuler 1 kb DNA Ladder (Thermofisher); lane 2, *mbaS*::CpentaA 'left' flank 1196 bp PCR product; lane 3, *mbaS*CpentaA 'right' flank 597 bp PCR product. **F.** Second round SOE PCR to amplify *mbaS*CpentaA with upstream and downstream flanking DNA. Lane 1, GeneRuler 1 kb DNA Ladder (Thermofisher); lane 2, *mbaS*CpentaA 1765 bp PCR product. **G.** pEX18Tp-*pheS-mbaS*CpentaA plasmid DNA. Lane 1, Supercoiled ladder (NEB); lane 2, pEX18Tp-*pheS*, 4.5 kb; lane 3, pEX18Tp-*pheS-mbaS*CpentaA, 6.2 kb.

146

4.5.2 Attempts at the introduction of *mbaS*_{CpentaA} into *B. thailandensis* by allelic exchange

Many attempts were made at introducing the *mbaS*$_{CpentaA}$ allele into *Bth* E264 Δ*mbaS* and *Bth* E264 Δ*mbaS* Δ*pchE* by allelic exchange. Initially, this was attempted using pEX18Tp-*pheS*-*mbaS*$_{CpentaA}$. *E. coli* SM10λ*pir* transformed with pEX18Tp-*pheS*-*mbaS*$_{CpentaA}$ was used as the donor strain for transfer of the mutant allele by conjugation into *Bth* E264 Δ*mbaS* and *Bth* E264 Δ*mbaS* Δ*pchE*. Resolution products were selected on M9 agar containing 25 µg ml^{-1} trimethoprim. Plasmid integration was further verified by PCR screening using the vector specific primers pEX18Tpfor2 and pEX18Tprev2.

The verified co-integrant strains, harbouring both Δ*mbaS* and *mbaS*$_{CpentaA}$, were then grown on M9-glucose agar containing 0.1% (w/v) cPhe and counter-screened on trimethoprim according to methods to isolate recombinant strains. Additionally, colonies were screened on CAS agar containing 10 µM FeCl$_3$ to identify colonies exhibiting gain of a yellow halo, indicative of restoration of the Mba$^+$ phenotype. Positive clones underwent PCR screening with the primer pair Δ*mbaS*-out-fwd/Δ*mbaS*-out-rev to identify recombinants with the *mbaS*$_{CpentaA}$ gene insertion and loss of the vector backbone.

Several hundred potential resolution products were screened in this way. However, most of the screened colonies did not have genomic DNA which gave rise to a PCR product of a size corresponding to a second homologous recombination event i.e. these colonies were cPhe resistant, but had not excised the integrated plasmid backbone.

Therefore, the I-SceI endonuclease method, which proved successful in inducing the second recombination event for the mutagenesis of *Bth* E264 Δ*pchE* (see section 4.3.2), was attempted. The *mbaS*$_{CpentaA}$ allele was subcloned by restriction digest with *Hin*dIII and *Bam*HI from pEX18Tp-*pheS* to pSNUFF3Cm, to produce pSNUFF3Cm-*mbaS*$_{CpentaA}$. This was plasmid construct introduced into *Bth* E264 Δ*mbaS* and *Bth* E264 Δ*mbaS* Δ*pchE* by conjugation using *E. coli* SM10λ*pir* donor cells. Resolution products were selected on LB agar containing 50 µg ml^{-1} gentamicin and 50 µg ml^{-1} chloramphenicol. Plasmid integration was further verified by PCR screening using the vector specific primers pEX18Tpfor2 and pEX18Tprev2.

The I-SceI endonuclease was then introduced into the verified co-integrant strain, harbouring both Δ*mbaS* and *mbaS*CpentaA, in order to select for a second recombination event. This was attempted by introduction of pDAI-SceI-*pheS* via conjugation with *E. coli* S17-1λ*pir* donor cells. Strains that had successfully taken up pDAI-Sce-*pheS* were selected for on Lnx agar containing 50 µg ml^{-1} gentamicin and 50 µg ml^{-1} tetracycline. Positive clones underwent PCR screening with the primer pair ΔmbaS-out-fwd/ΔmbaS-out-rev to identify recombinants with the *mbaS*CpentaA gene insertion and loss of the vector backbone (an example is show in Figure 4.8).
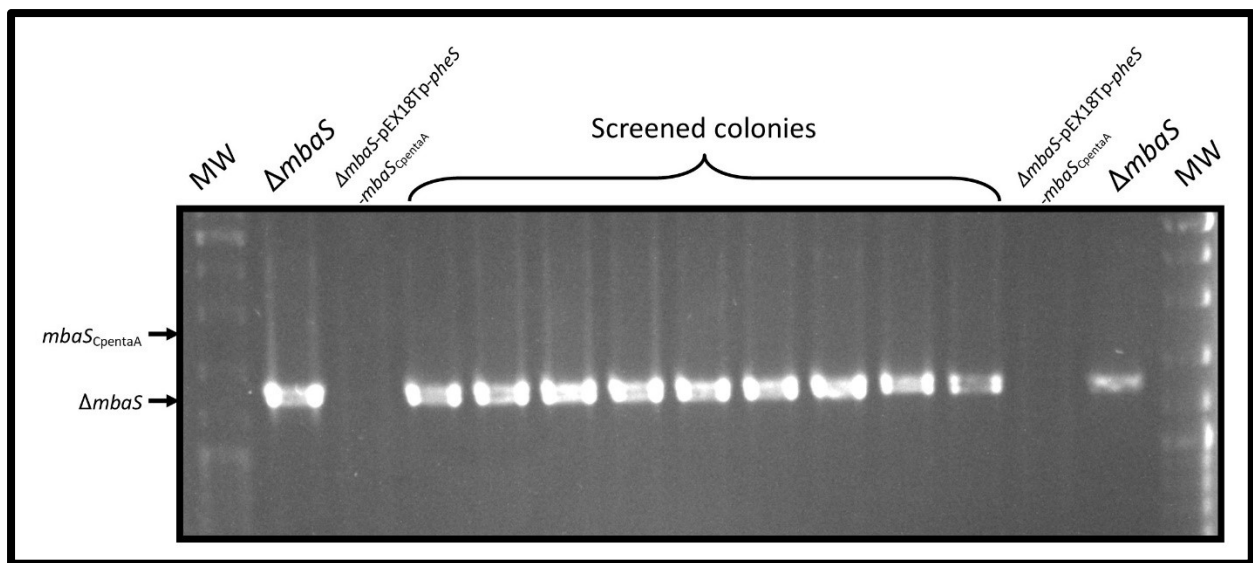
Figure 4.8. A representative example of PCR screening for introduction of the *mbaS*CpentaA allele into *Bth*.

Agarose gel electrophoresis analysis of DNA products from PCR screening of strains during an attempted introduction of mutant *mbaS*CpentaA allele into *Bth* E264 Δ*mbaS*, using the primer pair ΔmbaS-out-fwd/ΔmbaS-out-rev (expected molecular weights: *mbaS*CpentaA = 1797 bp, Δ*mbaS* = 1131 bp, shown to the left of the gel image). The bacterial strain from which the template DNA is extracted is denoted above the gel image. Screened colonies were selected as detailed in text. MW denotes GeneRuler 1 kb DNA Ladder (Thermofisher).

Again, several hundred potential resolution products were screened in this way. However, all of the screened colonies gave rise to a PCR product of a size corresponding to a second homologous recombination event that retained the Δ*mbaS* allele in place of the *mbaS*CpentaA allele.

An analogous method of isolating the $mbaS_{CpentaA}$ mutant by the I-SceI endonuclease using M9 minimal agar (supplemented with 0.5% (w/v) glucose and 0.1% (w/v) casamino acids) in place of Lnx agar was attempted. The rationale for this was that, on iron-limited media, there would be a selective advantage for *Bth* to maintain the $mbaS_{CpentaA}$ allele (and gain an Mba$^+$ phenotype) over retention of the $\Delta mbaS$ allele. Nonetheless, the resolution product strains that were isolated appeared to contain the $\Delta mbaS$ allele.

No explanation could be found for the perceived incompatibility for the $mbaS_{CpentaA}$ allele and *Bth* E264. However, it is possible that the cysteine-to-alanine substitutions introduced changes in either the genomic DNA sequence of the protein sequence that conferred a detrimental effect upon the organism. In particular, the C230A substitution introduces base substitutions within the *mbaH* promoter. Therefore, *mbaS* alleles with different cysteine-to-alanine substitutions were attempted to be introduced into *Bth* (see section 4.5.3).

4.5.3   Further attempts at the introduction of *mbaS* with cysteine-to-alanine substitutions into *B. thailandensis* by allelic exchange

Due to the problems encountered in generating mutants with the $mbaS_{CpentaA}$ allele, attempts were made at introducing both the $mbaS_{CdiA}$ allele (substituting cysteine 203 and cysteine 206 for alanines in *mbaS*) and $mbaS_{CtetraA}$ allele (substituting cysteines 203, 206, 216 and 220 for alanines in *mbaS*) that were generated in section 4.5.1. The pSNUFF3Cm vector was selected to be used for this mutagenesis ahead of pEX18Tp-*pheS*, due to the greater number of colonies that had undergone a second homologous recombination event. Both $mbaS_{CdiA}$ and $mbaS_{CtetraA}$ were subcloned into pSNUFF3Cm between the *Hind*III and *Bam*HI sites of the MCS. As an additional control, the 1765 bp *mbaS* wild-type allele was amplified from *Bth* E264 genomic DNA by PCR using the primers ΔmbaS-A and ΔmbaS-D, and this was also cloned into pSNUFF3Cm (verified by PCR screening and DNA sequencing analysis with the primers M13revBACTH and M13for).

In parallel, the four plasmids pSNUFF3Cm-*mbaS*, pSNUFF3Cm-*mbaS*$_{CdiA}$, pSNUFF3Cm-*mbaS*$_{CtetraA}$ and pSNUFF3Cm-*mbaS*$_{CpentaA}$ were introduced into *Bth* E264 Δ*mbaS* Δ*pchE* by conjugation using *E. coli* S17-1 donor cells. Resolution products were selected on LB agar

containing 50 µg ml^{-1} gentamicin and 50 µg ml^{-1} chloramphenicol. Plasmid integration was further verified by PCR screening using the vector specific primers pEX18Tpfor2 and pEX18Tprev2.

An additional PCR screening step using the primers mbaSmeroscreen-fwd and mbaSmeroscreen-rev was introduced to determine the location of the recombination event that led to the plasmid integration. If the recombination event occurred at the region of identical sequence upstream of the Δ*mbaS* allele, PCR using the co-integrant template DNA produces a 1012 bp product; if the recombination event occurred at the region of identical sequence downstream of the Δ*mbaS* allele, PCR using the co-integrant template DNA produces a 1678 bp product (an example is shown in Figure 4.9). For each mutant allele two co-integrants were selected, in which either an 'upstream' or a 'downstream' recombination had occurred.

The I-SceI endonuclease was then introduced into the co-integrant strains, harbouring both Δ*mbaS* and either *mbaS*, *mbaS*CdiA, *mbaS*CtetraA or *mbaS*CpentaA. This was achieved by introduction of pDAI-SceI-*pheS* via conjugation with *E. coli* S17-1λ*pir* donor cells. Strains that had successfully taken up pDAI-Sce-*pheS* were selected for on Lnx agar containing 50 µg ml^{-1} gentamicin and 50 µg ml^{-1} tetracycline. To screen for loss of the integrated vector backbone, clones were counter-screened by growth (or lack, thereof) on LB agar containing 50 µg ml^{-1} chloramphenicol. In each case, around 50 colonies were selected. However, PCR screening with the primer pair ΔmbaS-out-fwd/ΔmbaS-out-rev did not identify any recombinants with the desired *mbaS*CdiA, *mbaS*CpentaA or *mbaS*CpentaA gene mutations ('knock-in' mutagenesis with the *mbaS* allele was not screened for).

Ultimately, the *mbaS*CpentaA allele, or a similar allele with other C-terminal cysteine-to-alanine substitutions, was not introduced into *Bth* by allelic exchange.
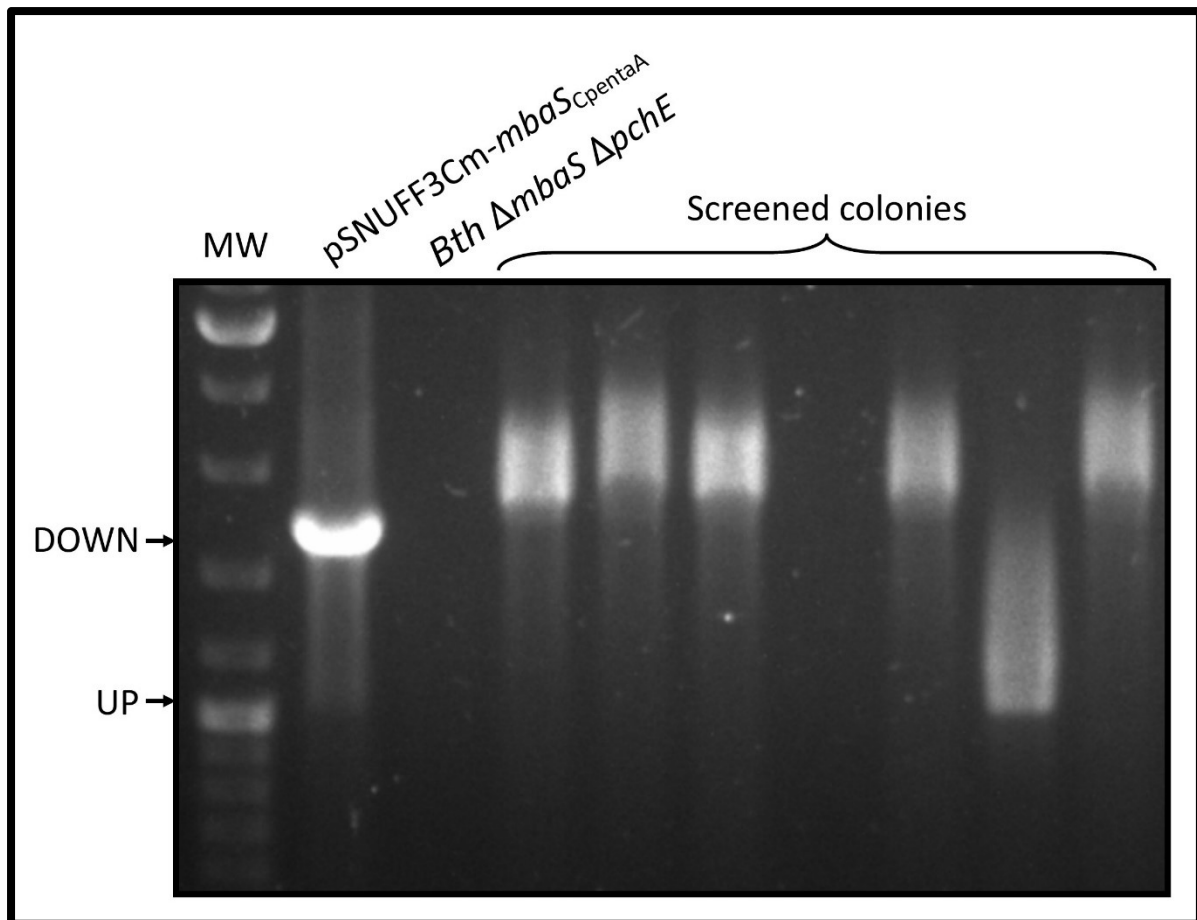
Figure 4.9. A representative example of PCR screening to the determine the location of the first homologous recombination event for introduction of the *mbaS*CpentaA allele into *Bth*.

Agarose gel electrophoresis analysis of DNA products from PCR screening of strains during an integration pSNUFF3Cm-*mbaS*CpentaA into *Bth* E264 Δ*mbaS* Δ*pchE*, using the primer pair mbaSmeroscreen-fwd/mbaSmeroscreen-rev (expected molecular weights: 'upstream' recombination = 1012 bp, 'downstream' recombination = 1678 bp, shown to the left of the gel image). PCR positive controls using pSNUFF3Cm-*mbaS*CpentaA and *Bth* E264 Δ*mbaS* Δ*pchE* as template DNA were used (denoted above lanes). Screened colonies were selected as detailed in text. MW denotes GeneRuler 1 kb DNA Ladder (Thermofisher).

4.6 Attempts at construction of Δ*fur* gene deletion mutants

With the aim of investigating the iron regulation of the sigma factor MbaS *in vivo*, specific to its cysteine-rich extension (see section 1.7.2), it was necessary to remove the iron-dependent transcriptional regulation of MbaS accomplished by the ferric uptake regulator, Fur (see section 1.5). Although Fur is a global transcriptional repressor and its deletion is likely to have widespread effects upon *Bth*, mutagenesis performed in *Bce* (A. Butt, unpublished data) and *Pseudomonas aeruginosa* (Pasqua *et al.*, 2017) has suggested that a *Bth fur* null mutant could be generated and be used in *in vivo* studies. This would remove the masking effect of iron-dependent Fur regulation, and enable direct iron regulation of MbaS to be investigated.

4.6.1 Construction of pSNUFF3Cm-Δ*fur*

For the introduction of Δ*fur*, the pSNUFF3Cm allelic exchange vector was used. The Δ*fur* mutant allele, with ≥500 bp of upstream and downstream flanking DNA, was amplified by SOE-PCR using primers Δfur-A, Δfur-B, Δfur-C and Δfur-D to produce a 1090 bp PCR product (Figure 4.10a,b). The Δ*fur* allele was cloned between the *Hin*dIII and *Bam*HI sites of the MCS of pSNUFF3Cm to give pSNUFF3-Cm-Δ*fur* (Figure 4.10c). The identity of the plasmid construct was confirmed by PCR screening and DNA sequencing analysis with primers M13revBACTH and M13for2.
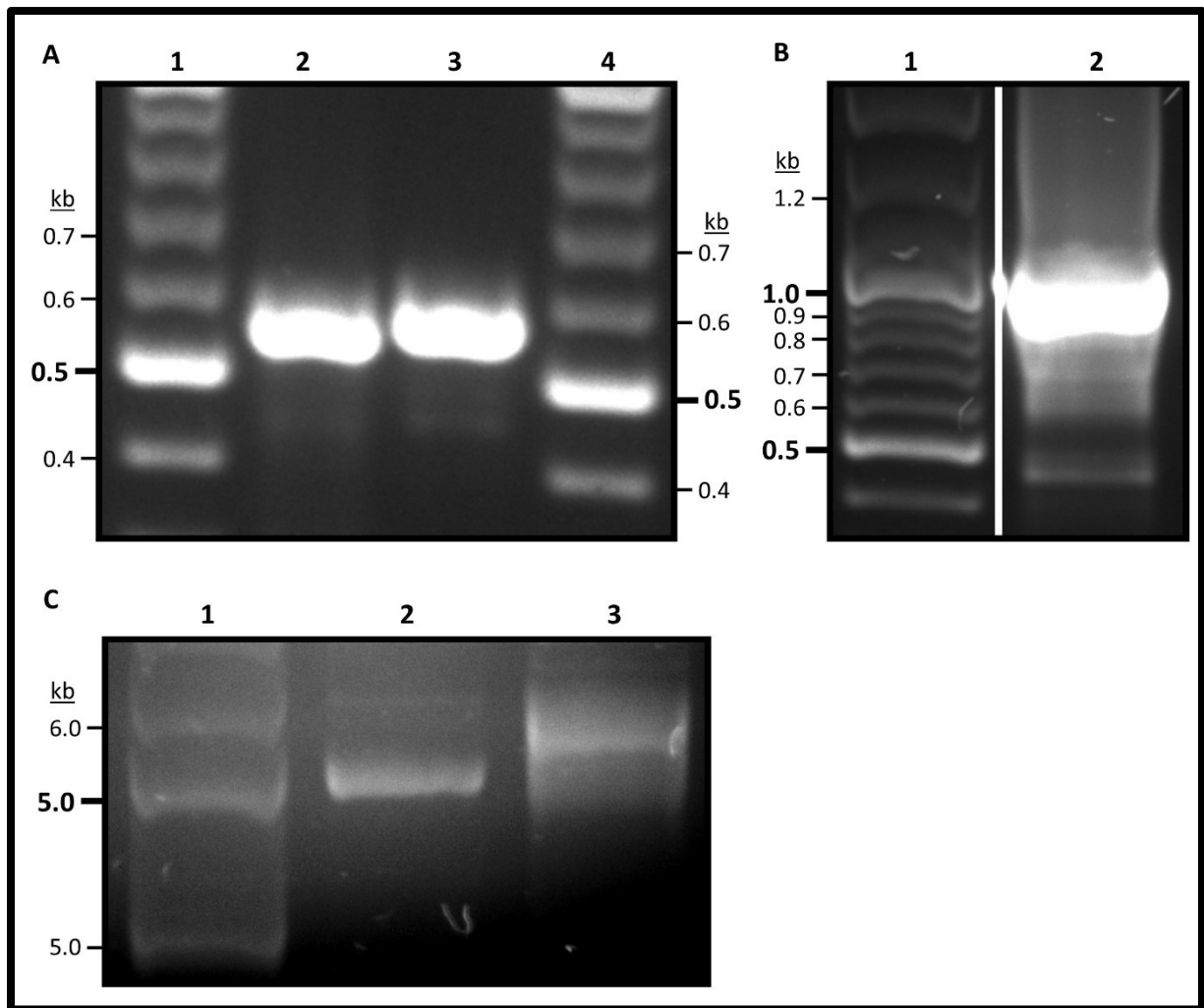
Figure 4.10. Construction of pSNUFF3Cm-Δ*fur*

Agarose gel electrophoresis analysis of DNA PCR products and plasmid DNA used in construction of pSNUFF3Cm-Δ*fur*. **A.** First round SOE PCR to amplify Δ*fur* with upstream and downstream flanking DNA. Lanes 1 and 4, GeneRuler 1 kb DNA Ladder (Thermofisher); lane 2, Δ*fur* 'left' flank, 554 bp PCR product; lane 3, Δ*fur* 'right' flank, 572 bp PCR product. **B.** Second round SOE PCR to amplify Δ*fur* with upstream and downstream flanking DNA. Lane 1, GeneRuler 1 kb DNA Ladder (Thermofisher); lane 2, Δ*fur*, 1090 bp PCR product. **C.** pSNUFF3Cm-Δ*fur*. Lane 1, Supercoiled ladder (NEB); lane 2, pSNUFF3Cm, 5.1 kb; lane 3, pSNUFF3Cm-Δ*fur*, 6.1 kb.

4.6.2 Construction of pSHAFT3-Δ*fur*::TpTer and pSHAFT2-Δ*fur*::TpTer

Due to difficulties encountered using pSNUFF3Cm-Δ*fur* to introduce the unmarked Δ*fur* allele into *Bth* (see section 4.6.3), a different approach using a marked mutant was attempted. A similar Δ*fur* allele was made, but with the insertion of an internal TpTer antibiotic selection marker.

153

SOE-PCR was used to produce a Δ*fur* mutant allele. This mutant allele contained an internal *Nde*I site, preceded by an in-frame stop codon, into which the TpTer cassette from p34E-TpTer (Shastri *et al.*, 2017) would be inserted. This Δ*fur*::*Nde*I allele was amplified from *Bth* E264 genomic DNA by SOE-PCR using the primers Δfur-A, Δfur-NdeI-B, Δfur-NdeI-C, and Δfur-D to produce a 1099 bp PCR product (Figure 4.11a,b). After gel extraction, this Δ*fur*::*Nde*I allele was cloned between the *Hin*dIII and *Bam*HI sites of the MCS of pBBR1MCS-2 to give the intermediate plasmid pBBR1MCS2-Δ*fur* (Figure 4.11c). The identity of this plasmid construct was confirmed by PCR screening and DNA sequencing analysis with the primers M13revBACTH and M13for2. Next, the TpTer cassette from p34E-TpTer was removed by restriction digest with *Nde*I, and inserted within the *Nde*I site of pBBR1MCS2-Δ*fur* to give pBBR1MCS2-Δ*fur*::TpTer (Figure 4.11d). Finally, the Δ*fur*::TpTer cassette from this plasmid was subcloned into pSHAFT3 using the restriction enzymes *Acc*65I and *Xba*I to construct pSHAFT3-Δ*fur*::TpTer (Figure 4.11e). The identity of this plasmid construct was confirmed by DNA sequencing analysis with the primers catendout and pUTcatrev.

The Δ*fur*::TpTer cassette was also subcloned in the same way into pSHAFT2 to give pSHAFT2-Δ*fur*::TpTer. The identity of this plasmid was also confirmed by DNA sequencing analysis using the primers catendout and pUTcatrev.
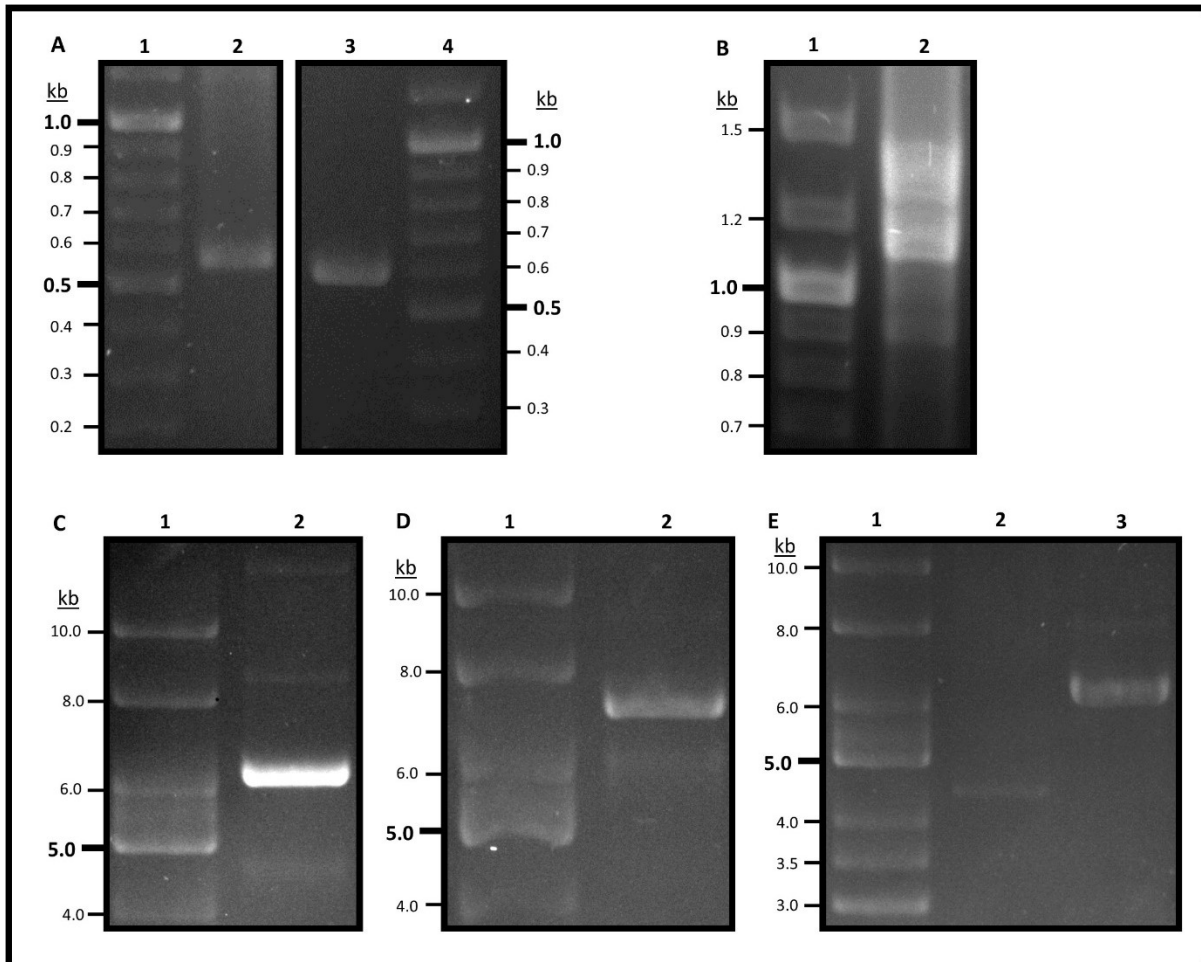
Figure 4.11. Construction of pSHAFT3-Δ*fur*::TpTer

Agarose gel electrophoresis analysis of DNA PCR products and plasmid DNA used in construction of pSHAFT3-Δ*fur*::TpTer. **A.** First round SOE PCR to amplify Δ*fur* with ≥500 bp upstream and downstream flanking DNA, and an internal *Nde*I site. Lanes 1 and 4, GeneRuler 1 kb DNA Ladder (Thermofisher); lane 2, Δ*fur* 'left' flank, 563 bp PCR product; lane 3, Δ*fur* 'right' flank, 581 bp PCR product. **B.** Second round SOE PCR to amplify Δ*fur*. Lane 1, GeneRuler 1 kb DNA Ladder (Thermofisher); lane 2, Δ*fur*, 1099 bp PCR product. **C.** pBBR1MCS2-Δ*fur*. Lane 1, Supercoiled ladder (NEB); lane 2, pBBR1MCS2-Δ*fur*, 6.2 kb. **D.** Insertion of TpTer cassette into pBBR1MCS2-Δ*fur*. Lane 1, Supercoiled ladder (NEB); lane 2, pBBR1MCS2-Δ*fur*::TpTer, 7.1 kb. **E.** Subcloning of Δ*fur*::TpTer into pSHAFT3. Lane 1, Supercoiled ladder (NEB); lane 2, pSHAFT3, 4.5 kb; lane 3, pSHAFT3-Δ*fur*::TpTer, 6.5 kb.

4.6.3   Attempts at the introduction of Δ*fur* into *B. thailandensis* by allelic exchange

Initially, *E. coli* S17-1λ*pir* transformed with pSNUFF3Cm-Δ*fur* was used as the donor strain

for transfer of the mutant allele by conjugation into wild-type *Bth* E264. Resolution products

were selected on Lnx agar containing 50 μg ml^{-1} kanamycin and 50 μg ml^{-1} chloramphenicol.

Plasmid integration was further verified by PCR screening using the vector specific primers pEX18Tpfor2 and pEX18Tprev2.

The I-SceI endonuclease was then introduced into the verified co-integrant strain, harbouring both *fur* and Δ*fur*, in order to select for a second recombination event. This was achieved by introduction of pDAI-SceI-*pheS* via conjugation with *E. coli* S17-1λ*pir* donor cells. Strains that had successfully taken up pDAI-Sce-*pheS* were selected for on EB agar containing 50 μg ml^{-1} gentamicin and 50 μg ml^{-1} tetracycline. Positive clones underwent PCR screening with the primer pairs Δfur-out-fwd/Δfur-out-rev to identify recombinants with the *fur* gene deletion. Approximately 200 colonies were screened in this way. However, no successful Δ*fur* strains were identified. Where a second recombination event was found to have occurred, cells had favoured retaining the wild-type *fur* allele ahead of the *fur* deletion, as judged by the presence of a 1688 bp PCR product rather than a 1312 bp PCR product.

This suggested that there was a strong selective disadvantage for the loss of *fur* in *Bth*. Therefore, attempts were made using the Δ*fur*::TpTer allele. Initially, this was attempted using pSHAFT3-Δ*fur*::TpTer. However, there were unexplained difficulties in introducing this plasmid into *E. coli* SM10λ*pir* and S17-1λ*pir* and pSHAFT2-Δ*fur*::TpTer was used instead. Additionally, research in *Pseudomonas aeruginosa* had suggested that the *fur* deletion may not be lethal in conjunction with a Pch$^-$ phenotype. Therefore, the Δ*fur*::TpTer allele was attempted to be introduced into *Bth* E264 Δ*mbaS* (see section 4.2), *Bth* E264 Δ*pchE* (see section 4.3) and *Bth* E264 Δ*mbaS* Δ*pchE* (see section 4.4) in addition to wild-type *Bth* E264.

pSHAFT2-Δ*fur*::TpTer vector was introduced into the *Bth* strains by conjugation via *E. coli* SM10λ*pir* donor cells, and cells that had undergone homologous recombination with the plasmid were selected for on EB agar containing 50 μg ml^{-1} gentamicin and 50 μg ml^{-1} trimethoprim. As *Bth* lacks the ability to utilise the oriR6K origin of replication of the plasmid, only homologous recombination between the chromosome and the plasmid confers trimethoprim resistance. This recombination can occur by a single crossover event, resulting in integration of the plasmid and co-integrant formation, with both the wild-type *fur* allele and the Δ*fur*::TpTer allele present. Alternatively, the recombination can occur by a double crossover event, resulting in the wild-type *fur* allele being replaced by the Δ*fur*::TpTer mutant allele. In this case, vector sequences are not permanently integrated

into the genome. The desired latter case was screened for by a subsequent counter-screening for chloramphenicol and/or ampicillin sensitivity. Approximately 1,000 colonies were screened in this way. However, in all cases, the bacteria displayed resistance to 50 µg ml^{-1} chloramphenicol and/or 100 µg ampicillin, indicating the occurrence of a single homologous recombination event, rather than the desired double recombination. PCR screening of selected colonies with the primer pair Δfur-out-fwd/Δfur-out-rev confirmed the retention of the wild-type *fur* gene (Figure 4.12). Ultimately, it was not possible to generate a *Bth* E264 *fur* null mutant in this study.
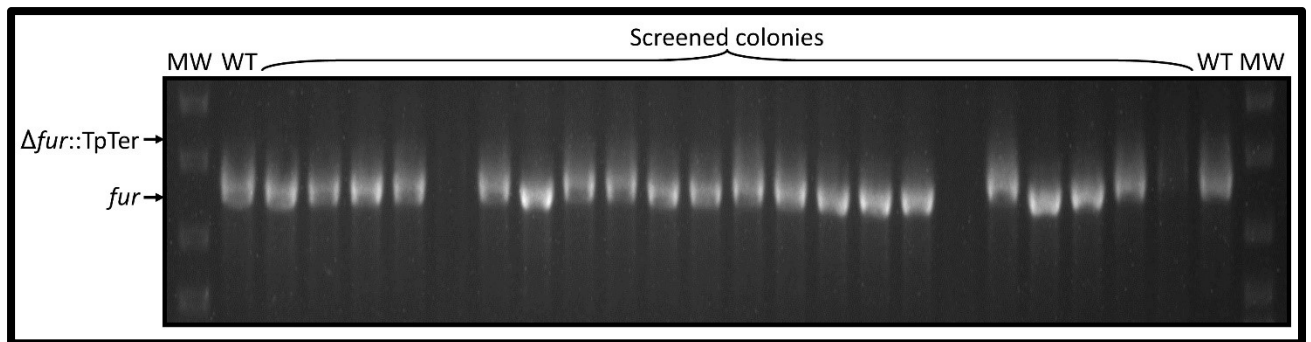
Figure 4.12. A representative example of PCR screening for introduction of the Δ*fur*::TpTer allele into *Bth*.

Agarose gel electrophoresis analysis of DNA products from PCR screening of strains during introduction of mutant Δ*fur*::TpTer allele into *Bth* E264 using the primer pair Δfur-out-fwd/Δfur-out-rev (expected molecular weights: *fur* = 1688 bp, Δ*fur*::TpTer = 2189 bp, shown to the left of the gel image). The bacterial strain from which the template DNA is extracted is denoted above the gel image (WT denoted *Bth* E264, screened colonies were selected as detailed in the main body of text). MW denotes GeneRuler 1 kb DNA Ladder (Thermofisher).

4.7 Phenotypic characterisation of *B. thailandensis* mutants

The three successfully generated mutant strains of *Bth* E264 harbouring Δ*mbaS* and/or Δ*pchE* gene deletions were further verified and characterised via a series of phenotypic assays. These included growth on CAS medium to analyse production of siderophores, monitoring the growth of culture under iron-limited and iron-replete conditions, and

promoter reporter analysis using selected target promoters. These experiments also required the construction of plasmids that express corresponding protein to complement the mutants, and transcriptional reporter plasmids, which are discussed forthwith.

4.7.1 Construction of pBBR1MCS2-*mbaS*, pBBR1MCS2-*mbaS*_{CpentaA} and pBBR1MCS2-*pchE*

For the expression of the MbaS protein and MbaS$_{CpentaA}$ mutant proteins *in vivo* and to complement the Δ*mbaS* mutants, the *mbaS* and *mbaS*$_{CpentaA}$ genes were cloned into the broad host range expression vector pBBR1MCS-2 (Kovach *et al.*, 1995). The *mbaS* gene was amplified by PCR from *Bth* E264 genomic template DNA, and the *mbaS*$_{CpentaA}$ was amplified by PCR from the plasmid pSNUFF3-Cm-*mbaS*$_{CpentaA}$ (see section 4.5.1) using the primers mbaS-fwd-HindIII and mbaS-rev-BamHI to produce a 774 bp PCR product in each case (Figure 4.13a,b). This included 30 bp immediately upstream of the translation start codon that contained the Shine-Dalgarno sequence, but not the native *mbaS* promoter. An in-frame stop codon was incorporated into the 5' end of the forward primer to terminate translation of the upstream *lacZα* gene segment of the vector to eliminate the possibility of generating a LacZα-MbaS protein fusion. The *mbaS* and *mbaS*$_{CpentaA}$ genes were cloned between the *Hin*dIII and *Bam*HI sites of the MCS of pBBR1MCS-2 to give pBBR1MCS2-*mbaS* and pBBR1MCS2-*mbaS*$_{CpentaA}$ (Figure 4.13c). The identities of the plasmid constructs were confirmed by PCR screening and DNA sequencing analysis with primers M13revBACTH and M13for2.
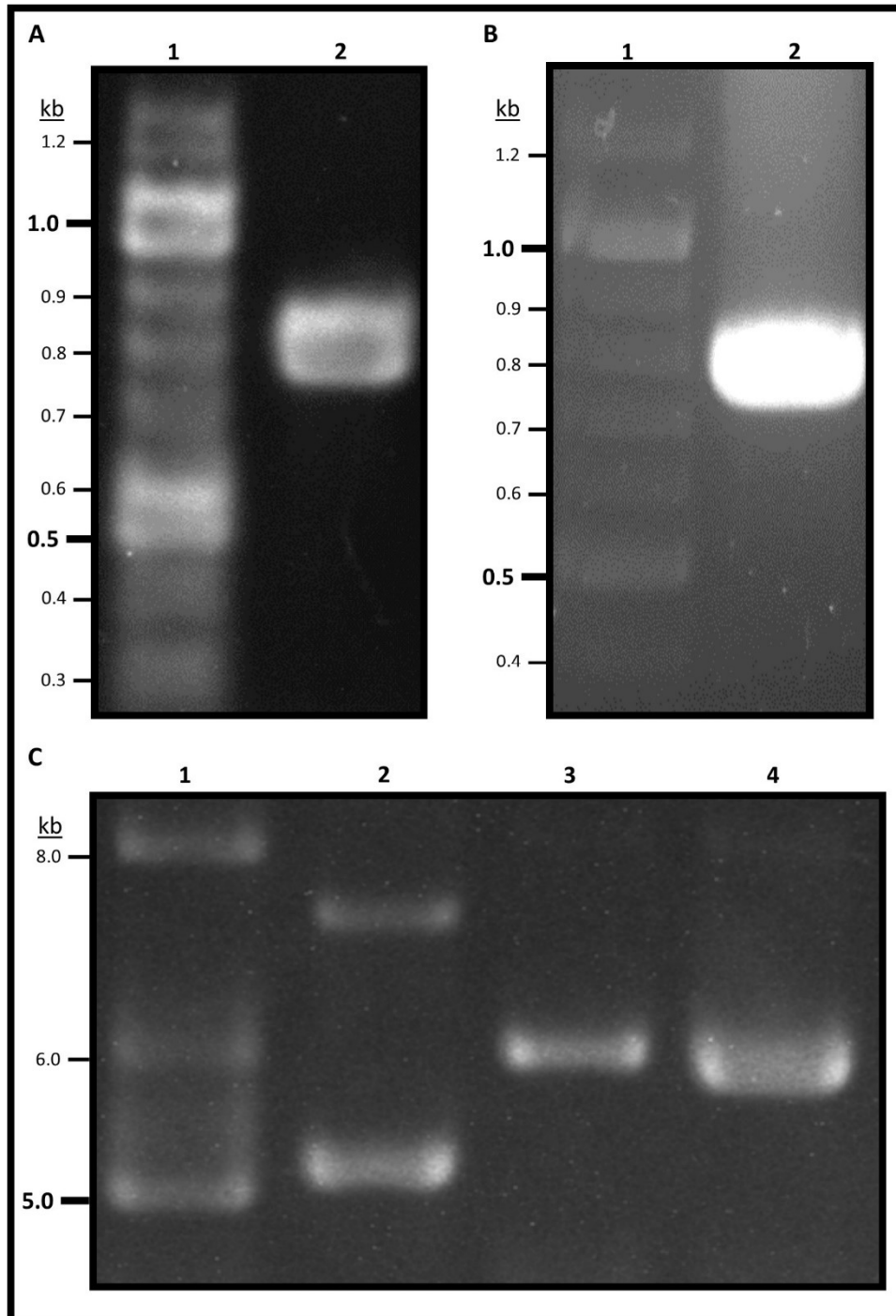
Figure 4.13. Construction of pBBR1MCS2-*mbaS* and pBBR1MCS2-*mbaS*CpentaA.

Agarose gel electrophoresis analysis of DNA PCR products and plasmid DNA used in construction of pBBR1MCS2-*mbaS* pBBR1MCS2-*mbaS*CpentaA. **A.** PCR to amplify *mbaS*. Lane 1, GeneRuler 1 kb DNA Ladder (Thermofisher); lane 2, *mbaS* PCR product, 774 bp. **B.** PCR to amplify *mbaS*CpentaA. Lane 1, GeneRuler 1 kb DNA Ladder (Thermofisher); lane 2, *mbaS*CpentaA PCR product, 774 bp. **C.** pBBR1MCS2-*mbaS* and pBBR1MCS2-*mbaS*CpentaA plasmid DNA. Lane 1, Supercoiled DNA Ladder (NEB); lane 2, pBBR1MCS-2, 5.1 kb; lane 3, pBBR1MCS2-*mbaS*, 5.9 kb; lane 4, pBBR1MCS2-*mbaS*CpentaA, 5.9 kb.

Likewise, for the expression of PchE and complementation of Δ*pchE* mutants *in vivo*, the *pchE* gene was also cloned into pBBR1MCS-2. The *pchE* gene was amplified by PCR from *Bth* E264 genomic DNA using the primers pchE-fwd-HindIII and pchE-rev-BamHI to produce a 4464 bp PCR product. As with *mbaS* and *mbaS*~CpentaA~, the cloned *pchE* gene was preceded by an in-frame stop codon. *pchE* was cloned between the *Hin*dIII and *Bam*HI sites of the MCS of pBBR1MCS-2 to give pBBR1MCS2-*pchE* (Figure 4.14). The identity of the plasmid was confirmed by PCR screening analysis with primers M13revBACTH and M13for2.
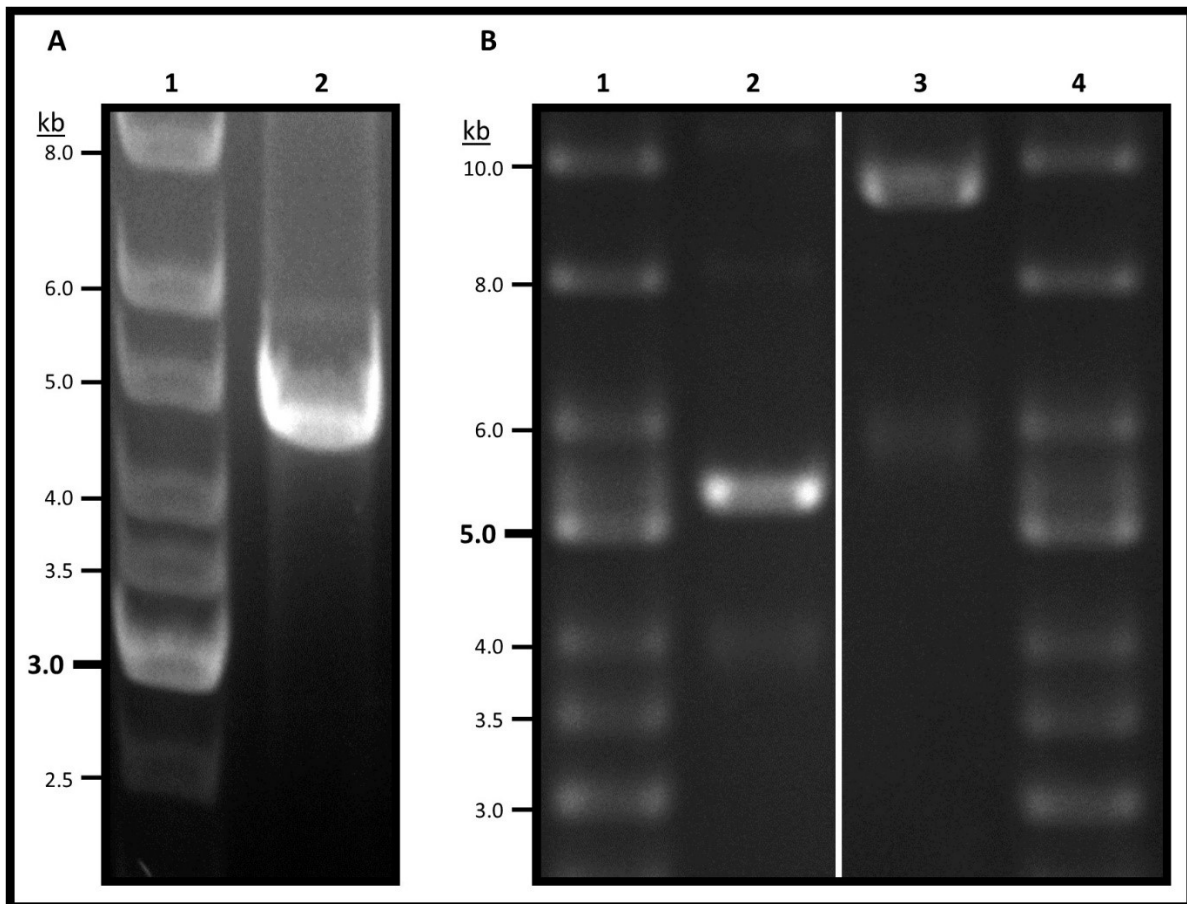
Figure 4.14. Construction of pBBR1MCS2-*pchE*.

Agarose gel electrophoresis analysis of DNA PCR products and plasmid DNA used in construction of pBBR1MCS2-*pchE*. **A.** PCR to amplify *pchE*. Lane 1, GeneRuler 1 kb DNA Ladder (Thermofisher); lane 2, *pchE* PCR product, 4464 bp. **B.** pBBR1MCS2-*pchE* plasmid DNA. Lanes 1 and 4, Supercoiled DNA Ladder (NEB); lane 2, pBBR1MCS-2, 5.1 kb; lane 3, pBBR1MCS2-*pchE*, 9.6 kb.

4.7.2 Comparison and complementation of siderophore production CAS agar

The deletion of both the *mbaS* and *pchE* genes was verified *in vivo* by complementation of their phenotypes using the plasmids constructed in section 4.7.1. The plasmids pBBR1MCS-2, pBBR2-*mbaS* or pBBR2-*pchE* were introduced into wild-type *Bth* E264, *Bth* E264 Δ*mbaS*, *Bth* E264 Δ*pchE* or *Bth* E264 Δ*mbaS* Δ*pchE* via conjugation with *E. coli* S17-1λ*pir* donor cells. *Bth* strains harbouring the plasmids were selected on Lnx medium containing 50 µg ml^{-1} gentamicin and 250 µg ml^{-1} kanamycin. Overnight cultures of these plasmid-harbouring strains were grown in M9 minimal medium supplemented with 0.5% (w/v) glucose and 250 µg ml^{-1} kanamycin. Additionally, overnight cultures of wild-type *Bth* E264, *Bth* E264 Δ*mbaS*, *Bth* E264 Δ*pchE* and *Bth* E264 Δ*mbaS* Δ*pchE* were also grown in M9 minimal medium supplemented with 0.5% (w/v) glucose. After normalisation, 1 µl of each bacterial culture was spotted onto CAS agar plates containing 10 µM FeCl$_3$, and incubated at 30 °C for approximately 48 hours.

Firstly, *Bth* E264 wild-type and Δ*mbaS* strains were grown on CAS agar to verify and analyse the effect of the *mbaS* deletion in *Bth* E264 Δ*mbaS*. This gene deletion was complemented in cells harbouring pBBR2-*mbaS* (Figure 4.15).

Both areas of growth of the wild-type *Bth* and the Δ*mbaS* mutant grown on CAS medium were surrounded by a distinctive halo, indicating the secretion of an iron-chelating molecule (Figure 4.15, left). The wild-type strain was surrounded by a yellow halo, and the Δ*mbaS* strain was surrounded by an orange halo. *Bce* strains that are to produce ornibactin, but not pyochelin, also display a large yellow/orange halo around their area of bacterial growth on CAS medium. Due to the high structural similarity between ornibactin and malleobactin, it is highly likely the yellow colour observed in Figure 4.15 derives from metal chelation by malleobactin. The loss of the *mbaS* gene, and therefore the assumed loss of malleobactin synthesis, is the most likely explanation for the loss of this yellow halo in the Δ*mbaS* mutant. An orange halo can be obseerved around the growth of the Δ*mbaS* mutant strain. It is likely that this orange colour derives from the secondary siderophore pyochelin. *Bce* grown on CAS medium that produce pyochelin, but not ornibactin, are characterised by red/violet halos.
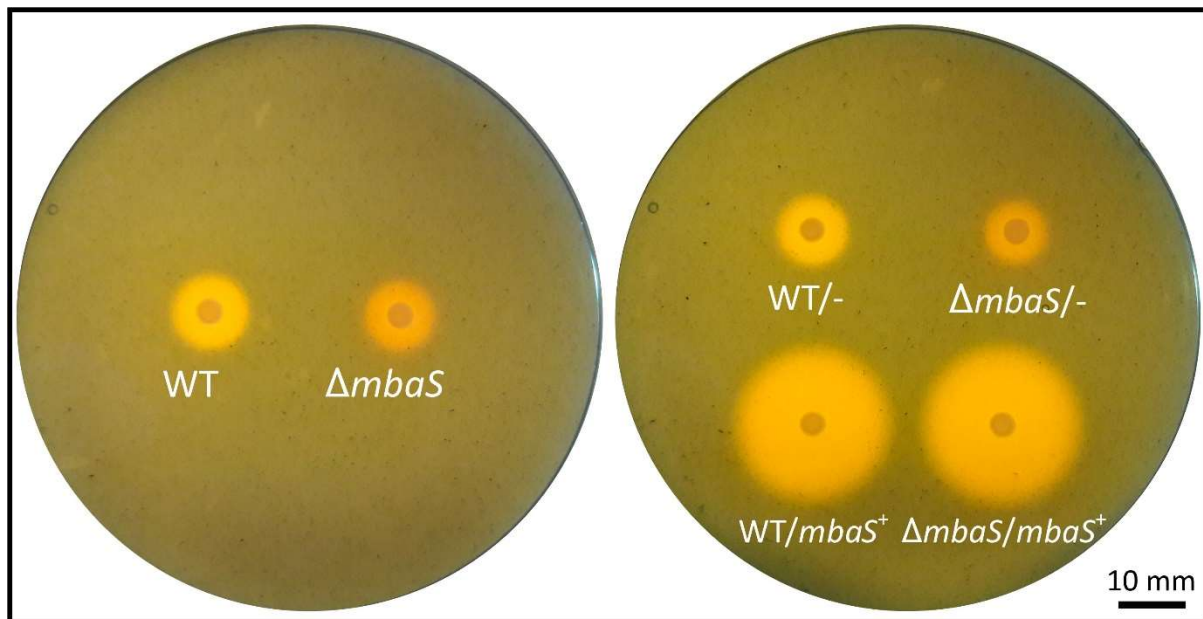
Figure 4.15. *Burkholderia thailandensis* **E264 Δ*mbaS* grown on CAS agar**

Bacterial cultures of *Bth* grown on CAS agar containing 10 μM FeCl$_3$. Cultures were incubated at 30 °C for approximately 48 hours (more detail provided in text). **Left.** *Bth* E264 (WT) and *Bth* E264 Δ*mbaS*. **Right.** *Bth* E264/pBBR2 (WT/-), *Bth* E264/pBBR2-*mbaS* (WT/*mbaS*$^+$), *Bth* E264 Δ*mbaS*/pBBR2 (Δ*mbaS*/-); *Bth* E264 Δ*mbaS*/pBBR2-*mbaS* (Δ*mbaS*/*mbaS*$^+$).

Providing further verification that the yellow halo colour on CAS agar is due to malleobactin, complementation of *Bth* with the plasmid pBBR2-*mbaS* gives rise to large yellow halos produced around the bacterial growth. These halos are larger than are observed for *Bth* that are not harbouring plasmid DNA. This suggests that pBBR2-*mbaS* is able to express and produce MbaS in much greater quantities than is achieved from the chromosomal copy of the gene, and that this has increased the MbaS-dependent transcription of the *mba* gene cluster. Hence, more malleobactin has been produced and secreted, giving rise to a greater yellow area due to iron-chelation and release of CAS dye.

Bth E264 wild-type and Δ*pchE* strains were grown on CAS agar to verify and analyse the effect of the *pchE* deletion in *Bth* E264 Δ*pchE*. This gene deletion was complemented in cells harbouring pBBR2-*pchE* (Figure 4.16).
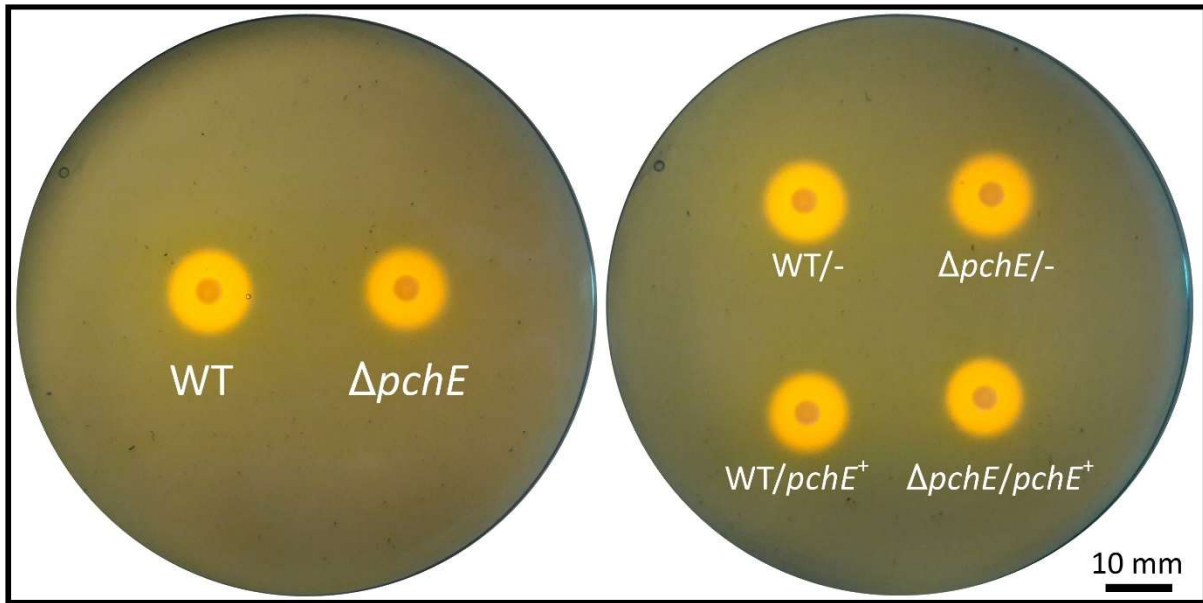
Figure 4.16. *Burkholderia thailandensis* **E264 Δ*pchE* grown on CAS agar**

Bacterial cultures of *Bth* grown on CAS agar containing 10 µM FeCl$_3$. Cultures were incubated at 30 °C for approximately 48 hours (more detail provided in text). **Left.** *Bth* E264 (WT) and *Bth* E264 Δ*pchE*. **Right.** *Bth* E264/pBBR2 (WT/-), *Bth* E264/pBBR2-*pchE* (WT/*pchE*+), *Bth* E264 Δ*pchE*/pBBR2 (Δ*pchE*/-); *Bth* E264 Δ*pchE*/pBBR2-*pchE* (Δ*pchE*/*pchE*+).

The *Bth* strains grown in Figure 4.16 ubiquitously displayed yellow halos around their bacterial growth on CAS medium regardless of whether *pchE* is deleted. This yellow halo is assumed to be due to the metal-chelation by malleobactin. In isolation, this makes it difficult to judge whether the Δ*pchE* allele has been successfully introduced.

However, the Δ*mbaS* was introduced into *Bth* E264 Δ*pchE* to generate *Bth* E264 Δ*mbaS* Δ*pchE*. Therefore, assuming there were no secondary site mutations co-introduced during the *mbaS* mutagenesis, the Pch⁻ phenotype of *Bth* E264 Δ*mbaS* Δ*pchE* should be consistent with the Pch⁻ phenotype of *Bth* E264 Δ*pchE*.

Bth E264 wild-type and *Bth* E264 Δ*mbaS* Δ*pchE* strains were grown on CAS agar to verify and analyse the effect of the *mbaS* and *pchE* deletions in *Bth* E264 Δ*mbaS* Δ*pchE*. These gene deletions were complemented in cells harbouring pBBR2-*mbaS* or pBBR2-*pchE* (Figure 4.17).
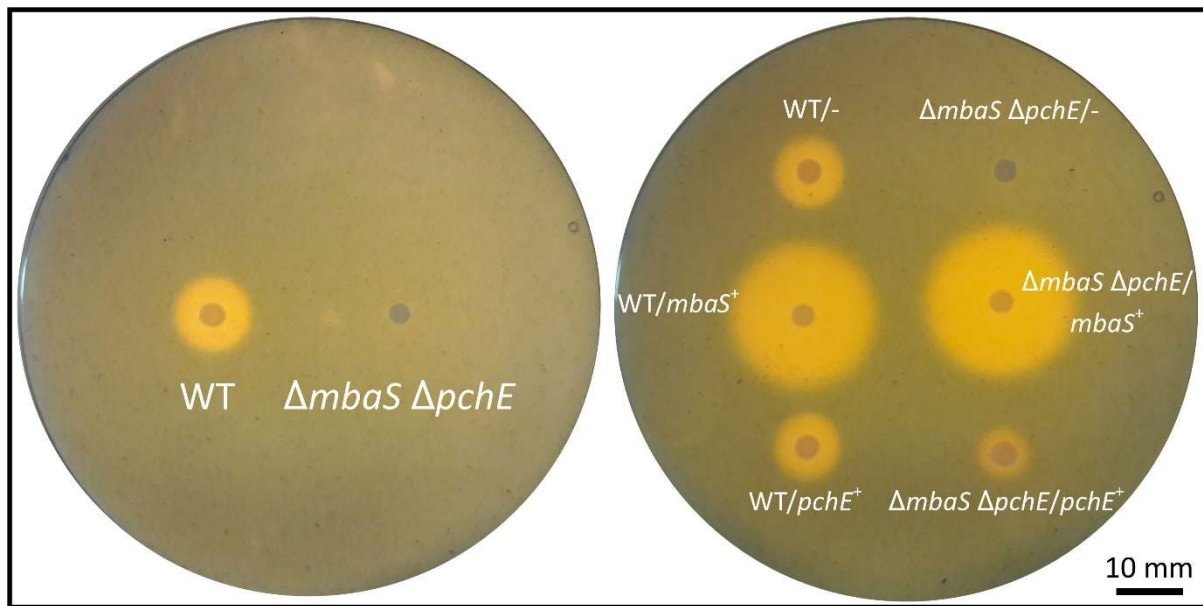
Figure 4.17. *Burkholderia thailandensis* E264 Δ*mbaS* Δ*pchE* grown on CAS agar

Bacterial cultures of *Bth* grown on CAS agar containing 10 μM FeCl₃. Cultures were incubated at 30 °C for approximately 48 hours (more detail provided in text). **Left.** *Bth* E264 (WT) and *Bth* E264 Δ*mbaS* Δ*pchE*. **Right.** *Bth* E264/pBBR2 (WT/-), *Bth* E264/pBBR2-*mbaS* (WT/*mbaS*⁺), *Bth* E264/pBBR2-*pchE* (WT/*pchE*⁺), *Bth* E264 Δ*mbaS* Δ*pchE*/pBBR2 (Δ*mbaS* Δ*pchE*/-), *Bth* E264 Δ*mbaS* Δ*pchE*/pBBR2-*mbaS* (Δ*mbaS* Δ*pchE*/*mbaS*⁺), *Bth* E264 Δ*mbaS* Δ*pchE*/pBBR2-*pchE* (Δ*mbaS* Δ*pchE*/*pchE*⁺).

The area of growth of *Bth* E264 Δ*mbaS* Δ*pchE* mutant did not show a distinctive halo in CAS agar (Figure 4.17. left). This was consistent with an Mba⁻ Pch⁻ phenotype, as there should be no iron-chelating siderophores produced by these strains. This strongly suggested that both *mbaS* and *pchE* have successfully been deleted. To verify this further, this *Bth* strain was complemented using pBBR2-*mbaS* and pBBR2-*pchE* (Figure 4.17, right). Both the Mba⁺ phenotype was restored (as judged by a large yellow halo), and the Pch⁺ phenotype was restored (as judged by a small orange halo). Taken together, the phenotypes of these *Bth* strains, and their *in trans* complementation, suggest it is very likely that both the Δ*mbaS* and Δ*pchE* alleles have been successfully introduced, and that they display the Mba⁻ and Pch⁻ phenotypes, respectively.

The phenotypes of the constructed *Bth* mutants grown on CAS agar are compared in Figure 4.18. Growth of wild-type *Bth* E264 and *Bth* E264 Δ*pchE* on CAS medium are surrounded by a yellow halo. This is assumed to be due to chelation of exogenous ferric iron by secreted malleobactin. Growth of *Bth* E264 Δ*mbaS* on CAS medium is surrounded by an orange halo.

This is assumed to be due to the chelation of exogenous ferric iron by secreted pyochelin. No such halos were observed around growth of *Bth* E264 Δ*mbaS* Δ*pchE*. This is assumed to be due to inability to produce either malleobactin or pyochelin, hence no chelation of exogenous ferric iron is observed.
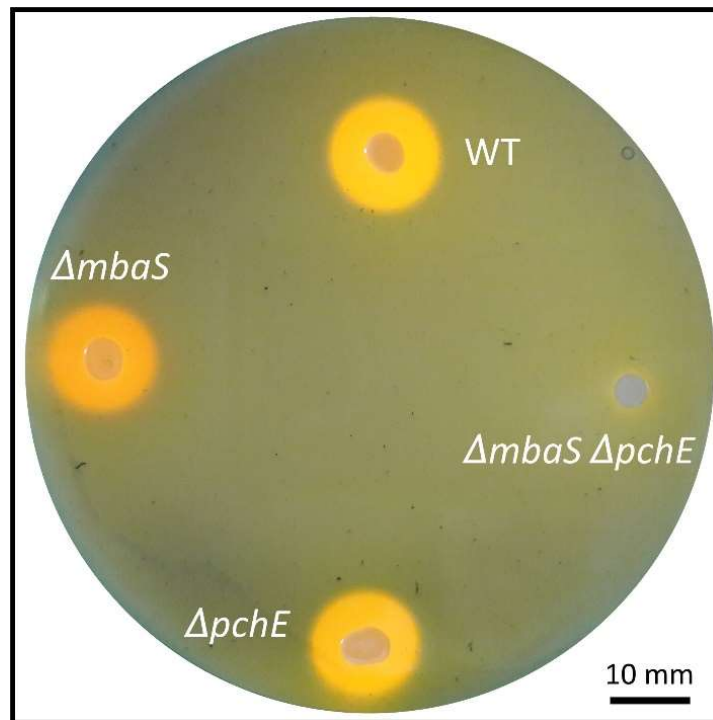
Figure 4.18. *Burkholderia thailandensis* **E264 mutant strains grown on CAS agar**

Bacterial cultures of *Bth* grown on CAS agar containing 10 μM FeCl₃. Cultures were incubated at 30 °C for approximately 48 hours (more detail provided in text). Bacterial cultures grown are *Bth* E264 (WT), *Bth* E264 Δ*mbaS*, *Bth* E264 Δ*pchE* and *Bth* E264 Δ*mbaS* Δ*pchE*.

4.7.3   Effect of temperature upon production of pyochelin

During the phenotypic characterisation of the *Bth* E264 siderophore deficient mutants, it was observed that the presence and area of the siderophore halo resulting from the secretion of pyochelin varied depending on incubation temperature. More specifically, plates grown at 37 °C appeared to show smaller halo areas due the secretion of iron chelating compounds (pyochelin) than those grown at 30 °C, and the pyochelin-derived halo was initially observed after longer incubation time compared to the malleobactin-derived halo.

This phenomenon was investigated further by growing Mba⁻ Pch⁺ *Bth* strains on CAS agar. *Bth* E264 Δ*mbaS* was grown in M9 minimal medium supplemented with 0.5% (w/v) glucose, and *Bth* E264 Δ*mbaS* Δ*pchE*/pBBR2-*pchE* was grown in the same medium supplemented with 250 µg ml⁻¹ kanamycin. After normalisation, 1 µl of each bacterial culture was spotted onto CAS agar plates containing 10 µM $FeCl_3$, and incubated at a range of temperatures. Images of the cultures were taken at a range of time points (Figure 4.19).
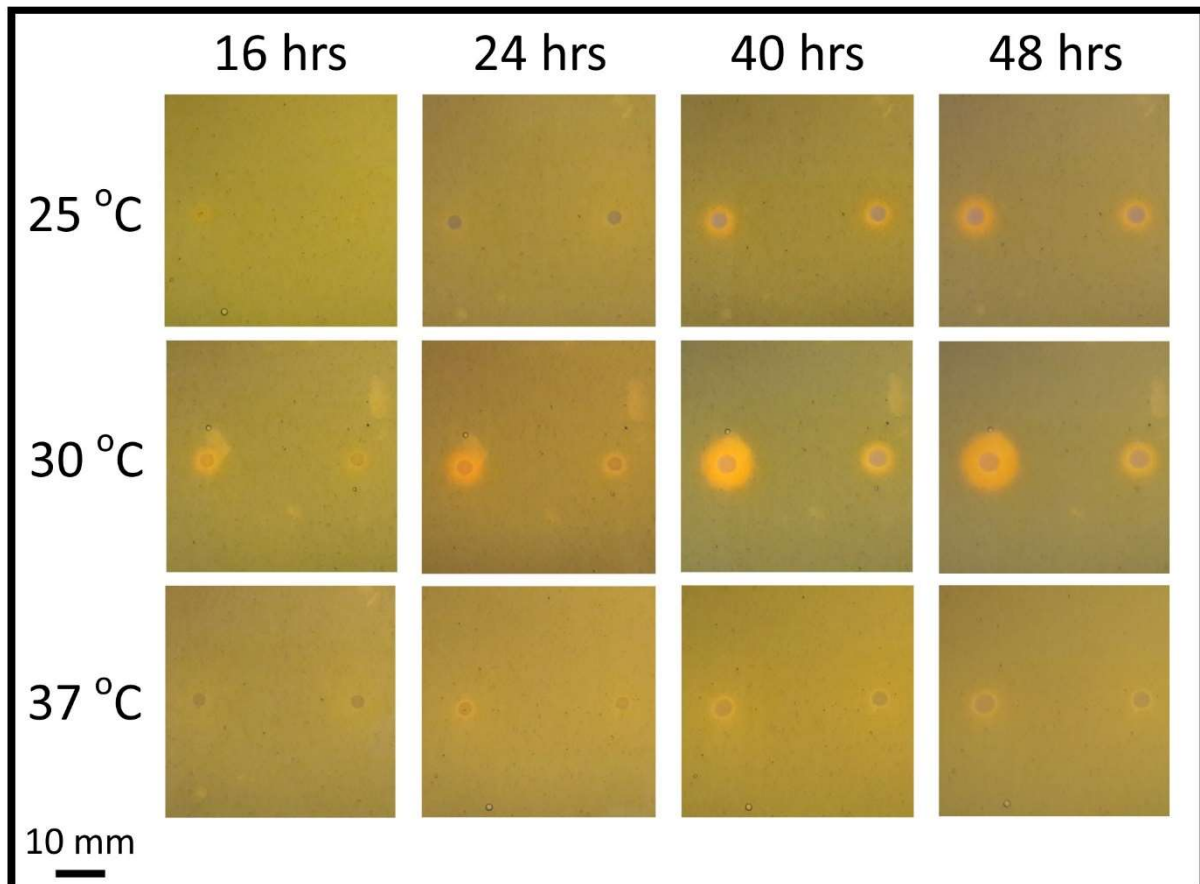
Figure 4.19 Effect of temperature upon production of pyochelin in *Burkholderia thailandensis* E264

Bacterial cultures of *Bth* grown on CAS agar containing 10 µM $FeCl_3$. Cultures were incubated at 25 °C, 30 °C or 37 °C. Each agar plate was imaged after approximately 16, 24, 40 and 48 hours of incubation. In each image, the bacterial cultures grown are: **Left:** *Bth* E264 Δ*mbaS*, **Right:** *Bth* E264 Δ*mbaS* Δ*pchE*/pBBR2-*pchE*.

The halos visible around these cultures suggest that pyochelin was secreted in greater quantities when grown at 30 °C, compared to when grown at 25 °C and 37 °C. Even when grown at 25 °C, the *Bth* cultures secreted more pyochelin then when grown at 37 °C. Furthermore, it typically took around 16 hours at 30 °C for the appearance of a yellow halo

166

(derived from malleobactin-mediated iron chelation) of considerable area to be observed around the growth of *Bth.* It took around 48 hours at 30°C for the appearance of an orange halo (derived from pyochelin-mediated iron chelation) of a similar area to be observed around the growth of *Bth*.

4.7.4   Comparison of bacterial growth rates of *Bth* mutants

To determine the effect that the *mbaS* and *pchE* gene deletions had upon the growth of *B. thailandensis* grown in minimal medium, the growth curves and rates of the strains were compared. Additionally, to demonstrate the complementation of the Δ*mbaS* and Δ*pchE* mutants, pBBR2-*mbaS* and pBBR2-*pchE* were introduced into these strains, and the growth curves and rates also compared. Bacterial growth curves were generated, and growth rates were calculated, according to the protocol in section 2.1.1.

The effect of the Δ*mbaS* deletion was investigated by comparison of wild-type *Bth* E264 and *Bth* E264 Δ*mbaS*. Both of these strains, harbouring either pBBR1MCS-2 or pBBR2-*mbaS*, were grown in M9 minimal medium containing 0.5% (w/v) glucose, 0.1% (w/v) casamino acids, and 250 µg ml^{-1} kanamycin (Figure 4.20). The OD$_{600}$ of these bacterial cultures was recorded every 30 minutes once the cultures were judged to have reached log phase.

The Δ*mbaS* mutant displays a lower growth rate compared to the wild-type. However, this appears to be somewhat alleviated by the *in trans* addition of MbaS. This confirms that MbaS, and by extension malleobactin, are factors for the growth of *Bth* under iron-limited conditions. It also provides further verification the Δ*mbaS* allele was implemented as intended.

The effect of the Δ*pchE* deletion was also investigated using the same conditions by comparison of wild-type *Bth* E264 and *Bth* E264 Δ*pchE*. These strains harboured either pBBR2 or pBBR2-*pchE*, and were grown in M9 minimal medium containing 0.5% (w/v) glucose, 0.1% (w/v) casamino acids, and 250 µg ml^{-1} kanamycin (Figure 4.21).
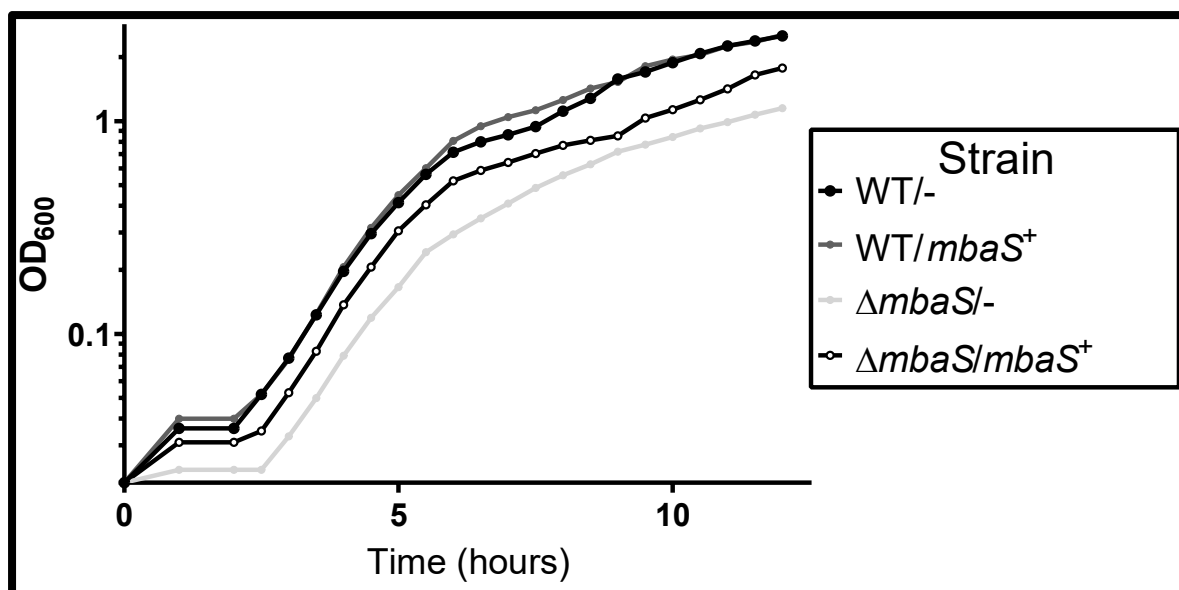
Figure 4.20. *Burkholderia thailandensis* E264 Δ*mbaS* growth curve

Burkholderia thailandensis E264 wild-type and Δ*mbaS* strains complemented with pBBR1MCS-2-*mbaS* grown in M9 minimal salts medium supplemented with 0.5% (w/v) glucose, 0.1% (w/v) casamino acids and 250 µg ml^{-1} kanamycin (n=1).

Table 4.1. Growth rate of *Bth* E264 and *Bth* E264 Δ*mbaS* supplied with *mbaS in trans*.

Strain	Growth rate (doubling hr^{-1}) [1]	
	pBBR1MCS-2 [2]	pBBR2-*mbaS* [2]
Bth E264	1.16	0.99
Bth E264 Δ*mbaS*	1.07	0.86

[1] Growth rates for the indicated strains were calculated as described in section 2.1.1, using the curves shown in Figure 4.20.
[2] Strains contained either pBBR1MCS-2 or pBBR2-*mbaS*, as indicated
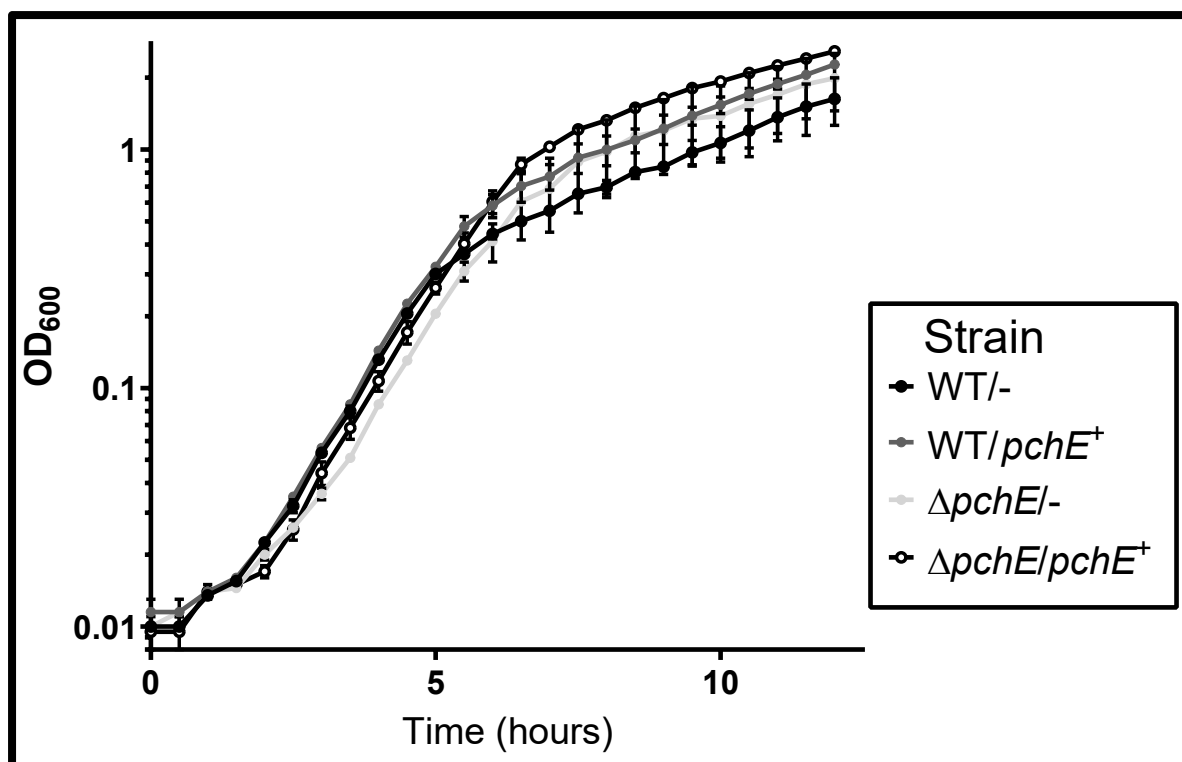
Figure 4.21. *Burkholderia thailandensis* E264 Δ*pchE* growth curve

Burkholderia thailandensis E264 wild-type and Δ*pchE* strains complemented with pBBR2-*pchE* grown in M9 minimal salts medium supplemented with 0.5% (w/v) glucose, 0.1% (w/v) casamino acids and 250 μg ml^{-1} kanamycin. Error bars show SEM (n=2).

Table 4.2. Growth rate of *Bth* E264 and *Bth* E264 Δ*pchE* supplied with *pchE in trans*.

Strain	Growth rate (doubling hr^{-1}) [1]	
	pBBR1MCS-2 [2]	pBBR2-*pchE* [2]
Bth E264	0.97	0.85
Bth E264 Δ*pchE*	0.82	0.79

[1] Growth rates for the indicated strains were calculated as described in section 2.1.1, using the curves shown in Figure 4.21.
[2] Strains contained either pBBR1MCS-2 or pBBR2-*pchE*, as indicated

This mutation appears less significant compared to the loss of *mbaS*, as there is no significant difference between the growth curves of the grown bacterial cultures. This is consistent with previous assertions that malleobactin is the major siderophore used by *Bth* and pyochelin is less significant to the bacteria's survival.

Aditionally, the growth rates of all of the generated *Bth* strains, including *Bth* E264 Δ*mbaS* Δ*pchE*, were investigated. These strains were grown in M9 minimal medium containing 0.5% (w/v) glucose, 0.1% (w/v) casamino acids. The effect of further iron starvation was examined by supplementing the growth medium with 100 µM 2,2-dipyridyl (Figure 4.22).
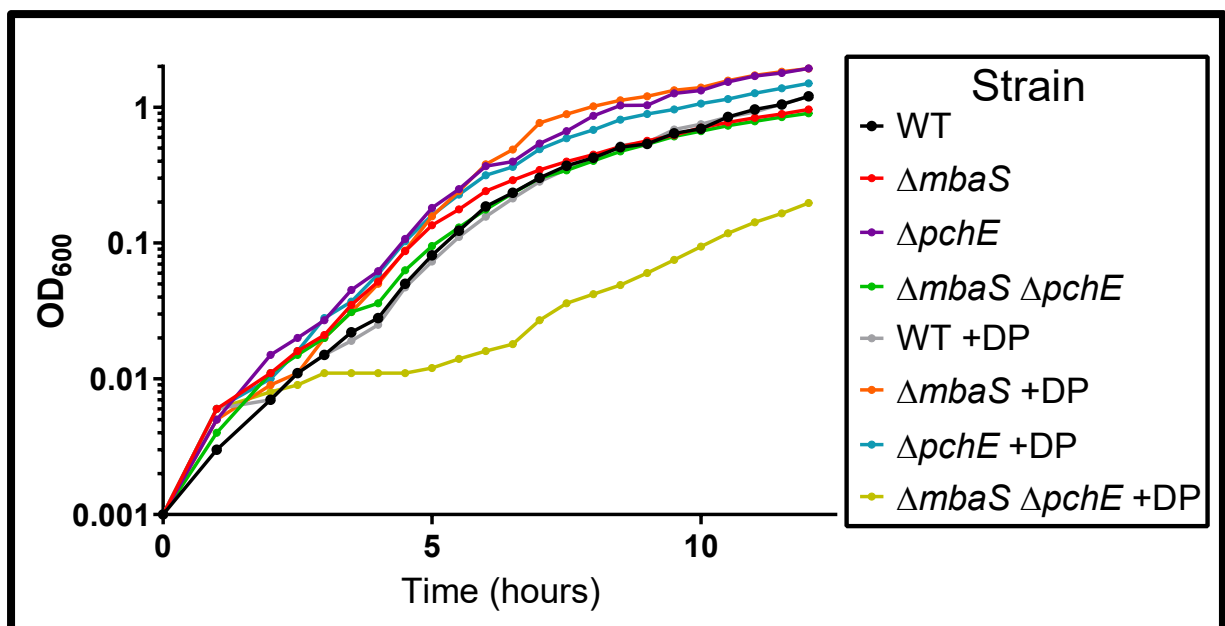
Figure 4.22. *Burkholderia thailandensis* **E264 Δ*mbaS* Δ*pchE* growth curve**

Burkholderia thailandensis E264 wild-type, Δ*mbaS*, Δ*pchE* and Δ*mbaS* Δ*pchE* strains grown in M9 minimal salts medium supplemented with 0.5% (w/v) glucose and 0.1% (w/v) casamino acids, and 100 µM 2,2-dipyridyl where indicated by '+DP' (n=1).

Table 4.3. Growth rate of *Bth* E264, *Bth* E264 Δ*mbaS*, *Bth* E264 Δ*pchE* and *Bth* E264 Δ*mbaS* Δ*pchE*.

Strain	Growth rate (doubling hr^{-1}) [1]	
	0 µM DP	100 µM DP
Bth E264	0.78	0.80
Bth E264 Δ*mbaS*	0.88	0.69
Bth E264 Δ*pchE*	0.81	0.81
Bth E264 Δ*mbaS* Δ*pchE*	0.92	3.54

[1] Growth rates for the indicated strains were calculated as described in section 2.1.1, using the curves shown in Figure 4.22.

There are only small differences in the growth rates of all of the grown bacteria cultures, in the absence and presence 100 µM 2,2-dipyridyl. The exception to this is the growth of *Bth* E264 Δ*mbaS* Δ*pchE* grown with 100 µM 2,2-dipyridyl, which has a significantly slower growth rate than the other strains. The effect of deleting both siderophores appears to have a greater effect than deleting either malleobactin or pyochelin individually.

In all of the *Bth* E264 growth curves, any difference due to the effect of deleting either *mbaS* or *pchE* appears to take place at the lag phase of growth. Furthermore, given that the secretion of pychelin is lower at 37 °C than at 30 °C (Figure 4.19), and in these experiments the bacteria were grown at 37 °C, the analysis of the effect of deleting *pchE* may be limited.

4.7.5 Comparison of *mbaS*-dependent promoter activity in Δ*mbaS* mutants

In order to confirm the loss of the *mbaS* gene in the mutants Δ*mbaS* and Δ*mbaS* Δ*pchE*, the activity of the ECF sigma factor upon its putative target promoter was compared by a β-galactosidase assay.

The DNA fragments containing the putative MbaS target promoter P*mbaH* and the *mbaS* promoter P*mbaS* were cloned into the transcriptional *lacZ* reporter plasmid pKAGd4 (Agnoli *et al.*, 2006). The promoter DNA was cloned into the MCS upstream of the promoter-less *lacZ* gene, allowing the promoter activity of the cloned DNA to be assayed by performing β-galactosidase assays. For each promoter, a 'long' DNA fragment of ~250 bp was cloned (to be distinguished from the 'short' promoters in section 5.2.2).

The 'long' *mbaS* promoter, P*mbaS-L*, was amplified using primers pmbaS-long-fwd and pmbaS-long-rev to produce a 186 bp PCR product, and the 'long' *mbaH* promoter, P*mbaH-L,* was amplified using primers pmbaH-long-fwd and pmbaH-long-rev to produce a 274 bp PCR product, by PCR from *Bth* E264 genomic template DNA. The cloned DNA was inserted between the *Hin*dIII and *Bam*HI sites of pKAGd4 to give the plasmids pKAGd4-P*mbaS-L* and pKAGd4-P*mbaH-L.* The identity of each plasmid construct was confirmed by PCR screening and DNA sequencing analysis using the primer AP10.

pKAGd4-P*mbaS-L* and pKAGd4-P*mbaH-L* were introduced into *Bth* E264, *Bth* E264 Δ*mbaS* and *Bth* E264 Δ*mbaS* Δ*pchE* by conjugation via *E. coli* S17-1 donor cells. The β-galactosidase assay was performed on cultures grown in M9 minimal medium, supplemented with 0.1% (w/v) casamino acids, 0.5% (w/v) glucose and 50 µg ml^{-1} chloramphenicol, according to the protocol outlined in section 2.5.1. The experiment was performed a total of three times across three days (Figure 4.23).
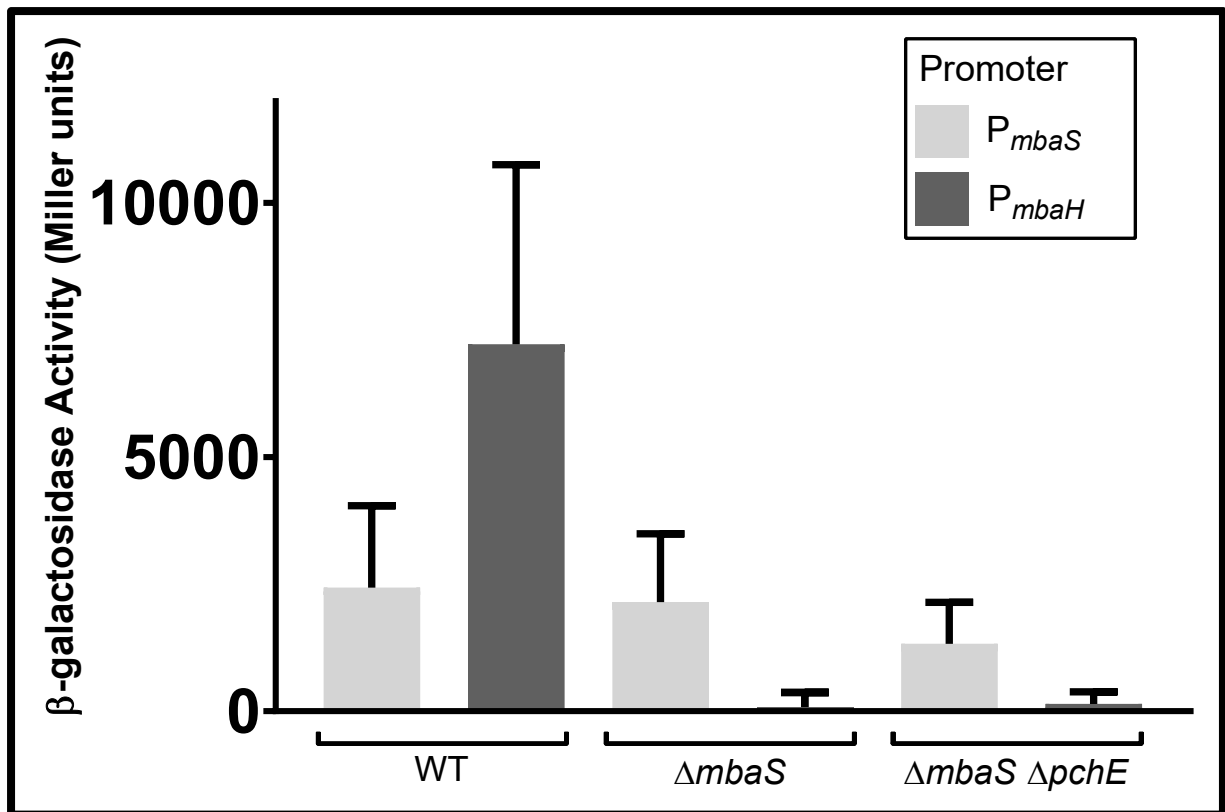
Figure 4.23. β-galactosidase assay of P*mbaS* and P*mbaH* in *B. thailandensis* E264 Δ*mbaS* mutants

β-galactosidase activity was measured in *Bth* E264 wild-type, Δ*mbaS* and Δ*mbaS* Δ*pchE* (denoted below data bars). Cells harboured either pKAGd4-P*mbaS-L* (light grey) or pKAGd4-P*mbaH-L* (dark grey). All β-galactosidase activities were corrected for the background vector activity by subtraction of activity derived from the same *Bth* E264 strain harbouring the parental plasmid pKAGd4. Error bars show standard deviation (n=9). Growth medium was M9 minimal salts medium supplemented with 0.5% (w/v) glucose, 0.1 % (w/v) casamino acids and 50 μg ml^{-1} chloramphenicol.

The activity from the *mbaS* remained at a consistent level in all of the assayed bacteria. However, the activity of the *mbaH* promoter was high in the wild-type strains, and completely abolished in the strains with the *mbaS* gene deletion. These observations are consistent with the hypothesis that *mbaS* promoter is acted upon by σ^{70}, and that the *mbaH* promoter is acted upon by MbaS (this is investigated further in section 5.2).

4.8 Identification of *B. thailandensis* E264 strain variant

During the process of this research, it was discovered there were two strain variants of *Bth* E264 in use. The strain used first, hereafter denoted as E264a, showed many key differences in comparison to the reference strain, hereafter denoted as E264b. These differences include colony morphology, antibiotic resistance, secretion of siderophores and sigma factor activity. Many DNA products were amplified by PCR from *Bth* E264a genomic DNA, but cloned DNA showed no difference from the reference *Bth* E264 genome. In the following section, figures and data are presented that uses *Bth* E264a – this has been clearly denoted. In all other experiments in this thesis, where the particular strain is not specified, the *Bth* E264b strain has been used.

4.8.1   Morphological distinction

The most striking difference between *Bth* E264a and *Bth* E264b is their colony morphology (Figure 4.24). *Bth* E264a produces smaller, circular, opaque colonies, whereas *Bth* E264b produces larger, circular, translucent colonies. This was observed when the bacteria were grown on both rich (LB) and limited (M9 minimal) media.
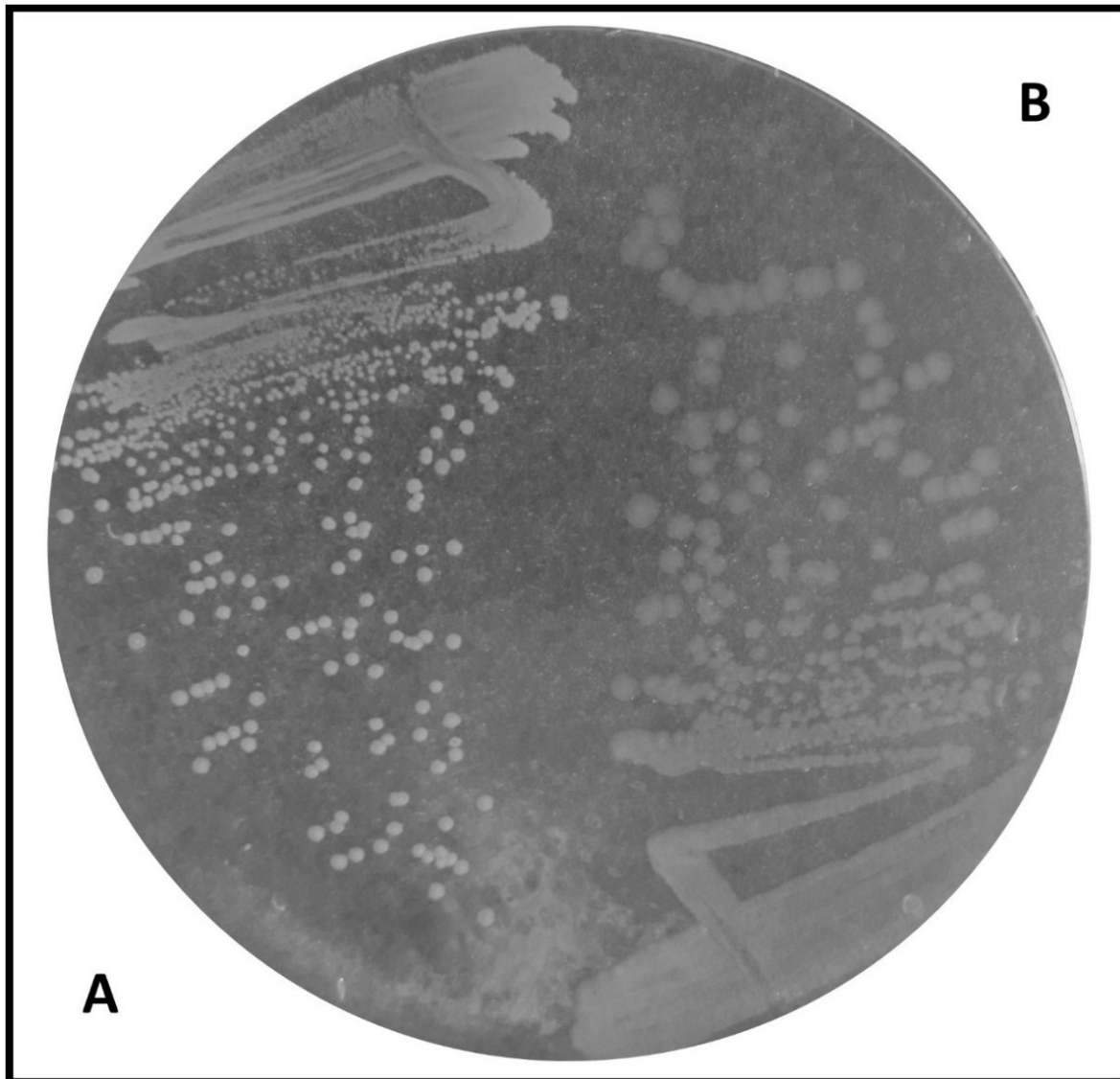
Figure 4.24. *Burkholderia thailandensis* **E264 Strains Colony Formation**

Burkholderia thailandensis E264 strains on M9 minimal agar supplemented with 0.5% (w/v) glucose and 0.1% (w/v) casamino acids. **A**: *Bth* E264a; **B**: *Bth* E264b.

4.8.2 Malleobactin secretion and transcriptional control of associated genes

In promoter reporter assays performed in *Bth* E264a, lower promoter activities than expected were consistently observed, irrespective of the DNA fragment containing putative promoters. This was explored further by direct comparison with *Bth* E264b. The relative promoter activity of two promoters was assayed; the σ^{70}-dependent P$_{mbaS}$ and the MbaS-dependent P$_{mbaH}$.

The pKAGd4 reporter vectors pKAGd4-P$_{mbaS-F}$ and pKAGd4-P$_{mbaH-F}$ (described in section 4.7.5) were introduced into *Bth* E264a and *Bth* E264b by conjugation via *E. coli* S17-1 donor cells. The β-galactosidase assay was performed in LB medium, supplemented with 100 µg ml^{-1} ampicillin according to the protocol outlined in section 2.5.1. The experiment was performed a total of three times across different days (Figure 4.25).
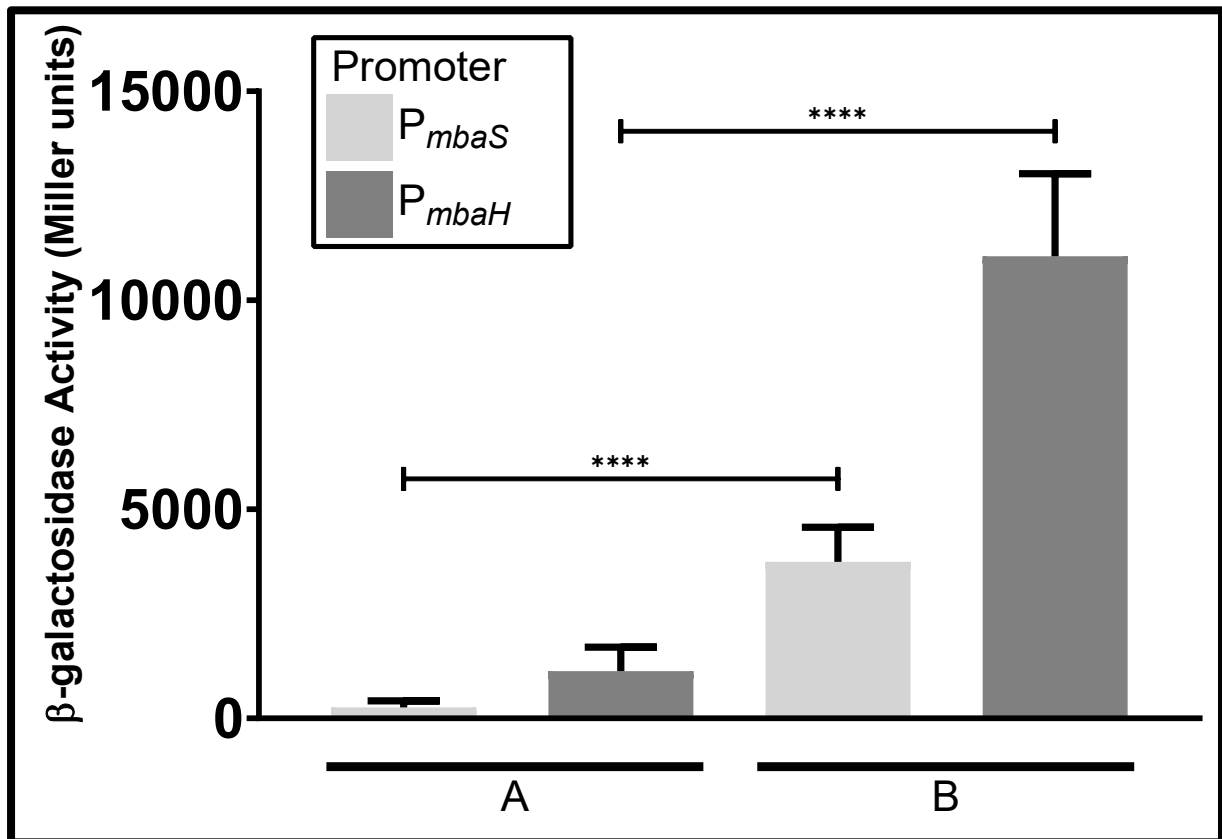
Figure 4.25. β-galactosidase assay of *B. thailandensis* E264a and E264b upon P$_{mbaS}$ and P$_{mbaH}$

β-galactosidase assays were performed in the *Bth* strains E264a and E264b (denoted below data bars). Cells harboured either pKAGd4-P$_{mbaS-F}$ (light grey) or pKAGd4-P$_{mbaHF}$ (dark grey). All β-galactosidase activities were corrected for the background vector activity by subtraction of activity derived from the same *Bth* E264 strain harbouring the parental plasmid pKAGd4. Growth medium was LB medium supplemented with 100 µg ml^{-1} ampicillin. Error bars show standard deviation (n=9).

In the promoter reporter assays shown in Figure 4.25, there was a statistically significant difference between groups (one-way ANOVA, F=174.8, P<0.0001). Tukey's multiple comparisons post hoc tests reveal that *Bth* E264a displays significantly lower transcriptional activity than *Bth* E264b. The activity from P$_{mbaS}$ was approximately 93% lower for E264a than for E264b (P<0.0001), and the activity from P$_{mbaH}$ was approximately 90% lower for E264a

than for E264b (P<0.0001). The low activity of the P_{mbaH} promoter is likely due to the same factors that result in the low activity of the P_{mbaS} promoter, as these would have an accumulative effect on the amount of MbaS present in the cell.

Furthermore, the activity of the MbaS regulon, and the production of malleobactin, was compared by growing the two strains of *Bth* E264 on CAS agar. Overnight cultures of both *Bth* E264a and *Bth* E264b were grown in LB medium, and 1 µl of normalised cultures of each were spotted on CAS medium containing 10 µM FeCl$_3$ (Figure 4.26).
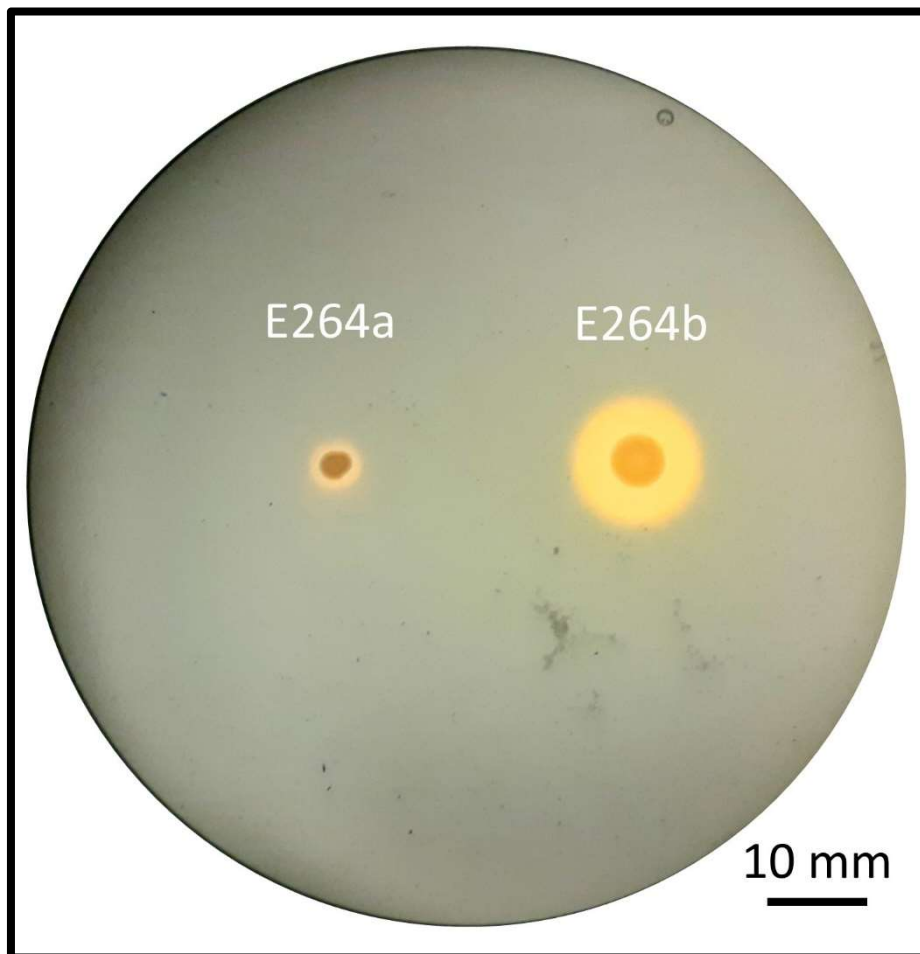
Figure 4.26. *Burkholderia thailandensis* **E264 Strains Colony Formation**

Burkholderia thailandensis E264 strains on CAS agar containing 10 µM FeCl$_3$. **A**: *Bth* E264a; **B**: *Bth* E264b.

Comparing the halos observed around growth of each bacterial strain on CAS agar, it is clear that *Bth* E264a produces a much smaller halo around the area of bacterial growth compared

to the large yellow halo produced around *Bth* E264b. This suggest that E264a produces less iron-chelating compound (likely predominantly malleobactin) than E264b. This could be linked the transcriptional activity data observed in Figure 4.25.

4.9 <u>Discussion</u>

In this chapter, the gene deletion mutant alleles Δ*mbaS*, Δ*pchE* and Δ*fur* (plus Δ*fur*::TpTer), and the substitution mutants alleles *mbaS*$_{C203+206A}$ (*mbaS*$_{CdiA}$), *mbaS*$_{C203+206+216+220A}$ (*mbaS*$_{CtetraA}$) and *mbaS*$_{C203+206+216+220+230A}$ (*mbaS*$_{CpentaA}$), were constructed using SOE-PCR. The mutant alleles were cloned into allelic exchange vectors to enable in-frame gene deletions or substitutions to be introduced into *Bth*.

The Δ*mbaS* and Δ*pchE* deletion alleles were successfully introduced to generate *Bth* E264 Δ*mbaS*, *Bth* E264 Δ*pchE* and *Bth* E264 Δ*mbaS* Δ*pchE*. These mutant strains were phenotypically characterised to verify the gene deletions and demonstrate the resulting loss of malleobactin and pyochelin production. However, attempts at introducing the Δ*fur*/Δ*fur*::TpTer and *mbaS*$_{CdiA}$/*mbaS*$_{CtetraA}$/*mbaS*$_{CpentaA}$ alleles was not achieved. All three of the allelic exchange vectors pEX18Tp-*pheS*, pSNUFF3Cm and pSHAFT2, containing the mutant alleles, successfully integrated into *Bth* chromosomal DNA to generate co-integrant strains. However, the stimulation of a second recombination event that excised the integrated plasmid and gave the desired gene deletion proved to be difficult. For the introduction of the Δ*pchE* allele using pSNUFF3Cm-Δ*pchE*, of the 50 candidate colonies that displayed tetracycline resistance (specified by pDAI-SceI-*pheS*) and chloramphenicol sensitivity (due to loss of the pSNUFF3Cm vector backbone), only one candidate colony had resolved the co-integrant state and retained the desired Δ*pchE* allele. For the introduction of the Δ*mbaS* allele into *Bth* using pEX18Tp-*pheS*-Δ*mbaS*, 600 candidate colonies in total (300 colonies each for the generation of *Bth* E264 Δ*mbaS* and *Bth* E264 Δ*mbaS* Δ*pchE*) displayed cPhe resistance (due to loss of the pEX18Tp-*pheS* vector backbone). Of these 600 colonies, only three colonies that had resolved the co-integrant state and retained the

desired Δ*mbaS* allele (two for *Bth* E264 Δ*mbaS*, one for *Bth* E264 Δ*mbaS* Δ*pchE*). Several hundred candidate colonies for the introduction of the *fur* deletion and the *mbaS*$_{CpentaA}$ replacement were isolated, but none possessed the desired mutant allele. These allelic exchange vectors have been shown to be effective in several species of *Burkholderia* (Barrett *et al.*, 2008; Shastri *et al.*, 2017)(H. Spiewak, unpublished). Indeed, pSNUFF3Cm was used to introduce gene deletions successfully in *Bce* (see Chapter VI). Therefore, it appears these allelic exchange vectors have poor efficiency in *Bth*. It is unclear what factors specific to *Bth* may affect this efficiency of mutant generation, but problems arose at the stage of resolving the co-integrant state of the *Bth* cells. It is likely that this was not specific to the mutant allele being introduced, as introduction of the *mbaS*$_{CpentaA}$ allele into *Bth* E264 Δ*mbaS* (which should introduce a relative advantageous phenotype) also proved to be difficult.

With regards to attempts to introduce the Δ*fur* mutation, the potentially essential nature of the global repressor may have contributed to the inability to isolate a gene deletion mutant. Efforts were made to overcome this in several ways. Mutagenesis was performed using EB agar, a partially nutrient-limited medium that has been demonstrated to support growth of a *Burkholderia multivorans fur* mutant (Yuhara *et al.*, 2008). Additionally, usage of a marked mutant allele conferring trimethoprim resistance was attempted in order introduce a selective advantage to *fur* null mutants. This was performed in *Bth* Mba⁻ and Pch⁻ strains, which could have decreased the excess of intracellular iron that may have been toxic for a *fur* mutant. Although none of these attempts worked, the choice of medium may have a significant effect upon the viability of *fur* null *Bth* mutants. Efforts could be made in the future to rationally select a different growth medium to generate a *Bth* Δ*fur* mutant, in which the *fur* gene is not essential. Despite this, it cannot be precluded that Fur is an essential protein in *Bth*.

The *Bth* E264 Δ*mbaS*, Δ*pchE* and Δ*mbaS* Δ*pchE* strains had their specific gene deletions verified *in vivo* by complementation with pBBR2-*mbaS* and pBBR2-*pchE*. However, *Bth* E264 Δ*pchE* displayed no observable phenotypic difference to the wild-type, making it difficult to confirm the *pchE* deletion and the complementation of this gene deletion. However, in combination with the phenotypic characterisation of the *Bth* E264 Δ*mbaS* and *Bth* E264 Δ*mbaS* Δ*pchE* it is unlikely that the gene deletions were not introduced as expected.

Additionally, when *Bth* was grown on CAS agar, the large yellow halo was assigned as being produced due to the secretion of malleobactin, and the large orange halo was assigned as the result of pyochelin production. This is assumption is based upon the known functions of the *mbaS* and *pchE* genes. However, empirical identification of these siderophores could be achieved by siderophore cross-feeding assays and/or isolation of the siderophore and mass spectroscopic analysis.

Assuming that the orange halo produced around *Bth* cultures when grown on CAS agar is due to the activity of pyochelin, there appears to be an effect of temperature upon pyochelin production. Two different Pch+ *Bth* cells cultures were used – the first produced pyochelin using a chromosomal copy of PchE (*Bth* E264 Δ*mbaS*), and the second produced pyochelin using the plasmid-based copy of PchE (*Bth* E264 Δ*mbaS* Δ*pchE*/pBBR2-*pchE*). Both strains display similar patterns of halo production on CAS agar. The explanation for this effect of temperature upon the production of pyochelin is unclear, and may be worthy of further investigation.

Finally, during the course of this study a strain variant of *Bth* E264 was discovered. Using a *Bth* strain (now designated as *Bth* E264a) originating from the Titball research group at the University of Exeter, attempts were made to analyse the production of siderophores by growing the bacteria on CAS agar. The failure of this strain to produce a large halo due to siderophore secretion prompted comparison with another *Bth* E264 strain (now designated as *Bth* E264b) originating from the Hertweck research group at the Leibniz Institute for Natural Product Research and Infection Biology. This second *Bth* E264 strain was able to produce a much larger halo due to siderophore secretion when grown on CAS agar, indicating the presence of two strain variants. Many experiments were performed in *Bth* E264a, until it was recognised as a strain variant. These experiments were repeated in *Bth* E264b. The discovery of this strain variant perhaps demonstrates the extent to which there may be genetic variation between strains of this model organism.

Chapter V: Metal-dependent regulation of MbaS and OrbS activity

5.1 Overview

As previously discussed in section **Error! Reference source not found.**, the *Burkholderia* ECF sigma factors MbaS and OrbS both contain extended C-terminal extensions that are rich in conserved cysteine residues. Within these cysteine-rich extensions (CREs), MbaS contains five cysteine residues (amino acid positions 203, 206, 216, 220 and 230) and OrbS contains four cysteine residues (amino acid positions 196, 199, 203 and 209) (Figure 1.13).

It is hypothesised that these residues perform a key role in the post-translational regulation of the sigma factors. The most likely possibility is that ferrous iron could bind to the cysteine thiol groups, conferring a conformational change which inhibits the activity of the sigma factor.

In the experiments described in this chapter, this hypothesis is tested through assaying the effect of iron and alternative metals upon the activity of MbaS and OrbS. Through comparison with constructed cysteine-to-alanine substitution mutants, the involvement of the CRE in metal-dependent regulation was also examined.

Objectives:

- To verify that MbaS is an ECF sigma factor, and to identify its target promoters

- To verify Fur-dependent regulation of *mbaS* transcription and the location of the Fur-regulated DNA binding region

- To investigate cross-activity between MbaS and OrbS with respect to promoter recognition

- To investigate metal-dependent inhibition of MbaS and OrbS activity via their cysteine-rich extensions

5.2 Identification of MbaS-dependent promoters using a reporter gene analysis

A significant body of work regarding the OrbS regulon has been published. The target promoters of OrbS, P$_{orbH}$, P$_{orbE}$ and P$_{orbI}$, have been experimentally verified via a transcription reporter analysis (Agnoli *et al.*, 2006), and their transcription start sites have been identified by primer extension analysis (Agnoli *et al.*, 2018). Furthermore, the precise -35 and -10 promoter elements of P$_{orbH}$ have been elucidated single base pair substitution analysis *in vivo* (Agnoli *et al.*, 2018). Additionally, it has been demonstrated that OrbS does not, as is the case with most ECF sigma factors, act upon its own promoter in an auto-regulatory fashion (Agnoli *et al.*, 2006).

There is a high degree of sequence identity between the genes of the *orb* gene cluster and the *mba* gene cluster. Therefore, it is highly likely that MbaS recognises the homologous promoters P$_{mbaH}$, P$_{mbaE}$ and P$_{mbaI}$, and does not interact with its own promoter. However, this has not been empirically demonstrated. Therefore, steps were taken to confirm these assumptions and characterise the MbaS regulon.

5.2.1   *in silico* identification of MbaS-dependent target promoters

Three MbaS-dependent promoters have been predicted in the *Bps* malleobactin gene cluster based upon DNA sequence similarity with the empirically determined and homologous PvdS-dependent promoter motifs, and RNAse protection assays (Alice *et al.*, 2006). These predicted MbaS-dependent promoter sequences have been used to predict the position of the MbaS-dependent promoters in the genome sequence of *Bth* E264, and to generate a consensus sequence motif using the predicted promoter sequences from several *Bth*, *Bps* and *Bma* strains that encode MbaS (Figure 5.1). Given the homology between the PvdS, OrbS and MbaS systems, it is highly likely that the sequences identified correspond to the target promoters of MbaS.

Figure 5.1. Sequences and consensus sequence motif of predicted MbaS-dependent promoters

A. DNA sequences predicted to be recognised by MbaS. **Top**. The consensus sequence motifs recognised by PvdS (Wilson, McMorran and Lamont, 2001) and OrbS (Agnoli *et al.*, 2018). **Bottom.** Aligned DNA sequences found upstream of the *Bth* E264 genes *mbaH*, *mbaE* and *mbaI*. Identified bases in all five sequences are shown with white font upon black background. **B.** The consensus sequence motif of the predicted MbaS-dependent promoter. Generated using WebLogo (Crooks *et al.*, 2004) with DNA upstream of the *mbaH*, *mbaE* and *mbaI* genes from the following species: *Bth* E264, *Bth* E254, *Bth* 34. *Bps* K96243, *Bps* TSV48, *Bps* 1710b, *Bma* FMH and *Bma* ATCC23344.

5.2.2 Construction of MbaS-dependent promoter-reporter fusion plasmids

The DNA fragments containing putative MbaS target promoters, and the *mbaS* promoter, were cloned into the transcriptional *lacZ* reporter plasmid pKAGd4 (Agnoli *et al.*, 2006). The promoter DNA was cloned into the MCS upstream of the promoter-less *lacZ* gene, allowing the promoter activity of the cloned DNA to be assayed by performing β-galactosidase assays. The promoters for the genes *mbaS*, *mbaH*, *mbaE* and *mbaI* were all to be assayed. For each promoter, a 'long' DNA fragment of ~250 bp, and a 'short' DNA fragment of 49 or 53 bp (both containing the putative -35 and -10 promoter elements) were cloned (

Table 5.1). 'Long' promoters were cloned by PCR amplification, whereas 'short' promoters were cloned by annealing of long single-stranded oligonucleotides to form double-stranded DNA fragments with sticky ends.

The cloning of the 'long' *mbaS* promoter, P$_{mbaS-L}$, and the 'long' *mbaH* promoter, P$_{mbaH-L}$, are described in section 4.7.5. The 'short' *mbaS* promoter, P$_{mbaS-S}$, was generated by annealing oligonucleotides pmbaS-short-fwd and pmbaS-short-rev to produce a 63 bp DNA product. The 'short' *mbaH* promoter, P$_{mbaH-S}$, was annealed using oligonucleotides pmbaH-short-fwd and pmbaH-short-rev to produce a 59 bp DNA product. The 'long' *mbaE* promoter, P$_{mbaE-L}$, was amplified by PCR from *Bth* E264 genomic template DNA using primers pmbaE-long-fwd and pmbaE-long-rev to produce a 308 bp DNA product. The 'short' *mbaE* promoter, P$_{mbaE-S}$, was generated by anneal oligonucleotides pmbaE-short-fwd and pmbaE-short-rev to produce a 59 bp DNA product. The 'long' *mbaI* promoter, P$_{mbaI-L}$, was amplified by PCR from *Bth* E264 genomic template DNA using primers pmbaI-long-fwd and pmbaI-long-rev to produce a 295 bp DNA product. The 'short' *mbaI* promoter, P$_{mbaI-S}$, was annealed using oligonucleotides pmbaI-short-fwd and pmbaI-short-rev to produce a 59 bp DNA product. All promoter DNA fragments were inserted between the *Hin*dIII and *Bam*HI sites of pKAGd4 to give the corresponding plasmid derivatives (excluding P$_{mbaI-L}$, cloned between *Hin*dIII and *Xba*I). The identity of each plasmid construct was confirmed by PCR screening and DNA sequencing analysis using the primer AP10.

Table 5.1. Cloned putative promoter endpoints from the malleobactin gene cluster

Promoter	Upstream endpoint[1]	Downstream endpoint[1]
P$_{mbaS-L}$	-141	+25
P$_{mbaS-S}$	-45	+8
P$_{mbaH-L}$	-193	+57
P$_{mbaH-S}$	-43	+6
P$_{mbaE-L}$	-150	+138
P$_{mbaE-S}$	-43	+6
P$_{mbaI-L}$	-202	+73
P$_{mbaI-S}$	-43	+6

[1] Endpoint distances are given relative to the experimentally determined transcription start site of the homologous *orb* system (Agnoli *et al.*, 2018)

P*mbaS*

aacgcaggatcgtaccgccgttcgttgcgccgccggcaatgatcgacgagcgaagtgctgcaaaa
cgacaaatcccgcgagattatcgggttatcaataaatcagattgagaacgattcgcgtttacgtt
agattgcttgccattgagcaaatatct**ggag**aatcc

P*mbaH*

cgcgaggagacgctgcagagcgccgcacgcgcgctgaacgtgtcgcagacgctcgtgcatttcat
ggtccgcgacgccgagcggcactgcgtcgcgtgcgtcgacgcgtccgagcgcgggctcgcgtgcc
cggcgttttgcggcgcgcgcgcgcggccggtaaaaaaatgcgtgcgcgattcgtctatcgagt**a**a
acgcggcgcgcccggcgcgccgtccttcgaactttttcca**g**c**gag**ctttcccgatc

P*mbaE*

tgcggtccggccgcacggttcccggcgcgcgcgacgccctcctgcgcgccgcacgggccaagcag
gaccaagcaggaccacgcagcaccaagcgcggccgagcaagccgagcgcgggtaaagattcggcg
cgcccattcgtctagcagac**t**gaaggggcctcttagcgccttgccgttcgcttcgccgccgaagc
gccgatccgattcctttattgacccgtgctctgccgatgaccgatgccatcgggcgtctcgacgc
cccgccccc**gaac**cga**ttcccgccccgcc

P*mbaI*

ttggtcctgcttggcccgtgcggcgcgcaggagggcgtcgcgcgcgccgggaaccgtgcggccgg
accgcaccgagccgccggcgctgcgcacccgagccgcaccggcgccgctgcggctgcgcgcggcc
gatgcgcgtgtccgtcgccgccaaacgtgaacaacccggtaaaaaatttcgagcgtgattcgtct
cacagtt**g**aagcggccctcttgtggccggcgacttgaacgaaacggccgaggcggccggatccaa
c**gga**cttcacgccct

Figure 5.2. Cloned putative promoter sequences from the malleobactin gene cluster

Full sequences shown correspond to the sequences of the 'long' cloned promoters. The sequences of the corresponding 'short' promoters are underlined. DNA bases enclosed in boxes correspond to the predicted -35 and -10 promoter elements, and bases in bold red font correspond to the predicted transcription start site, based upon the homologous *orb* system (Agnoli *et al.*, 2018). Predicted Shine-Dalgarno sequences are shown in bold black font. Bases with identity to the Fur consensus sequence (Baichoo and Helmann, 2002) at the predicted Fur binding site of P*mbaS* are highlighted in yellow.

5.2.3   Activity of MbaS-dependent promoters in *E. coli*

The pBBR1MCS2-*mbaS* expression plasmid and the pKAGd4 promoter reporter plasmids were co-introduced into *E. coli* MC1061 (Δ*lac*) by transformation, in addition to the parental plasmids as negative controls, in different combinations. The β-galactosidase assay was performed according to the protocol outlined in section 2.5.1. The assay was performed on

cultures grown in LB broth, supplemented with 100 μg ml^{-1} ampicillin and 50 μg ml^{-1} kanamycin, and the experiment was performed a total of four times on different days.

The results shown in Figure 5.3 demonstrate that both P$_{mbaS}$ derivatives are active even without the introduction of MbaS. Furthermore, the addition of MbaS does not significantly increase the β-galactosidase activity. This is consistent with the assumption that P$_{mbaS}$ is a σ^{70}-dependent promoter, as the high degree of conservation between the *E. coli* and *Bth* σ^{70} proteins results in β-galactosidase activity when the promoter-reporter is present. The absence of significantly increased β-galactosidase activity for either promoter fragment with the introduction of MbaS also verifies that, like OrbS, MbaS does not have auto-regulatory activity and P$_{mbaS}$ is not an MbaS-dependent promoter. This is the first demonstration of the σ^{70}-dependency of P$_{mbaS}$. These results localised the P$_{mbaS}$ core elements to a 53 bp DNA region and the P$_{mbaH}$, P$_{mbaE}$ and P$_{mbaI}$ core elements to a 49 bp region.

The results also demonstrate that P$_{mbaH}$, P$_{mbaE}$ and P$_{mbaI}$ are all MbaS-dependent promoters. For each of the promoters, there is no β-galactosidase activity when there is no MbaS present, indicating that they are not activated directly by *E. coli* σ^{70} is the same way that P$_{mbaS}$ is. When *mbaS* is introduced on a plasmid, each of the promoters gives rise to a high β-galactosidase activity, indicating that they are activated directly by MbaS. Interestingly, the 'long' P$_{mbaH}$ and P$_{mbaE}$ promoters give rise to lower β-galactosidase activities compared to the 'short' promoters. The 'long' and 'short' P$_{mbaI}$ promoters show no significant disparity. This possibly points towards an inhibitory regulatory element upstream of the P$_{mbaH}$ and P$_{mbaE}$ promoters that is present in the 'long' promoter variants, and an unknown factor of *E. coli* MC1061 is able to bind to give moderate repression of the β-galactosidase activity.
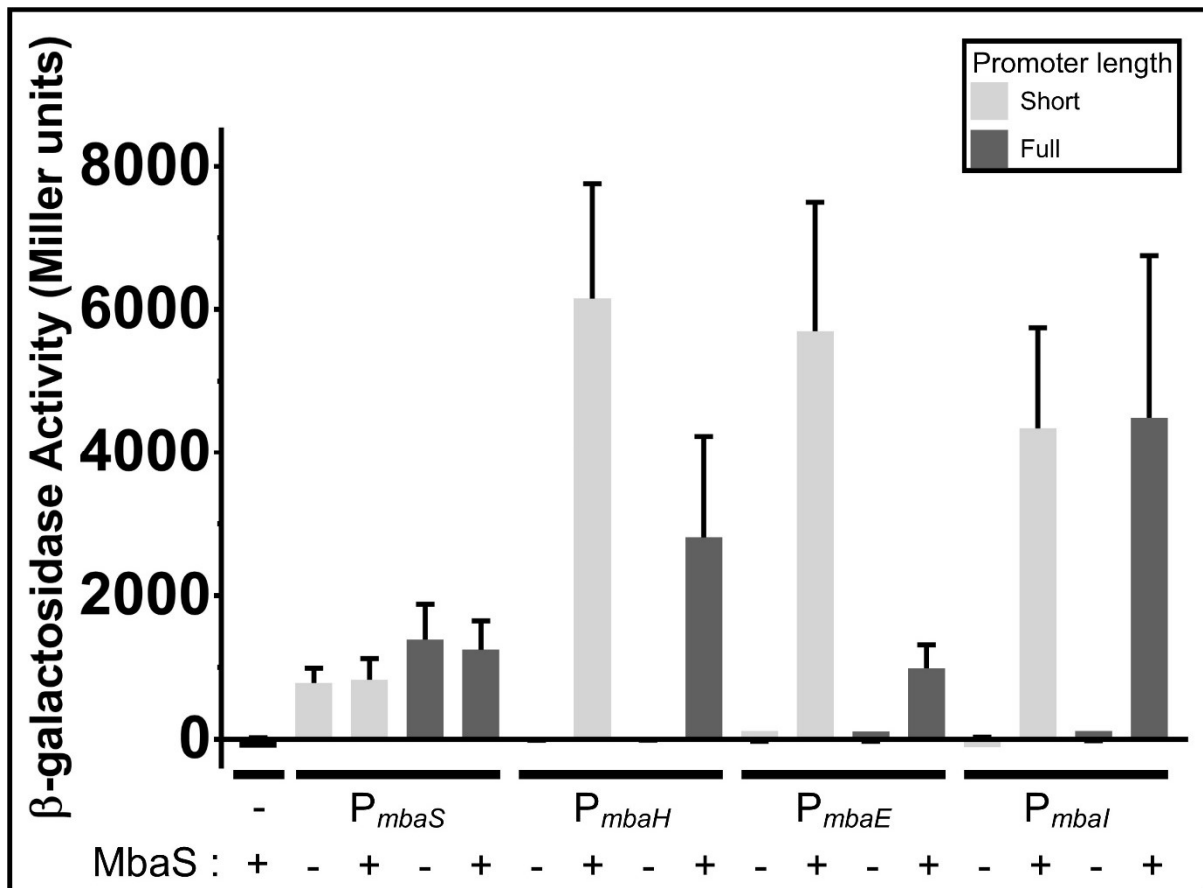
Figure 5.3. β-galactosidase assay of MbaS-dependent promoters in *E. coli* MC1061.

β-galactosidase activity was measured in *E. coli* MC1061 harbouring a) pBBR1MCS-2 (denoted by '-') or pBBR1MCS-2-*mbaS* (denoted by '+'), and b) pKAGd4 or pKAGd4 derivatives containing P*mbaS*, P*mbaH*, P*mbaE*, or P*mbaI* (denoted below data bars). All β-galactosidase activities were corrected for the background vector activity by subtraction of activity derived from *E. coli* MC1061 harbouring both parental plasmids pBBR1MCS-2 and pKAGd4. Error bars show standard deviation (n=12). Growth medium was LB supplemented with 100 μg ml^{-1} ampicillin and 50 μg ml^{-1} kanamycin.

5.2.4   Activity of MbaS-dependent promoters in *B. thailandensis*

After identification of the MbaS-dependent promoters in *E. coli*, the pKAGd4 promoter reporter plasmids (and the parental pKAGd4 plasmid as a negative control) were introduced into *Bth* E264 by conjugation to verify their activity in *Bth*. MbaS protein was provided by the chromosomal copy of the gene in *Bth*. The β-galactosidase assay was performed according to the protocol outlined in section 2.5.1 on cells grown in M9 minimal salts medium supplemented with 0.5% (w/v) glucose, 0.1 % (w/v) casamino acids and 50 μg ml^{-1} chloramphenicol. The experiment was performed a total of three times on three different days.
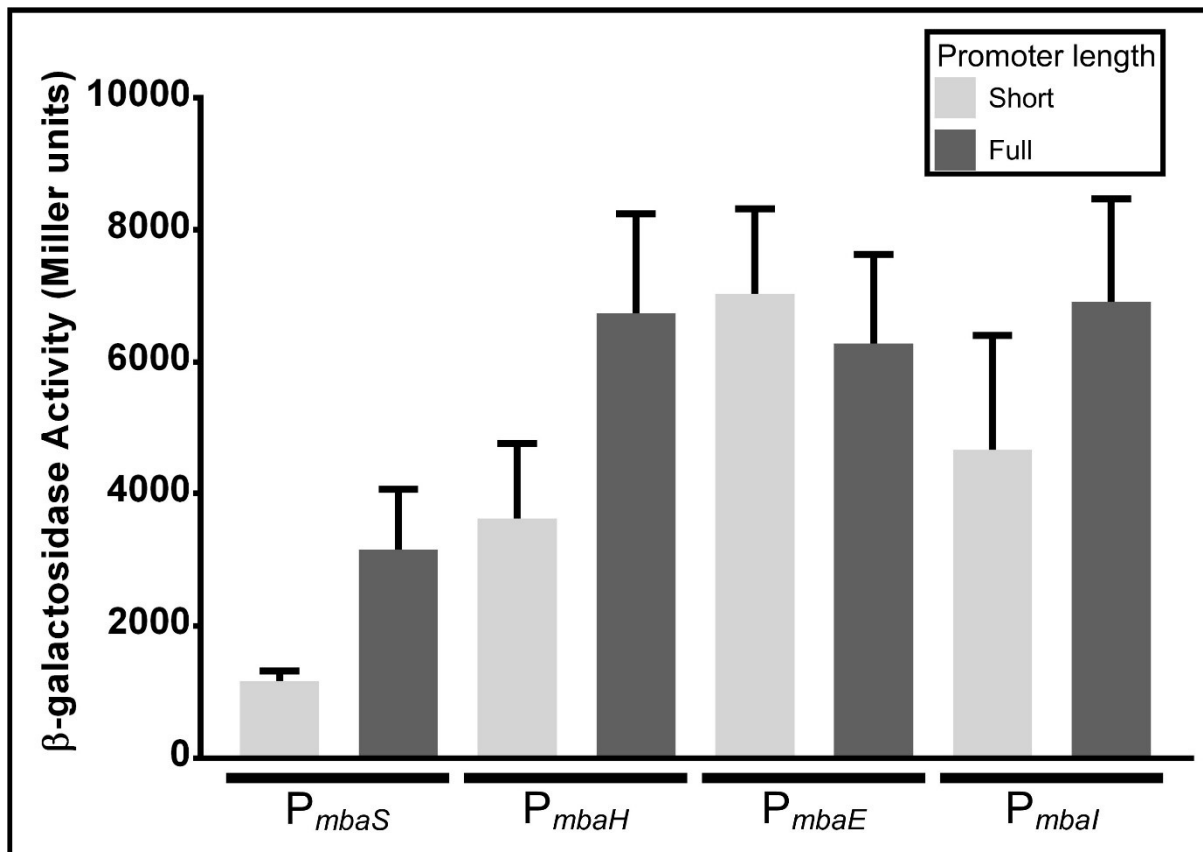
Figure 5.4. β-galactosidase assay of MbaS-dependent promoters in *B. thailandensis* E264.

β-galactosidase activity was measured in *Bth* E264 harbouring pKAGd4 derivatives containing P*mbaS*, P*mbaH*, P*mbaE*, or P*mbaI* (denoted below data bars). All β-galactosidase were activities corrected for background vector activity by subtraction of activity derived from *Bth* E264 harbouring the parental plasmid pKAGd4. Error bars show standard deviation (n=9). Growth medium was M9 minimal salts supplemented with 0.5% (w/v) glucose, 0.1 % (w/v) casamino acid and 50 μg ml^{-1} chloramphenicol.

The results from Figure 5.4 show that the assayed promoters are active in *Bth* E264. From this experiment alone, it is unclear what factor in *Bth* E264 acts upon the promoters, but taken in conjunction with the results in Figure 5.3 and Figure 4.23 it is highly likely that the factor acting upon P*mbaH*, P*mbaE* and P*mbaI* is the chromosomally-expressed MbaS sigma factor, and the factor acting upon P*mbaS* is the *Bth* E264 σ^{70} protein. The β-galactosidase activity for specified by the 'short' and 'long' P*mbaS* variants is lower than that of the activities for 'full' P*mbaH*, P*mbaE* and P*mbaI*, and 'short' P*mbaE* promoters.

5.3 Identification of an MbaS-dependent promoter by *in vitro* transcription assay

In addition to the *in vivo* methods used to verify the characterisation of MbaS as a sigma factor and the identities of the MbaS-dependent promoters, *in vitro* transcription (*iv*T) was also used. This method allows confirmation of MbaS as a sigma factor as there are no other protein factors present apart from core RNAP. This method required the purification of the MbaS and the cloning of a target promoter into a transcription reporter vector compatible with *iv*T. As MbaS stimulated high levels of transcription in *E. coli*, it was decided to use the *E. coli* core RNAP for *iv*T assays as it was commercially available.

5.3.1   Construction of pET14b-*mbaS* and pET14b-*mbaS*$_{CpentaA}$

To overexpress the MbaS and MbaS$_{CpentaA}$ sigma factor for protein-based assays, the corresponding genes were cloned into the bacterial expression vector pET14b (Novagen). Both the *mbaS* gene and the *mbaS*$_{CpentaA}$ genes were amplified using the primers mbaS-fwd-NdeI and mbaS-rev-BamHI to produce 740 bp PCR products (Figure 5.5a,b). The *mbaS* gene was amplified from *Bth* E264 genomic template DNA, whereas the *mbaS*$_{CpentaA}$ gene was amplified from the plasmid construct pSNUFF3Cm-*mbaS*$_{CpentaA}$ (see section 4.5.1) as template DNA. Both PCR products were cloned between the *Nde*I and *Bam*HI sites of the MCS of pET14b to give pET14b-*mbaS* and pET14b-*mbaS*$_{CpentaA}$ (Figure 5.5c). In both cases, the cloned genes were under the transcriptional control of a T7 promoter, and the translated product included an N-terminal hexahistidine tag followed by a thrombin cleavage site giving a total N-terminal tag length of 20 amino acids. The identities of the plasmid constructs were confirmed by PCR screening and DNA sequencing analysis with primers T7for and T7rev.
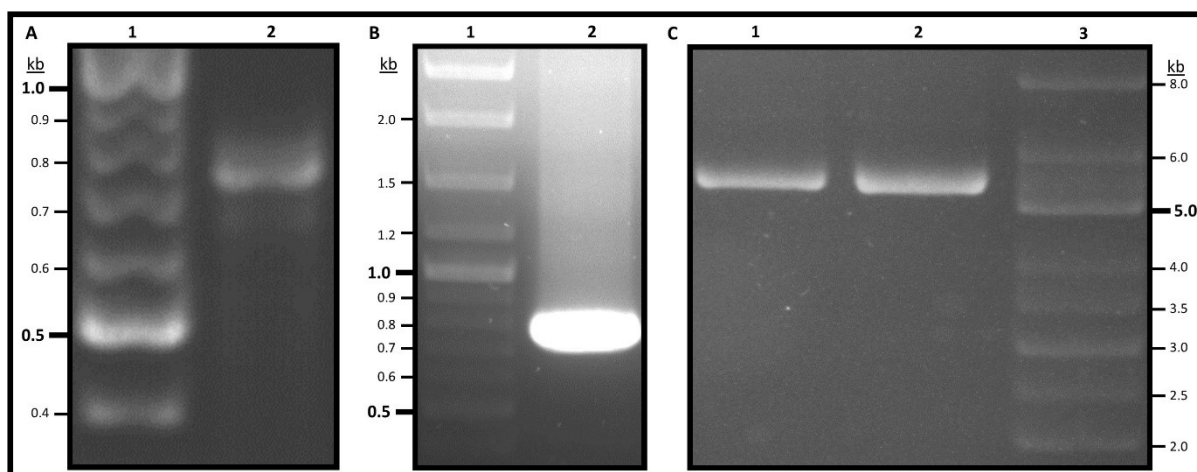
Figure 5.5. Construction of pET14b-*mbaS* and pET14b-*mbaS*CpentaA

Agarose gel electrophoresis analysis of DNA PCR products and plasmid DNA used in construction of pET14b-*mbaS* and pET14b-*mbaS*CpentaA. **A.** PCR to amplify *mbaS*. Lane 1, GeneRuler 1 kb DNA Ladder (Thermofisher); lane 2, *mbaS* PCR product, 740 bp. **B.** PCR to amplify *mbaS*CpentaA. Lane 1, GeneRuler 1 kb DNA Ladder (Thermofisher); lane 2, *mbaS*CpentaA PCR product, 740 bp. **C.** pET14b plasmid constructs. Lane 1, pET14b-*mbaS*, 5.4 kb; lane 2, pET14b-*mbaS*CpentaA, 5.4 kb; lane 3, Supercoiled DNA Ladder (NEB).

5.3.2 Purification of MbaS and MbaSCpentaA

The constructed plasmids pET14b-*mbaS* and pET14b-*mbaS*CpentaA were used to overexpress the corresponding ECF sigma factors in *E. coli* BL21(DE3). The overexpressed proteins were purified from cell lysates as described in sections 2.4.1 to 2.4.3. Typically, the MbaS and MbaSCpentaA proteins were extracted from cell pellets generated from 50 ml of culture. As with many ECF sigma factors, the proteins were found to be insoluble and required solubilisation with N-lauroylsarcosine (also referred to as sarkosyl). Examples of SDS-PAGE for analysis of the protein purification process are shown for MbaS (Figure 5.6) and MbaSCpentaA (Figure 5.7).
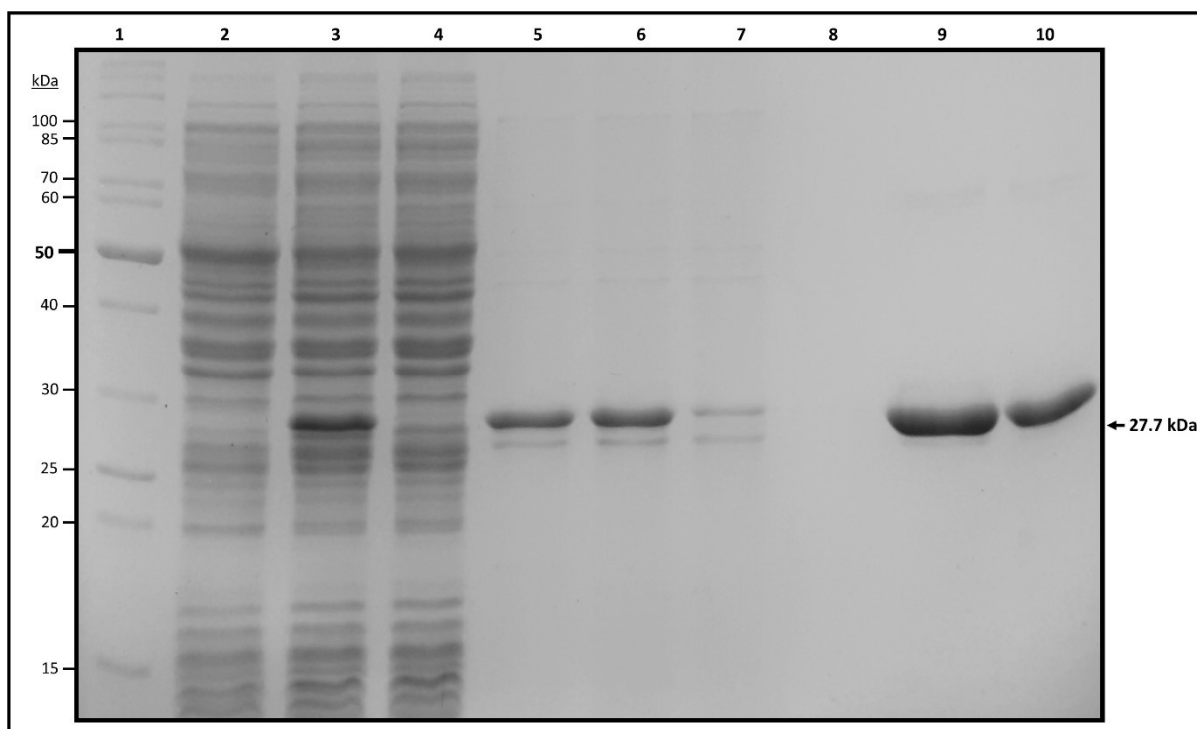
Figure 5.6. Purification of MbaS

SDS-PAGE analysis of protein samples from overexpression and purification of MbaS. Expected MW of MbaS is 27.7 kDa. Volume of sample loaded shown below in brackets. Lane 1, EZ-run *Rec* Protein Ladder (Fisher Bioreagents); lane 2, un-induced protein (5 µl); lane 3, total induced protein (5 µl); lane 4, total soluble protein (5 µl); lane 5, total protein post-sarkosyl treatment (10 µl); lane 6, total soluble protein post-sarkosyl treatment (10 µl); lane 7, protein unbound to IMAC column (10 µl); lane 8, flow-through of wash through protein-loaded IMAC column (10 µl); lane 9, eluted protein (10 µl); lane 10, final dialysed protein (5 µl).
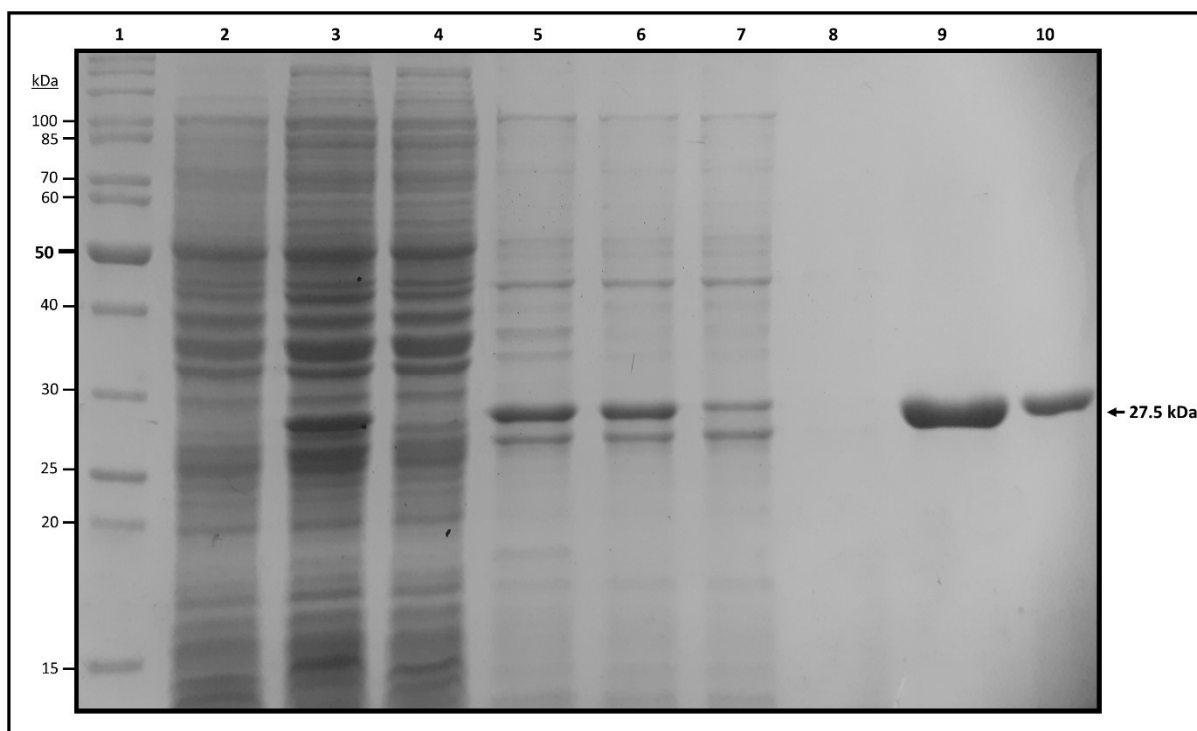
Figure 5.7. Purification of MbaS_{CpentaA}

SDS-PAGE analysis of protein samples from overexpression and purification of MbaS$_{CpentaA}$. Expected MW of MbaS$_{CpentaA}$ is 27.5 kDa. Volume of sample loaded shown below in brackets. Lane 1, EZ-run *Rec* Protein Ladder (Fisher Bioreagents); lane 2, un-induced protein (5 µl); lane 3, total induced protein (5 µl); lane 4, total soluble protein (5 µl); lane 5, total protein post-sarkosyl treatment (10 µl); lane 6, total soluble protein post-sarkosyl treatment (10 µl); lane 7, protein unbound to IMAC column (10 µl); lane 8, flow-through of wash through protein-loaded IMAC column (10 µl); lane 9, eluted protein (10 µl); lane 10, final dialysed protein (5 µl).

During the stages of dialysis into the storage buffer, the purified proteins would occasionally precipitate; this was corrected by titrating with N-lauroylsarcosine at final concentrations of 0.05-0.25% until resolubilisation was achieved. Although it was unclear whether ECF sigma factor treated in this way would refold into the native state, the proteins functioned identically in *ivT* (see section 5.3.4) and bio layer interferometry (see section 5.9.4) regardless of resolubilisation procedure. Typically, the final concentration of purified ECF sigma factor purified in storage buffer was 1.5-3.0 mg ml^{-1}. These proteins were then diluted in storage buffer to 1.0 mg ml^{-1} to be used directly in *iv*T assays and bio layer interferometry (BLI) assays.

5.3.3 Construction of pRLG770-derived transcription assay vector for analysis of MbaS-dependent transcription *in vitro*

A plasmid harbouring an MbaS-dependent promoter was required to serve as template DNA in the ivT assay. As the transcription assay procedure uses supercoiled DNA, the plasmid template must have a strong transcription terminator located downstream of the cloning site for the promoter DNA. pRLG770 is an *in* vitro transcription reporter vector that contains the tandem *rrnB* T_1T_2 terminator (Ross *et al.*, 1990). This would give an RNA transcript of an expected length that can be detected through incorporation of ^{32}P-UTP and thereby used as a probe for MbaS/MbaS$_{CpentaA}$ transcription activity. The *mbaH* promoter was selected as a representative MbaS-dependent promoter for cloning into pRLG770.

The 49 bp P_{mbaH} promoter DNA fragment was made by annealing the oligonucleotides pBTHI2426-EcoRI-fwd an pBTHI2426-HindIII-rev, and ligated between the *Eco*RI and *Hin*dIII sites of pRLG770 to give the plasmid pRLG770-P*mbaH* (Figure 5.8). The identity of the plasmid construct was confirmed by PCR screening and DNA sequencing analysis with the primers 1204 and RLG1620.

For use in ivT assays, the plasmid was prepared by maxiprep as described in section 2.3.3. The concentration of the template plasmid was typically at a concentration of around 100 µg ml^{-1}.
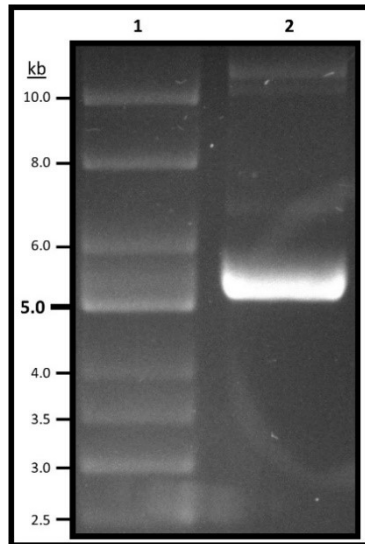
Figure 5.8. Construction of pRLG770-P*mbaH*

Agarose gel electrophoresis analysis of DNA products and plasmid DNA used in construction of pRLG770-P*mbaH*. Lane 1, Supercoiled DNA Ladder (NEB); lane 2, pRLG770-P*mbaH*, 5.1 kb.

5.3.4 Verification of MbaS as a sigma factor by *in vitro* transcription assay

Once all of the components of the *iv*T assay were prepared, a series of control reactions were performed (Figure 5.9). These reactions were set up to confirm that (a) *E. coli* σ^{70} does not direct synthesis of RNA from P*mbaH*, (b) MbaS/MbaS$_{CpentaA}$ do not direct synthesis of RNA from the P*mbaH* promoter in the absence of *E. coli* core RNAP, and (c) MbaS/MbaS$_{CpentaA}$ are able to direct synthesis of RNA from P*mbaH* when *E. coli* core RNAP is present. As a positive control, pRLG770-P*guaB* containing the σ^{70}-dependent *guaB* promoter was included in the assays. For the assays involving MbaS/MbaS$_{CpentaA}$, a 15-minute pre-incubation step was employed to allow for association of the σ factor with *E. coli* core RNAP. However, for σ^{70}-depednent transcription, preformed *E. coli* RNAP holoenzyme (NEB) was employed.
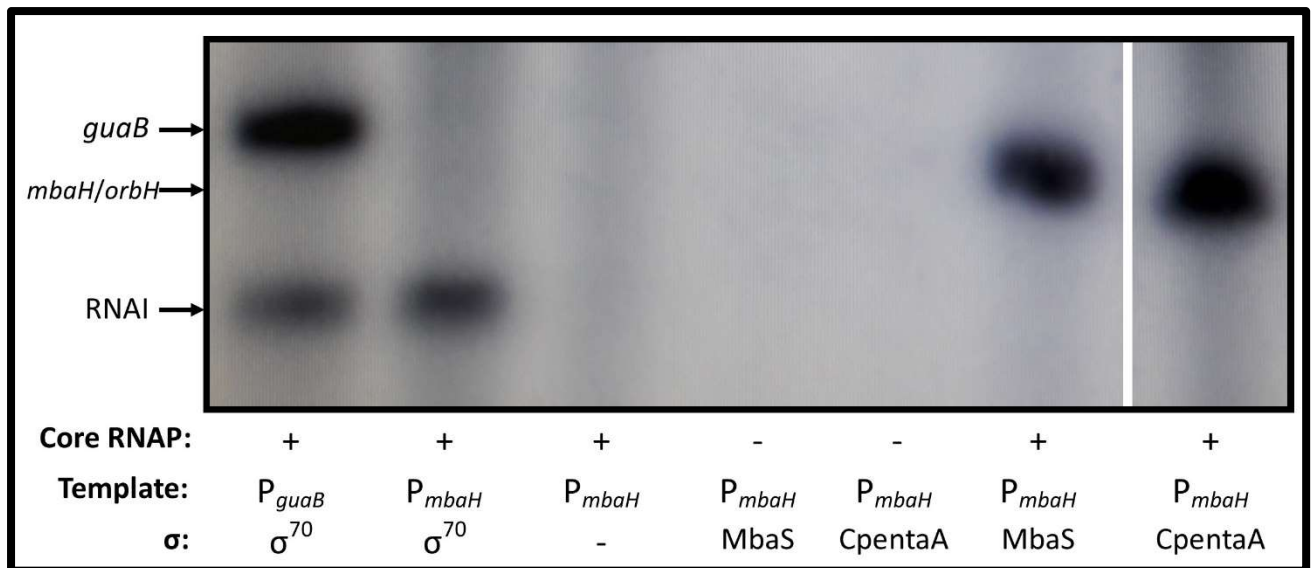
Figure 5.9. *in vitro* **transcription assay controls**

RNA transcripts were resolved in a 5.5% acrylamide, 7 M urea gel following an *in vitro* transcription assay. *E. coli* core RNA polymerase (NEB), in association with a sigma factor, was used to synthesise RNA from DNA fragments containing the promoters P$_{guaB}$, P$_{mbaH}$ or P$_{orbH}$ cloned into pRLG770 as indicated. The location of the transcripts originating from each promoter are indicated on the left of the image: the *guaB* promoter (186 nt transcript), the *mbaH* or *orbH* promoter (156 nt transcript). The location of the replicon-derived RNAI 108 nt transcript is also indicated. More detail is included within the text.

As expected, the reaction containing the *E. coli* σ^{70} holoenzyme and pRLG770-P$_{guaB}$ produces two RNA transcripts: one 186 nt product initiated from the cloned *guaB* promoter, and one 108 nt product initiated from the RNAI site within pRLG770. When pRLG770-P$_{mbaH}$ was used as template in place of pRLG770-P$_{guaB}$, only the RNAI transcript was produced, consistent with the hypothesis that the P$_{mbaH}$ is not a σ^{70}-dependent promoter. This was confirmed further when *E. coli* σ^{70} was not included in the reaction, and there is complete shutdown of transcription. Both MbaS and MbaS$_{CpentaA}$ are not able to stimulate RNA synthesis originating from the *mbaH* promoter in the absence of *E. coli* core RNAP, confirming there was no contaminating RNAP in the preparations of these sigma factors. Finally, it was observed that both MbaS and MbaS$_{CpentaA}$, when in association with core RNAP, can initiate transcription from P$_{mbaH}$ and produce a 156 nt RNA transcript. Both of these sigma factors show functional activity, and result in similar amounts of RNA transcript.

5.4 Demonstration of Fur-dependent regulation of *mbaS*

In order to investigate the putative iron-dependent regulation of MbaS sigma factor activity *in vivo*, it was necessary to empirically demonstrate that Fur acts upon P$_{mbaS}$, but not upon the MbaS-dependent promoters P$_{mbaH}$, P$_{mbaE}$ and P$_{mbaI}$. Doing so ensures that any observed iron-regulation of the activity of MbaS upon a target promoter is due solely to effects upon MbaS activity and/or abundance, and not upon the MbaS target promoters.

In the homologous *orbS* system of *Bce*, it has been demonstrated by bioinformatic prediction, Fur titration assay (FURTA) and EMSAs, that P$_{orbS}$ contains a Fur box, but P$_{orbH}$ and P$_{orbI}$/P$_{orbE}$ do not (Agnoli *et al.*, 2006). Additionally, in the *mbaS* system of *Bps*, a putative Fur box was identified at P$_{mbaS}$ bioinformatically and by FURTA (Alice *et al.*, 2006). In the latter experiment, the length of the P$_{mbaS}$ DNA fragment that was assayed was not specified and the precise location of the Fur box is yet to be identified experimentally. Therefore, investigations using both FURTA and transcriptional reporter fusions were performed to demonstrate Fur regulation of MbaS, and identify the Fur box with greater precision.

5.4.1   Construction of pBluescript II KS-derived Fur box probe vectors

The same 'long' promoter DNA fragments of ~200-300 bp from the malleobactin gene cluster that were cloned used to construct pKAGd4-P$_{mbaS-L}$, pKAGd4-P$_{mbaH-L}$, pKAGd4-P$_{mbaE-L}$ and pKAGd4-P$_{mbaI-L}$ were cloned into the high copy-number reporter plasmid pBluescript II KS to examine Fur binding by FURTA. The amplified DNA fragments containing the promoters are shown in Figure 5.10a-d. The P$_{mbaS}$, P$_{mbaH}$, and P$_{mbaE}$ DNA fragments were cloned between the *Hin*dIII and *Bam*HI sites of the pBluescript II SK MCS to give pBS-P$_{mbaS}$, pBS-P$_{mbaH}$ and pBS-P$_{mbaE}$, respectively (Figure 5.10e). The P$_{mbaI}$ DNA fragment was cloned between the *Hin*dIII and *Xba*I sites of the MCS of pBluescript II SK to give pBS-P$_{mbaI}$ (Figure

5.10e). The identities of the plasmid constructs were confirmed by PCR screening and DNA sequencing analysis with primers M13for2 and M13revBACTH.
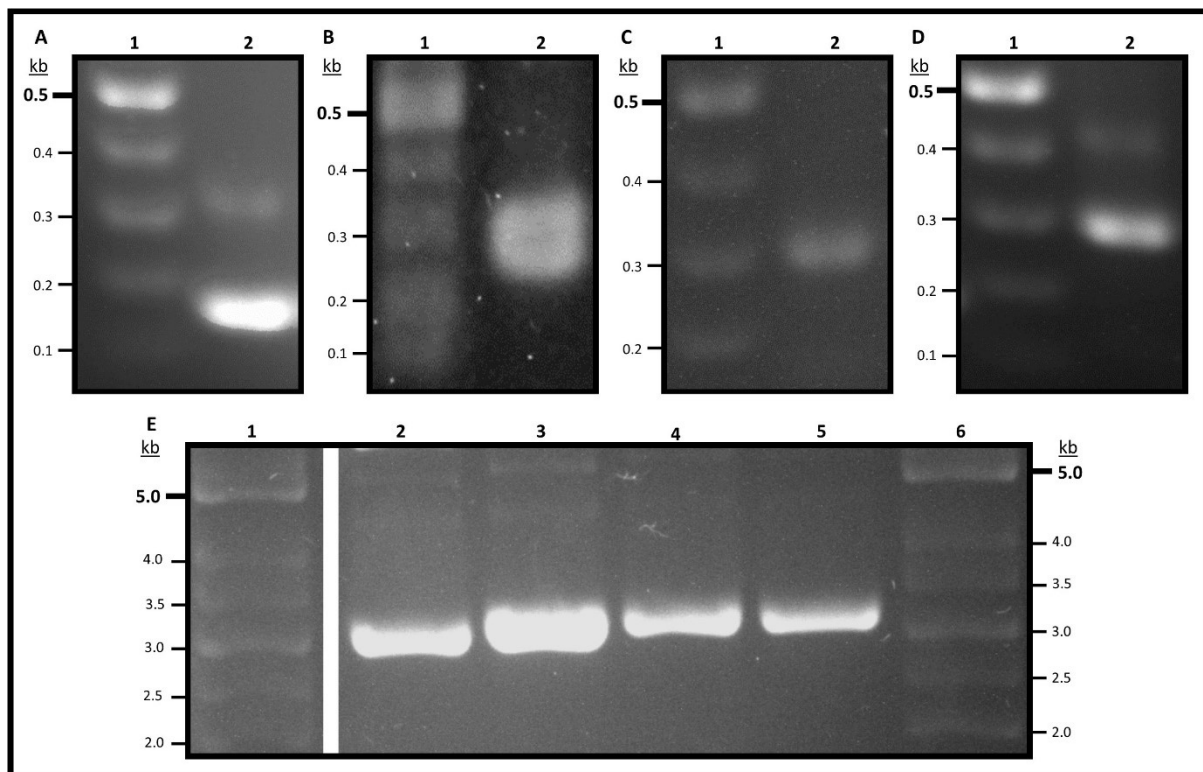
Figure 5.10. Construction of pBluescript II SK derivatives containing putative promoter DNA.

Agarose gel electrophoresis analysis of DNA PCR products and plasmid DNA used in construction of pBluescript II SK derivatives containing promoter DNA for the genes *mbaS*, *mbaH*, *mbaE* and *mbaI*. **A.** PCR to amplify P*mbaS*. Lane 1, GeneRuler 1 kb DNA Ladder (Thermofisher); lane 2, P*mbaS*, 186 bp PCR product. **B.** PCR to amplify P*mbaH*. Lane 1, GeneRuler 1 kb DNA Ladder (Thermofisher); lane 2, P*mbaH*, 274 bp PCR product. **C.** PCR to amplify P*mbaE*. Lane 1, GeneRuler 1 kb DNA Ladder (Thermofisher); lane 2, P*mbaE*, 308 bp PCR product. **D.** PCR to amplify P*mbaI*. Lane 1, GeneRuler 1 kb DNA Ladder (Thermofisher); lane 2, P*mbaI*, 295 bp PCR product. **E.** pBluescript II SK plasmid constructs. Lanes 1 and 6, Supercoiled DNA ladder (NEB); lane 2, pBS-P*mbaS*, 3.1 kb; lane 3, pBS-P*mbaH*, 3.2 kb; lane 4, pBS-P*mbaE*, 3.2 kb, lane 5, pBS-P*mbaI*, 3.2 kb.

5.4.2   Identification of Fur binding sites by FURTA

The pBluescript II KS derivatives containing P*mbaS*, P*mbaH*, P*mbaE* and P*mbaI*, in addition to pBluescript II KS and p3FZBS (positive control harbouring the *E. coli* consensus Fur box) were introduced into *E. coli* H1717 by transformation. These strains were streaked out onto MacConkey agar containing 1% (w/v) lactose and 40 μM $Fe(NH_4)_2(SO_4)_2$, and grown at 37 ^oC for 16 hours. More details are included in section 2.5.2.
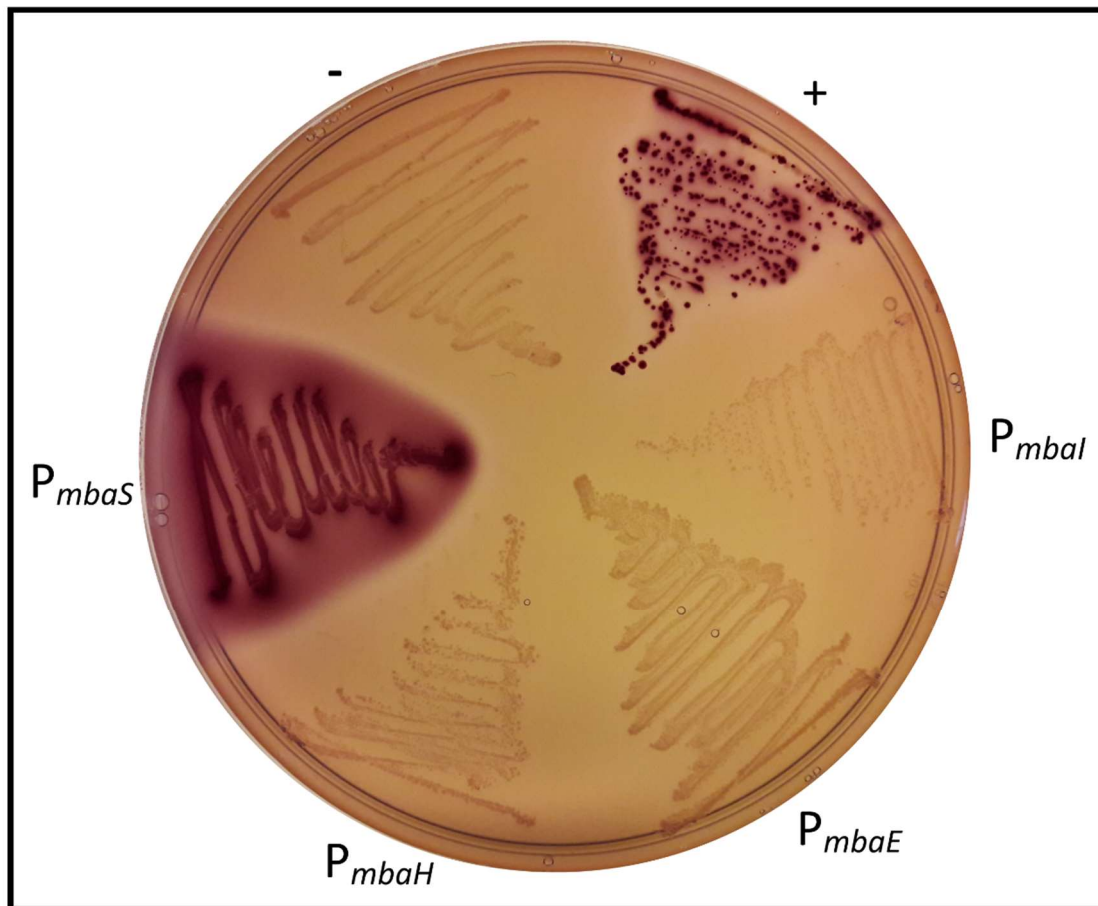
Figure 5.11. Identification of Fur-binding sites in MbaS-associated promoters by FURTA

E. coli H1717 transformants grown on a MacConkey agar plate, supplemented with 1% (w/v) lactose, 40 µM Fe(NH$_4$)$_2$(SO$_4$)$_2$ and 100 µM ampicillin. Plasmids harboured by *E. coli* H1717 are pBluescript II KS (-), p3ZFBS (+), and pBluescript II KS derivatives containing the promoters P$_{mbaS}$, P$_{mbaH}$, P$_{mbaE}$, and P$_{mbaI}$, as indicated.

The results from the FURTA indicate that the 186 bp DNA region located upstream of the *mbaS* translation initiation codon contains a Fur box, whereas the 274, 308 and 295 bp DNA regions upstream of *mbaH*, *mbaE* and *mbaI*, respectively, do not contain a Fur box. Therefore, analogous to the *orb* system, only the transcription of *mbaS* is directly regulated by Fur, and transcription of the MbaS target genes is directed independently of Fur.

5.4.3   Determination of optimum 2,2-dipyridyl concentration to induce iron-limited conditions

In order to simulate iron-deplete conditions, the metal ion-chelating molecule 2,2-dipyridyl (DP) was added to minimal salts medium to sequester any trace amounts of iron. DP is able to enter bacterial cells and bind Fe^{2+}, where three molecules of the bidentate ligand DP coordinate one ion of Fe^{2+} with high affinity.

A suitable concentration of DP in conjunction with *Bth* had to be determined for use in bacterial growth curves and transcription reporter analyses; this would be the highest concentration of metal chelator that did not significantly affect the bacterial growth rate. A concentration of DP that impacts bacterial growth may lead to physiological changes that could interfere with or mask iron regulatory mechanisms. Conversely, a concentration of DP too low may not induce iron-depleted conditions. The suitable concentration of DP to be used was determined by growing *Bth* E264 in medium containing different concentrations of DP (Figure 5.12).
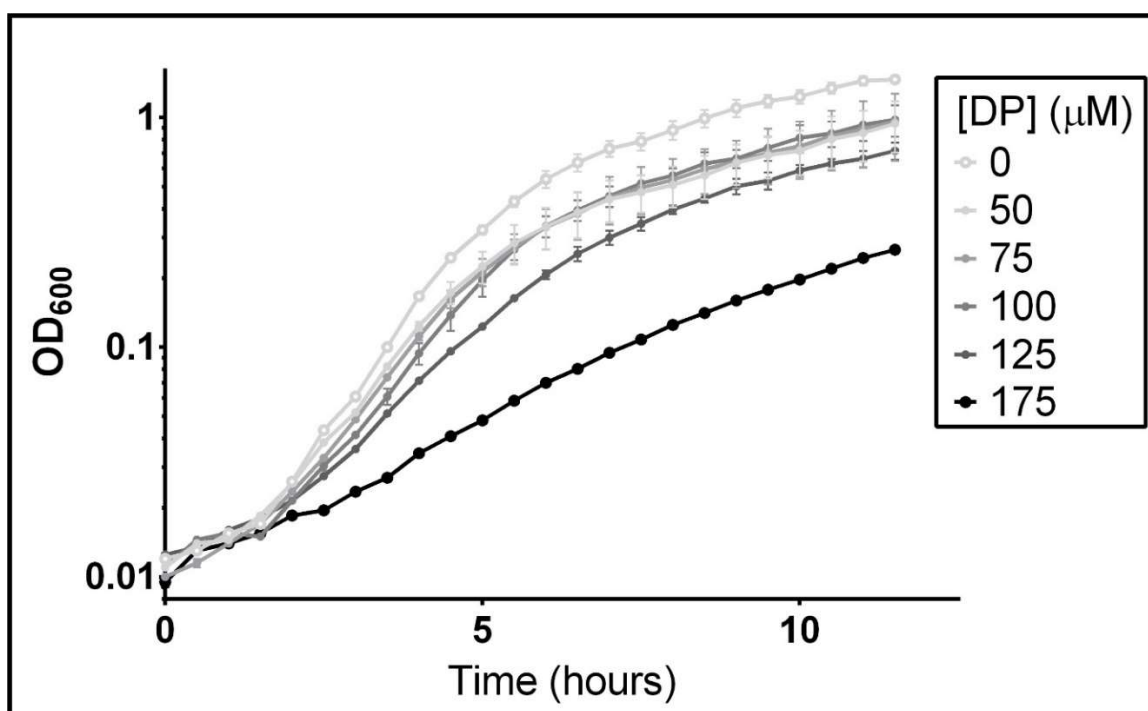
Figure 5.12. Growth curves of *Bth* E264 growth with different concentrations of 2,2-dipyridyl.

Growth curves carried out in M9 minimal salts medium supplemented with 0.5% (w/v) glucose, 0.1% (w/v) casamino acids and varying concentrations of 2,2-dipyridyl (DP). Concentration of DP is denoted in key. Error bars denote SEM (n=2). Error bars that are not visible are smaller than data point symbols.

Figure 5.12 suggests that a concentration of 100 µM DP is sufficient to induce iron-depleted conditions for *Bth* in M9 minimal salts medium supplemented with 0.5% (w/v) glucose and 0.1% (w/v) casamino acids, as this is the highest concentration of DP that results in only a small decrease in growth rate. This concentration was used in all subsequent experiments where iron starvation conditions were required.

5.4.4 Demonstration of Fur-dependent regulation of MbaS by transcription reporter analysis

It has previously been demonstrated that the expression of *mbaS* occurs in a Fur-dependent manner (see section 5.4.2) (Agnoli *et al.*, 2006), and therefore the transcription of the *mbaS* gene and its downstream target genes will be regulated by iron. Under iron-replete conditions, *mbaS* is downregulated; under iron-limiting conditions, *mbaS* is upregulated (Alice *et al.*, 2006). Although this has been observed in *Bps* K96243, it has not previously been shown *in vivo* in *Bth*.

To confirm that *mbaS* and its malleobactin-associated target genes are regulated by iron, the pKAGd4 reporter plasmids bearing the 'long' P_{mbaS}, P_{mbaH}, P_{mbaE} and P_{mbaI} promoters (and the parental pKAGd4 plasmid as a negative control) were introduced into *Bth* E264 by conjugation. β-galactosidase assays were performed on cells growing in M9 minimal salts medium supplemented with 0.5% (w/v) glucose, 0.1% casamino acids and 50 µg ml^{-1} chloramphenicol according to the protocol outlined in section 2.5.1. To induce iron-limiting conditions, cultures were supplemented with 100 µM 2,2-dipyridyl (see section 5.4.3). To induce iron-replete conditions, cultures were supplemented with 50 µM FeCl$_3$, as this concentration is regularly used to induce iron-replete conditions for many bacteria across many studies. The experiment was performed a total of three times on three different days.
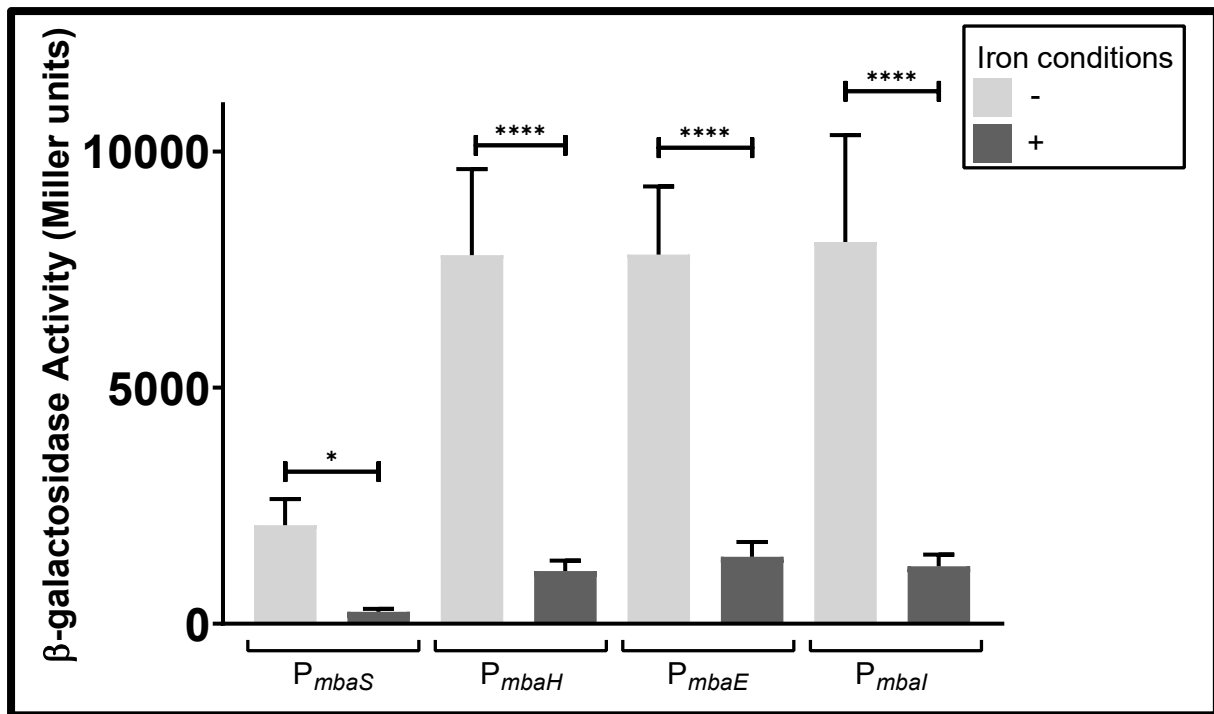
Figure 5.13. β-galactosidase assay of MbaS-dependent promoters in *B. thailandensis* E264 under iron-replete and iron-limited conditions.

Results of β-galactosidase assay investigating iron-dependent regulation of promoters *mbaS* and its target genes. β-galactosidase activity was measured in *Bth* E264 harbouring pKAGd4 derivatives containing P*mbaS*, P*mbaH*, P*mbaE*, or P*mbaI* (denoted below data bars). All β-galactosidase activities were corrected for the background vector activity by subtraction of activity derived from *Bth* E264 harbouring the parental plasmid pKAGd4 under identical conditions. Growth medium was M9 minimal salts supplemented with 0.5% (w/v) glucose, 0.1 % (w/v) casamino acid, 50 µg ml^{-1} chloramphenicol and either 100 µM 2,2-dipyridyl (iron-limited, light grey) or 50 µM FeCl$_3$ (iron-replete, dark grey). Error bars show standard deviation (n=9). There is a significant difference in β-galactosidase activity between cultures grown under iron-limited and iron-replete conditions for the promoters P*mbaS* (P=0.03), P*mbaH* (P<0.0001), P*mbaE* (P<0.0001) and P*mbaI* (P<0.0001) (one-way ANOVA, F=79.78, Tukey's multiple comparison's test).

The results in Figure 5.13 show that all four of the promoters are regulated by iron, with significantly higher activity in cells grown under iron-limited conditions compared to iron-replete conditions. The addition of iron results in an approximately 88% decrease in activity from the *mbaS* promoter (P=0.03), an approximately 86% decrease in activity from the *mbaH* promoter (P<0.0001), an approximately 82% decrease in activity from the *mbaE* promoter (P<0.0001), and an approximately 85% decrease in activity from the *mbaI* promoter (P<0.0001).

5.5 Construction of Fur-independent MbaS and OrbS expression vectors

To investigate the possibility of direct iron regulation of MbaS and OrbS activity *in vivo*, expression vectors to supply the sigma factors *in trans* were constructed, without their native promoters so that Fur-dependent regulation of sigma factor gene transcription was eliminated from the *in vivo* assay system. The effect of iron on the activity of these sigma factors could then be ascertained using a transcription reporter system. Fur-independent expression of *mbaS* and *orb Seas* achieved using pBBR1MCS-2 and pBBR1MCS-5 plasmids containing the genes for *mbaS*, *mbaS*$_{CpentaA}$, *orbS* and *orbS*$_{CtetraA}$.

5.5.1 Construction of pBBR1MCS2-*orbS* and pBBR1MCS2-*orbS*$_{CtetraA}$ expression vectors

Both the *orbS* and *orbS*$_{CtetraA}$ genes have been cloned into pBBR1MCS-based expression plasmids by previous researchers ((Agnoli *et al.*, 2006), A. Butt unpublished). However, in these constructs *orbS* and *orbS*$_{CtetraA}$ were cloned together with the native P$_{orbS}$ promoter, and so are therefore regulated by Fur. To express the OrbS protein and OrbS$_{CtetraA}$ mutant proteins *in vivo*, independently of Fur, these genes were cloned in an analogous manner as for construction of pBBR2-*mbaS* and pBBR2-*mbaS*$_{CpentaA}$ (see section 4.7.1).

The *orbS* gene was amplified from *Bce* H111 genomic template DNA and the *orbS*$_{CtetraA}$ gene was amplified from the plasmid pBBR1MCS-*orbS*$_{CtetraA}$ (Agnoli, 2007), using the primers orbS-fwd-HindIII and orbS-rev-BamHI to produce a 723 bp PCR product in each case (Figure 5.14a,b). This included 30 bp immediately upstream of the translation start codon that contained the Shine-Dalgarno sequence, but not the native *orbS* promoter. An in-frame stop codon was incorporated into the 5' end of the forward primer to terminate translation of the upstream *lacZα* gene segment of the vector to eliminate the possibility of generating a LacZα-OrbS protein fusion. The *orbS* and *orbS*$_{CtetraA}$ genes were cloned between the *Hin*dIII and *Bam*HI sites of the MCS of pBBR1MCS-2 to give pBBR1MCS2-*orbS*$_{ΔP}$ and pBBR1MCS2-

orbS~CtetraA-ΔP~ (Figure 5.14c). The identities of the plasmid constructs were confirmed by PCR screening and DNA sequencing analysis with primers M13revBACTH and M13for2. These plasmid constructs were given ΔP nomenclature to distinguish them previously constructed plasmids in which the the genes were cloned together with the native P*~orbS~* promoter.
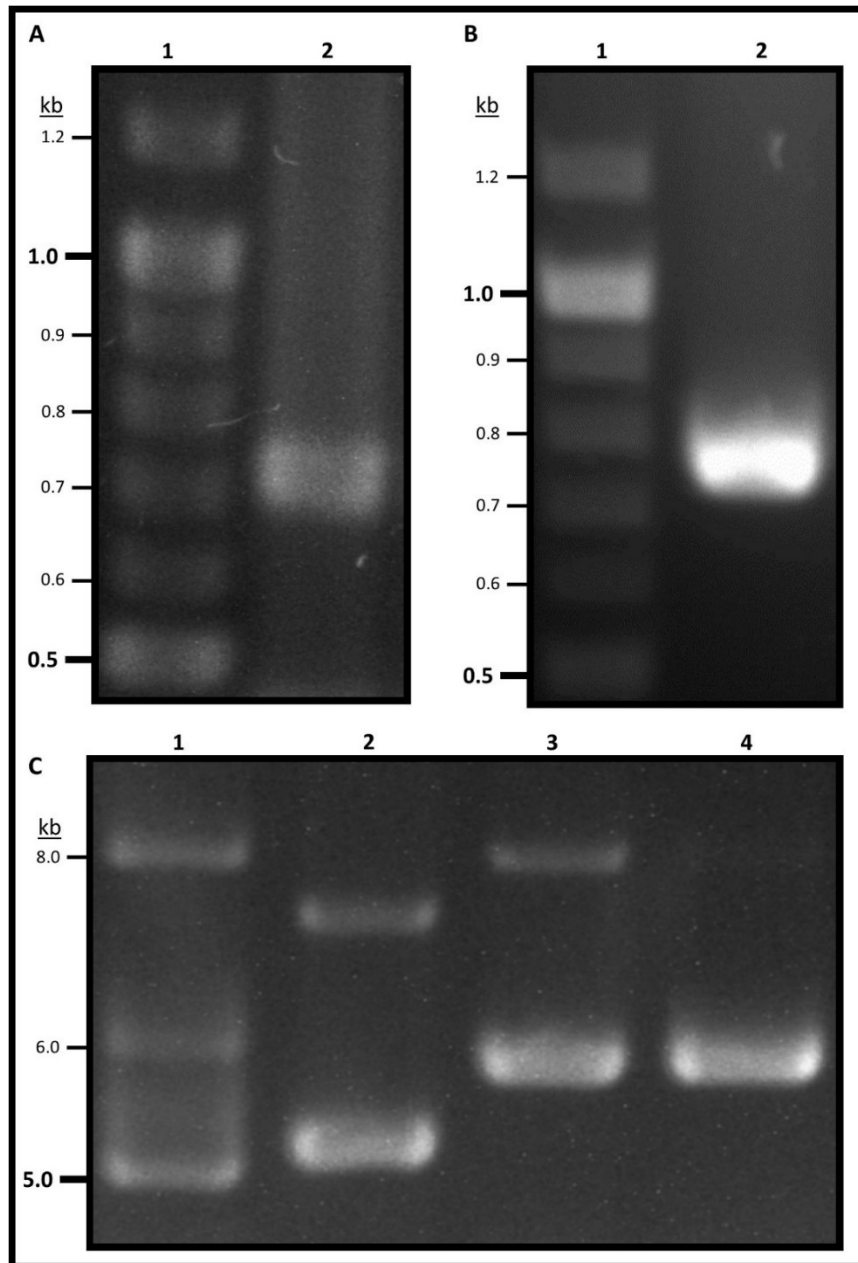
Figure 5.14. Construction of pBBR1MCS2-*orbS*~ΔP~ and pBBR1MCS2-*orbS*~CtetraA-ΔP~.

Agarose gel electrophoresis analysis of DNA PCR products and plasmid DNA used in construction of pBBR1MCS2-*orbS*~ΔP~ and pBBR1MCS2-*orbS*~CtetraA-ΔP~. **A.** PCR to amplify *orbS*. Lane 1, GeneRuler 1 kb DNA Ladder (Thermofisher); lane 2, *orbS* PCR product, 723 bp. **B.** PCR to amplify *orbS*~CtetraA~. Lane 1, GeneRuler 1 kb DNA Ladder (Thermofisher); lane 2, *orbS*~CtetraA~ PCR product, 723 bp. **C.** pBBR1MCS2-*orbS* and pBBR1MCS2-*orbS*~CtetraA~. Lane 1, Supercoiled DNA Ladder (NEB); lane 2, pBBR1MCS-2, 5.1 kb; lane 3, pBBR1MCS2-*orbS*~ΔP~, 5.8 kb, lane 4, pBBR1MCS2-*orbS*~CtetraA-ΔP~, 5.8 kb.

5.5.2 Construction of pBBR1MCS5-based expression vectors

To investigate Fur-dependent regulation of MbaS, the *E. coli fur* mutant strain QC1732 (Touati *et al.*, 1995) and its parent strain QC771 (Carlioz and Touati, 1986) were used. However, QC1732 contains a kanamycin antibiotic resistance cassette that was used to inactivate the *fur* gene, and so could not be used in conjunction with the pBBR1MCS2-based plasmid constructs (see section 4.7.1 and 5.5.1). Therefore, these genes were cloned into another plasmid of the pBBR1MCS series: pBBR1MCS-5 (Kovach *et al.*, 1995). This plasmid has an antibiotic selection marker that specifies gentamicin resistance, and could be used in conjunction with *E. coli* QC1732. As with the pBBR1MCS-2 based plasmid constructs (section 5.5.1), the plasmids that contained *orbS* and *orbS*$_{CtetraA}$ were given ΔP nomenclature.

The *mbaS*, *mbaS*$_{CpentaA}$, *orbS*, and *orbS*$_{CtetraA}$ genes were obtained by restriction digestion with *Hin*dIII and *Bam*HI from the plasmid constructs pBBR2-*mbaS*, pBBR2-*mbaS*$_{CpentaA}$, pBBR2-*orbS*$_{ΔP}$ and pBBR2-*orbS*$_{CtetraA-ΔP}$, respectively, and ligated into the MCS of pBBR1MCS-5 between the *Hin*dIII and *Bam*HI sites to give pBBR1MCS5-*mbaS*, pBBR1MCS5-*mbaS*$_{CpentaA}$, pBBR1MCS5-*orbS*$_{ΔP}$ and pBBR1MCS5-*orbS*$_{CtetraA}$ (Figure 5.15). The identities of the plasmid constructs were confirmed by PCR screening and DNA sequencing analysis with primers M13revBACTH and M13for2.
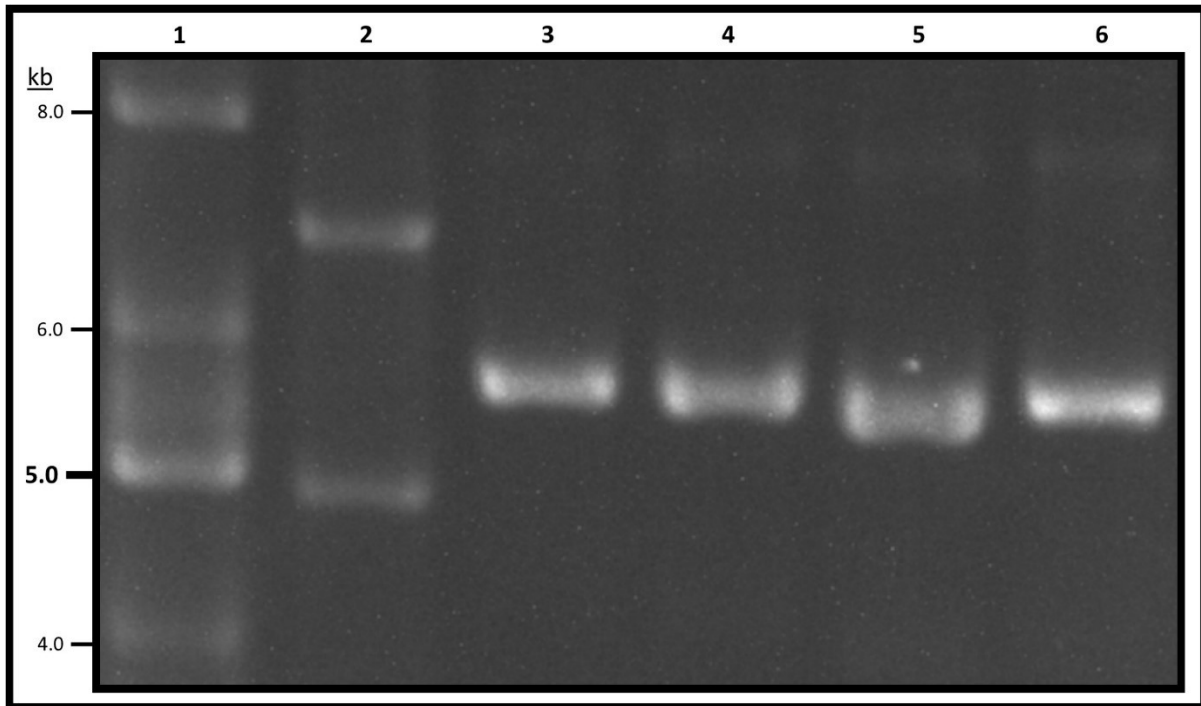
Figure 5.15. Construction of pBBR1MCS-5 vectors expressing MbaS, MbaS$_{CpentaA}$, OrbS and OrbS$_{CtetraA}$.

Agarose gel electrophoresis analysis of constructed plasmid DNA pBBR1MCS5-*mbaS*, pBBR1MCS5-*mbaS*$_{CpentaA}$, pBBR1MCS5-*orbS*$_{\Delta P}$ and pBBR1MCS2-*orbS*$_{CtetraA-\Delta P}$. Lane 1, Supercoiled DNA Ladder (NEB); lane 2, pBBR1MCS-5, 4.8 kb; lane 3, pBBR1MCS5-*mbaS*, 5.5 kb, lane 4, pBBR1MCS5-*mbaS*$_{CpentaA}$, 5.5 kb; lane 5, pBBR1MCS5-*orbS*$_{\Delta P}$, 5.4 kb; lane 6, pBBR1MCS5-*orbS*$_{CtetraA-\Delta P}$, 5.4 kb.

5.5.3 Construction of pKAGd4-P$_{orbH-S}$

Although pKAGd4 constructs containing P$_{orbH}$ have previously been constructed, a new variant of pKAGd4-P$_{orbH}$ was constructed that contained a promoter that corresponded in length and base pair coordinates to pKAGd4-P$_{mbaH-S}$ (-43 to +6 with respect to the predicted transcription start site) to allow direct comparison. The corresponding *orbH* promoter was assembled by annealing the oligonucleotides porbH-fwd-HindIII and porbH-rev-BamHI to produce a 59 bp DNA product. This was cloned between the *Hin*dIII and *Bam*HI sites of pKAGd4 to produce pKAGd4-P$_{orbH-S}$. The identity of this plasmid construct was confirmed by PCR screening and DNA sequencing analysis using the primer AP10.

5.5.4 Demonstration of loss of Fur-dependent regulation of *mbaS* and *orbS* expression on pBBR1MCS5-derived expression vectors lacking the native *mbaS* and *orbS* promoters

To confirm that by cloning the *mbaS* and *orbS* genes without their native promoter results in Fur-independent expression, the activity of the sigma factors expressed from pBBR5-*mbaS* and pBBR5-*orbS*$_{\Delta P}$ upon their target promoters was compared in both an *E. coli fur*$^+$ strain (QC771) and an *E. coli fur*$^-$ strain (QC1732). As positive controls for Fur dependency, the Fur-regulated promoters P$_{mbaS}$ and P$_{orbS}$ were also assayed.

Firstly, either pKAGd4, pKAGd4-P$_{mbaS-S}$, or pKAGd4-P$_{orbS}$ (Agnoli *et al.*, 2006) were introduced into each of *E. coli* QC771 or QC1732 by transformation. Also, a combination of (a) pKAGd4-P$_{mbaH-S}$ or pKAGd4-P$_{orbH-S}$ and (b) pBBR1MCS-5, pBBR5-*mbaS* or pBBR5-*orbS*$_{\Delta P}$ were introduced into either *E. coli* QC771 or QC1732 by co-transformation. β-galactosidase assays were performed on cells growing in M9 minimal salts medium supplemented with 0.5% (w/v) glucose, 0.1% casamino acids, and 25 μg ml^{-1} chloramphenicol, according to the protocol outlined in section 2.5.1. The medium was supplemented with 50 μg ml^{-1} gentamicin for bacteria harbouring pBBR1MCS-5 and its derivatives. To induce iron-limiting conditions, cultures were supplemented with 100 μM 2,2-dipyridyl (see section 5.4.3). To induce iron-replete conditions, cultures were supplemented with 50 μM FeCl$_3$.
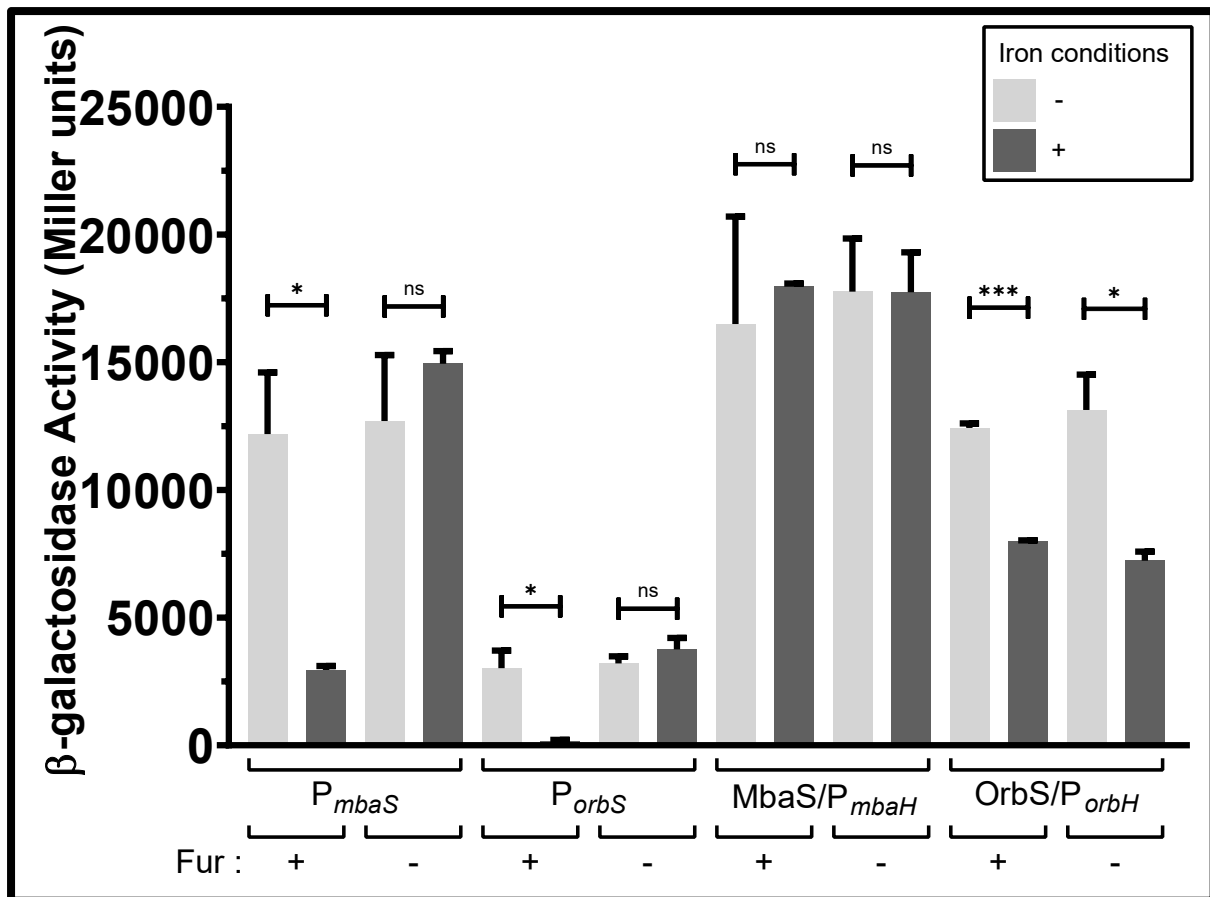
Figure 5.16. β-galactosidase assay demonstrating loss of Fur-dependent regulation of constructed ECF sigma factor expression plasmids under iron-replete and iron-limited conditions.

Results of β-galactosidase assay investigating iron-dependent regulation of the σ^{70}-dependent promoters P$_{mbaS}$ and P$_{orbS}$, and the loss of iron-dependent regulation upon the expression of MbaS and OrbS measured via their activity upon their target promoters. β-galactosidase activity was measured in either *E. coli* QC771 (*fur*[+]) or *E. coli* QC1732 (*fur*[-]) (denoted as '+' or '-' below data bars). The bacteria harboured either pKAGd4-P^{short}$_{mbaS}$ (P$_{mbaS}$), pKAGd4-P$_{orbS}$ (P$_{orbS}$), pBBR5-*mbaS* and pKAGd4-P^{short}$_{mbaH}$ (MbaS/P$_{mbaH}$) or pBBR5-*orbS* and pKAGd4-P$_{orbH}$ (OrbS/P$_{orbH}$), as denoted below data bars. All β-galactosidase activities are corrected against background by subtraction of activity derived from either *E. coli* QC771 or *E. coli* QC1732 harbouring pKAGd4, or harbouring pBBR5 with pKAGd4-P^{short}$_{mbaH}$ or pKAGd4-P$_{orbH}$, as appropriate, under identical conditions. Growth medium was M9 minimal salts supplemented with 0.5% (w/v) glucose, 0.1 % (w/v) casamino acid, 25 µg ml^{-1} chloramphenicol, 50 µg ml^{-1} gentamicin for pBBR5-containing strains, and either 100 µM 2,2-dipyridyl (iron-limited, light grey) or 50 µM FeCl$_3$ (iron-replete, dark grey). Error bars show standard deviation (n=2). There are significant differences of β-galactosidase activity between iron-limited and iron-replete conditions for P$_{mbaS}$ in QC771 (P=0.03), P$_{orbS}$ in QC771 (P=0.03), and OrbS/P$_{orbH}$ in both QC771 (P=0.0008) and QC1732 (P=0.03) (unpaired t-tests).

In this assay, there is clear Fur dependent iron regulation of both P$_{mbaS}$ and P$_{orbS}$ in the *fur*[+] strain (P=0.03 for both, unpaired t-tests), which has been abolished in the *fur*[-] strain (no significant difference, unpaired t tests). For the pBBR5-*mbaS*/pKAGd4-P$_{mbaH}$ system, where

mbaS is being expressed from the vector *lacZ* promoters but not its native promoter, there is no iron regulation in the *fur*⁺ strain (no significant difference, unpaired t tests). This demonstrates that MbaS expressed from pBBR1MCS-5 is no longer under the regulatory control of Fur. For the pBBR5-*orbS*/pKAGd4-P$_{orbH}$ system, there is some iron regulation of P$_{orbH}$ present. However, this is assumed to not be due to Fur, as this regulation is present in both the *fur*⁺ and *fur*⁻ strains of *E. coli* (P=0.0008 and P=0.03, respectively, unpaired t tests). Therefore, the pBBR1MCS-based expression plasmids containing *mbaS*, *mbaS*$_{CpentaA}$, *orbS* and *orbS*$_{CtetraA}$ were used to investigate the effect of regulation upon the sigma factors independently of Fur.

5.6 Demonstration of cross-activity between MbaS and OrbS

Due to the homology between MbaS and OrbS, and their target promoters, the degree to which they show cross-activity was investigated. Although this may not occur in nature, this would demonstrate the high conservation shown by these IS sigma factors found in different *Burkholderia* species.

5.6.1 Cross-activity by CAS assay

The plasmids pBBR1MCS-2, pBBR1MCS2-*mbaS* and pBBR1MCS2-*orbS*$_{ΔP}$ were introduced by conjugation into the strains *Bth* E264 Δ*mbaS* and *Bce* H111 Δ*orbS* to compare the ability of the expressed sigma factors to complement the malleobactin/ornibactin-deficient phenotypes. This was assayed using the observed production of siderophore observed on CAS agar. Although pyochelin is still produced by both strains of *Burkholderia*, the production is much lower compared to that of malleobactin/ornibactin (in the case of *Bth* E264 Δ*mbaS* it is not seen after 16 hours at 37 °C) and can be clearly distinguished by its orange/red colour compared to the yellow of malleobctin/ornibactin.

Overnight cultures of each strain were grown in M9 minimal medium supplemented with 0.5% (w/v) glucose and 250 µg ml^{-1} (for *Bth*) or 50 µg ml^{-1} (for *Bce*) kanamycin. Cultures were normalised according to their OD$_{600}$ and 1 µl spotted onto CAS agar containing 10 µM FeCl$_3$ in triplicate. The areas of the siderophore halos was calculated manually.
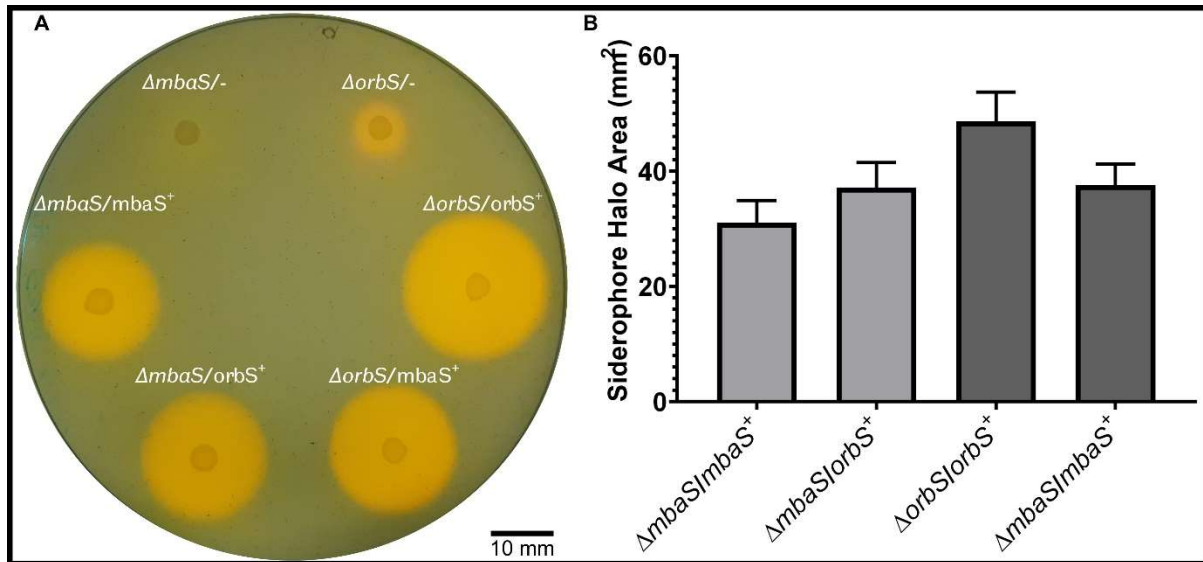
Figure 5.17. CAS assay demonstrating cross activity of MbaS and OrbS.

Bth E264 Δ*mbaS* and *Bce* H111 Δ*orbS* containing pBBR2 expression plasmids harbouring pBBR2, pBBR2-*mbaS* or pBBR2-*orbS*$_{ΔP}$ grown on CAS agar plates supplemented with 10 µM FeCl$_3$. Strain and plasmid harboured denoted above spotted culture. **B.** Area of siderophore halos produced. Error bars show standard deviation (n=3).

Both MbaS and OrbS expressed from the pBBR1MCS-2 plasmid are able to complement the Mba$^-$ and Orb$^-$ phenotypes of both *Bth* and *Bce*, respectively. This occurs irrespective of which sigma factor is present i.e. MbaS from *Bth* is able to complement the Δ*orbS* deletion of *Bce* and regulate the production of ornibactin, and OrbS from *Bce* is able to complement the Δ*mbaS* deletion of *Bth* and regulate the production of malleobactin. OrbS appears to show a greater ability to complement the Mba$^-$ and Pch$^-$ phenotypes, but this is small and not statistically significant.

5.6.2 Cross-activity by transcription reporter analysis

To quantify the *in vivo* cross activity observed in section 5.6.1 further, a combination of the expression vectors pBBR1MCS-2, pBBR2-*mbaS* and pBBR2-*orbS*$_{\Delta P}$ and the transcriptional reporter vectors pKAGd4-P$_{mbaH-S}$ and pKAGd4-P$_{orbH-S}$ were introduced into *E. coli* MC1061 by transformation. The β-galactosidase assay was performed according to the protocol outlined in section 2.5.1, and performed on cells grown in Lnx medium supplemented with 50 µg ml^{-1} kanamycin and 100 µg ml^{-1} ampicillin.
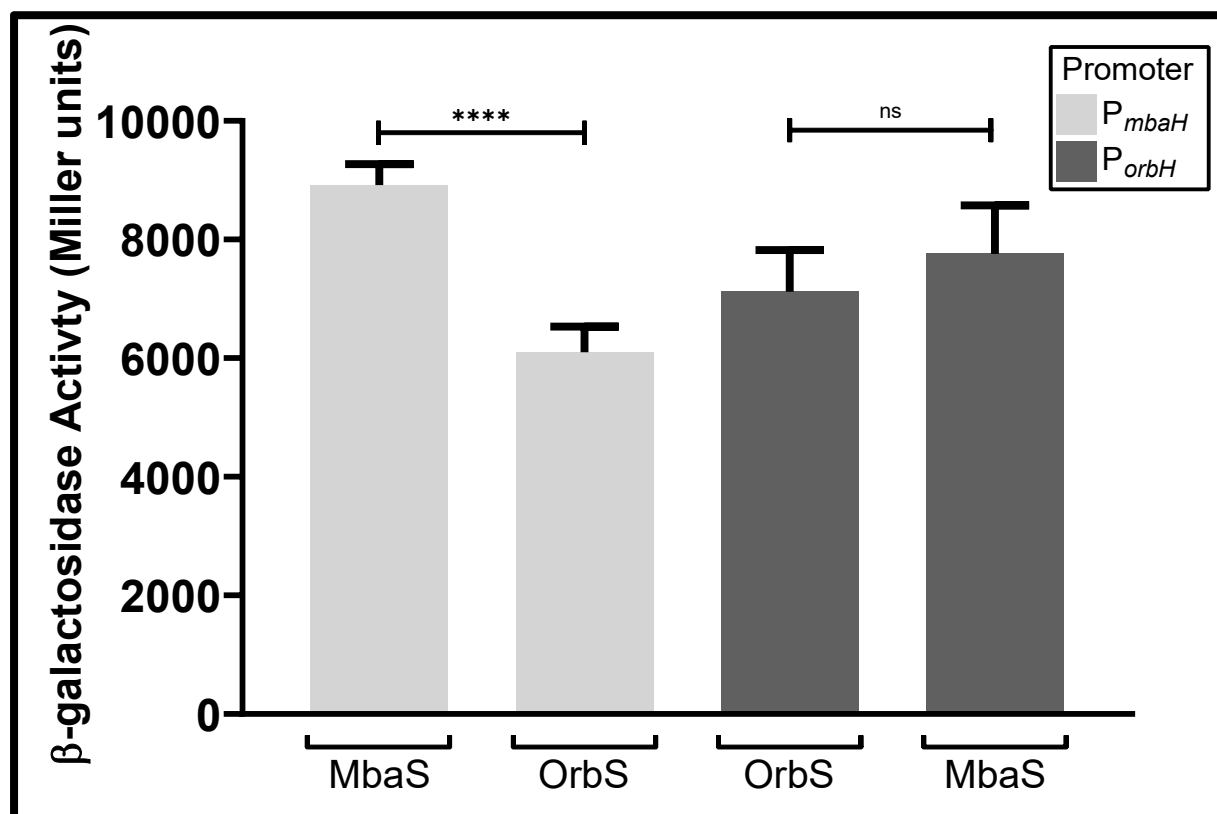
Figure 5.18. β-galactosidase assay demonstrating cross activity of MbaS and OrbS.

Results of β-galactosidase assay cross-activity of MbaS and OrbS upon their target promoters. β-galactosidase activity was measured in *E. coli* MC1061 harbouring (a) the transcriptional reporter vectors pKAGd4-P$_{mbaH-S}$ (light grey) or pKAGd4-P$_{orbH-S}$ (dark grey), and (b) the expression vector pBBR2-*mbaS* or pBBR2-*orbS*$_{\Delta P}$ (denoted below data bars). All β-galactosidase activities were corrected against background vector activity by subtraction of activity derived from *E. coli* MC1061 harbouring both the parental plasmid pBBR2 and either pKAGd4-P$_{mbaH-S}$ or pKAGd4-P$_{orbH-S}$. Strains were grown in Lnx medium supplemented with 50 µg ml^{-1} kanamycin and 100 µg ml^{-1} ampicillin. Error bars show standard deviation (n=6). There is a significant difference between the activities of MbaS and OrbS upon P$_{mbaH}$ (P<0.0001), but no significant different between the activities of MbaS and OrbS upon P$_{orbH}$ (one-way ANOVA, Tukey's multiple comparisons test).

Again, it can be observed that both sigma factors are able to recognise and initiate transcription from the other's target promoter. Both MbaS and OrbS display similar activity upon the *orbH* promoter (no significant difference), but OrbS displays a smaller activity upon the *mbaH* promoter compared to MbaS (P<0.0001).

5.6.3   Purification of OrbS and OrbS$_{CtetraA}$

The previously constructed plasmids pET14b-*orbS* (Agnoli, 2007) and pET14b-*orbS*$_{CtetraA}$ (A. Butt unpublished data) were used to overexpress the corresponding ECF sigma factors in *E. coli*BL21(DE3). The overexpressed proteins were purifiedfrom cell lysates in an analogous manner to MbaS and MbaS$_{CpentaA}$ (section 5.3.2) and as described in sections 2.4.1 to 2.4.3. Protein yields were typically lower for OrbS/OrbS$_{CtetraA}$. To overcome this, proteins were extracted from cell pellets generated from 500 ml of cell culture, supplemented with 100 µg ml^{-1} carbenicillin. Examples of SDS-PAGE for analysis of the protein purification process are shown for OrbS (Figure 5.19) and OrbS$_{CtetraA}$ (Figure 5.20).
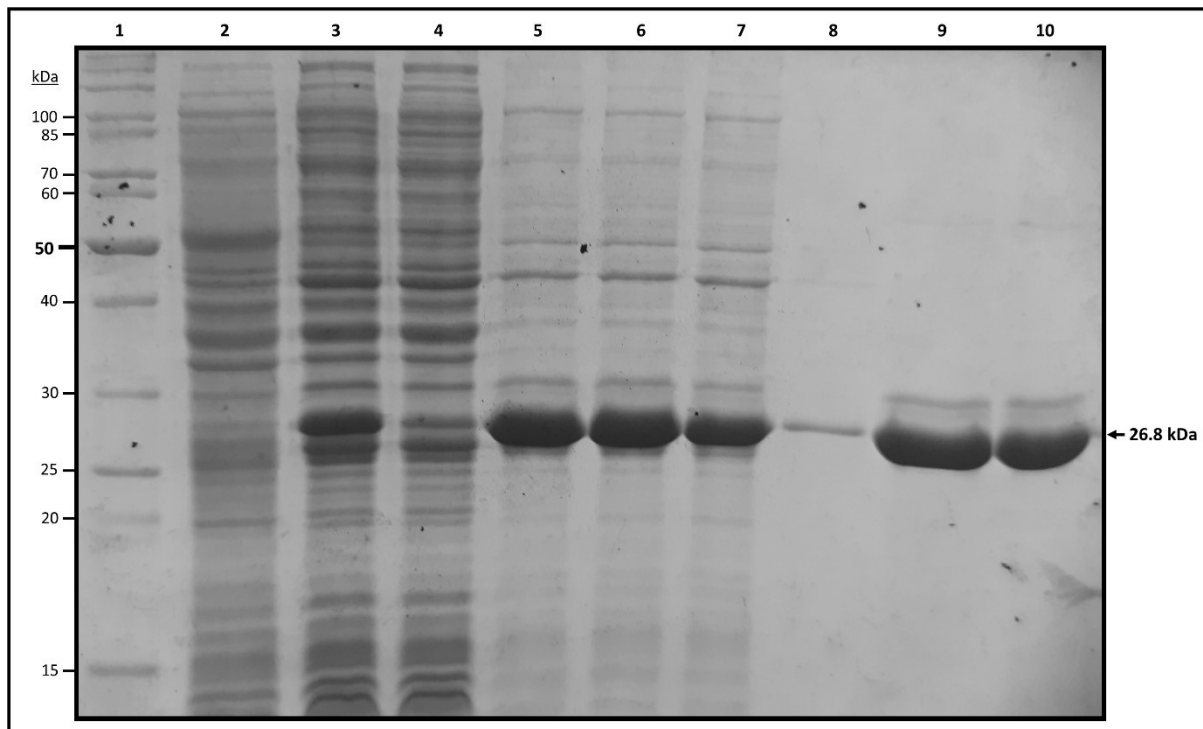
Figure 5.19. Purification of OrbS

SDS-PAGE analysis of protein samples from overexpression and purification of OrbS. Expected MW of OrbS is 26.8 kDa. Volume of sample loaded shown below in brackets. Lane 1, EZ-run *Rec* Protein Ladder (Fisher Bioreagents); lane 2, un-induced protein (5 µl); lane 3, total induced protein (5 µl); lane 4, total soluble protein (5 µl); lane 5, total protein post-sarkosyl treatment (10 µl); lane 6, total soluble protein post-sarkosyl treatment (10 µl); lane 7, protein unbound to IMAC column (10 µl); lane 8, flow-through of wash through protein-loaded IMAC column (10 µl); lane 9, eluted protein (10 µl); lane 10, final dialysed protein (5 µl).
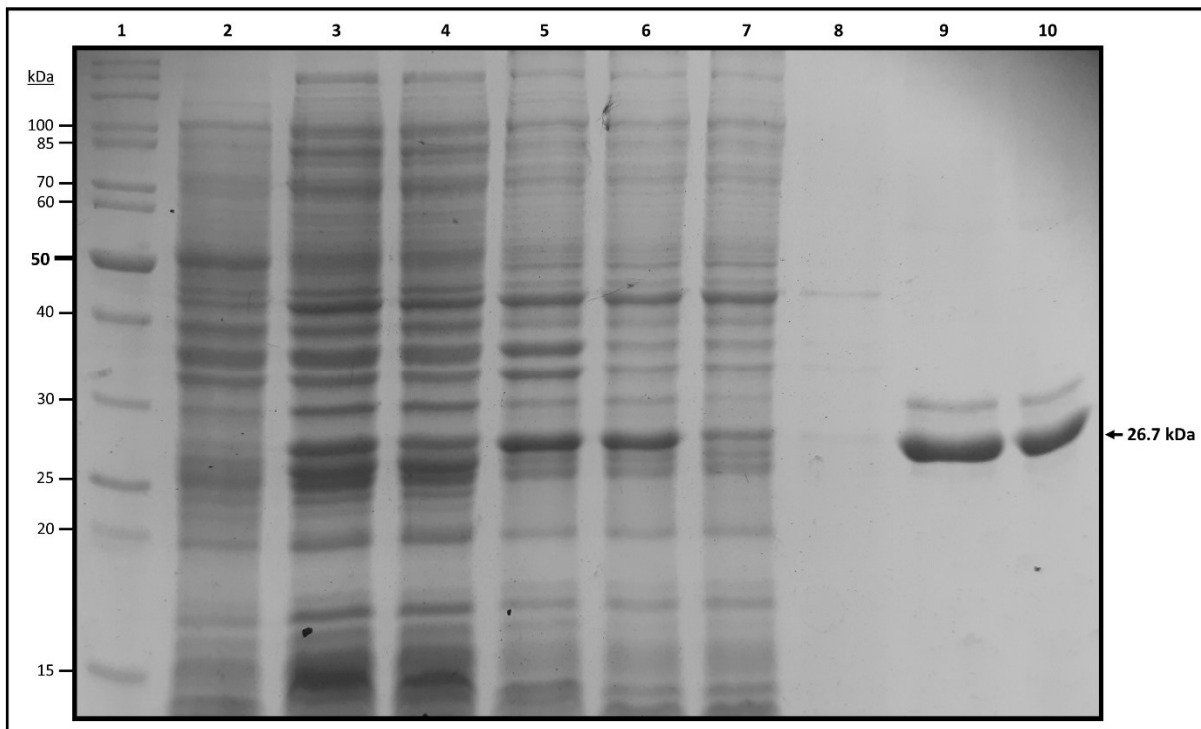
Figure 5.20. Purification of OrbS$_{CtetraA}$

SDS-PAGE analysis of protein samples from overexpression and purification of OrbS$_{CtetraA}$. Expected MW of OrbS$_{CtetraA}$ is 26.7 kDa. Volume of sample loaded shown below in brackets. Lane 1, EZ-run *Rec* Protein Ladder (Fisher Bioreagents); lane 2, un-induced protein (5 µl); lane 3, total induced protein (5 µl); lane 4, total soluble protein (5 µl); lane 5, total protein post-sarkosyl treatment (10 µl); lane 6, total soluble protein post-sarkosyl treatment (10 µl); lane 7, protein unbound to IMAC column (10 µl); lane 8, flow-through of wash through protein-loaded IMAC column (10 µl); lane 9, eluted protein (10 µl); lane 10, final dialysed protein (5 µl).

5.6.4   Cross-activity by *in vitro* transcription assay

To further examine this cross-activity further, both the MbaS and OrbS sigma factors were used in *iv*T assays in combination with *E. coli* core RNAP (NEB) and the pRLG770 plasmids containing either P$_{mbaH}$ or P$_{orbH}$. Reactions were set up with core RNAP in conjunction with (a) pRLG770-P$_{mbaH}$ with MbaS, OrbS, or the absence of sigma factor, and (b) pRLG770-P$_{orbH}$ds6 (A. Butt, unpublished) with MbaS, OrbS, or the absence of sigma factor (Figure 5.21).

214
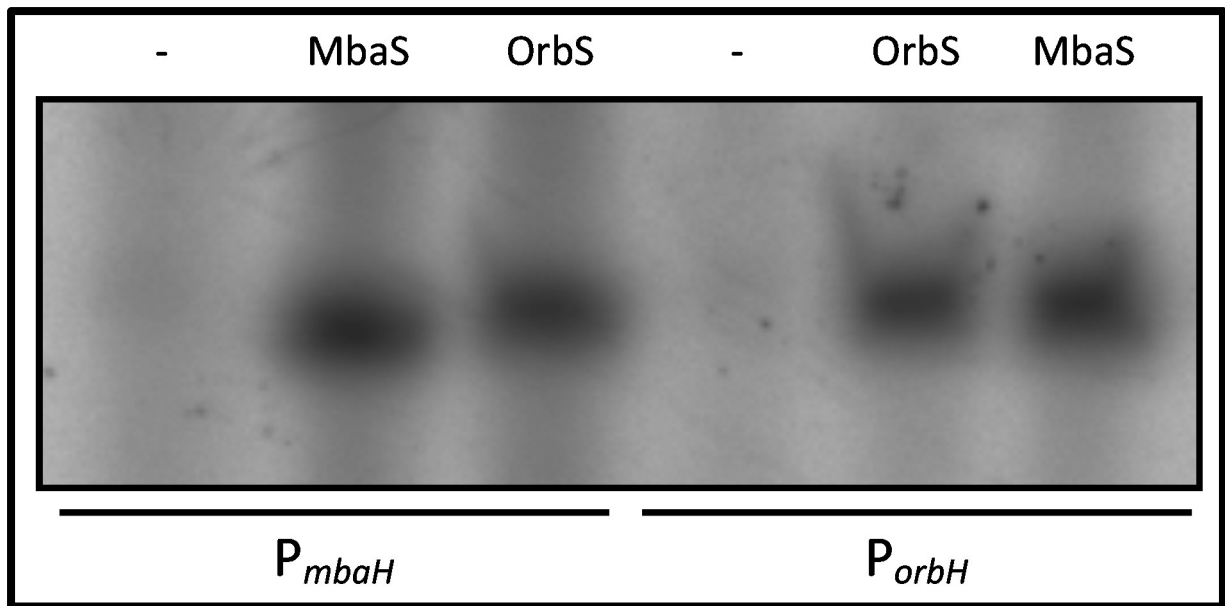
Figure 5.21. *in vitro* **transcription assay demonstrating cross-activity of MbaS and OrbS upon their target promoters.**

RNA transcripts were resolved in a 5.5% acrylamide, 7 M urea gel following an *in vitro* transcription assay. *E. coli* core RNA polymerase (NEB), in association with either MbaS, OrbS or no sigma factor (denoted above gel image), was used to synthesise RNA from a DNA fragments containing the promoters P*mbaH* or P*orbH* cloned into pRLG770 (denoted below gel image). RNA transcripts were synthesised from the *mbaH* or *orbH* promoter (156 nt transcripts).

Both MbaS and OrbS, when present with *E. coli* core RNAP, can initiate transcription to synthesise an RNA product from both the P*mbaH* and P*orbH* promoters. Again, this demonstrates the homology between both these ECF sigma factors and their target promoters.

5.7 Investigation of iron-dependent regulation of MbaS and OrbS *in vivo*

It has been observed in previous work, and in experimental data presented here (see Chapter III), that there appears to be a Fur-independent iron regulation of OrbS activity. It has been hypothesised that this regulation occurs via the four cysteine residues found

within the CRE of OrbS. Experimental work using OrbS$_{CtetraA}$, and mutant form of OrbS with four cysteine-to-alanine substitutions within the CRE, also provides some evidence that this iron regulation is lost when the cysteine residues are not present (see section 3.3-3.4). The homologous protein MbaS also contains a CRE, with five cysteine residues. So far, preliminary experiments (Figure 5.16) have not demonstrated any iron regulation.

The putative regulatory effect of iron, independent of Fur, upon both MbaS and OrbS was investigated further. If iron regulation is observed, the dependency of the cysteine residues of the CREs was examined by comparison of the wild-type sigma factors with their cysteine-to-alanine substitution mutants. Firstly, *in vivo* transcription reporter analysis and growth of *Bth* cultures on CAS medium were used to investigate this iron regulation.

5.7.1 Effect of iron availability upon MbaS and OrbS independent of Fur in *E. coli* MC1061

Using the Fur-independent expression vectors pBBR2-*mbaS* and pBBR2-*mbaS*$_{CpentaA}$ (see section 4.7.1), and the MbaS-dependent promoter contained within the transcriptional reporter vector pKAGd4-P$_{mbaH-S}$ (see section 5.2.2), it was possible to investigate the effect of iron upon the activity of MbaS via the five cysteine residues of its CRE through transcription reporter analysis. As the sigma factors genes are expressed independently of Fur (see section 5.5.4) it was possible to use the *fur*+ *E. coli* MC1061 strain. A combination of the plasmids pKAGd4 or pKAGd4-P$_{mbaH-S}$ and pBBR1MCS-2, pBBR2-*mbaS* or pBBR2-*mbaS*$_{CpentaA}$ were introduced into *E. coli* MC1061 by transformation. β-galactosidase assays were performed in cells grown in M9 minimal salts medium supplemented with 0.5% (w/v) glucose, 0.1% (w/v) casamino acids, 100 µg ml^{-1} ampicillin and 50 µg ml^{-1} kanamycin, according to the protocol outlined in section 2.5.1. Iron-limited conditions were introduced by the addition of 100 µM 2,2-dipyridyl, and iron-replete conditions were introduced by the addition of 50 µM FeCl$_3$. The experiment was performed a total of two times on two different days.
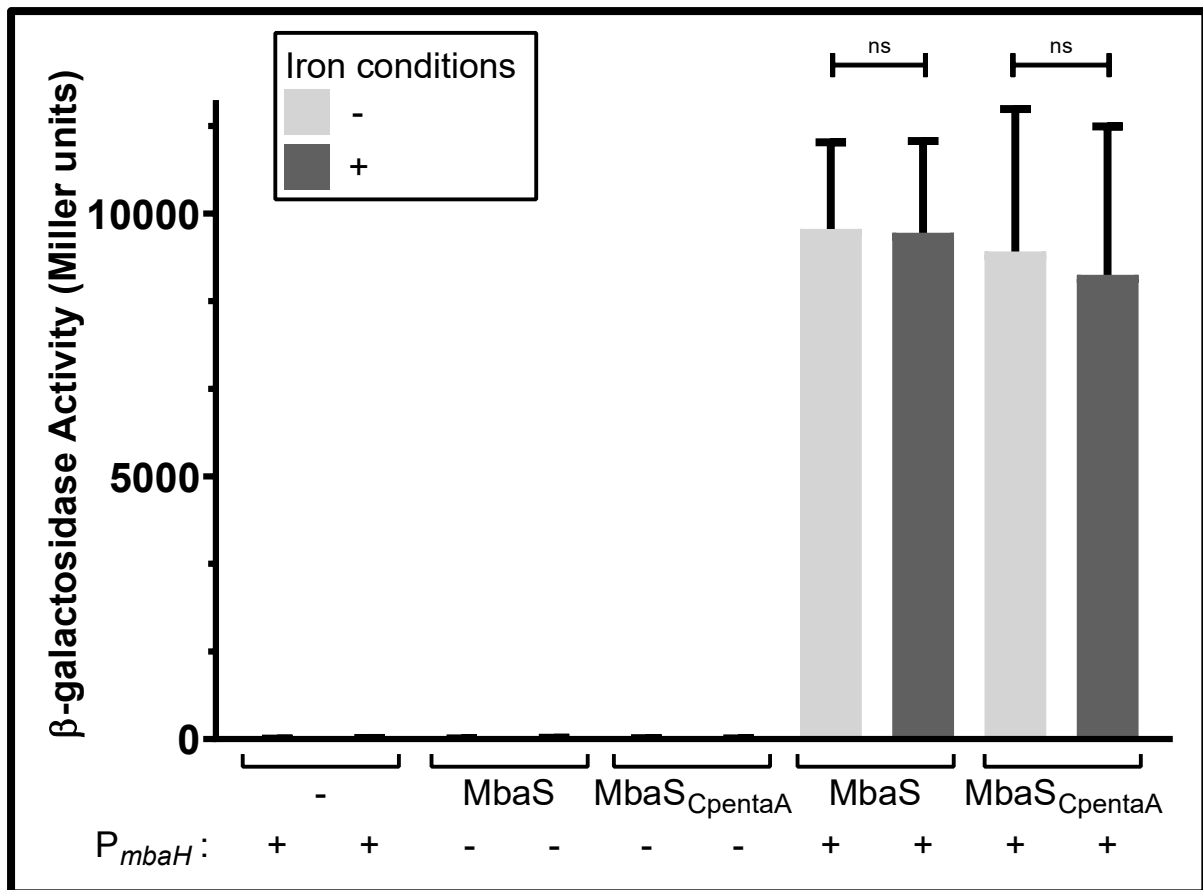
Figure 5.22. β-galactosidase assay of MbaS and MbaS$_{CpentaA}$ upon P$_{mbaH}$ in *E. coli* MC1061 under iron-limited and iron-replete conditions.

Results of β-galactosidase assay investigation iron-dependent regulation of MbaS and MbaS$_{CpentaA}$ upon an MbaS-dependent promoter. β-galactosidase activity was measured in *E. coli* MC1061 harbouring (a) pKAGd4, (-) or pKAGd4-P$_{mbaH-S}$ (+), and (b) pBBR1MCS-2 (-), pBBR2-*mbaS* or pBBR2-*mbaS*$_{CpentaA}$, as denoted below data bars. All β-galactosidase activities were corrected against background vector activity by subtraction of activity derived from *E. coli* MC1061 harbouring both parental plasmids pBBR2 and pKAGd4. Growth medium was M9 minimal salts supplemented with 0.5% (w/v) glucose, 0.1% (w/v) casamino acids, 100 µg ml^{-1} ampicillin and 50 µg ml^{-1} kanamycin and either 100 µM 2,2-dipyridyl (iron-limited, light grey) or 50 µM FeCl$_3$ (iron-replete, dark grey). Error bars show standard deviation (n=6). There are no significant differences between the activities of MbaS and MbaS$_{CpentaA}$ upon the *mbaH* promoter under iron-limited and iron-replete conditions (one-way ANOVA, Tukey's multiple comparisons test).

The β-galactosidase activity from the fused *mbaH* promoter remained high regardless of whether MbaS or MbaS$_{CpentaA}$ were included, and whether conditions were iron-limited or iron-replete. This strongly suggests there is no iron-regulation of MbaS. As a positive control for iron-dependent regulation of the sigma factors, it was decided to include OrbS and OrbS$_{CtetraA}$ in the transcription reporter analysis. The β-galactosidase assay was performed in

217

an analagous way, but included pBBR2-*orbS*ΔP or pBBR2-*orbS*CtetraA-ΔP, in combination with pKAGd4-P*orbH-S*, introduced into *E. coli* MC1061 by transformation. The experiment was performed a total of two times on two days.
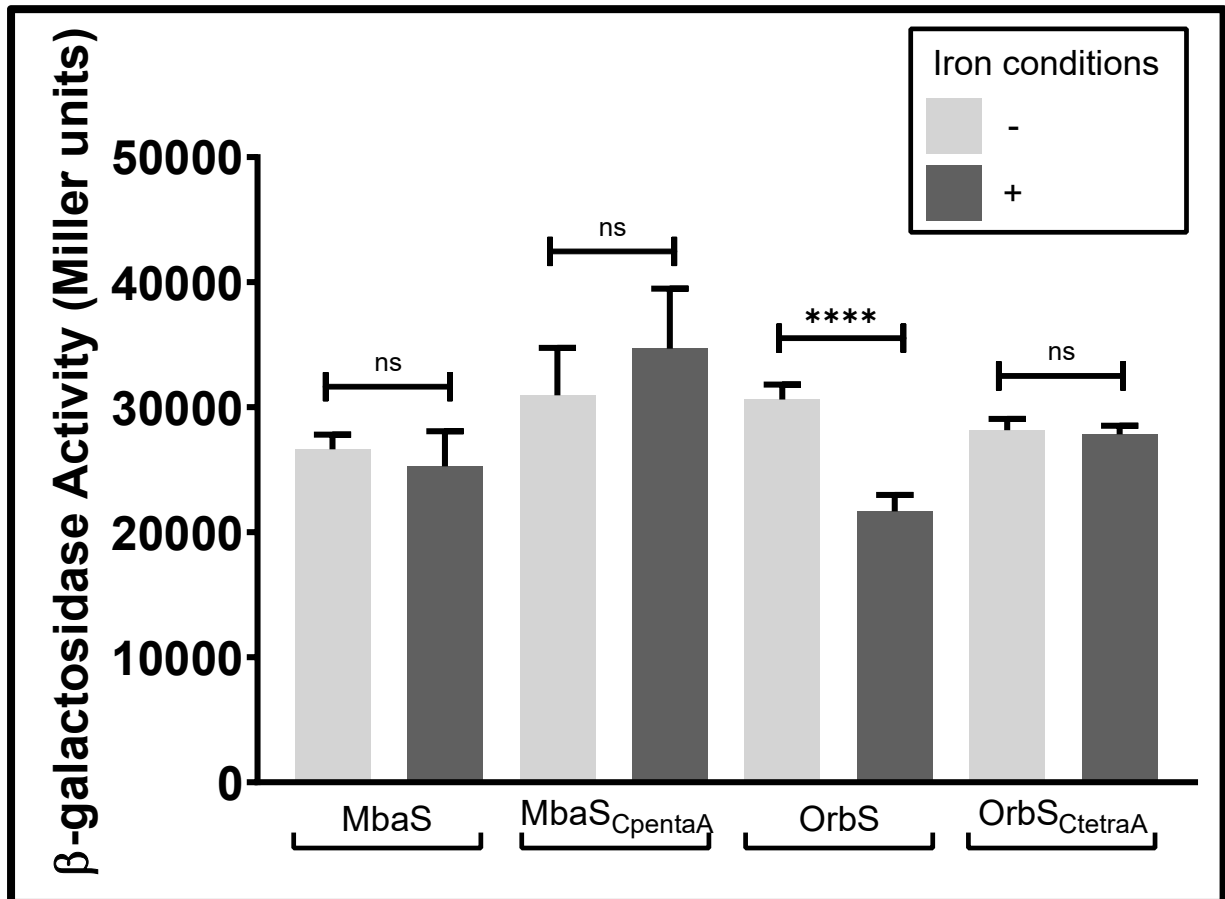
Figure 5.23. β-galactosidase assay of MbaS, MbaS CpentaA**, OrbS and OrbS**CtetraA **upon their target promoters in *E. coli* MC1061 under iron-limited and iron-replete conditions.**

Results of β-galactosidase assay investigation iron-dependent regulation of MbaS and MbaS$_{CpentaA}$ upon an MbaS-dependent promoter, and OrbS and OrbS$_{CtetraA}$ upon an OrbS-dependent promoter. β-galactosidase activity was measured in *E. coli* MC1061 harbouring (a) pKAGd4-P*mbaH-S* for MbaS and MbaS$_{CpentaA}$ or pKAGd4-P*orbH-S* for OrbS and OrbS$_{CtetraA}$, and (b) pBBR2-*mbaS*, pBBR2-*mbaS*$_{CpentaA}$, pBBR2-*orbS*ΔP or pBBR2-*orbS*CtetraA-ΔP as denoted below data bars. All β-galactosidase activities were corrected for background vector activity by subtraction of activity derived from *E. coli* MC1061 harbouring both plasmids pBBR2 and pKAGd4-P*mbaH-S* (for MbaS and MbaS$_{CpentaA}$) or pKAGd4-P*orbH-S* (for OrbS and OrbS$_{CtetraA}$). Growth medium was M9 minimal salts supplemented with 0.5% (w/v) glucose, 0.1% (w/v) casamino acids, 50 µg ml^{-1} chloramphenicol and 50 µg ml^{-1} kanamycin and either 100 µM 2,2-dipyridyl (iron-limited, light grey) or 50 µM FeCl$_3$ (iron-replete, dark grey). Error bars show standard deviation (n=6). There is a significant difference between the activity of OrbS under iron-limited and iron-replete conditions (P<0.0001), but not for the other sigma factors (one-way ANOVA, Sidak's multiple comparisons test).

Again, there appears to be no regulation of MbaS by iron. However, with OrbS there is a approximately 29% reduction in activity under iron-replete conditions compared to iron-limited conditions (P<0.0001, one-way ANOVA, Sidak's multiple comparisons test). The four cysteine residues of the CRE appear to be integral to this regulation mechanism, as there is no reduction of activity observed for OrbS$_{CtetraA}$.

5.7.2 Effect of iron availability upon MbaS and OrbS independently of Fur in *E. coli* QC1732

Although it has been demonstrated that the pBBR1MCS-based plasmids containing the *mbaS* and *orbS* genes are not regulated by Fur (see section 5.5.4), it is possible that the Fur protein may still influence the results when performing β-galactosidase assays investigating the effect of iron in the *E. coli fur$^+$* strain MC1061. For instance, under iron-replete conditions, the Fur repressor may regulate chromosomal genes of the *E. coli* MC1061 host strain that could ultimately impact the β-galactosidase activity measured from the LacZα-fused promoters cloned into pKAGd4. To overcome this potential issue, the β-galactosidase assays performed in section 5.7.1 were repeated in the *E. coli fur$^-$* QC1732 strain. Additionally, to demonstrate the loss of Fur regulation in parallel, pKAGd4 containing the σ^{70}-dependent, Fur-regulated, P$_{mbaS}$ was included.

A combination of the plasmids pKAGd4, pKAGd4-P$_{mbaS-L}$ or pKAGd4-P$_{mbaH-L}$ and pBBR1MCS-5, pBBR5-*mbaS* or pBBR5-*mbaS*$_{CpentaA}$ were introduced into *E. coli* QC1732 by transformation. The β-galactosidase assay was performed in cells grown in M9 minimal salts medium supplemented with 0.5% (w/v) glucose, 0.1% (w/v) casamino acids, 100 µg ml^{-1} ampicillin and 50 µg ml^{-1} gentamicin, according to the protocol outlined in section 2.5.1. Iron-limited conditions were introduced by the addition of 100 µM 2,2-dipyridyl, and iron-replete conditions were introduced by the addition of 50 µM FeCl$_3$. The experiment was performed a total of two times on two days.
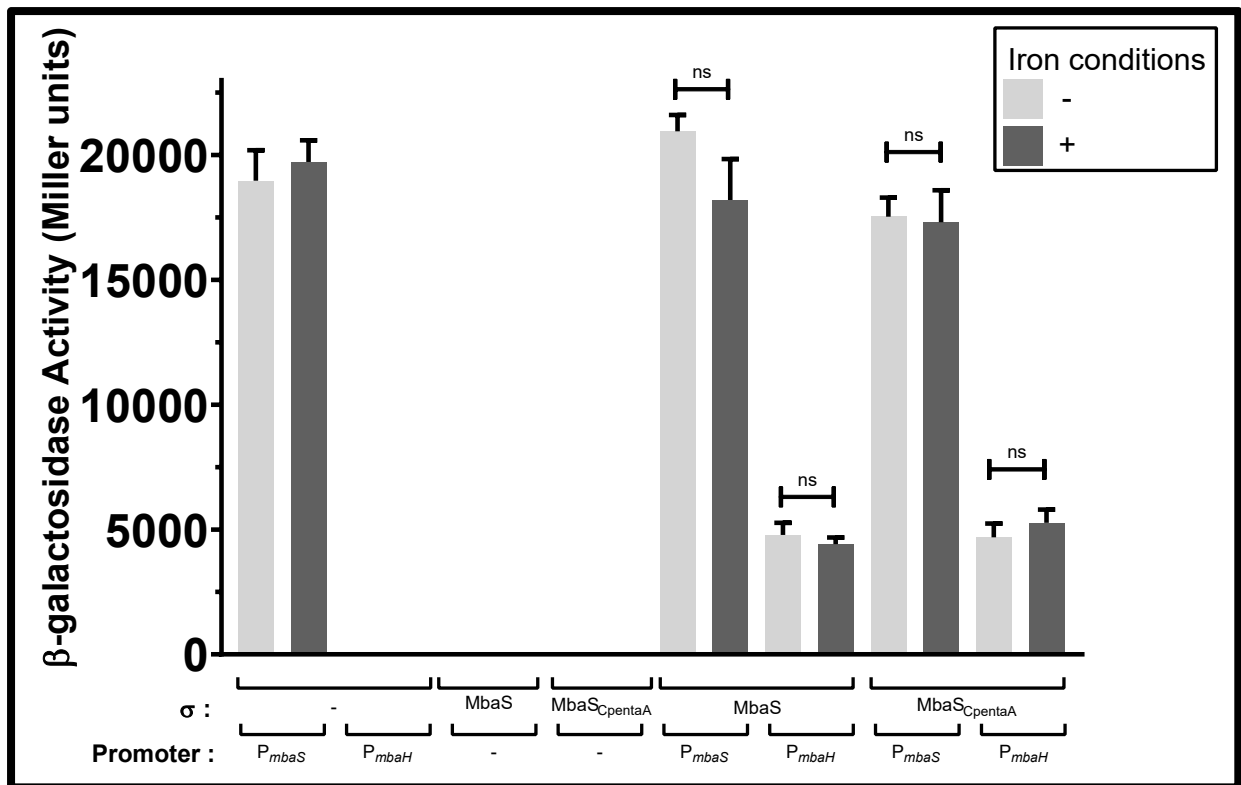
Figure 5.24. β-galactosidase assay of MbaS and MbaS$_{CpentaA}$ upon P$_{mbaS}$ and P$_{mbaH}$ in *E. coli* QC1732 under iron-limited and iron-replete conditions.

Results of β-galactosidase assay investigation iron-dependent regulation of MbaS and MbaS$_{CpentaA}$ upon the P$_{mbaS}$ and P$_{mbaH}$ promoters. β-galactosidase activity was measured in *E. coli* QC1732 harbouring (a) pBBR1MCS-5 (-), pBBR5-*mbaS* or pBBR5-*mbaS*$_{CpentaA}$, and (b) pKAGd4 (-), pKAGd4-P$_{mbaS-L}$ or pKAGd4-P$_{mbaH-L}$, as denoted below data bars. All β-galactosidase activities were corrected for background vector activity by subtraction of activity derived from *E. coli* QC1732 harbouring both parental plasmids pBBR1MCS-5 and pKAGd4. Growth medium was M9 minimal salts supplemented with 0.5% (w/v) glucose, 0.1% (w/v) casamino acids, 100 µg ml^{-1} ampicillin and 50 µg ml^{-1} gentamicin and either 100 µM 2,2-dipyridyl (iron-limited, light grey) or 50 µM FeCl$_3$ (iron-replete, dark grey). Error bars show SEM (n=6). There are no significant differences between the activities of the *mbaS* promoter or the activities of MbaS and MbaS$_{CpentaA}$ upon the *mbaH* promoter under iron-limited and iron-replete conditions (one-way ANOVA, F=0.58, P=0.63, Tukey's multiple comparisons post-hoc test).

As with the assay performed in *E. coli* MC1061, there is no iron-dependent inhibition effect upon MbaS. The β-galactosidase activity from the Fur-regulated σ^{70}-dependent *mbaS* promoter remains high regardless of the iron conditions, confirming that there no Fur-regulation is present in this system.

As with *E. coli* MC1061 in section 5.7.1, OrbS and OrbS$_{CtetraA}$ were included as a positive control for Fur-independent iron regulation. The assay was performed in an analogous manner, but included pBBR5-*orbS*$_{ΔP}$ or pBBR5-*orbS*$_{CtetraA-ΔP}$, in combination with pKAGd4-

P$_{orbH\text{-}S}$, introduced into *E. coli* QC1732 by transformation. The experiment was performed a total of two times on two days.
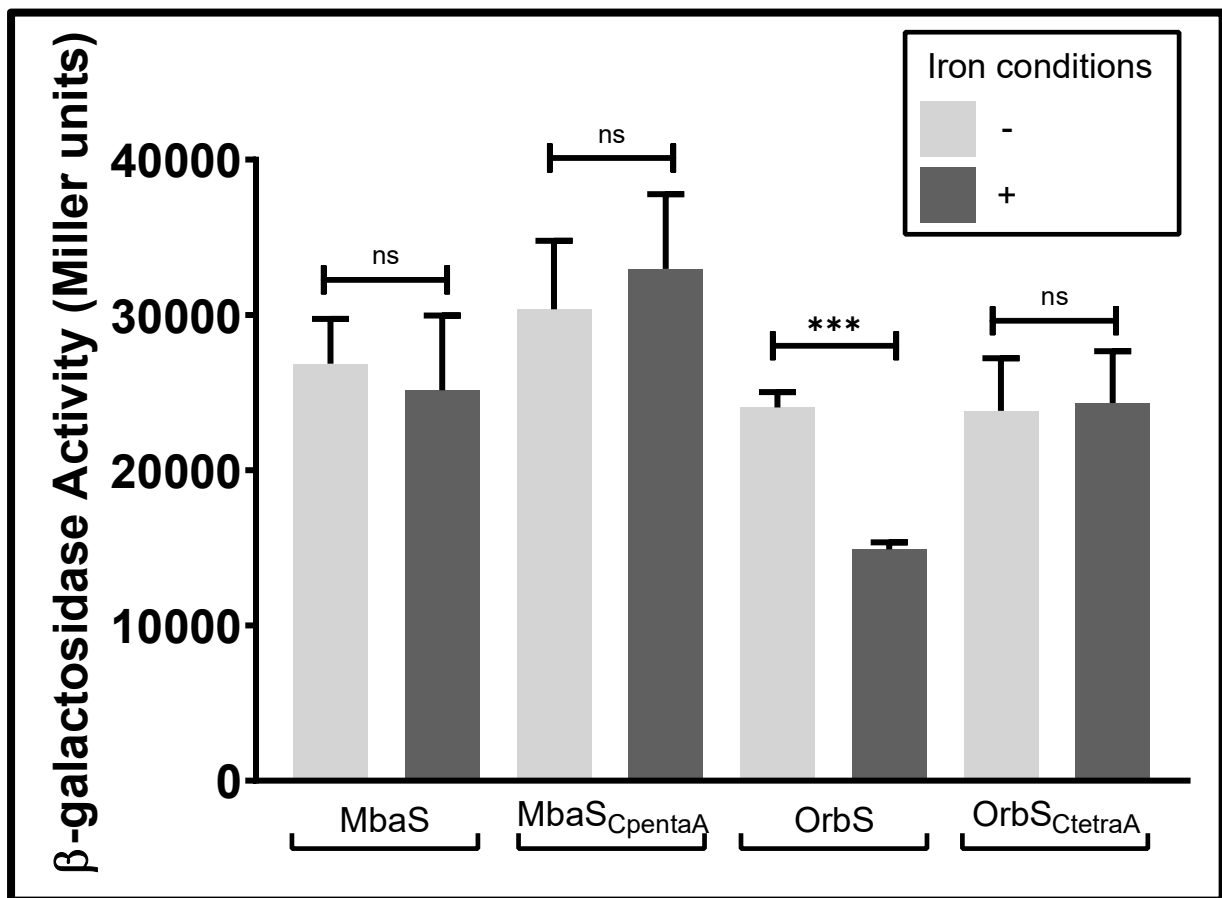
Figure 5.25. β-galactosidase assay of MbaS, MbaS$_{CpentaA}$, OrbS and OrbS$_{CtetraA}$ upon their target promoters in *E. coli* QC1732 under iron-replete and iron-limited conditions.

Results of β-galactosidase assay investigation iron-dependent regulation of MbaS and MbaS$_{CpentaA}$ upon an MbaS-dependent promoter, and OrbS and OrbS$_{CtetraA}$ upon an OrbS-dependent promoter. β-galactosidase activity was measured in *E. coli* QC1732 harbouring (a) pKAGd4-P$_{mbaH\text{-}S}$ for MbaS and MbaS$_{CpentaA}$ or pKAGd4-P$_{orbH\text{-}S}$ for OrbS and OrbS$_{CtetraA}$, and (b) pBBR5-*mbaS*, pBBR5-*mbaS*$_{CpentaA}$, pBBR5-*orbS*$_{ΔP}$ or pBBR5-*orbS*$_{CtetraA\text{-}ΔP}$ as denoted below data bars. All β-galactosidase activities were corrected for background vector activity by subtraction of activity derived from *E. coli* QC1732 harbouring both plasmids pBBR1MCS-5 and pKAGd4-P$_{mbaH\text{-}S}$ (for MbaS and MbaS$_{CpentaA}$) or pKAGd4-P$_{orbH\text{-}S}$ (for OrbS and OrbS$_{CtetraA}$). Growth medium was M9 minimal salts supplemented with 0.5% (w/v) glucose, 0.1% (w/v) casamino acids, 50 µg ml^{-1} chloramphenicol and 50 µg ml^{-1} gentamicin and either 100 µM 2,2-dipyridyl (iron-limited, light grey) or 50 µM FeCl$_3$ (iron-replete, dark grey). Error bars show standard deviation (n=6). There is a significant difference between the activity of OrbS under iron-limited and iron-replete conditions (P=0.0002), but not for the other sigma factors (one-way ANOVA, Sidak's multiple comparisons test).

As previously observed, there appears to be no regulation of MbaS by iron. This remains the case regardless of whether *E. coli* MC1061, QC771 or QC1732 is used. However, OrbS displays an approximately 38% reduction in activity upon P$_{orbH-S}$ under iron-replete conditions compared to iron-limited conditions (P=0.0002, one-way ANOVA, Sidak's multiple comparisons test). Further evidence is provided that this is due to the four cysteine residues of the CRE, as there is no reduction of activity observed for OrbS$_{CtetraA}$.

5.7.3 Effect of iron availability upon MbaS by transcription reporter analysis in *B. thalandensis ΔmbaS*

The transcription reporter analyses from sections 5.7.1 and 5.7.2 were performed in heterologous *E. coli* systems. However, there may be factors present in *Bth*, which are not found in *E. coli*, that could be involved in the iron-dependent regulation of MbaS. Therefore, the β-galactosidase assays were also performed using a *Bth* host strain. Ideally, these assays would be performed in a *Bth fur⁻* strain to remove Fur-regulation of the chromosomal copy of MbaS. However, there were many difficulties in isolating a *Bth* E264 *Δfur* mutant. Instead, the Fur-independent pBBR2-*mbaS* and pBBR2-*mbaS*$_{CpentaA}$ were utilised in a *Bth* E264 *ΔmbaS* host strain (to remove interference from chromosomally-encoded MbaS). However, this strain still possessed the Fur repressor, so P$_{mbaS}$ was assayed in parallel with P$_{mbaH}$ to examine the effect Fur-regulation may have on the system.

A combination of pKAGd4, pKAGd4-P$_{mbaS-L}$ and pKAGd4-P$_{mbaH-L}$ were introduced into *Bth* E264 *ΔmbaS* by conjugation using *E. coli* S17-1 donor cells. Subsequently, either pBBR1MCS-2, pBBR2-*mbaS* or pBBR2-*mbaS*$_{CpentaA}$ were introduced into these strains by conjugation, also using *E. coli* S17-1 donor cells. β-galactosidase assays were performed in M9 minimal salts medium supplemented with 0.5% (w/v) glucose, 0.1% (w/v) casamino acids, 50 µg ml^{-1} chloramphenicol and 250 µg ml^{-1} kanamycin according to the protocol outlined in section 2.5.1. Iron-limited conditions were introduced by the addition of 100 µM 2,2-dipyridyl, and iron-replete conditions were introduced by the addition of 50 µM FeCl$_3$. The experiment was performed a total of three times on three different days.

Figure 5.26. β-galactosidase assay of MbaS and MbaS$_{CpentaA}$ upon P$_{mbaS}$ and P$_{mbaH}$ in *B. thailandensis* E264 Δ*mbaS* under iron-limited and iron-replete conditions.

Results of β-galactosidase assay investigation iron-dependent regulation of MbaS and MbaS$_{CpentaA}$ upon the P$_{mbaS}$ and P$_{mbaH}$ promoters. β-galactosidase activity was measured in *Bth* E264 Δ*mbaS* harbouring (a) pBBR1MCS-2 (-), pBBR2-*mbaS* or pBBR2-*mbaS*$_{CpentaA}$, and (b) pKAGd4 (-), pKAGd4-P$_{mbaS-L}$ or pKAGd4-P$_{mbaH-L}$, as denoted below data bars. All β-galactosidase activities were corrected for background vector activity by subtraction of activity derived from *Bth* E264 Δ*mbaS* harbouring both parental plasmids pBBR1MCS-2 and pKAGd4. Growth medium was M9 minimal salts supplemented with 0.5% (w/v) glucose, 0.1% (w/v) casamino acids, 50 µg ml^{-1} chloramphenicol and 250 µg ml^{-1} kanamycin and either 100 µM 2,2-dipyridyl (iron-limited, light grey) or 50 µM FeCl$_3$ (iron-replete, dark grey). Error bars show SEM (n=9). There is a significant difference between the activities of MbaS upon the *mbaH* promoter under iron-limited and iron-replete conditions (unpaired t-test, P=0.04), and no significant difference between the activities of MbaS$_{CpentaA}$ upon the *mbaH* promoter under iron-limited and iron-replete conditions (unpaired t-test, P=0.40).

In Figure 5.26, it can be observed that the Fur repressor is active in the *Bth* E264 Δ*mbaS* host. This is seen in the reduction of activity from the P$_{mbaS}$ promoter under iron-replete conditions compared to iron-limited conditions. However, it is unlikely that this has had an effect upon the expression of MbaS/MbaS$_{CpentaA}$ from pBBR1MCS-5, or their activity upon P$_{mbaH}$, as the β-galactosidase activity from pKAGd4-P$_{mbaH-L}$ in combination with pBBR5-*mbaS*

or pBBR5-*mbaS*$_{CpentaA}$ does not display this magnitude of inhibition. A small, but significant, approximately 19% decrease in activity by MbaS upon P$_{mbaH}$ under iron-replete conditions compared to iron-limited conditions is observed (P=0.04, unpaired t-test). This inhibition is not observed in the parallel MbaS$_{CpentaA}$ system (P=0.40, unpaired t-test). This is the first indication that MbaS may respond to iron via its five cysteine residues present in its CRE. However, it should be noted that this inhibition effect is smaller than the effect seen with OrbS.

5.7.4 Effect of iron upon MbaS and OrbS-regulated siderophore production in *B. thailandensis* Δ*mbaS* and *B. cenocepacia* Δ*orbS* grown on CAS agar

In addition to the transcription reporter analyses in sections 5.7.1 to 5.7.3, *Burkholderia* strains were grown on CAS agar to investigate the effect of iron upon the regulation of MbaS and OrbS. Rather than judging the activity of the sigma factors via their target promoter expression, this *in vivo* method analysed the activity of the sigma factors via the production of siderophores.

To examine the iron-regulation of MbaS, the plasmids pBBR1MCS-2, pBBR2-*mbaS* and pBBR2-*mbaS*$_{CpentaA}$ were each introduced into *Bth* E264 Δ*mbaS* by conjugation using *E. coli* S17-1 donor cells. Likewise, to examine the iron-regulation of OrbS, the plasmids pBBR1MCS-2, pBBR2-*orbS*$_{\Delta P}$ and pBBR2-*orbS*$_{CtetraA-\Delta P}$ were each introduced into *Bce* H111 Δ*orbS* (A. Butt, unpublished) using *E. coli* S17-1 donor cells. Strains were grown overnight in M9 minimal medium containing 0.5% (w/v) glucose, 0.1% (w/v) casamino acids and either 250 μg ml^{-1} kanamycin (for *Bth*) or 50 μg ml^{-1} kanamycin (for *Bce*). Cultures were normalised according to their OD$_{600}$ and 1 μl spotted onto CAS agar containing either 10 μM FeCl$_3$ or 60 μM FeCl$_3$ in quadruplicate (Figure 5.27 and Figure 5.28). The areas of the siderophore halos was calculated by measuring their diameter.
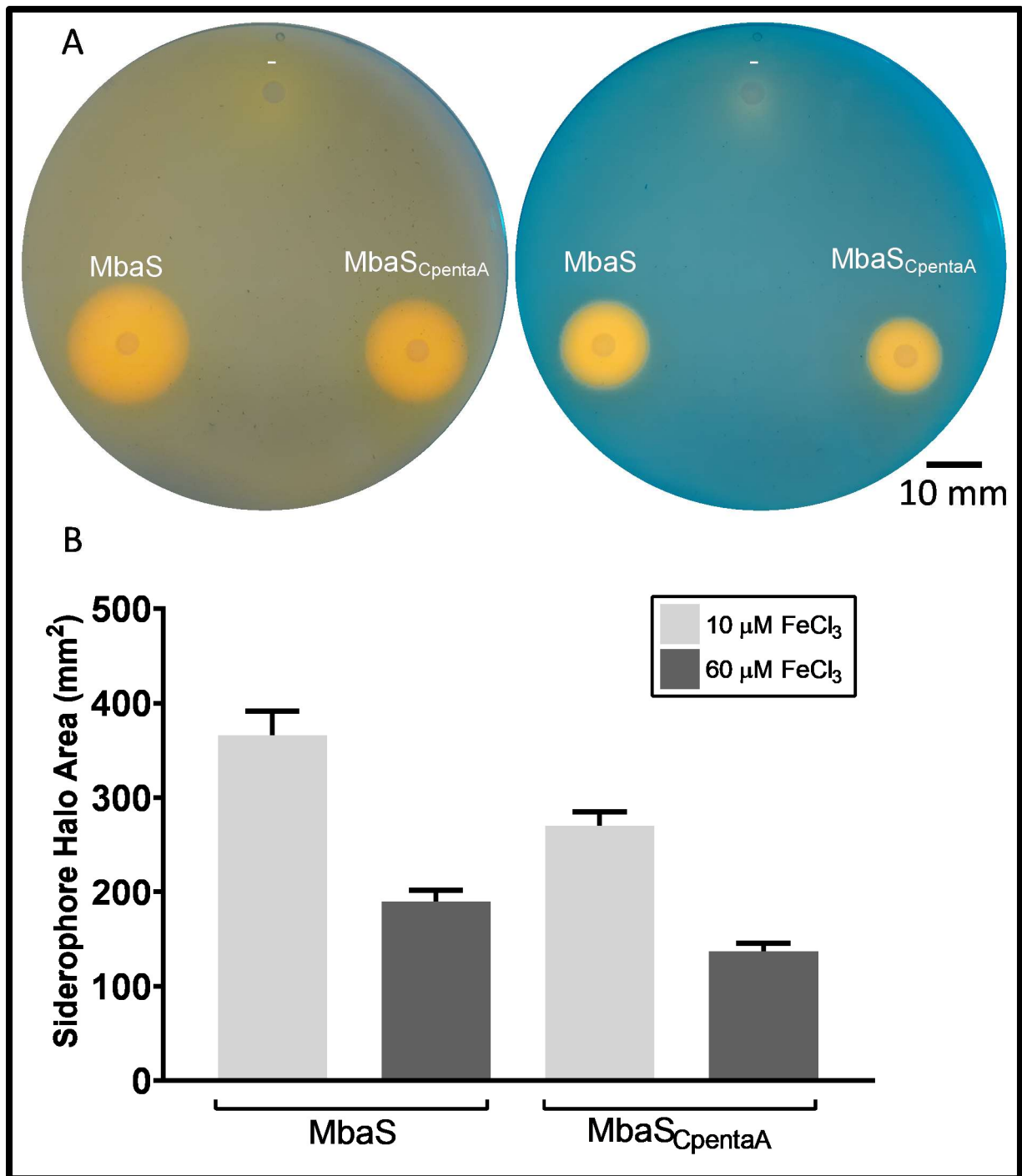
Figure 5.27. Comparison of *Bth* E264 Δ*mbaS* grown on iron-limited and iron-replete CAS medium supplied *in trans* with MbaS or MbaS$_{CpentaA}$

A. *Bth* E264 Δ*mbaS* containing either pBBR1MCS-2 (-), pBBR2-*mbaS* or pBBR2-*mbaS*$_{CpentaA}$ (indicated by white text above bacterial growth) grown on CAS agar plates supplemented with either 10 µM FeCl$_3$ (green plate, left) or 60 µM FeCl$_3$ (blue plate, right). **B.** Calculated areas of siderophore halos produced. Error bars show standard deviation (n=4).
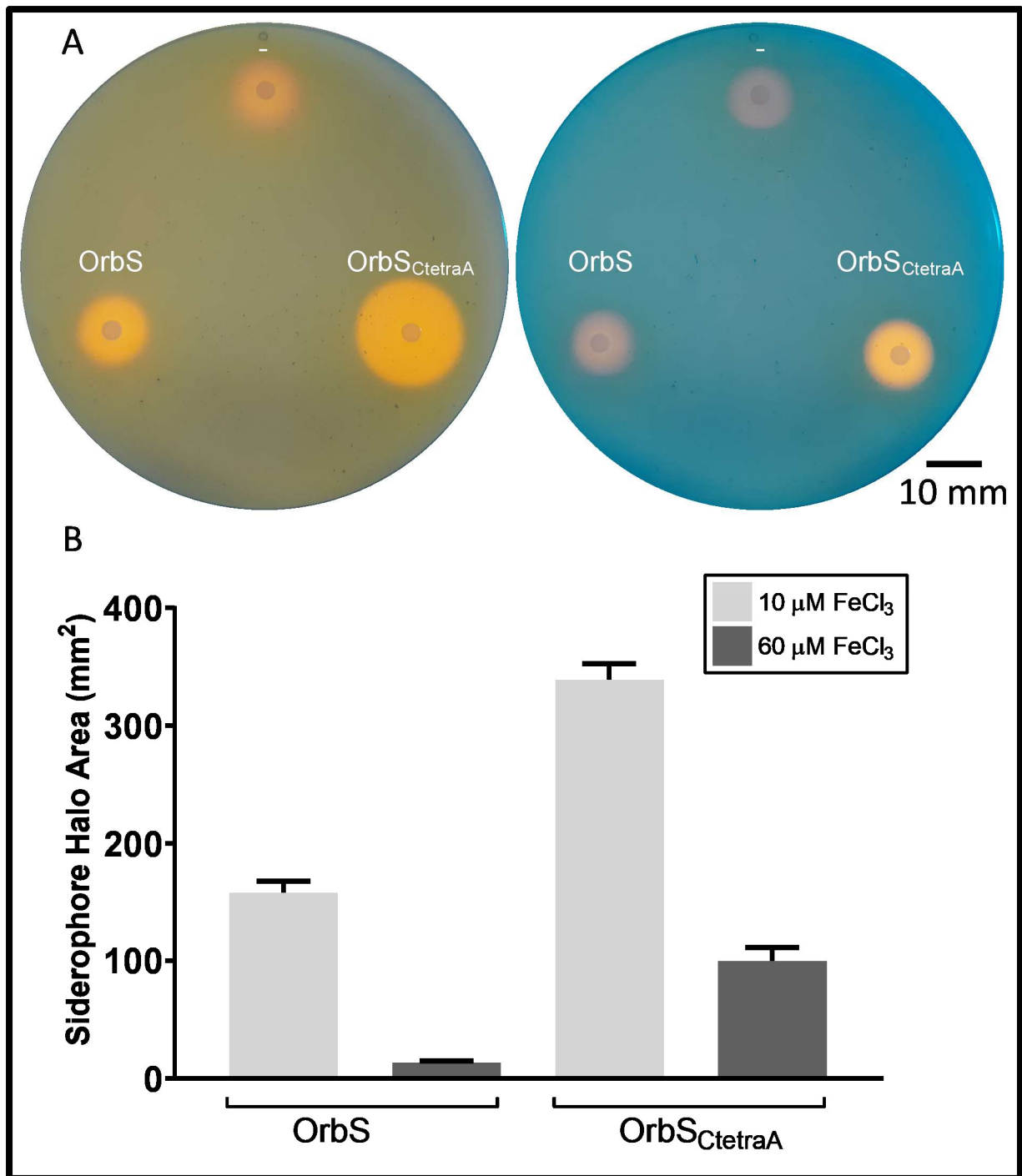
Figure 5.28. Comparison of *Bce* H111 Δ*orbS* grown on iron-limited or iron-replete CAS medium supplied *in trans* with OrbS or OrbS_CtetraA

A. *Bce* H111 Δ*orbS* containing either pBBR1MCS-2 (-), pBBR2-*orbS* or pBBR2-*orbS*_CtetraA (indicated by white text above spotted culture) grown on CAS agar plates supplemented with either 10 μM FeCl$_3$ (green plate, left) or 60 μM FeCl$_3$ (blue plate, right). **B.** Calculated areas of siderophore halos produced. Error bars show standard deviation (n=4).

In the *Bth* E264 Δ*mbaS* CAS assay (Figure 5.27), introduction of both MbaS and MbaS$_{CpentaA}$ complement the Δ*mbaS* gene deletion and initiate transcription of the malleobactin-associated genes, as judged by the production of a large yellow halo surrounding the bacterial growth. The halo observed due to the production of malleobactin is similar for both the wild-type and mutant sigma factors. Additionally, this malleobactin-induced halo is slightly smaller when the cultures are grown on the 60 μM FeCl$_3$ CAS agar, compared to when grown on 10 μM FeCl$_3$ CAS agar. However, these halos are relatively large, indicating that there is no Fur-regulation of the plasmid-supplied sigma factor. Furthermore, regardless of whether they are grown in iron-limited or iron-replete medium, the relative size of the halos produced by cultures harbouring pBBR2-*mbaS* and pBBR2-*mbaS*$_{CpentaA}$ remains the same i.e. they both decrease in area by approximately 48% and 49%, respectively. This suggests that, although there is some non-specific iron regulation occurring, it is not specific to the regulation of MbaS via the cysteine residues of the CRE.

Likewise, in the *Bce* H111 Δ*orbS* CAS assay (Figure 5.28), both OrbS and OrbS$_{CtetraA}$ can complement the Orb$^-$ phenotype and give rise to the production of ornibactin, observed through the production of a large yellow halo. Where no sigma factor has been supplied *in trans*, halos produced through the secretion of pyochelin can be observed (orange on CAS agar containing 10 μM FeCl$_3$, violet on CAS agar containing 60 μM FeCl$_3$). As with the *Bth* experiment, there appears to be a non-specific reduction of the production of siderophores on CAS agar containing 60 μM FeCl$_3$ compared to 10 μM FeCl$_3$. However, there is a larger reduction of the area of the yellow ornibactin halo when OrbS is introduced to the system (approximately 91%) compared to when OrbS$_{CtetraA}$ is introduced (approximately 70%). This provided further evidence that OrbS bears an iron regulation mechanism specific to the four cysteine residues within the CRE.

5.8 Investigation of alternative metal ions upon regulation of MbaS and OrbS *in vivo*

As there was no observable effect of iron upon the activity of MbaS compared to MbaS$_{CpentaA}$ *in vivo*, except the small effect seen in *Bth* E264 Δ*mbaS*, the inhibitory effect of alternative metal ions that could interact with the CRE were investigated. The biologically-relevant metals copper (a cofactor of cytochrome *c* oxidase), zinc (a cofactor in RNA and DNA polymerases and many DNA-binding proteins), nickel (found in most hydrogenases), manganese (an activator of a range of enzymes) and cobalt (a cofactor of vitamin B$_{12}$) were tested. As it was initially hypothesised that MbaS and OrbS interacted with Fe(II) via their CRE, the selected metals were assayed using ions with an oxidation state of 2+ i.e. Cu(II), Zn(II) etc. Again, transcription reporter analysis and growth on CAS agar was used to investigate the effect of these metals upon the activity of MbaS and OrbS compared to their cysteine-to-alanine substitution mutant forms.

5.8.1 Effect of alternative metal ions upon MbaS by transcription reporter analysis in *E. coli*

Using the same *E. coli* QC1732 strains used in section 5.7.2, a β-galactosidase assay was repeated using other biologically important transition metal ions. The metals copper, zinc, nickel, manganese and cobalt were selected. 50 µM of each of these metals was used in the β-galactosidase assay to parallel the concentration used for iron with the exception of copper: 10 µM was used as copper displays toxicity at higher concentrations (Mathew *et al.*, 2016).

Firstly, the effect of the metal ions upon MbaS and MbaS$_{CpentaA}$ was investigated. The *E. coli* QC1732 strain harbouring pKAGd4-P$_{mbaH-S}$ and either pBBR1MCS-5, pBBR5-*mbaS* or pBBR5-*mbaS*$_{CpentaA}$, (see section 5.7.2) were used. β-galactosidase assays were performed in cells grown in M9 minimal salts medium supplemented with 0.5% (w/v) glucose, 0.1% (w/v) casamino acids, 100 µg ml^{-1} ampicillin and 50 µg ml^{-1} gentamicin according to the protocol

outlined in section 2.5.1. Metal-limited conditions were introduced by the addition of 100 µM 2,2-dipyridyl, iron-replete conditions by the addition of 50 µM FeCl$_3$, copper-replete conditions by the addition of 10 µM CuCl$_2$, zinc-replete conditions by the addition of ZnCl$_2$, nickel-replete conditions by the addition of 50 µM NiSO$_4$, manganese-replete conditions by the addition of 50 µM MnCl$_2$, and cobalt-replete conditions by the addition of 50 µM CoCl$_2$.

Figure 5.29. β-galactosidase assay of MbaS and MbaS$_{CpentaA}$ upon a target promoter in *E. coli* QC1732 with a selection of biologically-relevant metals.

Results of β-galactosidase assay investigation metal-dependent regulation of MbaS and MbaS$_{CpentaA}$ upon an MbaS-dependent promoter. β-galactosidase activity was measured in *E. coli* QC1732 harbouring pKAGd4-P$_{mbaH-S}$ and pBBR5-*mbaS* (light grey) or pBBR5-*mbaS*$_{CpentaA}$ (dark grey). All β-galactosidase activities were corrected for background vector activity by subtraction of activity derived from *E. coli* QC1732 harbouring both plasmids pBBR1MCS-5 and pKAGd4-P$_{mbaH-S}$. Growth medium was M9 minimal salts supplemented with 0.5% (w/v) glucose, 0.1% (w/v) casamino acids, 25 µg ml^{-1} chloramphenicol and 50 µg ml^{-1} gentamicin and either 100 µM 2,2-dipyridyl (DP), 50 µM FeCl$_3$ (Fe), 10 µM CuCl$_2$ (Cu), 50 µM ZnCl$_2$ (Zn), 50 µM NiSO$_4$ (Ni), 50 µM MnCl$_2$ (Mn) or 50 µM CoCl$_2$ (Co). Error bars show standard deviation (n=3). There are no significant differences between MbaS and MbaS$_{CpentaA}$ under each metal condition (one-way ANOVA, Sidak's multiple comparisons test).

Again, no iron-dependent regulation of MbaS was demonstrated in this analysis. Moreover, it appears none of the other metals assayed exhibit any regulatory activity upon MbaS. The β-galactosidase activities for cultures grown in 50 μM CoCl$_2$ display lower activity than for the other metals, but this is observed in both the addition of MbaS and MbaS$_{CpentaA}$. Therefore, it is likely that this is a non-specific effect, possibly a result of cobalt toxicity upon the *E. coli* cells.

5.8.2   Effect of alternative metal ions upon MbaS by transcription reporter analysis in *B. thailandensis ΔmbaS*

Although no metal regulation upon MbaS could be observed in the heterologous *E. coli* QC1732 system, the β-galactosidase assay was repeated in the *Bth* E264 *ΔmbaS* system. Given that a small iron-inhibition effect was observed in this system previously (Figure 5.26), it could be that regulation by other metal ions may also be observed.

The assay was performed using the same *Bth* E264 *ΔmbaS* strains from section 5.7.3, harbouring pKAGd4-P$_{mbaH-S}$ and either pBBR1MCS-5, pBBR5-*mbaS* or pBBR5-*mbaS*$_{CpentaA}$. Bacterial cultures were grown in analogous conditions as in section 5.8.1, with the exception of the antibiotics used: the medium was supplemented with 50 μg ml^{-1} chloramphenicol and 250 μg ml^{-1} kanamycin.
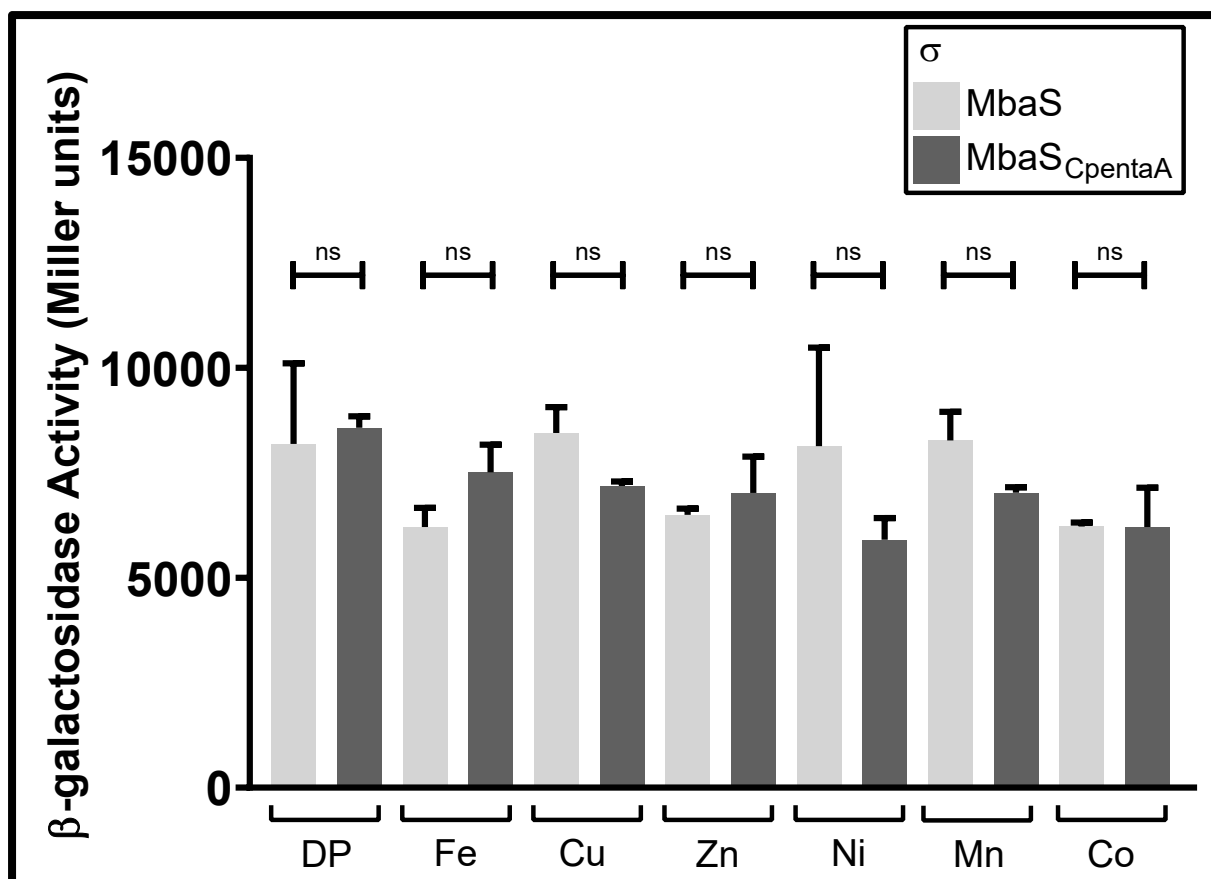
Figure 5.30. β-galactosidase assay of MbaS and MbaS$_{CpentaA}$ upon a target promoter in *B. thailandensis* E264 Δ*mbaS* with a selection of biologically-relevant metals.

Results of β-galactosidase assay investigation metal-dependent regulation of MbaS and MbaS$_{CpentaA}$ upon an MbaS-dependent promoter. β-galactosidase activity was measured in *B. thailandensis* E264 Δ*mbaS* harbouring pKAGd4-P$_{mbaH-S}$ and pBBR5-*mbaS* (light grey) or pBBR5-*mbaS*$_{CpentaA}$ (dark grey). All β-galactosidase activities were corrected for background vector activity by subtraction of activity derived from *B. thailandensis* E264 Δ*mbaS* harbouring both plasmids pBBR1MCS-5 and pKAGd4-P$_{mbaH-S}$. Growth medium was M9 minimal salts medium supplemented with 0.5% (w/v) glucose, 0.1% (w/v) casamino acids, 50 μg ml^{-1} chloramphenicol and 250 μg ml^{-1} kanamycin and either 100 μM 2,2-dipyridyl (DP), 50 μM FeCl$_3$ (Fe), 10 μM CuCl$_2$ (Cu), 50 μM ZnCl$_2$ (Zn), 50 μM NiSO$_4$ (Ni), 50 μM MnCl$_2$ (Mn) or 50 μM CoCl$_2$ (Co). Error bars show standard deviation (n=3). There are no significant differences between MbaS and MbaS$_{CpentaA}$ under each metal condition (one-way ANOVA, Sidak's multiple comparisons test).

However, again it can be observed that there are no significant differences between the β-galactosidase activities resulting from the addition of MbaS or MbaS$_{CpentaA}$ in the presence of metal ions. It appears none of the selected metals exhibit an inhibition effect upon MbaS specific to the CRE.

5.8.3 Effect of alternative metal ions upon OrbS by transcription reporter analysis in *E. coli*

Although an iron inhibition effect has been demonstrated upon OrbS, the effect of alternative metals ions was also assayed. The assay was performed using the *E. coli* QC1732 strains used in section 5.7.2, harbouring pKAGd4-P$_{orbH-S}$ and either pBBR1MCS-5, pBBR5-*orbS*$_{\Delta P}$ or pBBR5-*orbS*$_{CtetraA-\Delta P}$. The β-galactosidase assay was performed in an analogous manner as described in section 5.8.1.
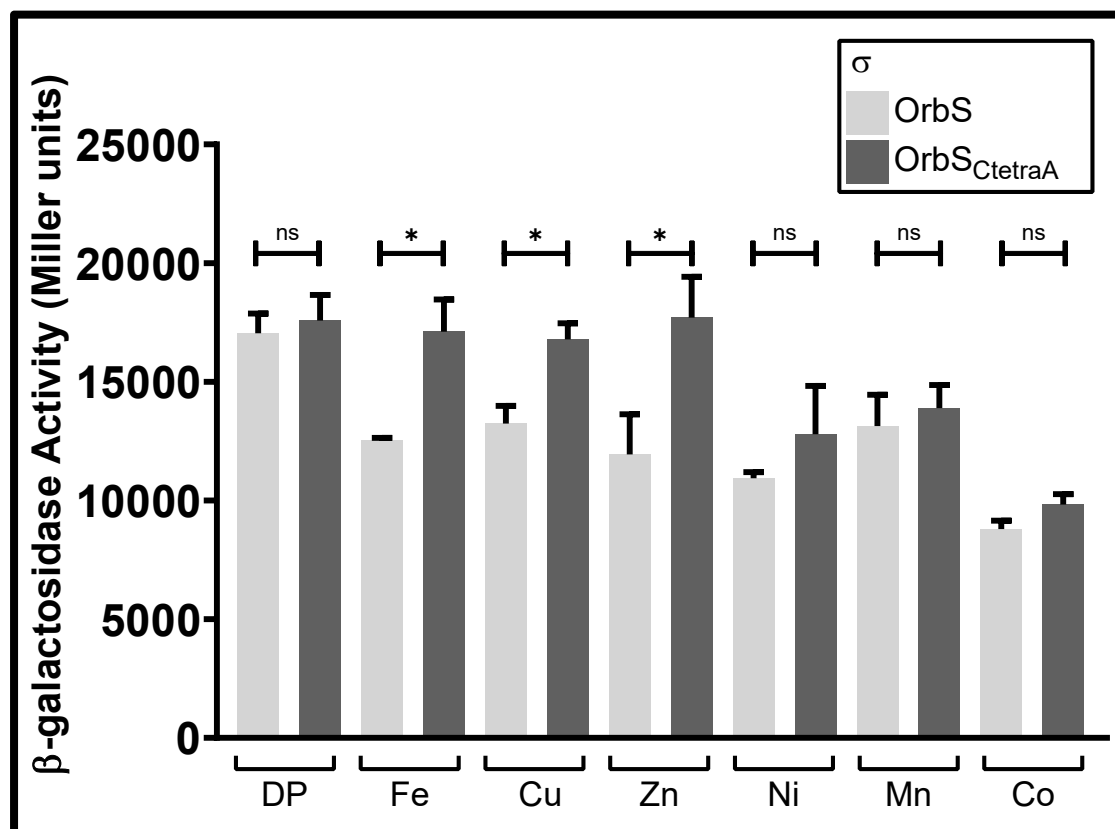
Figure 5.31. β-galactosidase assay of OrbS and OrbS$_{CtetraA}$ upon a target promoter in *E. coli* QC1732 with a selection of biologically-relevant metals.

Results of β-galactosidase assay investigation metal-dependent regulation of OrbS and OrbS$_{CtetraA}$ upon an OrbS-dependent promoter. β-galactosidase activity was measured in *E. coli* QC1732 harbouring pKAGd4-P$_{orbH-S}$ and pBBR5-*orbS*$_{\Delta P}$ (light grey) or pBBR5-*orbS*$_{CtetraA-\Delta P}$ (dark grey). All β-galactosidase activities were corrected for background vector activity by subtraction of activity derived from *E. coli* QC1732 harbouring both plasmids pBBR1MCS-5 and pKAGd4-P$_{orbH-S}$. Growth medium was M9 minimal salts medium supplemented with 0.5% (w/v) glucose, 0.1% (w/v) casamino acids, 25 μg ml^{-1} chloramphenicol and 50 μg ml^{-1} gentamicin and either 100 μM 2,2-dipyridyl (DP), 50 μM FeCl$_3$ (Fe), 10 μM CuCl$_2$ (Cu), 50 μM ZnCl$_2$ (Zn), 50 μM NiSO$_4$ (Ni), 50 μM MnCl$_2$ (Mn) or 50 μM CoCl$_2$ (Co). Error bars show standard deviation (n=3). There are significant differences between the activities of OrbS and OrbS$_{CtetraA}$ under iron-replete conditions (P=0.0002), copper-replete conditions (P=0.0044) and zinc-replete conditions (P<0.0001) (one-way ANOVA, Sidak's multiple comparisons test).

As previously observed, there is a significant difference in the β-galactosidase activities resulting from the activity of OrbS and OrbS$_{CtetraA}$ in the presence of iron (P=0.0002). In addition, there appears to be differences in these activities in the presence of copper and zinc, too (P=0.0044 and P<0.0001, respectively, one-way ANOVA, Sidak's multiple comparisons test). There are no differences in these β-galactosidase activities in the presence of nickel, manganese, or cobalt (again, a non-specific reduction of β-galactosidase activity in the presence of cobalt is observed). This data suggests that in addition to Fe(II), both Cu(II) and Zn(II) ions could interact with the putative key cysteine residues of the CRE to regulate the activity of OrbS.

5.8.4   Effect of alternative metal ions upon OrbS by transcription reporter analysis in *B. cenocepacia* Δ*orbS*

To explore the effect of metal ions upon OrbS further, the β-galactosidase assay was repeated in the *Bce* H111 Δ*orbS* system. The assay was performed using the same *Bce* H111 Δ*orbS* harbouring pKAGd4-P$_{orbH-S}$ and either pBBR1MCS-2, pBBR2-*orbS*$_{ΔP}$ or pBBR2-*mbaS*$_{CtetraA-ΔP}$, introduced by sequential conjugation using *E.coli* S17-1 donor cells. Bacterial cultures were grown in analogous conditions as in section 5.8.1, with the exception of the antibiotics used: the medium was supplemented with 50 μg ml^{-1} chloramphenicol and 50 μg ml^{-1} kanamycin.
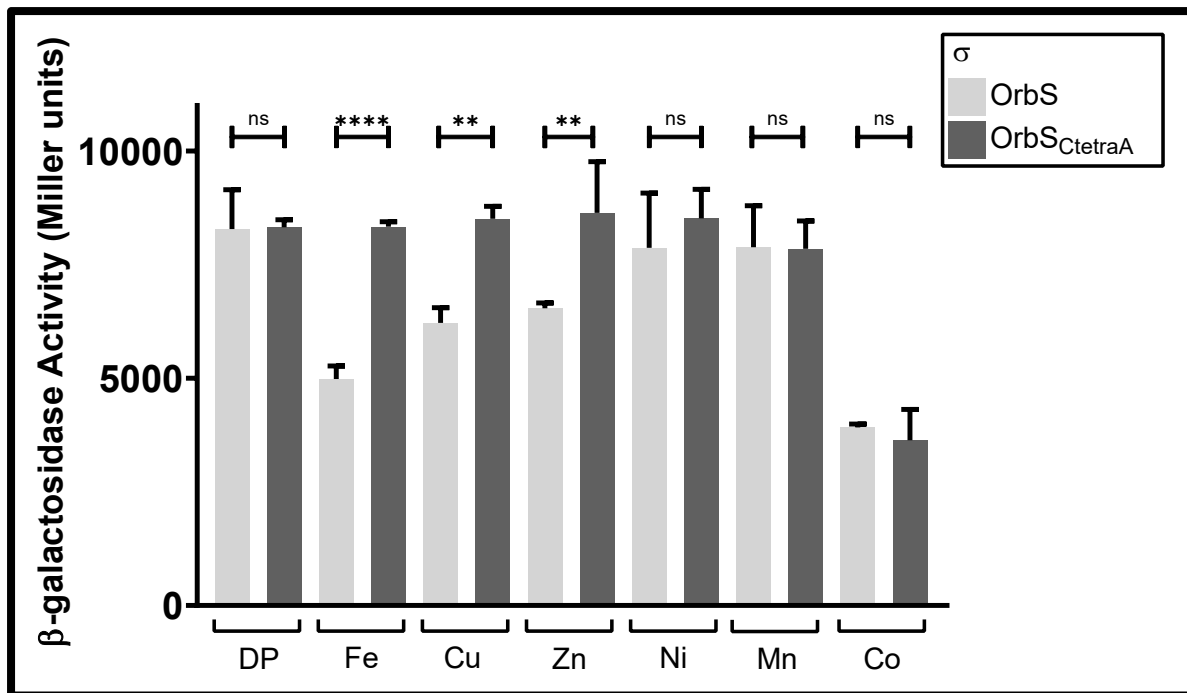
Figure 5.32. β-galactosidase assay of OrbS and OrbS$_{CtetraA}$ upon a target promoter in *B. cenocepacia* E264 Δ*orbS* with a selection of biologically-relevant metals.

Results of β-galactosidase assay investigation metal-dependent regulation of OrbS and OrbS$_{CtetraA}$ upon an OrbS-dependent promoter. β-galactosidase activity was measured in *B. cenocepacia* H111 Δ*orbS* harbouring pKAGd4-P$_{orbH-S}$ and pBBR2-*orbS*$_{ΔP}$ (light grey) or pBBR2-*orbS*$_{CtetraA-ΔP}$ (dark grey). All β-galactosidase activities were corrected for background vector activity by subtraction of activity derived from *B. cenocepacia* H111 Δ*orbS* harbouring both plasmids pBBR1MCS-2 and pKAGd4-P$_{orbH-S}$. Growth medium was M9 minimal salts medium supplemented with 0.5% (w/v) glucose, 0.1% (w/v) casamino acids, 50 μg ml^{-1} chloramphenicol and 250 μg ml^{-1} kanamycin and either 100 μM 2,2-dipyridyl (DP), 50 μM FeCl$_3$ (Fe), 10 μM CuCl$_2$ (Cu), 50 μM ZnCl$_2$ (Zn), 50 μM NiSO$_4$ (Ni), 50 μM MnCl$_2$ (Mn) or 50 μM CoCl$_2$ (Co). Error bars show standard deviation (n=3). There are significant differences between the activities of OrbS and OrbS$_{CtetraA}$ under iron-replete conditions (P<0.0001), copper-replete conditions (P=0.0012) and zinc-replete conditions (P=0.0033) (one-way ANOVA, Sidak's multiple comparisons test).

As was observed in *E. coli*, there are significant differences in the β-galactosidase activities from the *orbH* promoter between when OrbS or OrbS$_{CtetraA}$ are supplied *in trans* in the presence of iron (P<0.0001), copper (P=0.0012) and zinc (P=0.0033, one-way ANOVA, Sidak's multiple comparisons test). There are no differences in the presence of nickel, manganese or cobalt. This corroborates the finding that Fe(II), Cu(II) and Zn(II) may interact with and inhibit the activity of OrbS via the conserved cysteine residues of the protein's CRE.

5.8.5 Effect of alternative metal ions upon siderophore production in *B. thailandensis* Δ*mbaS* and *B. cenocepacia* Δ*orbS* grown on CAS agar

As a further attempt to assay the regulatory effect of metal ions upon the sigma factors MbaS and OrbS, specific to their CREs, selected *Bth* and *Bce* cultures were grown in CAS agar supplemented with different metal ions. Different CAS agar recipes have been used to demonstrate the production of siderophore analogues that chelate non-iron metal ions, for example the copper-binding chalkophores produced by several methanotroph species (Yoon *et al.*, 2010). However, CAS agar was desired that contained alternative metal ions (to analyse their effect upon the regulation of siderophore production) in addition to iron (to colormetrically identify and quantify siderophore production). No research literature could be found that described such CAS medium, therefore it was unclear whether this dual-metal CAS agar would be viable.

Overnight cultures of *Bth* E264 Δ*mbaS* harbouring pBBR2-*mbaS* or pBBR2-*mbaS*$_{CpentaA}$, and cultures of *Bce* H111 Δ*orbS* harbouring pBBR2-*orbS*$_{ΔP}$ or pBBR2-*orbS*$_{CtetraA-ΔP}$, were grown in M9 minimal medium supplemented with 0.5% (w/v) glucose and 250 µg ml^{-1} (for *Bth*) or 50 µg ml^{-1} (for *Bce*) kanamycin. Cultures were normalised according to their OD$_{600}$ and 1 µl spotted, in triplicate, onto CAS agar containing either 10 µM FeCl$_3$, 60 µM FeCl$_3$, 10 µM FeCl$_3$ and 50 µM ZnCl$_2$, 10 µM FeCl$_3$ and 10 µM CuCl$_2$, 10 µM FeCl$_3$ and 50 µM NiSO$_4$, and 10 µM FeCl$_3$ and 50 µM MnCl$_2$. Cultures were grown at 37 °C for 24 hours. *Burkholderia* cultures were also attempted to be grown on CAS agar containing 10 µM FeCl$_3$ and 50 µM CoCl$_2$, but there was no bacterial growth upon this medium.
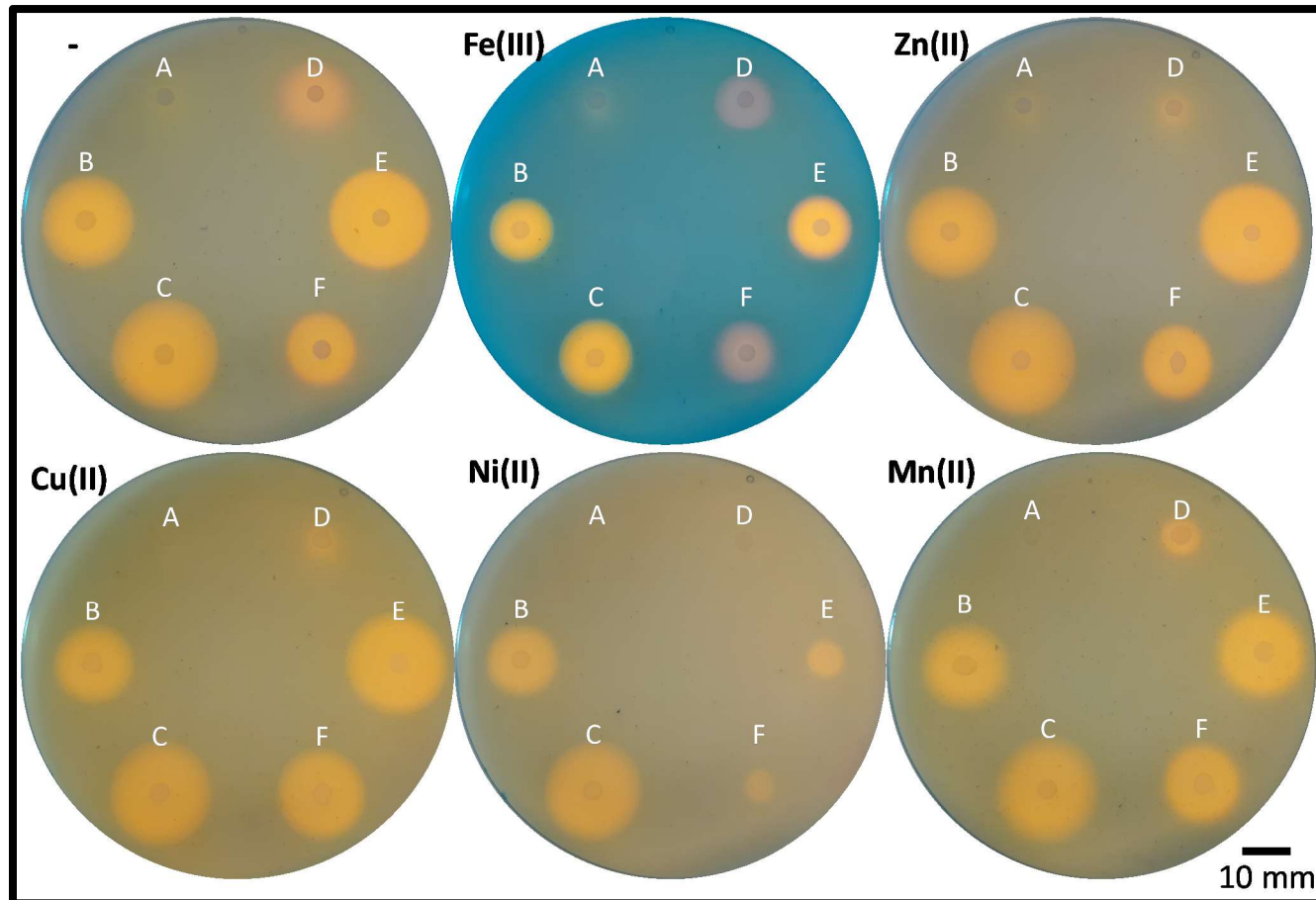
Figure 5.33. Comparison of *Bth* E264 Δ*mbaS*, supplied *in trans* with MbaS or MbaS_{CpentaA}, and *Bce* H111 Δ*orbS*, supplied *in trans* with OrbS or OrbS_{CtetraA}, grown on iron-limited CAS medium further supplemented with iron, zinc, copper, nickel and manganese.

Bth and *Bce* grown on CAS agar plates supplemented with 10 µM FeCl$_3$ (**-**) in addition to a further 50 µM FeCl$_3$ (**Fe(III)**), 50 µM ZnCl$_2$ (**Zn(II)**), 10 µM CuCl$_2$ (**Cu(II)**), 50 µM NiSO$_4$ (**Ni(II)**) or 50 µM MnCl$_2$ (**Mn(II)**), denoted at the top left of each plate image. The *Burkholderia* cultures were as follows: **A:** *Bth* E264 Δ*mbaS*/pBBR1MCS-2; **B:** *Bth* E264 Δ*mbaS*/pBBR2-*mbaS*$_{CpentaA}$; **C:** *Bth* E264 Δ*mbaS*/pBBR2-*mbaS*; **D:** *Bce* H111 Δ*orbS*/pBBR1MCS-2; **E:** *Bce* H111 Δ*orbS*/pBBR2-*orbS*$_{CtetraA-ΔP}$; **F:** *Bce* H111 Δ*orbS*/pBBR2-*orbS*$_{ΔP}$. Cultures were grown at 37 °C for 24 hours (n=4).

On all of the dual-metal CAS agar used in Figure 5.33, halos resulting from the removal of Fe(III) from CAS-HDTMA can be observed. In all cases, it is likely that this results from the secretion of the siderophores malleobactin and ornibactin. On CAS agar containing 60 µM $FeCl_3$, an inhibition of ornibactin production initiated by OrbS, but not $OrbS_{CtetraA}$, is observed (similar to as seen in Figure 5.28). Based upon the results of Figure 5.31 and Figure 5.32, it could also be expected that a similar pattern of ornibactin regulation would be observed for CAS agar containing 10 µM $FeCl_3$ and 50 µM $ZnCl_2$, and 10 µM $FeCl_3$ and 10 µM $CuCl_2$. However, this is not the case; the *Bce* H111 Δ*orbS* cultures produce similar sized halos on all of the dual-metal CAS media, relative to those observed on CAS agar containing only 10 µM $FeCl_3$. This is also the case for all of the *Bth* E264 Δ*mbaS* cultures grown on these CAS media.

5.9 Investigation of metal-dependent regulation of MbaS and OrbS *in vitro*

Following on from *in vivo* data investigating the effect of metal regulation upon MbaS and OrbS, *in vitro* methods were also employed to analyse the influence of Fe(II) and Zn(II) upon the activity of MbaS and OrbS, and their association with core RNAP. The recombinant proteins MbaS, $MbaS_{CpentaA}$, OrbS and $OrbS_{CtetraA}$ (produced and purified using the methods described in sections 2.4.1 to 2.4.3, and shown in sections 5.3.2 and 5.6.3) were used in these experiments. A combination of *in vitro* transcription (*iv*T) assays (see section 2.6.1), examining the RNA synthesis performed by core RNAP is association with the *Burkholderia* sigma factors, and bio layer interferometry (BLI) (see section 2.6.2), examining the binding affinity of the *Burkholderia* sigma factors for core RNAP, were used.

5.9.1 Determination of optimum Fe(II) concentration to be used in *in vitro* transcription

Preliminary experiments examining the effect of Fe(II) on the association of *E. coli* core RNAP with the heterologous *Burkholderia* sigma factors presented the issue of non-specific iron-inhibition. Therefore, it was necessary to determine the optimum concentration of Fe(II) to use. This would be the highest concentration at which there is no non-specific inhibition effect upon the transcription reaction. To do this, *E. coli* holo RNAP (NEB) (comprising *E. coli* σ^{70}) was used in conjunction with pRLG770-P$_{guaB}$ containing the σ^{70}-dependent *guaB* promoter. The synthesis of RNA was examined by performing the *iv*T assay in the presence of different concentrations of Fe(NH$_4$)(SO$_4$) (Figure 5.34).
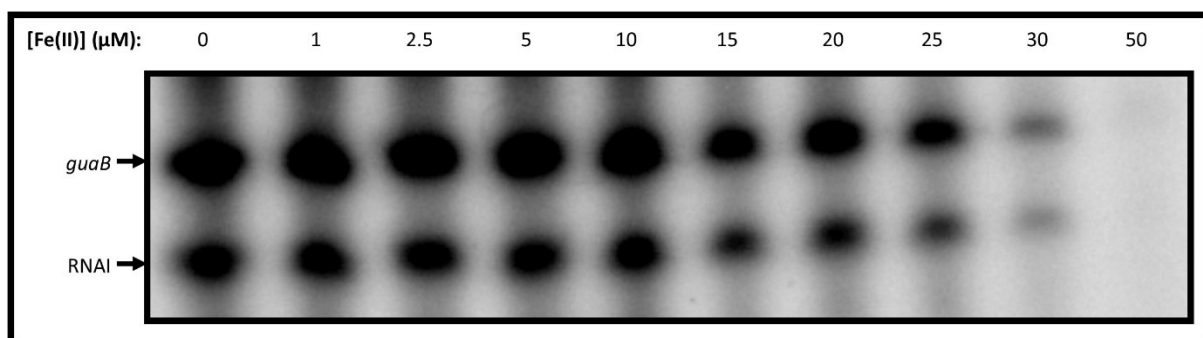
Figure 5.34. *in vitro* transcription assay to determine the optimum concentration of Fe(NH$_4$)$_2$(SO$_4$)$_2$.

RNA transcripts were resolved in a 5.5% acrylamide, 7 M urea gel following an *in vitro* transcription assay. RNA transcripts were synthesised by *E. coli* holo σ^{70} RNA polymerase (NEB). The location of the RNA transcript originating from the cloned *guaB* promoter (186 nt) and from the replicon-derived RNAI transcript (108 nt) is indicated to the left of the image. The concentrations of Fe(NH$_4$)$_2$(SO$_4$)$_2$ in the the transcription reaction is denoted above the image.

From this data, it can be concluded that the efficiency of the transcription reactions decreases in the presence of higher concentrations of Fe(NH$_4$)$_2$(SO$_4$)$_2$. This appears to take effect at concentrations from 15 μM onwards. Therefore, it was decided to use 10 μM Fe(NH$_4$)$_2$(SO$_4$)$_2$ in *iv*T assays investigating the effect of Fe(II) (see section 5.9.2).

5.9.2   Effect of Fe(II) upon MbaS and OrbS in *in vitro* transcription

The influence of Fe(II) upon the RNA transcription achieved by *E. coli* core RNAP in association with the *Burkholderia* sigma factors, upon their target promoters, was investigated. Transcription reactions were prepared containing (a) *E. coli* core RNAP, (b) MbaS, MbaS$_{CpentaA}$, OrbS or OrbS$_{CtetraA}$, and (c) pRLG770-P$_{mbaH}$ (for MbaS/MbaS$_{CpentaA}$) or pRLG770-P$_{orbH\text{ds6}}$ (for OrbS/OrbS$_{CtetraA}$). Reactions contained either 0 µM or 10 µM Fe(NH$_4$)$_2$(SO$_4$)$_2$. This *iv*T assays was performed in duplicate (Figure 5.35).

The amount of RNA transcribed by core RNAP in association with MbaS$_{CpentaA}$ and OrbS$_{CtetraA}$ remains the same, regardless of the addition of Fe(II) (P=0.17 and P=0.88, respectively, one-way ANOVA, Sidak's multiple comparisons test). In the presence of 10 µM Fe(II), there is a statistically significant approximately 61% decrease in the amount of RNA produced by RNAP in association with MbaS (P=0.02), and a non-statistically significant approximately 85% decrease in the amount of RNA produced by RNAP in association with OrbS (P=0.07, one-way ANOVA, Sidak's multiple comparisons test). It appears Fe(II) may have a specific effect, via the cysteine residues of their respective CREs, upon the activity of MbaS and OrbS to promote transcription.
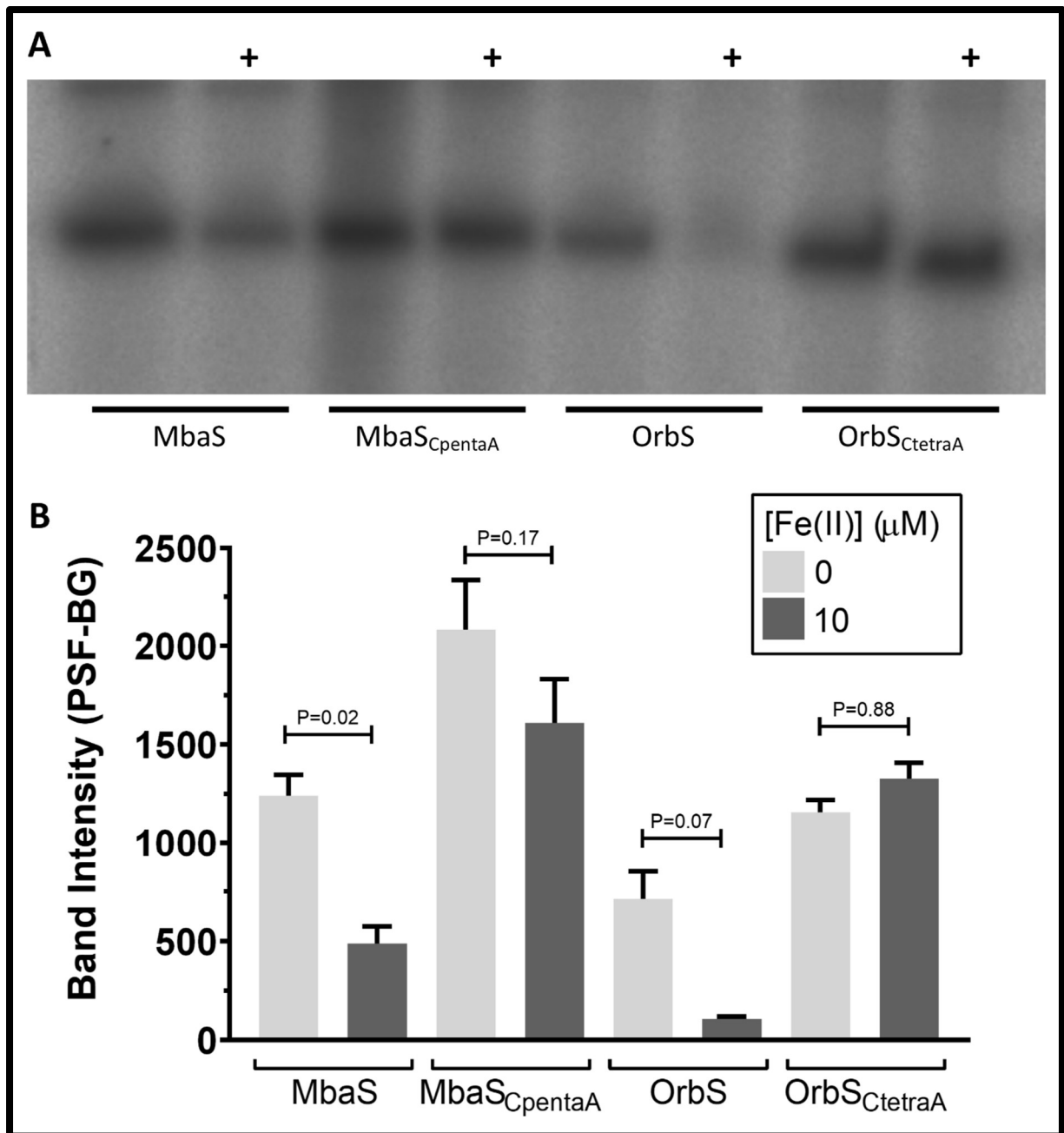
Figure 5.35. *in vitro* transcription assay examining the effect of 10 μM Fe(NH₄)₂(SO₄)₂ upon transcription initiated by MbaS, MbaS_CpentaA, OrbS and OrbS_CtetraA in association with core RNA polymerase.

A. RNA transcripts were resolved in a 5.5% acrylamide, 7 M urea gel following an *in vitro* transcription assay. *E. coli* core RNA polymerase (NEB), in association with either MbaS, MbaS_CpentaA, OrbS or OrbS_CtetreA (denoted below gel image) was used to synthesise 156 nt RNA from a DNA fragments containing promoters P_mbaH (for MbaS and MbaS_CpentaA) or P_orbH (for OrbS and OrbS_CtetraA) cloned into pRLG770. The reaction was performed in the absence (-) or in the presence (+) of 10 μM Fe(NH₄)₂(SO₄)₂ (denoted above the gel image). **B.** Quantification RNA transcripts from the *in vitro* transcription assays. The sigma factors used in the reactions are denoted below data bars. Reactions were performed in the presence of 0 μM Fe(NH₄)₂(SO₄)₂ (light grey) or 10 μM Fe(NH₄)₂(SO₄)₂ (dark grey). Error bars show standard deviation (n=2). P value results from one-way ANOVA, Sidak's multiple comparisons test, are shown above corresponding pairs of data bars.

5.9.3 Effect of Zn(II) upon MbaS and OrbS in *in vitro* transcription

In an analogous method as was performed in section 5.9.2, the influence of Zn(II) upon the RNA transcription achieved by *E. coli* core RNAP in association with the *Burkholderia* sigma factors was investigated. Preliminary experiments using MbaS and MbaS$_{CpentaA}$ suggested that there was no non-specific inhibition effect of Zn(II) upon the transcription reaction. Therefore, a concentration of 25 µM ZnCl$_2$ was selected to be used in these *iv*T assays (to be consistent with metal concentrations used in BLI, see section 5.9.4). The experiment was performed identically to those in section 5.9.2, with the exception that reactions contained either 0 µM or 25 µM ZnCl$_2$. The *iv*T assay was performed in triplicate. Although, these assays displayed qualitative consistency, ^{32}P-UTP decay resulted in large quantitative discrepancies between data sets. Therefore, only one set of data is presented (Figure 5.36).

There appears to be a large decrease in the amount of RNA transcribed by core RNAP in association with MbaS in the presence of zinc (72%), whereas there is only a small decrease when core RNAP is in association with MbaS$_{CpentaA}$ in the presence of zinc (25%). In the transcription reactions containing OrbS or OrbS$_{CtetraA}$, there appears to be a non-specific inhibition of transcription in the presence of zinc which masks any specific inhibition of the sigma factors. Nonetheless, the reduction in RNA synthesis by core RNAP in the presence of zinc is greater when the enzyme is in association with OrbS (99.5%) than it is for in association with OrbS$_{CtetraA}$ (93.8%). This data requires much greater statistical power, yet qualitatively is appears Zn(II) could exhibit specific regulation upon MbaS and OrbS their respective CREs.
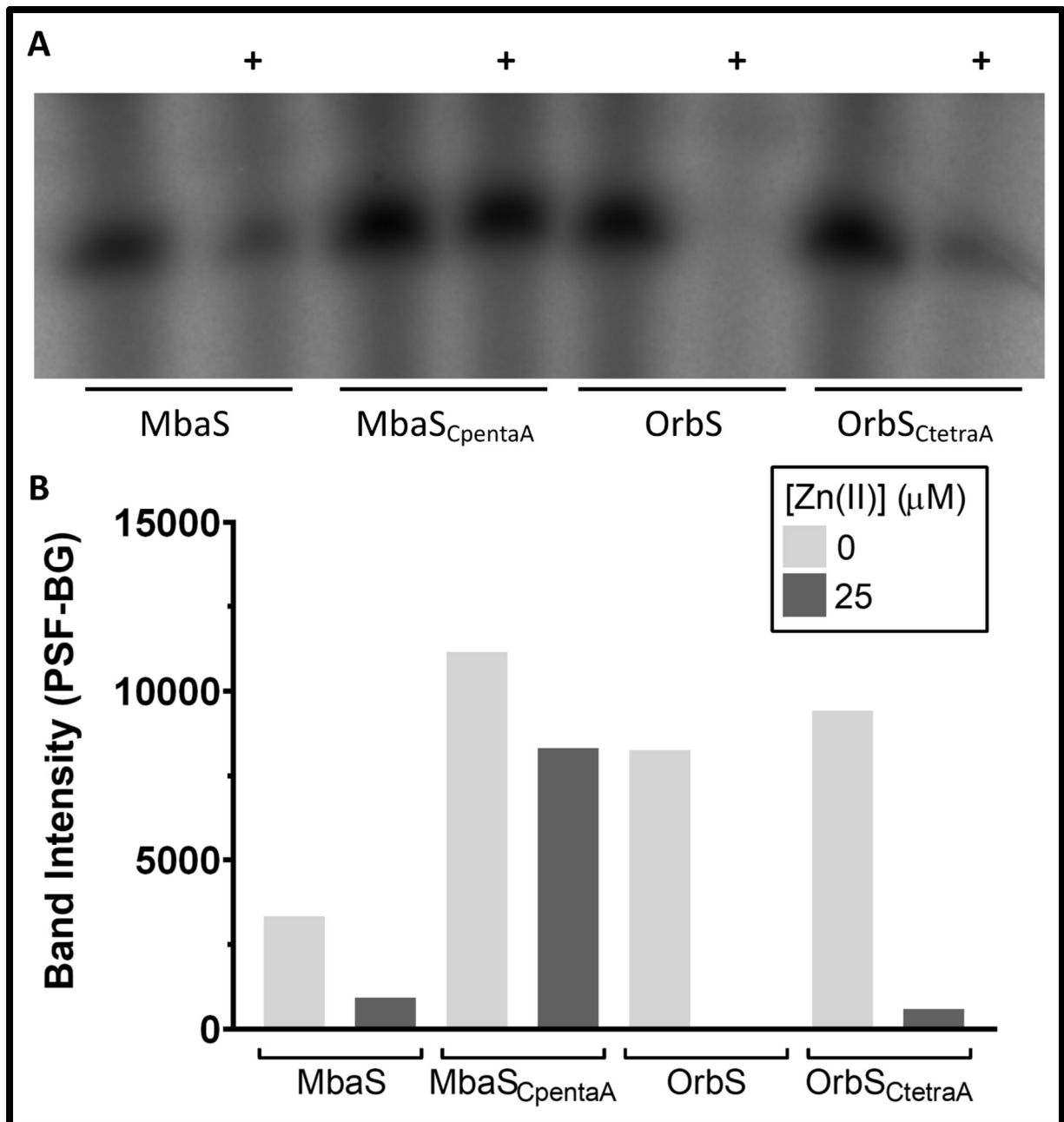
Figure 5.36. *in vitro* **transcription assay examining the effect of 25 µM ZnCl₂ upon transcription initiated by MbaS, MbaS$_{CpentaA}$, OrbS and OrbS$_{CtetraA}$ in association with core RNA polymerase.**

A. RNA transcripts were resolved in a 5.5% acrylamide, 7 M urea gel following an *in vitro* transcription assay. *E. coli* core RNA polymerase (NEB), in association with either MbaS, MbaS$_{CpentaA}$, OrbS or OrbS$_{CtetreA}$ (denoted below gel image) was used to synthesise 156 nt RNA from a DNA fragment containing the promoters P$_{mbaH}$ (for MbaS and MbaS$_{CpentaA}$) or P$_{orbH}$ (for OrbS and OrbS$_{CtetraA}$) cloned into pRLG770. The reaction was performed in the absence (**-**) or in the presence (**+**) of 25 µM ZnCl₂ (denoted above the gel image). **B.** Quantification RNA transcripts from the *in vitro* transcription assays. The sigma factors used in the reactions are denoted below data bars. Reactions were performed in the presence of 0 µM ZnCl₂ (light grey) or 10 µM ZnCl₂ (dark grey) (n=1).

5.9.4 Effect of selected metals upon the binding affinity of core RNAP for MbaS and OrbS

In the putative metal-responsive regulatory mechanism for MbaS and OrbS, it has been hypothesised that the sigma factors are inhibited by interaction with metal ions via the cysteine residues within their CRE. This could regulate the activity of the sigma factor either by (a) inhibiting the association of the sigma factor with core RNAP, or (b) by inhibiting the interaction of the sigma factor with its target promoter. Previous work using EMSAs (A. Butt, unpublished) has suggested that it may be the former mechanism. Therefore, the effect of metals upon the association of the *Burkholderia* sigma factors and *E. coli* core RNAP polymerase was investigated using bio layer interferometry (BLI).

BLI provides binding kinetics data about protein-protein interactions, enabling quantification of the interaction between a sigma factor and core RNAP. This binding interaction was compared in the presence of the metal ions $FeCl_2$, $CuCl_2$, $ZnCl_2$ and $MnCl_2$. The assays were performed according to the protocol outlined in section 2.6.2, and a representative examples using real data (for the interaction between MbaS and core RNAP in the presence of 25 µM Mn(II)) is presented in Figure 5.37. Optimisation and development of the assays was performed by Dr. Srdjan (Guta) Vitovski, whom also obtained the data for the association of OrbS with core RNAP in the absence of metal, the presence of Fe(II), Cu(II) and Zn(II), and of $OrbS_{CtetraA}$ with core RNAP in the absence of metal, the presence of Fe(II) and Zn(II). All of the binding affinities of the ECF sigma factors MbaS, $MbaS_{CpentaA}$, OrbS and $OrbS_{CtetraA}$ for core RNAP in the absence of metal ions, or in the presence of 25 µM Fe(II), Cu(II), Zn(II) or Mn(II), are shown in Table 5.2.

All four of the *Burkholderia* sigma factors display a strong binding affinity, in the nanomolar range, for core RNAP in the absence of metal. There is some variation in the binding affinity between sigma factors, and in the presence of different metal ions. Based upon the data presented, a subjectively significant change in the binding affinity was judged to have occurred in cases where the relative fold decrease in binding affinity is greater than two orders of magnitude i.e. a 100-fold change or higher.

For MbaS and $MbaS_{CpentaA}$, the presence of Fe(II), Cu(II) or Mn(II) ions has no large scale effect on the binding of the sigma factors to core RNAP. However, when Zn(II) is present,

MbaS displays a 77,544-fold decrease in binding affinity for core RNAP, whereas MbaS$_{CpentaA}$ displays only a 2-fold decrease. This strongly suggests that Zn(II) is able to inhibit the interaction of MbaS and core RNAP via the C-terminal cysteine residues.

For OrbS and OrbS$_{CtetraA}$, both the presence of Fe(II) ions and Zn(II) ions exhibit 435-fold and 934-fold decreases in binding affinity for core RNAP, respectively. This large decrease in binding affinity is not observed for OrbS$_{CtetraA}$ under identical conditions. Additionally, the presence of Cu(II) and Mn(II) does not appear to significantly affect the binding of either OrbS or OrbS$_{CtetraA}$ for core RNAP.
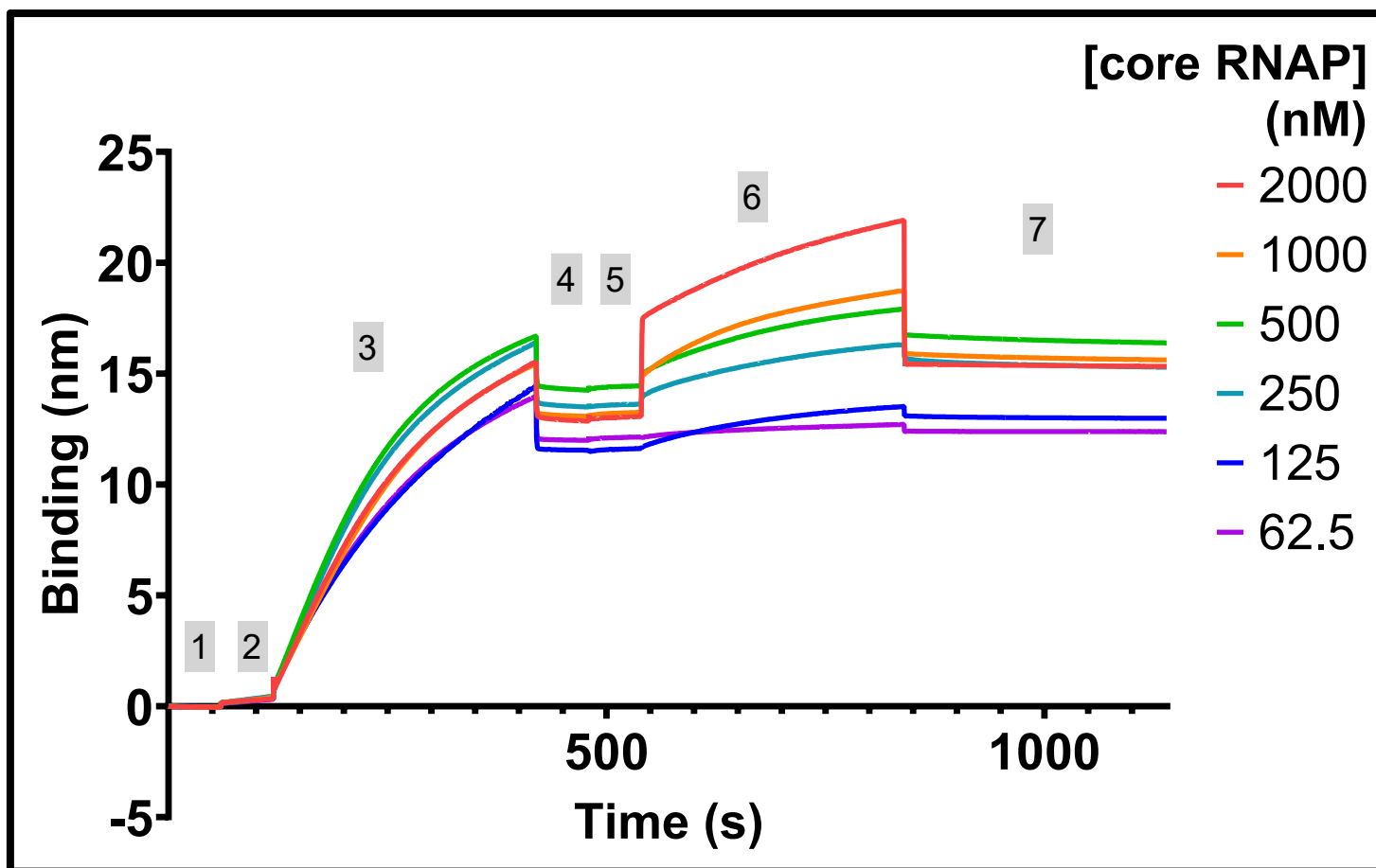
Figure 5.37. Representative example of binding kinetics data for a bio layer interferometry experiment using core RNAP and MbaS.

Time course of BLI experiment investigating the binding affinity (K_D) of ECF sigma factors for core RNA polymerase in the presence of different metal ions. For the determination of the K_D for each protein-protein interaction in the presence of metal ions, six concentrations of core RNAP were used (right). The numbers in grey boxes are positioned above the distinct steps of the BLI assay, corresponding to those described in Table 2.16. ECF sigma factor is loaded upon the biosensor to form a bio layer in step 3, core RNAP associates to the bio layer in step 6, and core RNAP dissociates from the bio layer in step 7. The association constant (k_a) and dissociation constant (k_d) are calculated by analysis of kinetic data from the start of step 6 to the end of step 7.

Table 5.2 Binding affinity of ECF sigma factors for core RNA polymerase in the presence of different metal ions.

	Sigma factor											
	MbaS			**MbaS$_{CpentaA}$**			**OrbS**			**OrbS$_{CtetraA}$**		
Metal	K_D (M)	K_d (s^{-1})/ K_a (M^{-1} s^{-1})	Fold change[1]	K_D (M)	K_d (s^{-1})/ K_a (M^{-1} s^{-1})	Fold change[1]	K_D (M)	K_d (s^{-1})/ K_a (M^{-1} s^{-1})	Fold change[1]	K_D (M)	K_d (s^{-1})/ K_a (M^{-1} s^{-1})	Fold change[1]
None	1.71×10^{-8}	2.98×10^{-4}/ 1.74×10^{4}		1.97×10^{-8}	7.54×10^{-4}/ 3.82×10^{4}		8.38×10^{-8}	4.50×10^{-4}/ 5.37×10^{3}		1.96×10^{-8}	3.02×10^{-4}/ 1.54×10^{4}	
Fe(II)	1.58×10^{-7}	1.47×10^{-3}/ 9.28×10^{3}	9	4.28×10^{-8}	7.23×10^{-4}/ 1.69×10^{4}	2	3.65×10^{-5}	2.43×10^{-4}/ 6.67×10^{0}	435	8.40×10^{-8}	7.64×10^{-4}/ 9.09×10^{3}	4
Cu(II)	1.56×10^{-7}	1.37×10^{-3}/ 8.79×10^{3}	9	4.41×10^{-7}	5.40×10^{-3}/ 1.23×10^{4}	22	1.10×10^{-7} [2]	9.53×10^{-4}/ 8.69×10^{3}	1	$1.18\ 10^{-7}$	8.83×10^{-4}/ 7.04×10^{3}	6
Zn(II)	1.33×10^{-3}	1.33×10^{-2}/ 1.00×10^{1}	77,544	3.39×10^{-8}	4.74×10^{-3}/ 1.40×10^{5}	2	7.82×10^{-5}	3.02×10^{-4}/ 3.86×10^{0}	934	2.98×10^{-8}	4.67×10^{-4}/ 1.57×10^{4}	2
Mn(II)	7.82×10^{-8}	6.94×10^{-4}/ 8.87×10^{3}	5	2.65×10^{-7}	4.38×10^{-3}/ 1.65×10^{4}	13	7.43×10^{-8} [2]	5.68×10^{-4}/ 7.65×10^{3}	1	8.76×10^{-8}	5.29×10^{-4}/ 6.04×10^{3}	4

[1] The relative fold decrease in the binding of each sigma factor to *E. coli* RNAP in the presence of each metal, to the nearest integer, is calculated as the ratio of the K_D value in the presence of the metal to the K_D in the absence of metal.

[2] Note that these values were measured using a different protein preparation of OrbS than other values.

K_D binding affinities (M) are calculated from the dissociation constant K_d (s^{-1}) and the association constant K_a (M^{-1} s^{-1}).

5.10   Discussion

In this chapter, it has been empirically demonstrated that MbaS is a sigma factor. This has been shown through its capacity to stimulate transcription from target gene promoters in promoter reporter assays and *in vitro* transcription assays in the presence of core RNAP. Additionally, the association of MbaS and core RNAP has been demonstrated by bio layer interferometry, and a binding affinity for this association has been determined. Although the designation of MbaS as an ECF sigma factor has been established for some time (Alice *et al.*, 2006), this study presents the first empirical demonstration of this.

Furthermore, the target promoters of MbaS have been formally identified. Again, based upon homology with the *orb* gene cluster and RNase protection assays of MbaS-regulated genes, the P*mbaH* and P*mbaE* promoters were assumed to be transcribed in an MbaS-dependent manner. A 562 bp DNA region containing the P*mbaI* promoter DNA was shown to be activated in an MbaS-dependent manner by an *in vivo* promoter reporter assay (Alice *et al.*, 2006). Through further *in vivo* promoter reporter assays presented in this study, this has been empirically demonstrated for all three promoters. Moreover, these promoters have been identied with precision to a 49 bp DNA region. It is very likely that the core promoter elements are present within this region, and that they correspond to those precisely identified in the *orbH* promoter (see Figure 5.2) (Agnoli *et al.*, 2018).

The *mbaS* promoter has also been characterised to a greater degree. Through *in* vivo promoter reporter assays, it has been established that activity from the *mbaS* promoter does not increase in the presence of MbaS, and therefore it can be concluded MbaS does not autoregulate its own promoter. It is highly likely that the *mbaS* promoter is regulated in a σ^{70}-dependent manner, although this has not been demonstrated unequivocally. Previous work identified that transcription of *mbaS* was downregulated under high-iron conditions, likely due to a Fur box sequence identified *in silico* in a DNA region upstream of the translation start codon (Alice *et al.*, 2006). It was also reported that this was demonstrated by FURTA (although the data was not shown and the length of DNA assayed was not

specified). Using FURTA, this study has limited the location of the Fur box to an 186 bp DNA of region. Nonetheless, this could be identified with greater precision in the future.

Cross-activity between MbaS and OrbS has also been demonstrated. Due to the homology between the two IS sigma factors, it was likely that they would recognise target promoters of a similar sequence. MbaS was shown to stimulate transcription from the *orbH* promoter, and OrbS shown to stimulate transcription from the *mbaH* promoter. This cross-activity is unlikely to occur in nature, but it demonstrates that these two sigma factors likely possess highly similar mechanisms of DNA binding.

Evidence has been presented that supports the hypothesis that MbaS and OrbS possess on-board metal-responsive regulatory domains. A series of methods were developed and employed to investigate the influence that the presence of metal ions had on MbaS and OrbS activity upon dependent promoters, and upon association with core RNAP. Through comparison with the cysteine-to-alanine substitution mutants MbaS$_{CpentaA}$ and OrbS$_{CtetraA}$, the dependency of the conserved cysteine residues of the CRE upon this metal regulation could be inferred.

In *in vivo* promoter reporter analyses, inhibition of the activity of OrbS could be observed in the presence of 50 µM iron chloride, copper chloride and zinc chloride. The presence of 10 µM Fe(II) and 25 µM Zn(II) was also demonstrated to inhibit the OrbS-dependent transcription of a target promoter *in vitro*. Finally, the presence of 25 µM Fe(II) and Zn(II) decreased the binding affinity of core RNAP and OrbS by 435-fold and 934-fold, respectively. This strongly suggests that OrbS is able to respond to the presence of Fe(II), Zn(II), and possibly Cu(II) ions. In the same experiments performed upon MbaS *in vivo*, the presence of the selected metal showed no effect upon the activity of MbaS upon its target promoter. However, *in vitro* transcription assays demonstrated that presence of 25 µM Zn(II) and 10 µM Fe(II) resulted in reduced MbaS-dependent transcription from a target promoter, and presence of 25 µM Zn(II) decreased the binding affinity between MbaS and core RNAP 77,544-fold. This suggests that MbaS is able to respond to the presence of Zn(II), and possibly Fe(II) ions.

Importantly, these metal inhibition effects were not observed to occur to the same degree upon the activity of MbaS$_{CpentaA}$ OrbS$_{CtetraA}$. Therefore, it is highly likely that this influence the metal ions exhibit upon the sigma factor activity and association with core RNAP occurs via the thiol groups of some or all of the conserved cysteine residues of the CREs present in both OrbS and MbaS. Nonetheless, direct binding of iron to these sigma factors has not been demonstrated.

It is unclear why, despite displaying a strong inhibitory effect upon the association of MbaS and core RNAP *in vitro*, presence of Zn(II) does not demonstrate this inhibition of MbaS activity in *in vivo* promoter reporter analyses. It could possibly be due that the intracellular concentration of zinc is very low, and MbaS does not sense or interact with Zn(II). Also, the effect of six common metals found in biology were investigated. However, it cannot be discounted that additional metals, or other moieties, could regulate the activity of MbaS and OrbS via the thiol groups of their CRE.

Chapter VI: Characterisation of *B. cenocepacia* ECF sigma factor BCAM0001

6.1 Overview

BCAM0001 is a putative uncharacterised ECF13 group sigma factor. The gene annotated as BCAM0001 is located upstream of a gene annotated as BCAM0001a, encoding a putative anti-sigma factor. These genes overlap by 25 bp, suggesting that they are co-transcribed.

No work has previously been performed upon this sigma factor system, and therefore it was important to demonstrate that BCAM0001 displays sigma factor activity. It is unclear what genes could be regulated by BCAM0001 are, or what their function is. However, most ECF

sigma factors act upon the own promoter, so BCAM0001 was predicted to stimulate expression of its own promoter. Additionally, ECF sigma factors are often located in proximity to the genes that they regulate (Figure 6.1). Therefore, the neighbouring genes annotated as BCAM2840 and BCAM0002 were predicted to be to be transcribed from BCAM0001-dependent promoters.
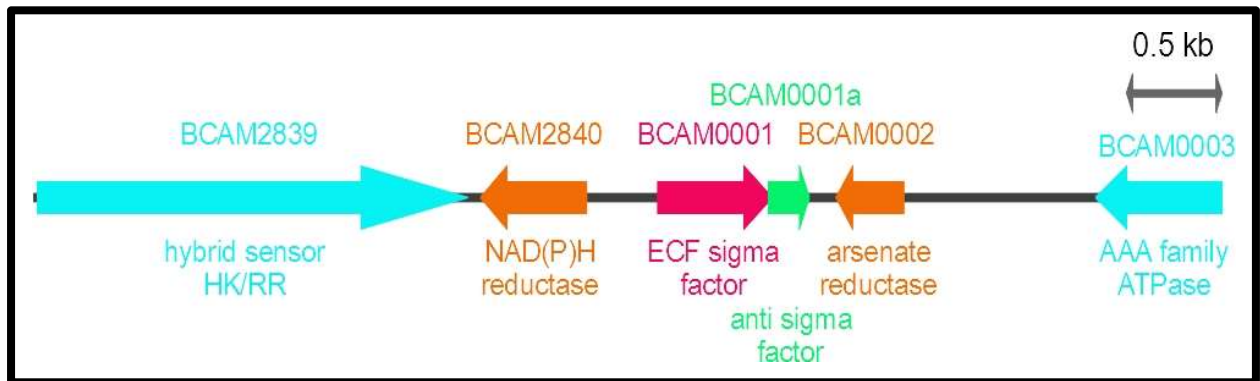
Figure 6.1. Schematic representation of the DNA region around BCAM0001.

Genes are shown as block arrows, and are annotated above with their gene annotation and below with their protein homologies and/or predicted functions. Genes are as follows: BCAM2839 (blue), hybrid sensor histidine kinase/ response regulator; BCAM2840 (orange), NAD(P)H reductase and/or chromate reductase; BCAM0001 (pink), RNA polymerase ECF sigma factor; BCAM0001a (green), zinc-finger domain containing anti-sigma factor; BCAM0002 (orange), arsenate reductase; BCAM0003 (blue), AAA family ATPase and/or ParA-like protein. Genes predicted to be regulated by BCAM0001 are shown in orange.

Objectives:

- To demonstrate a protein-protein interaction between BCAM0001 and BCAM0001a

- To introduce gene deletions of BCAM0001 and BCAM0001a in *Bce* H111 and characterise the mutant phenotypes

- To demonstrate that BCAM0001 has sigma factor activity, identify the BCAM0001-dependent promoters in *Bce* H111

6.2 Investigating the protein-protein interaction between BCAM0001 and BCAM0001a

The protein-protein interaction between the ECF sigma factor BCAM0001 and its anti-sigma factor BCAM0001a was analysed *in vivo* using the bacterial adenylate cyclase two-hybrid assay (more detail in section 2.6.3). This was performed to investigate the protein-protein interaction between the anti-sigma factor and the full-length sigma factor, and additionally the individual sigma domains domain 2 and domain 4. Furthermore, the self-interaction of the anti-sigma factor BCAM0001a was investigated.

6.2.1 Construction of BACTH assay plasmids

The ECF sigma factor gene BCAM0001 was amplified by PCR using the primers BACTH-BCAM1-Fwd and BACTH-BCAM1-Rev to produce a 617 bp product (Figure 6.2a). This was cloned between the *Acc*65I and *Xba*I restriction sites of the MCS of all four BACTH assay plasmids to give adenylate cyclase domain protein fusions resulting from the plasmids pUT18-BCAM0001, pUT18C-BCAM0001, pKT25-BCAM0001 and pKNT25-BCAM0001 (Figure 6.2b). The identity of the plasmids was verified by PCR screening and DNA sequencing analysis with the primers M13revBACTH and BACTH-BCAM1-rev.

The N-terminus of BCAM0001, from Pro2-Thr82 and comprising the σ2 domain, was amplified by PCR using the primers BACTH-BCAM1-Fwd and BACTH-BCAM1r2-Rev to produce a 266 bp product (Figure 6.3a). This was cloned between the *Acc*65I and *Xba*I restriction sites of the MCS of all four BACTH assay plasmids to give adenylate cyclase domain protein fusions resulting in the plasmids pUT18-BCAM0001σ2, pUT18C-BCAM0001σ2, pKT25-BCAM0001σ2 and pKNT25-BCAM0001σ2 (Figure 6.3b). The identity of the plasmids was verified by PCR screening and DNA sequencing analysis with the primers M13revBACTH and BACTH-BCAM1σ2-rev.
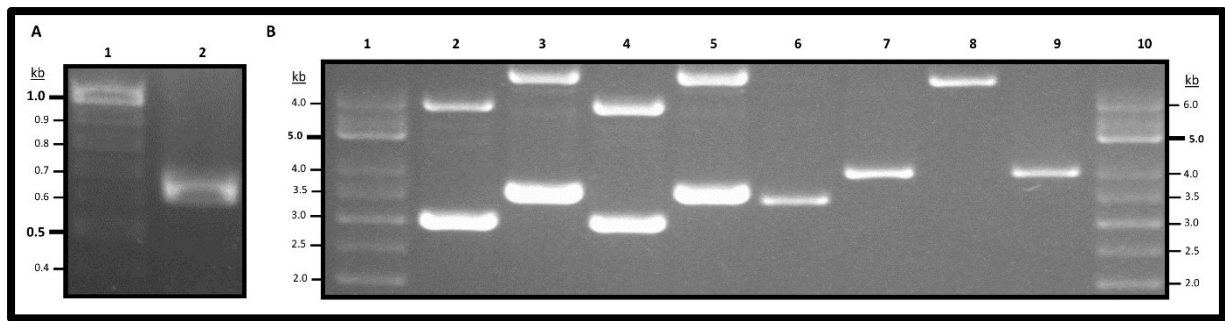
Figure 6.2. Construction of BACTH plasmids expressing BCAM0001

Agarose gel electrophoresis analysis of PCR products and constructed bacterial two-hybrid assay plasmid DNA expressing BCAM0001. **A.** PCR to amplify *bcam0001*. Lane 1, GeneRuler 1 kb DNA Ladder (Thermofisher); lane 2, *bcam0001*, 617 bp PCR product. **B.** BACTH plasmid DNA. Lanes 1 and 10, Supercoiled ladder (NEB); lane 2, pUT18, 3.0 kb; lane 3, pUT18-*bcam0001*, 3.6 kb; lane 4, pUT18C, 3.0 kb; lane 5, pUT18C-*bcam0001*, 3.6 kb; lane 6, pKT25, 3.4 kb; lane 7, pKT25-*bcam0001*, 4.0 kb; lane 8, pKNT25, 3.5 kb; lane 9, pKNT25-*bcam0001*, 4.1 kb. Note the pKNT25 is only observed in the concatenated form.

The C-terminus of BCAM0001, from Gln122-Tyr199, comprising the σ4 domain, was amplified by PCR using the primers BACTH-BCAM1r4-Fwd and BACTH-BCAM1-Rev to produce a 257 bp product (Figure 6.4a). This was cloned between the *Acc*65I and *Xba*I restriction sites of the MCS of all four BACTH assay plasmids to give adenylate cyclase domain protein fusions resulting in the plasmids pUT18-*bcam0001*σ4, pUT18C-*bcam0001*σ4, pKT25-*bcam0001*σ4 and pKNT25-*bcam0001*σ4 (Figure 6.4b). The identity of the plasmids was verified by PCR screening and DNA sequencing analysis with the primers M13revBACTH and BACTH-BCAM1-rev.

The anti-sigma factor gene BCAM0001a was amplified by PCR using the primers BACTH-BCAM1a-Fwd and BACTH-BCAM1a-Rev to produce a 233 bp product (Figure 6.5a). This was cloned between the *Acc*65I and *Xba*I restriction sites of the MCS of all four BACTH assay plasmids to give adenylate cyclase domain protein fusions resulting from the plasmids pUT18-*bcam0001a*, pUT18C-*bcam0001a*, pKT25-*bcam0001a* and pKNT25-*bcam0001a* (Figure 6.5b). The identity of the plasmids was verified by PCR screening and DNA sequencing analysis with the primers M13revBACTH and BACTH-BCAM1a-rev.
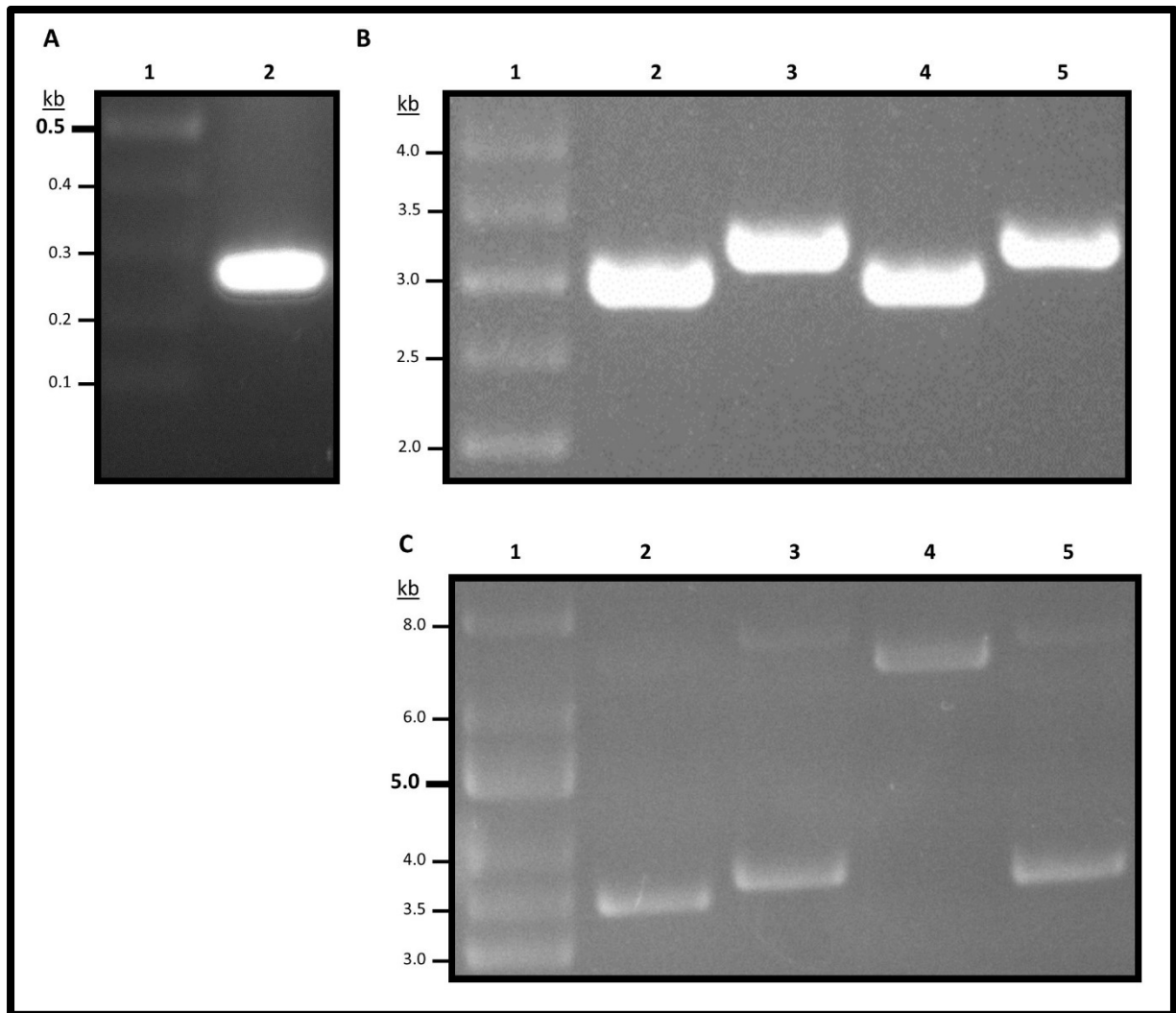
Figure 6.3. Construction of BACTH plasmids expressing BCAM0001σ2

Agarose gel electrophoresis analysis of PCR products and constructed bacterial two-hybrid assay plasmid DNA expressing BCAM0001σ2. **A.** PCR to amplify *bcam0001σ2*. Lane 1, GeneRuler 1 kb DNA Ladder (Thermofisher); lane 2, *bcam0001σ2*, 266 bp PCR product. **B.** BACTH plasmid DNA. Lane 1, Supercoiled ladder (NEB); lane 2, pUT18, 3.0 kb; lane 3, pUT18-*bcam0001σ2*, 3.3 kb; lane 4, pUT18C, 3.0 kb; lane 5, pUT18C-*bcam0001σ2*, 3.3 kb. **C.** BACTH plasmid DNA. Lane 1, Supercoiled ladder (NEB); lane 2, pKT25, 3.4 kb; lane 3, pKT25-*bcam0001σ2*, 3.7 kb; lane 4, pKNT25, 3.5 kb; lane 5, pKNT25-*bcam0001σ2*, 3.7 kb. Note the pKNT25 is only observed in the concatenated form.
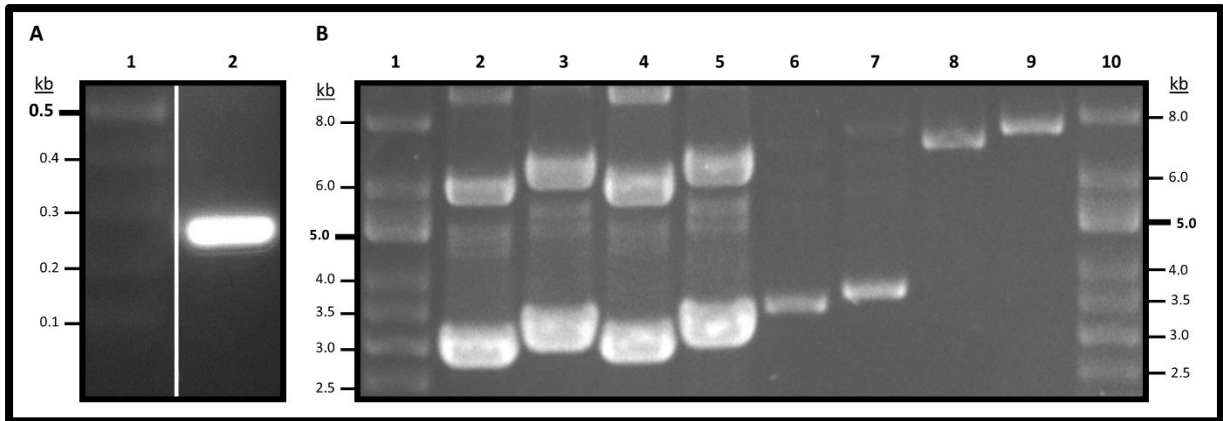
Figure 6.4. Construction of BACTH plasmids expressing BCAM0001σ4

Agarose gel electrophoresis analysis of PCR products and constructed bacterial two-hybrid assay plasmid DNA expressing BCAM0001σ4. **A.** PCR to amplify *bcam0001σ4*. Lane 1, GeneRuler 1 kb DNA Ladder (Thermofisher); lane 2, *bcam0001σ4*, 257 bp PCR product. **B.** BACTH plasmid DNA. Lanes 1 and 10, Supercoiled ladder (NEB); lane 2, pUT18, 3.0 kb; lane 3, pUT18-*bcam0001σ4*, 3.3 kb; lane 4, pUT18C, 3.0 kb; lane 5, pUT18C-*bcam0001σ4*, 3.2 kb; lane 6, pKT25, 3.4 kb; lane 7, pKT25-*bcam0001σ4*, 3.7 kb; lane 8, pKNT25, 3.5 kb; lane 9, pKNT25-*bcam0001σ4*, 3.7 kb. Note that both pKNT25 and pKNT25-bcam0001σ4 are only observed in the concatenated form.
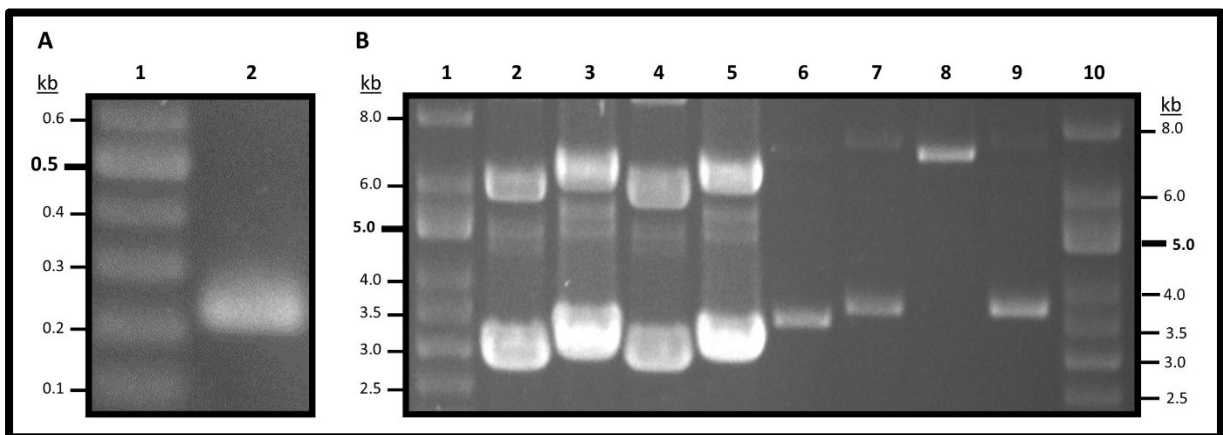
Figure 6.5. Construction of BACTH plasmids expressing BCAM0001a

Agarose gel electrophoresis analysis of PCR products and constructed bacterial two-hybrid assay plasmid DNA expressing BCAM0001a. **A.** PCR to amplify *bcam0001a*. Lane 1, GeneRuler 1 kb DNA Ladder (Thermofisher); lane 2, *bcam0001a*, 233 bp PCR product. **B.** BACTH plasmid DNA. Lanes 1 and 10, Supercoiled ladder (NEB); lane 2, pUT18, 3.0 kb; lane 3, pUT18-*bcam0001*, 3.2 kb; lane 4, pUT18C, 3.0 kb; lane 5, pUT18C-*bcam0001*, 3.2 kb; lane 6, pKT25, 3.4 kb; lane 7, pKT25-*bcam0001*, 3.6 kb; lane 8, pKNT25, 3.5 kb; lane 9, pKNT25-*bcam0001*, 3.7 kb.

6.2.2   Demonstration of BCAM0001-BCAM0001a interaction *in vivo*

The interaction between the BCAM0001 and BCAM0001a was investigated using the bacterial two-hybrid assay (see section 2.6.3). Proteins or protein domains are fused to the complementary subunits T25 or T18 of *Bordetella pertussis* adenylate cyclase (CyaA) in the constructed plasmids described in section 6.2.1. If a protein-protein interaction occurs, a distinctive deep pink colony colour can be observed on indicator medium.

The phenotype consistent with a protein-protein interaction occurring is observed between full-length BCAM0001 and BCAM0001a when BCAM0001 is fused to both T25 and T18 via its N-terminus (Figure 6.6) and via its C-terminus (Figure 6.7). A phenotype consistent with a protein-protein interaction with BCAM0001 is not observed when BCAM0001 containing only its σ2 domain or only its σ4 domain are assayed, regardless of the terminal location of the protein fusion (Figure 6.6 and Figure 6.7).

Additionally, a phenotype suggesting a self-interaction by BCAM0001a is not observed in the BACTH assay, irrespective of the terminal location of the protein fusion (Figure 6.8).
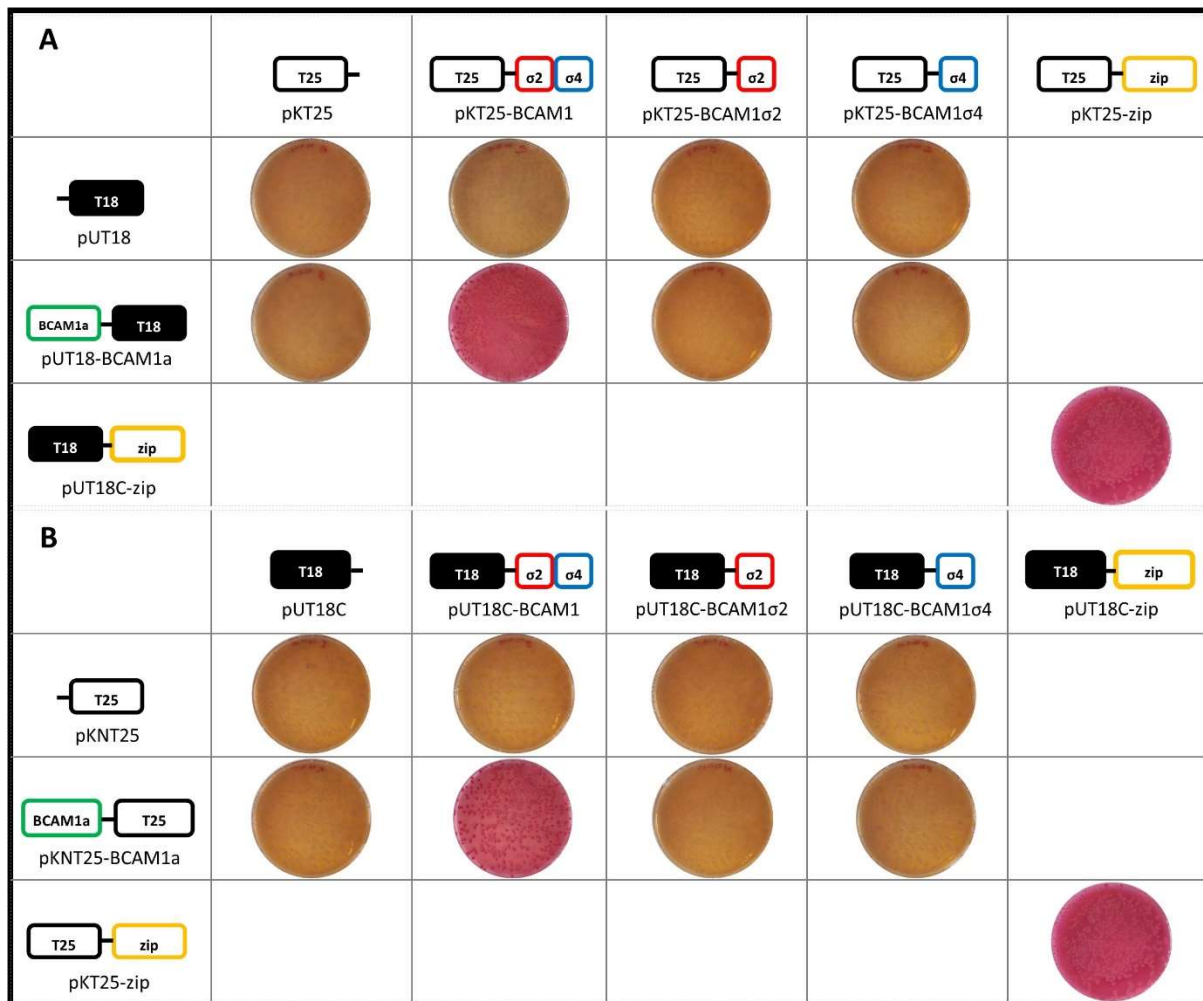
Figure 6.6. Bacterial two-hybrid analysis of interaction N-terminally linked BCAM0001, and its domains, and C-terminally linked BCAM0001a

BTH101 cells were grown on MacConkey medium containing 1% (w/v) maltose, 0.5 mM IPTG, 100 µg ml^{-1} ampicillin and 50 µg ml^{-1} kanamycin at 30 °C for five nights. The combinations assayed are denoted by the box representations: T18 domain, black; T25 domain, white; full-length BCAM0001, linked red and blue boxes; BCAM0001σ2, red; BCAM0001σ2, blue; BCAM0001a, green; the leucine zipper component of GNC4, yellow.
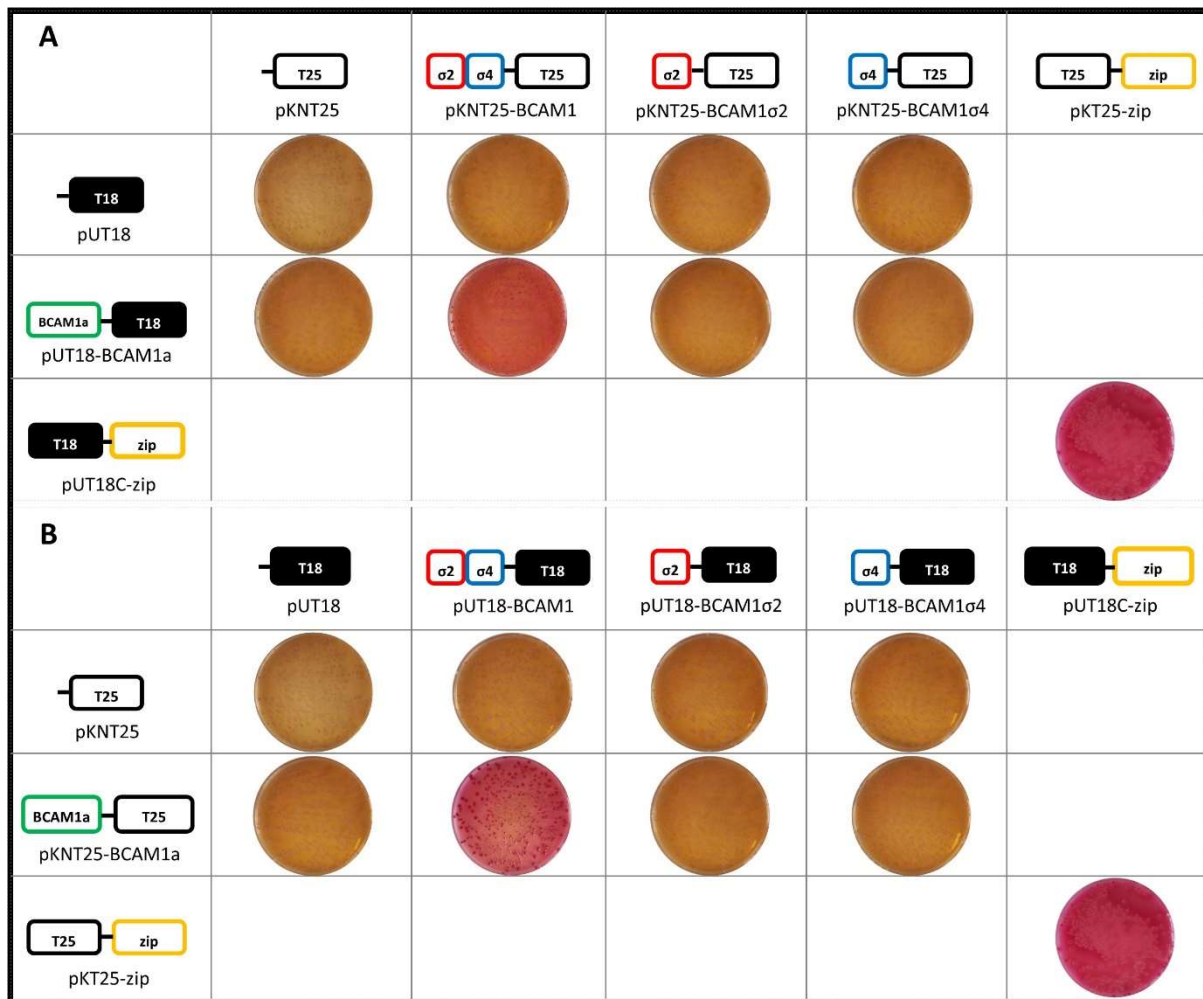
Figure 6.7. Bacterial two-hybrid analysis of interaction C-terminally linked BCAM0001, and its domains, and C-terminally linked BCAM0001a

BTH101 cells were grown on MacConkey medium containing 1% (w/v) maltose, 0.5 mM IPTG, 100 μg ml^{-1} ampicillin and 50 μg ml^{-1} kanamycin at 30 °C for five nights. The combinations assayed are denoted by the box representations: T18 domain, black; T25 domain, white; full-length BCAM0001, linked red and blue boxes; BCAM0001σ2, red; BCAM0001σ2, blue; BCAM0001a, green; the leucine zipper component of GNC4, yellow.
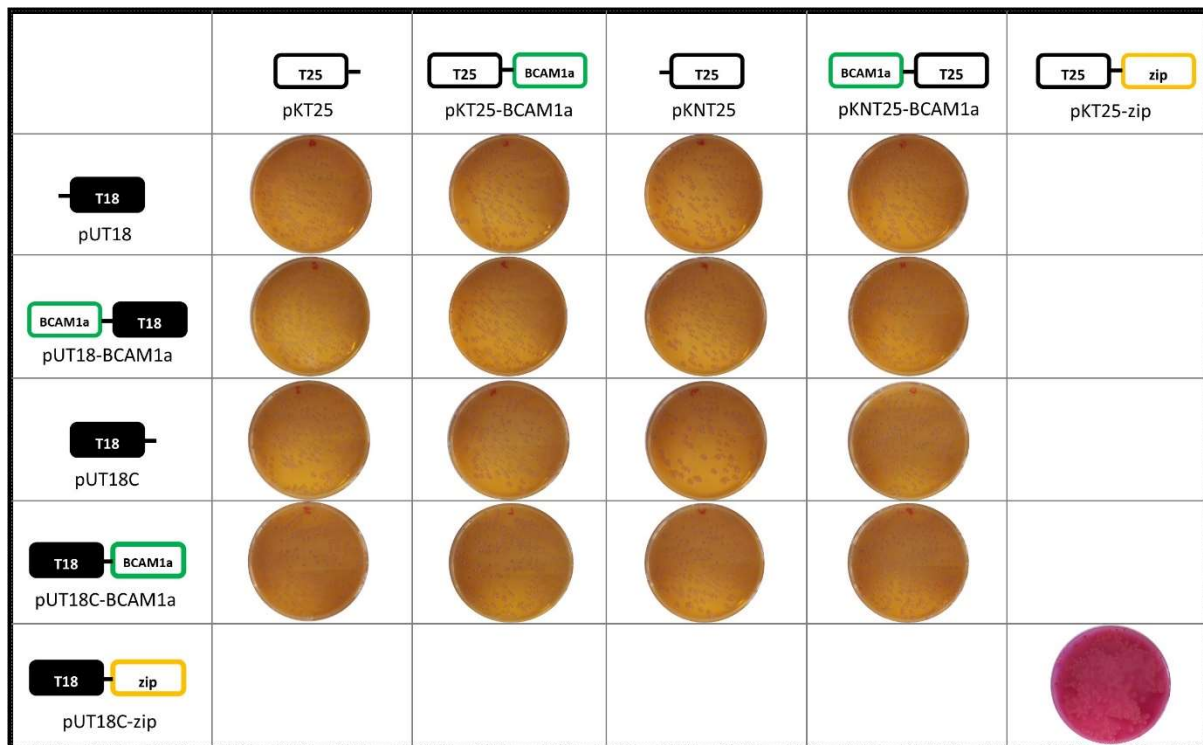
Figure 6.8. Bacterial two-hybrid analysis of BCAM0001a-BCAM0001a interaction

BTH101 cells were grown on MacConkey medium containing 1% (w/v) maltose, 0.5 mM IPTG, 100 μg ml^{-1} ampicillin and 50 μg ml^{-1} kanamycin at 30 ^{o}C for five nights. The combinations assayed are denoted by the box representations: T18 domain, black; T25 domain, white; BCAM0001a, green; the leucine zipper component of GNC4, yellow.

6.3 Attempts a construction of a ΔBCAM0001 gene deletion mutant

To investigate function of the genes regulated by BCAM0001, a gene deletion was attempted in *Bce* H111. This was attempted by introduction of in-frame marker-less ΔBCAM0001 allele using the allelic exchange vector pSNUFF3Cm (H. Spiewak, unpublished).

6.3.1   Construction of pSNUFF3Cm-Δ*bcam0001*

The in-frame marker-less Δ*bcam0001* mutant allele was amplified by SOE-PCR using primers Δbcam1-A, Δbcam1-B, Δbcam1-C and Δbcam1-D to produce a 1073 bp PCR product (Figure

6.9a,b). This gene deletion maintained the start of the *bcam0001a* gene and the 25 bp immediately upstream of its start codon, which overlaps with the *bcam0001* gene. The Δ*bcam0001* allele was cloned between the *Bam*HI and *Hin*dIII sites of the MCS of pSNUFF3Cm to give pSNUFF3Cm-Δ*bcam0001* (Figure 6.9c). The identity of the plasmid construct was confirmed by PCR screening and DNA sequencing analysis with primers M13revBACTH and M13for2.
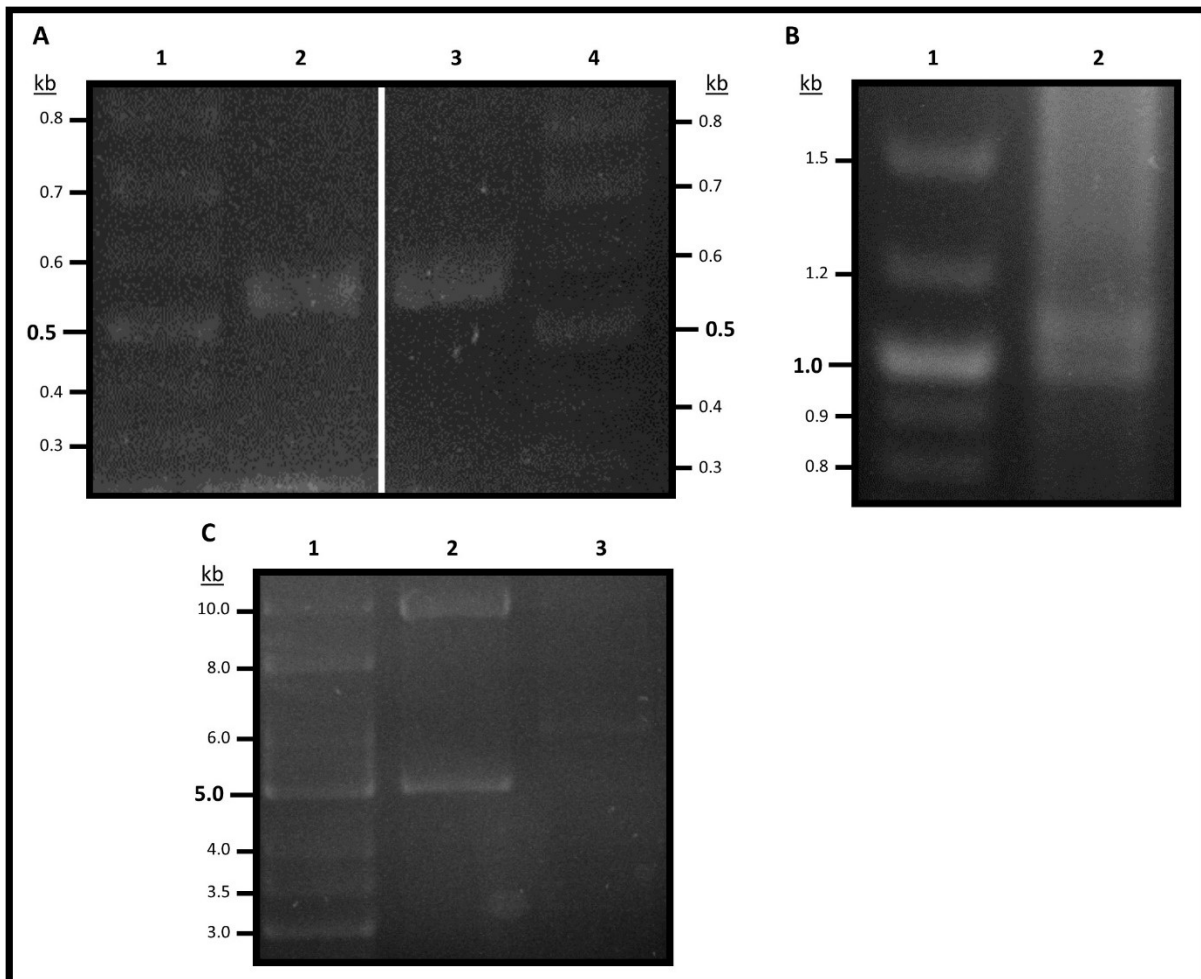
Figure 6.9. Construction of pSNUFF3Cm-Δ*bcam0001*

Agarose gel electrophoresis analysis of DNA PCR products and plasmid DNA used in construction of pSNUFF3Cm-Δ*bcam0001*. **A.** First round SOE PCR to amplify Δ*bcam0001* with upstream and downstream flanking DNA. Lanes 1 and 4, GeneRuler 1 kb DNA Ladder (Thermofisher); lane 2, Δ*bcam0001* 'left' flank, 543 bp PCR product; lane 3, Δ*bcam0001* 'right' flank, 565 bp PCR product. **B.** Second round SOE PCR to amplify Δ*bcam0001* with upstream and downstream flanking DNA. Lane 1, GeneRuler 1 kb DNA Ladder (Thermofisher); lane 2, Δ*bcam0001*, 1073 bp PCR product. **C.** pSNUFF3Cm-Δ*bcam0001* plasmid DNA. Lane 1, Supercoiled ladder (NEB); lane 2, pSNUFF3Cm, 5.1 kb; lane 3, pSNUFF3Cm-Δ*bcam0001*, 6.1 kb.

6.3.2   Attempts to introduce Δ*bcam0001* into *B. cenocepacia* by allelic exchange

E. coli SM10λ*pir* transformed with pSNUFF3Cm-Δ*bcam0001* was used as the donor strain for transfer of the mutant allele by conjugation into wild-type *Bce* H111. Resolution products were selected on LB agar containing 100 μg ml^{-1} ampicillin and 50 μg ml^{-1} chloramphenicol. Plasmid integration was further verified by PCR screening using the *bcam0001*-specific primers Δbcam1-A and Δbcam1-D, and the vector specific primers pEX18Tpfor2 and pEX18Tprev2.

E. coli SM10λ*pir* transformed with pDAI-SceI-*pheS* was used to introduce the constitutively-expressed I-SceI endonuclease into the verified co-integrant strain, harbouring both *bcam0001* and Δ*bcam0001*, via a second conjugation. Strains that had successfully undergone a second recombination event to remove the vector backbone were selected for on Lnx agar containing 100 μg ml^{-1} ampicillin and 125 μg ml^{-1} tetracycline. However, no clones that contained the desired gene deletion were identified by PCR screening with the primer pair Δbcam1-1a-out-fwd/Δbcam1-1a-out-rev.

6.4 Construction of Δ*bcam0001a* gene deletion mutant

As another approach to investigate the function of the genes regulated by BCAM0001, a gene deletion of its putative anti-sigma factor, BCAM0001a, was attempted in *Bce* H111. Without the its inhibitory partner, the BCAM0001 may be free to associated with core RNAP and stimulate the expression of genes of its regulon. This was attempted by introduction of in-frame marker-less ΔBCAM0001a allele using the allelic exchange vector pSNUFF3Cm (H. Spiewak, unpublished).

6.4.1   Construction of pSNUFF3Cm-Δ*bcam0001a*

The in-frame marker-less Δ*bcam0001a* mutant allele was amplified by SOE-PCR using primers Δbcam1a-A, Δbcam1a-B, Δbcam1a-C and Δbcam1a-D to produce a 1056 bp PCR product (Figure 6.10a,b). The Δ*bcam0001a* allele was cloned between the *Bam*HI and *Hin*dIII sites of the MCS of pSNUFF3Cm to give pSNUFF3Cm-Δ*bcam0001a* (Figure 6.10c). The identity of the plasmid construct was confirmed by PCR screening and DNA sequencing analysis with primers M13revBACTH and M13for2.
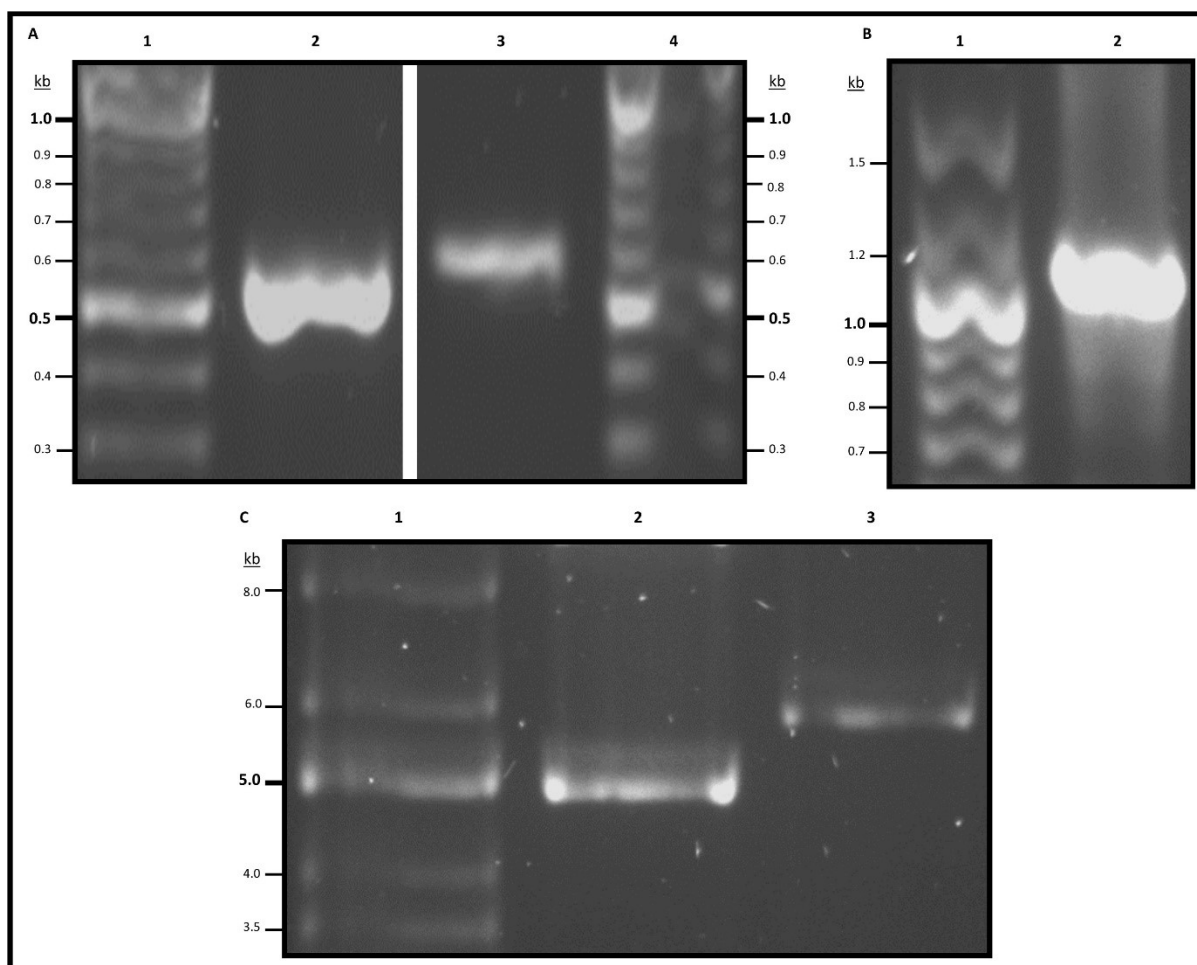
Figure 6.10. Construction of pSNUFF3Cm-Δ*bcam0001a*

Agarose gel electrophoresis analysis of DNA PCR products and plasmid DNA used in construction of pSNUFF3Cm-Δ*bcam0001a*. **A.** First round SOE PCR to amplify Δ*bcam0001a* with upstream and downstream flanking DNA. Lanes 1 and 4, GeneRuler 1 kb DNA Ladder (Thermofisher); lane 2, Δ*bcam0001a* 'left' flank, 532 bp PCR product; lane 3, Δ*bcam0001a* 'right' flank, 555 bp PCR product. **B.** Second round SOE PCR to amplify Δ*bcam0001a* with upstream and downstream flanking DNA. Lane 1, GeneRuler 1 kb DNA Ladder (Thermofisher); lane 2, Δ*bcam0001a*, 1056 bp PCR product. **C.** pSNUFF3Cm-Δ*bcam0001a* plasmid DNA. Lane 1, Supercoiled ladder (NEB); lane 2, pSNUFF3Cm, 5.1 kb; lane 3, pSNUFF3Cm-Δ*bcam0001a*, 6.1 kb.

6.4.2   Introduction of ΔBCAM0001a into *B. cenocepacia* by allelic exchange

E. coli SM10λ*pir* transformed with pSNUFF3Cm-Δ*bcam0001a* was used as the donor strain for transfer of the mutant allele by conjugation into wild-type *Bce* H111. Resolution products were selected on LB agar containing 100 µg ml^{-1} ampicillin and 50 µg ml^{-1} chloramphenicol. Plasmid integration was further verified by PCR screening using the *bcam0001a*-specific primers Δbcam1a-A and Δbcam1a-D, and the vector specific primers pEX18Tpfor2 and pEX18Tprev2.

E. coli SM10λ*pir* transformed with pDAI-SceI-*pheS* was used to introduce the constitutively-expressed I-SceI endonuclease into the verified co-integrant strain, harbouring both *bcam0001a* and Δ*bcam0001a*, via a second conjugation. Strains that had successfully undergone a second recombination event to remove the vector backbone were selected for on Lnx agar containing 100 µg ml^{-1} ampicillin and 125 µg ml^{-1} tetracycline. Positive clones underwent PCR screening with the primer pairs Δbcam1-1a-out-fwd/ Δbcam1-1a-out-rev, Δbcam1a-A/ Δbcam1a-D, and pEX18Tpfor2/ pEX18Tprev2, to identify recombinants with the *bcam0001a* gene deletion and loss of the vector backbone (Figure 6.11). Mutants were then cured of the pDAI-SceI-*pheS* plasmid by growth on M9 minimal medium with 0.1% (w/v) cPhe.
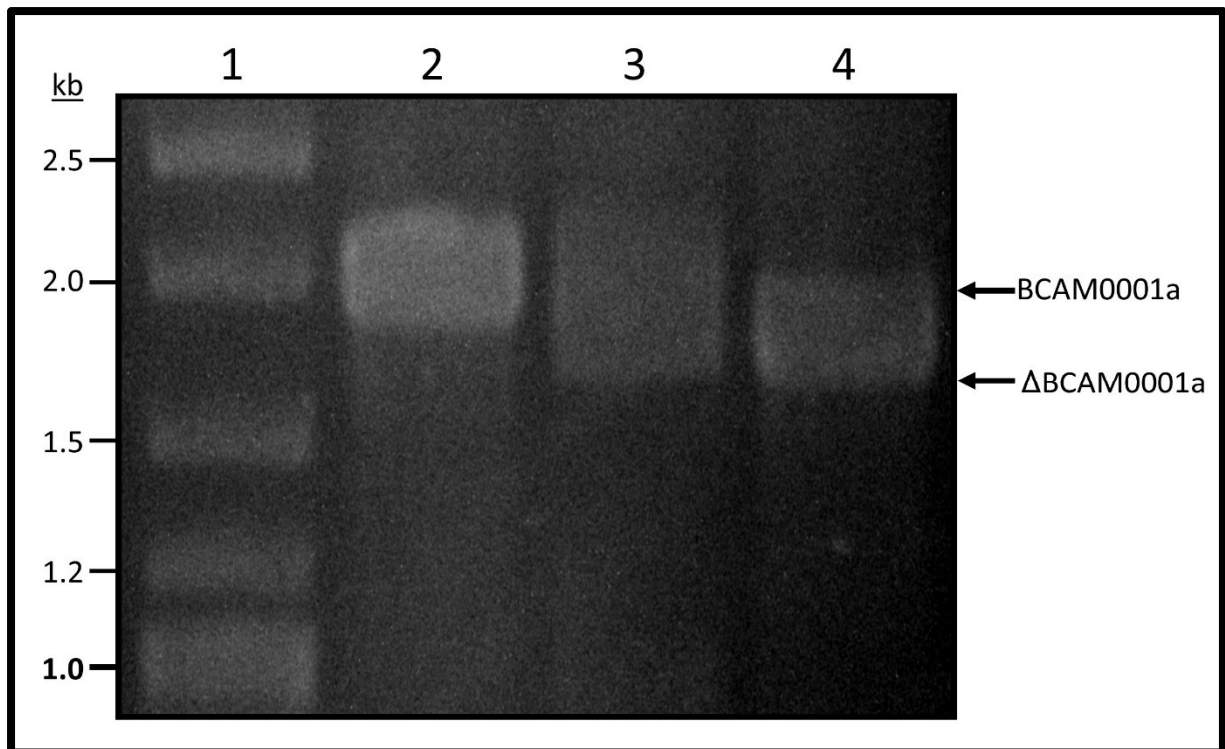
Figure 6.11. Verification of *Bce* H111 ΔBCAM0001a deletion mutant by PCR screen

Agarose gel electrophoresis analysis of DNA products from PCR screening of strains during introduction of mutant ΔBCAM0001a allele into *Bce* H111 using the primer pair Δbcam1-1a-out-fwd/ Δbcam1-1a-out-rev (expected molecular weights: BCAM0001a = 1869 bp, ΔBCAM0001a = 1703 bp). Lane 1, GeneRuler 1 kb DNA Ladder (Thermofisher). The bacterial strain from which the template DNA is extracted is as follows: lane 2, *Bce* H111; lane 3, *Bce* H111-pSNUFF3Cm-ΔBCAM0001a (co-integrant); lane 4, *Bce* H111 ΔBCAM0001a.

6.5 Construction of Δ*bcam0001-bcam0001a* gene deletion mutant

6.5.1   Construction of pSNUFF3Cm-Δ*bcam0001-bcam0001a*

The in-frame marker-less Δ*bcam0001-bcam0001a* mutant allele was amplified by SOE-PCR using primers Δbcam1-A, Δbcam1-1a-B, Δbcam1-1a-C and Δbcam1a-D to produce a 1064 bp PCR product (Figure 6.12a,b). This mutant allele deletes both the *bcam0001* and *bcam0001a* genes, and leaves a small fused gene formed of the first eight codons of *bcam0001* and the last eight codons of *bcam0001a*. The Δ*bcam0001-bcam0001a* allele was cloned between the *Bam*HI and *Hin*dIII sites of the MCS of pSNUFF3Cm to give pSNUFF3Cm-Δ*bcam0001-*

bcam0001a (Figure 6.12c). The identity of the plasmid construct was confirmed by PCR screening and DNA sequencing analysis with primers M13revBACTH and M13for2.
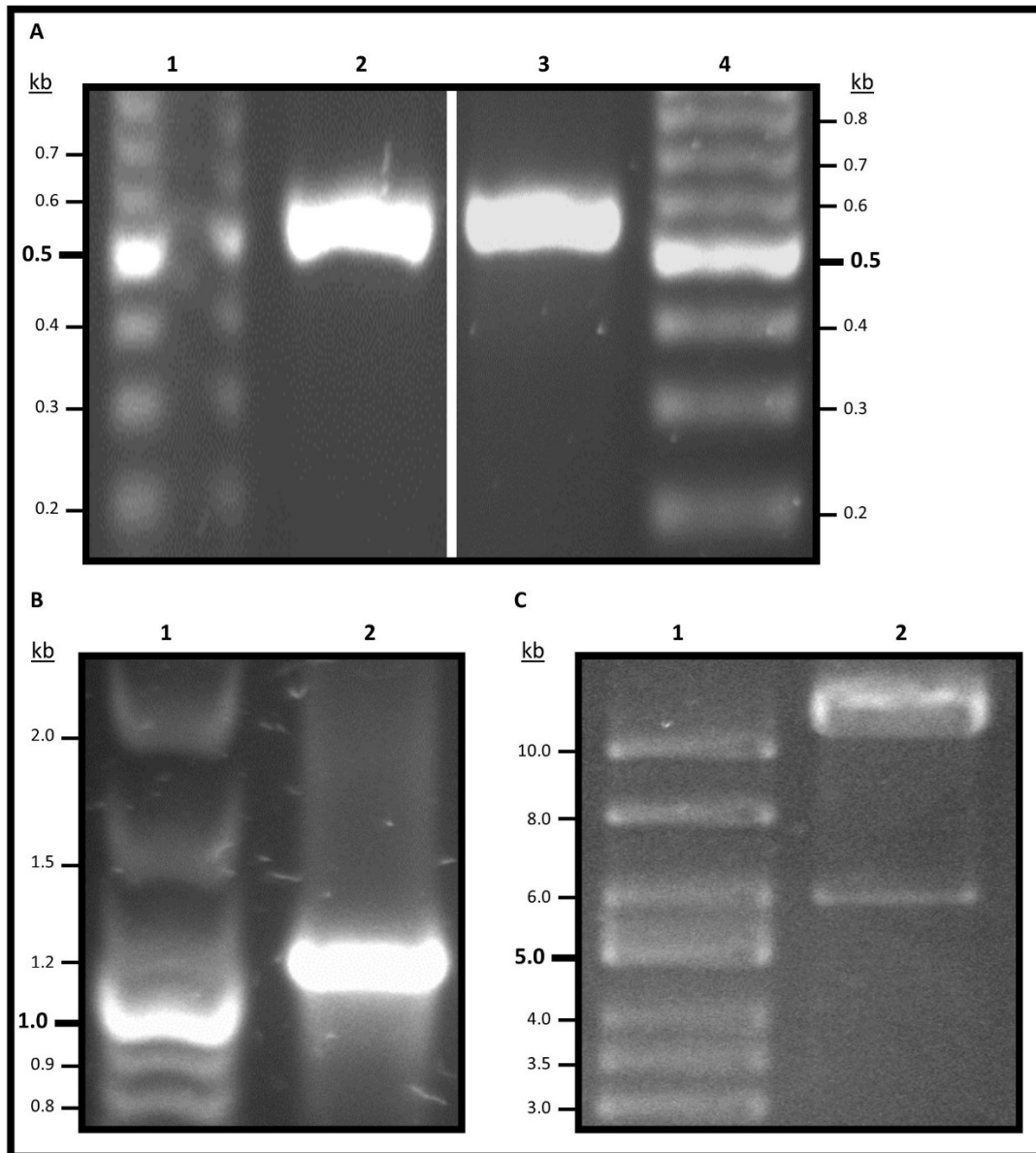
Figure 6.12. Construction of pSNUFF3Cm-Δ*bcam0001-bcam0001a*

Agarose gel electrophoresis analysis of DNA PCR products and plasmid DNA used in construction of pSNUFF3Cm-Δ*bcam0001-bcam0001a*. **A.** First round SOE PCR to amplify Δ*bcam0001-bcam0001a* with upstream and downstream flanking DNA. Lanes 1 and 4, GeneRuler 1 kb DNA Ladder (Thermofisher); lane 2, Δ*bcam0001-bcam0001a* 'left' flank, 544 bp PCR product; lane 3, Δ*bcam0001-bcam0001a* 'right' flank, 555 bp PCR product. **B.** Second round SOE PCR to amplify Δ*bcam0001-bcam0001a* with upstream and downstream flanking DNA. Lane 1, GeneRuler 1 kb DNA Ladder (Thermofisher); lane 2, Δ*bcam0001-bcam0001a*, 1064 bp PCR product. **C.** pSNUFF3Cm-Δ*bcam0001-bcam0001a* plasmid DNA. Lane 1, Supercoiled ladder (NEB); lane2, pSNUFF3Cm-Δ*bcam0001-bcam0001a*, 6.1 kb.

6.5.2 Introduction of Δ*bcam0001-bcam0001a* into *B. cenocepacia* by allelic exchange

E. coli SM10λ*pir* transformed with pSNUFF3Cm-Δ*bcam0001-bcam0001a* was used as the donor strain for transfer of the mutant allele by conjugation into wild-type *Bce* H111. Resolution products were selected on LB agar containing 100 μg ml^{-1} ampicillin and 50 μg ml^{-1} chloramphenicol. Plasmid integration was further verified by PCR screening using the *bcam0001-0001a*-specific primers Δbcam1-A and Δbcam1a-D, and the vector specific primers pEX18Tpfor2 and pEX18Tprev2.

E. coli SM10λ*pir* transformed with pDAI-SceI-*pheS* was used to introduce the constitutively-expressed I-SceI endonuclease into the verified co-integrant strain, harbouring both *bcam0001-bcam0001a* and Δ*bcam0001-bcam0001a*, via a second conjugation. Strains that had successfully undergone a second recombination event to remove the vector backbone were selected for on Lnx agar containing 100 μg ml^{-1} ampicillin and 125 μg ml^{-1} tetracycline. Positive clones underwent PCR screening with the primer pairs Δbcam1-1a-out-fwd/ Δbcam1-1a-out-rev, Δbcam1-A/ Δbcam1a-D, and pEX18Tpfor2/ pEX18Tprev2, to identify recombinants with the *bcam0001-bcam0001a* gene deletion and loss of the vector backbone (Figure 6.13). Mutants were then cured of the pDAI-SceI-*pheS* plasmid by growth on M9 minimal medium with 0.1% (w/v) cPhe.
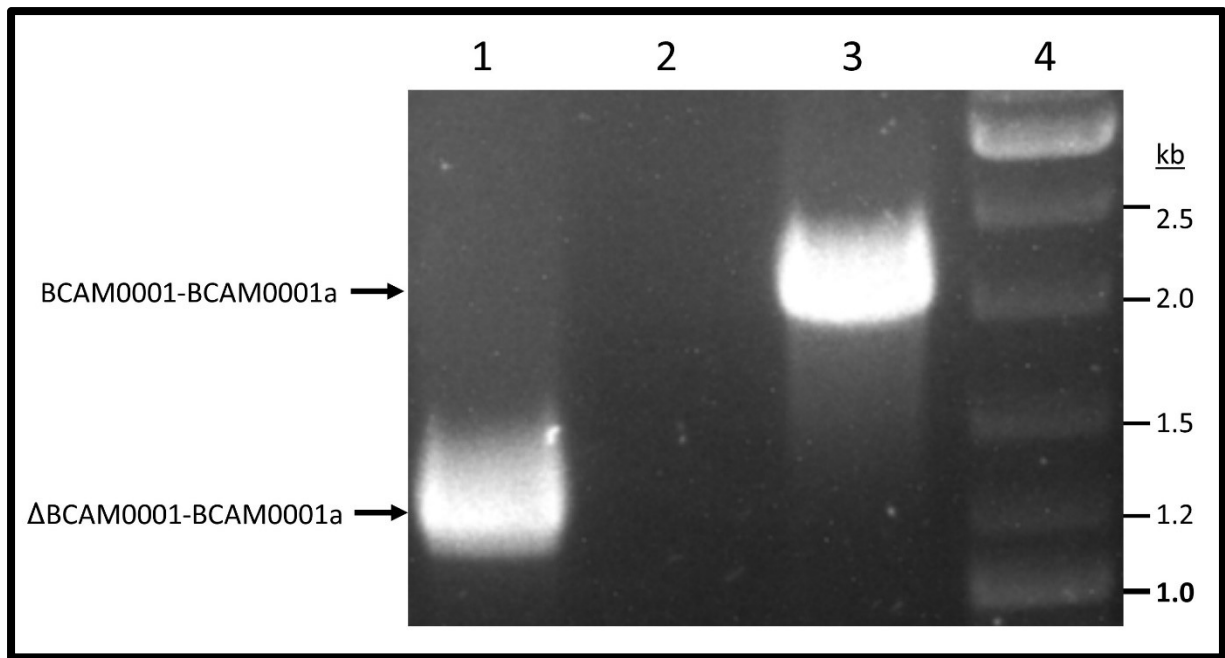
Figure 6.13. Verification of *Bce* H111 ΔBCAM0001-BCAM0001a deletion mutant by PCR screen

Agarose gel electrophoresis analysis of DNA products from PCR screening of strains during introduction of mutant ΔBCAM0001-BCAM0001a allele into *Bce* H111 using the primer pair Δbcam1-1a-out-fwd/ Δbcam1-1a-out-rev (expected molecular weights: BCAM0001-BCAM0001a = 1869 bp, ΔBCAM0001-BCAM001a = 1125 bp). The bacterial strain from which the template DNA is extracted is as follows: lane 1, *Bce* H111 ΔBCAM0001-BCAM0001a; lane 3, *Bce* H111-pSNUFF3Cm-ΔBCAM0001-BCAM0001a (co-integrant); lane 4, *Bce* H111. Lane 4, GeneRuler 1 kb DNA Ladder (Thermofisher).

6.6 Identification of BCAM0001-dependent promoters

6.6.1   Construction of pBBR1MCS-2-*bcam0001*

For the analysis of the BCAM0001 ECF sigma factor *in vivo*, the *bcam0001* gene was cloned into the broad host range expression vector pBBR1MCS-2 (Kovach *et al.*, 1995). The *bcam0001* gene was amplified by PCR from *Bce* H111 genomic template DNA using the primers bcam1-fwd-HindIII and bcam1-rev-BamHI to produce a 672 bp PCR product (Figure 6.14a). This included 30 bp immediately upstream of the start codon containing the Shine-Dalgarno sequence, and preceded by an in-frame stop codon to terminate translation of the upstream *lacZα* gene of the vector to eliminate LacZα-BCAM0001 fusion. The *bcam0001*

gene was cloned between the *Hind*III and *Bam*HI sites of the MCS of pBBR1MCS-2 to give pBBR1MCS-2-*bcam0001* (Figure 6.14b). The identity of the plasmid construct was confirmed by PCR screening and DNA sequencing analysis with primers M13revBACTH and M13for2.
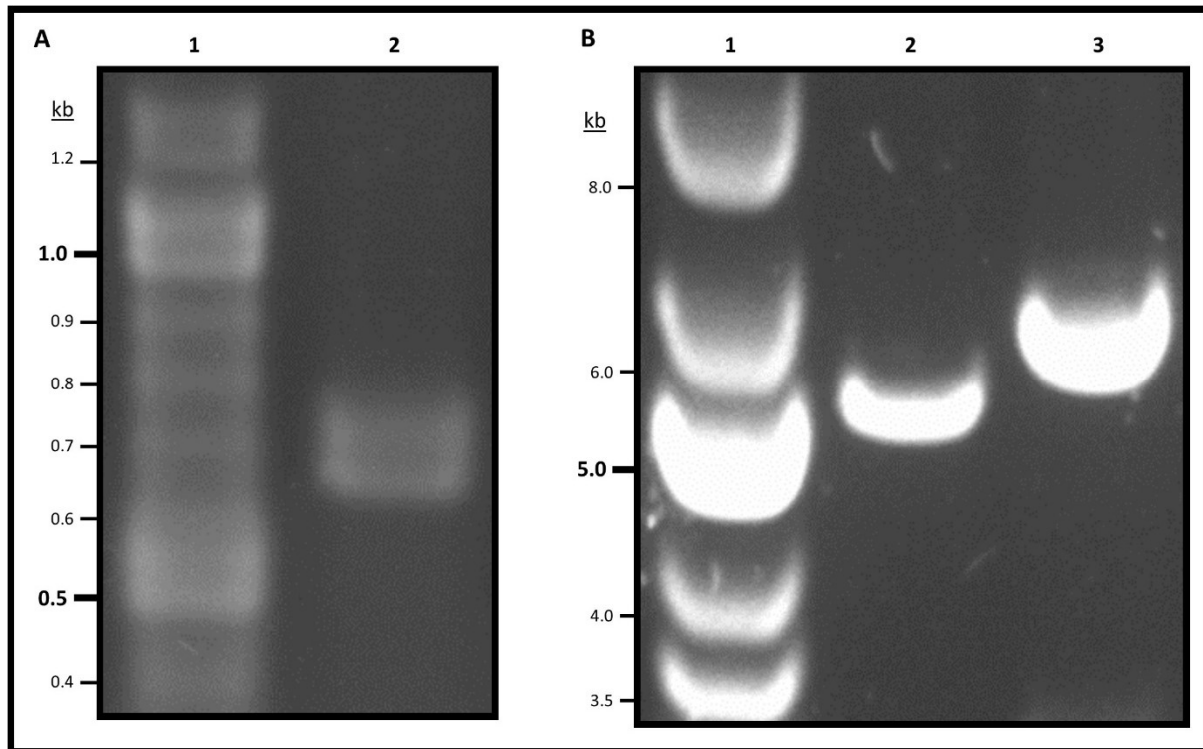
Figure 6.14. Construction of pBBR1MCS-2-*bcam0001*.

Agarose gel electrophoresis analysis of DNA PCR products and plasmid DNA used in construction of pBBR1MCS-2-*bcam0001*. **A.** PCR to amplify *bcam0001*. Lane 1, GeneRuler 1 kb DNA Ladder (Thermofisher); lane 2, *bcam0001* PCR product, 672 bp. **B.** pBBR1MCS-2-*bcam0001* plasmid DNA. Lane 1, Supercoiled DNA Ladder (NEB); lane 2, pBBR1MCS-2, 5.1 kb; lane 3, pBBR1MCS-2-*bcam0001*, 5.8 kb.

6.6.2 Construction of pKAGd4-derived transcriptional reporter plasmids

To investigate the activity of BCAM0001 upon its putative target promoters by β-galactosidase assay, the promoters $P_{bcam2840}$, $P_{bcam0001}$ and $P_{bcam0002}$ were cloned into the transcription reporter plasmid pKAGd4 (Agnoli *et al.*, 2006). All promoters were amplified by PCR from *Bce* H111 genomic template DNA. The primers p-bcam2840-fwd and p-bcam2840-rev were used to produce a 388 bp PCR product, containing 368 bp of the 5'-UTR of the *bcam2840* gene (Figure 6.15a); the primers p-bcam0001-fwd and p-bcam0001-rev were used to produce a 388 bp PCR product, containing 368 bp of the 5'-UTR of the *bcam0001*

gene (Figure 6.15b); the primers p-bcam0002-fwd and p-bcam0002-rev were used to produce a 294 bp PCR product, containing 274 bp of the 5'-UTR of the *bcam2840* gene (Figure 6.15c). All promoter DNA was cloned between the *Hin*dIII and *Bam*HI sites of the MCS of pKAGd4, upstream of the *lacZα* gene, to give pKAGd4-P*bcam2840*, pKAGd4-P*bcam0001* and pKAGd4-P*bcam0002* (Figure 6.15d). The identities of the plasmid constructs were confirmed by PCR screening and DNA sequencing analysis using the primer AP10.
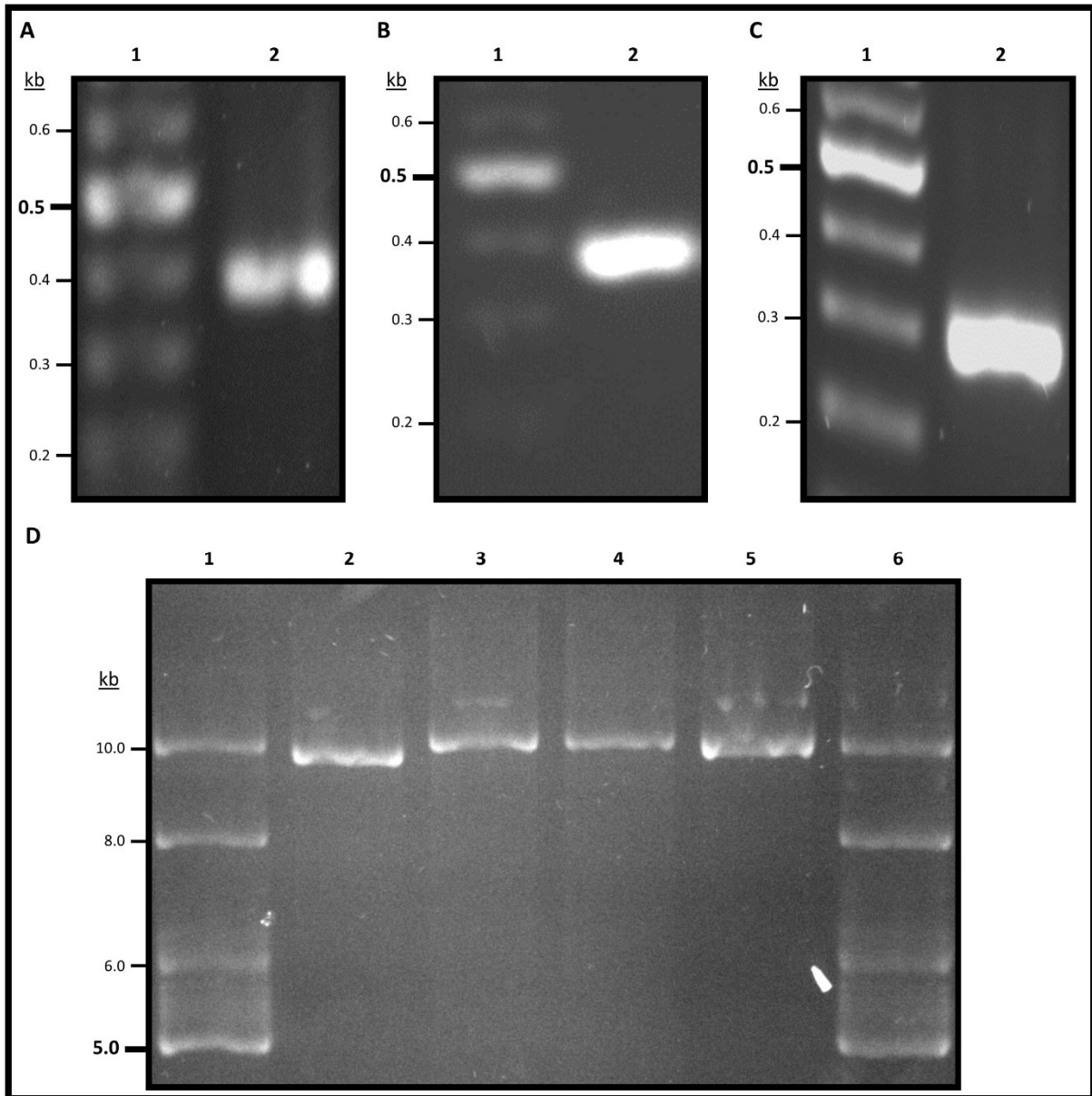
Figure 6.15. Construction of pKAGd4 derivatives containing putative promoter DNA.

Agarose gel electrophoresis analysis of DNA PCR products and plasmid DNA used in construction of pKAGd4 derivatives containing putative promoter DNA for the genes *bcam2840*, *bcam0001* and *bcam0002*. **A.** PCR to amplify P$_{bcam2840}$. Lane 1, GeneRuler 1 kb DNA Ladder (Thermofisher); lane 2, P$_{bcam2840}$ PCR product, 388 bp. **B.** PCR to amplify P$_{bcam0001}$. Lane 1, GeneRuler 1 kb DNA Ladder (Thermofisher); lane 2, P$_{bcam0001}$ PCR product, 388 bp. **C.** PCR to amplify P$_{bcam0002}$. Lane 1, GeneRuler 1 kb DNA Ladder (Thermofisher); lane 2, P$_{bcam0002}$ PCR product, 294 bp. **D.** pKAGd4 derivatives plasmid DNA. Lanes 1 and 6, Supercoiled DNA Ladder (NEB); lane 2, pKAGd4, 9.60 kb; lane 3, pKAGd4-P$_{bcam2840}$, 9.94 kb; lane 4, pKAGd4-P$_{bcam0001}$, 9.94 kb; lane 5, pKAGd4-P$_{bcam0002}$, 9.85 kb.

6.6.3 Promoter reporter analyses of putative BCAM0001-dependent promoters

The pBBR1MCS2-BCAM0001 expression plasmid and the pKAGd4 promoter reporter plasmids containing the putative BCAM0001-dependent promoters were co-introduced into *E. coli* MC1061 (Δ*lac*) by transformation, in addition to the parental plasmids as negative controls, in different combinations. The β-galactosidase assay was performed according to the protocol outlined in section 2.5.1. The assay was performed on cultures grown in LB broth, supplemented with 100 μg ml^{-1} ampicillin and 50 μg ml^{-1} kanamycin. However, none of the three assayed promoters displayed any activity in the presence of BCAM0001 (data not shown).

This could be explained by the lack of a *Bce* specific factor necessary for the activity of the sigma factor. Therefore, the pKAGd4 promoter reporter plasmids (and the parental pKAGd4 plasmid as a negative control) were introduced into *Bce* H111 by conjugation to verify their activity in *Bce*. The β-galactosidase assay was performed according to the protocol outlined in section 2.5.1 on cells grown in LB medium supplemented with 50 μg ml^{-1} chloramphenicol. However, again, none of the three assayed promoters displayed any activity (data not shown).

6.7 Discussion

In this chapter, the start of an investigation into characterising the BCAM0001 sigma factor of *Bce* has been described. The protein-protein interaction between BCAM0001 and its putative anti-sigma factor has be demonstrated *in vivo*. Although this does not verify that these two protein constitute a sigma-anti-sigma factor pair in isolation, it strongly suggests that their activity is linked. This could be explored further with *in vitro* experiments.

Attempts were made to generate a BCAM0001 gene deletion mutant. However, this proved to be difficult. However, a deletion of the anti-sigma factor BCAM0001a, and a tandem deletion of the BCAM0001-BCAM0001a pair were introduced into *Bce* H111. These strains

could be used to determine the function of the genes regulated by BCAM0001. This could take the form of experiments to characterise the phenotypes of the mutant strains grown in the presence of different stressors.

Finally, the identification of the BCAM0001-dependent promoters was undertaken. Although it was predicted that the DNA fragments upstream of the translation start codon of the genes located proximal to BCAM0001 would contain BCAM0001-dependent promoters, these regions of DNA showed no activity in promoter reporter analyses. As with the phenotypic characterisation of the *Bce* H111 mutant strains, analysing the activities of these promoters in the presence of different stressors may be necessary to activate the BCAM0001-dependent promoters. As the predicted functions of BCAM2840 are an NAD(P)H reductase or chromate reductase, and the predicted function of BCAM0002 is an arsenate reductase, oxidative stress or heavy metal ions may induce the activity of BCAM0001.

Chapter VII: Final discussion

7.1 Final discussion and remarks

The body of research presented in this thesis has provided several new insights into the OrbS, MbaS and BCAM0001 sigma factor systems of *Burkholderia*, and their metal-responsive regulatory domains. In adition to delivering novel information about these systems, and new tools whith which to study them, this research has also generated new questions to pursue.

Firstly, the regulation of MbaS has been elucidated in greater detail. It has been demonstrated that, like OrbS, MbaS is regulated by the ferric uptake regulator, Fur, and the location of the Fur-binding DNA element has been limited to a 186 bp region of DNA (shown in Figure 5.2. Within this region of DNA, is a sequence that shows similarity to the 19-mer

Fur box consensus sequence. It is highly likely that this the Fur site in P$_{mbaS}$, but further FURTA experiments or promoter-reporter analyses with base substitutions could be performed to identify this site beyond doubt. Additionally, three MbaS-dependent promoters have been validated.

An *mbaS* deletion mutant has also been constructed in *B. thailandensis*, a useful tool for the study of the sigma factor and its function. This work enabled the investigation of the regulatory mechanism or MbaS, alongside its homologue OrbS. Further gene deletions and insertions using a variety of techniques were attempted, but proved to be unsuccessful. It is unclear why this was the case, but it may by that the allelic exchange vectors used have low effectiveness when used in conjunction with *Bth*, and different methods may need to be used. With respect to the introduction of the *mbaS*$_{CpentaA}$ allele, a potential solution may be directly replacing the wild-type *mbaS* with *mbaS*$_{CpentaA}$ (rather than the 'knock-in' mutagenesis attempted). This would require the use of specific screening primers that bind to the mutated CRE region of *mbaS*$_{CpentaA}$, but not *mbaS*, or *vice versa*.

An interesting observation that arose though the deletion of *mbaS* and the NRPS gene *pchE* in *Bth* was the effect of temperature upon the secretion of pyochelin. It appears that a greater amount of pyochelin is produced and/or secreted by *Bth* at 30 °C, compared to at 37 °C. It is unclear why this may be the case, but could be linked to the utilisation of more than one siderophore by *Bth* and many other siderophore-producing bacteria. Perhaps the secondary siderophore pyochelin is the favoured siderophore of use, over malleobactin, under some environmental conditions. When found in its soil environment, temperatures are around 30 °C and pyochelin production could be increased; during infection of mammalian hosts, temperatures are around 37 °C and the pyochelin production could be decreased. Therefore, the regulation of dual-siderophore systems may be pertintent to infection, and this temperature regulation effect of pyochelin is worthy of future investigation.

In the course of this research, a strain variant of *Bth* E264 was discovered. Although obstensibly the same as the reference strain *Bth* E264, this strain differed in some key aspects, particularly the loss of malleobactin production. This suggests that the usage of malleobactin is not essential to *Bth* E264 under laboratory conditions. This could also imply

that the siderophore system provides a selective advantage to *Bth* in its soil environment and/or during infection, given that this system is retained in other strains of the bacterium. The identification of this strain also raise the possibility that there is large variation between *Bth* E264 strains widely used across many laboratories, which could have profound implications upon the research performed upon hypothetically identical bacterial strains.

Examination of the N-terminal extension of OrbS was performed through analysis of an OrbS variant encoding a deletion of the N-terminal region. However, this N-terminally deleted OrbS variant appeared to act identically to the wild-type protein, and was not studied further. It is unclear what the function of this N-terminal extension, present in both MbaS and OrbS, is. More experimental work could be carried out on this variant. In particular, examining the effect of the N-terminal deletion in conjunction with the C-terminal deletion, or substitutions of the C-terminal cysteines, could investigate any cooperativity between the two terminal regions.

Examination of the function of the C-terminal extension in OrbS by sequential truncations of the C-terminus revealed that this extension contributed to the activity of the sigma factor. When short C-terminal deletions were made in OrbS, the resulting activity from a target promoter was decreased. However, this activity was not completely lost, suggesting the C-terminal extension only confers a partial influence upon the sigma factor's activity. Additionally, when C-terminal truncation impinged upon the C-terminal helix-turn-helix of region 4.2, there was abolition of the sigma factor's activity.

These preliminary studies also provided evidence of iron regulation upon the activity of OrbS, independently of Fur. The presence of iron was shown to result in lower activity from an OrbS-dependent promoter. The C-terminally truncated variants displayed a loss of this iron regulation. This indicated that the C-terminal region of OrbS contains elements that were able to transduce the presence of iron, and regulate the activity of the sigma factor. This C-terminal extension contains four cysteine residues, and was referred to as a cysteine-rich extension (CRE). Substitution of the four cysteines for alanine encoded an OrbS variant that, like the C-terminally truncated variants, was not regulated in the presence of iron. This indicated that the four cysteine residues, almost certainly via their thiol groups, were the elements within the C-terminal extension that transduced the presence of iron.

This regulatory mechanism was investigated further for OrbS and MbaS through a series of *in vivo* promoter reporter analyses and *in vitro* examination of transcription and RNAP holoenzyme reconstitution. These were performed in parallel with variant of each sigma factor with cysteine-to-alanine substitutions of the C-terminal cysteine residues with the CRE. It was determined that OrbS was regulated both *in vivo* and *in vitro* by the presence of iron, copper and zinc, and that MbaS was regulated only *in vitro* by the presence of iron and zinc. This meal regulation was shown to be specific to the cysteines of the CRE.

For the *in vitro* experiments, concentrations of the metal ions assayed were selected empirically at 10 µM or 25 µM. However, these concentrations may not truly reflect the concentrations of the metals in nature. The total concentrations of iron and zinc in bacterial cells are around 0.2 mM, but much of this is bound by metalloproteins (Outten and O'Halloran, 2001). Therefore, the pool of free metal ions in *E. coli* is estimated to be around 10^{-6} to 10^{-7} M for Fe(II), and 10^{-15} to 10^{-16} M for Zn(II) (effectively no free Zn(II) ions in the cytoplasm under normal growth conditions) (Outten and O'Halloran, 2001; Williams, 2012). So, the concentrations of Fe(II) used are around one order of magnitude greater than found in the cell, and the concentration of Zn(II) used is around 10 orders of magnitude greater than found in the cell. This raises that the possibility that the concentrations used in *iv*T and BLI assays do not have relevance for the binding of metal the the sigma factors in nature. Nonetheless, these simple *in vitro* systems do not account for the complexity of the cell, and the influence other metalloproteins and metal chaperone proteins may have in the bacterial cytoplasm and upn the effective concentration of metal ions. Plus, if the influence of iron, zinc and copper upon the sigma factors was an artefactual effect due to high concentrations of metal, one might expect to see similar levels of sigma factor inhibition in the presence of other metal ions, which is not observed. Therefore, despite the concentrations of metal ions used in the *iv*T and BLI experiments being much higher than would be present in a bacterial cell, it is still probable that the metal-dependent inhibitory effect upon the sigma factor activity is genuine and likely to be at work in nature.

Through biolayer interferometry assays, a series of binding affinities for MbaS, MbaS$_{CpentaA}$, OrbS and OrbS$_{CtetraA}$ with *E. coli* core RNAP were generated (Table 5.3). In the absence of metal, these interactions had and mean K_D values of 3.5×10^{-8} M. Binding affinity for core RNAP and sigma factor interactions is limited, and varies somewhat depending on the

specific protein pair and the techniques used to derive the data. However, the interaction of *E. coli* core RNAP and σ^{FecI}, determined by holoenzyme reconstitution followed by gel filtration column chromatography, protein staining and image-based quantification, has a K_D value of 1.73×10^{-9} M (Maeda, Fujita and Ishihama, 2000). This represents a 20-fold discrepancy of binding affinity between the two K_D values. Nonetheless, BLI assays are a more accurate method of determining binding kinetic data, and perhaps should be considered with greater validity than data generated through methods that are more inaccurate and/or modelling.

Further examination of the binding kinetics values generated in Table 5.3 could provide some insights into the inhibitory mechanism of the metal-dependent regulation. It has been demonstrated that specific metals inhibit the association of MbaS and OrbS with core RNAP via their CREs; this could occur via decreasing the association of the holoenzyme complex, or by increasing the dissociation of the holoenzyme complex. In the case of Orbs, regardless of the presence of metal, the K_d values remain within the same order of magnitude (around 5×10^{-4} s^{-1}). However, when Fe(II) or Zn(II) are added, the K_a values decrease by 805-fold and 1,391-fold, respectively. This indicates that it is the association of OrbS and core RNAP that is inhibited by the presence of Fe(II) and Zn(II). In the case of MbaS interacting with core RNAP, however, both the association and dissociation constants are altered with the addition of Zn(II): the K_a decreases 1,740-fold, and the K_d increases 45-fold, when Zn(II) is present compared to when it is not. This could indicate that both the association and dissociation of MbaS and core RNAP is affected by the presence of Zn(II), although the assocoiation is the more significantly influenced step of the protein-protein interaction. Nonetheless, this could suggest subtley different metal-dependent inhibitory mechanisms between MbaS and OrbS.

In conclusion, the research presented in this study has provided evidence that the iron starvation (IS) sigma factors OrbS and MbaS contain on-board regulatory domains. These domains are able to transduce the presence of specific metal ions. This could represent a novel regulatory mechanism of this class of ECF sigma factors.

Given that both MbaS and OrbS are regulated by iron via Fur, and they regulate the transcription of Fe(III)-specific siderophores, it is unclear why this secondary metal-

dependent regulation mechanism via the CREs exists, and why additional non-iron metal ions are able to regulate the sigma factors. Firstly, it suggests that the post-translational regulation of sigma factor activity is important and there is a selective advantage for maintaining or evolving such a mechanism. Normally, ECF sigma factors have an anti-sigma factor to regulate this activity at the protein level. Even PvdS, an IS sigma factor with iron-dependent transcriptional regulation by Fur, is regulated by the anti-sigma factor FpvR. The expression and utilisation of siderophore systems much be a metabolically intensive process to warrant this level of stringent control. Perhaps the degradation of MbaS and OrbS within the bacterial cell is a relatively slow process, and simply repressing the transcription of the sigma factors via Fur is insufficient to repress the transcription of the malleobactin/ornibactin apparatus effectively. Secondly, this additional post-translational regulation may allow further modulation of the sigma factor activity. Given that iron-dependent regulation occurs via Fur, alternative metal-dependent regulation could be able to occur via the sigma factor's CREs. These alternative metals could acts proxy stimuli for iron limitation, and could be selected for as they provide further detection of metal starvation conditions in an example of metal homeostasis.

7.2 Future work

Nonetheless, further elucidation of this regulatory mechanism is required. Data from bio layer interferometry experiments, which examined the association of core RNAP with the *Burkholderia* sigma factors, suggests that it is this reconstitution step that is inhibited by the presence of the metal ions. However, the association of sigma factor and DNA was not specifically examined, and the metal ions could inhibit this association, too. Further bio layer interferometry assays, or EMSAs, investigated this interaction could be employed.

Additionally, because all of the cysteine residues of the CRE were substituted, it is unclear what influence the individual cysteines had upon the regulatory activity. Performing these experiments with a series of individual or combined cysteine-to-alanine substitutions could

explore this further. Moreover, there are additional conserved amino acids residues within the CRE. It is conceivable that they, too, may transduce the presence of metal ions. In particular, a histidine residue located in region 4.2, and conserved among ECF09 IS sigma factors containing a CRE (highlighted in Figure 1.13), and a conserved aspartate residue (amino acid position 201 in OrbS, 208 in MbaS), could be capable of coordinating metal ions via their imidazole and carboxylate groups, respectively.

It also appears that the differences in the CREs of MbaS and OrbS influence the metal ions that can be transduced. OrbS is regulated in the presence of copper *in vivo* whereas MbaS is not. To examine this further, and truly characterise the CRE as a protein domain, protein constructs could be engineered in which the CREs are swapped. This may result in changing the specificity of the metal ions that the sigma factors are regulated by.

This study looked solely at the influence of metal ions upon the activity of the sigma factors OrbS and MbaS via their CREs. However, the CRE may respond to other stimuli to affect the activity of the sigma factors. For instance, cysteine residues are readily oxidised and reduced, and this greatly affects the ability of the side chains to acts as nucleophiles and form disulphide bridges. Therefore, redox stress could be another stimulus that regulates the activity of OrbS and MbaS through their CREs.

Most importantly, direct binding of metal ions to the sigma factors MbaS and OrbS has not been demonstrated. The binding metal ions to the sigma factors could be inferred from a series of experiements. Circular dichroism could be used to demonstrate a shift in secondary protein structure upon binding of metal to the sigma factors. This could also be demonstrated by isothermal titration calorimetry experiments, which enabes calculation of a binding affinity. In the case of iron binding, proteins containing iron-sulphur clusters typically produce orange-coloured solutions; this phenomonen could be exploited by titrating OrbS/MbaS with iron to form iron-sulphur clusters *in vitro*, and spectrometrically measure the colour change. Alternatively, metal-binding could be measured using NMR spectroscopy, with the added nuance that the residues responsible for the binding could be determined by 2D-NMR analysis. Mass spectroscopy, specifically ESI-MS, would also identify whether metal binding occurs by ascertaining the precise molecular weight; this molecular weight would also elucidate the ratio metal ions bound and (in the case of iron-binding) the

coordination of the iron-sulphur cluster. A further method of determining the metal-protein stoichiometry with high precision is inductively coupled plasma optical emission spectroscopy (ICP-OES). Ultimately, the elucidation of the protein structures of OrbS or MbaS with bound metal ions would provide considerable data, including identification of the metal-coordinating residues and the inactive conformation of the sigma factors. If binding of the metal ion by the thiols is accommodated by the formation of a metal-sulphur cluster, the coordination of this cluster could also be examined.

However, to perform these experiements the proteins analysed must be compatible. There were significant difficulties in handling the purified OrbS and MbaS proteins. These IS sigma factors were prone to denaturation and/or degradation, often precipitating out of solution. This would occur at temperatures above 4 ^{O}C, at high concentrations above ~1 mg ml^{-1}, and in buffers that did not contain high concentrations of glycerol. Given that most of the biochemical techniques with the potential to examine metal binding to these sigma factors require the proteins to be in solutions at high concentrations/amounts, in compatible buffers, and at room temperature or higher, this poses serious difficulties. For this further work to be achieved, the purification and handling of the proteins must be developed and optimised to increase their stability and compatibility with these experiements.

References

Agnoli, K. (2007) *Regulation of ornibactin synthesis and utilisation in Burkholderia cenocepacia.*

Agnoli, K., Haldipurkar, S. S., Tang, Y., Butt, A. T. and Thomas, M. S. (2018) 'Distinct modes of promoter recognition by two iron starvation sigma factors with overlapping promoter specificities', *J Bacteriol*.

Agnoli, K., Lowe, C. A., Farmer, K. L., Husnain, S. I. and Thomas, M. S. (2006) 'The ornibactin biosynthesis and transport genes of Burkholderia cenocepacia are regulated by an extracytoplasmic function σ factor which is a part of the Fur regulon', *Journal of Bacteriology,* 188(10), pp. 3631-3644.

Agochukwu, N. Q., Rastinehad, A. R., Richter, L. A., Barak, S., Zerbe, C. S., Holland, S. M. and Pinto, P. A. (2012) 'Prostatic abscess in a pediatric patient with chronic granulomatous

disease: report of a unique case and review of the literature', *Journal of Pediatric Surgery,* 47(2), pp. 400-403.

Alice, A. F., Lopez, C. S., Lowe, C. A., Ledesma, M. A. and Crosa, J. H. (2006) 'Genetic and transcriptional analysis of the siderophore malleobactin biosynthesis and transport genes in the human pathogen Burkholderia pseudomallei K96243', *J Bacteriol,* 188(4), pp. 1551-66.

Andrews, S. C., Robinson, A. K. and Rodriguez-Quinones, F. (2003) 'Bacterial iron homeostasis', *FEMS Microbiol Rev,* 27(2-3), pp. 215-37.

Angus, A. A., Agapakis, C. M., Fong, S. M., Yerrapragada, S., Estrada-de Los Santos, P., Yang, P., Song, N., Kano, S., Caballero-Mellado, J., de Faria, S. M., Dakora, F. D., Weinstock, G. and Hirsch, A. M. (2014) 'Plant-Associated Symbiotic Burkholderia Species Lack Hallmark Strategies Required in Mammalian Pathogenesis', *PLOS ONE,* 9(1), pp. e83779.

Ashdown, L. R. (1979) 'Nosocomial infection due to Pseudomonas pseudomallei: two cases and an epidemiologic study', *Rev Infect Dis,* 1(5), pp. 891-4.

Aunkham, A., Schulte, A., Winterhalter, M. and Suginta, W. (2014) 'Porin involvement in cephalosporin and carbapenem resistance of Burkholderia pseudomallei', *PLoS One,* 9(5), pp. e95918.

Bae, J. B., Park, J. H., Hahn, M. Y., Kim, M. S. and Roe, J. H. (2004) 'Redox-dependent changes in RsrA, an anti-sigma factor in Streptomyces coelicolor: Zinc release and disulfide bond formation', *Journal of Molecular Biology,* 335(2), pp. 425-435.

Baichoo, N. and Helmann, J. D. (2002) 'Recognition of DNA by Fur: a reinterpretation of the Fur box consensus sequence', *Journal of Bacteriology,* 184(21), pp. 5826-5832.

Balla, J., Jacob, H. S., Balla, G., Nath, K., Eaton, J. W. and Vercellotti, G. M. (1993) 'Endothelial-cell heme uptake from heme proteins: induction of sensitization and desensitization to oxidant damage', *Proc Natl Acad Sci U S A,* 90(20), pp. 9285-9.

Barne, K., Bown, J., Busby, S. and Minchin, S. (1997) 'Region 2.5 of the Escherichia coli RNA polymerase sigma(70) subunit is responsible for the recognition of the 'extended -10' motif at promoters', *Embo Journal,* 16(13), pp. 4034-4040.

Barrett, A. R., Kang, Y., Inamasu, K. S., Son, M. S., Vukovich, J. M. and Hoang, T. T. (2008) 'Genetic tools for allelic replacement in Burkholderia species', *Applied and Environmental Microbiology,* 74(14), pp. 4498-4508.

Bastiaansen, K. C., Otero-Asman, J. R., Luirink, J., Bitter, W. and Llamas, M. A. (2015a) 'Processing of cell-surface signalling anti-sigma factors prior to signal recognition is a conserved autoproteolytic mechanism that produces two functional domains', *Environmental Microbiology,* 17(9), pp. 3263-3277.

Bastiaansen, K. C., van Ulsen, P., Wijtmans, M., Bitter, W. and Llamas, M. A. (2015b) 'Self-cleavage of the Pseudomonas aeruginosa Cell-surface Signaling Anti-sigma Factor FoxR Occurs through an N-O Acyl Rearrangement', *J Biol Chem,* 290(19), pp. 12237-46.

Baysse, C., De Vos, D., Naudet, Y., Vandermonde, A., Ochsner, U., Meyer, J. M., Budzikiewicz, H., Schafer, M., Fuchs, R. and Cornelis, P. (2000) 'Vanadium interferes with siderophore-mediated iron uptake in Pseudomonas aeruginosa', *Microbiology,* 146 (Pt 10), pp. 2425-34.

Biggins, J. B., Ternei, M. A. and Brady, S. F. (2012) 'Malleilactone, a Polyketide Synthase-Derived Virulence Factor Encoded by the Cryptic Secondary Metabolome of Burkholderia pseudomallei Group Pathogens', *Journal of the American Chemical Society,* 134(32), pp. 13192-13195.

Biot, F. V., Valade, E., Garnotel, E., Chevalier, J., Villard, C., Thibault, F. M., Vidal, D. R. and Pages, J. M. (2011) 'Involvement of the efflux pumps in chloramphenicol selected strains of Burkholderia thailandensis: proteomic and mechanistic evidence', *PLoS One,* 6(2), pp. e16892.

Birnie, E., van 't Hof, S., Bijnsdorp, A., Mansaray, Y., Huizenga, E., van der Ende, A., Hugenholtz, F., Grobusch, M. P. and Wiersinga, W. J. (2019) 'Identification of Burkholderia thailandensis with novel genotypes in the soil of central Sierra Leone', *PLoS Negl Trop Dis,* 13(6), pp. e0007402.

Bory, S., Daily, F., Khim, G., Letchford, J., Sok, S., Kol, H., Seang Lak, M., Tuseo, L., Vibol, C., Oeng, S. and Turner, P. (2018) 'A Report from the Cambodia Training Event for Awareness of Melioidosis (C-TEAM), October 2017', *Trop Med Infect Dis,* 3(1).

Bradbeer, C. (1993) 'The proton motive force drives the outer membrane transport of cobalamin in Escherichia coli', *Journal of Bacteriology,* 175(10), pp. 3146-3150.

Braun, V. and Mahren, S. (2005) 'Transmembrane transcriptional control (surface signalling) of the Escherichia coli Fec type', *Fems Microbiology Reviews,* 29(4), pp. 673-684.

Braun, V., Mahren, S. and Sauter, A. (2006) 'Gene Regulation by Transmembrane Signaling', *Biometals,* 19(2), pp. 103-113.

Brett, P. J., DeShazer, D. and Woods, D. E. (1998) 'Burkholderia thailandensis sp. nov., a Burkholderia pseudomallei-like species', *Int J Syst Bacteriol,* 48 Pt 1, pp. 317-20.

Brickman, T. J. and Armstrong, S. K. (2012) 'Iron and pH-responsive FtrABCD ferrous iron utilization system of Bordetella species', *Mol Microbiol,* 86(3), pp. 580-93.

Burtnick, M. N. and Brett, P. J. (2013) 'Burkholderia mallei and Burkholderia pseudomallei cluster 1 type VI secretion system gene expression is negatively regulated by iron and zinc', *PloS one,* 8(10), pp. e76767-e76767.

Burtnick, M. N., Brett, P. J., Harding, S. V., Ngugi, S. A., Ribot, W. J., Chantratita, N., Scorpio, A., Milne, T. S., Dean, R. E., Fritz, D. L., Peacock, S. J., Prior, J. L., Atkins, T. P. and Deshazer, D. (2011) 'The cluster 1 type VI secretion system is a major virulence determinant in Burkholderia pseudomallei', *Infect Immun,* 79(4), pp. 1512-25.

Busche, T., Silar, R., Picmanova, M., Patek, M. and Kalinowski, J. (2012) 'Transcriptional regulation of the operon encoding stress-responsive ECF sigma factor SigH and its anti-sigma

factor RshA, and control of its regulatory network in Corynebacterium glutamicum', *Bmc Genomics,* 13.

Butt, A. T. and Thomas, M. S. (2017) 'Iron Acquisition Mechanisms and Their Role in the Virulence of Burkholderia Species', *Front Cell Infect Microbiol,* 7, pp. 460.

Campagne, S., Damberger, F. F., Kaczmarczyk, A., Francez-Charlot, A., Allain, F. H. T. and Vorholt, J. A. (2012) 'Structural basis for sigma factor mimicry in the general stress response of Alphaproteobacteria', *Proceedings of the National Academy of Sciences of the United States of America,* 109(21), pp. E1405-E1414.

Campagne, S., Marsh, M. E., Capitani, G., Vorholt, J. A. and Allain, F. H. T. (2014) 'Structural basis for-10 promoter element melting by environmentally induced sigma factors', *Nature Structural & Molecular Biology,* 21(3), pp. 269-276.

Campbell, E., Muzzin, O., Chlenov, M., Sun, J., Olson, C., Weinman, O., Trester-Zedlitz, M. and Darst, S. (2002) 'Structure of the bacterial RNA polymerase promoter specificity sigma subunit', *Molecular Cell,* 9(3), pp. 527-539.

Campbell, E. A., Greenwell, R., Anthony, J. R., Wang, S., Lim, L., Das, K., Sofia, H. J., Donohue, T. J. and Darst, S. A. (2007) 'A conserved structural module regulates transcriptional responses to diverse stress signals in bacteria', *Molecular Cell,* 27(5), pp. 793-805.

Campbell, E. A., Tupy, J. L., Gruber, T. M., Wang, S., Sharp, M. M., Gross, C. A. and Darst, S. A. (2003) 'Crystal structure of Escherichia coli sigmaE with the cytoplasmic domain of its anti-sigma RseA', *Mol Cell,* 11(4), pp. 1067-78.

Campos, C. G., Byrd, M. S. and Cotter, P. A. (2013) 'Functional characterization of Burkholderia pseudomallei trimeric autotransporters', *Infect Immun,* 81(8), pp. 2788-99.

Cao, J., Woodhall, M. R., Alvarez, J., Cartron, M. L. and Andrews, S. C. (2007) 'EfeUOB (YcdNOB) is a tripartite, acid-induced and CpxAR-regulated, low-pH Fe2+ transporter that is cryptic in Escherichia coli K-12 but functional in E. coli O157:H7', *Mol Microbiol,* 65(4), pp. 857-75.

Carlioz, A. and Touati, D. (1986) 'Isolation of superoxide dismutase mutants in Escherichia coli: is superoxide dismutase necessary for aerobic life?', *The EMBO journal,* 5(3), pp. 623-630.

Carver, T., Harris, S. R., Berriman, M., Parkhill, J. and McQuillan, J. A. (2012) 'Artemis: an integrated platform for visualization and analysis of high-throughput sequence-based experimental data', *Bioinformatics,* 28(4), pp. 464-9.

Casadaban, M. J. and Cohen, S. N. (1980) 'Analysis of gene-control signals by DNA-fusion and cloning in Escherichia coli', *Journal of Molecular Biology,* 138(2), pp. 179-207.

Cassat, J. E. and Skaar, E. P. (2013) 'Iron in infection and immunity', *Cell Host Microbe,* 13(5), pp. 509-519.

Chaba, R., Grigorova, I. L., Flynn, J. M., Baker, T. A. and Gross, C. A. (2007) 'Design principles of the proteolytic cascade governing the sigma(E)-mediated envelope stress response in Escherichia coli: keys to graded, buffered, and rapid signal transduction', *Genes & Development,* 21(1), pp. 124-136.

Chan, Y. Y., Tan, T. M., Ong, Y. M. and Chua, K. L. (2004) 'BpeAB-OprB, a multidrug efflux pump in Burkholderia pseudomallei', *Antimicrob Agents Chemother,* 48(4), pp. 1128-35.

Chansrichavala, P., Wongsuwan, N., Suddee, S., Malasit, M., Hongsuwan, M., Wannapinij, P., Kitphati, R., Day, N. P., Michie, S., Peacock, S. J. and Limmathurotsakul, D. (2015) 'Public awareness of melioidosis in Thailand and potential use of video clips as educational tools', *PLoS One,* 10(3), pp. e0121311.

Cheng, A. C. and Currie, B. J. (2005) 'Melioidosis: Epidemiology, pathophysiology, and management', *Clinical Microbiology Reviews,* 18(2), pp. 383-+.

Chodimella, U., Hoppes, W. L., Whalen, S., Ognibene, A. J. and Rutecki, G. W. (1997) 'Septicemia and Suppuration in a Vietnam Veteran', *Hospital Practice,* 32(5), pp. 219-221.

Coenye, T. and Vandamme, P. (2003) 'Diversity and significance of Burkholderia species occupying diverse ecological niches', *Environmental Microbiology,* 5(9), pp. 719-729.

Cohn, R. C., Rudzienski, L. and Putnam, R. W. (1995) 'Verapamil-Tobramycin Synergy in <i>Pseudomonas cepacia </i>but Not <i>Pseudomonas aeruginosa </i>in vitro', *Chemotherapy,* 41(5), pp. 330-333.

Cosgrove, S., Chotirmall, S. H., Greene, C. M. and McElvaney, N. G. (2011) 'Pulmonary proteases in the cystic fibrosis lung induce interleukin 8 expression from bronchial epithelial cells via a heme/meprin/epidermal growth factor receptor/Toll-like receptor pathway', *J Biol Chem,* 286(9), pp. 7692-704.

Cox, C. D. and Graham, R. (1979) 'Isolation of an iron-binding compound from Pseudomonas aeruginosa', *J Bacteriol,* 137(1), pp. 357-64.

Crooks, G. E., Hon, G., Chandonia, J. M. and Brenner, S. E. (2004) 'WebLogo: a sequence logo generator', *Genome Res,* 14(6), pp. 1188-90.

Cruz-Migoni, A., Hautbergue, G. M., Artymiuk, P. J., Baker, P. J., Bokori-Brown, M., Chang, C. T., Dickman, M. J., Essex-Lopresti, A., Harding, S. V., Mahadi, N. M., Marshall, L. E., Mobbs, G. W., Mohamed, R., Nathan, S., Ngugi, S. A., Ong, C., Ooi, W. F., Partridge, L. J., Phillips, H. L., Raih, M. F., Ruzheinikov, S., Sarkar-Tyson, M., Sedelnikova, S. E., Smither, S. J., Tan, P., Titball, R. W., Wilson, S. A. and Rice, D. W. (2011) 'A Burkholderia pseudomallei toxin inhibits helicase activity of translation factor eIF4A', *Science,* 334(6057), pp. 821-4.

Cuppels, D. A., Stipanovic, R. D., Stoessl, A. and Stothers, J. B. (1987) 'The constitution and properties of a pyochelin–zinc complex', *Canadian Journal of Chemistry,* 65(9), pp. 2126-2130.

Currie, B. J. (2015) 'Melioidosis: evolving concepts in epidemiology, pathogenesis, and treatment', *Semin Respir Crit Care Med,* 36(1), pp. 111-25.

Currie, B. J., Jacups, S. P., Cheng, A. C., Fisher, D. A., Anstey, N. M., Huffam, S. E. and Krause, V. L. (2004) 'Melioidosis epidemiology and risk factors from a prospective whole-population study in northern Australia', *Trop Med Int Health,* 9(11), pp. 1167-74.

Currie, B. J., Ward, L. M. and Cheng, A. C. (2010) 'The epidemiology and clinical spectrum of melioidosis: 540 cases from the 20 year Darwin prospective study', *PLoS neglected tropical diseases,* 4(11), pp. e900-e900.

Dance, D. A. B., Sihalath, S., Rith, K., Sengdouangphachanh, A., Luangraj, M., Vongsouvath, M., Newton, P. N., Lubell, Y. and Turner, P. (2019) 'The cost-effectiveness of the use of selective media for the diagnosis of melioidosis in different settings', *PLoS Negl Trop Dis,* 13(7), pp. e0007598.

Darling, P., Chan, M., Cox, A. D. and Sokol, P. A. (1998) 'Siderophore production by cystic fibrosis isolates of Burkholderia cepacia', *Infect Immun,* 66(2), pp. 874-7.

Deng, Z., Wang, Q., Liu, Z., Zhang, M., Machado, A. C., Chiu, T. P., Feng, C., Zhang, Q., Yu, L., Qi, L., Zheng, J., Wang, X., Huo, X., Qi, X., Li, X., Wu, W., Rohs, R., Li, Y. and Chen, Z. (2015) 'Mechanistic insights into metal ion activation and operator recognition by the ferric uptake regulator', *Nat Commun,* 6, pp. 7642.

Depoorter, E., Bull, M. J., Peeters, C., Coenye, T., Vandamme, P. and Mahenthiralingam, E. (2016) 'Burkholderia: an update on taxonomy and biotechnological potential as antibiotic producers', *Applied Microbiology and Biotechnology,* 100(12), pp. 5215-5229.

DeShazer, D., Brett, P. J., Carlyon, R. and Woods, D. E. (1997) 'Mutagenesis of Burkholderia pseudomallei with Tn5-OT182: isolation of motility mutants and molecular characterization of the flagellin structural gene', *J Bacteriol,* 179(7), pp. 2116-25.

Devanga, R., Naveen, K. and Veeraraghavan, B. (2019) 'Accurate identification and epidemiological characterization of Burkholderia cepacia complex: an update', *Annals of clinical microbiology and antimicrobials,* 18(1), pp. 7-7.

Dobritsa, A. P. and Samadpour, M. (2016) 'Transfer of eleven species of the genus Burkholderia to the genus Paraburkholderia and proposal of Caballeronia gen. nov. to accommodate twelve species of the genera Burkholderia and Paraburkholderia', *International Journal of Systematic and Evolutionary Microbiology,* 66(8), pp. 2836-2846.

Duangurai, T., Indrawattana, N. and Pumirat, P. (2018) 'Burkholderia pseudomallei Adaptation for Survival in Stressful Conditions', *Biomed Res Int,* 2018, pp. 3039106.

Edgar, R. J., Hampton, G. E., Garcia, G. P. C., Maher, M. J., Perugini, M. A., Ackerley, D. F. and Lamont, I. L. (2017) 'Integrated activities of two alternative sigma factors coordinate iron acquisition and uptake by Pseudomonas aeruginosa', *Mol Microbiol,* 106(6), pp. 891-904.

Elhassanny, A. E., Anderson, E. S., Menscher, E. A. and Roop, R. M., 2nd (2013) 'The ferrous iron transporter FtrABCD is required for the virulence of Brucella abortus 2308 in mice', *Mol Microbiol,* 88(6), pp. 1070-82.

Essex-Lopresti, A. E., Boddey, J. A., Thomas, R., Smith, M. P., Hartley, M. G., Atkins, T., Brown, N. F., Tsang, C. H., Peak, I. R., Hill, J., Beacham, I. R. and Titball, R. W. (2005) 'A type IV pilin, PilA, Contributes To Adherence of Burkholderia pseudomallei and virulence in vivo', *Infect Immun,* 73(2), pp. 1260-4.

Estrada-de Los Santos, P., Palmer, M., Chavez-Ramirez, B., Beukes, C., Steenkamp, E. T., Briscoe, L., Khan, N., Maluk, M., Lafos, M., Humm, E., Arrabit, M., Crook, M., Gross, E., Simon, M. F., Dos Reis Junior, F. B., Whitman, W. B., Shapiro, N., Poole, P. S., Hirsch, A. M., Venter, S. N. and James, E. K. (2018) 'Whole Genome Analyses Suggests that Burkholderia sensu lato Contains Two Additional Novel Genera (Mycetohabitans gen. nov., and Trinickia gen. nov.): Implications for the Evolution of Diazotrophy and Nodulation in the Burkholderiaceae', *Genes (Basel),* 9(8).

Estrada-de los Santos, P., Vinuesa, P., Martínez-Aguilar, L., Hirsch, A. M. and Caballero-Mellado, J. (2013) 'Phylogenetic Analysis of Burkholderia Species by Multilocus Sequence Analysis', *Current Microbiology,* 67(1), pp. 51-60.

Fazli, M., Harrison, J. J., Gambino, M., Givskov, M. and Tolker-Nielsen, T. (2015) 'In-Frame and unmarked gene deletions in Burkholderia cenocepacia via an allelic exchange system compatible with gateway technology', *Applied and Environmental Microbiology,* 81(11), pp. 3623-3630.

Fehlberg, L. C. C., Andrade, L. H. S., Assis, D. M., Pereira, R. H. V., Gales, A. C. and Marques, E. A. (2013) 'Performance of MALDI-ToF MS for species identification of Burkholderia cepacia complex clinical isolates', *Diagnostic Microbiology and Infectious Disease,* 77(2), pp. 126-128.

Feklistov, A. and Darst, S. A. (2011) 'Structural Basis for Promoter-10 Element Recognition by the Bacterial RNA Polymerase sigma Subunit', *Cell,* 147(6), pp. 1257-1269.

Fong, S. M., Wong, K. J., Fukushima, M. and Yeo, T. W. (2015) 'Thalassemia major is a major risk factor for pediatric melioidosis in Kota Kinabalu, Sabah, Malaysia', *Clin Infect Dis,* 60(12), pp. 1802-7.

Francez-Charlot, A., Kaczmarczyk, A., Fischer, H. M. and Vorholt, J. A. (2015) 'The general stress response in Alphaproteobacteria', *Trends in Microbiology,* 23(3), pp. 164-171.

Franke, J., Ishida, K. and Hertweck, C. (2014) 'Evolution of Siderophore Pathways in Human Pathogenic Bacteria', *Journal of the American Chemical Society,* 136(15), pp. 5599-5602.

Franke, J., Ishida, K. and Hertweck, C. (2015) 'Plasticity of the Malleobactin Pathway and Its Impact on Siderophore Action in Human Pathogenic Bacteria', *Chemistry-a European Journal,* 21(22), pp. 8010-8014.

Franke, J., Ishida, K., Ishida-Ito, M. and Hertweck, C. (2013) 'Nitro versus hydroxamate in siderophores of pathogenic bacteria: effect of missing hydroxylamine protection in malleobactin biosynthesis', *Angew Chem Int Ed Engl,* 52(32), pp. 8271-5.

French, C. T., Toesca, I. J., Wu, T.-H., Teslaa, T., Beaty, S. M., Wong, W., Liu, M. F., Schroeder, I., Chiou, P.-Y., Teitell, M. A. and Miller, J. F. (2011) 'Dissection of the Burkholderia intracellular life cycle using a photothermal nanoblade', *Proceedings of the National Academy of Sciences of the United States of America,* 108(29), pp. 12095-12100.

Gaballa, A., Guariglia-Oropeza, V., Durr, F., Butcher, B. G., Chen, A. Y., Chandrangsu, P. and Helmann, J. D. (2018) 'Modulation of extracytoplasmic function (ECF) sigma factor promoter selectivity by spacer region sequence', *Nucleic Acids Res,* 46(1), pp. 134-145.

Gardella, T., Moyle, H. and Susskind, M. M. (1989) 'A mutant Escherichia coli sigma-70 subunit of RNA polymerase with altered promoter specificity', *Journal of Molecular Biology,* 206(4), pp. 579-590.

Gasteiger, E., Hoogland, C., Gattiker, A., Duvaud, S., Wilkins, M. R., Appel, R. D. and Bairoch, A. (2005) 'Protein Identification and Analysis Tools on the ExPASy Server', in Walker, J.M. (ed.) *The Proteomics Protocols Handbook*: Humana Press, pp. 571-607.

Gee, J. E., Elrod, M. G., Gulvik, C. A., Haselow, D. T., Waters, C., Liu, L. and Hoffmaster, A. R. (2018) 'Burkholderia thailandensis Isolated from Infected Wound, Arkansas, USA', *Emerging infectious diseases,* 24(11), pp. 2091-2094.

Glass, M. B., Steigerwalt, A. G., Jordan, J. G., Wilkins, P. P. and Gee, J. E. (2006) 'Burkholderia oklahomensis sp. nov., a Burkholderia pseudomallei-like species formerly known as the Oklahoma strain of Pseudomonas pseudomallei', *Int J Syst Evol Microbiol,* 56(Pt 9), pp. 2171-6.

Gomez-Santos, N., Perez, J., Sanchez-Sutil, M. C., Moraleda-Munoz, A. and Munoz-Dorado, J. (2011) 'CorE from Myxococcus xanthus is a copper-dependent RNA polymerase sigma factor', *PLoS Genet,* 7(6), pp. e1002106.

González, L. J., Bahr, G., Nakashige, T. G., Nolan, E. M., Bonomo, R. A. and Vila, A. J. (2016) 'Membrane anchoring stabilizes and favors secretion of New Delhi metallo-β-lactamase', *Nature chemical biology,* 12(7), pp. 516-522.

Gotschlich, A., Huber, B., Geisenberger, O., Togl, A., Steidle, A., Riedel, K., Hill, P., Tummler, B., Vandamme, P., Middleton, B., Camara, M., Williams, P., Hardman, A. and Eberl, L. (2001) 'Synthesis of multiple N-acylhomoserine lactones is wide-spread among the members of the Burkholderia cepacia complex', *Systematic and Applied Microbiology,* 24(1), pp. 1-14.

Goutam, K., Gupta, A. K. and Gopal, B. (2017) 'The fused SnoaL_2 domain in the Mycobacterium tuberculosis sigma factor sigmaJ modulates promoter recognition', *Nucleic Acids Res,* 45(16), pp. 9760-9772.

Gruber, T. and Gross, C. (2003) 'Multiple sigma subunits and the partitioning of bacterial transcription space', *Annual Review of Microbiology,* 57, pp. 441-466.

Hall, T. A. (1999) 'BioEdit: a user-friendly biological sequence alignment editor and analysis program for Windows 95/98/NT', *Nucleic Acids Symposium,* 41, pp. 95-98.

Hanahan, D. (1983) 'Studies on transformation of Escherichia coli with plasmids', *Journal of Molecular Biology,* 166(4), pp. 557-580.

Hantke, K. (1987) 'Selection procedure for deregulated iron transport mutants (fur) in Escherichia coli K 12: fur not only affects iron metabolism', *Mol Gen Genet,* 210(1), pp. 135-9.

Hassan, A. A., Coutinho, C. P. and Sa-Correia, I. (2019) 'Burkholderia cepacia Complex Species Differ in the Frequency of Variation of the Lipopolysaccharide O-Antigen Expression During Cystic Fibrosis Chronic Respiratory Infection', *Front Cell Infect Microbiol,* 9, pp. 273.

Hauser, N. and Orsini, J. (2015) 'Cepacia Syndrome in a Non-Cystic Fibrosis Patient', *Case Rep Infect Dis,* 2015, pp. 537627.

Heinrich, J. and Wiegert, T. (2009) 'Regulated intramembrane proteolysis in the control of extracytoplasmic function sigma factors', *Research in Microbiology,* 160(9), pp. 696-703.

Heinrichs, D. E. and Poole, K. (1993) 'Cloning and sequence analysis of a gene (pchR) encoding an AraC family activator of pyochelin and ferripyochelin receptor synthesis in Pseudomonas aeruginosa', *J Bacteriol,* 175(18), pp. 5882-9.

Helmann, J. D. (2002) 'The extracytoplasmic function (ECF) sigma factors', *Advances in Microbial Physiology, Vol 46,* 46, pp. 47-110.

Henry, D., Campbell, M., McGimpsey, C., Clarke, A., Louden, L., Burns, J. L., Roe, M. H., Vandamme, P. and Speert, D. (1999) 'Comparison of isolation media for recovery of Burkholderia cepacia complex from respiratory secretions of patients with cystic fibrosis', *Journal of Clinical Microbiology,* 37(4), pp. 1004-1007.

Herrero, M., de Lorenzo, V. and Timmis, K. N. (1990) 'Transposon vectors containing non-antibiotic resistance selection markers for cloning and stable chromosomal insertion of foreign genes in gram-negative bacteria', *J Bacteriol,* 172(11), pp. 6557-67.

Hider, R. C. and Kong, X. (2010) 'Chemistry and biology of siderophores', *Natural Product Reports,* 27(5), pp. 637-657.

Ho, T. D. and Ellermeier, C. D. (2012) 'Extra cytoplasmic function sigma factor activation', *Curr Opin Microbiol,* 15(2), pp. 182-8.

Hoffmaster, A. R., AuCoin, D., Baccam, P., Baggett, H. C., Baird, R., Bhengsri, S., Blaney, D. D., Brett, P. J., Brooks, T. J., Brown, K. A., Chantratita, N., Cheng, A. C., Dance, D. A., Decuypere, S., Defenbaugh, D., Gee, J. E., Houghton, R., Jorakate, P., Lertmemongkolchai, G., Limmathurotsakul, D., Merlin, T. L., Mukhopadhyay, C., Norton, R., Peacock, S. J., Rolim, D. B., Simpson, A. J., Steinmetz, I., Stoddard, R. A., Stokes, M. M., Sue, D., Tuanyok, A., Whistler, T., Wuthiekanun, V. and Walke, H. T. (2015) 'Melioidosis diagnostic workshop, 2013', *Emerg Infect Dis,* 21(2).

Holden, M. T., Titball, R. W., Peacock, S. J., Cerdeno-Tarraga, A. M., Atkins, T., Crossman, L. C., Pitt, T., Churcher, C., Mungall, K., Bentley, S. D., Sebaihia, M., Thomson, N. R., Bason, N., Beacham, I. R., Brooks, K., Brown, K. A., Brown, N. F., Challis, G. L., Cherevach, I., Chillingworth, T., Cronin, A., Crossett, B., Davis, P., DeShazer, D., Feltwell, T., Fraser, A., Hance, Z., Hauser, H., Holroyd, S., Jagels, K., Keith, K. E., Maddison, M., Moule, S., Price, C., Quail, M. A., Rabbinowitsch, E., Rutherford, K., Sanders, M., Simmonds, M., Songsivilai, S., Stevens, K., Tumapa, S., Vesaratchavest, M., Whitehead, S., Yeats, C., Barrell, B. G., Oyston, P. C. and Parkhill, J. (2004) 'Genomic plasticity of the causative agent of melioidosis, Burkholderia pseudomallei', *Proc Natl Acad Sci U S A,* 101(39), pp. 14240-5.

Hong, H. J., Paget, M. S. B. and Buttner, M. J. (2002) 'A signal transduction system in Streptomyces coelicolor that activates the expression of a putative cell wall glycan operon in response to vancomycin and other cell wall-specific antibiotics', *Molecular Microbiology,* 44(5), pp. 1199-1211.

Howard, K. and Inglis, T. J. (2003) 'The effect of free chlorine on Burkholderia pseudomallei in potable water', *Water Res,* 37(18), pp. 4425-32.

Husnain, S. I. and Thomas, M. S. (2008) 'Downregulation of the Escherichia coli guaB promoter by FIS', *Microbiology,* 154(Pt 6), pp. 1729-1738.

Ibrahim, M., Tang, Q., Shi, Y., Almoneafy, A., Fang, Y., Xu, L., Li, W., Li, B. and Xie, G.-L. (2012) 'Diversity of potential pathogenicity and biofilm formation among Burkholderia cepacia complex water, clinical, and agricultural isolates in China', *World Journal of Microbiology and Biotechnology,* 28(5), pp. 2113-2123.

Imlay, J. A., Chin, S. M. and Linn, S. (1988) 'Toxic DNA damage by hydrogen peroxide through the Fenton reaction in vivo and in vitro', *Science,* 240(4852), pp. 640-2.

Ishihama, A. (1969) 'Subunits of E coli RNA polymerase in function and structure', *Journal of Cellular Physiology,* 74(2P2S), pp. 223-&.

Isles, A., Maclusky, I., Corey, M., Gold, R., Prober, C., Fleming, P. and Levison, H. (1984) 'Pseudomonas cepacia infection in cystic fibrosis: An emerging problem', *The Journal of Pediatrics,* 104(2), pp. 206-210.

Jenjaroen, K., Chumseng, S., Sumonwiriya, M., Ariyaprasert, P., Chantratita, N., Sunyakumthorn, P., Hongsuwan, M., Wuthiekanun, V., Fletcher, H. A., Teparrukkul, P., Limmathurotsakul, D., Day, N. P. and Dunachie, S. J. (2015) 'T-Cell Responses Are Associated with Survival in Acute Melioidosis Patients', *PLoS Negl Trop Dis,* 9(10), pp. e0004152.

Jogler, C., Waldmann, J., Huang, X. L., Jogler, M., Glockner, F. O., Mascher, T. and Kolter, R. (2012) 'Identification of Proteins Likely To Be Involved in Morphogenesis, Cell Division, and Signal Transduction in Planctomycetes by Comparative Genomics', *Journal of Bacteriology,* 194(23), pp. 6419-6430.

Juang, Y. and Helmann, J. (1994) 'A promoter melting region in the primary sigma-factor of Bacillus subtilis - Identification of functionally important aromatic amino acids', *Journal of Molecular Biology,* 235(5), pp. 1470-1488.

Kaestli, M., Schmid, M., Mayo, M., Rothballer, M., Harrington, G., Richardson, L., Hill, A., Hill, J., Tuanyok, A., Keim, P., Hartmann, A. and Currie, B. J. (2012) 'Out of the ground: aerial and exotic habitats of the melioidosis bacterium Burkholderia pseudomallei in grasses in Australia', *Environ Microbiol,* 14(8), pp. 2058-70.

Kalish, L. A., Waltz, D. A., Dovey, M., Potter-Bynoe, G., McAdam, A. J., LiPuma, J. J., Gerard, C. and Goldmann, D. (2006) 'Impact of Burkholderia dolosa on lung function and survival in cystic fibrosis', *American Journal of Respiratory and Critical Care Medicine,* 173(4), pp. 421-425.

Karimova, G., Ullmann, A. and Ladant, D. (2001) 'Protein-protein interaction between Bacillus stearothermophilus tyrosyl-tRNA synthetase subdomains revealed by a bacterial two-hybrid system', *J Mol Microbiol Biotechnol,* 3(1), pp. 73-82.

Kelley, L. A., Mezulis, S., Yates, C. M., Wass, M. N. and Sternberg, M. J. E. (2015) 'The Phyre2 web portal for protein modeling, prediction and analysis', *Nature Protocols,* 10, pp. 845.

Khakhum, N., Bharaj, P., Myers, J. N., Tapia, D., Walker, D. H., Endsley, J. J. and Torres, A. G. (2019) 'Evaluation of Burkholderia mallei DeltatonB Deltahcp1 (CLH001) as a live attenuated vaccine in murine models of glanders and melioidosis', *PLoS Negl Trop Dis,* 13(7), pp. e0007578.

Khan, S. R., Gaines, J., Roop, R. M., II and Farrand, S. K. (2008) 'Broad-host-range expression vectors with tightly regulated promoters and their use to examine the influence of TraR and TraM expression on Ti plasmid quorum sensing', *Applied and Environmental Microbiology,* 74(16), pp. 5053-5062.

Klaus, J. R., Deay, J., Neuenswander, B., Hursh, W., Gao, Z., Bouddhara, T., Williams, T. D., Douglas, J., Monize, K., Martins, P., Majerczyk, C., Seyedsayamdost, M. R., Peterson, B. R., Rivera, M. and Chandler, J. R. (2018) 'Malleilactone Is a Burkholderia pseudomallei Virulence Factor Regulated by Antibiotics and Quorum Sensing', *J Bacteriol,* 200(14).

Klumpp, C., Burger, A., Mislin, G. L. and Abdallah, M. A. (2005) 'From a total synthesis of cepabactin and its 3:1 ferric complex to the isolation of a 1:1:1 mixed complex between iron (III), cepabactin and pyochelin', *Bioorganic & Medicinal Chemistry Letters,* 15(6), pp. 1721-1724.

Kohler, C., Dunachie, S. J., Muller, E., Kohler, A., Jenjaroen, K., Teparrukkul, P., Baier, V., Ehricht, R. and Steinmetz, I. (2016) 'Rapid and Sensitive Multiplex Detection of Burkholderia pseudomallei-Specific Antibodies in Melioidosis Patients Based on a Protein Microarray Approach', *PLoS Negl Trop Dis,* 10(7), pp. e0004847.

Kovach, M. E., Elzer, P. H., Hill, D. S., Robertson, G. T., Farris, M. A., Roop, R. M. and Peterson, K. M. (1995) 'Four new derivatives of the broad-host range cloning vector pBBR1MCS, carrying different antibiotic-resistance cassettes', *Gene,* 166(1), pp. 175-176.

Kovach, M. E., Phillips, R. W., Elzer, P. H., Roop, R. M., 2nd and Peterson, K. M. (1994) 'pBBR1MCS: a broad-host-range cloning vector', *Biotechniques,* 16(5), pp. 800-2.

Kovacs-Simon, A., Hemsley, C. M., Scott, A. E., Prior, J. L. and Titball, R. W. (2019) 'Burkholderia thailandensis strain E555 is a surrogate for the investigation of Burkholderia pseudomallei replication and survival in macrophages', *BMC Microbiol,* 19(1), pp. 97.

Kumar, A., Chua, K. L. and Schweizer, H. P. (2006) 'Method for regulated expression of single-copy efflux pump genes in a surrogate Pseudomonas aeruginosa strain: identification of the BpeEF-OprC chloramphenicol and trimethoprim efflux pump of Burkholderia pseudomallei 1026b', *Antimicrob Agents Chemother,* 50(10), pp. 3460-3.

Kumar, M., Gupta, A., Sahoo, R. K., Jena, J., Debata, N. K. and Subudhi, E. (2016) 'Functional Genome Screening to Elucidate the Colistin Resistance Mechanism', *Scientific Reports,* 6, pp. 23156.

Kvitko, B. H., Goodyear, A., Propst, K. L., Dow, S. W. and Schweizer, H. P. (2012) 'Burkholderia pseudomallei Known Siderophores and Hemin Uptake Are Dispensable for Lethal Murine Melioidosis', *Plos Neglected Tropical Diseases,* 6(6).

Lafontaine, E. R., Balder, R., Michel, F. and Hogan, R. J. (2014) 'Characterization of an autotransporter adhesin protein shared by Burkholderia mallei and Burkholderia pseudomallei', *BMC microbiology,* 14, pp. 92-92.

Lan, L. F., Deng, X., Zhou, J. M. and Tang, X. Y. (2006) 'Genome-wide gene expression analysis of Pseudomonas syringae pv. tomato DC3000 reveals overlapping and distinct pathways regulated by hrpL and hrpRS', *Molecular Plant-Microbe Interactions,* 19(9), pp. 976-987.

Lee, J. W. and Helmann, J. D. (2007) 'Functional specialization within the Fur family of metalloregulators', *Biometals,* 20(3-4), pp. 485-99.

Lee, J. W., Kim, Y. E. and Park, S. J. (2018) 'Burkholderia alba sp. nov., isolated from a soil sample on Halla mountain in Jeju island', *J Microbiol,* 56(5), pp. 312-316.

Lessie, T. G., Hendrickson, W., Manning, B. D. and Devereux, R. (1996) 'Genomic complexity and plasticity of Burkholderia cepacia', *FEMS Microbiology Letters,* 144(2-3), pp. 117-128.

Li, W., Bottrill, A. R., Bibb, M. J., Buttner, M. J., Paget, M. S. B. and Kleanthous, C. (2003) 'The role of zinc in the disulphide stress-regulated anti-sigma factor RsrA from Streptomyces coelicolor', *Journal of Molecular Biology,* 333(2), pp. 461-472.

Limmathurotsakul, D., Golding, N., Dance, D. A., Messina, J. P., Pigott, D. M., Moyes, C. L., Rolim, D. B., Bertherat, E., Day, N. P., Peacock, S. J. and Hay, S. I. (2016a) 'Predicted global distribution of Burkholderia pseudomallei and burden of melioidosis', *Nature microbiology,* 1(1), pp. 15008.

Limmathurotsakul, D., Golding, N., Dance, D. A. B., Messina, J. P., Pigott, D. M., Moyes, C. L., Rolim, D. B., Bertherat, E., Day, N. P. J., Peacock, S. J. and Hay, S. I. (2016b) 'Predicted global distribution of Burkholderia pseudomallei and burden of melioidosis', *Nature Microbiology,* 1, pp. 15008.

Limmathurotsakul, D., Jamsen, K., Arayawichanont, A., Simpson, J. A., White, L. J., Lee, S. J., Wuthiekanun, V., Chantratita, N., Cheng, A. C., Day, N. P. J., Verzilli, C. and Peacock, S. J. (2010a) 'Defining the true sensitivity of culture for the diagnosis of melioidosis using Bayesian latent class models', *PloS one,* 5(8), pp. e12485-e12485.

Limmathurotsakul, D., Kanoksil, M., Wuthiekanun, V., Kitphati, R., deStavola, B., Day, N. P. J. and Peacock, S. J. (2013) 'Activities of daily living associated with acquisition of melioidosis in northeast Thailand: a matched case-control study', *PLoS neglected tropical diseases,* 7(2), pp. e2072-e2072.

Limmathurotsakul, D., Wongratanacheewin, S., Teerawattanasook, N., Wongsuvan, G., Chaisuksant, S., Chetchotisakd, P., Chaowagul, W., Day, N. P. and Peacock, S. J. (2010b) 'Increasing incidence of human melioidosis in Northeast Thailand', *Am J Trop Med Hyg,* 82(6), pp. 1113-7.

Liu, P. V. and Shokrani, F. (1978) 'Biological activities of pyochelins: iron-chelating agents of Pseudomonas aeruginosa', *Infect Immun,* 22(3), pp. 878-90.

Liu, Q., Pinto, D. and Mascher, T. (2018) 'Characterization of the Widely Distributed Novel ECF42 Group of Extracytoplasmic Function σ Factors in Streptomyces venezuelae

', *Journal of Bacteriology,* 200(21), pp. e00437-18.

Llamas, M. A., Imperi, F., Visca, P. and Lamont, I. L. (2014) 'Cell-surface signaling in Pseudomonas: stress responses, iron transport, and pathogenicity', *Fems Microbiology Reviews,* 38(4), pp. 569-597.

Lopes-Santos, L., Castro, D. B. A., Ferreira-Tonin, M., Correa, D. B. A., Weir, B. S., Park, D., Ottoboni, L. M. M., Neto, J. R. and Destefano, S. A. L. (2017) 'Reassessment of the taxonomic position of Burkholderia andropogonis and description of Robbsia andropogonis gen. nov., comb. nov', *Antonie Van Leeuwenhoek,* 110(6), pp. 727-736.

Loprasert, S., Sallabhan, R., Whangsuk, W. and Mongkolsuk, S. (2003a) 'Compensatory increase in ahpC gene expression and its role in protecting Burkholderia pseudomallei against reactive nitrogen intermediates', *Arch Microbiol,* 180(6), pp. 498-502.

Loprasert, S., Whangsuk, W., Sallabhan, R. and Mongkolsuk, S. (2003b) 'Regulation of the katG-dpsA operon and the importance of KatG in survival of Burkholderia pseudomallei exposed to oxidative stress', *FEBS Lett,* 542(1-3), pp. 17-21.

Loprasert, S., Whangsuk, W., Sallabhan, R. and Mongkolsuk, S. (2004) 'DpsA protects the human pathogen Burkholderia pseudomallei against organic hydroperoxide', *Arch Microbiol,* 182(1), pp. 96-101.

Maeda, H., Fujita, N. and Ishihama, A. (2000) 'Competition among seven Escherichia coli sigma subunits: relative binding affinities to the core RNA polymerase', *Nucleic Acids Res,* 28(18), pp. 3497-503.

Mahenthiralingam, E., Campbell, M., Speert, D. P., Govan, J. R. W., Lipuma, J. J., Stull, T. L., Steinbach, S. F. and Goldstein, R. (1995) 'Burkholderia cepacia in Cystic Fibrosis', *New England Journal of Medicine,* 332(12), pp. 819-821.

Mahenthiralingam, E., Urban, T. A. and Goldberg, J. B. (2005) 'The multifarious, multireplicon Burkholderia cepacia complex', *Nature Reviews Microbiology,* 3(2), pp. 144-156.

Mahren, S. and Braun, V. (2003) 'The FecI Extracytoplasmic-Function Sigma Factor of Escherichia coli Interacts with the β′ Subunit of RNA Polymerase', *Journal of Bacteriology,* 185(6), pp. 1796-1802.

Maillard, A. P., Girard, E., Ziani, W., Petit-Härtlein, I., Kahn, R. and Covès, J. (2014) 'The crystal structure of the anti-σ factor CnrY in complex with the σ factor CnrH shows a new structural class of anti-σ factors targeting extracytoplasmic function σ factors', *J Mol Biol,* 426(12), pp. 2313-27.

Maniam, P., Nurul Aiezzah, Z., Mohamed, R., Embi, N. and Hasidah, M. S. (2015) 'Regulatory role of GSK3beta in the activation of NF-kappaB and modulation of cytokine levels in Burkholderia pseudomallei-infected PBMC isolated from streptozotocin-induced diabetic animals', *Trop Biomed,* 32(1), pp. 36-48.

Mannaa, M., Park, I. and Seo, Y.-S. (2018) 'Genomic Features and Insights into the Taxonomy, Virulence, and Benevolence of Plant-Associated Burkholderia Species', *International Journal of Molecular Sciences,* 20(1), pp. 121.

Marcos-Torres, F. J., Pérez, J., Gómez-Santos, N., Moraleda-Muñoz, A. and Muñoz-Dorado, J. (2016) 'In depth analysis of the mechanism of action of metal-dependent sigma factors: characterization of CorE2 from Myxococcus xanthus', *Nucleic Acids Research*.

Marr, M. and Roberts, J. (1997) 'Promoter recognition as measured by binding of polymerase to nontemplate strand oligonucleotide', *Science,* 276(5316), pp. 1258-1260.

Mascher, T. (2013) 'Signaling diversity and evolution of extracytoplasmic function (ECF) sigma factors', *Curr Opin Microbiol,* 16(2), pp. 148-55.

Mathew, A., Eberl, L. and Carlier, A. L. (2014) 'A novel siderophore-independent strategy of iron uptake in the genus Burkholderia', *Mol Microbiol,* 91(4), pp. 805-20.

Mathew, A., Jenul, C., Carlier, A. L. and Eberl, L. (2016) 'The role of siderophores in metal homeostasis of members of the genus Burkholderia', *Environ Microbiol Rep,* 8(1), pp. 103-9.

Matsumoto, T., Nakanishi, K., Asai, K. and Sadaie, Y. (2005) 'Transcriptional analysis of the ylaABCD operon of Bacillus subtilis encoding a sigma factor of extracytoplasmic function family', *Genes & Genetic Systems,* 80(6), pp. 385-393.

McLeod, C., Morris, P. S., Bauert, P. A., Kilburn, C. J., Ward, L. M., Baird, R. W. and Currie, B. J. (2015) 'Clinical presentation and medical management of melioidosis in children: a 24-

year prospective study in the Northern Territory of Australia and review of the literature', *Clin Infect Dis,* 60(1), pp. 21-6.

McLoughlin, T. J., Quinn, J. P., Bettermann, A. and Bookland, R. (1992) 'Pseudomonas cepacia suppression of sunflower wilt fungus and role of antifungal compounds in controlling the disease', *Applied and Environmental Microbiology,* 58(5), pp. 1760-1763.

McNicholas, S., Potterton, E., Wilson, K. S. and Noble, M. E. M. (2011) 'Presenting your structures: the CCP4mg molecular-graphics software', *Acta Crystallographica Section D,* 67(4), pp. 386-394.

McRobb, E., Kaestli, M., Mayo, M., Price, E. P., Sarovich, D. S., Godoy, D., Spratt, B. G. and Currie, B. J. (2013) 'Melioidosis from contaminated bore water and successful UV sterilization', *Am J Trop Med Hyg,* 89(2), pp. 367-8.

Mettrick, K. A. and Lamont, I. L. (2009) 'Different roles for anti-sigma factors in siderophore signalling pathways of Pseudomonas aeruginosa', *Molecular Microbiology,* 74(5), pp. 1257-1271.

Meyer, J. M., Van, V. T., Stintzi, A., Berge, O. and Winkelmann, G. (1995) 'Ornibactin production and transport properties in strains of Burkholderia vietnamiensis and Burkholderia cepacia (formerly Pseudomonas cepacia)', *Biometals,* 8(4), pp. 309-17.

Michel, L., Bachelard, A. and Reimmann, C. (2007) 'Ferripyochelin uptake genes are involved in pyochelin-mediated signalling in Pseudomonas aeruginosa', *Microbiology,* 153(5), pp. 1508-1518.

Miller, J. H. (1972) *Experiments in Molecular Genetics.* Cold Spring Harbor, NY: Cold Spring Harbor Laboratory Press.

Miller, R. R., Hird, T. J., Tang, P. and Zlosnik, J. E. A. (2015) 'Whole-Genome Sequencing of Three Clonal Clinical Isolates of B. cenocepacia from a Patient with Cystic Fibrosis', *PLOS ONE,* 10(11), pp. e0143472.

Mills, S. A. and Marletta, M. A. (2005) 'Metal binding characteristics and role of iron oxidation in the ferric uptake regulator from Escherichia coli', *Biochemistry,* 44(41), pp. 13553-9.

Mima, T. and Schweizer, H. P. (2010) 'The BpeAB-OprB efflux pump of Burkholderia pseudomallei 1026b does not play a role in quorum sensing, virulence factor production, or extrusion of aminoglycosides but is a broad-spectrum drug efflux system', *Antimicrob Agents Chemother,* 54(8), pp. 3113-20.

Mohd Ali, M. R., Lih Huey, L., Foo, P. C., Goay, Y. X., Ismail, A. S., Mustaffa, K. M. F., Aziah, I., Kia Kien, P., Harun, A., Ismail, N. and Yean Yean, C. (2019) 'Duplex TaqMan Hydrolysis Probe-Based Molecular Assay for Simultaneous Detection and Differentiation of Burkholderia pseudomallei and Leptospira spp. DNA', *Biomed Res Int,* 2019, pp. 9451791.

Moore, R. A. and Hancock, R. E. (1986) 'Involvement of outer membrane of Pseudomonas cepacia in aminoglycoside and polymyxin resistance', *Antimicrobial Agents and Chemotherapy,* 30(6), pp. 923.

Moore, R. A., Reckseidler-Zenteno, S., Kim, H., Nierman, W., Yu, Y., Tuanyok, A., Warawa, J., DeShazer, D. and Woods, D. E. (2004) 'Contribution of gene loss to the pathogenic evolution of Burkholderia pseudomallei and Burkholderia mallei', *Infect Immun,* 72(7), pp. 4172-87.

Moraleda-Munoz, A., Marcos-Torres, F. J., Perez, J. and Munoz-Dorado, J. (2019) 'Metal-responsive RNA polymerase extracytoplasmic function (ECF) sigma factors', *Mol Microbiol,* 112(2), pp. 385-398.

Morici, L., Torres, A. G. and Titball, R. W. (2019) 'Novel multi-component vaccine approaches for Burkholderia pseudomallei', *Clin Exp Immunol,* 196(2), pp. 178-188.

Murakami, K. S. (2013) 'X-ray crystal structure of Escherichia coli RNA polymerase sigma70 holoenzyme', *J Biol Chem,* 288(13), pp. 9126-34.

Murakami, K. S., Masuda, S., Campbell, E. A., Muzzin, O. and Darst, S. A. (2002) 'Structural basis of transcription initiation: An RNA polymerase holoenzyme-DNA complex', *Science,* 296(5571), pp. 1285-1290.

Murakami, K. S., Masuda, S. and Darst, S. A. (2002) 'Structural basis of transcription initiation: RNA polymerase holoenzyme at 4 angstrom resolution', *Science,* 296(5571), pp. 1280-1284.

Muruato, L. A. and Torres, A. G. (2016) 'Melioidosis: where do we stand in the development of an effective vaccine?', *Future Microbiol,* 11(4), pp. 477-80.

Narayanaswamy, V. P., Giatpaiboon, S., Baker, S. M., Wiesmann, W. P., LiPuma, J. J. and Townsend, S. M. (2017) 'Novel glycopolymer sensitizes Burkholderia cepacia complex isolates from cystic fibrosis patients to tobramycin and meropenem', *PLOS ONE,* 12(6), pp. e0179776.

Nguyen, L. H., Jensen, D. B. and Burgess, R. R. (1993) 'Overproduction and purification of sigma-32, the Escherichia coli heat-shock transcription factor', *Protein Expression and Purification,* 4(5), pp. 425-433.

Nierman, W. C., DeShazer, D., Kim, H. S., Tettelin, H., Nelson, K. E., Feldblyum, T., Ulrich, R. L., Ronning, C. M., Brinkac, L. M., Daugherty, S. C., Davidsen, T. D., Deboy, R. T., Dimitrov, G., Dodson, R. J., Durkin, A. S., Gwinn, M. L., Haft, D. H., Khouri, H., Kolonay, J. F., Madupu, R., Mohammoud, Y., Nelson, W. C., Radune, D., Romero, C. M., Sarria, S., Selengut, J., Shamblin, C., Sullivan, S. A., White, O., Yu, Y., Zafar, N., Zhou, L. W. and Fraser, C. M. (2004) 'Structural flexibility in the Burkholderia mallei genome', *Proceedings of the National Academy of Sciences of the United States of America,* 101(39), pp. 14246-14251.

Norris, M. H., Schweizer, H. P. and Tuanyok, A. (2017) 'Structural diversity of Burkholderia pseudomallei lipopolysaccharides affects innate immune signaling', *PLoS Negl Trop Dis,* 11(4), pp. e0005571.

Ochsner, U. A., Vasil, A. I. and Vasil, M. L. (1995) 'Role of the ferric uptake regulator of Pseudomonas aeruginosa in the regulation of siderophores and exotoxin A expression: purification and activity on iron-regulated promoters', *J Bacteriol,* 177(24), pp. 7194-201.

Ong, K. S., Aw, Y. K., Lee, L. H., Yule, C. M., Cheow, Y. L. and Lee, S. M. (2016) 'Burkholderia paludis sp. nov., an Antibiotic-Siderophore Producing Novel Burkholderia cepacia Complex Species, Isolated from Malaysian Tropical Peat Swamp Soil', *Frontiers in microbiology,* 7, pp. 2046-2046.

Osman, D. and Cavet, J. S. (2010) 'Bacterial metal-sensing proteins exemplified by ArsR-SmtB family repressors', *Nat Prod Rep,* 27(5), pp. 668-80.

Outten, C. E. and O'Halloran, T. V. (2001) 'Femtomolar sensitivity of metalloregulatory proteins controlling zinc homeostasis', *Science,* 292(5526), pp. 2488-92.

Paget, M. S. B. (2015) 'Bacterial Sigma Factors and Anti-Sigma Factors: Structure, Function and Distribution', *Biomolecules,* 5(3), pp. 1245-65.

Paget, M. S. B., Bae, J. B., Hahn, M. Y., Li, W., Kleanthous, C., Roe, J. H. and Buttner, M. J. (2001) 'Mutational analysis of RsrA, a zinc-binding anti-sigma factor with a thiol-disulphide redox switch', *Molecular Microbiology,* 39(4), pp. 1036-1047.

Papp-Wallace, K. M., Becka, S. A., Zeiser, E. T., Ohuchi, N., Mojica, M. F., Gatta, J. A., Falleni, M., Tosi, D., Borghi, E., Winkler, M. L., Wilson, B. M., LiPuma, J. J., Nukaga, M. and Bonomo, R. A. (2017) 'Overcoming an Extremely Drug Resistant (XDR) Pathogen: Avibactam Restores Susceptibility to Ceftazidime for Burkholderia cepacia Complex Isolates from Cystic Fibrosis Patients', *ACS Infectious Diseases,* 3(7), pp. 502-511.

Parke, J. L. and Gurian-Sherman, D. (2001) 'DIVERSITY OF THE BURKHOLDERIA CEPACIA COMPLEX AND IMPLICATIONS FOR RISK ASSESSMENT OF BIOLOGICAL CONTROL STRAINS', *Annual Review of Phytopathology,* 39(1), pp. 225-258.

Pasqua, M., Visaggio, D., Lo Sciuto, A., Genah, S., Banin, E., Visca, P. and Imperi, F. (2017) 'Ferric Uptake Regulator Fur Is Conditionally Essential in Pseudomonas aeruginosa', *J Bacteriol,* 199(22).

Payne, G. W., Vandamme, P., Morgan, S. H., LiPuma, J. J., Coenye, T., Weightman, A. J., Jones, T. H. and Mahenthiralingam, E. (2005) 'Development of a recA Gene-Based Identification Approach for the Entire Burkholderia Genus', *Applied and Environmental Microbiology,* 71(7), pp. 3917.

Perard, J., Coves, J., Castellan, M., Solard, C., Savard, M., Miras, R., Galop, S., Signor, L., Crouzy, S., Michaud-Soret, I. and de Rosny, E. (2016) 'Quaternary Structure of Fur Proteins, a New Subfamily of Tetrameric Proteins', *Biochemistry,* 55(10), pp. 1503-15.

Pinto, D. and Mascher, T. (2016) 'The ECF Classification: A Phylogenetic Reflection of the Regulatory Diversity in the Extracytoplasmic Function σ Factor Protein Family', in J, d.B.F. (ed.) *Stress and Environmental Regulation of Gene Expression and Adaptation in Bacteria*.

Podnecky, N. L., Rhodes, K. A. and Schweizer, H. P. (2015) 'E ffl ux pump-mediated drug resistance in Burkholderia', *Front Microbiol,* 6, pp. 305.

Podnecky, N. L., Wuthiekanun, V., Peacock, S. J. and Schweizer, H. P. (2013) 'The BpeEF-OprC efflux pump is responsible for widespread trimethoprim resistance in clinical and environmental Burkholderia pseudomallei isolates', *Antimicrob Agents Chemother,* 57(9), pp. 4381-6.

Pohl, E., Haller, J. C., Mijovilovich, A., Meyer-Klaucke, W., Garman, E. and Vasil, M. L. (2003) 'Architecture of a protein central to iron homeostasis: crystal structure and spectroscopic analysis of the ferric uptake regulator', *Mol Microbiol,* 47(4), pp. 903-15.

Randall, L. B., Dobos, K., Papp-Wallace, K. M., Bonomo, R. A. and Schweizer, H. P. (2015) 'Membrane-Bound PenA beta-Lactamase of Burkholderia pseudomallei', *Antimicrob Agents Chemother,* 60(3), pp. 1509-14.

Ratledge, C. and Dover, L. G. (2000) 'Iron Metabolism in Pathogenic Bacteria', *Annual Review of Microbiology,* 54(1), pp. 881-941.

Regan, K. H. and Bhatt, J. (2019) 'Eradication therapy for Burkholderia cepacia complex in people with cystic fibrosis', *Cochrane Database of Systematic Reviews,* (4).

Reimmann, C., Patel, H. M., Serino, L., Barone, M., Walsh, C. T. and Haas, D. (2001) 'Essential PchG-dependent reduction in pyochelin biosynthesis of Pseudomonas aeruginosa', *J Bacteriol,* 183(3), pp. 813-20.

Rhodes, K. A. and Schweizer, H. P. (2016) 'Antibiotic resistance in Burkholderia species', *Drug Resist Updat,* 28, pp. 82-90.

Rodriguez, J. Y., Alvarez-Moreno, C. A., Cortes, J. A., Rodriguez, G. J., Esquea, K., Pinzon, H., Mendoza, M. J. and Acosta, Y. (2019) 'Melioidosis in Colombia, description of a clinical case and epidemiological considerations', *Biomedica,* 39, pp. 10-18.

Ronnebaum, T. A. and Lamb, A. L. (2018) 'Nonribosomal peptides for iron acquisition: pyochelin biosynthesis as a case study', *Current Opinion in Structural Biology,* 53, pp. 1-11.

Ronnebaum, T. A., McFarlane, J. S., Prisinzano, T. E., Booker, S. J. and Lamb, A. L. (2019) 'Stuffed Methyltransferase Catalyzes the Penultimate Step of Pyochelin Biosynthesis', *Biochemistry,* 58(6), pp. 665-678.

Ross, W., Thompson, J. F., Newlands, J. T. and Gourse, R. L. (1990) 'Escherichia coli Fis protein activates ribosomal-RNA trnascription in vitro and in vivo', *Embo Journal,* 9(11), pp. 3733-3742.

Sachdeva, V., Pathengay, A., Joseph, J., Sharma, S. and Das, T. (2011) 'Burkholderia cepacia endophthalmitis: clinico-microbiologic profile and outcomes', *Retina,* 31(9), pp. 1801-5.

Saiman, L., Siegel, J. D., LiPuma, J. J., Brown, R. F., Bryson, E. A., Chambers, M. J., Downer, V. S., Fliege, J., Hazle, L. A., Jain, M., Marshall, B. C., O'Malley, C., Pattee, S. R., Potter-Bynoe,

G., Reid, S., Robinson, K. A., Sabadosa, K. A., Schmidt, H. J., Tullis, E., Webber, J. and Weber, D. J. (2014) 'Kadinfection prevention and control guideline for cystic fibrosis: 2013 update', *Infection Control and Hospital Epidemiology,* 35(SUPPL.1), pp. S1-S67.

Salsgiver, E. L., Fink, A. K., Knapp, E. A., LiPuma, J. J., Olivier, K. N., Marshall, B. C. and Saiman, L. (2016) 'Changing Epidemiology of the Respiratory Bacteriology of Patients With Cystic Fibrosis', *Chest,* 149(2), pp. 390-400.

Sawana, A., Adeolu, M. and Gupta, R. S. (2014) 'Molecular signatures and phylogenomic analysis of the genus Burkholderia: proposal for division of this genus into the emended genus Burkholderia containing pathogenic organisms and a new genus Paraburkholderia gen. nov. harboring environmental species', *Front Genet,* 5, pp. 429.

Schaffer, S., Hantke, K. and Braun, V. (1985) 'Nucleotide sequence of the iron regulatory gene fur', *Mol Gen Genet,* 200(1), pp. 110-3.

Schmidt, I. H. E., Gildhorn, C., Boning, M. A. L., Kulow, V. A., Steinmetz, I. and Bast, A. (2018) 'Burkholderia pseudomallei modulates host iron homeostasis to facilitate iron availability and intracellular survival', *PLoS Negl Trop Dis,* 12(1), pp. e0006096.

Schumacher, M. A., Bush, M. J., Bibb, M. J., Ramos-Leon, F., Chandra, G., Zeng, W. and Buttner, M. J. (2018) 'The crystal structure of the RsbN-sigmaBldN complex from Streptomyces venezuelae defines a new structural class of anti-sigma factor', *Nucleic Acids Res,* 46(14), pp. 7405-7417.

Schwartz, E., Shekhtman, A., Dutta, K., Pratt, M., Cowburn, D., Darst, S. and Muir, T. (2008) 'A Full-Length Group 1 Bacterial Sigma Factor Adopts a Compact Structure Incompatible with DNA Binding', *Chemistry & Biology,* 15(10), pp. 1091-1103.

Schywyn, B. and Neilands, J. B. (1987) 'Universal chemical assay for the detection and determination of siderophores', *Analytical Biochemistry,* 160, pp. 47-56.

Sfeir, M. M. (2018) 'Burkholderia cepacia complex infections: More complex than the bacterium name suggest', *Journal of Infection,* 77(3), pp. 166-170.

Shalom, G., Shaw, J. G. and Thomas, M. S. (2007) 'In vivo expression technology identifies a type VI secretion system locus in Burkholderia pseudomallei that is induced upon invasion of macrophages', *Microbiology,* 153(Pt 8), pp. 2689-99.

Shastri, S., Spiewak, H. L., Sofoluwe, A., Eidsvaag, V. A., Asghar, A. H., Pereira, T., Bull, E. H., Butt, A. T. and Thomas, M. S. (2017) 'An efficient system for the generation of marked genetic mutants in members of the genus Burkholderia', *Plasmid,* 89, pp. 49-56.

Siegele, D. A., Hu, J. C., Walter, W. A. and Gross, C. A. (1989) 'Altered promoter recognition by mutant forms of the sigma-70 subunit of Escherichia coli RNA polymerase', *Journal of Molecular Biology,* 206(4), pp. 591-603.

Simon, R., Priefer, U. and Puhler, A. (1983) 'A broad host range mobilization system for in vivo genetic-engineering - Transposon mutagenesis in Gram-negative bacteria', *Bio-Technology,* 1(9), pp. 784-791.

Smith, M. D., Angus, B. J., Wuthiekanun, V. and White, N. J. (1997) 'Arabinose assimilation defines a nonvirulent biotype of Burkholderia pseudomallei', *Infect Immun,* 65(10), pp. 4319-21.

Sommerstein, R., Führer, U., Lo Priore, E., Casanova, C., Meinel, D. M., Seth-Smith, H. M., Kronenberg, A., On Behalf Of, A., Koch, D., Senn, L., Widmer, A. F., Egli, A., Marschall, J. and On Behalf Of, S. (2017) 'Burkholderia stabilis outbreak associated with contaminated commercially-available washing gloves, Switzerland, May 2015 to August 2016', *Euro surveillance : bulletin Europeen sur les maladies transmissibles = European communicable disease bulletin,* 22(49), pp. 17-00213.

Song, W. C., Tong, X. J., Zhang, J. S., Meng, P. and Li, J. (2017) 'Autotrophic and heterotrophic components of soil respiration caused by rhizosphere priming effects in a plantation', *Plant, Soil and Environment,* 63(7), pp. 295-299.

Sorenson, M. K., Ray, S. S. and Darst, S. A. (2004) 'Crystal structure of the flagellar sigma/anti-sigma complex sigma(28)/FlgM reveals an intact sigma factor in an inactive conformation', *Molecular Cell,* 14(1), pp. 127-138.

Spilker, T., Baldwin, A., Bumford, A., Dowson, C. G., Mahenthiralingam, E. and LiPuma, J. J. (2009) 'Expanded Multilocus Sequence Typing for Burkholderia Species', *Journal of Clinical Microbiology,* 47(8), pp. 2607.

Staron, A., Sofia, H. J., Dietrich, S., Ulrich, L. E., Liesegang, H. and Mascher, T. (2009) 'The third pillar of bacterial signal transduction: classification of the extracytoplasmic function (ECF) sigma factor protein family', *Mol Microbiol,* 74(3), pp. 557-81.

Stephan, H., Freund, S., Beck, W., Jung, G., Meyer, J. M. and Winkelmann, G. (1993) 'Ornibactins--a new family of siderophores from Pseudomonas', *Biometals,* 6(2), pp. 93-100.

Stevens, M. P., Stevens, J. M., Jeng, R. L., Taylor, L. A., Wood, M. W., Hawes, P., Monaghan, P., Welch, M. D. and Galyov, E. E. (2005) 'Identification of a bacterial factor required for actin-based motility of Burkholderia pseudomallei', *Mol Microbiol,* 56(1), pp. 40-53.

Stock, A. M., Robinson, V. L. and Goudreau, P. N. (2000) 'Two-component signal transduction', *Annual Review of Biochemistry,* 69, pp. 183-215.

Stojiljkovic, I., Baumler, A. J. and Hantke, K. (1994) 'Fur regulon in Gram-negative bacteria - Identification and characterization of new iron-regulated Escherichia coli gene by a Fur titration assay', *Journal of Molecular Biology,* 236(2), pp. 531-545.

Studier, F. W. (2005) 'Protein production by auto-induction in high density shaking cultures', *Protein Expr Purif,* 41(1), pp. 207-34.

Studier, F. W. and Moffatt, B. A. (1986) 'Use of bacteriophage-T7 RNA-polymerase to direct selective high-level expression of cloned genes', *Journal of Molecular Biology,* 189(1), pp. 113-130.

Studier, F. W., Rosenberg, A. H., Dunn, J. J. and Dubendorff, J. W. (1990) 'Use of T7 RNA polymerase to direct expression of cloned genes', *Methods Enzymol,* 185, pp. 60-89.

Tamura, K., Sugimoto, H., Shiro, Y. and Sugita, Y. (2019) 'Chemo-Mechanical Coupling in the Transport Cycle of a Heme ABC Transporter', *J Phys Chem B.*

Taneja, S., Kumar, P., Gautam, V., Duseja, A., Singh, V., Dhiman, R. K. and Chawla, Y. (2017) 'Spontaneous Bacterial Peritonitis by Burkholderia cepacia Complex: A Rare, Difficult to Treat Infection in Decompensated Cirrhotic Patients', *Journal of Clinical and Experimental Hepatology,* 7(2), pp. 102-106.

Titball, R. W., Burtnick, M. N., Bancroft, G. J. and Brett, P. (2017) 'Burkholderia pseudomallei and Burkholderia mallei vaccines: Are we close to clinical trials?', *Vaccine,* 35(44), pp. 5981-5989.

Toesca, I. J., French, C. T. and Miller, J. F. (2014) 'The Type VI secretion system spike protein VgrG5 mediates membrane fusion during intercellular spread by pseudomallei group Burkholderia species', *Infect Immun,* 82(4), pp. 1436-44.

Touati, D., Jacques, M., Tardat, B., Bouchard, L. and Despied, S. (1995) 'Lethal oxidative damage and mutagenesis are generated by iron in delta-fur mutants of Escherichia coli - Protective role of superoxide dismutase', *Journal of Bacteriology,* 177(9), pp. 2305-2314.

Trepreau, J., Girard, E., Maillard, A. P., de Rosny, E., Petit-Haertlein, I., Kahn, R. and Coves, J. (2011) 'Structural Basis for Metal Sensing by CnrX', *Journal of Molecular Biology,* 408(4), pp. 766-779.

Trottmann, F., Franke, J., Ishida, K., Garcia-Altares, M. and Hertweck, C. (2019a) 'A Pair of Bacterial Siderophores Releases and Traps an Intercellular Signal Molecule: An Unusual Case of Natural Nitrone Bioconjugation', *Angew Chem Int Ed Engl,* 58(1), pp. 200-204.

Trottmann, F., Franke, J., Richter, I., Ishida, K., Cyrulies, M., Dahse, H.-M., Regestein, L. and Hertweck, C. (2019b) 'Cyclopropanol Warhead in Malleicyprol Confers Virulence of Human- and Animal-Pathogenic Burkholderia Species', *Angewandte Chemie International Edition,* 0(0).

Trunck, L. A., Propst, K. L., Wuthiekanun, V., Tuanyok, A., Beckstrom-Sternberg, S. M., Beckstrom-Sternberg, J. S., Peacock, S. J., Keim, P., Dow, S. W. and Schweizer, H. P. (2009) 'Molecular basis of rare aminoglycoside susceptibility and pathogenesis of Burkholderia pseudomallei clinical isolates from Thailand', *PLoS Negl Trop Dis,* 3(9), pp. e519.

Truong, T. T., Seyedsayamdost, M. R., Greenberg, E. P. and Chandler, J. R. (2015) 'A Burkholderia thailandensis Acyl-Homoserine Lactone-Independent Orphan LuxR Homolog That

Activates Production of the Cytotoxin Malleilactone', *Journal of Bacteriology,* 197(21), pp. 3456-3462.

Tseng, C. F., Burger, A., Mislin, G. L., Schalk, I. J., Yu, S. S., Chan, S. I. and Abdallah, M. A. (2006) 'Bacterial siderophores: the solution stoichiometry and coordination of the Fe(III) complexes of pyochelin and related compounds', *J Biol Inorg Chem,* 11(4), pp. 419-32.

Tuanyok, A., Mayo, M., Scholz, H., Hall, C. M., Allender, C. J., Kaestli, M., Ginther, J., Spring-Pearson, S., Bollig, M. C., Stone, J. K., Settles, E. W., Busch, J. D., Sidak-Loftis, L., Sahl, J. W., Thomas, A., Kreutzer, L., Georgi, E., Gee, J. E., Bowen, R. A., Ladner, J. T., Lovett, S., Koroleva, G., Palacios, G., Wagner, D. M., Currie, B. J. and Keim, P. (2017) 'Burkholderia humptydooensis sp. nov., a New Species Related to Burkholderia thailandensis and the Fifth Member of the Burkholderia pseudomallei Complex', *Appl Environ Microbiol,* 83(5).

Tyrrell, J., Whelan, N., Wright, C., Sa-Correia, I., McClean, S., Thomas, M. S. and Callaghan, M. (2015) 'Investigation of the multifaceted iron acquisition strategies of Burkholderia cenocepacia', *Biometals,* 28(2), pp. 367-380.

Ulrich, L. E., Koonin, E. V. and Zhulin, I. B. (2005) 'One-component systems dominate signal transduction in prokaryotes', *Trends in Microbiology,* 13(2), pp. 52-56.

Van Zandt, K. E., Greer, M. T. and Gelhaus, H. C. (2013) 'Glanders: an overview of infection in humans', *Orphanet journal of rare diseases,* 8, pp. 131-131.

Vanaporn, M., Wand, M., Michell, S. L., Sarkar-Tyson, M., Ireland, P., Goldman, S., Kewcharoenwong, C., Rinchai, D., Lertmemongkolchai, G. and Titball, R. W. (2011) 'Superoxide dismutase C is required for intracellular survival and virulence of Burkholderia pseudomallei', *Microbiology,* 157(Pt 8), pp. 2392-400.

Vander Broek, C. W. and Stevens, J. M. (2017) 'Type III Secretion in the Melioidosis Pathogen Burkholderia pseudomallei', *Front Cell Infect Microbiol,* 7, pp. 255.

Vanderpool, C. K. and Armstrong, S. K. (2001) 'The Bordetella bhu locus is required for heme iron utilization', *Journal of Bacteriology,* 183(14), pp. 4278-4287.

Vargas-Straube, M. J., Camara, B., Tello, M., Montero-Silva, F., Cardenas, F. and Seeger, M. (2016) 'Genetic and Functional Analysis of the Biosynthesis of a Non-Ribosomal Peptide Siderophore in Burkholderia xenovorans LB400', *PLoS One,* 11(3), pp. e0151273.

Vassylyev, D. G., Sekine, S., Laptenko, O., Lee, J., Vassylyeva, M. N., Borukhov, S. and Yokoyama, S. (2002) 'Crystal structure of a bacterial RNA polymerase holoenzyme at 2.6 angstrom resolution', *Nature,* 417(6890), pp. 712-719.

Visca, P., Colotti, G., Serino, L., Verzili, D., Orsi, N. and Chiancone, E. (1992) 'Metal regulation of siderophore synthesis in Pseudomonas aeruginosa and functional effects of siderophore-metal complexes', *Applied and environmental microbiology,* 58(9), pp. 2886-2893.

Visca, P., Imperi, F. and Lamont, I. L. (2007) 'Pyoverdine siderophores: from biogenesis to biosignificance', *Trends Microbiol,* 15(1), pp. 22-30.

Volpe-Chaves, C. E., Rodrigues, A. C. S., Lacerda, M., Oliveira, C. T. F., Castilho, S. B., Franciscato, C., Santos, I. C. O., Assef, A., Roever, L., Oliveira, S. and Paniago, A. M. M. (2019) 'Melioidosis, an emerging infectious disease in the Midwest Brazil: A case report', *Medicine (Baltimore),* 98(16), pp. e15235.

Vuthoori, S., Bowers, C., McCracken, A., Dombroski, A. and Hinton, D. (2001) 'Domain 1.1 of the sigma(70) subunit of Escherichia coli RNA polymerase modulates the formation of stable polymerase/promoter complexes', *Journal of Molecular Biology,* 309(3), pp. 561-572.

Wecke, T., Halang, P., Staron, A., Dufour, Y. S., Donohue, T. J. and Mascher, T. (2012) 'Extracytoplasmic function sigma factors of the widely distributed group ECF41 contain a fused regulatory domain', *Microbiologyopen,* 1(2), pp. 194-213.

Whitby, P. W., Vanwagoner, T. M., Springer, J. M., Morton, D. J., Seale, T. W. and Stull, T. L. (2006) 'Burkholderia cenocepacia utilizes ferritin as an iron source', *J Med Microbiol,* 55(Pt 6), pp. 661-8.

Whitmore, A. (1913) 'An Account of a Glanders-like Disease occurring in Rangoon', *J Hyg (Lond),* 13(1), pp. 1-34.1.

Wiersinga, W. J., Currie, B. J. and Peacock, S. J. (2012) 'Melioidosis', *N Engl J Med,* 367(11), pp. 1035-44.

Wiersinga, W. J., Virk, H. S., Torres, A. G., Currie, B. J., Peacock, S. J., Dance, D. A. B. and Limmathurotsakul, D. (2018) 'Melioidosis', *Nat Rev Dis Primers,* 4, pp. 17107.

Wilken, C., Kitzing, K., Kurzbauer, R., Ehrmann, M. and Clausen, T. (2004) 'Crystal structure of the DegS stress sensor: How a PDZ domain recognizes misfolded protein and activates a protease', *Cell,* 117(4), pp. 483-494.

Williams, R. J. (2012) 'Iron in evolution', *FEBS Lett,* 586(5), pp. 479-84.

Wilson, M. J., McMorran, B. J. and Lamont, I. L. (2001) 'Analysis of Promoters Recognized by PvdS, an Extracytoplasmic-Function Sigma Factor Protein fromPseudomonas aeruginosa', *Journal of Bacteriology,* 183(6), pp. 2151-2155.

Wong, J., Chen, Y. and Gan, Y. H. (2015) 'Host Cytosolic Glutathione Sensing by a Membrane Histidine Kinase Activates the Type VI Secretion System in an Intracellular Bacterium', *Cell Host Microbe,* 18(1), pp. 38-48.

Woods, C. W., Brasslar, A. M., LiPuma, J. J., Alexander, B. D., Clements, D. A., Weber, D. J., Moore, C. M., Reller, L. B. and Kaye, K. S. (2004) 'Virulence associated with outbreak-related strains of Burkholderia cepacia complex among a cohort of patients with bacteremia', *Clinical Infectious Diseases,* 38(9), pp. 1243-1250.

Wu, H., Liu, Q., Casas-Pastor, D., Dürr, F., Mascher, T. and Fritz, G. (2019) 'The role of C-terminal extensions in controlling ECF σ factor activity in the widely conserved groups ECF41 and ECF42', *Molecular Microbiology,* 0(ja).

Yabuuchi, E., Kosako, Y., Oyaizu, H., Yano, I., Hotta, H., Hashimoto, Y., Ezaki, T. and Arakawa, M. (1992) 'Proposal of Burkholderia gen. nov. and Transfer of Seven Species of the Genus Pseudomonas Homology Group II to the New Genus, with the Type Species Burkholderia cepacia (Palleroni and Holmes 1981) comb. nov', *Microbiology and Immunology,* 36(12), pp. 1251-1275.

Yang, H. M., Chaowagul, W. and Sokol, P. A. (1991) 'Siderophore production by Pseudomonas pseudomallei', *Infection and Immunity,* 59(3), pp. 776-780.

Yang, H. M., Kooi, C. D. and Sokol, P. A. (1993) 'Ability of Pseudomonas pseudomallei malleobactin to acquire transferrin-bound, lactoferrin-bound, and cell-derived iron', *Infect Immun,* 61(2), pp. 656-62.

Yanisch-Perron, C., Vieira, J. and Messing, J. (1985) 'Improved M13 phage cloning vectors and host strains - Nucleotide sequences of the M13MP18 and PUC19 vectors', *Gene,* 33(1), pp. 103-119.

Yee, K. C., Lee, M. K., Chua, C. T. and Puthucheary, S. D. (1988) 'Melioidosis, the great mimicker: a report of 10 cases from Malaysia', *J Trop Med Hyg,* 91(5), pp. 249-54.

Yoon, S., Kraemer, S. M., DiSpirito, A. A. and Semrau, J. D. (2010) 'An assay for screening microbial cultures for chalkophore production', *Environmental Microbiology Reports,* 2(2), pp. 295-303.

Yoshimura, M., Asai, K., Sadaie, Y. and Yoshikawa, H. (2004) 'Interaction of Bacillus subtilis extracytoplasmic function (ECF) sigma factors with the N-terminal regions of their potential anti-sigma factors', *Microbiology-Sgm,* 150, pp. 591-599.

Yu, Y., Kim, H. S., Chua, H. H., Lin, C. H., Sim, S. H., Lin, D., Derr, A., Engels, R., DeShazer, D., Birren, B., Nierman, W. C. and Tan, P. (2006) 'Genomic patterns of pathogen evolution revealed by comparison of Burkholderia pseudomallei, the causative agent of melioidosis, to avirulent Burkholderia thailandensis', *BMC Microbiology,* 6(1), pp. 46.

Yuhara, S., Komatsu, H., Goto, H., Ohtsubo, Y., Nagata, Y. and Tsuda, M. (2008) 'Pleiotropic roles of iron-responsive transcriptional regulator Fur in Burkholderia multivorans', *Microbiology,* 154(Pt 6), pp. 1763-74.

Zahariadis, G., Levy, M. H. and Burns, J. L. (2003) 'Cepacia-Like Syndrome Caused by Burkholderia mutivorans', *Canadian Journal of Infectious Diseases,* 14(2).

Zhang, Y., Feng, Y., Chatterjee, S., Tuske, S., Ho, M., Arnold, E. and Ebright, R. (2012) 'Structural Basis of Transcription Initiation', *Science,* 338(6110), pp. 1076-1080.

Appendix: Plasmid Maps
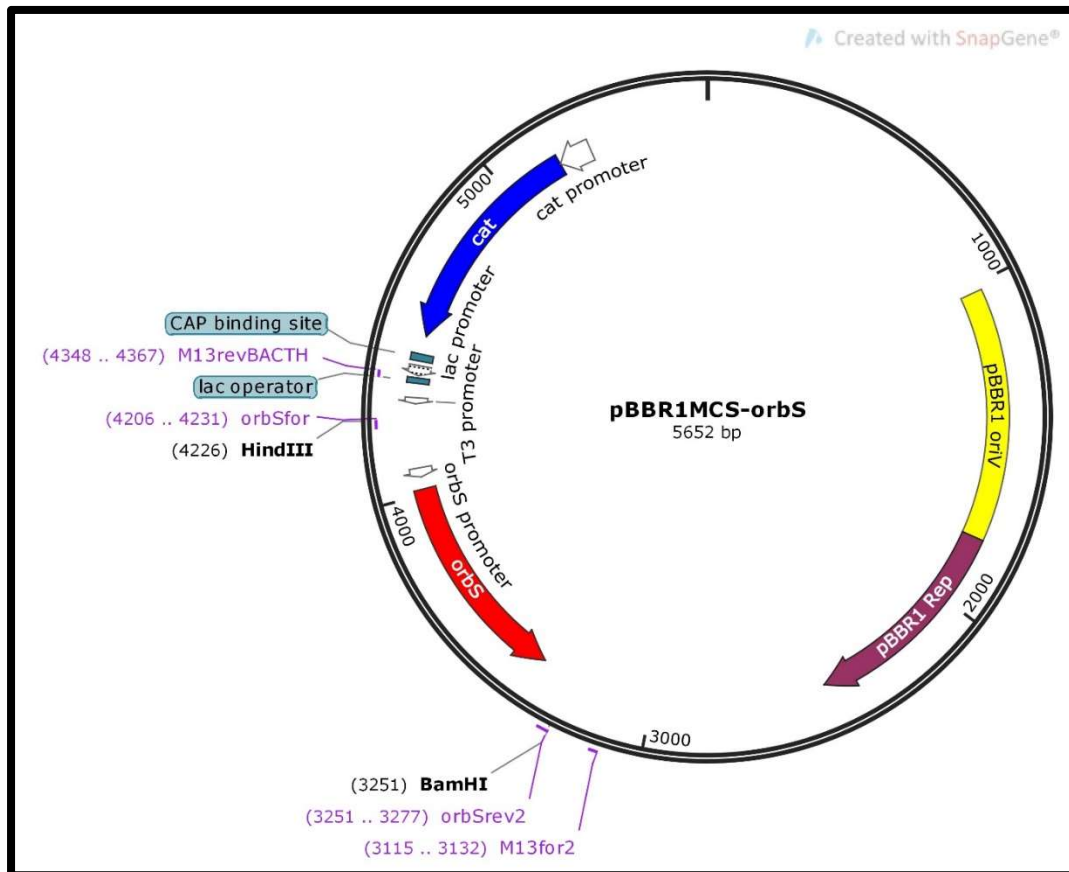
Figure A.1. Plasmid map of pBBR1MCS-*orbS*.

The locations of each of the following are shown: the *orbS* gene (red), the chloramphenicol resistance-conferring gene *cat* (blue), the *Bordetella bronchiseptica* gene encoding the plasmid replication protein Rep (purple), the Rep-dependent *Bordetella bronchiseptica* plasmid replication origin *oriV* (yellow), the *cat*, *lac*, T3 and *orbS* promoters (white), the CAP binding site and *lac* operator (teal), the *Hind*III and *Bam*HI restriction sites used in plasmid construction, and the binding sites for relevant DNA primers.
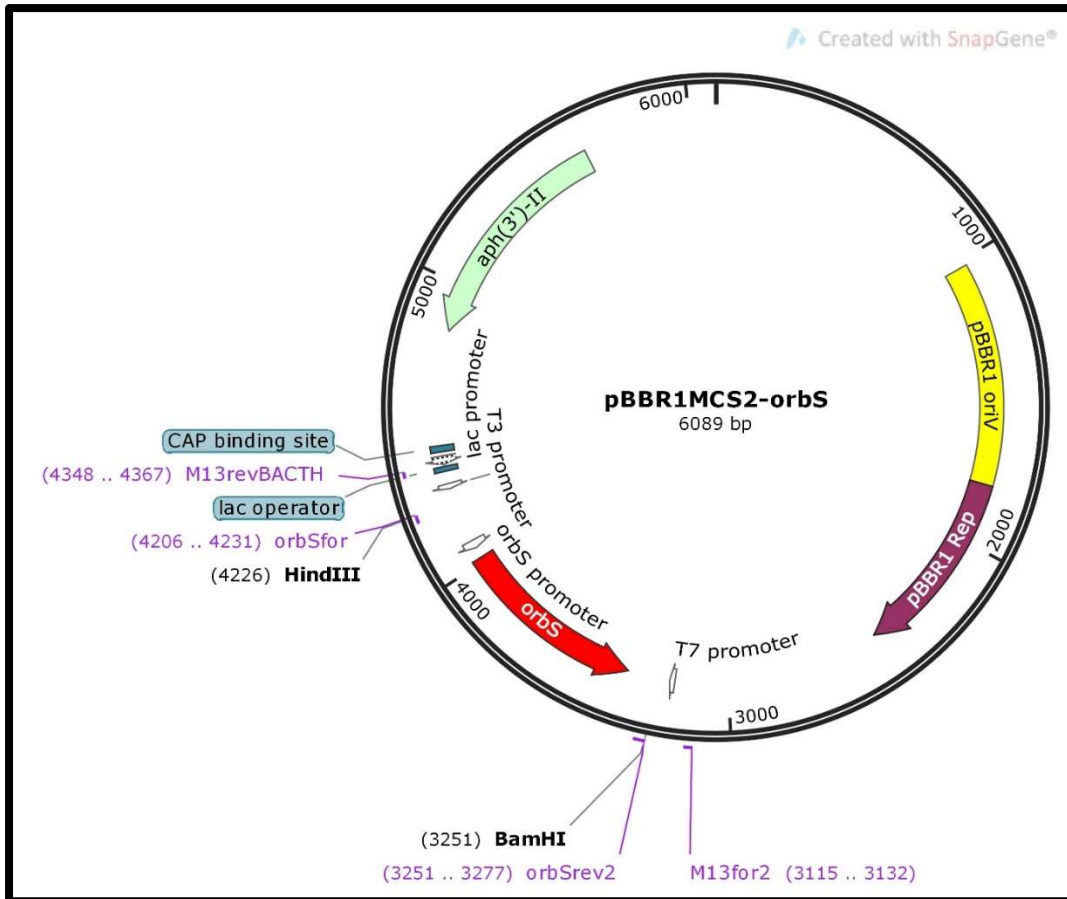
Figure A.2. Plasmid map of pBBR1MCS2-*orbS*.

The locations of each of the following are shown: the *orbS* gene (red), the kanamycin resistance-conferring gene *aph*(3')-II (light green), the *Bordetella bronchiseptica* gene encoding the plasmid replication protein Rep (purple), the Rep-dependent *Bordetella bronchiseptica* plasmid replication origin *oriV* (yellow), the *lac*, T3, T7 and *orbS* promoters (white), the CAP binding site and *lac* operator (teal), the *Hin*dIII and *Bam*HI restriction sites used in plasmid construction, and the binding sites for relevant DNA primers.
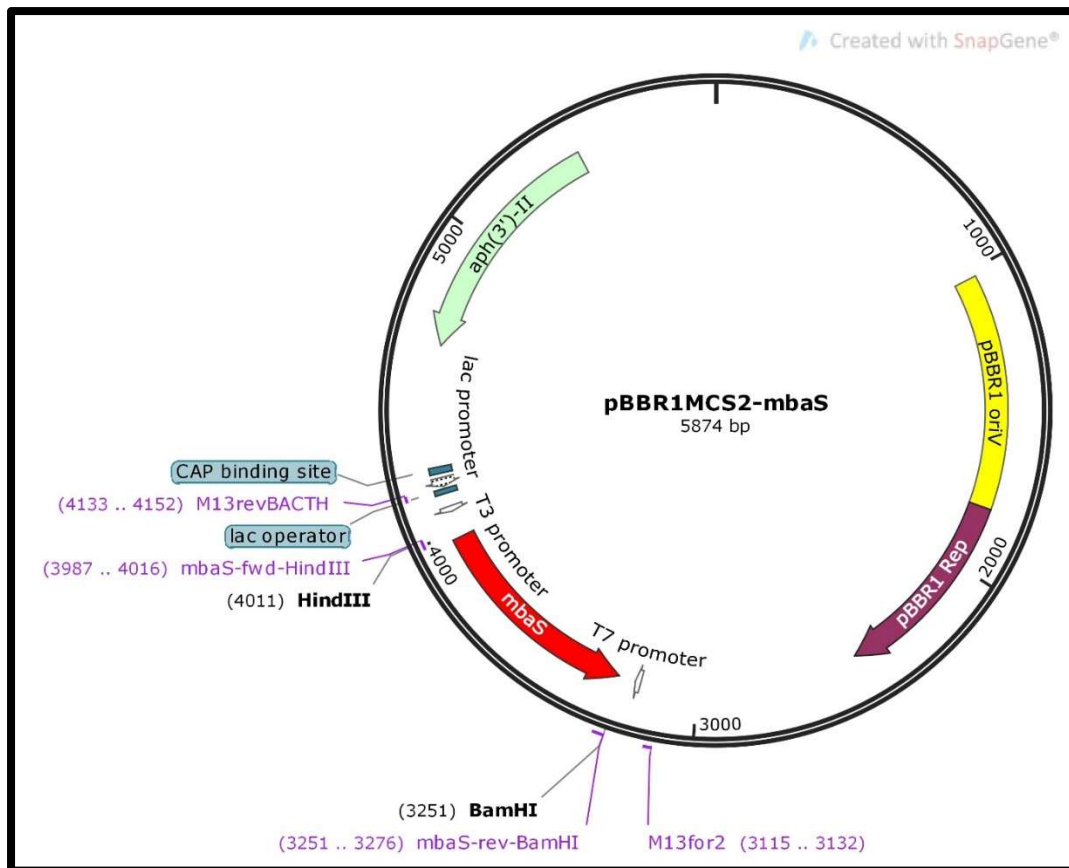
Figure A.3. Plasmid map of pBBR1MCS2-*mbaS*.

The locations of each of the following are shown: the *mbaS* gene (red), the kanamycin resistance-conferring gene *aph*(3')-II (light green), the *Bordetella bronchiseptica* gene encoding the plasmid replication protein Rep (purple), the Rep-dependent *Bordetella bronchiseptica* plasmid replication origin *oriV* (yellow), the *lac*, T3 and T7 promoters (white), the CAP binding site and *lac* operator (teal), the *Hin*dIII and *Bam*HI restriction sites used in plasmid construction, and the binding sites for relevant DNA primers.
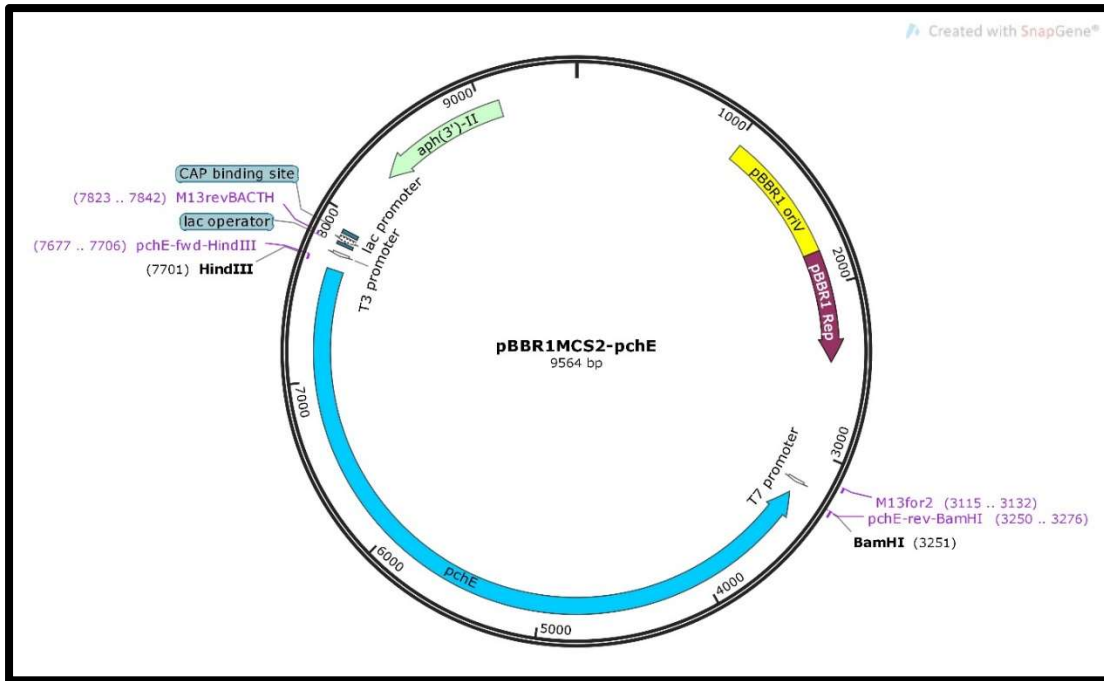
Figure A.4. Plasmid map of pBBR1MCS2-*pchE*.

The locations of each of the following are shown: the *pchE* gene (blue), the kanamycin resistance-conferring gene *aph*(3')-II (light green), the *Bordetella bronchiseptica* gene encoding the plasmid replication protein Rep (purple), the Rep-dependent *Bordetella bronchiseptica* plasmid replication origin *oriV* (yellow), the *lac*, T3 and T7 promoters (white), the CAP binding site and *lac* operator (teal), the *Hin*dIII and *Bam*HI restriction sites used in plasmid construction, and the binding sites for relevant DNA primers.
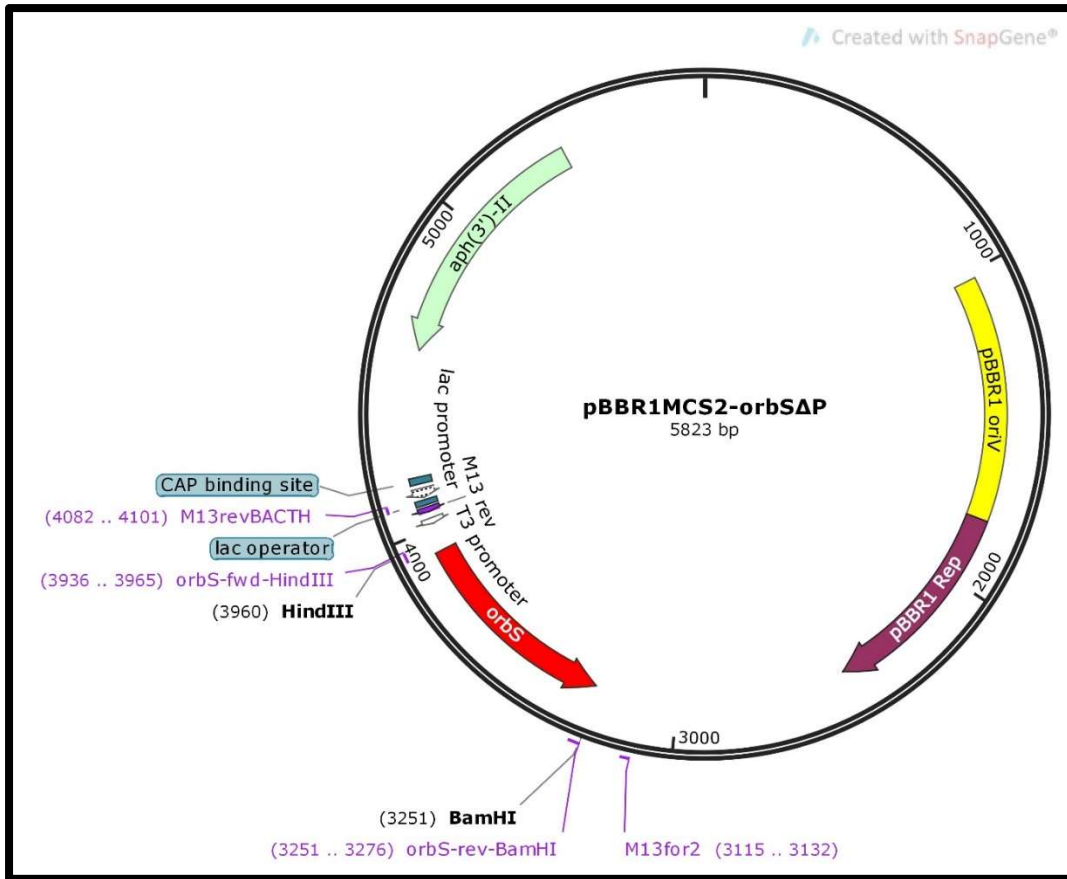
Figure A.5. Plasmid map of pBBR1MCS2-orbS$_{\Delta P}$.

The locations of each of the following are shown: the *orbS* gene (red), the kanamycin resistance-conferring gene *aph*(3')-II (light green), the *Bordetella bronchiseptica* gene encoding the plasmid replication protein Rep (purple), the Rep-dependent *Bordetella bronchiseptica* plasmid replication origin *oriV* (yellow), the *lac* and T3 promoters (white), the CAP binding site and *lac* operator (teal), the *Hind*III and *Bam*HI restriction sites used in plasmid construction, and the binding sites for relevant DNA primers.
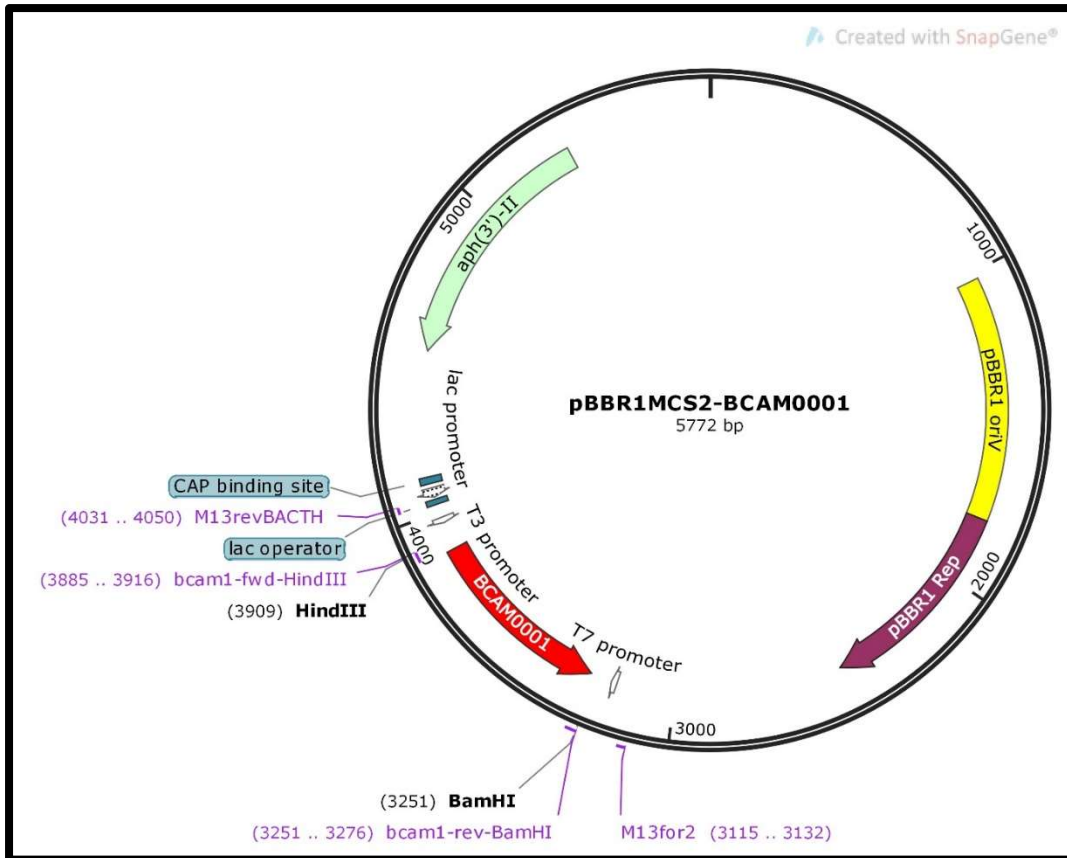
Figure A.6. Plasmid map of pBBR1MCS2-BCAM0001.

The locations of each of the following are shown: the BCAM0001 gene (red), the kanamycin resistance-conferring gene *aph*(3')-II (light green), the *Bordetella bronchiseptica* gene encoding the plasmid replication protein Rep (purple), the Rep-dependent *Bordetella bronchiseptica* plasmid replication origin *oriV* (yellow), the *lac*, T3 and T7 promoters (white), the CAP binding site and *lac* operator (teal), the *Hin*dIII and *Bam*HI restriction sites used in plasmid construction, and the binding sites for relevant DNA primers.
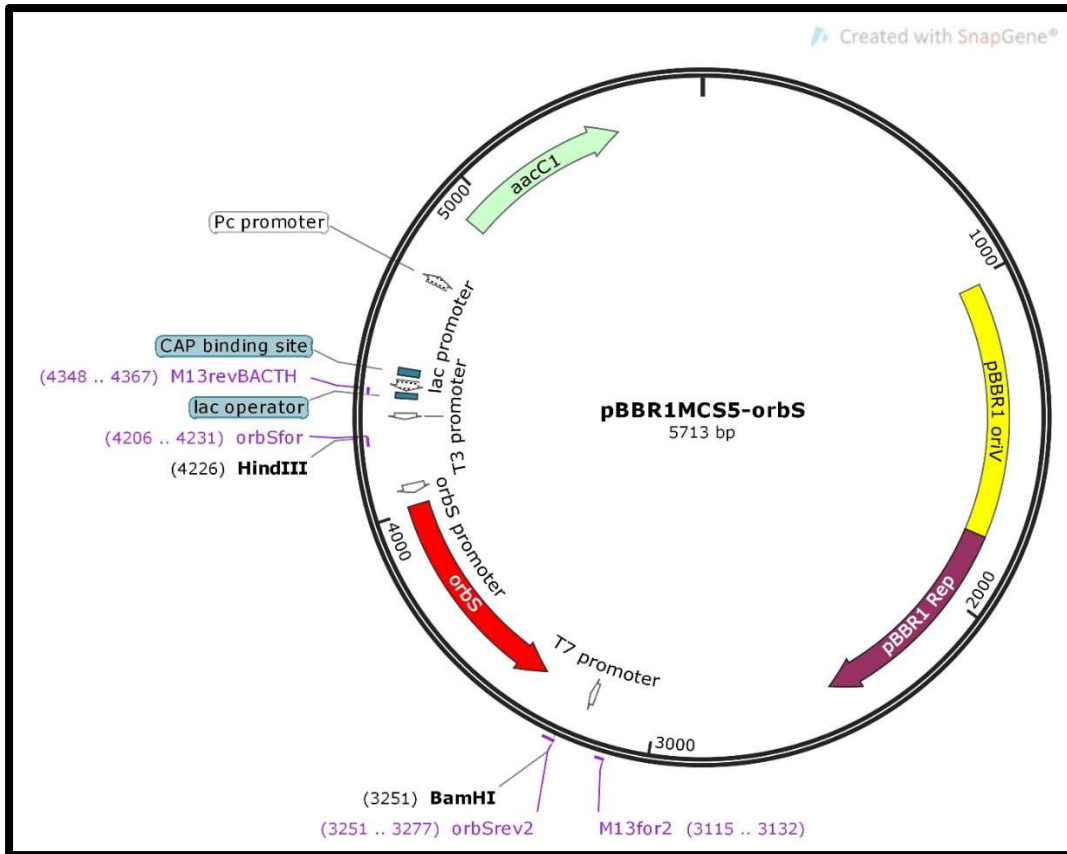
Figure A.7. Plasmid map of pBBR1MCS5-*orbS*.

The locations of each of the following are shown: the *orbS* gene (red), the gentamycin resistance-conferring gene *aac*C1 (light green), the *Bordetella bronchiseptica* gene encoding the plasmid replication protein Rep (purple), the Rep-dependent *Bordetella bronchiseptica* plasmid replication origin *oriV* (yellow), the Pc, *lac*, T3, *orbS* and T7 promoters (white), the CAP binding site and *lac* operator (teal), the *Hin*dIII and *Bam*HI restriction sites used in plasmid construction, and the binding sites for relevant DNA primers.
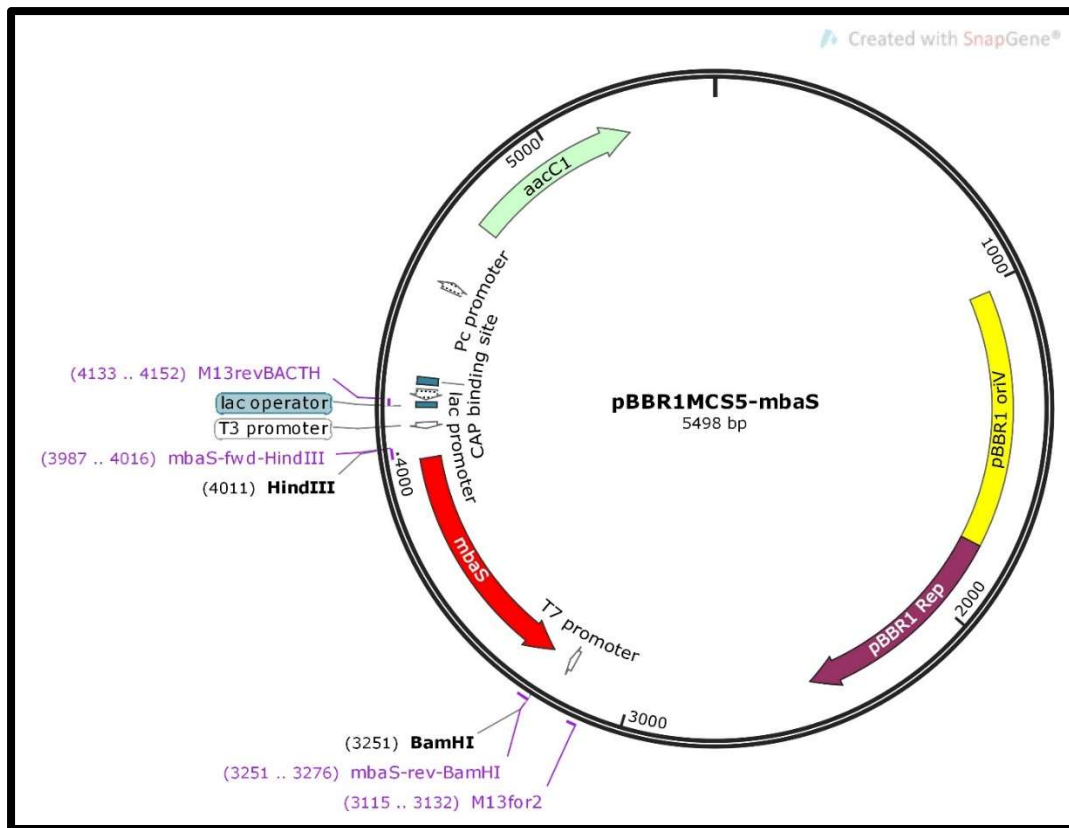
Figure A.8. Plasmid map of pBBR1MCS5-*mbaS*.

The locations of each of the following are shown: the *mbaS* gene (red), the gentamycin resistance-conferring gene *aac*C1 (light green), the *Bordetella bronchiseptica* gene encoding the plasmid replication protein Rep (purple), the Rep-dependent *Bordetella bronchiseptica* plasmid replication origin *oriV* (yellow), the Pc, *lac*, T3 and T7 promoters (white), the CAP binding site and *lac* operator (teal), the *Hin*dIII and *Bam*HI restriction sites used in plasmid construction, and the binding sites for relevant DNA primers.
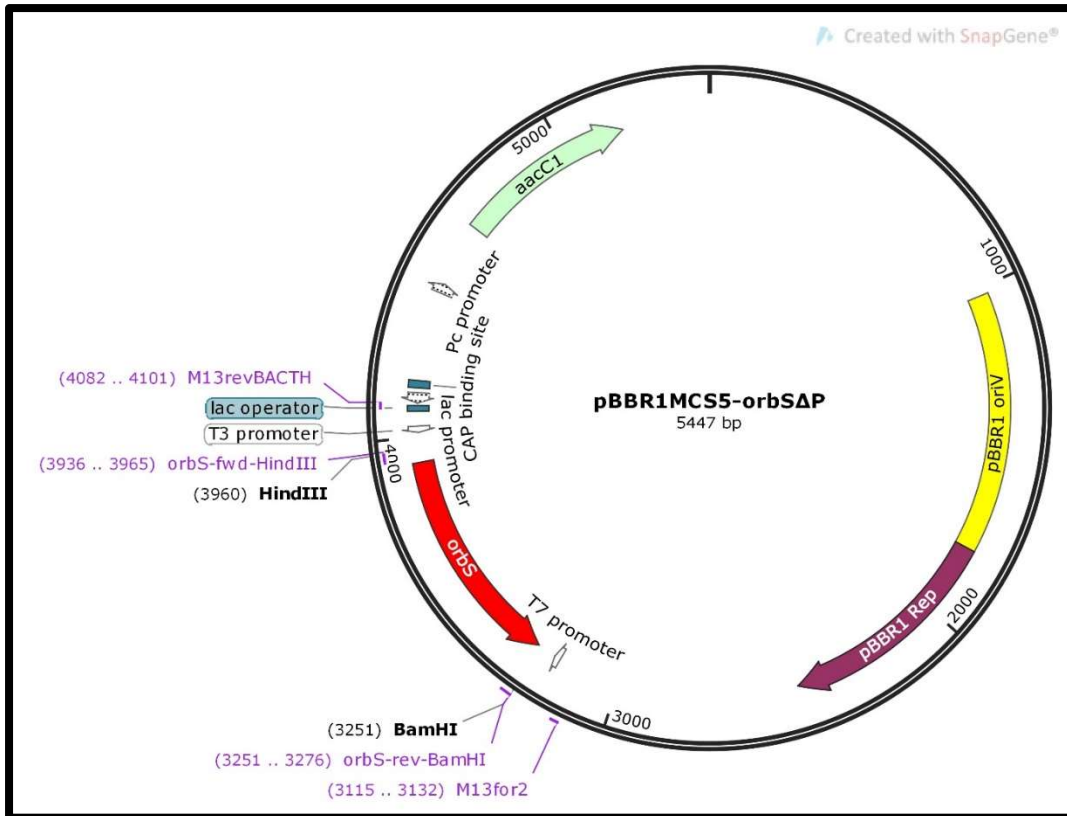
Figure A.9. Plasmid map of pBBR1MCS5-*orbS*ₐₚ.

The locations of each of the following are shown: the *orbS* gene (red), the gentamycin resistance-conferring gene *aac*C1 (light green), the *Bordetella bronchiseptica* gene encoding the plasmid replication protein Rep (purple), the Rep-dependent *Bordetella bronchiseptica* plasmid replication origin *oriV* (yellow), the Pc, *lac*, T3, and T7 promoters (white), the CAP binding site and *lac* operator (teal), the *Hin*dIII and *Bam*HI restriction sites used in plasmid construction, and the binding sites for relevant DNA primers.
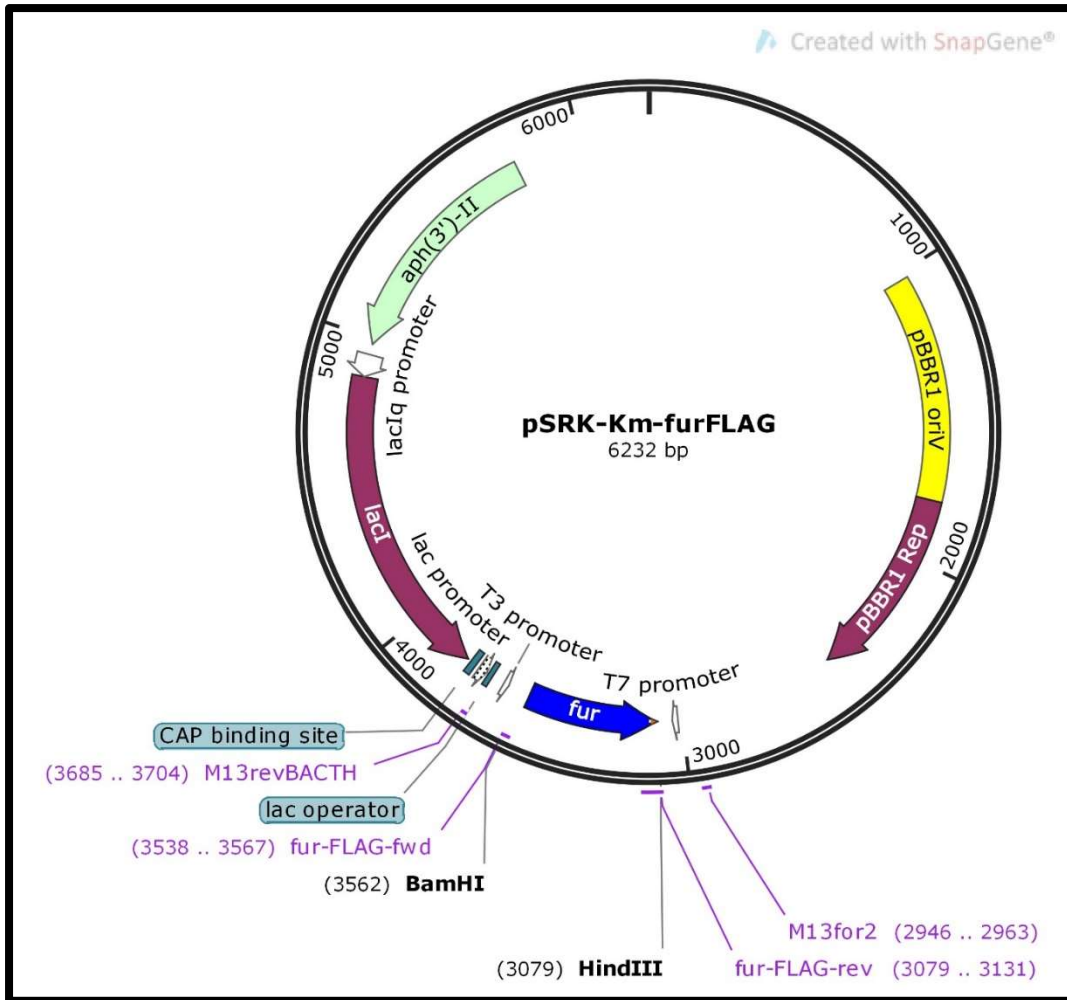
Figure A.10. Plasmid map of pSRK-Km-*fur*FLAG

The locations of each of the following are shown: the *fur*FLAG gene (blue, with FLAG epitope residues in orange), the kanamycin resistance-conferring gene *aph*(3')-II (light green), the *Bordetella bronchiseptica* gene encoding the plasmid replication protein Rep (purple), the Rep-dependent *Bordetella bronchiseptica* plasmid replication origin *oriV* (yellow), the *lacI* gene (purple), the *lacI*q, *lac*, T3, and T7 promoters (white), the CAP binding site and *lac* operator (teal), the *Hin*dIII and *Bam*HI restriction sites used in plasmid construction, and the binding sites for relevant DNA primers.
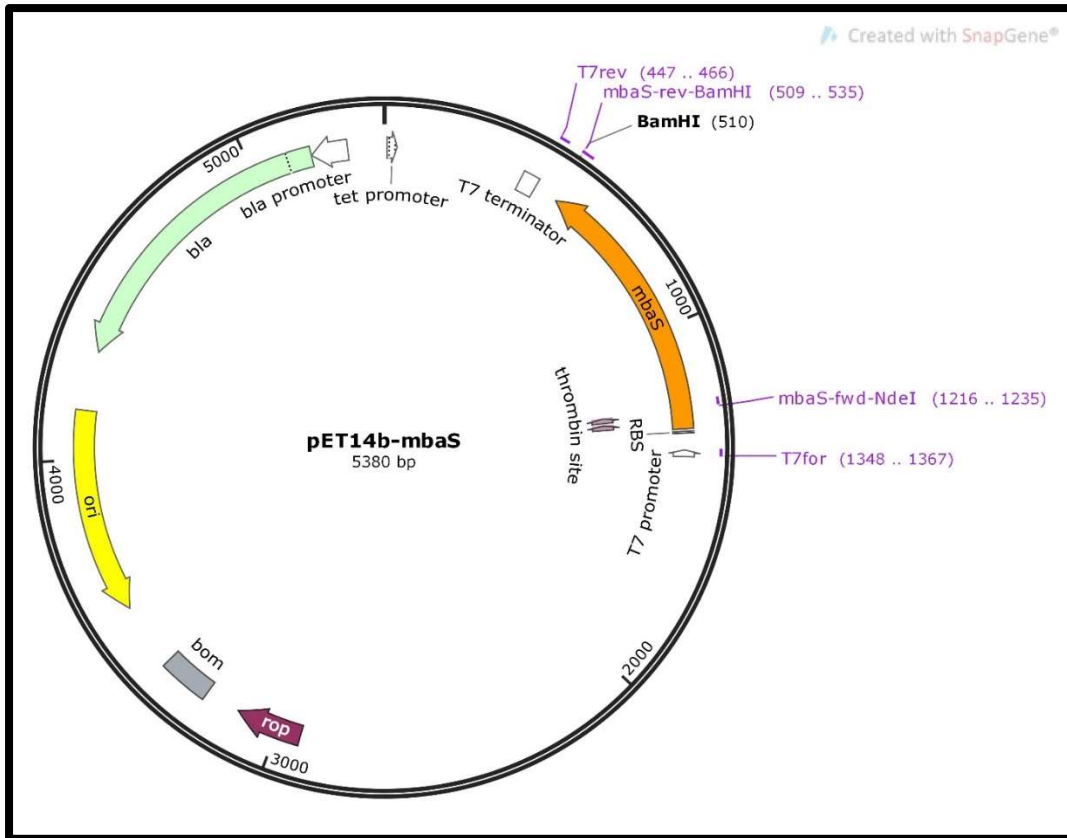
Figure A.11. Plasmid map of pET14b-*mbaS*

The locations of each of the following are shown: the *mbaS* gene containing an N-terminal His-tag (orange), the ampicillin resistance-conferring gene *bla* (light green), the plasmid ColE1 replication origin *ori* (yellow), the gene encoding the *E. coli* regulatory protein Rop (purple), the T7, *tet* and *bla* promoters (white), the T7 terminator (white), the plasmid pBR322 basis of mobility region *bom* (grey), the thrombin cleavage site (purple), the ribosome binding site (grey), the *Nde*I and *Bam*HI restriction sites used in plasmid construction, and the binding sites for relevant DNA primers.
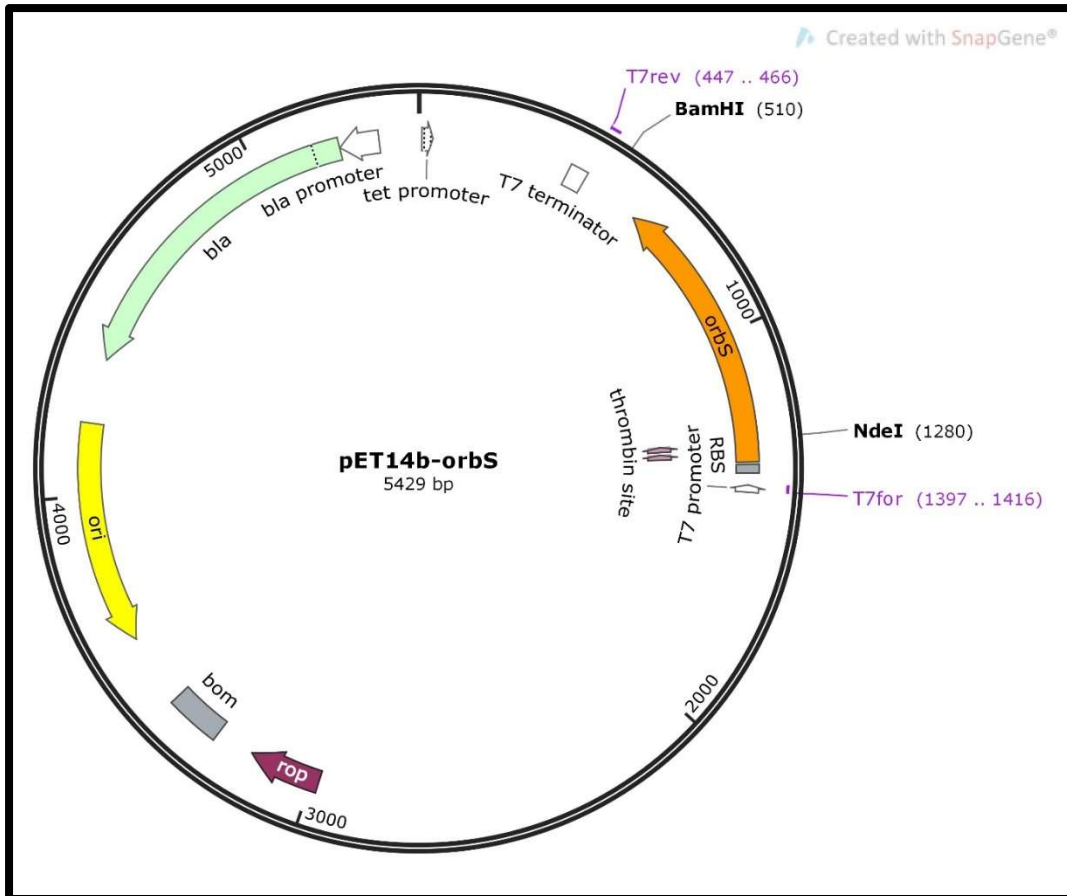
Figure A.12. Plasmid map of pET14b-*orbS*

The locations of each of the following are shown: the *orbS* gene containing an N-terminal His-tag (orange), the ampicillin resistance-conferring gene *bla* (light green), the plasmid ColE1 replication origin *ori* (yellow), the gene encoding the *E. coli* regulatory protein Rop (purple), the T7, *tet* and *bla* promoters (white), the T7 terminator (white), the plasmid pBR322 basis of mobility region *bom* (grey), the thrombin cleavage site (purple), the ribosome binding site (grey), the *Nde*I and *Bam*HI restriction sites used in plasmid construction, and the binding sites for relevant DNA primers.
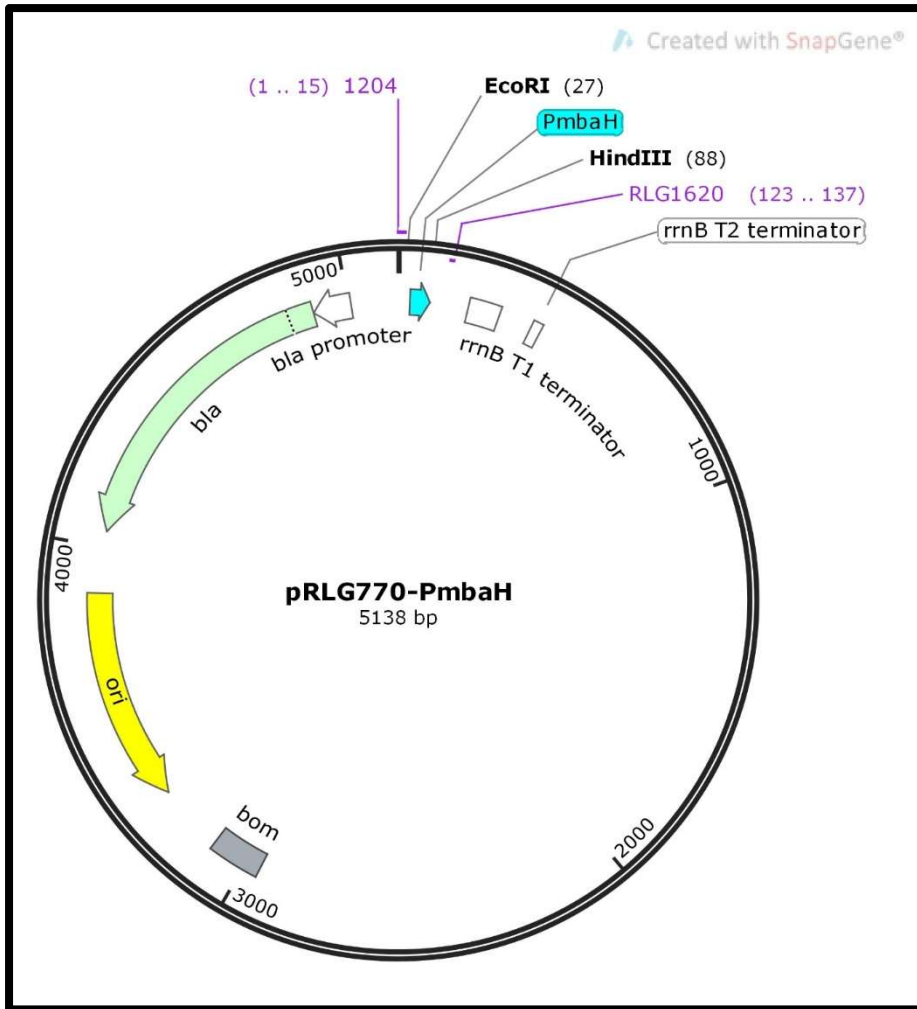
Figure A.13. Plasmid map of pRLG770-P$_{mbaH}$.

The locations of each of the following are shown: the P$_{mbaH}$ promoter (blue), the ampicillin resistance-conferring gene *bla* (light green), the plasmid ColE1 replication origin *ori* (yellow), the *bla* promoter (white), the *rrnB* T1 and T2 terminators (white), the plasmid pBR322 basis of mobility region *bom* (grey), the *Eco*RI and *Hin*dIII restriction sites used in plasmid construction, and the binding sites for relevant DNA primers.
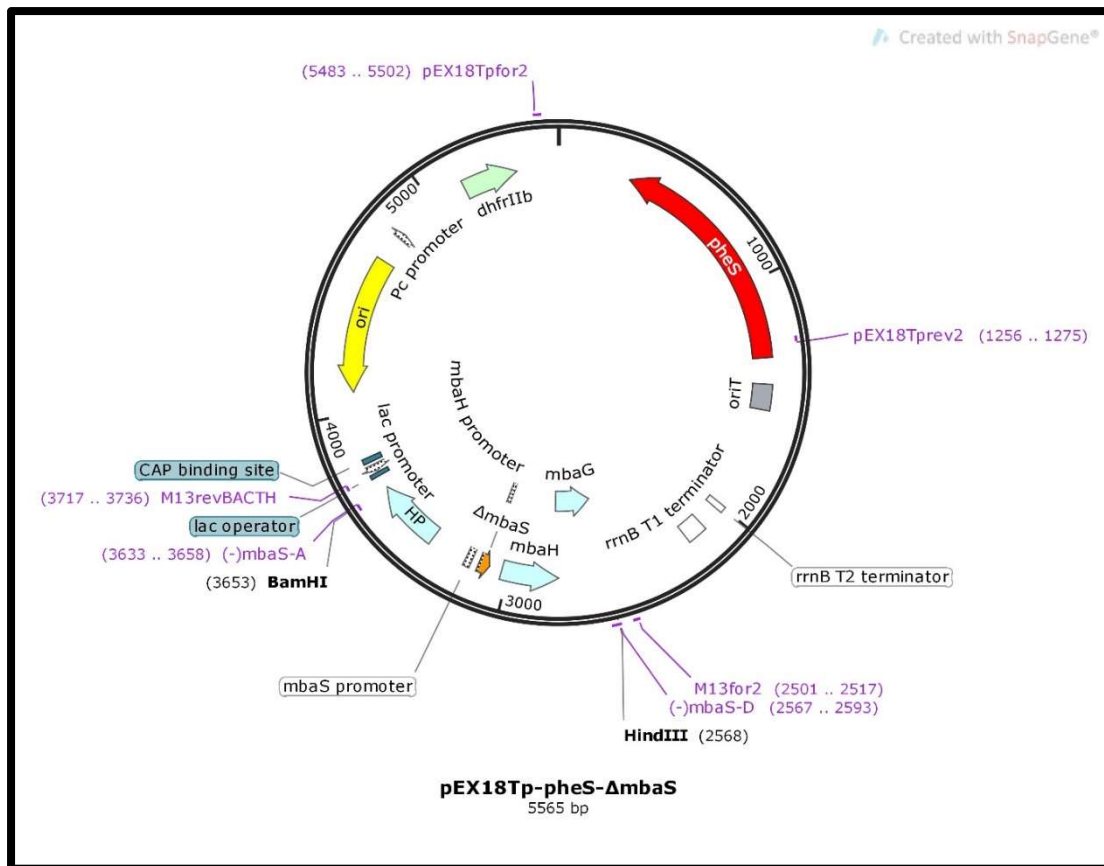
Figure A.14. Plasmid map of pEX18Tp-*pheS*-Δ*mbaS*.

The locations of each of the following are shown: the Δ*mbaS* gene (orange), the trimethoprim resistance-conferring gene *dhfr*IIb (light green), the plasmid ColE1 replication origin *ori* (yellow), the *Bps* mutant gene *pheS* (red), the *Bth* genes encoding MbaH, MbaG, and a hypothetical protein (HP) (light blue), the Pc, *lac*, *mbaS* and *mbaH* promoters (white), the *rrnB* T1 and T2 terminators (white), the CAP binding site and *lac* operator (teal), the conjugal origin of transfer *oriT* (grey), the *Bam*HI and *Hin*dIII restriction sites used in plasmid construction, and the binding sites for relevant DNA primers.
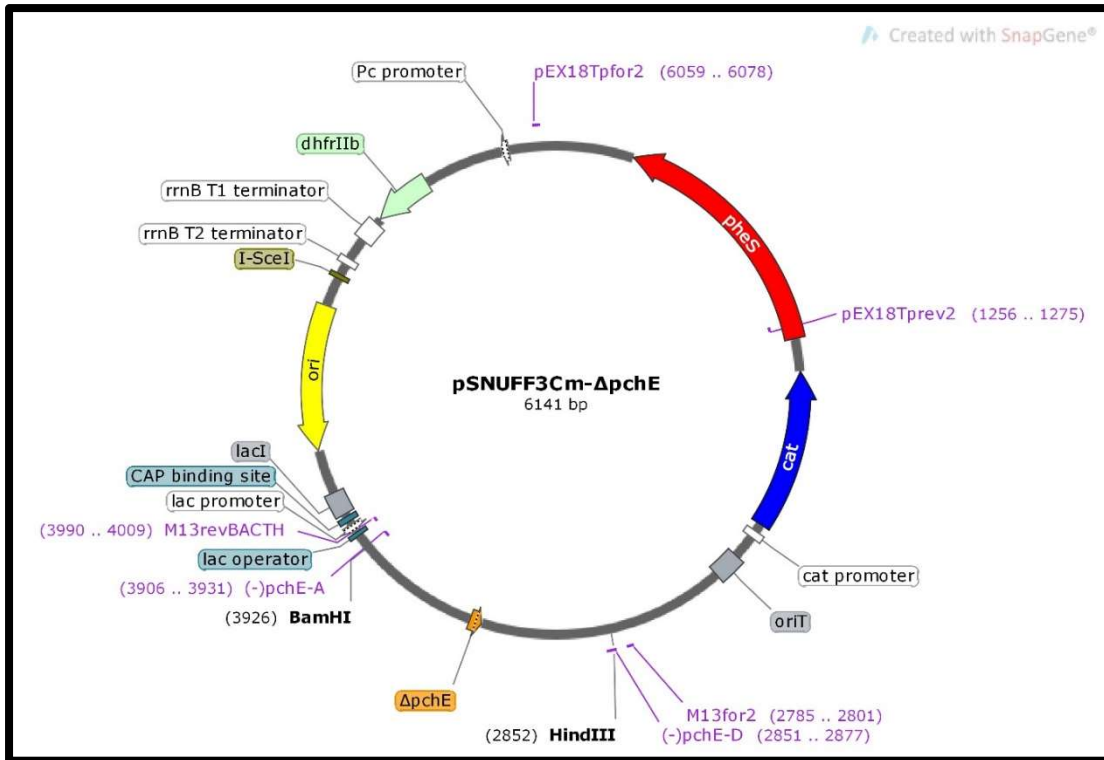
Figure A.15. Plasmid map of pSNUFF3Cm-Δ*pchE*.

The locations of each of the following are shown: the Δ*pchE* gene (orange), the trimethoprim resistance-conferring gene *dhfr*IIb (light green), the chloramphenicol resistance-conferring gene *cat* (blue), the plasmid ColE1 replication origin *ori* (yellow), the *Bps* mutant gene *pheS* (red), the Pc, *lac*, and *cat* promoters (white), the *rrnB* T1 and T2 terminators (white), the CAP binding site and *lac* operator (teal), the *lacI* attenuator region (grey), the conjugal origin of transfer *oriT* (grey), the I-SceI meganuclease restriction site (olive), the *Bam*HI and *Hin*dIII restriction sites used in plasmid construction, and the binding sites for relevant DNA primers.
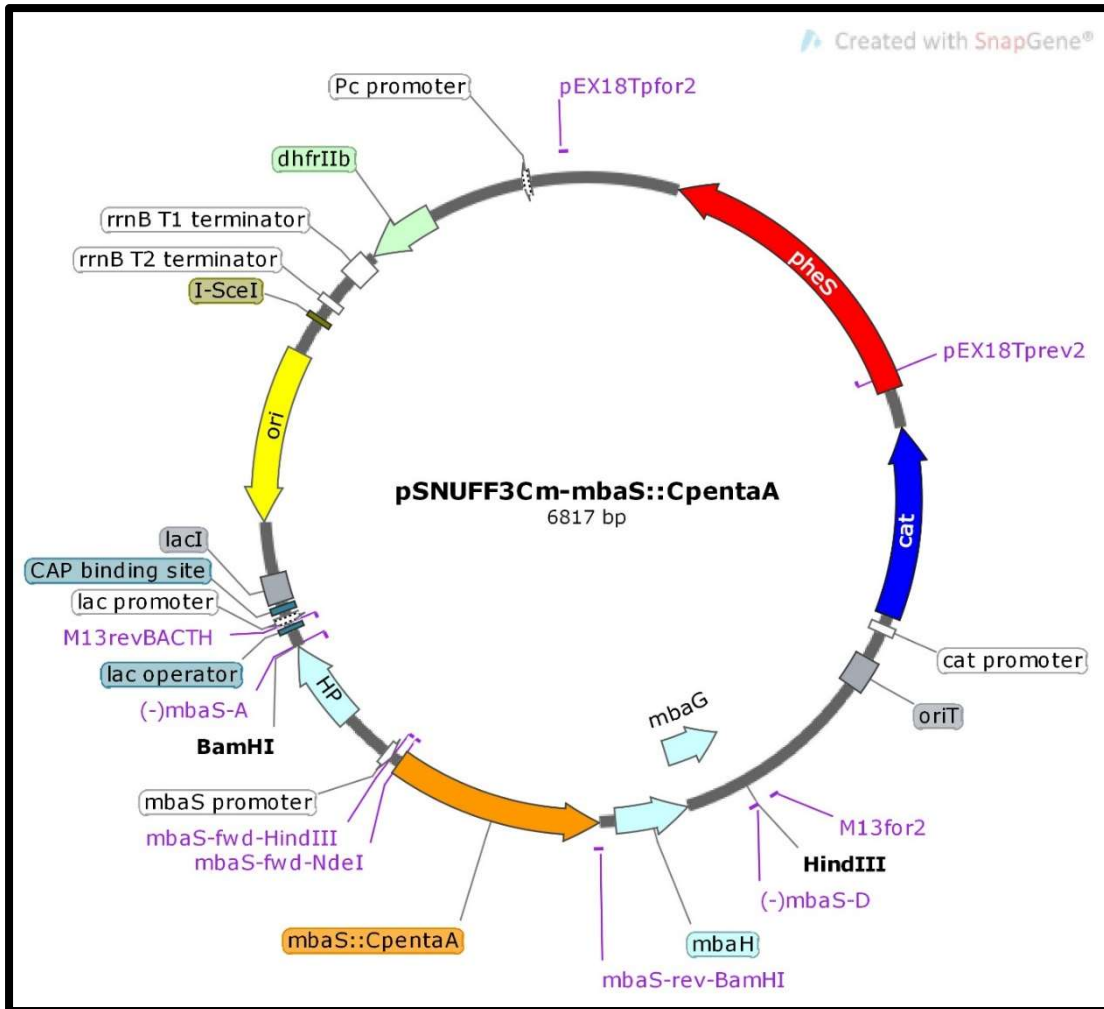
Figure A.16. Plasmid map of pSNUFF3Cm-*mbaS*CpentaA.

The locations of each of the following are shown: the *mbaS*CpentaA gene (orange), the trimethoprim resistance-conferring gene *dhfr*IIb (light green), the chloramphenicol resistance-conferring gene *cat* (blue), the *Bth* genes encoding MbaH, MbaG, and a hypothetical protein (HP) (light blue), the plasmid ColE1 replication origin *ori* (yellow), the *Bps* mutant gene *pheS* (red), the Pc, *lac*, *cat* and *mbaS* promoters (white), the *rrnB* T1 and T2 terminators (white), the CAP binding site and *lac* operator (teal), the *lacI* attenuator region (grey), the conjugal origin of transfer *oriT* (grey), the I-SceI meganuclease restriction site (olive), the *Bam*HI and *Hin*dIII restriction sites used in plasmid construction, and the binding sites for relevant DNA primers.
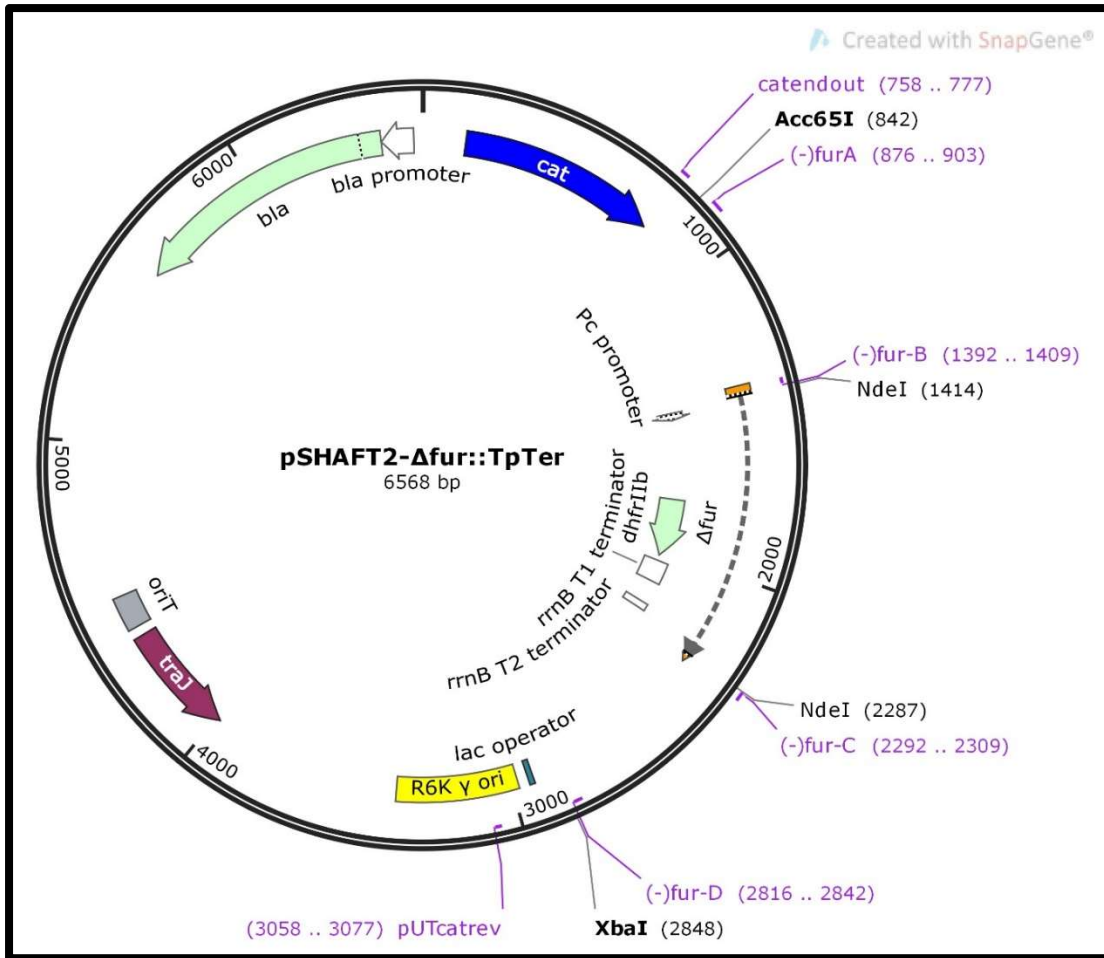
Figure A.17. Plasmid map of pSHAFT2-Δ*fur*::TpTer.

The locations of each of the following are shown: the disrupted Δ*fur* gene (orange), the trimethoprim resistance-conferring gene *dhfr*IIb (light green), the chloramphenicol resistance-conferring gene *cat* (blue), the ampicillin resistance-conferring gene *bla* (light green), the *E. coli* plasmid transfer gene *traJ* (purple), the R6Kγ replication origin *ori* (yellow), the Pc and *bla* promoters (white), the *rrnB* T1 and T2 terminators (white), the *lac* operator (teal), the conjugal origin of transfer *oriT* (grey), the *Nde*I, *Xba*I and *Acc*65I restriction sites used in plasmid construction, and the binding sites for relevant DNA primers.